30ᴛʜ Annual
Precise Time and Time Interval (PTTI) Systems and Applications Meeting

Proceedings of a meeting held at
The Hyatt Regency Hotel
at Reston Town Center
Reston, Virginia
1 — 3 December 1998

20030612 120

The U.S. Naval Observatory
Washington, DC

NONPRINT FORM

1. Type of Product: softcover book	2. Operating System/Version:	3. New Product or Replacement: New	4. Type of File: Text

5. Language/Utility Program:

6. # of Files/# of Products:	7. Character Set:	8. Disk Capacity:
	9. Compatibility:	10. Disk Size:

11. Title:
Proceedings of the 30th Annual Precise Time and Time Interval (PTTI) Systems and Applications Meeting

12. Performing Organization: U.S. Naval Observatory 3450 Massachusetts Ave., NW Washington, DC 20392-5420	13. Performing Report #:	14. Contract #:
		15. Program Element #:

16. Sponsor/Monitor: U.S. Naval Observatory 3450 Massachusetts Ave., NW Washington, DC 20392-5420	17. Sponsor/Monitor # Acronym:	19. Project #:
	18. Sponsor/Monitor #:	20. Task #:
		21. Work Unit #:

22. Date: 1999	23. Classification of Product: Unclassified
24. Security Classification Authority: DOD	25. Declassification/Downgrade Schedule: none

26. Distribution/Availability:
A   Approved for public release; distribution is unlimited.

27. Abstract: This document is a compilation of technical papers presented at the 30th Annual Precise Time and Time Interval (PTTI) Systems and Applications Meeting held 1-3 December 1998 at the Hyatt Regency Hotel at Reston Town Center, Reston, Virginia. Papers are in the following categories:
- Recent developments in rubidium, cesium, and hydrogen-based atomic frequency standards, and in trapped-ion and space clock technology;
- National and international applications of PTTI technology with emphasis on GPS and GLONASS timing, atomic time scales, and telecommunications;
- Applications of PTTI technology to evolving military navigation and communication systems; geodesy; aviation; and pulsars;
- Dissemination of precise time and frequency by means of GPS, geosynchronous communication satellites, computer networks, WAAS, and LORAN.

28. Classification of Abstract:
Unclassified

29. Limitation of Abstract:
Unclassified Unlimited

30. Subject Terms: time, atomic time, time scales, precise time, frequency standards, precision oscillators, cesium, rubidium, hydrogen masers, trapped ion, time transfer, frequency transfer, synchronization, GPS, navigation, telecommunications, communication satellites, computer networks, geodesy, WAAS, LORAN, pulsars

30a. Classification of Subject Terms:
Unclassified

31. Required Peripherals:

32. # of Physical Records:

33. # of Logical Records:

34. # of Tracks:

35. Record Type:

36. Color:
Black and White

37. Recording System:

38. Recording Density:

39. Parity:

40. Playtime:

41. Playback Speed:

42. Video:
No

43. Text:
Yes

44. Still Photos:
No

45. Audio:
No

46. Other:

47. Documentation/Supplemental Information:
Bound hardcopies are available from POC. Hardcopies may also be ordered via http://tycho.usno.navy.mil/ptti/orderform.html. Table of contents, abstracts, and texts available at http://tycho.usno.navy.mil/ptti/index.html.

48. Point of Contact and Telephone Number: Lee A. Breakiron
Time Service Department, U.S. Naval Observatory, 3450 Massachusetts Ave., NW, Washington, DC 20392-5420
(202) 762-1092
lab@kepler.usno.navy.mil

30TH ANNUAL PRECISE TIME AND TIME INTERVAL (PTTI) SYSTEMS AND APPLICATIONS MEETING

Editor
Lee A. Breakiron
U.S. Naval Observatory

United States Naval Observatory
Washington, DC 20392-5420

1999

ORDER FORM FOR PROCEEDINGS

You can order back issues of the Proceedings from either PTTI or NTIS

Year	PTTI Price	NTIS Number	NTIS Price in U.S.; higher elsewhere
1 - 1969	unavailable	unavailable	unavailable
2 - 1970	$ 25.00	AD-881014 (incl. Vols. 1 and 2)	inquire
3 - 1971	unavailable	AD-758739	inquire
4 - 1972	unavailable	AD-A010785/4	inquire
5 - 1973	$ 25.00	AD-A010786/2	inquire
6 - 1974	$ 25.00	AD-A018192/5	inquire
7 - 1975	$ 25.00	AD-A040774/2	inquire
8 - 1976	unavailable	AD-A043856/4	inquire
9 - 1977	unavailable	AD-A123920/1	inquire
10 - 1978	$ 25.00	N79-24731/8	inquire
11 - 1979	unavailable	N80-29096/8	inquire
12 - 1980	$ 25.00	N81-27467/2	inquire
13 - 1981	$ 25.00	N82-20494/2	inquire
14 - 1982	unavailable	N83-35351/6	inquire
15 - 1983	$ 25.00	AD-A149163/8	inquire
16 - 1984	unavailable	N85-29221/7	inquire
17 - 1985	$ 25.00	inquire	inquire
18 - 1986	$ 25.00	inquire	inquire
19 - 1987*	$ 25.00	inquire	inquire
20 - 1988	$ 35.00	AD-A217145/2INZ	$ 77.50
21 - 1989	$ 65.00	inquire	inquire
22 - 1990	$ 69.50	N91-25755/0INZ	inquire
23 - 1991	$ 69.50	AD-A255837/7INZ	$ 31.50
23 - Tutorial	included	AD-A254745/3INZ	$ 45.00
24 - 1992	$ 69.50	AD-A267301/0INZ	$ 86.50
25 - 1993	$ 69.50	N94-30639/6INZ	$ 103.50
26 - 1994*	$ 69.50	N95-32319/2INZ	$ 86.50
27 - 1995	$ 69.50	N19960042616INZ	$ 69.50
28 - 1996	$ 115.00	inquire	inquire
28 - Tutorial	$ 35.00	inquire	inquire
29 - 1997	$ 135.00	inquire	inquire
30 - 1998	$ 135.00	inquire	inquire

*Includes an Errata volume

When ordering from PTTI, return order form with payment to:

PTTI Executive Committee
U.S. Naval Observatory
3450 Massachusetts Avenue, NW
Washington, DC 20392-5420
Tel: 202-762-1414, Fax: 202-762-1511

Make checks payable to "Treasurer, PTTI." Do not send cash. We cannot accept credit card orders. When you register for the PTTI meeting or order the Proceedings, your name is added to the PTTI mailing list to receive future meeting information.

When ordering from NTIS, contact:

U.S. Department of Commerce
Technology Administration
National Technical Information Service
5285 Port Royal Road
Springfield, VA 22161
Tel: 800.553.6847, Fax: 703.605.6900

E-mail: orders@ntis.fedworld.gov
WWW: www.ntis.gov

NTIS prices are subject to change without notice. There is also a handling fee. Microfiche is available.

OFFICERS

General Chairman
MR. DONALD H. MITCHELL
TrueTime, Inc.

Technical Program Committee Chairman
DR. DENNIS D. MCCARTHY
U.S. Naval Observatory

TECHNICAL PROGRAM COMMITTEE
DR. HENRY F. FLIEGEL
The Aerospace Corporation

MR. PAUL F. KUHNLE
NASA Jet Propulsion Laboratory

DR. RICHARD L. SYDNOR
NASA Jet Propulsion Laboratory (Ret.)

MS. FRANCINE M. VANNICOLA
U.S. Naval Observatory

MR. S. CLARK WARDRIP
SFA, INC.

EDITORIAL COMMITTEE CHAIRMAN
DR. LEE A. BREAKIRON
U.S. Naval Observatory

TREASURER
DR. LEE A. BREAKIRON
U.S. Naval Observatory

EXHIBITS AND PUBLICITY COMMITTEE CHAIRMAN
MR. DONALD H. MITCHELL
TrueTime, Inc.

AUDIO-VISUAL CHAIRMAN
MR. PAUL F. KUHNLE
Jet Propulsion Laboratory

TECHNICAL ASSISTANCE
MR. JEFFREY S. INGOLD
AlliedSignal Technical Services Corporation

MEETING ARRANGEMENTS
MS. SHEILA FAULKNER
SFA, Inc.

v

Distinguished PTTI Service Award Committee

Dr. Joseph D. White, Chairman
U.S. Naval Research Laboratory

Dr. Leonard S. Cutler
Hewlett-Packard Company

Dr. Henry F. Fliegel
The Aerospace Corporation

Dr. Richard L. Sydnor
NASA Jet Propulsion Laboratory (Ret.)

Past Recipients of the Distinguished PTTI Service Award

1994
Dr. Gernot M. R. Winkler
U.S. Naval Observatory
(Retired)

1995
Dr. James A. Barnes
National Institute of
Standards and Technology
(Retired)

1996
Professor Sigfrido M. Leschiutta
Politenico di Torino and
Instituto Elettrotecnico Nazionale G. Ferraris

1997
Professor Bernard R. Guinot
Bureau International des Poids et Mesures
(Retired)

ADVISORY BOARD MEMBERS

SESSION CHAIRMEN

SESSION I
DR. EDWARD D. POWERS
U.S. Naval Observatory

SESSION VI
DR. GERARD PETIT
Bureau International des
Poids et Mesures

SESSION II
MR. WILLIAM J. RYAN
Defense Information Systems Agency

SESSION VII
DR. GERARD PETIT
Bureau International des
Poids et Mesures

SESSION III
DR. MARK A. WEISS
National Institute of
Standards and Technology

SESSION VIII
DR. DIETER KIRCHNER
Technische Universität Graz

SESSION IV
MR. IVAN J. GALYSH
U.S. Naval Research Laboratory

SESSION IX
MR. T. (JAY) JAYAWARENDA
AT&T Laboratories

SESSION V
DR. WLODZIMIERZ LEWANDOWSKI
Bureau International des
Poids et Mesures

SESSION X
DR. WILLIAM J. KLEPCZYNSKI
Innovative Solutions International

POSTER SESSION
MR. JEFFREY S. INGOLD
AlliedSignal Technical Services Corporation

ARRANGEMENTS

MRS. SHEILA FAULKNER
SFA, Inc.

MR. PAUL F. KUHNLE
NASA Jet Propulsion Laboratory

FINANCE COMMITTEE

MR. RONALD L. BEARD
U.S. Naval Research Laboratory

DR. JOSEPH D. WHITE
U.S. Naval Research Laboratory

DR. LEE A. BREAKIRON
U.S. Naval Observatory

THE RECEPTIONISTS AT THE 30TH ANNUAL PTTI MEETING WERE:

MS. NICOLETTE JARDINE
MRS. ALINE KUHNLE
MS. CARMEN LÓPEZ
MS. TERESA SMITH
MRS. BETTY WARDRIP

TABLE OF CONTENTS

Session II

New Products for the Timing Community

William J. Ryan, Chairman
Defense Information Systems Agency

Presentations were made by representatives of Absolute Time Corporation; Allen Osborne Associates, Inc.; Brandywine Communications; Datum, Inc.; Femtosecond Systems, Inc.; Navtech Seminars & GPS Supply; Quartzlock UK Ltd.; TeleComm Solutions/Symetracom; Temex, Inc.; 3S Navigation; TimeTech, GmbH; Timing Solutions Corporation; TRAK Microwave Corporation; TrueTime, Inc.; and WR, Inc.

Session III

Algorithms and Analysis

Marc A. Weiss, Chairman
National Institute of Standards and Technology

POSTER SESSION

Jeffrey S. Ingold, Chairman
AlliedSignal Technical Services Corporation
(Papers have been reassigned to Sessions III, IV, VII, and IX)

SESSION IV

GPS/GLONASS I

Ivan J. Galysh, Chairman
U.S. Naval Research Laboratory

Session V

GPS/GLONASS II

**Wlodzimierz Lewandowski, Chairman
Bureau International des Poids et Mesures**

Session VI

Applying GPS Carrier Phase to Time and Frequency Transfer I

**Gerard Petit, Chairman
Bureau International des Poids et Mesures**

Session VII

Applying GPS Carrier Phase to Time and Frequency Transfer II

Gerard Petit, Chairman
Bureau International des Poids et Mesures

SESSION VIII

TWO-WAY SATELLITE TIME TRANSFER

Dieter Kirchner, Chairman
Technische Universität Graz

SESSION IX

FREQUENCY DISTRIBUTION

T. (Jay) Jayawardena, Chairman
AT&T Laboratories

SESSION X

NAVIGATION APPLICATIONS/GPS ENHANCEMENTS

William J. Klepczynski, Chairman
Innovative Solutions International

OPENING ADDRESS

Captain Dennis G. Larsen
Superintendent
U.S. Naval Observatory
Washington, DC

Good morning. I have a small book here of opening remarks that was prepared for me. I have been assured by my timing experts that it will take precisely ten minutes, which I think is the time allotted, assuming that I use the right frequency. I will try to keep on track here.

It is my pleasure to open the Thirtieth Annual Precise Time and Time Interval Meeting. The series, as most of you know, was started about 30 years ago to bring together the Department of Defense users of time with the experts to provide precise time and time interval. Since then, these PTTI meetings have expanded to include the international timing community and provide an opportunity for various users to bring forward their ideas and timing requirements for improving not only the Defense Department's needs, but also the needs of the world.

Similarly, these conferences have allowed time and time interval providers to make system developers aware of the latest improvements in the field. The objective of this series of meetings is mainly to disseminate and coordinate PTTI information at the user level; to review present and future PTTI requirements; to inform engineers, technicians, and managers of developing precise time and frequency technologies; and to provide an opportunity for an active dialog that is more important today than ever before.

In the past 30 years the accuracy with which time and time interval are measured and transferred has improved by three orders of magnitude, or an order of magnitude every decade. We have also witnessed remarkable growth in the use of time. It is safe to say that the development of precise time has played a critical role in the growth of technology that touches all of our lives today. The Global Positioning System is a prime example of a system based on timing that has had a remarkable impact on the world. There are many others.

Glancing at the program for this meeting, we will see that this year's schedule includes topics that promise even more significant developments for the future. Potential improvements in time and frequency standards provide a new challenge to develop timescale algorithms to steer the clocks of the next millennium. Our ability to transfer time is tested by the expected precision of these new standards, and significant improvements in time transfer will be required. A number of papers devoted to carrier-phase time transfer test this interest in the technique for improved time transfer.

All of these developments, however, bring on new issues that this meeting, and also future PTTI conferences, will have to address. The first concern that I would like to mention is the need to recognize operational standards for the timekeeping and time transfer. The Department of Defense and the U.S. has clearly recognized that inter-operability is a major issue. It has become evident that standards for time and time interval play an increasingly important role in assuring that modern systems can communicate among themselves and function effectively. We must strive to eliminate the costly practice of developing systems independently, without regard for the requirement to operate with other existing

and future systems. The application of advanced technology to address the world security needs demands that these systems adhere to standards in timing and in time transfer.

In 1998, Chairmen of the Joint Chiefs of Staff Master Position, Navigation, and Timing Plan and the Federal Radionavigation Plan assigned responsibility for DoD timekeeping to the U.S. Naval Observatory. We stand ready to assist those who are improving current systems and those who are developing new systems to eliminate needless and expensive duplication in the area of PTTI. One specific step the Naval Observatory is currently taking is hosting a meeting of the Naval Sea Systems Command-sponsored Timing and Synchronization Working Group, the Common Time Requirements System Engineering Team, or CTRSET, at the U.S. Naval Observatory on 12 January. This group is addressing the implementation of the common-time reference in the Navy and will eventually elevate this issue to the joint level. We will take that opportunity to hold a DoD PTTI meeting on the afternoon of the 12th to discuss future timing requirements for the Department of Defense.

A second issue being recognized at the CTRSET is that precise time is becoming a utility, much like that of electricity and communications. The ability to obtain precise time and time interval is assumed in the infrastructure of modern society. We often deal with users of precise time who are unaware of the dependence on availability of precise timing information. It is a product that most take for granted. Therefore, we must recognize the need to manage this new utility and meet society's current and future requirements.

Another interesting recognition came from the recent proposal by the GPS Independent Review Team for the GPS Joint Program Office to create a national GPtS – and that is a small "t." The initials stand for "Global Positioning and time System," with the "t" being small to show its fundamental importance. This management responsibility involves not only the productive stewardship of national resources, but also the recognition that a society makes increasing demands on time; we also make ourselves vulnerable to its disruption. National and international laboratories must work together to make sure that the world's timing needs are not compromised; requirements for redundant systems must also be evaluated carefully; and systems designers will have to deal with making provisions for adequate backups.

We who are in the business of providing time to users often complain how difficult it is to establish definitive requirements for time and time interval at these PTTI meetings. While we need to document requirements for budgetary purposes, users are often wary of being specific about their needs, feeling that they will be asked to fiscally support their timing demands. The need for documented requirements still exists, and I hope that this and future meetings will continue to address that need.

In addition, I would like to challenge users of time to think creatively about new possibilities that take advantage of our ability to provide time and time interval with much improved precision. Utility of precise time will in the future provide improvements to us all. We need to plan now to take advantage of this resource.

While we spend the next few days here discussing the latest developments in time and time transfer and innovative uses of timing. We also need to keep in mind these broader issues: standards for inter-operability, managing time as a national and international utility, PTTI vulnerabilities and backup systems, and creative planning for future utilization of precise timing.

I am looking forward to the presentations and discussions, and I thank you all for your attendance and for your participation. Thank you.

PTTI DISTINGUISHED SERVICE AWARD

**Presented to
Dr. Jacques Vanier
Director General
Institute for National measurements Standards
National Research Council
Canada
(Retired)**

**by
Dr. Richard L. Sydnor
Jet Propulsion Laboratory
(Retired)**
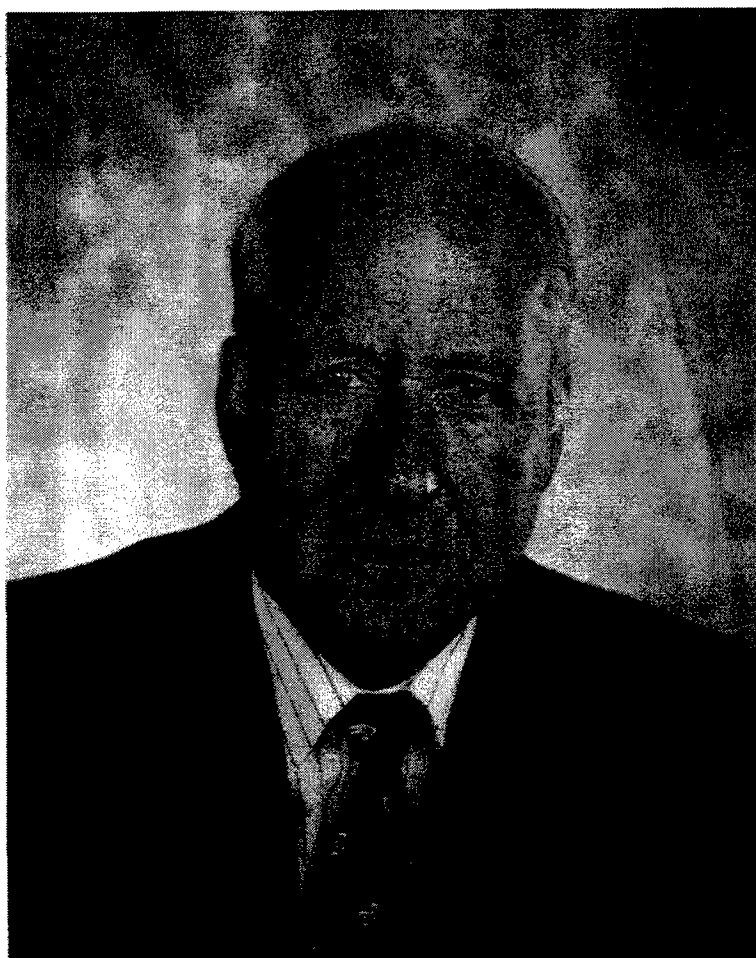
As you can see, I am not Leonard Cutler. Len had a recurrence of an illness and was hospitalized. He is doing well and is now home but could not make this trip. I am going to read what he has given us. The Distinguished Service Award Committee has selected Dr. Jacques Vanier from Canada this year.

Jacques Vanier was born in Canada. He received his B.A. and B.Sc. degrees in physics from the University of Montreal and his M.Sc. and Ph.D. in physics from McGill University, Montreal.

During his career Dr. Vanier has worked in various institutions, organizations and companies, such as University of Montreal, McGill University, Laval University, Defence Research Establishment, Varian Associates, Hewlett-Packard and the National Research Council of Canada. In this last institution, he was Director General of the Institute for National Measurement Standards. He is now Adjunct Professor of Physics at the University of Montreal. His teaching and research have been concentrated in solid state physics, semiconductors, thermodynamics, electromagnetism and quantum electronics. His most vivid souvenir of all his research activities is the day he dropped in the vacuum system of a hydrogen maser a cigar that a proud, new father had given him. To retrieve it, he had to take to pieces the whole system. This gave him solid experience to act as consultant for several companies such as Varian Associates, CA, Communication Components, CA, and EG&G, MA. He is now pursuing this activity for Kernco, MA. He also acted as Guest Worker in several organizations such as: the Centre National de la Recherche Scientifique (CNRS), France; the National institute of Standards and Technology (NIST), USA; the Instituto Elettrotecnico Nazionale (IEN) and the Universita di Pisa, Italy.

While pursuing these activities he could not resist being pulled into various committees and functions. Those he feels he may have made a contribution worth mentioning are: Union Radio Scientifique Internationale (URSI), President of Commission A (1990-1993); Conference of Precision Electromagnetic Measurements (CPEM), President of the 1990 Conference in Ottawa, and president of the Executive Committee (1990-1994); Frequency Standards and Metrology Symposium (initiator and co-founder); Administrative Committee of the I&M Society of the IEEE (1987-1993); Comité International des Poids et Mesures (1990-1996).

He is: Fellow of the Royal Society of Canada (RSC); Fellow of the American Physical Society (APS); and Fellow of the Institute of Electrical and Electronics Engineers (IEEE). In 1984, he received the IEEE Centennial Medal. In 1994, he was presented the Symposium on Frequency Control Rabi Award for his contributions to the field of atomic frequency standards.

He has written and published over ninety papers in scientific journals and conference proceedings. He spent six years in the writing of a book (with C. Audoin, Université de Paris as co-author): "The Quantum Physics of Atomic frequency Standards." To the question "Why that long?", his reply is, "With two authors it is twice as long."

Dr. Vanier is a dedicated painter. He presently pursues this activity and participates in various exhibitions. He uses oil as a medium and concentrates on Canadian landscapes. Dr. Vanier is also adept at boating. Confident in the usefulness of atomic clocks he has installed a Loran-C receiver in his boat. He says that the device can tell him accurately that the boat is in the Saint-Lawrence River and not on Saint-Catherine Street in downtown Montreal. He is thinking of switching to GPS.

Jacques, please come up to the podium, I would like to present you with the award. It is a clock.

Jacques Vanier

Thank you very much, Dick, for the kind words and for the humor contained in them.

I wish also to thank the committee which selected me for this award. In looking at this room and looking at the faces, I can see a lot of persons who deserve recognition in this field. I can only wish that one day they will experience the joy that I am enjoying at this moment in receiving this award.

Some time ago I decided to retire and do something else with my life. After an occasion like this one, I had questioned this decision. After a few years and after filling my house with paintings and creating the great collections of Vanier, in my house, I really questioned that. Then I received a timely invitation from Professor Leschiutta, from the IEN, to visit his institute and start doing something useful again. It did not take me long, maybe 50 microseconds in time interval, to make a decision. I am glad to say that I am back to quantum mechanics of atomic clocks again and trying to contribute. It was quite successful.

It is very exciting. Actually, I will say that it is a very privileged life. You do what you like most, and you get paid for it. Love this stuff, and people recognize you once in awhile. So, I would like to thank you again for this recognition. I feel that I belong to this group, and I find an identity in it. Thank you again very much.

30 YEARS OF PTTI – A RETROSPECTIVE

William J. Klepczynski
Innovative Solutions International
1608 Spring Hill Toad, Vienna, VA 22182
(202) 651-7670, *Bill.Klepczynski@faa.dot.gov*

Five years ago, my predecessor at the US Naval Observatory gave a history of PTTI which covered 25 years [1]. It is an excellent, informative and insightful review and I refer everyone to it. I do not think that you can find a better and more meaningful article.

This year I was asked to give a retrospective look at 30 years of PTTI. If you look up "retrospective" in a thesaurus, you will find a group of words which imply that a retrospective look of a subject is done from a personal point of view. These words include: looking back, contemplating the past, recollection, considering past events, remembering, perspective from the present, and memory. I will draw upon some of these different synonyms in this look based somewhat on personal experience. However, I will do it in a way which avoids mentioning the names of individuals, because, alas, I may miss a few and I do not wish to slight any of the people whom I might miss and for whom I have fond memories.

In the early 60's, I started at USNO in the Nautical Almanac Office. It was there that I became associated with the Institute of Navigation. This exposed me to the intrinsic and intimate relation of navigation with timing. It was with the ION that I first heard of Omega, Loran-C, TRANSIT, and vaguely something about 621B and Timation, the forerunners of GPS. It was an exciting experience because one could see the change that was rapidly taking place during that decade. In fact, the impact and role of navigation systems on timekeeping has been, is, and will continue to be dramatic. The land-based navigation systems that impacted timekeeping, such as Omega and Loran-C, gave way to GPS and now the role of GPS may be supplemented by the Satellite-Based Augmentation Systems currently being developed. These latter systems include the WAAS, EGNOS, and MSAS. They will enable global, real-time nanosecond synchronization to UTC.

On transferring to the Time Service Division in the early 70's, I immediately became involved with two entirely different aspects of practical timekeeping. The first being atomic time through participation in portable clock trips and the second being astronomical time through the construction of a 65 cm Photographic Zenith Tube (PZT) used in Earth Rotation studies. I believe portable clock trips led to the development of advanced time transfer techniques. There had to be an easier way to compare clocks than through the costly transport of 150 lb. behemoths. Also, for the first time I became aware of the National Bureau of Standards, now National Institute of Standards and Technology. During these last 30 years, both NIST and USNO have flourished. NIST developed its Cesium VII and USNO became the time reference for GPS.

While many here may not be aware of it, astronomy had played an important role in timekeeping during the early part of these last 3 decades. The definition of the second had just undergone great turmoil and change in the late 60's and early 70's. Relatively quickly, the basis of the SI second changed from the ephemeris second (astronomical) to the cesium second (atomic) and leap seconds were introduced into UTC.

Going back to astronomical time for the moment, the optical PZT was an instrument used to measure the rate of rotation of the Earth. It did this by comparing the time of transit of stars to time scales based on an ensemble of cesium clocks. While this instrument was productive over several decades, it became replaced by radio astronomy techniques. Such is the natural course of events. But the overall impact of astronomy in timekeeping was and is dwindling. UTC is no loner based on a purely astronomical measure. But, to this day, knowledge of Earth rotation for navigation is still extremely important. It is what limits the long-term, total, self-sufficiency of GPS. GPS needs to know how the Earth is rotating underneath it.

During the 70's, we saw the development of the improved cesium-beam tube (HP 5061, 004 option). This gave way to the HP 5071 cesium-beam frequency standard in the 80's. This was a very significant step in timekeeping. Also this era started to see the production of reliable hydrogen maser clocks. Now, masers are capable of running for extended periods of time without the need for a cast of thousands to keep them running. The role of the rubidium clock has more recently changed. Improvements in their design and construction have led to their choice in the next generation of GPS satellites.

The improvements in clock technology subsequently led to improvements in time scale calculation. A significant number of improvements in time scale algorithms included better weighting of clocks and the incorporation of different kinds of clocks into them. We are now seeing the development of time scale algorithms using Kalman filtering techniques, another significant milestone. Simultaneously with these improvements, there were significant advances in the characterization of the statistical behavior of clocks and the description their noise processes.

While portable clock trips were reaching their peak in the late 70's and the early 80's, alternative methods for time transfer were being developed and tested. The use of Omega and Loran-C gave way to GPS, probably the most significant factor affecting timekeeping during this period. It allowed global time transfer at the level of several nanoseconds. Experiments in two-way satellite time transfer using the ATS and Symphonie satellites led to the development of the Mitrex modem, which utilized PRN coded signals locked to the 1 PPS of a user's clock.

As my predecessor did at the end of his twenty-five year history of PTTI, I will also make some predictions for the future. However, mine may not be so conservative. In the not too distant future, it is entirely possible that UTC may yet undergo another revision and do away with the leap second. And, I already have mentioned the possibility of having a global, real-time synchronization capability at the 1 nanosecond level. Lastly, I see a possible restructuring of the major timing institutions in the United States.

I really feel blessed to have participated in this period of PTTI. There have been many advances and developments within a relatively short time span in which many of us at this meeting have taken part. We are in a unique field. It is composed of individuals who have developed an extraordinary sense of camaraderie. I am glad to have been a part of this exciting time in our history.

REFERENCES

[1] G. M. R. Winkler 1994, *"Twenty-five Years of PTTI,"* Proceedings of the 25th Annual Precise and Time Interval (PTTI) Applications and Planning Meeting, 29 November-2 December 1993, Marina del Rey, California, USA, NASA CP-3267, pp. 1-10.

Questions and Answers

DENNIS D. McCARTHY (USNO): Do you have any ideas on the redefinition of UTC?

WILLIAM KLEPCZYNSKI (ISI): What I see happening, where I work now, with the Satellite-based Augmentation System, many of the countries want to use existing systems, such as GPS and GLONASS. However, GLONASS has in its prime base UTC, which introduces the leap second. Whenever there is a leap second, GLONASS becomes unavailable for anywhere from two minutes to 20 hours. This last year there was a very significant outage because they also did a very big time step. To use it as the reliance on a safety-critical navigation system, I feel that it will not be accepted, that easily, until some change is made in the time basis. This may be one way to achieve that, or there might some momentum gathering for something like that.

GPS WEEK ROLL-OVER AND Y2K COMPLIANCE FOR NBS-TYPE RECEIVERS, AND ABSOLUTE CALIBRATION OF THE NIST PRIMARY RECEIVER*

M. Weiss, V. Zhang
National Institute of Standards and Technology
325 Broadway, Boulder, CO 80303

E. Powers
U.S.Naval Observatory

R. Loiler
Allan Osborne Associates

Abstract

The NBS-type receiver software was modified to account for both the GPS end-of-week crossover and for the Y2K event. Receivers using this software were tested by personnel from the National Institute of Standards and Technology and the U.S. Naval Observatory using a simulator at the Naval Research Laboratory. An independent test was performed by a private company. The software now appears to be fully compliant with requirements for both the GPS week roll-over and the Y2K events. Since the NBS-type receivers are still the predominant receiver for time transfer among laboratories which generate International Atomic Time, this receiver was given significant attention. In the process, an absolute calibration of the delay through the primary NIST GPS common-view receiver was completed. This calibration agrees within its 2.8 ns uncertainty both with the value from an estimate in June 1986, which has been used continuously since then, and with an absolute calibration in April of 1987.

GPS WEEK ROLL-OVER AND Y2K COMPLIANCE

Receivers of signals from Global Positioning System satellites decode time and date information from the satellite's 50 Hz bit stream [1]. The date is transmitted as a 10-bit week number plus the second of the week. With 10 bits, the week value can range from 0 to 1023. Week 1023 corresponds to the week ending August 21, 1999. The week starting August 22, 1999 will be broadcast as week 0 again. This event is called the GPS week roll-over. NBS-type receivers are those patterned after the time transfer receiver completed by the National Bureau of Standards (NBS, now called the National Institute of Standards or NIST) in the early 1980's. Software for these receivers is usually written by personnel of NIST.

---

*Contribution of U.S. Government not subject to copyright.

The GPS week number is used by the NBS-type receivers to synchronize the receiver clock. Unless the software is upgraded, NBS-type GPS receivers will not be able to update the clock after the GPS roll-over. The receiver clock will walk off, unless it is manually updated, resulting in incorrect time-tagging, shortened tracks, and loss of track.

NBS-type receivers keep track of the year using the two low-order digits, the ones and tens digits, since they can be held in one byte. At and after the year 2000, the routine in the receiver which converts the calendar date to the modified Julian day (MJD) will fail without an upgrade. Since this conversion is used as a test to see if the year was entered correctly, the receiver will also fail to back up the current date to its internal fail-safe clock. Consequently, the MJD will never be set correctly, and the date will be lost if power is cycled. If power is not cycled, the MJD will be incremented properly at the end of each day. Thus, users may not notice a problem until the receiver is turned off and on again.

An update which complies with both the GPS week roll-over and the roll over of the low-order digits of the calendar year at the year 2000, the so-called Y2K event, has been created. The GPS week roll-over software update, version V9802, for NBS-type receivers was tested at the Naval Research Laboratory (NRL) in February, 1998 [2]. V9802 was also tested by Allen Osborne Associates (AOA) in May, 1998. The test showed that V9802 handles the GPS week roll-over properly [3]. However, V9802 failed to set the receiver clock correctly when the receiver was powered up after the year 2000.

V9802 was modified to create the second version of software update, V9806. This version was tested by AOA in June of 1998, and passed the week roll-over and Y2K power-cycling tests without problems. Version V9806 was also tested at NRL using a GPS simulator [2] on August 25, 1998. The software was installed in a NIST GPS receiver (serial number NIST57, model TTR-5). The purpose of the test was to verify that the NBS-type GPS receiver with the software update will operate properly before and after the following events which were simulated during the test:

(1)   GPS week roll-over
(2)   Year 2000
(3)   Leap year after year 2000.

For the GPS week roll-over and year 2000 tests, the following were tested for the dates before and after the event:
--   if the receiver can correctly set its clock (MJD, date, time) when powered up,
--   if the receiver can track GPS satellites according to the schedule and lock on the GPS signal,
--   if the receiver can synchronize its clock when locked on the GPS signal (when the receiver clock is off by less than 15 minutes).

For the leap year test, we observed for the date from February 28 to March 1:
-- if the receiver can correctly set its clock (MJD, date, time) when powered up on February 29 of year 2000 and year 2004,
-- if the receiver clock (MJD, date, time) is correct during the track and in the idle state for the leap years (year 2000 and year 2004) and non-leap years (year 1999 and year 2001),
-- if the receiver can track GPS satellites according to schedule and lock on the GPS signal,
-- if the receiver can synchronize its clock when locked on the GPS signal (when the receiver clock is off by less than 15 minutes).

The tests have shown, with V9806:
-- the receiver clock (MJD, date, time) is set correctly when powered up before and after the roll-over, before and after the year 2000 and on February 29 after year 2000,
-- the receiver has no problem tracking GPS satellites and locking on the GPS signal,
-- the receiver can synchronize its clock when locked on the GPS signal (when the receiver clock is off by less than 15 minutes),
-- the receiver clock is correct during tracks and in the idle state for the leap years and non-leap years.

The test did reveal a few imperfections in V9806, minor things used for housekeeping purposes. Some of the imperfections were corrected to generate the new version V9809.

The test results indicate that the software update, V9809, is fully compliant with the requirements for both the GPS week roll-over and year 2000.

CALIBRATION OF THE NIST PRIMARY GPS RECEIVER

The receiver NIST57 was calibrated for its total timing delay in addition to being used to test the software for compliance with events as above. This calibration was transferred to the NIST reference receiver NBS10. The NIST57 was calibrated against the primary receiver, NBS10 from August 3, 1998 to August 13, 1998, before it was shipped to Naval Research Laboratory (NRL). At NRL, the NIST57 was calibrated using a simulator on August 25, 1998 [2]. The NIST57 was then returned to NIST and re-calibrated against NBS10 from September 6, 1998 to September 16, 1998.

During the calibration at NIST, the antenna for NIST57 was positioned in a location close to the antenna of NBS10. The two receivers were set up for a common-clock calibration [4,5,6,7]: they were given the same track schedule; the 5 MHz reference frequency and the local 1 pps (with known 1 pps cable delays) were derived from the same source, UTC(NIST) in this case. The receiver measures reference clock time minus GPS time (REF-GPS) via individual satellites [8]. To determine the relative

13

delay, NBS10 - NIST57, values of REF-GPS were differenced for matching satellites at the mid-point of full length tracks (track length of 780 s). Because both NBS10 and NIST57 were driven by the same clock, the REF-GPS differences yielded the differential receiver delays, once known cable delays were accounted for. The NIST57 was set up in the same condition before and after the trip to NRL, for closure.

During the simulator calibration at NRL, the C/A code at L1 frequency from the simulator was injected into the low-noise amplifier (LNA) of the NIST57's antenna/down converter, as indicated in block form in Figure 1. The signal power injected into the LNA was comparable to the GPS signal power received by the antenna. The 5 MHz reference frequency for NIST57 was taken from the same source as used by the simulator. The local 1 pps signal for NIST57 was generated by the simulator. The timing relationship between the local 1 pps signal for NIST57 and the C/A code transition for REF-GPS was estimated before the calibration.

The NIST57 took three standard 780 s tracks during the calibration. The third track was made after power-down/power-up of the receiver. Because the third track showed a warm-up trend with the measurements converging to the value before the power-down, only the mid-point REF-GPS value of the first two 780-second tracks were used to determine the absolute receiver delay. Since we know the simulator's REF-GPS offset from its 1 pps signal, the absolute NIST57 receiver delay can be obtained by:

Simulator - NIST57 = [(REF-GPS)simulator - (REF-GPS)NIST57] + cable delays.

With the NIST57 absolute receiver delay calibrated by the simulator and relative receiver delay calibrated by NBS10, the NBS10 receiver delay of this calibration is given as an offset from the current NBS10 delay by:

(NBS10 delay)cal = NBS10 delay + [(Simulator - NIST57) - (NBS10 - NIST57)].

The calibration results are presented in Table I. The comparisons between the traveling receiver, NIST57, and the primary receiver, NBS10, are in rows 2-3 with the number, N, of measurements, the mean, μ, of these measurements, the formal standard deviation σ, and the standard deviation of mean $\sigma/\sqrt{N}$. The noise type of each of the calibrations was determined to be consistent with a white phase noise model. Hence, the standard deviation of the mean is a valid statistic. Row 4 gives the value used for the transfer, 54.8 ns.

Below the transfer numbers Table I gives the values for the calibration with the simulator in rows 5-6. NIST57 was calibrated to have a delay of 56.2 ns. The difference of the NIST57 calibration, 56.2 ns, minus the transfer calibration of 54.8 ns gives the calibrated offset of NBS10, 1.4 ns. Adding this to the current receiver delay of 53 ns for NBS10 gives the calibrated delay of 54.4 ns.

The uncertainty of this NBS10 receiver delay calibration is about 2.8 ns, which is estimated from the uncertainty of the relative receiver calibration and the uncertainty of the absolute receiver calibration. The uncertainty of the relative receiver delay calibration is 2.0 ns, which mainly comes from the delay change of the antenna electronics as a function of the outdoor temperature change. The uncertainty of the absolute receiver delay calibration is 2.0 ns, which is the error in estimating REF-GPS of the simulator.

The historical values of the NBS10 delay are illustrated in Table II. The current value of the NBS10 receiver delay, 53 ns, was estimated in June, 1986. In April, 1987, the NBS10 receiver delay was calibrated via the absolute calibration of a traveling receiver at the United States Naval Observatory (USNO) with a calibrator of NRL. The NBS10 receiver delay of that calibration was 57 ns with an uncertainty of 5 ns. It was decided not to change the delay in NBS10 because the +4 ns delay change was within the uncertainty of the calibration. The NBS10 receiver delay of this calibration differs from the previous two calibrations by +1.4 ns and -2.6 ns, respectively. Because these values are within the uncertainty of this calibration, we conclude there is no significant change in the NBS10 receiver delay since June, 1986. Since the NIST receiver is part of the network of common-view GPS receivers used for generating TAI, this result implies that the delay used among the receivers in this network is consistent with the capabilities of current calibration equipment. NIST has verified the constancy of this delay at the level of a few ns over 12 years by constant inter-comparisons among three receivers. Some of the variations in these receivers are shown to be of order a few ns over the past 6 years in [9].

TABLE I: AUGUST- SEPTEMBER 1998 CALIBRATION

Calibrations at NIST: NBS10 - NIST57	N	μ (ns)	σ (ns)	$\sigma/\sqrt{N}$ (ns)
Before trip (8/3/98 - 8/13/98)	526	54.9	2.89	0.13
After trip: (9/6/98 - 9/16/98)	505	54.7	2.57	0.11
Mean value		54.8		
Simulator Calibration: Simulator - NIST57	N	μ (ns)	Uncertainty (ns)	
NRL: (8/25/98)	2	56.2	2.0	
Simulator - NBS10 Calibration	1.4 ns		2.8	
NBS10 receiver delay (9/98)	54.4 ns		2.8	

TABLE II: HISTORICAL CALIBRATIONS

Calibration	Value (ns)	uncertainty (ns)
June 1986, Theoretical Estimate — Used Continuously SinceThen	53	unknown
April 1987, at USNO with NRL Calibrator	57	5

REFERENCES

[1]   Interface Control Document, ICD-GPS-200, available from Arinc Research Corp., 11770 Warner Aver, Suite 210, Fountain Valley, CA 92708.

[2]   E.D. Powers, M. Miranian, J.D. White, J. Brad, "Absolute Time Error Calibration of GPS Receivers Using Advanced GPS Simulators," *Proc. 29th Precise Time and Time Interval (PTTI) Meeting*, pp 193-198, 1997.

[3]   This test was done with an Estel 7200 satellite simulator. Trade names are reported for completeness. No endorsement by NIST is implied.

[4]   J.A. Buisson, O.J. Oaks, and M.J. Lister, "Remote Calibration and Time Synchronization (R-CATS) Between Major European Time Observatories and the U.S. Naval Observatory Using GPS," *Proc. 17th PTTI*, pp.201-222, 1985.

[5]   W. Lewandowski, M.A. Weiss, and D. Davis, " A Calibration of GPS Equipment at Time and Frequency Laboratories in the USA and Europe," *Proc. 18th PTTI*, pp. 265-279, 1986, [also in *Metrologia*, 24, pp. 181-186, 1987].

[6]   M.A. Weiss, and D. Davis, " A Calibration of GPS Equipment in Japan," *Proc. 20th PTTI*, pp. 101-106, 1988.

[7]   W. Lewandowski, "Determination of the Differential Time Correction Between GPS Time Receivers Located at the Observatoire de Paris, the Observatoire de la Côte d'Azur and the Technical University of Graz," *Rapport BIPM — 91/6*, 1991.

[8]   D.W. Allan, C. Thomas, "Technical Directives for Standardization of GPS Time Receiver Software," *Metrologia*, 1994, 31, pp.69-79.

[9]   M.A. Weiss, V. Zhang, L. Nelson, V. Hanns, M.G.L. Regalado, "Delay Variations in Some Timing Receivers," *Proc. 1997 IEEE International Frequency Symposium*, pp.304-312.

ACKNOWLEDGMENTS
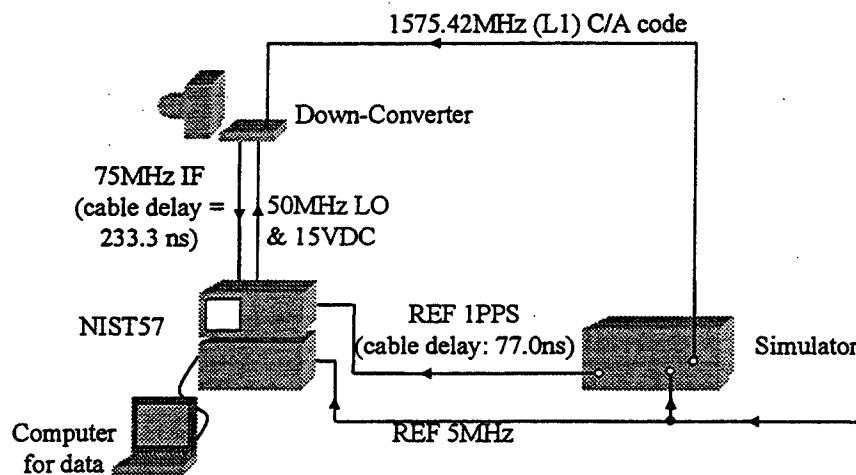
Figure 1. Test setup for the absolute calibration of NIST57.

Questions and Answers

ROBERT M. GRAHAM (Sandia National Laboratories): During the simulated end-of-week rollover tests, why was the GPS operational status (or rollover period) monitored for two minutes before the rollover and only 12 minutes after the rollover?

MARC WEISS (NIST): The GPS receiver is limited to accepting a programmed time change - via the simulator - of less than 15 minutes. We chose to begin monitoring GPS-operational status two minutes prior to the end-of-week rollover. Therefore, we were limited to the 12 minutes after the rollover.

POSTPROCESSED TIMESCALES AT THE U.S. NAVAL OBSERVATORY

Demetrios Matsakis and Lee A. Breakiron
U.S. Naval Observatory
Washington, DC 20392, USA

Abstract

A set of free-running timescales is generated using 9 years of data from the USNO clock ensemble. Cesium and maser clock phases and frequencies are characterized by global fits to first- or second-order polynomials, and the timescales are generated from the clocks' detrended frequencies using a variety of weighting functions. These timescales are compared to those generated by USNO's A.1, BIPM's ALGOS and TT98, and NIST's AT1 algorithms from the perspective of algorithm choice and frequency stability.

1 THE ALGORITHM

Since its derivation and implementation by Don Percival, the U.S. Naval Observatory (USNO)'s mean algorithm[1] has proven robust and adaptable for over 20 years. It is the basis of the USNO free-running mean timescale A.1, which is used to form the USNO mean timescale that is frequency-steered to International Atomic Time (TAI) or, equivalently, UTC(BIPM). In turn, the USNO Master Clock (MC2) is steered to the USNO mean timescale to generate UTC(USNO), providing the most precise on-line realization of UTC in the world today.

The A.1 timescale is actually an integrated frequency scale. In its current formulation, clock frequencies (rates) are generated by averaging the hourly first differences of clock timing data referenced to the USNO Master Clock (MC2). Individual clock frequencies are detrended, using the past A.1 as a reference, through a first-order fit (effectively, to clock rate and drift) over time ranges of uniform clock behavior, as determined by experienced USNO data analysts. Clocks showing poor performance, or not yet well-determined rates and drifts, are ignored, while all others are included with a weight depending upon clock type and, for masers, the time since the present[2]. For example, this dynamic weighting system initially weights day-old data from cavity-tuned masers up to 12 times more than data from cesium clocks, and 3-day-old maser data 5 times more than contemporaneous cesium data. It completely deweights maser data older than 75 days.

The A.1 timescale was always intended to be a compromise between stability and robustness. Its algorithm was motivated by the need to optimize on-line precision for a clock ensemble with a limited number of masers; different algorithms are now under consideration for the 12-maser ensemble currently maintained at the USNO. One innovation introduced in January, 1999 is to detrend cesiums and masers against a reference timescale composed of only cesium standards, as opposed to A.1. Another innovation under test is to realize UTC through a timescale composed of only masers that have been detrended against the unsteered cesium average.

Another possible problem with the current A.1 algorithm is that clocks are detrended individually, instead of all at once. The differences between the global and local minima for the values of the clock characterization polynomials are not very important in an on-line timescale whose main purpose is to provide a template for monthly steers to TAI; however, they are more important for work relating to comparisons with other free-running time scales or pulsar data.

We report here timescales generated using a postprocessed algorithm, informally titled SuperP, whose detrending polynomial models are determined through a global fit to inter-clock phase difference data which has been differenced from the temporally preceding clock difference N times. For example, phase data differenced once ("first differences") are equivalent to frequency data. Note that because the clock data are recorded only in the form of differences between clocks, the choice of reference is irrelevant. Also, the SuperP and A.1 timescales are underdetermined, by a polynomial of order M, if the timescale is generated from N integrations of a scale based upon Nth-order differences, which are detrended using a polynomial of order M-N. For solutions involving drift-corrections (M=2), any parabola may be added to the final timescale without affecting the consistency of the solution for optimal polynomial detrending coefficients. The free-running timescales TA(NIST), generated by NIST using their AT1 algorithm, and EAL, generated by the BIPM using their algorithm ALGOS[3], are also sensitive to the initial timescale reference (Table 1); if the initial values of one of these timescales had differed by an constant and slope, that same difference would have persisted to the present. If a perfectly calibrated set of drift differences between external timescales were available, it would be possible to determine the parabolic term from a limited set. One consequence of using all the data to resolve the indeterminacy, as opposed to a subset that is assumed to be better calibrated, is that long-term variations, such as would be expected due to white frequency noise, are masked and the effective errors in the comparisons are increased[4].

2 THE DATA

The USNO maintains an on-line archive of (currently) 9 years of clock data from its maser and cesium ensemble, beginning on MJD 47752 (11 August, 1989) and ending on MJD 51086 (30 September, 1998). Although lower-noise measurement systems are also being used, this work is based only on data taken with a time-interval counter and switch system, whose measurement accuracy is better than 100 ps. For brevity, only measurements at 0 hours UT were used in this analysis. In Figure 1, the numbers of each type of clock producing acceptable data are presented. Unfortunately, the decisions made by data analysts for maser data previous to MJD 50079 were not permanently recorded; thus, maser data previous to that time are here ignored, although re-analysis may be made at a later date. It is also possible that the editing information available for the oldest data is not accurate, and that a re-analysis will improve the results slightly. As is evident in the later figures, timescales are of lesser stability previous to about MJD 49400 (17 February, 1994); the subsequent improvement is due to the dramatic increase in the number and quality of clocks maintained at the USNO and contributing to TAI (cavity-tuned Sigma-Tau/Datum masers and HP5071 cesiums). The natural division of the data into three time ranges is the reason why different analyses presented below will begin at different MJD's. Comparisons with TT98 are limited by its cutoff in December, 1997.

This work is based on only data recorded as acceptable by USNO data analysts, with some additional automatic editing of outliers identified through a simple median-based scheme. The time ranges of the on-line polynomial clock characterizations determined by the data analysts were used to define the break points in the global least-squares solution to the polynomials. The important question of whether these time ranges are optimal in the determination of rate

and drifts is not addressed here. The A.1 used here differs somewhat from what has been reported to the BIPM due to the effect of dynamic weighting and occasional refinements in editing or clock characterization made after submission to the BIPM.

For comparisons with non-USNO timescales, time-transfer noise has always been a serious problem. Although much better than previous modes of time transfer, even common-view GPS time transfer has been shown to have systematic errors on the order of tens of nanoseconds. In 1995 and 1996 a BIPM-organized calibration effort revealed a total 29-ns calibration error in the common-view chain between USNO, NIST, and the Observatory of Paris (OP), and somewhat lower errors in the links between many other institutions and OP. Although most of the institutions involved immediately had their data adjusted with a single time-step, USNO's data were gradually corrected, in 3-ns steps, over the year 1997 (MJD 50482-50783), in consideration of USNO's users, most of whom require greater frequency stability. It is possible to verify the results of this procedure in a rough manner, by comparing the values for GPS time reported in Circular T with those measured at the USNO (Figure 2). Although this comparison does not benefit from the common-view removal of Selective Availability (SA), the 29-ns change is apparent, along with what appears to be a small (4 ns) residual error. This small error may be due to remaining calibration errors anywhere in the measurement chain. In the comparisons with UTC, EAL, and TT98, it was found that correcting the differences as if this problem had never occurred did not improve the comparisons, nor was there any improvement after crude allowance was made for the high weight USNO clocks have in the generation of EAL. It is possible that improvement would be evident if adjustments could be made for the fact that many other institutions had time-transfer corrections made at the same time.

3 THE SuperP FAMILY OF TIMESCALES

Perhaps the most important of the controversial issues related to timescale algorithms is the determination of clock weights, which need not be the same in the clock characterization and the timescale generation, and at times could be zero.

Although clocks whose frequency data display Gaussian statistics should theoretically be weighted by the inverse variance of their frequency data, in practice the USNO has found it more robust to weight all clocks of the same type equally[5]. This approach is justified because the accuracy and precision of measurement systems and clocks are difficult to assess, partly due to nonzero covariances in clock performance data[6,7], and because clock time series are not statistically stationary; in particular, past performance is not always a good indicator of future performance.

To study the effect of weighting, a very incomplete set of 9 functions was explored for weighting individual differences between clocks in the clock characterization solution. In all cases, measured difference data for each pair of clocks were weighted as the inverse root-sum-square (RSS) of the set of clock weights given in Table 2.

In applying the weights to the clock characterization, all possible clock pairs at each MJD were used without allowance for the strong correlation between pairs that include the same clock. Although solutions could be generated restricting all pairs to those involving any single reference clock (which may change between measurement times), this would complicate any solutions involving a variance-based weighting scheme. A more robust approach would involve using the full covariance function in determining a non-diagonal weight matrix for clock characterization. Of these weighting schemes, the best one (based on the 3-cornered-hat analysis described in the next section), effectively removes masers from the characterization process by down-weighting them by a factor of 1000.

Once the clocks were detrended using the clock characterization determined by the fitting, timescales were generated as averages of all clocks, one point per day, using the same weighting schemes as for clock characterization. For clarity in the analysis, the problem of combining data from masers with cesiums to form a timescale was bypassed through the generation of separate pure-maser and pure-cesium timescales. We note that modern steering theory would provide an optimal way to steer a supposedly less-accurate, but more stable, maser-based timescale to a cesium-based one[8].

4 THE INTERNAL ERRORS

The different weighting options were examined through the consistency of timescales generated using independent subsets of 1/3 of the data, and performing a 3-cornered-hat analysis which allowed for possible data correlations using a technique that minimizes covariances [7]. The subsets were chosen by assigning clocks in the order they were encountered by the computer, and excluded data before MJD 49400. The resulting stability assessments for cesium-only and maser-only averages (Figures 3) indicate a weak preference for a weighting scheme in which maser and cesium clocks are characterized by comparison with a unity-weighted pure-cesium mean, but the improvement of ignoring masers for clock characterization should be larger in an on-line timescale generated using our current dynamic weighting scheme.

Using the SuperP formalism, it is simple to generate timescales from other than the data's first differences, and to compare their results. Through determination of the internal errors, using the same technique as above, it was found that fitting first-order polynomials to the first differences (frequencies, as is done for A.1, AT1, and EAL) was preferable to fitting second-order polynomials to phase data, constants to second difference data, or nothing to third difference data (Figures 4). This was also found using the A.1 formalism[9], and is expected in a situation dominated by white FM. Once the clock characterization has been determined, differencing to order N also has the effect of smoothing over phase discontinuities of order N-1 that may be associated with gaps in the data. Since all the free-running timescales considered here are generated from first differences, this result validates what has long been done in practice.

Figures 5 show how the 3-cornered-hat analysis estimates the stability of HP5071-only and Sigma-Tau/Datum-only timescales derived by integrating average detrended frequencies, for which the clock characterization was determined through a weighting scheme sensitive only to cesiums and down-weighting non-HP5071 cesiums by a factor of 0.65. Also shown are a curve for the mean timescale of one-half of the clocks relative to the mean timescale of the other half, where the deviations were reduced in size by a factor of $\sqrt{2}$ to convert them from relative error to absolute error (neglecting covariances), and a curve for the mean of the entire HP5071 ensemble (assuming the three subsets could be weighted according to their inverse variances, hence also neglecting covariances).

5 THE EXTERNAL ERRORS

To estimate the external errors in the USNO data, comparisons were made between the USNO timescales and the BIPM timescales EAL and TT98 (the latter is in essence a postprocessed UTC, determined from EAL using information available at the end of 1997[10]), and their frequency stabilities relative to TT98 are shown in Figure 6. The most stable timescales are those generated by SuperP using only the most recent data; however, the disparity between

the size of the clock ensembles utilized and the existence of unmodelled time transfer noise obscures these comparisons.

Figures 7-11 compare the A.1, SuperP pure-maser average, SuperP pure-cesium average, and TA(NIST) with EAL and TT98. Here, A.1 is essentially a pure-cesium timescale because all the maser data have been phased out except for the last 75 days by the dynamic weighting. Again, for recent data the smallest RMS errors relative to TT98 were found for the SuperP timescales. For comparisons going further back into the past, A.1 provides the best fit to EAL. It is difficult to draw firm conclusions from these comparisons because it is evident that the statistics are not stationary. It would be better to simply note that the comparisons reflect the considerable improvement in recent years. This improvement is also evident in the USNO's ability to better steer our Master Clock to UTC—as reported in BIPM's last Circular T, all the timing differences between the USNO Master Clock and UTC were less than 2 ns. While we don't expect this close alignment to continue in the near future, it is entirely possible that pending improvements in time transfer and frequency standards may result in such differences between UTC and UTC(USNO) becoming routine in several more years.

6 CONCLUSIONS

A set of free-running timescales were generated using 9 years of USNO clock data and an algorithm dubbed SuperP, which made global fits of phases and frequencies to first-order and second-order polynomials. USNO clock frequencies and drifts are currently determined with respect to a pure cesium-based timescale. The procedure proved to be the best of those treated herein.

Timescales were generated from the clocks' detrended frequencies and a variety of weighting functions. Frequency stability assessments indicated a preference for fitting first-order polynomials to first differences, rather than other polynomials or other types of data.

Comparisons of A.1, SuperP, and TA(NIST) timescales to TT98 showed the greatest frequency stability for those of SuperP, while the A.1 provided the best fit to EAL. Partial allowance for past USNO/BIPM calibration errors does not improve the comparison between USNO data and the BIPM-generated timescales.

7 ACKNOWLEDGMENTS

8 REFERENCES

[1] D. B. Percival 1978, *"The U.S. Naval Observatory clock time scales,"* IEEE Trans. Instr. Meas., IM-27, 376-385.

[2] L. A. Breakiron 1992, *"Timescale algorithms combining cesium clocks and hydrogen masers,"* Proceedings of the 23rd Annual Precise Time and Time Interval (PTTI)

Applications and Planning Meeting, 3-5 December, 1991, Pasadena, California, USA, pp. 297-305.

[3] C. Thomas, P. Wolf, and P. Tavella 1994, **Time Scales**, Monograph 94/1, Bureau International des Poids et Mesures, Sèvres, France.

[4] J. A. Barnes 1984, *"The measurement of linear frequency drift in oscillators,"* Proceedings of the 15th Annual Precise Time and Time Interval (PTTI) Applications and Planning Meeting, 6-8 December 1983, Washington, DC, USA, pp. 551-582.

[5] L. A. Breakiron 1995, *"The effects of clock errors on timescale stability,"* Proceedings of the 26th Annual Precise Time and Time Interval (PTTI) Applications and Planning Meeting, 6-8 December, 1994, Reston, Virginia, USA, pp. 369-380 (see Errata volume #2).

[6] A. Premoli and P. Tavella 1993, *"A revisited three-cornered hat method for estimating frequency standard instability,"* **IEEE Trans. Instr. Meas., IM-42,** 7-13.

[7] F. Torcaso, C. R. Ekstrom, E. A. Burt, and D.N. Matsakis 1999, *"Estimating frequency stability and cross-correlations,"* these Proceedings.

[8] D. Matsakis, M. Miranian, and P. Koppang 1999, *"Steering the U.S. Naval Observatory (USNO) Master Clock,"* Proceedings of 1999 Institute of Navigation Technical Meeting, 25-27 January 1999, San Diego, California, USA, in press.

[9] L. A. Breakiron 1994, *"A comparative study of clock rate and drift estimation,"* Proceedings of the 25th Annual Precise Time and Time Interval (PTTI) Applications and Planning Meeting, 29 November-2 December 1993, Marina del Rey, California, USA, pp. 401-412.

[10] B. Guinot 1988, *"Atomic time scales for pulsar studies and other demanding applications,"* **Astronomy and Astrophysics, 192,** 370-373.

Table 1. Comparison of several algorithms with SuperP.

Algorithm	Timescale Weights	Constant Correction?	Freq Corr?	Drift Corr?	Detrending Time (days)
NIST (AT1)	(exp)*	N/A	yes	(exp)*	20-30
EAL(BIPM)**	(1-year var)	N/A	yes	no	30 (was 60)
UTC,TT(BIPM)	***	N/A	***	0***	-
USNO (A.1)	dynamic	N/A	yes	yes	as needed****
SuperP					
Ave phase	8 options	option	option	option	as needed
Ave 1st diff	"	N/A	option	option	"
Ave 2nd diff	"	N/A	N/A	option	"
Ave 3rd diff	"	N/A	N/A	N/A	"

* NIST AT1 based on exponential filter: last frequency estimate averaged with most recent estimate, with time constant set to 20-30 days. Weights are based upon the inverse variance and a similar exponential filter[3].

** BIPM-EAL subtracts from each clock phase a term: A+B*time, where A is the previous phase and B is the frequency estimate. This would be 100% equivalent to second diff if their "B" were related to frequency obtained from two adjacent 5-day points instead of the past 30 days (formerly 60). Clocks with significant drifts are deweighted[3].

*** UTC and TT are generated by steering UTC to the primary (calibrated) frequency standards, hence the drift is zero by definition. Of course time-transfer noise and frequency measurement errors are not completely negligible.

**** Typically 30-360 days.

Table 2. Clock-based weight schemes explored in this work. Schemes 4 through 9 are based upon the performance (statistical properties) of the clock, as measured through an initial computation of the difference between the detrended clock data and an average of all clocks, using unity weights to characterize and average the initial estimate, which is performed in the same difference mode as the final computations.

1. 1.0 for all clocks

2. 1.0 for HP5071 cesiums, .65 for other cesiums, .001 for masers

3. 1.0 for HP5071 cesiums and all masers, .65 for other cesiums

4. Inverse of squared sum of temporarily adjacent points

5. Inverse of variance, computed after removal of mean difference

6. Inverse variance

7. Inverse variance times the time range of the data in MJD

8. Inverse variance times the time-range of the data squared

9. Inverse variance times the time-range of the data cubed
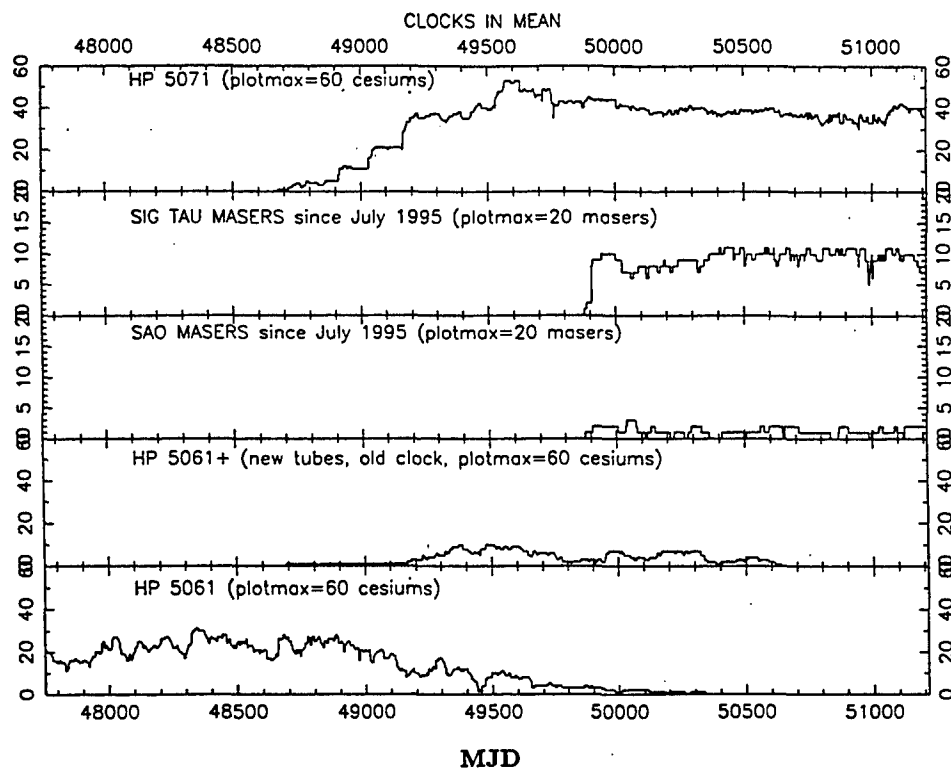
Figure 1. Number of USNO clocks used in SuperP and A.1. Maser data previous to MJD 50079 are available, but the associated editing and trend-break decisions would have to be re-evaluated.
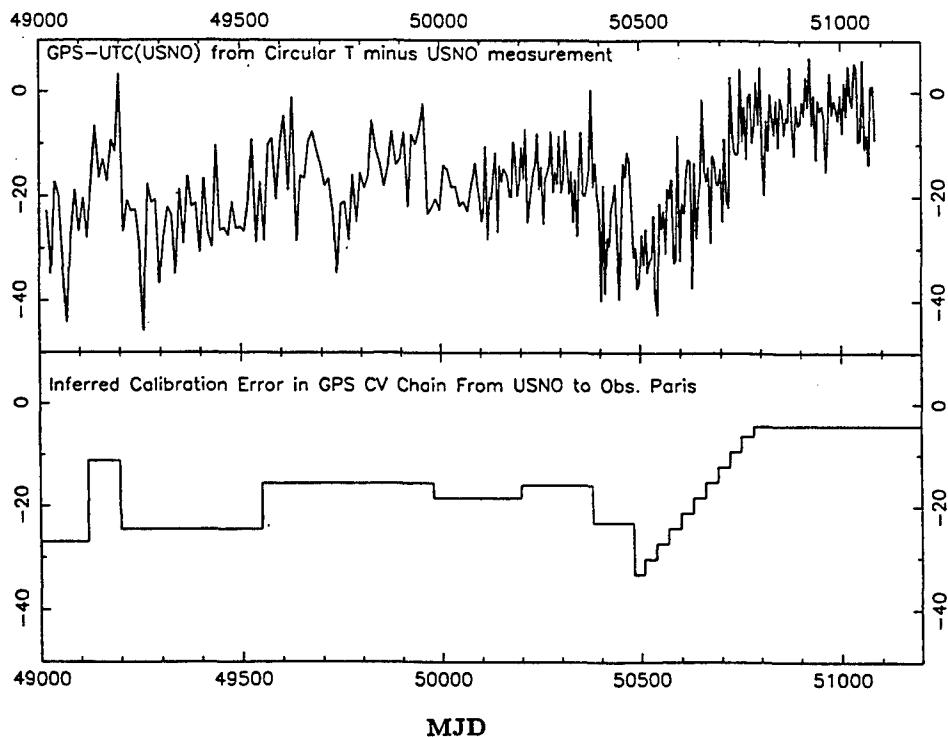
Figure 2. Calibration errors in chain USNO-NIST-OP, as estimated from USNO and BIPM measurements of GPS.
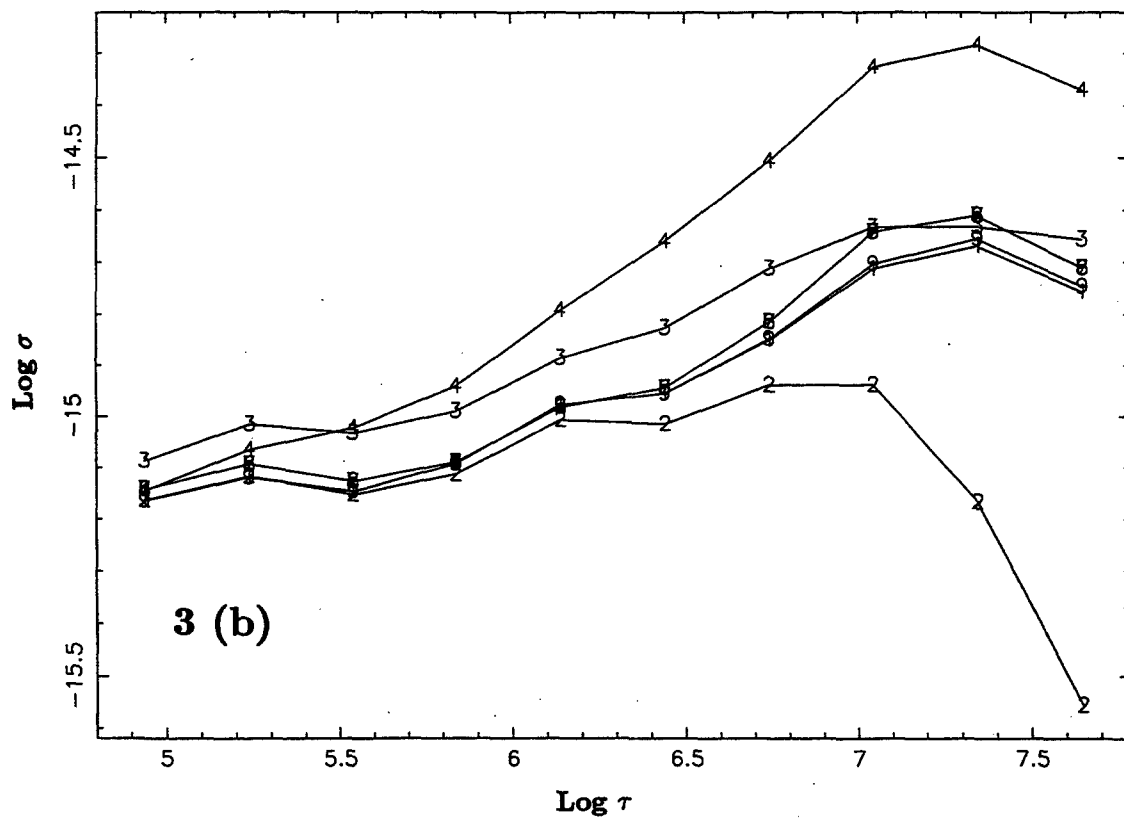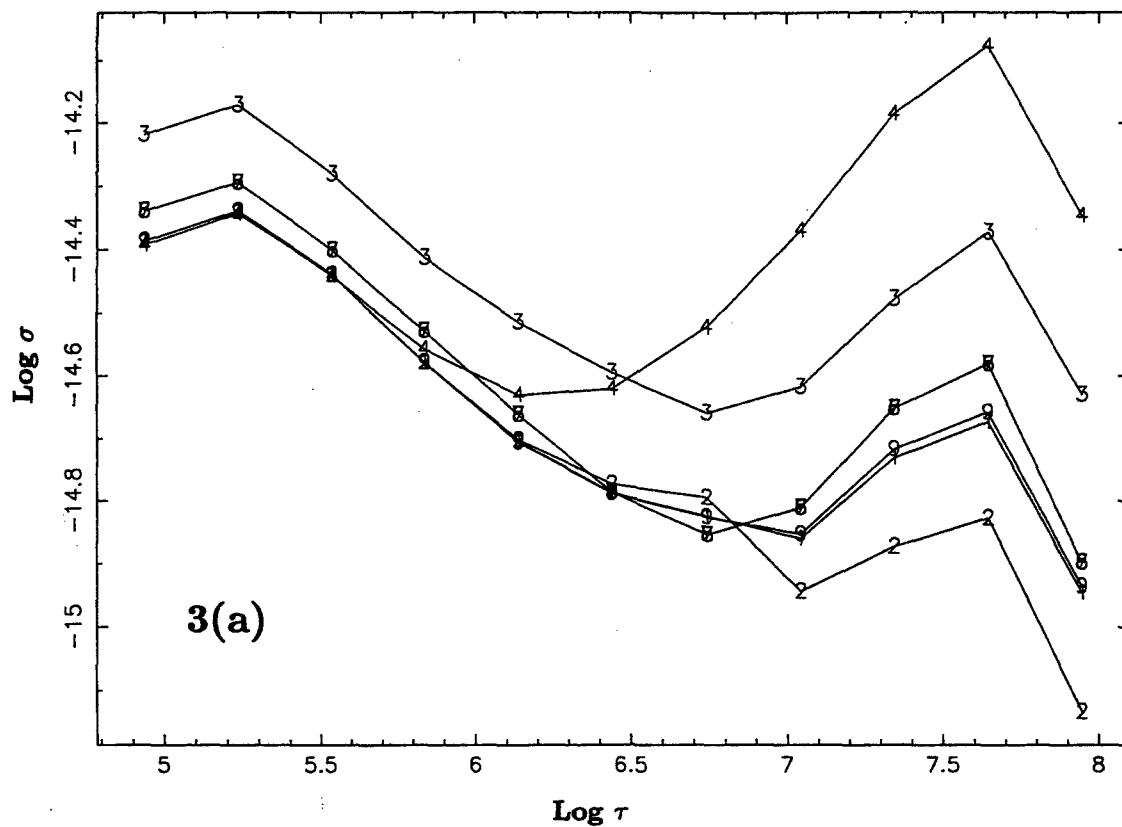
Figure 3. Frequency stabilities for integrated first-difference timescales derived using weighting schemes in Table 2. (a) is for cesium-only data since MJD 49400. (b) is for maser-only data since MJD 50079. Plot characters correspond to rows of Table 2. σ is the Allan deviation for frequency and τ is the sampling time in seconds.
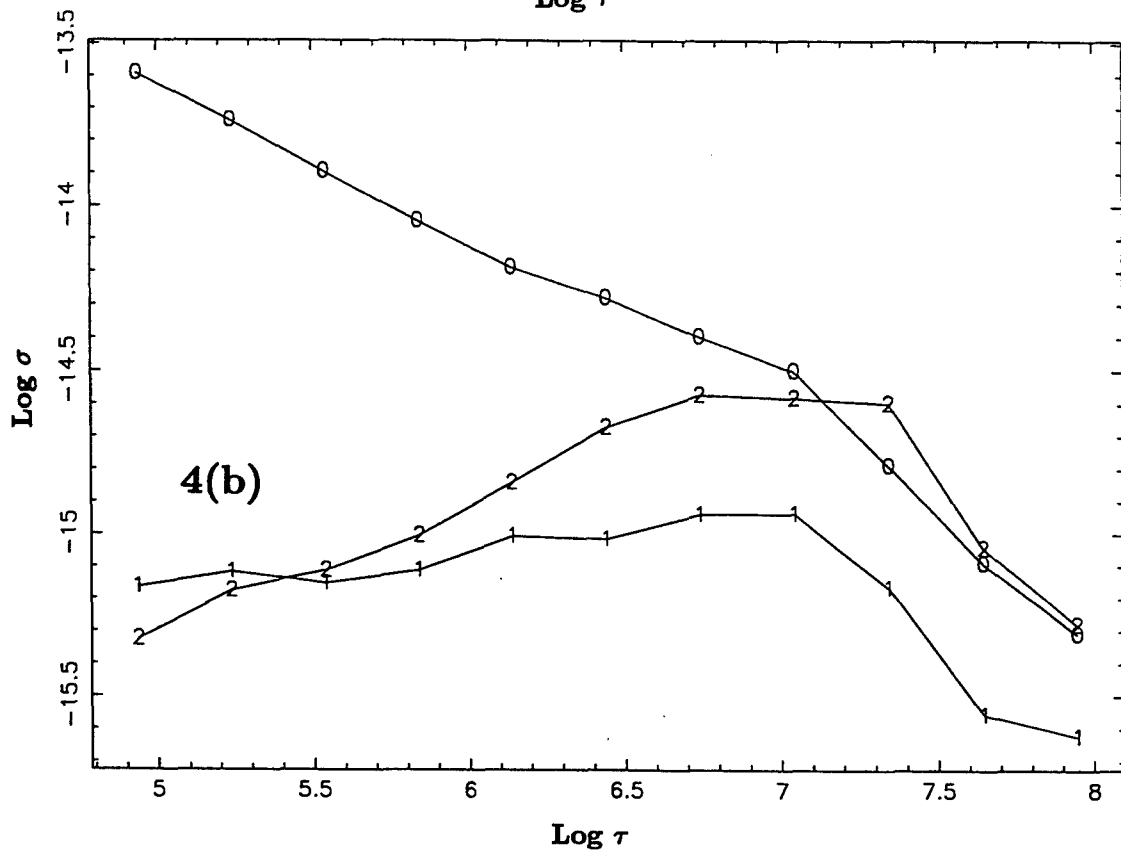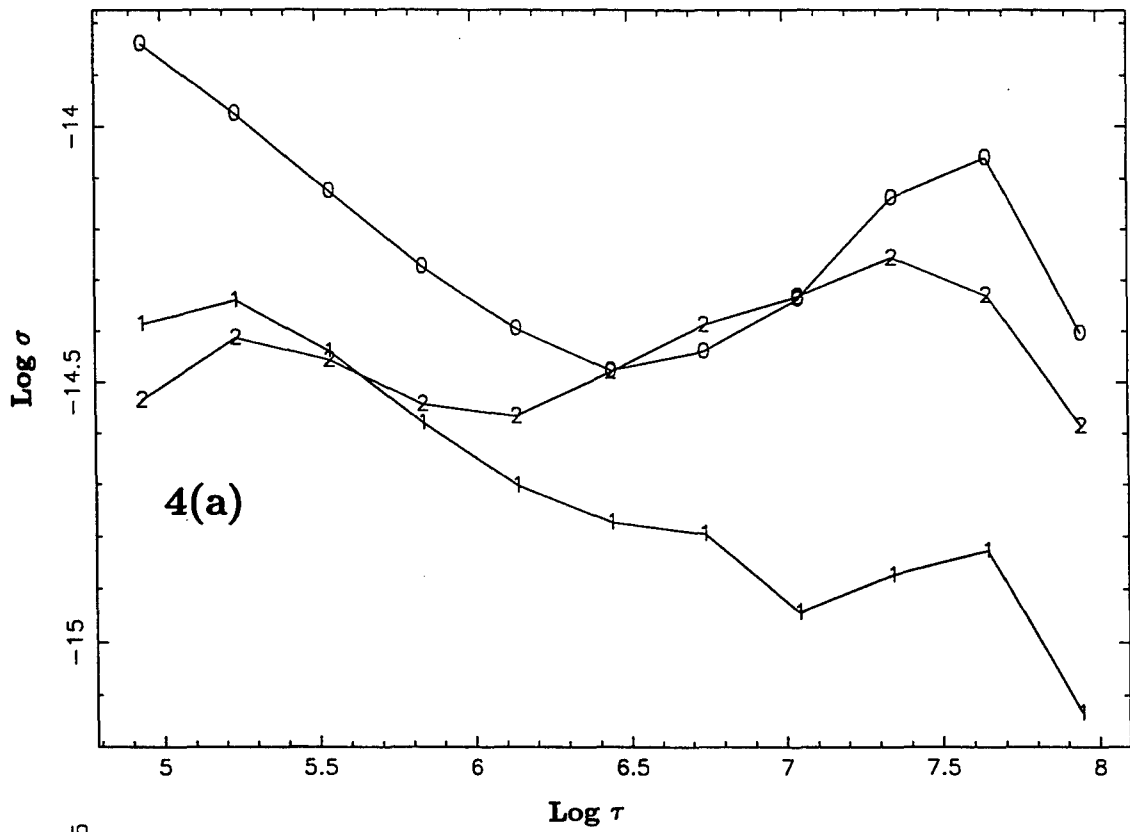
Figure 4. Frequency stabilities for timescales derived using temporal Nth-order data differences and cesium-dominated weight scheme "2." (a) is for cesium-only timescales using data since MJD 49400. (b) is for maser-only timescales derived using data since MJD 50079. Plot characters correspond to order of pre-fit differencing.
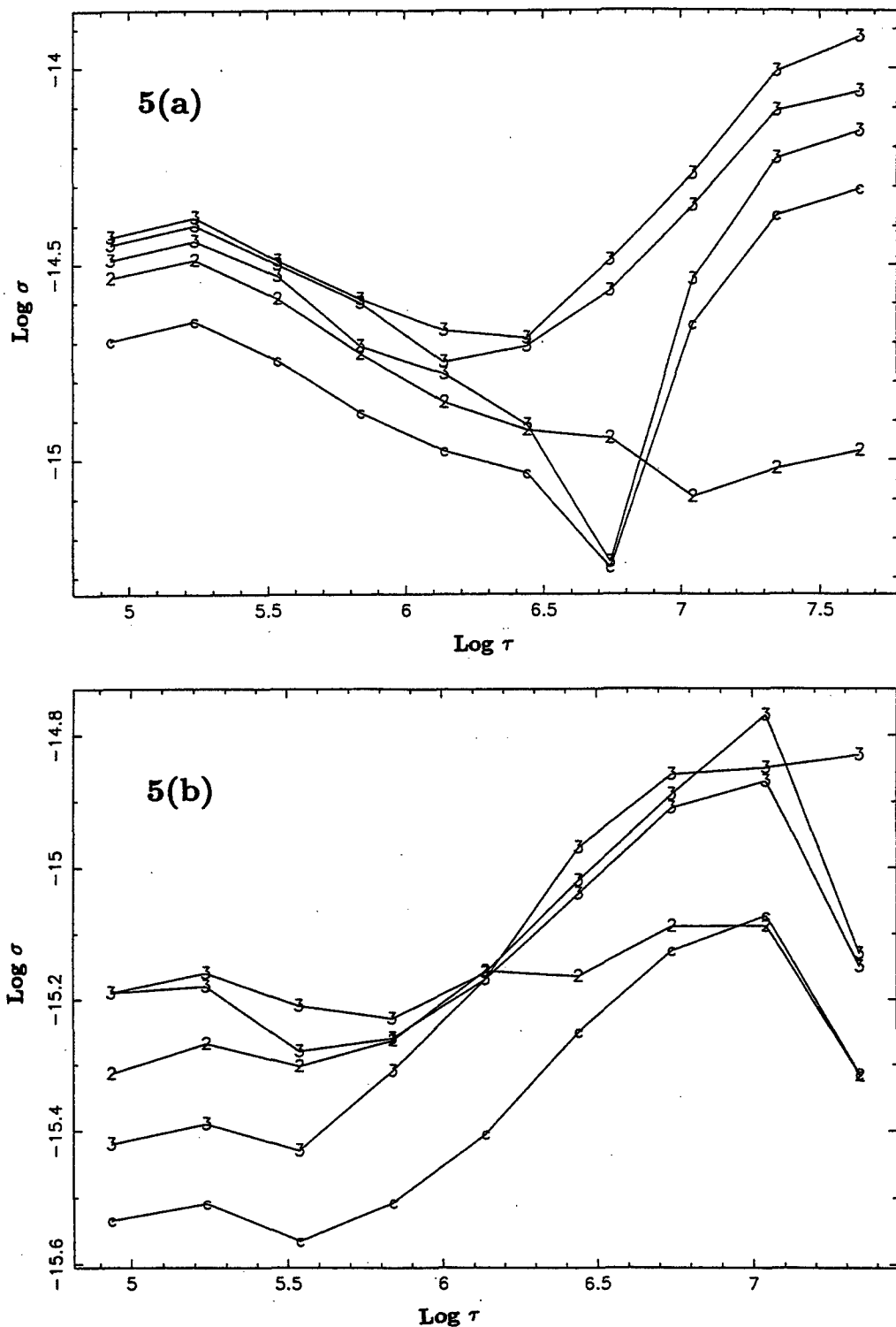
Figure 5. Frequency stabilities for mean timescales generated using only one type of clock and three independent subsets, derived from a 3-cornered-hat analysis of timescales that allowed for covariances. (a) is for an HP5071-only timescale and is based upon data since MJD 49400. (b) is for a Sigma Tau/Datum maser-only timescale and is based on data since MJD 50079. The curve indicated by "2" is for a mean timescale of one-half of the clocks relative to a mean timescale of the other half, and the curve indicated by "c" is for the complete USNO HP5071 ensemble (in both, covariances were neglected).
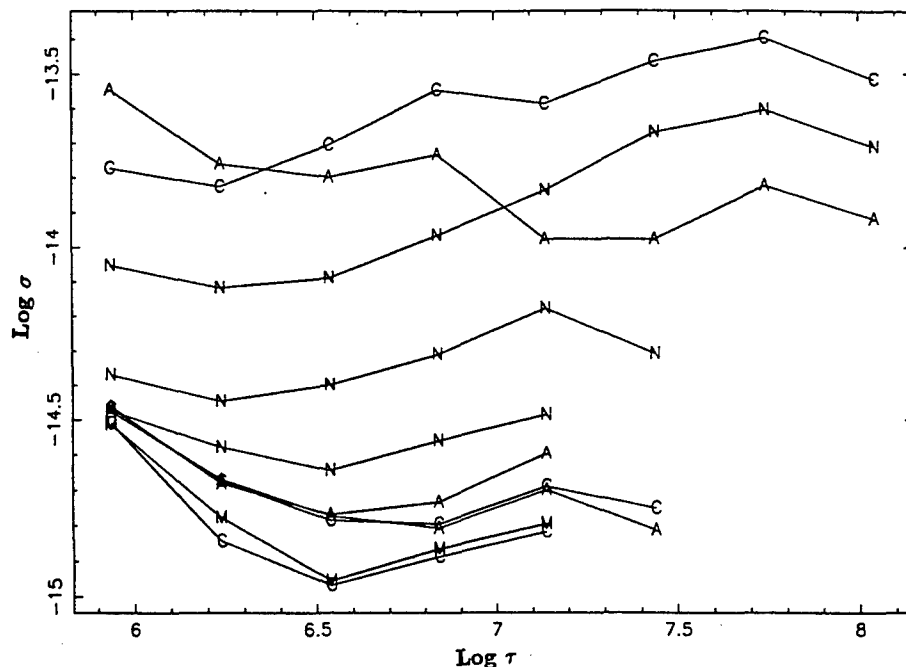
Figure 6. Frequency stability plots comparing timescales to TT98 over three different sampling times τ. Those of TT98-A.1 are denoted **A**, TT98-SuperP cesium-only average are denoted **C**, TT98-SuperP maser-only averages are denoted **M**, and TT98-TA(NIST) are denoted **N**. The three curves that extend over the longest range of log τ include all data since MJD 44752; the cesium-only average is the only such to include non-HP5071 cesiums. The three curves of shortest range in log τ are for data since MJD 50079, and the three of intermediate range are for data since MJD 49400.
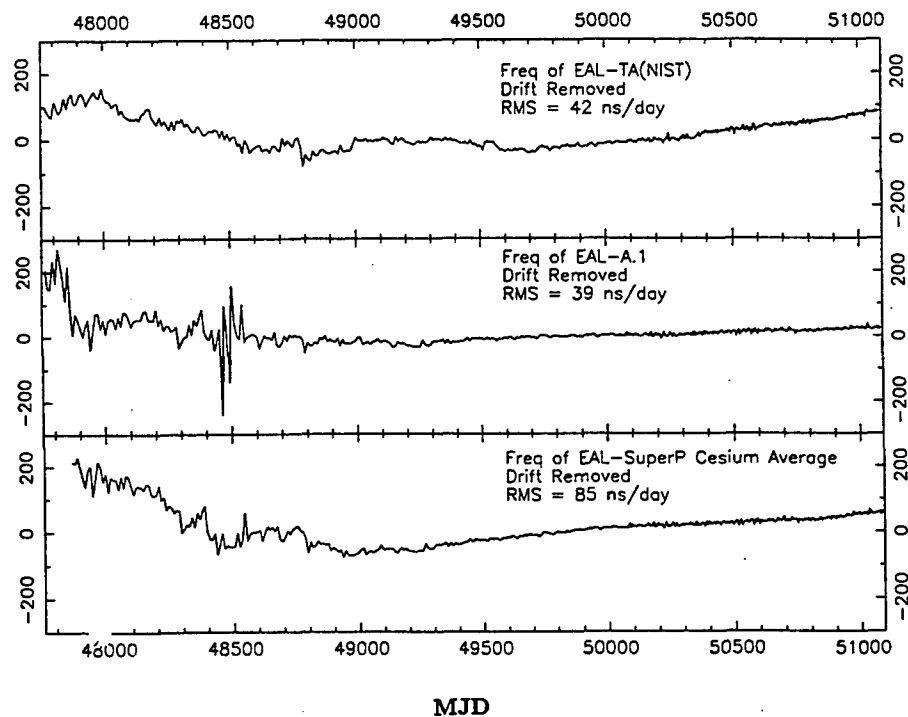
Figure 7. Frequencies in ns/day of EAL-TA(NIST), EAL-A.1, and EAL-SuperP cesium-only average. For display purposes, some high-frequency data from the SuperP timescale were removed previous to MJD 47900; however, they are still included in the RMS calculation.

30
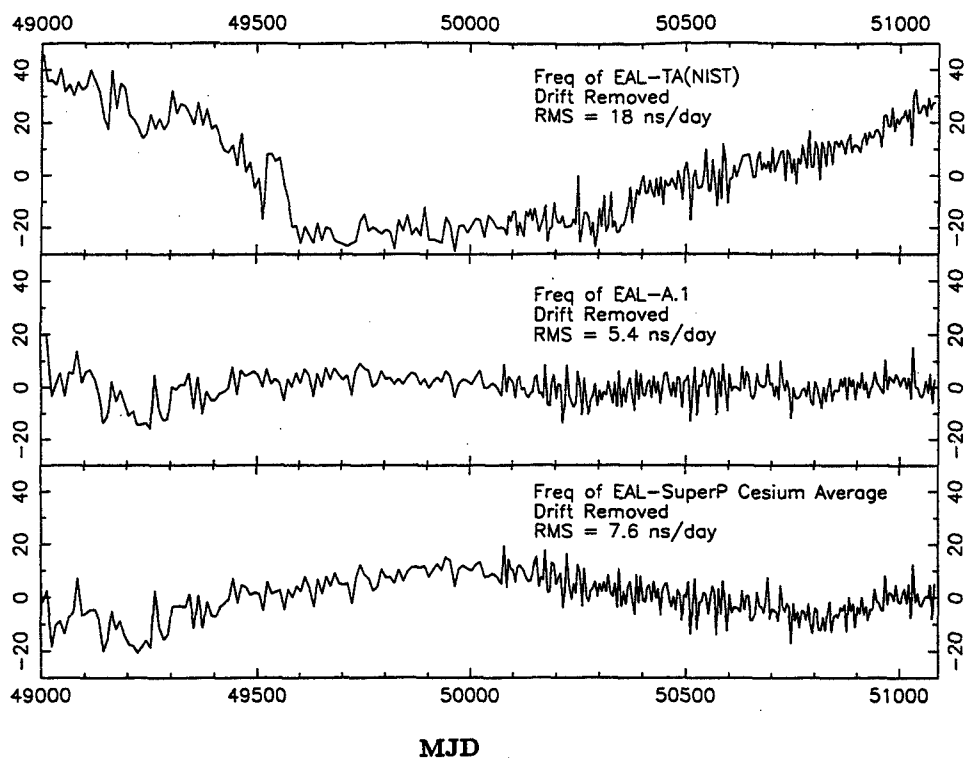
Figure 8. Frequencies in ns/day of EAL-TA(NIST), EAL-A.1, and EAL-SuperP using only data since MJD 49000.
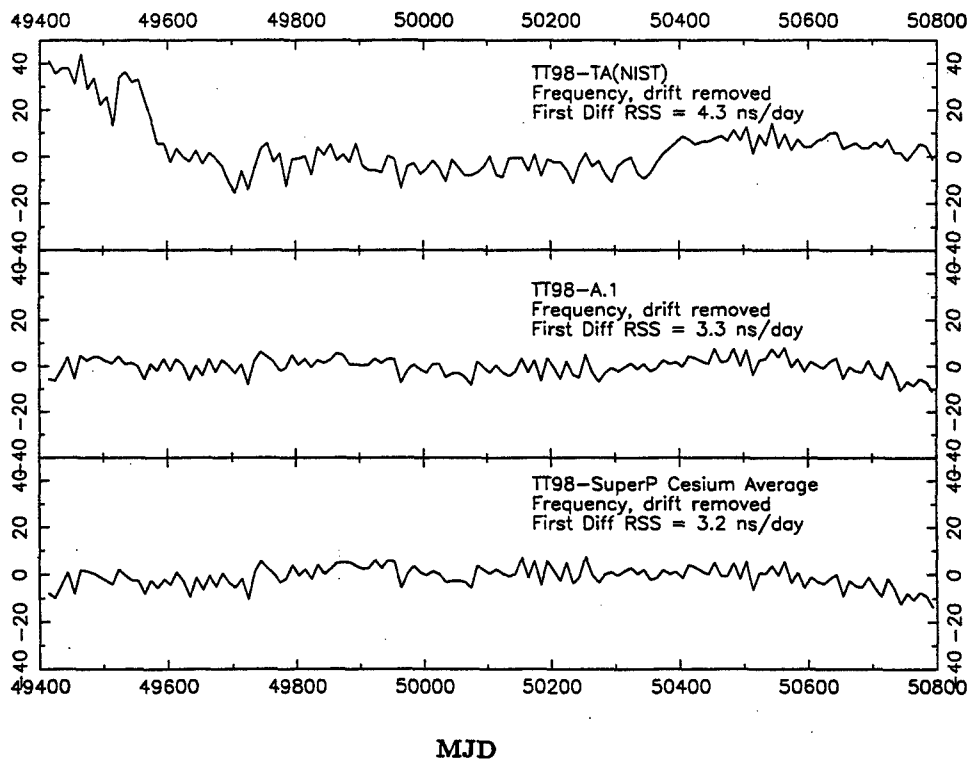
Figure 9. Frequencies in ns/day of TT98-TA(NIST), TT98-A.1, and TT98-SuperP using only data since MJD 49400.

31
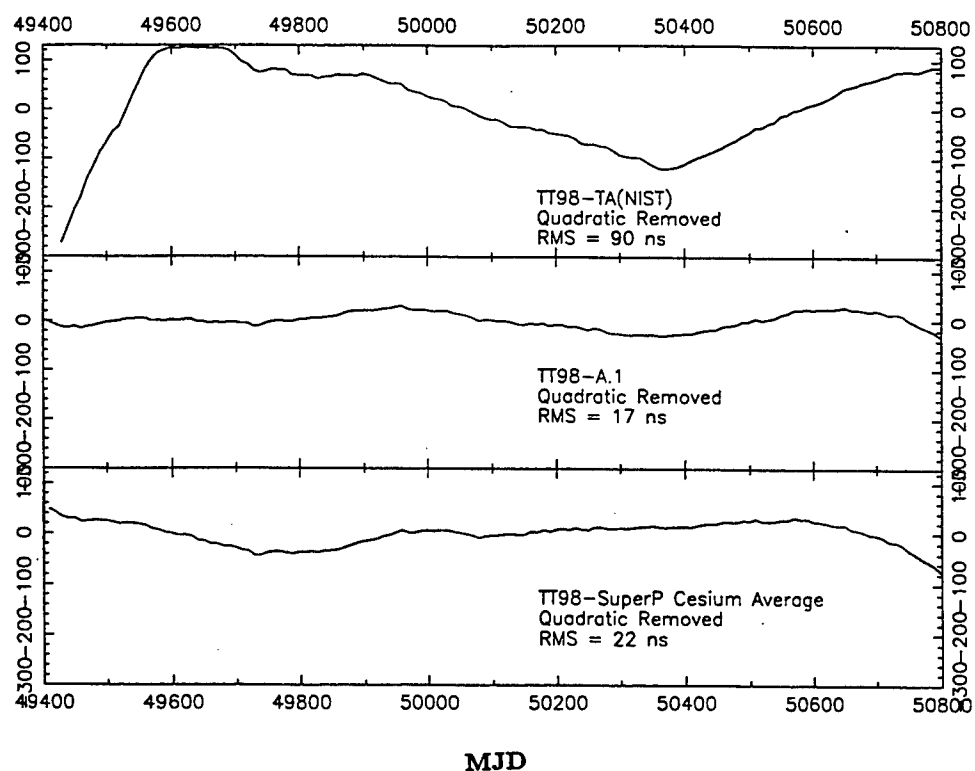
Figure 10. Differences in ns between timescales and TT98 using only data since MJD 49400.
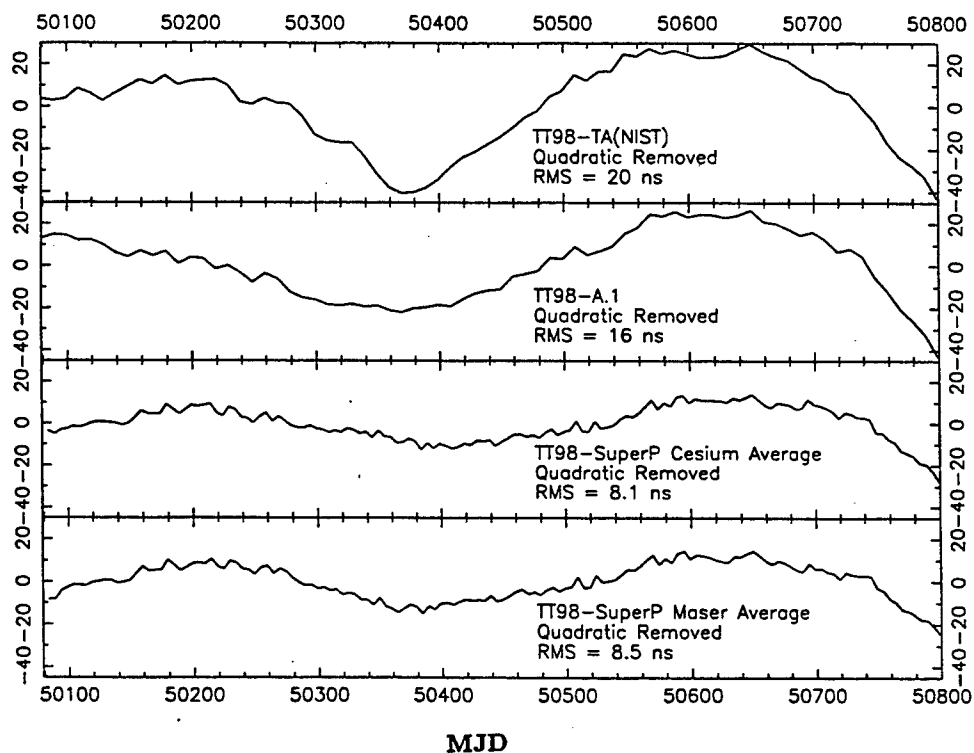
Figure 11. Differences in ns between timescales and TT98 using only data since MJD 50079.

32

Questions and Answers

GERARD PETIT (BIPM): Your comparison with TT-BIPM is, of course, comparing two different kinds of scales. TT-BIPM is one algorithm designed to provide the longest possible time span, one scale based upon existing primary standards. It provides something, which has been done consistently for 20 years and your plot is over 20 years. Maybe one confusion is that data from the primary standards are not sufficient compared to the quality of the clocks in the past two years.

DEMETRIOS MATSAKIS (USNO): I think that is absolutely the case. I think we have to look to the future, not to the past. Certainly those kinds of errors which consider 2-nanosecond variations 10 or 15 years ago would be impossible; you would not even think about it. Everything was much worse back then; but now everything is getting better.

MARC WEISS (NIST): I have a question: In the removal of a quadratic in order to compare time scales, I would be concerned that first of all, when you remove a quadratic, you remove a fair amount of the random walk from the scale; so it is difficult to see the difference between a quadratic and a random walk over a short period of time, even over years. Secondly, the drift of the clocks comes in and produces a quadratic, and it seems like modeling the drift is a big problem. I think it is problematic to remove a drift, that is, to remove a third of a quadratic from the time scale in order to compare them.

DEMETRIOS MATSAKIS: Well, it is in there. I could change my original estimate of the drift 10 years ago, and it would show right now. So you can keep it in and pretend it is not there, but you would only be fooling yourself. You could compare frequencies instead of time because this is really a frequency scale which is integrated. You would get the same results. I mean the same general conclusions.

STATISTICAL PROBLEMS IN THE ANALYSIS OF UNEQUALLY SPACED DATA

Patrizia Tavella
Istituto Elettrotecnico Nazionale G. Ferraris,
Strada delle Cacce 91, 10135 Torino, Italy
tavella@tf.ien.it

Mauro Leonardi
Politecnico di Torino, Dip. Elettronica,
C.so Duca degli Abruzzi 24, 10129 Torino, Italy
leonardi@tf.ien.it

Abstract

The statistical analysis of irregularly spaced data or the handling of series with missing data asks for particular care because results may be biased. In particular, in PTTI applications, two points seems to be addressed:

- *the noise analysis in terms of Allan or related variances;*
- *the estimation of a missing datum on a particular date.*

Both these issues are examined in the particular case of the current TWSTT measurement, by means of an analytical and theoretical approach that can be of more general interest. Some numerical estimates based on the TWSTT measures are eventually reported.

1 INTRODUCTION

Time and frequency comparisons repeated with an irregular periodicity are today the possible results of the new clock comparison technologies or the new working principles of atomic frequency standards. For example, the TWSTT (Two-Way Satellite Time Transfer) is currently operated on Mondays, Wednesdays, and Fridays, thus with a time interval between measures of 2, 2, and 3 days. But the problems of handling unevenly spaced data is of more general interest, for example in case of optical synchronization links, in case of inter-satellite links, and in case of the repeatability analysis of the new frequency standards which do not work continuously. The statistical treatment of unevenly spaced data deserves some attention. In particular, in this paper, the issues of noise analysis and of missing datum estimation are investigated.

As far as noise analysis is concerned, type and amount of noise are commonly estimated by the use of the Allan or a related variance. Such estimation requires a series of equally spaced data. When data are not equally spaced they are usually filled in by means of some reconstruction technique, e.g., linear interpolation. The reconstruction technique induces a modification on the true noise of the data series, but it should give the possibility to identify the real noise, at least in some spectral bandwidth. By the introduction of the Allan covariance matrices and by using the transformation laws of such matrices, the effect of interpolating missing data was inferred with

an analytical treatment and its effect on typical clock noises was previously reported [1]. In this paper some other possibilities of estimating ADEV without or with minor data manipulation are also presented.

The second task of interpolating a missing measure on a particular date is here approached with the double aim of smoothing the noise added by the comparison link and of retaining the clock noise for a correct evaluation of the clock behavior. The uncertainty of the reconstructed data is also evaluated by means of the least square theory and the use of the Kalman filter.

Finally, the above procedures are applied to some TWSTT measures performed in the last months to provide an example of application and a preliminary evaluation of TWSTT data. This work was performed in the frame of a collaboration with the CCTF Study Group on TWSTT [2].

2. NOISE ANALYSIS

When dealing with time and frequency measure sequences, the statistical tools commonly used to characterize the noise are the Allan variance or the associated Time variance (TVAR). These tools must be applied on equally spaced series. In case of unevenly data series, first of all it is thus necessary to obtain some evenly spaced sequences. With the aim of developing a general treatment, an analytical formulation was preferred instead than a simulative approach. This gives the advantages of allowing an insight on those parameters that most affect the results and of examining with a minimal effort another measurement periodicity or another noise case or a different reconstruction technique. The analytical processing requires the introduction of covariance matrices and the noise properties are examined by the transformation laws of such covariance matrices. In particular, the Allan covariance matrix and the TVAR(τ) matrix are introduced. Mathematical details and discussion are reported in [1].

Three possible approaches are examined in the case of a statistical analysis of unevenly data sequence:
1) identifying some regularities in the irregular sequence;
2) considering the original data as equally spaced by a "fictitious" τ_0. In the particular case of the current TWSTT measures an equal separation with an average gap of τ_0=2.33 days between the data can be assumed;
3) reconstructing the missing data on Tuesdays, Thursdays, Saturdays and Sundays with some specific interpolation rules, in order to obtain a daily spaced series.

2.1 CHECKING FOR SOME REGULARITIES IN THE IRREGULAR SEQUENCE

This approach consists in the research of those possible regularities that are present in the unevenly series. The interest is to highlight in the sequence those particular triads of phase samples spaced in such a way as to permit the estimation of a single two-sample variance i.e. a single phase second difference. Let's remind ourselves, in fact, that the ADEV estimation is performed by averaging a certain number of phase second differences $\Delta_2 x$ as:

$$ADEV\,(\tau) = \sqrt{\frac{1}{2\tau^2}\left\langle\left(x(t) - 2x(t+\tau) + x(t+2\tau)\right)^2\right\rangle} = \sqrt{\frac{1}{2\tau^2}\left\langle\left(\Delta_2 x\right)^2\right\rangle}$$

The three phase measures $x(t)$, $x(t+\tau)$ and $x(t+2\tau)$ must be subsequent and spaced by the same τ interval. Other second differences $\Delta_2 x$ can be obtained from following triads of phase measures even if not subsequent to the first considered triad. The ADEV determination in fact asks for the estimation of the variation of the mean frequency averaged over two subsequent τ intervals. Then, other phase second differences $\Delta_2 x$ can be estimated over whichever 2τ interval provided that another series of three phase measures, evenly spaced by a τ interval, is available. As an example, the case of the integration time equal to 2 days can be considered (Figure 1). For each week, the estimation of two adjacent mean frequencies is possible (one averaged between Monday and Wednesday and one between Wednesday and Friday). This implies that for each week it is possible to estimate one second difference $\Delta_2 x$. The higher is the number of weeks in the sequence, the higher the number of the possible $\Delta_2 x$ estimations to determine the final estimation of the ADEV(2 days) and the better the degree of confidence.

Analogously this is possible for any $\tau = 2, 5, 7, 9,..., 7n, 7n\pm2$ days. The case of $\tau = 7, 14, ... 7n$ days is trivial because for example all the Monday measures form a sequence of weekly equally spaced data. In this case, moreover, the overlapping estimation technique can be applied and also the MDEV and TDEV can be estimated. In case of $\tau = 2, 5, 9, .. 7n\pm2$ days, the triad of phase measures are not subsequent; therefore the overlapping ADEV and the classical estimation of MDEV and TDEV is not possible. In such cases, a *point estimate* of TDEV was proposed [2]. In case of a missing measure, the only consequence is that a particular triad of phase measures cannot be used and the number of possible estimates $\Delta_2 x$ is decreased, but if the number of measurement weeks is large, the confidence on the ADEV estimation can be assured. In conclusion, with an accurate analysis on the measurement date regularities, it is possible to find out specific values of τ for which ADEV estimation can be determined directly from real data, without any manipulation.

2.2 CONSIDERING DATA AS EQUALLY SPACED BY AN "AVERAGE" τ_0.

A second approach when dealing with irregularly spaced data series is based on the assumption that all the data are indeed equally spaced with an average gap. In the case of the current two-way measurements, an artificial separation of $\tau_0 = 2.33$ days can be assumed for the values in the sequence. In each week, in fact, three measures are available and $7/3 \cong 2.33$ days.

The effects of this treatment on the noise recognition depend on the kind of noise and on the true separation between data. If WPM is considered, the noise analysis turns out to be always correct because data are completely uncorrelated and there is no difference in considering them at a certain date or another. Only in case of TDEV evaluation, attention is to be paid because TDEV

values depend on the stated τ_0 value. With other noise types the assumption, instead, is nearly correct when the data aperiodicity is small. Otherwise the result may be highly biased. In the particular case of the TWSTT periodicity, it was found [2] that, in case of WFM and RWFM, such technique leads to a noise overestimation for small τ. Since the repetition rate of TWSTT has only a slight aperiodicity, the bias in the results is only a minor one, but other data sequences affected by different aperiodicities could present more critical problems if treated as equally spaced.

Despite the fact that the evaluation technique with an "average" τ_0 is quite simple and allows the use of the commonly made software that requires evenly spaced data, some underhand pitfalls can cause significant errors. For example, always in the case of the TWSTT periodicity, the average spacing of 2.33 days can be assumed when all the scheduled measures are performed, i.e. each Monday, Wednesday, and Friday. In reality it may happen that some measures fail or that entire measurement weeks are absent. The easiest procedure is to make a list of all the available measures regardless of their dates and to evaluate the ADEV with an overlapping procedure as if the data were equally spaced by an average τ_0 (estimated by total measurement period divided by the number of actual measurements). This can be very dangerous. In case of colored noises, the noise identification can be misleading, because data spaced for example by one or more weeks are treated as if they were spaced only by two or three days.

2.3 MISSING DATA RECONSTRUCTION

A third approach consists in the reconstruction of the missing data by using interpolation techniques. This solution was examined in [1], and also in [3]. It presents the disadvantage that results are biased because the interpolation acts as a filter. The results obtained in the case of WPM, WFM, and RWFM, considering the current TWSTT periodicity and a straight line or a 5th order polynomial interpolation of the missing data, are illustrated in [1]. Here only the example of white PM is reported in Figure 2, from which it can be seen that the technique of a fictitious τ_0=2.33 days seems to lead to overestimation, while the interpolation leads to underestimation of the true noise, particularly for small values of the integration time. It is worthwhile to stress that the overestimation of the first method is due to the dependency of TDEV on τ_0 value, while with colored noises, the overestimation is effective.

3. THE ESTIMATE OF MISSING DATA AND UNCERTAINTY EVALUATION

Particular applications need the knowledge of the clock comparison exactly at a certain date which is not in the measurement schedule. The complete evaluation of the missing data asks for its estimate and also for the uncertainty of such estimate.

To this aim, it is necessary to know:
1. the uncertainty on the measured values and the kind of noise due to the comparison technique;

2. the dynamical model describing the evolution in time of the clock difference and the noise affecting the clocks over the observation intervals of interest.

Let's consider, for example, in the typical TWSTT sequence, measurements performed on Monday and Wednesday, but the necessity of estimating the clock difference on Tuesday. As a first step let's consider the simple case of measurements affected by negligible uncertainty. Two hypothesis are then assumed:
1. measurements with negligible uncertainty;
2. clocks affected by phase random walk (i.e. white FM) and clock difference (e.g. UTC[i]-UTC[j]) described by the following equation:

$$x(t + \tau) = x(t) + y \cdot \tau + \varepsilon(t)$$

where τ represents the interval of one day, $x(t)$ the clock difference, y the relative frequency deviation, and $\varepsilon(t)$ a random Gaussian noise yielding the white FM and thus the random walk PM. The latter assumption is reasonable in case of cesium clocks compared daily. From one day to the following one the dominant noise driving the clock behavior is a white FM, resulting in a phase random walk. It is also assumed that the relative frequency deviation y is known. That may not always be true because the y also has to be estimated from the measures. The estimation of y can follow different ways (long or short observation interval, different number of measures...) and we will not discuss here this topic. If comparison measures are available for a certain period of time (e.g. months), it is reasonable to assume that the frequency deviation can be easily estimated and thus, for the Tuesday interpolation, it may be supposed known. The situation is thus depicted in Figure 3 where the knowledge on Monday and Wednesday is "perfect," but in the middle the random behavior of the clocks can follow different paths. The estimate of the clock state and its uncertainty follows from the theory of random walks.

A random walk is a process defined by the accumulation of independent random steps and it is a particular Markov process [4], whose peculiarities is that the knowledge of the future state depends only on the present state and not on the past. In case of clocks, it means that the "position" on Tuesday depends only on the position on Monday and not on the previous behavior. The knowledge of the Monday value is then sufficient to estimate the possible state on Tuesday. Since the state on Wednesday is also known by measurement, estimation on Tuesday can also be seen as a "backward" estimation problem. From the theory of least squares and its dynamical version (Kalman filter) it can be demonstrated that the best estimate $\hat{x}_{Tue}$ of the Tuesday value, knowing Monday and Wednesday measures and with the assumptions above, is the average value (corresponding to a straight line interpolation) between the measures of Monday and Wednesday. Such estimate is described by a Gaussian probability density centered on the average value $\hat{x}_{Tue}=(x_{Mon}+x_{Wed})/2$ and its uncertainty is given by $u_{Tue} = \sqrt{\frac{\sigma_{r.w.}^2}{2}}$, where $\sigma_{r.w.}^2$ is the "diffusion coefficient" describing the daily random walk and that can be easily

estimated by observing [5] that $\sigma_{rw}^2 = AVAR(\tau) \cdot \tau$, with dimensions of $[\sigma_{rw}^2] = ns^2/day$, when x is measured in ns and τ in days. The estimation of the Tuesday value is thus obtained as depicted in Figure 4.

Let's now consider a more realistic case with the following assumptions:
1. measurements with an uncertainty due to the comparison system, corresponding to a white PM (thus uncorrelated from one measure to the following and uncorrelated from clock noise) with zero average and variance σ_{ms}^2;
2. (as before) clocks affected by phase random walk (i.e. white FM) and clock difference (e.g. UTC(i)-UTC(j)) described by the following equation:

$$x(t+\tau) = x(t) + y \cdot \tau + \varepsilon(t)$$

In this case, the measurements are executed with an uncertainty σ_{ms}; therefore the knowledge of the clock state on Monday and Wednesday is not perfect. From Monday to Wednesday, the evolution of the clock state is always described by random walk in phase. The best estimate is also in this case obtained by the average of the Monday and Wednesday values, but the uncertainty of this estimate contains also the contribution of the measurement uncertainty, leading to a final Tuesday uncertainty u_{Tue} equal to:

$$u_{Tue} = \sqrt{\frac{(\sigma_{rw}^2 + \sigma_{ms}^2)}{2}}$$

In this situation also the previous and following measures become useful. By the knowledge of clock behavior and the characteristics of the involved noises, the measures performed before that Monday can be inserted in a Kalman filter and the estimation of the clock state on that Monday can improve. That means reducing the uncertainty on the knowledge of the clock state on Monday, i.e. reducing the σ_{ms} by the use of previous measurements. Let's indicate by $\sigma_{b.e}$ i.e. "best estimate," the resulting uncertainty on the knowledge of the clock state on such particular Monday. If the model is correct the following relationship holds:

$$\sigma_{b.e} < \sigma_{ms}$$

The same can be done backwards, for improving the knowledge of the Wednesday state by filtering the measures at disposal after that particular Wednesday. We are now in the same situation of the beginning but with the estimates on Monday and Wednesday affected by a minor uncertainty $\sigma_{b.e}$. Nevertheless the clock random walk between Monday and Wednesday is unchanged and unaffected by the knowledge of previous and following data. The previous and the following data can be used to reduce the uncertainty of the Monday and Wednesday estimates, but nothing can be done to reduce the noise contribution σ_{rw}. Therefore the best estimate of the Tuesday datum is always obtained by the average $\hat{x}_{Tue} = [(x_{Mon}+x_{Wed})/2]$ with uncertainty given by $\sqrt{(\sigma_{rw}^2 + \sigma_{be}^2)/2}$ as depicted in Figure 5.

Let's now briefly examine the case of a reconstruction on Saturday or Sunday datum based on the Friday and Monday measures. In the case of measures without uncertainty, the best estimate of the Saturday value is obtained from the linear interpolation of the Friday and Monday values, but, if the measures are affected by an uncertainty σ_{ms}, the estimate on Saturday is not directly the linear interpolation of Friday and Monday data, but it has a term depending on the σ_{ms} and the frequency deviation y also. The best estimate $\hat{x}_{Sat}$ of the Saturday value can be written as:

$$\hat{x}_{Sat} = x_{Fri} \frac{(\sigma_{ms}^2 + 2\sigma_{rw}^2)}{2\sigma_{ms}^2 + 3\sigma_{rw}^2} - y \frac{\sigma_{ms}^2}{2\sigma_{ms}^2 + 3\sigma_{rw}^2} + x_{Mon} \frac{(\sigma_{ms}^2 + \sigma_{rw}^2)}{2\sigma_{ms}^2 + 3\sigma_{rw}^2}$$

and it can be seen that, in case $\sigma_{ms}=0$, the estimate reduces to the linear interpolation given by :

$$\hat{x}_{Sat} = \frac{2}{3} x_{Fri} + \frac{1}{3} x_{Mon}$$

The uncertainty u_{Sat} on such best estimate can be written as:

$$u_{Sat} = \sqrt{\frac{\sigma_{ms}^4 + 3\sigma_{rw}^2 \cdot \sigma_{ms}^2 + 2\sigma_{rw}^4}{2\sigma_{ms}^2 + 3\sigma_{rw}^2}}$$

the same expressions are valid for the Sunday reconstruction, by interchanging the role of Friday and Monday.

The assumptions herewith considered can be quite realistic in the case of TWSTT comparing two high performance Cs clocks. Actually, the model of the clock noise could be incomplete because a pure random walk was considered with frequency deviation y assumed to be known and fed as an external input. In case the frequency offset had to be estimated inside the same estimation process, the estimate would depend on the technique chosen for the estimation of the frequency deviation. In this case a complete Kalman filter has to be examined and some runs can give an estimate on the uncertainty of reconstructed values [2].

If the frequency offset is not known, the Kalman filter has to estimate both frequency and phase offsets between clocks, so some uncertainty is added on the Tuesday estimate because there is one more state element to be estimate and thus introducing uncertainty. Therefore, by adding in the model an unknown frequency deviation, the result is that the Tuesday estimate is obtained with larger uncertainty than the case here evaluated. The cases presented above can then be considered as the case leading to the minor uncertainty on the Tuesday reconstruction. Let's recall that the estimate is optimal only if the model, concerning clock dynamics and noise as well as measurement noise, is correct.

4. RESULTS OBTAINED USING THE TWSTT MEASURES

The developed theory was applied to TWSTT experimental measures supplied by the TWSTT Study Group, through the BIPM, and concerning three different data sequences as summarized in the following table

UTC(i)-UTC(j)	First Datum	Last datum	Days in the period	Weeks in the period
PTB-NIST	01-08-97	08-05-98	281	40
TUG-NIST	01-08-97	08-05-98	281	40
TUG-PTB	21-02-97	06-05-98	440	62

The results on experimental data are to be considered examples of how the theory can be applied and which can be the consequent estimates in the frame of particular assumptions, with the aim of helping the following development and understanding of particular aspects of TWSTT and the use of their measures.

4.1 NOISE ANALYSIS

In order to evaluate the noise affecting these series, the three different approaches described in Sec. 2 were followed. In the case of ADEV evaluation, with the method referred as "true ADEV," i.e. the first of the outlined methods (Sec. 2.1), only the measures at disposal were used without any prior manipulation. The other two methods need some kind of missing data reconstruction, in fact also by using the method of a fictitious $\tau_0=2.33$ days, the missing scheduled measures (i.e. on Monday, Wednesday, and Friday) need to be reconstructed to preserve the spacing of 2-2-3 days between measures. This was done by linear interpolation, because it seemed safer than leaving the "holes" and evaluating a new average τ_0. The new sequences obtained are affected only by the typical uneven periodicity of the TWSTT. The last method (Sec. 2.3) asks for a complete reconstruction (i.e. also of Tuesday, Thursday, Saturday, and Sunday) in order to obtain a daily sampled data series. ADEV and TDEV were estimated according to the three procedures [2].

Let's here examine only a particular interesting result concerning only the "true ADEV." From an inspection of Figure 6 some important hints can be obtained. First, the ADEV behaviors are very similar to the high performance HP clock stability, indicating that, at least on such observation intervals, the noise added by the TWSTT link is negligible and clock instabilities are dominating. This is particularly true for the sequences TUG-PTB and TUG-NIST, where a first part due to white FM is recognizable. In the second part of the plot something similar to a flicker FM appears and that could be perhaps due to the combined effect of true clock noise together with the steering or clock correction effect. If it is assumed that the ADEV of the sequences TUG-PTB and TUG-NIST represent clock noise, it is possible to trace the slope corresponding to white FM and estimating the white FM level of clock noise over $\tau=1$ day. This leads to the

estimation of $\text{ADEV}(1day) \approx 3 \cdot 10^{-14}$.

On the other hand, the ADEV corresponding to the sequence PTB-NIST shows the typical clock instability behavior except maybe for the first point on $\tau=2$ days, which seems a bit higher than it should be if belonging to a white FM slope. Since we don't have here other information on the measurement system noise, let's assume that this first point belongs to a white PM slope representing the noise added by the comparison link. This is a conservative estimate of the synchronization noise; the actual noise could be lower. Also, this is an hypothesis on the TWSTT noise, and other hypotheses would be possible. The white PM assumption is certainly the simplest and often it is reasonable, but the final statement concerning TWSTT system noise come from experimental evidences and not from assumptions. Since we are here interested in the evaluation of missing data, such hypotheses are necessary for the following treatment, but results are valid only as long as the assumptions of the theoretical model can reasonably represent reality.

If a white PM is assumed, by tracing the corresponding slope, a value of $\text{ADEV}(1day) \approx 3 \cdot 10^{-14}$ is obtained, representing the noise added by the measurement system. Since, in the following evaluations, the classical variance σ_{ms}^2 of the measurement system is needed, it can be evaluated by remembering that in case of white PM the classical variance is equal to $\text{TVAR}(\tau_0)$ and that, when $\tau=\tau_0=1$ day, $\text{ADEV}(\tau_0)=\text{MDEV}(\tau_0)$. Therefore,

$$\sigma_{ms}^2 = TVAR(\tau_0) = AVAR(\tau_0) \cdot \frac{\tau_0}{3} \qquad \Rightarrow \qquad \sigma_{ms} \approx 1.7 \text{ ns}$$

4.2 MISSING DATA EVALUATIONS

The second problem of estimating UTC(i)-UTC(j) values on a certain date is also addressed in the frame of the following working assumptions:

1. measurements with an uncertainty due to the comparison system, corresponding to a white PM (thus uncorrelated from one measure to the following and uncorrelated from clock noise) with zero average and variance σ_{ms}^2;

2. clocks affected by phase random walk (i.e. white FM) characterized by a "diffusion coefficient" σ_{rw}^2 and known relative frequency deviation y.

From the noise analysis illustrated in the previous section and in particular from the discussion concerning Figure 6, some estimates of the noise are assumed, with the aim of providing an example on how the estimation of the missing data can be performed. Therefore, the following numbers are not to be considered definitive, but only an illustrative example.

As far as the noise of the comparison link is concerned, it was estimated that:

$$\sigma_{ms}^2 = TVAR(\tau_0) = AVAR(\tau_0) \cdot \frac{\tau_0}{3} \qquad \Rightarrow \qquad \sigma_{ms} \approx 1.7 \text{ ns}$$

43

As far as the clock noise σ_{rw}^2 is concerned, it was estimated that $ADEV(1day) \approx 3 \cdot 10^{-14}$. By recalling the relationship, $\sigma_{rw}^2 = AVAR(\tau) \cdot \tau$, with dimensions of $[\sigma_{rw}^2] = ns^2/day$, it can be estimated:

$$\sigma_{rw}^2 = AVAR(1day) \cdot 1day = 9 \cdot 10^{-28} \cdot 86400s = 9\left(\frac{ns^2}{day}\right)\left(\frac{86400s}{10^5}\right)^2 \approx 7.8\frac{ns^2}{day}$$

With these noise values, it appears that the best estimate of Tuesday value, when measurements are performed on Monday and Wednesday, is the average value of the Monday and Wednesday measures with uncertainty u_{Tue}:

$$u_{Tue} = \sqrt{(\sigma_{rw}^2 + \sigma_{ms}^2)\big/_2} \approx 2.3\,ns$$

while the best estimate of the Saturday value, when measures are performed on Friday and Monday depends on the value of the relative frequency deviation y, and its uncertainty is:

$$u_{Sat} = \sqrt{\frac{\sigma_{ms}^4 + 3\sigma_{rw}^2 \cdot \sigma_{ms}^2 + 2\sigma_{rw}^4}{2\sigma_{ms}^2 + 3\sigma_{rw}^2}} \approx 2.6\,ns$$

5. CONCLUSION

The statistical problems that arise in the treatment of irregularly sampled data were investigated and some possible procedure to overcome such problems were proposed. Firstly, the ADEV and TDEV analysis can be performed by following three approaches:

1) finding some regularities in the irregularly sampled sequence. For example, in case of TWSTT, for τ=2, 5, 7, 9, 12, 14 ... days the ADEV can be evaluated without any manipulation of data;

2) proceedings as if the data were equally spaced of a fictitious τ_0=2.33 days. Particular care is to be taken: results are correct only in case of pure white PM, if not the noise is overestimated;

3) interpolating missing measures with the aim of obtaining a daily spaced sequence. Noise results depend on the real noise and on the data reconstruction which filters the faster noise frequencies. Therefore, for small values of τ, ADEV and TDEV are underestimated.

The second aim is the best estimate of the clock difference on a certain date when TWSTT measurements are not available and the uncertainty of such estimate. By using the theory of least squares and the Kalman filter it was possible to evaluate the best estimate and its uncertainty, which depends on the noise of the TWSTT measure as well as on the random noise of the clocks and on the clock model. To provide an example, the following working assumptions were formulated:

- TWSTT comparison noise corresponding to a WPM;
- clock noise over one day corresponding to a WFM;
- relative frequency deviation of the compared clocks known with negligible uncertainty.

In this frame the best estimates of the missing data and the uncertainties were inferred.

It is worthwhile to remember that different level of noise or different models would lead to different estimates, therefore each particular situation has to be suitably evaluated, accordingly to the main lines here developed. In particular, the final uncertainty added by the measurement system should be derived from experimental tests and not only be based on assumptions. As a last remark, if the measurement was performed on the requested Tuesday or Saturday, the only uncertainty would be due to the measurement system.

6 REFERENCES

[1] P.Tavella, M.Leonardi, *"Noise characterisation of irregularly spaced data,"* European Frequency and Time Forum, Warsaw, Poland, 1998, pp. 209-214.
[2] W. Lewandowski, *"Report of the meeting of the participating stations of the CCTF working group on TWSTT,"* San Fernando, Spain, 28-30 October 1998.
[3] C. Hackman, T. Parker, *"Noise analysis of unevenly spaced time series data,"* Metrologia, 1996, 33, pp. 457-466.
[4] D.R.Cox, H.D.Miller, The theory of stochastic processes, Science Paperbacks, Chapman and Hall, London, 1965.
[5] J. W. Chaffee, *" Relating the Allan variance to the diffusion coefficients of a linear stochastic differential equation model for precision oscillators,"* IEEE Trans UFFC, vol. 34, n. 6, November 1987.
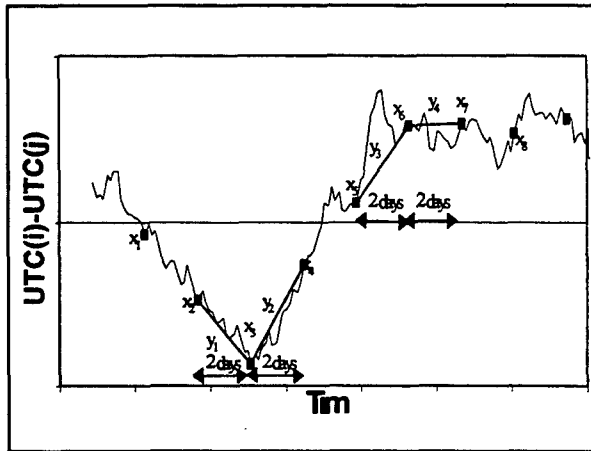
Figure 1. *Estimation of ADEV(2 Days). Measures are executed on Monday, Wednesday and Friday. For any $\Delta_2 x$ estimation, the three consecutive measures are considered for each week.*
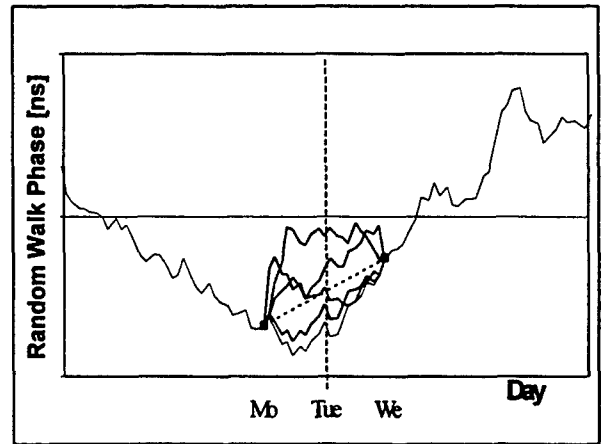
Figure 3. *Random walk behavior between Monday and Wednesday.*

Figure 4. *Least squares estimation of Tuesday value*
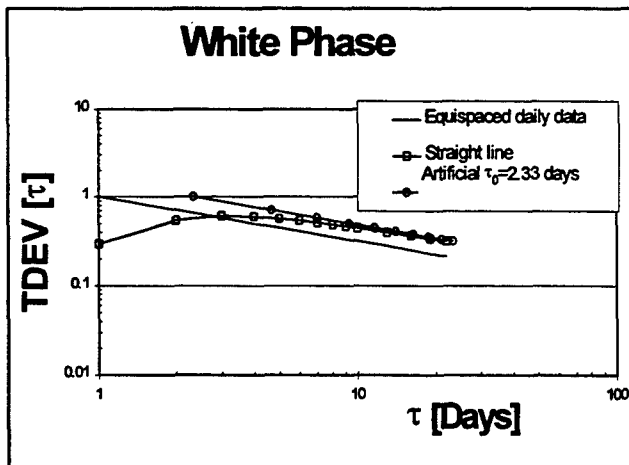
Figure 2. *Theoretical behavior in case of white PM as estimated by: a) true daily equally spaced series, b) TWSTT spaced series considered as equally spaced by $\tau_0 = 2.33$, c) daily series reconstructed by a straight line interpolation.*
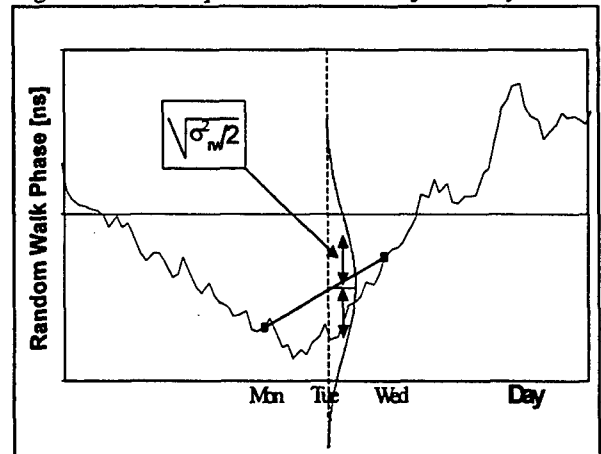
in case of negligible measurement uncertainty
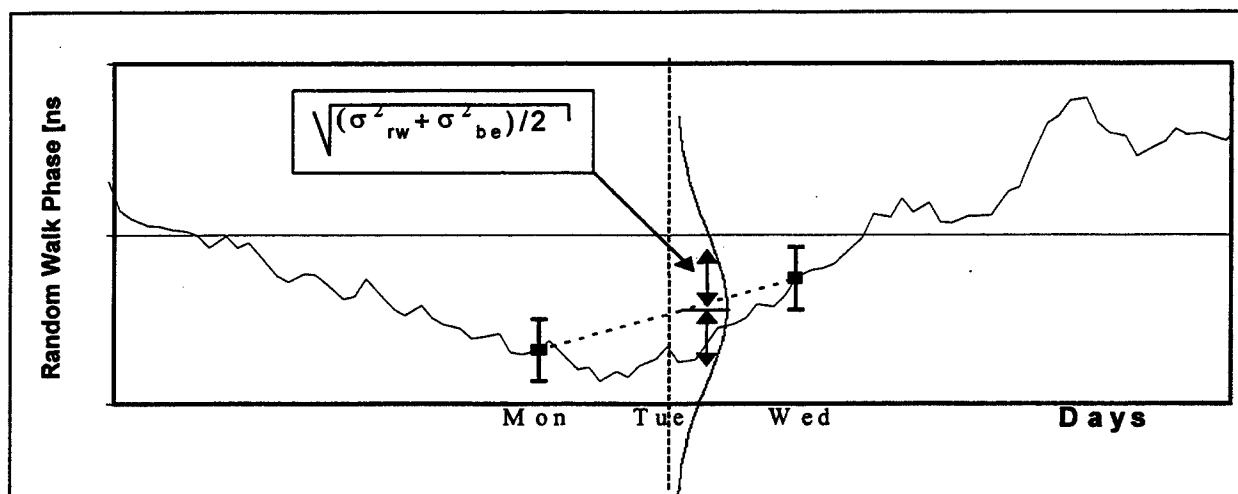
Figure 5. *Least square estimate of Tuesday value in case of measurement uncertainty.*
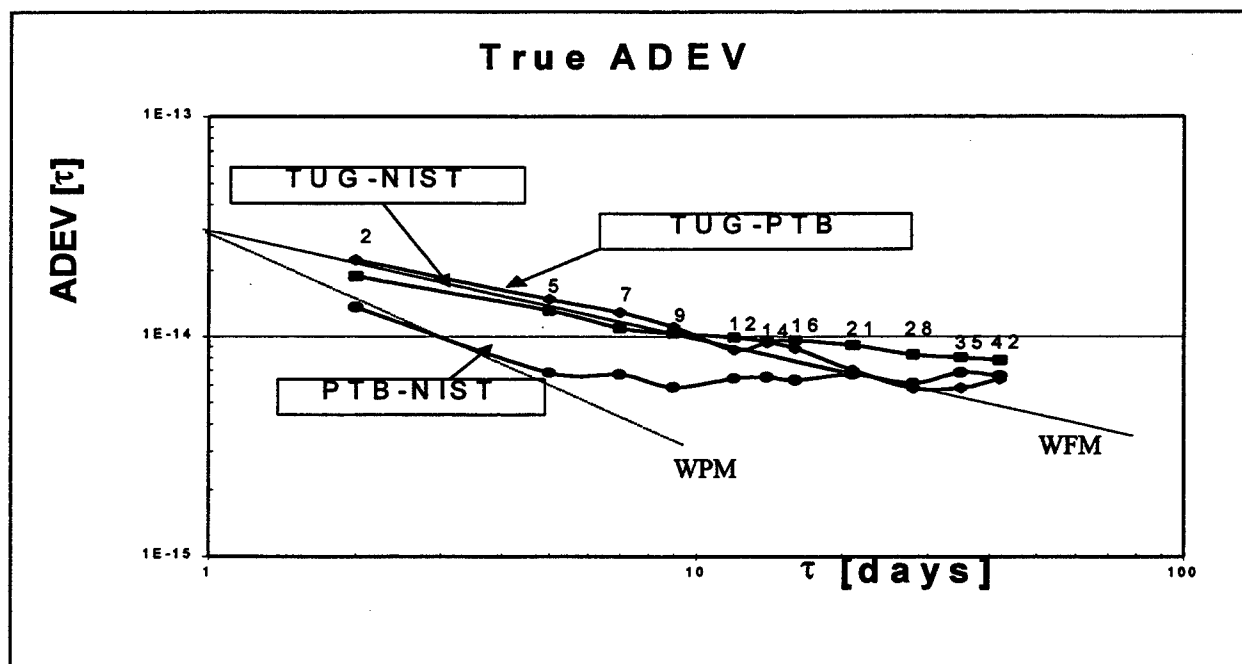
Figure 6. *True ADEV estimates for the three different links with the slope of the white PM and white FM.*

Questions and Answers

ROBERT DOUGLAS (NRC): For the uncertainty in the hydrogen maser comparison, were you including the flicker floor noise?

PATRIZIA TAVELLA (IEN):: Actually, I used white frequency and a drift, because I had some drift specifications on the hydrogen maser, which I used. I spoke with persons making the measurements, and I asked for the actual measurement, which seems to have a flicker. Since all these evaluations are done in an analytical way, the flicker is difficult to be treated analytically. I suppose that even if we consider something that is worse than flicker, for example, random walk frequency, it will be at such a lower level that in any case it will be negligible. The random part of the hydrogen maser will be negligible, I guess.

THE RANGE COVERED BY A CLOCK ERROR IN THE CASE OF WHITE FM

Patrizia Tavella* and Daniela Meo°

*Istituto Elettrotecnico Nazionale G. Ferraris
Strada delle Cacce 91 10135 TORINO
tel +39-11-3919235 fax +39-11-3487046 e-mail tavella@tf.ien.it
° Università di Torino, Dip. Matematica,
V. Carlo Alberto 10, 10124 Torino, Italy

Abstract

The range covered by the time error of a clock affected by a white frequency noise is studied by means of the theory of the Wiener process and its probability distribution is inferred. The application to atomic clocks and the MTIE characterization used in the telecommunication standards is also examined.

1. INTRODUCTION

In these last years, mostly due to the input of the telecommunication community, it became of interest to know of the possible range spanned by the time error of a clock, since it helps in correctly designing the memory buffers. The problem may be illustrated as follows: suppose we have an atomic clock used as a synchronization unit in a telecommunication network and we know that the clock signal is mostly affected by a certain random noise. Which is the "time error," i.e. the phase deviation, that such a clock may accumulate in a certain time interval? Apart from deterministic trends, the answer regarding the random component may only be a probabilistic one in view of the stochastic the nature of the process. So the problem can be better expressed as: knowing the spectral density of phase fluctuations, which is the probability law of the range spanned by such phase fluctuations?

The case of white phase noise was recently examined and it was possible to infer the probability law of the spanned range [1, 2, 3]. Also the relationship between the amount of white PM noise stated by the Allan deviation or the spectral density and the Maximum Time Interval Error MTIE, largely used in the telecom community and recently defined as a percentile quantity [4], was evinced. In this paper, the case of Gaussian white frequency modulation, which results in a phase random walk is considered and the range probability law is inferred, by the study of Wiener

processes and their characteristics. This study yields to the estimation of the "maximum" range that can be spanned by the clock error by the identification of a certain percentile in the range distribution, i.e. a range value which is not exceeded more than a certain small percentage of times. The relationship of the percentile range and the MTIE is again investigated and some examples of atomic clock white frequency noise and possible percentile MTIE are given.

2 MATHEMATICAL BACKGROUND

In the following the theoretical definition and characterization of the Wiener process are introduced [5]. Symbols used hereafter are typical in the description of stochastic processes and are different from the common symbols used in PTTI descriptions. The application to the time error of a clock and to the telecommunication standards will be addressed in the next section.

Let $\{X_k\}$ be a sequence of mutually independent random variables with a common distribution, zero mean and variance σ^2. The discrete variable S_n

$$S_n = X_1 + \ldots + X_n, \qquad (S_0 = 0),$$

denoting the position at time n (integer) of a moving particle, describes a random walk. The range R_n spanned by the discrete process S_n is defined as the difference between the maximum and the minimum value, therefore:

$$R_n = max\ [0,\ S_1,\ldots,S_n] - min\ [0,\ S_1,\ldots,S_n].$$

The discrete sums S_n are asymptotically normally distributed and can be considered as the value at time $t=n$ of a continuous Wiener process. For the evaluation of the spanned range, the continuous approximation is more convenient, therefore, the sum S_n is replaced by the Wiener process $S(t)$ where $S(0) = 0$. Moreover, the introduction of the Wiener process is not only useful for the following analytical development, but also because the Wiener process itself can be a convenient description of reality, for example when describing the error of an atomic clock. Therefore, in the following only the continuous Wiener process will be examined. At any instant t, $S(t)$ is a normal variable with zero mean and variance $\sigma^2 t$, therefore probability that the process $S(t)$ is in the position s can be described by the probability law:

$$p(s;t) = Prob\{S(t)=s\} = \frac{1}{\sigma\sqrt{2\pi t}}\exp\left\{-\frac{s^2}{2\sigma^2 t}\right\} \tag{1}$$

A Wiener process with drift μ, can also be introduced as $Y(t) = S(t)+\mu t$, but for sake of simplicity the case with $\mu=0$ is here examined. Nevertheless, the range distribution can be found also in case of $\mu \neq 0$. In the new notation, the range of $S(t)$ is defined as:

$$R(0,t) = max_{0 \leq T \leq t}\ S(T) - min_{0 \leq T \leq t}\ S(T).$$

assuming that $S(0) =0$. Studies on the peculiarities of the Wiener processes are reported in many papers and reference texts [5,6,7]. Particular attention is devoted to the study of the *survival probability* of a restricted process, i.e. the probability that the Wiener process evolves till the instant t without having touched upper and lower boundaries a and b ($a>0$, $b<0$). The survival probability benefits from many analytical results and it can be seen that there is an intimate relationship between the probability distribution of the range and the survival probability [8, 9, 10, 11]. We will investigate such a relationship. The study of the range probability distribution requires evaluating the joint probability distribution $F_{m,M}(t)$ of the maximum and the minimum value of the process, indicated respectively with M and m. $F_{m,M}(t,b,a)$ represents the probability that the minimum value m doesn't exceed the value b and the maximum M doesn't exceed the value a:

$$F_{m,M}(t;b,a)= P\{M(t) \leq a,\ m(t) \leq b\}.$$

This probability can be expressed as:

$$F_{m,M}(t;b,a)= P\{M(t) \leq a,\ m(t) \leq b\}=P\{M(t) \leq a\} - P\{M(t) \leq a,\ m(t) > b\}.$$

where the survival probability $P\{M(t) \leq a,\ m(t) > b\}$ of the process restricted by the barriers a and b is introduced. Let's consider the joint density function $f_{m,M}(b,a)$ of the maximum and the minimum, i.e. the probability that the larger value falls between a and $a+da$ and that the smaller value falls between b and $b+db$, obtained, by definition, as:

$$f_{m,M}(b,a) = \frac{\partial^2 F_{m,M}(t;b,a)}{\partial b \partial a}$$

Since we consider the Wiener process $S(t)$ with $S(0)=0$, the existence field of the joint density function $f_{m,M}(b,a)$ is given by the region in which a is positive and b negative. Moreover, in such a region, a certain sub-region D_r can be identified where the following relationship concerning the range holds:

$$D_r = \{ 0 \le R(0,t) = M(t) - m(t) \le r \}$$

The region D_r can be identified by the following relationships:

$$\begin{cases} b \le 0, \; a \ge 0 \\ a - b \le r. \end{cases} \qquad \text{that is} \qquad \begin{cases} -r \le b \le 0, \\ 0 < a \le r + b. \end{cases}$$

The range probability distribution, i.e. the probability that the range $R(0,t)$ doesn't exceed a certain value r, is given by the integral extended to the region D_r of the joint density function of the maximum and the minimum, i.e.:

$$F_R(r) = P\{R(0,t) \le r\} = \iint_{D_r} f_{m,M}(b,a)\,db\,da = \int_{-r}^{0}\left[\frac{\partial F_{m,M}(t;b,a)}{\partial b}\right]_{a=0}^{a=b+r} db$$

From this writing it is intuitive that the range probability distribution depends on the survival probability, which is known in case of a Wiener process. By several laborious calculations, the range probability distribution can be obtained as:

$$F_R(r) = P\{R(0,t) \le r\} = \tag{2}$$

$$= \sum_{k=1}^{+\infty}\left\{-6kErf\left[\frac{2kr}{\sigma\sqrt{2t}}\right] + 4kErf\left[\frac{(1+2k)r}{\sigma\sqrt{2t}}\right] + 4kErf\left[\frac{(2k-1)r}{\sigma\sqrt{2t}}\right] + k\left(Erf\left[\frac{2(1-k)r}{\sigma\sqrt{2t}}\right] - Erf\left[\frac{2(1+k)r}{\sigma\sqrt{2t}}\right]\right)\right\},$$

where $Erf[y] = \frac{2}{\sqrt{\pi}}\int_{0}^{y} e^{-x^2}\,dx$ stands for the error function.

An analogous but more complicated expression holds for the range distribution in case of a Wiener process with drift μ [10]. In Fig. 1 the range probability distribution (2) is represented for a Wiener process with variance $\sigma^2 = 1$. We can note that, for fixed t, the probability distribution increases when the value r is rising. It means that, for a fixed t, it becomes more and more probable to observe a range below the threshold level r, if r is high. For fixed r, instead, it can be seen that the probability that the covered range is below the threshold value r, is initially high, but then it decreases with time. If we consider an horizontal section of the Fig.1, we can identify the curves relating t and r that guarantee a certain percentile in the range distribution, i.e., for each t, a range threshold r which is not exceeded

more than a certain percentage of times. By fixing the probability level at the values 95%, 90%, and 80%, the Fig. 2 is obtained, where the range thresholds r are on the vertical axis and the time instants t on the horizontal one. It can be observed that the curve referred to the largest percentile increases more rapidly, that makes sense because, for fixed t, the threshold range r that guarantees to be larger than the observable ranges in 95 out of 100 cases, should be larger than the threshold ranges corresponding to smaller percentages.

3 RELATIONSHIP WITH THE MAXIMUM TIME INTERVAL ERROR (MTIE)

The study of the probability of the range spanned by a Wiener process can find immediate application in the characterization of clocks. This is of particular interest in case of digital telecommunication networks. Digital switching equipment in fact require synchronization in order to avoid slips in the input elastic stores [12,13,14]. To specify the clock stability requirements in telecommunication standards, the International Telecommunication Union (ITU-T) defined the quantity MTIE (Maximum Time Interval Error) [4]. It measures the range covered by the error of a clock with respect to a known reference. Let $x(t)$ be the time error of a clock and τ the observation time, the range of the clock error is defined as (Fig. 3):

$$\text{MTIE}_{t_0}(\tau) = \max_{t_0 \le t \le t_0 + \tau} (x(t)) - \min_{t_0 \le t \le t_0 + \tau} (x(t)).$$

Recently ITU-T defined MTIE(τ, β) as a specified β–percentile of the random variable MTIE(τ), that is to say as the range value which is not exceeded more than a certain small percentage (1-β) of times, for any t_0.

The clock phase error $x(t)$ is usually due to deterministic variations and to stochastic noises of different nature. In most of the commercially available clocks and reference oscillators one of the dominant noises, over certain observation intervals, is due to a white frequency modulation, which results in a phase random walk. Therefore, the previous study of the range covered by a Wiener process is of immediate utilization to study the range covered by the phase error of a clock affected by white FM. Let's consider a white FM with zero average that corresponds, in the stochastic process language, to a phase error described by a Wiener process $S(t)$ without drift (μ=0) and with variance σ^2. The range spanned by the phase error $x(t)$ is thus the range spanned by the process $S(t)$ as studied in the previous section, where we replace the elapsed time t with the observation interval τ. For sake of convenience, let's consider the new variable $R_N = R/\sigma$, i.e. the range normalized over the square root of the variance for unit of time of the Wiener process, R_N is dimensionless. According to the results obtained in the previous section, the probability distribution (2) of R_N can be written as :

53

$$F_{R_N}(r_N) = P\{R_N(\tau) \le r_N\} =$$ (3)

$$= \sum_{k=1}^{+\infty} \left\{ -6kErf\left[\frac{2kr_N}{\sqrt{2\tau}}\right] + 4kErf\left[\frac{(1+2k)r_N}{\sqrt{2\tau}}\right] + 4kErf\left[\frac{(2k-1)r_N}{\sqrt{2\tau}}\right] + \right.$$

$$\left. + k\left(Erf\left[\frac{2(1-k)r_N}{\sqrt{2\tau}}\right] - Erf\left[\frac{2(1+k)r_N}{\sqrt{2\tau}}\right]\right)\right\}.$$

Such distribution probability allows the interpretation of the percentile range as contained in the percentile definition of MTIE(τ,β), in fact, by fixing the percentile level $F_{R_N}(r_N) = \beta = 0.80$, 0.90, and 0.95 respectively, as done before, the percentile curves of Fig. 2 are obtained and they describe the range threshold values that are not exceed in the β percentage of observations. The same percentile curves are also represented in Fig. 4 in logarithmic co-ordinates and with the normalized range values. From Fig. 4 some numerical estimations of the MTIE(τ,β) are possible, when the level of random walk noise is known; for example, for $\tau = 10^5$ units of time, the normalized range threshold level corresponding to the 90th percentile is about equal to the value 750. From the expressions (3) of the probability distribution $F_{R_N}(r_N)$, it is difficult to analytically solve for the expression relating τ and r for a fixed probability. The percentile curve represented in Fig. 2 and 4 are thus found by numerical evaluations, but it can be seen that such percentile curves are nicely approximated by the curves

$$r_N = k_\beta \sqrt{2\tau},$$

where k_β is a real number depending on the probability levels and that in the represented cases amounts to: $k_{80} = 1.39$, $k_{90} = 1.59$, and $k_{95} = 1.77$
This approximated relationship allows to find a direct, through approximated, connection between the percentile range, thus the MTIE(τ,β) and the noise variances. Let's evaluate that.
In the language of stochastic processes, the Wiener process is described by a drift μ and a variance σ^2. In clock stability characterization, we are more familiar to Allan variances or spectral densities. The relationship between the Allan variance AVAR and the σ^2 of the Wiener process is given by [15] $\sigma^2 = AVAR(\tau) \cdot \tau$, where the dimension of σ are [ps/$\sqrt{s}$], when the phase error $x(t)$ is measures in ps and τ in s. The square root of the variance for unit of time of the Wiener process, used for normalizing the range, is therefore $\sigma \cdot \sqrt{1s}$. By using the approximated relationship above, the known [16] time domain/frequency domain relationships, by choosing the

range and τ units in ps and s respectively, the percentile range MTIE(τ,β) as a function of τ can be written as:

$$MTIE(\tau,\beta) \approx k_\beta\sqrt{2\tau}\cdot\sigma = k_\beta\sqrt{2\tau}\cdot(ADEV(\tau)\cdot\sqrt{\tau}) = k_\beta\sqrt{2\tau}\cdot\frac{\sqrt{h_0}}{\sqrt{2}}$$

where h_0 is the constant that determines the amount of white frequency noise in the polynomial model for the frequency spectral density $S_y(f)$. It remains to evaluate what can be the numerical values of MTIE(τ,β) for some typical clocks. This is discussed in the next section.

4 NUMERICAL EXAMPLE

Let's evaluate the percentile range, thus MTIE(τ,β), for example of a typical commercial high stability cesium clock. Let's assume that the noise of the clock is due to a white FM with zero average, that means that the cesium clock is considered on observation intervals of about $1 \leq \tau \leq 10^6$ s, and that its frequency deviation is equal to zero (corresponding to $\mu=0$). Let's suppose that the WFM noise of such a Cs clock amounts to a typical value given by

$$ADEV(\tau) = 1\cdot10^{-11}\cdot\tau^{-1/2} \qquad\qquad 1 \leq \tau \leq 10^6 \ \ s$$

By using the relationship between the Allan variance AVAR and the σ^2 of the Wiener process, it is found:

$$\sigma = ADEV(1s)\cdot\sqrt{1s} = 1\cdot10^{-11}\cdot\sqrt{1s} = 10\frac{ps}{s}\cdot\sqrt{1s} = 10\frac{ps}{\sqrt{s}}$$

The square root of the variance for unit of time of the Wiener process, used for normalizing the range, is therefore $\sigma\cdot\sqrt{1s} = 10\,ps$. Now the values of the threshold percentile range reported in Fig. 4 can be interpreted as a percentile range, thus MTIE(τ,β), provided that τ is measured in seconds and the normalized range values (dimensionless) reported in Fig. 4 are multiplied by the normalization factor that is, in this case, $\sigma\cdot\sqrt{1s} = 10\,ps$. Therefore, the MTIE($\tau,\beta$) that could be observed on the phase error $x(t)$ of the considered Cs clock are reported in Fig. 5 and, for example, for $\tau=10^5$s, it amounts to about 7.5 ns, which makes sense considering the stability of the considered clock. By using the approximate relationship discussed in the previous section it can also be written that, for the particular clock: MTIE(τ,β) $\approx$ $k_\beta\sqrt{2\tau}$ 10 ps .

It can be worth comparing there results with the MTIE(τ,β) prescribed by ITU standards. For example, the case of a Cs clock is considered in the standard [17] concerning primary reference clocks (PRC), which reports the limits for MTIE(τ,β) values, giving:

$$\text{MTIE} \quad 0.275 \cdot 10^{-3} \cdot \tau + 0.025 \ \mu s \qquad \text{for} \qquad 0.1 \le \tau \le 1000 \ \text{s}$$

$$10^{-5} \cdot \tau + 0.29 \ \mu s \qquad \text{for} \qquad \tau > 1000 \ \text{s}$$

Some numerical values are for example:

τ=1 s	MTIE $\approx$ 25 ns
τ=10 s	MTIE $\approx$ 27.8 ns
τ=100 s	MTIE $\approx$ 52.5 ns
τ=1000 s	MTIE $\approx$ 300 ns
τ=10 000 s	MTIE $\approx$ 390 ns

which are represented by a dotted line in Fig. 5 and that are largely achieved by the stability of the considered Cs standard.

CONCLUSION

By the analytical study of the properties of random walks and Wiener processes, it was possible to infer the probability distribution of the range covered by the process. This helps in understanding the percentile MTIE(τ,β) used in telecommunication for describing the range covered by a clock time error, when the noise of the clock is due to a white FM and thus random walk of phase. An example concerning a high stability commercial Cs clock gives estimates of the expected MTIE(τ,β) which largely comply with the requests of telecommunication standards.

REFERENCES

[1]P. Tavella, A. Godone, S. Leschiutta, *The range covered by a random process and the new definition of MTIE*, in Proc. 28th Precise Time and Time Interval PTTI, Reston, Virginia, Dec. 1996, pp.119-124.

[2] S. Bregni, P. Tavella, *Estimation of the percentile Maximum Time Interval Error of Gaussian white phase noise*, in Proc. IEEE ICC97 Int. Conf. on Communications, Montreal, Canada 1997, n. 0-7803-3928-2/97/$10.00 (c) IEEE.

[3] P. Tavella, *On the integral frequency-domain/time-domain relationship of MTIE(τ,β)*, European Transactions on Telecommunications, n. 6, 1998.

[4]International Telecommunication Union ITU-T Recommendation G.810, *Definition and terminology for synchronisation networks*, Geneva, July 1995.

[5]D.R.Cox, H.D.Miller, The theory of stochastic processes, Science   Paperbacks, Chapman and Hall, London, 1965, Cap. 2,5.

[6]A. Papoulis, Probability, random variables, and stochastic processes McGraw-Hill Book Company, New York, 1965

[7]L. M. Ricciardi, Diffusion processes and related topics in biology, Lecture Notes in Biomathematics, Springer-Verlag, Berlin, 1942

[8]D.A. Darling, A.J. Siegert, *The first passage problems for a continuous Markov process*, Ann. Math. Stat. 24, 1953, pp. 624-639.

[9]W. Feller, *The asymptotic distribution of the range of sums of independent random variables,* Ann. Math, Statist. 22, 1951, pp. 427-432

[10]J. Nadler and N.B. Robbins, *Some characteristics of Page's two sided procedure for detecting a change in a location parameter*, Ann. Math. Statist., v. 42, No. 2, 1971, pp. 538-591.

[11]P.Vallois, *The range of a simple random walk on Z*, Adv. Appl. Prob. 28, 1996, pp. 1014-1033.

[12]S.Bregni, *Measurement of Maximum Time Interval Error for Telecommunications Clock Stability Characterization*, IEEE Trans. Instr. Meas., Vol. 45, No. 5, Oct.1996.

[13]H. L. Hartmann, E. Steiner, *Synchronization Techniques for Digital Networks*, IEEE JSAC, vol. SAC-4, No. 4, July 1986, pp. 506–13.

[14] S.Bregni, *A Historical Perspective on Network Synchronization*, IEEE Communications Magazine, Vol. 36, No. 6, June 1998.

[15] J. W. Chaffee, *Relating the Allan variance to the diffusion coefficients of a linear stochastic differential equation model for precision oscillators*, IEEE Trans UFFC, vol. 34, n. 6, Nov. 1987

[16] International Telecommunication Union ITU-R Rec. TF.538-2, *"Frequency and Time (Phase) Instability Measures"*, Geneva, July 1995.

[17]International Telecommunication Union ITU-T Rec. G.811, *Timing characteristics of Primary Reference Clocks PRC*, Geneva, Sept 1997.
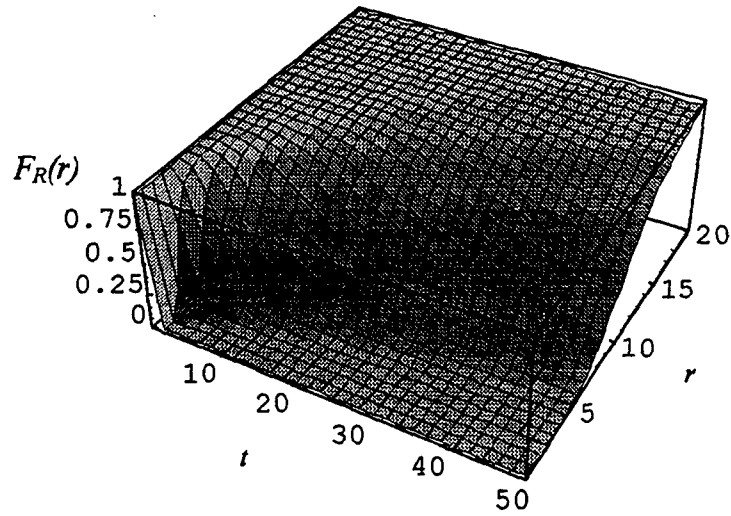
Fig.1: range probability distribution $F_R(r)$ for a Wiener process with zero average and $\sigma^2 = 1$.
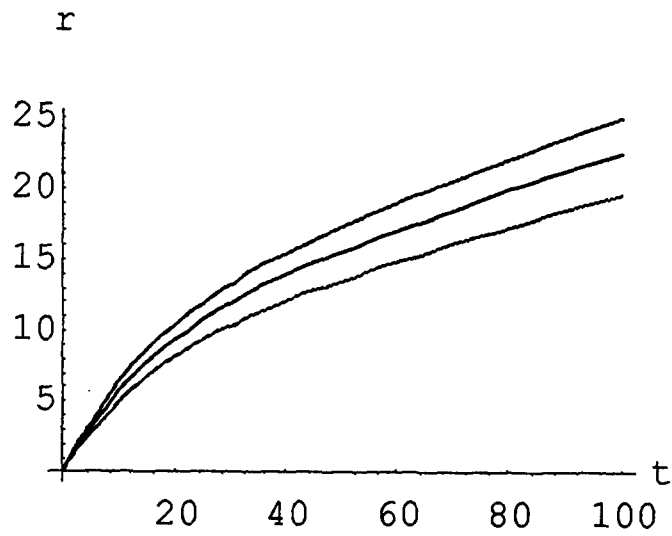
Fig. 2: Horizontal section of the surface in Fig. 1 representing, for each t, the threshold percentile value of the range r in the case of the 80th, 90th, and 95th percentile.
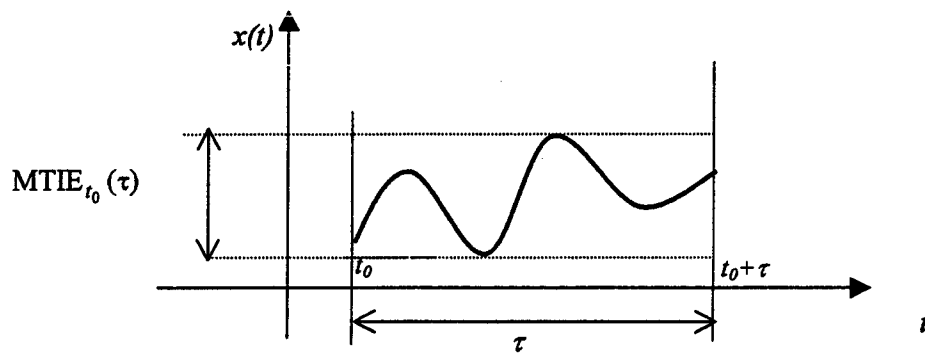
Fig. 3: graphical representation of the quantity MTIE [4]
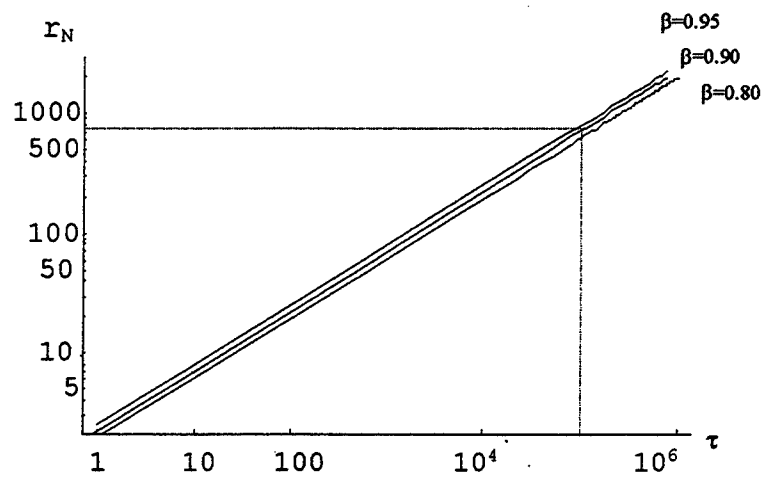
Fig. 4: normalized range threshold values, versus observation time for different percentile levels.
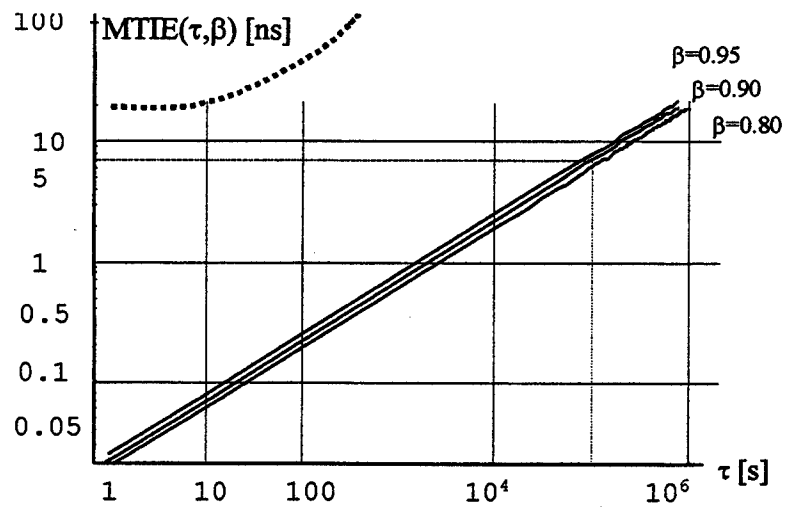
Fig. 5: MTIE(τ,β) as expected from an high stability Cs standard and ITU requests (dotted line, top left)

Questions and Answers

JUDAH LEVINE (NIST): The anti-specification usually has a requirement on the frequency accuracy as well, but you do not have that in your method.

PATRIZIA TAVELLA (IEN): No, the frequency accuracy for such a finite standard is that the frequency deviation should not exceed 10^{-11} over the long term. In the case of cesium, I think it is very well done.

JUDAH LEVINE : But, it might not be true for rubidium.

PATRIZIA TAVELLA: Yes, you are right.

BRIDGING THE GAP BETWEEN DESIGN AND USE OF PTTI SYSTEM: AN OPERATIONS PERSPECTIVE

Steven T. Hutsell
USNO Alternate Master Clock
400 O'Malley Avenue, Suite 44
Schriever AFB, CO 80912-4044, USA

William V. Bollwerk
USNO Alternate Master Clock

Abstract

Factors such as the unbounded growth in technology, as well as the desire for better, faster, and cheaper products, will always increase the pressure for advancing time transfer systems in the foreseeable future. Timing users will continually need systems with more features than before, improved robustness over previous systems, and better timing precision, stability, and accuracy than ever.

Often lost in the pursuit of timing system advancements is the perspective of the operator (user) of the system. This paper addresses elements of operations that are essential to the cohesiveness between a system and its operator. These often forgotten elements include system training, system continuity, operational simplicity, operator responsibility, and common sense in implementation.

INTRODUCTION

"A time transfer system is only as sophisticated as the confidence level of the operator/user." How often will the designers of time transfer systems stop to reflect on this simple thought?

The great technological growth the world is currently experiencing, especially since the dawn of the information superhighway, has opened the door for countless innovations for countless products in countless time transfer applications. Ultimately, though, if a customer doesn't feel comfortable with the operation of a new product, the countless innovations may prove to be more counterproductive than useful.

Advances in the determination, maintenance, and distribution of PTTI will require additional insight in the needs that drive such advances, and will also require improved understanding of how to best implement such advances with minimal risks of service interruption.

While continuing to advance on the technological front of timing systems, we must not forget the need to ensure that the operators of these timing systems have the confidence to accept the systems that utilize state-of-the-art advancements.

61

DESIGNING FOR OPERATIONS

Typically, the two major factors developers take into consideration in the design of a timing system are performance and price—a customer will show interest in a product if it meets timing specifications, without incurring an unacceptable financial tradeoff.

While not interfering with these two important goals, the design of a timing system should also incorporate theory about the *realistic operation* of that system. How a system should theoretically work only matters when that theory is allowed to operate in a realistic environment. In the real world, life isn't perfect, and the greatness of a system will depend on how it performs when adversity arises. Timing systems should be ready to respond to adversities—"nominal case" software coding *will* eventually become a problem—*at the worst possible time*! After all, a PTTI system is only as good as its worst day.

System Documentation

Documenting the design of a system is not always the most enjoyable aspect of system development. But, for many reasons, it is arguably the most important aspect. Documentation should never be considered an "afterthought" of system development. Rather, the designers should treat documentation as an activity parallel to such activities of coding, building, and testing.

Documentation is essential to configuration control and management. When a customer is trying to operate a system, he/she must know how it's *supposed* to operate, for two reasons: a) to keep the customer protected from the pain of undesirable surprises, and b) to allow the customer to know when something *isn't* working the way it's supposed to, and thereby allow the operator to intervene, as appropriate.

Documentation ensures accountability. Many timing applications involve the use of multiple systems interconnected in a typically complicated fashion. By understanding each component of a system, the user/operator can proactively configure his/her application such that no components will interfere with the optimal operation of the other components. And, when something doesn't work, accountability, through documentation, expedites the anomaly resolution process. In essence, documentation can significantly reduce confusion, and can also help to resolve disagreements quickly.

The format of documentation may not be as important as the existence of documentation. However, the format becomes most useful when it's geared towards optimal absorption of content by the reader, who, again, is the operator/user. Different applications will suggest the need for differing formats. Often, though, similar designs can benefit from the use of similar documentation formats.

The purpose of documentation is to describe the purpose of the system, for the perspective of the operator. Documentation provides understandable information, in an efficient manner, to the system user. Documentation is optimal when it can serve the knowledge needs of the user, without *overwhelming* the user.

System Training

In many military operations, the operational readiness of an organizational mission literally lives or dies in the execution of approved standard operating procedures. The 2d Space Operations Squadron (2 SOPS), responsible for command and control of all operational Global Positioning System (GPS)

satellites, is perhaps today's flagship example of this principle. The enormous success of GPS has resulted, in large part, from certified space operations crewmembers who exhibit outstanding checklist discipline, and to the others within the squadron who facilitate accurate checklists for use by those operators.

In 2 SOPS, classroom training provides only *preparation* for on-the-job training. Many can relate to the necessity for having this understanding. How many times have we taken a C class, a UNIX Introduction, or a Windows seminar, only to find out that once we get back to our desks, we require more familiarization? The reason for this is simple. Though the classes we pay for may serve as excellent building blocks for training, each particular operational environment is unique. This becomes increasingly true as technologies become more and more diversified. As such, from now on, truly no one can reasonably expect any classroom training to completely fill the whole training square. Nothing beats the familiarization and orientation that on-the-job training provides.

System training proves itself sufficient if it can serve the purpose of adequately describing how a system will work, but truly excels when it describes *how the human being will work with the system.*

Operational Continuity

"The more something changes....." You know the rest. This statement hits home more than we realize. We must ask ourselves, "How much of our work time do we spend creating something innovative, compared to the time we spend re-inventing the wheel?" Many of us share the experience of spending many hours re-working something, simply because the originators of a system didn't take the time to properly envision the need for system modularity.

We often forget the importance of not sacrificing the future for the present. Short-term fixes are no substitute for *long-term solutions.* While alleviating symptoms of problems, true accomplishment occurs when we can identify and correct the *causes* of our problems.

Operational Simplicity

Simplicity isn't always that simple. Additional system features can add robustness, but can also increase confusion. The more bells and whistles a system has, the less each one may be understandable to the operator/user. When more bells and whistles sound, the higher the likelihood of operators tending to ignore alarms, simply because they're receiving too many.

Often, designers will add features that, on paper, seem to show potential for improving operational performance. However, if the designers don't have a solid perspective of what the true needs of the operator are, such designers may end up complicating matters more than improving matters.

Such confusion often finds its way into the GPS community. One particular example involves the classic *accuracy vs. stability* debate. To many experts in the clock community, the natural intuition is to believe that the more accurate the clocks at the GPS monitor stations, the better. To an extent, and in the right context, this intuition has some truth. However, what many in the timing community may not always understand is that the performance of GPS actually depends much more on *stability* than accuracy. Whether in navigation or time transfer, the performance of GPS is largely dependent on the stability of the GPS Composite Clock. The stability of the individual frequency standards (in both monitor stations and satellites) contributing to GPS time is paramount to ensuring Composite Clock stability. Sacrificing

stability for absolute frequency or time accuracy at GPS monitor stations can actually *degrade* GPS performance [1].

The above issue is merely one example. Many military communication systems prefer accuracy over stability. Many digital communication systems, such as local area networks and the World Wide Web, may not care too much about accuracy and stability, and actually may care more about simple operational continuity. Most operators of PTTI systems look for the right combination of stability, accuracy, and operational continuity. The mix will invariably be user-dependent.

Often, the best solution to a challenge will be the least intuitive, but the simplest in design and infrastructure. Remember the KISS principle: *Keep It Simple, Scientist!*

OPERATIONS IN PRACTICE

The success of a timing system, of course, doesn't merely rest on its design. Yes, operators make or break a well-designed system. Though 2 SOPS commands and controls a superbly designed satellite system (GPS), using sophisticated navigation and time transfer software, much of 2 SOPS's operational success over the years is directly attributable to the dedication of the personnel who make the day-to-day difference in the operational availability and accuracy of GPS.

Coordination

The importance of coordination in the operation of a system is as follows: our activities may affect more people than we might think—our activities might be more *important* than we may think.

How many times in our corporate world have we felt "cubicles away, yet worlds apart"? How often do we forget that simply taking the time to walk over to our co-worker could help prevent a problem before it can even occur? How simple it seems, yet how uncommon in practice it occurs, that we take a minute or two to pick up the phone to check with others before making decisions that could affect them significantly?

How eager many are to offer suggestions and recommendations, but how often are we too lazy to *ask* for them? Ultimately, if we are working on something that others will eventually use, we best benefit when we actively solicit their feedback. And, sometimes simply opening the door for the opinions of others isn't enough--sometimes we absolutely have to *fight* for feedback.

The problem with blind spots is that we never know just how large they are! We must be careful when we make assumptions. When we assume, what we truly assume is responsibility for the repercussions incurred if we're wrong! One of the most common mistakes we make is when we assume that communication lines are foolproof. Unfortunately, in this technological age, along with advances in communications comes the increased likelihood of communication breakdowns. E-mails can get lost, people can misinterpret tone, and *others* will sometimes make incorrect assumptions. The key to alleviating these natural problems is the never-ending conviction to *always follow up*.

Responsibility

We all must accept various levels of responsibility in our particular, unique work environments. We must be reasonable, not just to others, but to ourselves, when we accept responsibility, explicitly or implicitly. We must set *reasonable* goals, and prioritize.

By accepting responsibility for a system, we must think not only in terms of immediate explicit responsibility, but also in terms of *long-term, implicit* responsibility. We all have learned international lessons about the impacts of when we don't responsibly act with foresight—we've seen many time bombs—Y2K is perhaps our generation's most egregious example.

Though easier said than done, we shouldn't ever cover up problems; rather we should learn from problems, and *let others learn from them as well*. People will respect us more in the long term. The more one tries to cover up a problem, the less likely that problem will be able to experience the benefits of a *solution*!

When we take control of a project (and subsequently take credit for that project), we must simultaneously take *accountability* for that project. Trust is integral to the transfer of responsibility. We can best earn the trust of others when we're willing to accept the accountability that parallels the control over particular projects. If we're going to take advantage of people to further our careers, we should first take advantage of ourselves, and our own integrity.

Common Sense

"It's realistic to be optimistic, but even more optimistic to be realistic." The best solution for a problem will most likely be *situation-dependent*. One makes the best progress in problem solving when he/she approaches and examines each problem uniquely.

For many years, many in the timing community had, via empirical analysis, identified what appeared to be a 12-hour timing periodic in the broadcast GPS signal. Many inferred that what they were observing was a 12-hour periodic in GPS time, and some even concluded that the periodic somehow must have been due to some quirk in the GPS steering algorithm. In reality, however, as presented in the previous year's PTTI Meeting, the 2 SOPS Ephemeris Enhancement Endeavor (EEE) was able to reduce the 12-hour periodic to the noise level of the GPS Master Control Station estimator, strictly by improving satellite ephemeris and solar pressure state estimation [2]. The EEE team was able to rule out the GPS time steering algorithm as the culprit of this periodic, and, at the same time, for the most part, alleviate the periodic, without even touching the GPS steering algorithm.

The above example points out that, when one takes the time to give the unique attention that a unique problem deserves, he/she will often take the course of action best suited for his/her long-term interests, and help to prevent making the original problem worse. Knee-jerk reactions can result in injury! Taking the time to properly assess what's truly going on can ensure safe, progressive improvements in operations.

CONCLUSION

No portion of the above text truly presents anything new or innovative. The thoughts conveyed in the above text are convictions most all of us have, whether consciously or subconsciously. Often, a natural progression in our technological revolution is to become preoccupied with the technical aspects of a great system, while forgetting to consider properly the operational needs of the user of the system itself. This behavior is a perfectly natural characteristic of human nature in the technological age.

Designers of PTTI systems excel by staying cognizant of the requirements, goals, and expectations of the operator. Effective lines of communication are essential. Designers who fail to recognize the time-honored "customer first" principle will fail to grow and may eventually fade into a caretaker status, or much worse.

We all want to harness the benefits of the many technical advances that are occurring literally on a daily basis. At the same time, however, in order to take advantage of those technically advanced systems, we must understand how to bridge the gap between the design of those advances, and the operational use of those advances. The road to failure is paved with good intentions. The road to success is best driven by confident, responsible, trained, qualified operators.

ACKNOWLEDGMENTS

REFERENCES

[1] S. Hutsell, 1996, Discussion comments during the 27th Annual Precise Time and Time Interval (PTTI) Applications and Planning Meeting, 29 November – 1 December 1995, San Diego, California, USA, pp. 48-49.

[2] J. Crum, S. Hutsell, and R. Smetek Jr. 1998, "The 2 SOPS Ephemeris Enhancement Endeavor," in Proceedings of the 29th Annual Precise Time and Time Interval (PTTI) Applications and Planning Meeting, 2-4 December 1997, Long Beach, California, USA, pp. 117-130.

Questions and Answers

MIHRAN MIRANIAN (USNO): Steve, you might want to comment on the fact that UTC did not run off.

STEVEN HUTSELL (USNO): Yes, good point. Mihran pointed out the fact that because GPS provides the correction term for the GPS minus UTC offset in Sub-Frame 4, page 18 of the NAV Message, the 270-nanosecond runoff that you saw did not directly translate into 270 nanoseconds of UTC time recovery to users, because for the most part daily updates as a result of downloads from USNO to 2SOPS did occur. So that at least it minimized the degradation and thankfully was able to keep the very top blue number under 28 nanoseconds, which is the specification.

LT. DAVID CRATER (2SOPS, Schriever AFB): Steven, I wanted just to ask if you had a chance to get a group of people in a room, people that designed navigation and time-transfer systems for solving those types of problems. What would you say to them in terms of improving their thinking on solving these problems and incorporating the types of principles that you have talked about, as opposed to solving a type of problem that has a well defined set of things that need to be addressed? From a technical point of view, how would you tell them to incorporate the types of operational issues that you have talked about?

STEVEN HUTSELL: Obviously I am going to bias my opinion on the fact that I have spent most of my time being an operator as opposed to being an analyst outside of operations. Therefore, my opinion is going to be inherently conservative; and part of that opinion was formed by working in a squadron, which you are now in, that runs very efficiently and very effectively because you have proven procedures and check lists. I guess my biased suggestion would be to examine the problem very carefully and not to make hasty decisions. In the case of this Colorado Springs event, there was enough time to get enough people together as a "Tiger Team." Unfortunately, for various reasons, that just did not happen.

We are not in a business where we have to make decisions so quick that the safety of the world is going to depend on it over a few minutes. We are not launching ICBMs, for instance; but, at the same time, we do not have that much time to resolve a problem. In the case of GPS, everything is geared around 24-hour predictions; uploads are done 24 hours a day; downloads from USNO are done once every 24 hours. That is basically the general time frame you have to respond in.

The answer to your question is: Just try to maintain a delicate balance of getting a concrete answer, but not taking much too much time so that the problem lingers on – if that is any help.

JAMES DeYOUNG (USNO): I just have one comment. At the Naval Observatory we have had a number of people who had a great deal of experience retire in the last few years. We have already gone through that experience. There are other places – especially in this room, I see a lot of people that have been around PTTI for a long time who will potentially be retiring in the near future. The goal is that basic knowledge is already out there, but there is still no replacement for experience in time and frequency. There are so many complex systems in the field today that we have to get younger people experienced in and understanding of the systems. It is great to approximate a clock with power-on noise and all of these things; but in the data I look at day to day, there are so many noise processes involved together that the simple models are not going to be sufficient. In my opinion, in the out-years, when you go to two-way time transfer and especially GPS carrier phase over long distances; you are going to be risking a lot. There is a lot of stuff going on that is scientifically interesting and are goals for bigger budgets in the future years.

STEVEN HUTSELL: Right. It enforces the tradeoff of how much performance you want versus how much redundancy and safety you have. As we are getting more technical in our systems, the more risks we have of things breaking and more people being around not really understanding the quickest way to solve it. It is a dilemma.

ESTIMATING FREQUENCY STABILITY AND CROSS-CORRELATIONS

F. Torcaso, C. R. Ekstrom, E. A. Burt, D. N. Matsakis

U. S. Naval Observatory
3450 Massachusetts Ave., NW
Washington, DC 20392 USA

Abstract

We present a method for estimating the absolute frequency stability of N clocks separate from a reference. The method introduced is a modification of the one proposed by Tavella and Premoli (1993). After developing the theory we apply the method to atomic clock data gathered from the USNO.

INTRODUCTION

The estimation of absolute frequency stability of clocks separate from a reference clock is usually required in order to produce a mean time scale. The usual method which can be employed for this task is the so-called "N-cornered-hat" method. As first presented by Gray and Allan [1], this method estimates the stability of a fixed clock among an ensemble of N clocks by forming all $(N-1)(N-2)/2$ triads of time differences which include those of the clock under test. The reason for triads is to avoid overdetermination in the estimation problem. From each of these triads one obtains stability estimates for each of the clocks in the triad under the assumption that clocks are uncorrelated − these are the "three-cornered-hat" estimates. These estimates are then weighted by a "triad uncertainty" to yield a stability estimate for each clock. Another version, developed by Barnes [2], simultaneously uses all $N-1$ time differences with a least-squares-type approach to estimate the individual stabilities. These approaches sometimes lead to stability estimates that are negative. Some attribute the negative estimate to its uncertainty [3], while others suggest the possibility that the assumption of uncorrelation is not always valid [4]; both are probably true to a significant extent.

Recently, Tavella and Premoli [4] developed an approach which avoids the problem of negative stability estimates by allowing the possibility of correlations among the ensemble of clocks. Their approach is consistent and formally equivalent to the three-cornered-hat method when clocks are uncorrelated, that is, both methods produce the same result in this situation. Their method,

however, will not produce a negative variance estimate even when a three-cornered-hat approach would. Since the problem of estimating absolute frequency stability is underdetermined, they impose the condition that if correlations exist they should be "small." They propose a condition which amounts to finding the smallest correlations possible which keep a certain matrix positive-definite. This will be explained in greater detail below. Since Tavella and Premoli's work [4] was done in the framework of three clocks, a weighted triad uncertainty approach can be used to improve the estimates if there are more than three clocks in the ensemble.

In a later paper [5] Tavella and Premoli refined their analysis. They show that when the number of clocks in a comparison increases, the amount of arbitariness in determining absolute frequency stability decreases.

The goal of this paper is to generalize the methods of [4] and [5] and to estimate absolute frequency stability for N clocks ($N > 3$). The results of this analysis will be discussed and applied to atomic clock time difference data from the U. S. Naval Observatory (USNO).

NOTATIONS AND DEFINITIONS

Let $x^i = \{x_k^i : k \geq 1\}$ for $i = 1, \cdots, N - 1$ be the time differences of clock i with respect to a fixed reference clock, say clock N, which is sampled every τ_0 seconds. We let $X^j = \{X_k^j : k \geq 1\}$ for $j = 1, \cdots, N$ represent the time differences with respect to a noiseless "ideal" clock, so that $x^i = X^i - X^N$.

Define the fractional frequencies:

$$y_k^i = \frac{x_{k+1}^i - x_k^i}{\tau_0}, \ k \geq 1 \tag{1}$$

and the process of averaging such fractional frequencies of order $m \geq 1$:

$$\bar{y}_k^i(m\tau_0) = \frac{y_{(k-1)m+1}^i + y_{(k-1)m+2}^i + \cdots + y_{km}^i}{m} = \frac{1}{m} \sum_{l=1}^{m} y_{(k-1)m+l}^i. \tag{2}$$

Notice that (2) reduces to (1) for $m = 1$. We define Y_k^i and $\bar{Y}_k^i(m\tau_0)$ by replacing x with X appropriately. As a measure of time domain frequency stability we use the Allan variance. The Allan variance of clock i referenced to clock N is defined as

$$s_{ii}(\tau) = \frac{1}{2} \langle (\bar{y}_2^i(\tau) - \bar{y}_1^i(\tau))^2 \rangle \tag{3}$$

where $\langle \rangle$ denotes mathematical expectation. We assume here, of course, that the process of averaged fractional frequencies is stationary and ergodic so that the definition (3) is well-defined. Most authors use the notation $\sigma_{i,N}^2(\tau)$ to represent the quantity in (3), but we will use the notation set forth in the works [4] and [5]. For what follows we need to define the Allan covariance of clocks i and j referenced to clock N to be

$$s_{ij}(\tau) = \frac{1}{2} \langle (\bar{y}_2^i(\tau) - \bar{y}_1^i(\tau))(\bar{y}_2^j(\tau) - \bar{y}_1^j(\tau)) \rangle. \tag{4}$$

This statistic appears in [6] with different notation. It is worth mentioning at this point that a covariance reduces to a variance for $i = j$; therefore we will refer to variances as covariances when no confusion can arise. Furthermore, it is clear from the definition (4) that $s_{ij}(\tau) = s_{ji}(\tau)$. However, all these quantities are usually never available in practice and can only be estimated through a large stretch of data (at least for $\tau = m\tau_0$ and integer $m \geq 1$) by the samples

$$\hat{s}_{ij} = \frac{1}{2(n-2m)} \sum_{k=1}^{n-2m} (\bar{y}_{k+1}^i(m\tau_0) - \bar{y}_k^i(m\tau_0))(\bar{y}_{k+1}^j(m\tau_0) - \bar{y}_k^j(m\tau_0)) \tag{5}$$

where n is the data length. The goal of this paper is estimate the dereferenced quantities:

$$r_{ii} = \frac{1}{2}\langle (\bar{Y}_2^i(\tau) - \bar{Y}_1^i(\tau))^2 \rangle \tag{6}$$

and

$$r_{ij} = \frac{1}{2}\langle (\bar{Y}_2^i(\tau) - \bar{Y}_1^i(\tau))(\bar{Y}_2^j(\tau) - \bar{Y}_1^j(\tau)) \rangle. \tag{7}$$

Again, some authors use the notation $\sigma_i^2(\tau)$ to represent the quantity shown in (6). The associated sample quantity is defined similar to (4):

$$\hat{r}_{ij} = \frac{1}{n-2m} \sum_{k=1}^{n-2m} (\bar{Y}_{k+1}^i(m\tau_0) - \bar{Y}_k^i(m\tau_0))(\bar{Y}_{k+1}^j(m\tau_0) - \bar{Y}_k^j(m\tau_0)) \tag{8}$$

By noting that $y_k^i = Y_k^i - Y_k^N$ we deduce from (4)-(8) the following relations:

$$s_{ij} = r_{ij} + r_{NN} - r_{iN} - r_{jN} \tag{9}$$

and

$$\hat{s}_{ij} = \hat{r}_{ij} + \hat{r}_{NN} - \hat{r}_{iN} - \hat{r}_{jN}. \tag{10}$$

If $N = 3$ and all $\hat{r}_{ij} = 0$ for $i \neq j$ then the usual three-cornered-hat estimates fall out of (10):

$$\begin{aligned} \hat{r}_{11} &= \hat{s}_{11} - \hat{s}_{12} \\ \hat{r}_{22} &= \hat{s}_{22} - \hat{s}_{12} \\ \hat{r}_{33} &= \hat{s}_{12} \end{aligned} \tag{11}$$

This was noted in references [4] and [6].

THE TAVELLA-PREMOLI APPROACH

Let's first outline the approach followed by Tavella and Premoli [4]. Suppose we are interested in obtaining estimates of absolute frequency stabilities for three clocks, say clocks 1, 2, and 3. That is, we wish to estimate the matrix

$$R = \begin{bmatrix} r_{11} & r_{12} & r_{13} \\ r_{12} & r_{22} & r_{23} \\ r_{13} & r_{23} & r_{33} \end{bmatrix}. \tag{12}$$

Notice the matrix R is inherently symmetric. Now consider the matrix

$$S = \begin{bmatrix} s_{11} & s_{12} \\ s_{12} & s_{22} \end{bmatrix}.$$

S is symmetric and we know a priori S is also positive-definite. The relation (9) can be rewritten to give the relations:

$$
\begin{aligned}
r_{11} &= s_{11} - r_{33} + 2r_{13} \\
r_{22} &= s_{22} - r_{33} + 2r_{23} \\
r_{12} &= s_{12} - r_{33} + r_{13} + r_{23}.
\end{aligned}
$$

This means that all the entries of R can be written as functions of the elements $\mathbf{r} = (r_{13}, r_{23})$ and the reference stability r_{33}. To find estimates for the entries of R, Tavella and Premoli proposed the following. We should find values of covariances r_{12}, r_{13} and r_{23}, which are small in some sense, but keep the matrix R positive-definite. To understand in what sense they mean small define

$$G(r_{12}, r_{13}, r_{23}) = r_{12}^2 + r_{13}^2 + r_{23}^2. \tag{13}$$

Clearly, the minimum value of G is 0 exactly when $r_{13} = r_{23} = r_{12} = 0$, and, given (9), this implies $r_{33} = s_{12}$. That is, we arrive at the three-cornered-hat estimates (11):

$$\hat{R}_{3\text{-corner}} = \begin{bmatrix} s_{11} - s_{12} & 0 & 0 \\ 0 & s_{22} - s_{12} & 0 \\ 0 & 0 & s_{12} \end{bmatrix}. \tag{14}$$

As long as

$$
\begin{aligned}
s_{11} &> s_{12} \\
s_{22} &> s_{12} \\
s_{12} &> 0
\end{aligned}
\tag{15}
$$

we have valid estimates of stability. However, if one of the diagonal elements in (14) is negative, we obtain a negative stability estimate. This can be ruled out if we insist that the estimated matrix $\hat{R}$ be positive-definite. Tavella and Premoli are able to show that the function

$$H(r_{13}, r_{23}, r_{33}) = r_{33} - (r_{13} - r_{33}, r_{23} - r_{33})S^{-1}(r_{13} - r_{33}, r_{23} - r_{33})^T \tag{16}$$

is positive if and only if R is positive-definite. T denotes transpose here. Therefore they suggest the r_{ij} should be chosen in a way that minimizes the following expression:

$$\frac{r_{12}^2 + r_{13}^2 + r_{23}^2}{H(r_{13}, r_{23}, r_{33})} \tag{17}$$

where the minimum is taken over all values r_{13}, r_{23}, r_{33} for which H is positive (i.e., R is positive-definite). Notice that if $H(0, 0, s_{12}) > 0$ then the minimum of (17) is 0 and we again achieve the three-cornered-hat estimates. This procedure, however, will not lead to a negative stability

estimate. To see this just notice that the minimization occurs over a convex region, namely the elliptic paraboloid region

$$P = \{(x, y, z) : H(x, y, z) > 0\}.$$

The boundary of P, ∂P, contains all the points where the function H identically equals 0. Since the objective function (17) is convex, it is well known that the minimizer of this problem is unique. The minimizer $(r_{13}^*, r_{23}^*, r_{33}^*)$ of (17) will always satisfy $H(r_{13}^*, r_{23}^*, r_{33}^*) > 0$ since points on the boundary of P yield undefined values in (17). Now $H > 0$ implies R is positive-definite. The result follows from the fact that positive-definite matrices have positive diagonal elements. The minimization of (17) was carried out explicitly for $N = 3$ clocks [4] and its solution was formulated through the zeroes of a sixth-degree polynomial.

The implementation of this method does show some subtle inadequacies however. As noted in the introduction, a three-cornered-hat approach may give a negative stability estimate. Although the Tavella-Premoli approach will not produce such a negative value, it may produce an optimistically small estimate of stability. Let's see why this may happen. It is easy to show that if the conditions (15) are all satisfied then $(0, 0, \hat{s}_{12}) \in P$. Therefore, if $\hat{s}_{12}$ is arbitrarily small and positive, our estimate for r_{33} will also be arbitrarily small. Similarly, if $\hat{s}_{11} < \hat{s}_{22}$ and $\hat{s}_{12}$ is close to $\hat{s}_{11}$, our estimate for r_{11} may also be optimistically small. These effects have appeared in time difference data gathered at the USNO.

This optimism can be attributed to the rather large domain of admissible values in (17). The admissible region is an elliptic paraboloid in $\Re^3$. If more clocks are in our comparison then, as shown in [5], this admissible region is substantially reduced and points that would be admissible when considered through triads would be disallowed when considered in a multiple comparison. We can use this substantial reduction in admissible values to generalize the Tavella-Premoli scheme. We will take this up next.

A MODIFIED APPROACH

Suppose we have time differences from $N - 1$ clocks with a fixed reference clock N ($N > 3$) and we wish to estimate the stabilities. We could, of course, apply the method of Tavella and Premoli [4] to triads of clocks and weight appropriately. As noted earlier, this approach may produce optimistic values of stability.

Let's consider the following approach. In analogy to the method proposed by [4], we suggest an obvious modification to (17) and find the values of covariances that minimize the following Tavella-Premoli function:

$$\frac{\sum_{i<j} r_{ij}^2}{H^2(r_{1N}, \cdots, r_{NN})} \tag{18}$$

where

$$H(r_{1N}, \cdots, r_{NN}) = r_{NN} - (r_{1N} - r_{NN}, \cdots, r_{1N} - r_{NN})S^{-1}(r_{1N} - r_{NN}, \cdots, r_{1N} - r_{NN})^T$$

the superscript T denotes transpose and the minimization is over those points r_{iN} which keep H positive. Here, the function $H > 0$ if and only if the matrix R is positive-definite [5]. Dividing

by H above as mentioned earlier keeps the points r_{iN} away from the boundary of the admissible region and, consequently, will keep the matrix R positive-definite. Notice the function (18) is now a function of the N variables $(r_{1N}, \cdots, r_{NN})$ as well as, of course, the s_{ij}. Also notice that function (18) has H squared in the denominator. This squaring is suggested in order to keep the minimization problem scale-invariant. This will also be helpful in order to do the minimization from a numerical point of view. The problem of minimizing (18) is a constrained minimization problem since we are only allowing values of r_{ij} which keep the matrix R positive-definite, that is, those r_{ij} for which $H(r_{1N}, \cdots, r_{NN}) > 0$. From the same convexity considerations the minimization problem (18) has a unique solution. Usually constrained minimization problems are difficult to solve, but one can apply numerical techniques if care is taken in scaling and choice of initial data. We used a conjugate gradient method to produce the minimizer. As far as the choice of initial data we chose

$$r_{iN} = 0 \text{ for } i < N,$$
$$r_{NN} = \frac{1}{2} \cdot \frac{1}{s^*}$$

$s^* \equiv (1, \cdots, 1) S^{-1} (1, \cdots, 1)^T > 0$ from the positive-definiteness of the matrix S and thus S^{-1}. The factor $\frac{1}{2}$ above is used to force the initial data to lie within the constraint (using convexity of admissible values here). This choice of initial data conforms with our belief that clocks are close to uncorrelated. Of course, from the uniqueness of the solution any reasonable point we choose initially will converge to the minimizer and this, in fact, is observed. We should mention that problems can arise if the initial datum is too close to the boundary of the admissible region. If this is the case a conjugate gradient direction may lead you outside the admissible region.

It is interesting to note that if clocks are uncorrelated ($r_{ij} = 0$ for all $i \neq j$) the minimization of (18) leads to the estimate

$$\hat{r}_{NN} = \frac{2 \sum_{i<j} \hat{s}_{ij}}{(N-1)(N-2)},$$

that is, the straight average of the values that one would obtain by performing the usual Tavella-Premoli procedure on all triads of clocks.

One implicit point we have stressed in this paper is the possibility of the existence of clock noise correlations. In order to convince the reader that clock correlations are a reality we have developed a preliminary statistical test which, although heuristic, may be used to determine if clock noise correlations exist between clocks in the comparison.

A STATISTICAL TEST OF CORRELATION

Tavella and Premoli have shown [5] that if $r_{ij} = 0$ for all $i \neq j$ then the matrix S of "true" Allan covariances has the form

$$S = \begin{bmatrix} r_{11} - r_{NN} & r_{NN} & r_{NN} & \cdots & r_{NN} \\ r_{NN} & r_{22} - r_{NN} & r_{NN} & \cdots & r_{NN} \\ r_{NN} & r_{NN} & r_{33} - r_{NN} & \cdots & r_{NN} \\ \vdots & \vdots & \vdots & & \vdots \\ r_{NN} & r_{NN} & r_{NN} & \cdots & r_{N-1,N-1} - r_{NN} \end{bmatrix} \quad (19)$$

As mentioned in the previous section, the matrix S can only be estimated by the matrix $\hat{S} = (\hat{s}_{ij})$. Thus, if the clocks are uncorrelated then the $\hat{s}_{ij}$ for $i \neq j$ are all estimating the reference stability r_{NN}. If the data length n is large, one should expect $\hat{r}_{ij} \approx 0$ for $i \neq j$. If this is the case then from (10) and (19) the statistic $\hat{s}_{ij} \approx \hat{r}_{NN}$ for $i \neq j$. Now since the distribution of $\hat{r}_{NN}$ can be shown to behave as a chi-square with some number of degrees of freedom (we consider here overlapping sample estimates), which in general varies with the noise type present [3], we can test if the off-diagonal terms of $\hat{S}$ actually differ up to some statistical significance. The problem can be formulated as follows:

Consider as the null hypothesis all clocks are uncorrelated. We would like to test whether the alternative hypothesis that some pair of clocks exhibit correlations is true. So we would like to test for the simultaneous equality of the off-diagonal elements of the matrix $\hat{S}$. This is a multiple comparison problem whose analysis can be quite difficult. We instead will be content to work with pair-wise comparisons of the off-diagonal elements $\hat{s}_{ij}$. For this problem we test whether the ratio

$$ f = \frac{\hat{s}_{ij}}{\hat{s}_{i'j'}} $$

for different pairs of clocks $i \neq j$ and $i' \neq j'$ is significantly different from 1. Now since the chi-squares all have the same degrees of freedom, d, for a fixed integration time τ, the test statistic f has the $F_{d,d}$-distribution, that is, the ratio of two chi-squares with d degrees of freedom each. Assume that for fixed $\tau > 0$ all the off-diagonal terms of $\hat{S}$ are positive. For 90% confidence we choose to reject the null in favor of the alternative if either

$$ f > F_{d,d,.95} \quad \text{or} \quad f < F_{d,d,.05} $$

where $F_{d,d,\alpha}$ represents the αth percentile of the F distribution. Since all estimates $\hat{s}_{ij}$ share the same degrees of freedom, the problem is simplified considerably since we only need to check if the statistic

$$ f^* = \max \frac{\hat{s}_{ij}}{\hat{s}_{i'j'}} $$

satisfies $f^* > F_{d,d,.95}$. The above argument is only heuristic and the resulting statistical test is not entirely substantiated since significant accidental covariances for increasingly smaller sample sizes can corrupt the distributional properties of the f-statistic, that is, if $n - 2m$ is not "large" then the values $\hat{r}_{kl}$ for $k \neq l$ in (10) may not be close to zero and can bias the $\hat{s}_{ij}$-statistic away from $\hat{r}_{NN}$. However, at least for very large sample sizes n and relatively small m, the above approximation seems reasonable. Of course, a better statistical test can be achieved if one can characterize the distribution of the Allan covariance statistics.

We applied the above analysis to a group of four cesium-beam frequency standards rereferenced to a fifth cesium-beam standard (see Table 1). The time differences had data length $n = 167,513$. We made the assumption that for the integration times observed the dominant noise type was white frequency modulation and computed the appropriate degrees of freedom for the overlapping estimates:

$$ d = \left[\frac{3(n-1)}{2m} - \frac{2(n-2)}{n} \right] \frac{4m^2}{4m^2 + 5}. $$

We found the corresponding F quantile and applied the above arguments. We noticed that although the off-diagonal entries of $\hat{S}$ may seem to be the same, at least for short integration times (from

20 seconds out to about 320 seconds) we were able to reject the null hypothesis and conclude that statistically significant correlations exist. This does not say that a correlation is "large"; indeed, $\hat{r}_{ij}$ can be relatively quite small (by orders of magnitude) when compared to the diagonal entries $\hat{r}_{ii}$ and $\hat{r}_{jj}$. However, some small covariance seems quite reasonable when we consider that some of the clocks in the above analysis were in the same environmental chamber. An exhaustive treatment of the above ideas would certainly be interesting from both a practical and theoretical point of view.

$$\hat{S}(20) = \begin{bmatrix} 7.10826E-24 & 3.81328E-24 & 3.79768E-24 & 3.79259E-24 \\ 3.81328E-24 & 7.95851E-24 & 3.82652E-24 & 3.83888E-24 \\ 3.79768E-24 & 3.82652E-24 & 7.89671E-24 & 3.82095E-24 \\ 3.79259E-24 & 3.83888E-24 & 3.82095E-24 & 6.99711E-24 \end{bmatrix}$$

$$\hat{S}(40) = \begin{bmatrix} 3.22437E-24 & 1.69300E-24 & 1.69913E-24 & 1.69097E-24 \\ 1.69300E-24 & 3.42756E-24 & 1.69388E-24 & 1.70435E-24 \\ 1.69913E-24 & 1.69388E-24 & 3.58596E-24 & 1.71195E-24 \\ 1.69097E-24 & 1.70435E-24 & 1.71195E-24 & 3.15194E-24 \end{bmatrix}$$

$$\hat{S}(320) = \begin{bmatrix} 3.55895E-25 & 1.82808E-25 & 1.85889E-25 & 1.84763E-25 \\ 1.82808E-25 & 3.65834E-25 & 1.89250E-25 & 1.85393E-25 \\ 1.85889E-25 & 1.89250E-25 & 4.04481E-25 & 1.89242E-25 \\ 1.84763E-25 & 1.85393E-25 & 1.89242E-25 & 3.55988E-25 \end{bmatrix}$$

Table 1.

Averaging Time	F-statistic	f^*-statistic	
20 sec.	1.009893	1.012205	$f^* > F$: can reject in favor of alternative.
40 sec.	1.010690	1.012407	$f^* > F$: can reject in favor of alternative.
320 sec.	1.026667	1.035239	$f^* > F$: can reject in favor of alternative.

The $\hat{S}$ matrices above were computed for $\tau =20$, 40 and 320 seconds. Table 1 shows the results of the statistical test for these integration times.

RESULTS

We have applied the technique described in the previous section to time difference data obtained from atomic clocks at the U.S. Naval Observatory (USNO). USNO has a large ensemble of clocks consisting of both commercial cesium-beam standards and active hydrogen masers. Data from both types of clocks were considered separately.

Figures 1a and 1b show sigma-tau plots generated by a three-cornered-hat and Tavella-Premoli analysis respectively. For comparison, both analyses were carried out on cesium-beam standards labelled 229, 260, and 253 over a period of five years. The three time series were rereferenced to one of the clocks (253) to avoid the obvious problem of correlation between the time scales. We used overlapping estimates of Allan covariance over all τ, instead of just $\tau = 2^m \tau_0$ (integer $m \geq 1$) where τ_0 is the sampling time.

There are several things to notice about these plots. First, both approaches coincide where the three-cornered-hat approach produces positive stability estimates, so that the primary difference between the two is that the Tavella-Premoli scheme is able to produce an "extension" of the reference stability. Second, by plotting the data for all τ, a "pathological" behavior is apparent in both approaches. There are two "dips" in each graph: one at 60 days and the other at about 590 days. Neither of these dips are likely to be physical, since cesium-beam standards integrate down with a $1/\sqrt{\tau}$ dependence until they reach their flicker floor or begin to drift significantly. One approach to this situation might be to add another clock to the ensemble and use the additional three triads. However, even if a straight average of the resulting estimates coming from each triad were used, one would still find that the dip creates a large bias in the result.

Instead, the extra clock can be used with the modified approach outlined in the previous section. The corresponding frequency stability plot is shown in Figure 2. This approach is in close agreement with the other two until $\tau \approx 30$ days. At this point, the first spike apparent in the other approaches is smoothed out. Most importantly, the new approach now maintains the expected $1/\sqrt{\tau}$ behavior at this point in the data. The second spike is smoothed out as well.

We performed this modified approach on the data with two more clocks added in. The results are shown in Figures 3a and 3b. Again the absence of non-physical dips is apparent and agreement between this and results shown in Figure 2 is good. In all plots we noticed that one of the cesium clocks appeared to be much worse than the others. Later we were able to show that this particular clock had a significant drift component that wasn't compensated for.

We also applied the modified approach to active hydrogen maser data. We, unfortunately, were not able to extract such a long stretch of data as with the cesiums. The resulting plot is in Figure 4.

We would also like to mention that the modified approach did not differ significantly with the manufacturer specifications, and, in most cases, conformed to them closely. Although the results of this analysis are by no means complete, we believe this method shows significant promise in achieving estimates of absolute frequency stability.

CONCLUSIONS

The modified approach for estimating frequency stability generally performs well: it gives essentially the same results for short-term stabilities ($\tau < 30$ days) and non-pathological behavior for long-term stabilities ($\tau \sim 1$ year). We are encouraged by these preliminary results and are hopeful that the method can be used to give an accurate representation of long-term stability in atomic clocks.

ACKNOWLEDGMENTS

REFERENCES

[1] J. E. Gray and D. W. Allan, 1974, "A method for estimating the frequency stability of an individual oscillator," in Proceedings of the 28th Frequency Control Symposium, 29-31 May 1974, Atlantic City, New Jersey, pp. 243-246.

[2] J. A. Barnes, 1982, Notes from NBS 2nd Symposium Atomic Time Scale Algorithms, June, National Bureau of Standards, Boulder, Colorado.

[3] S. R. Stein, 1985, "Frequency and time – their measurement and characterization," in *Precision Frequency Control*, Vol. 2, edited by E. A. Gerber and A. Bollato (Academic Press, New York), pp. 191-416.

[4] P. Tavella and A. Premoli, 1993, "A revisited three-cornered-hat method for estimating frequency standard instability," *IEEE Transactions on Instrumemtation and Measurement*, IM-42, 7-13.

[5] P. Tavella and A. Premoli, 1993, "Estimation of instabilities of N clocks by measuring differences of their readings," *Metrologia*, **30**, 479-486.

[6] A. Lepek and F. Walls, 1993, "Cross correlation analysis improves time domain measurements," in Proceedings of the IEEE International Frequency Control Symposium, 2-4 June 1993, Salt Lake City, Utah, pp. 312-321.
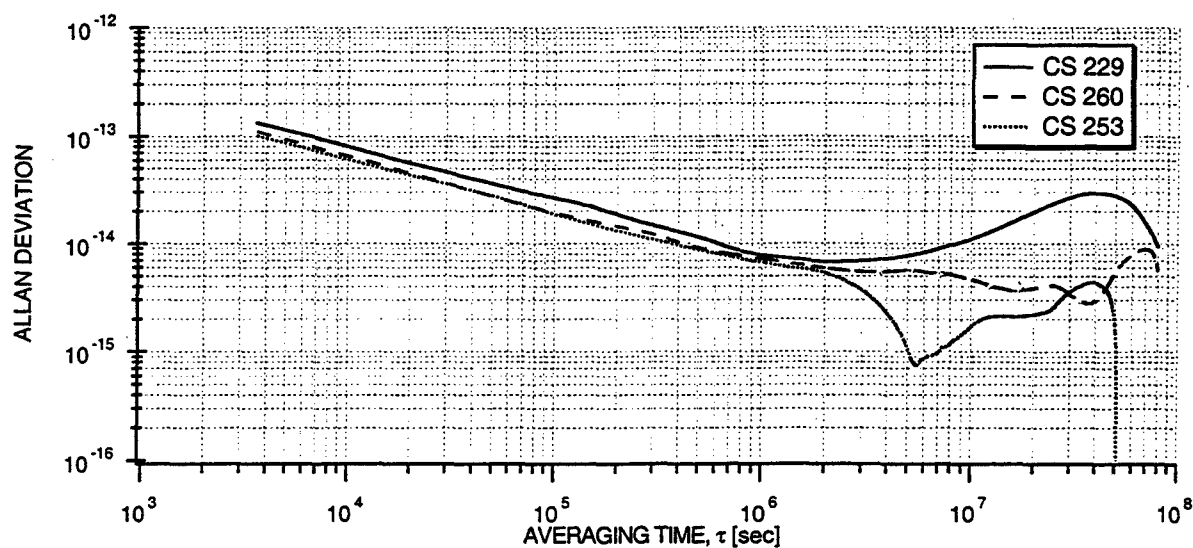
Fig. 1a: Plot of absolute frequency stability calculated using the three-cornered-hat approach.
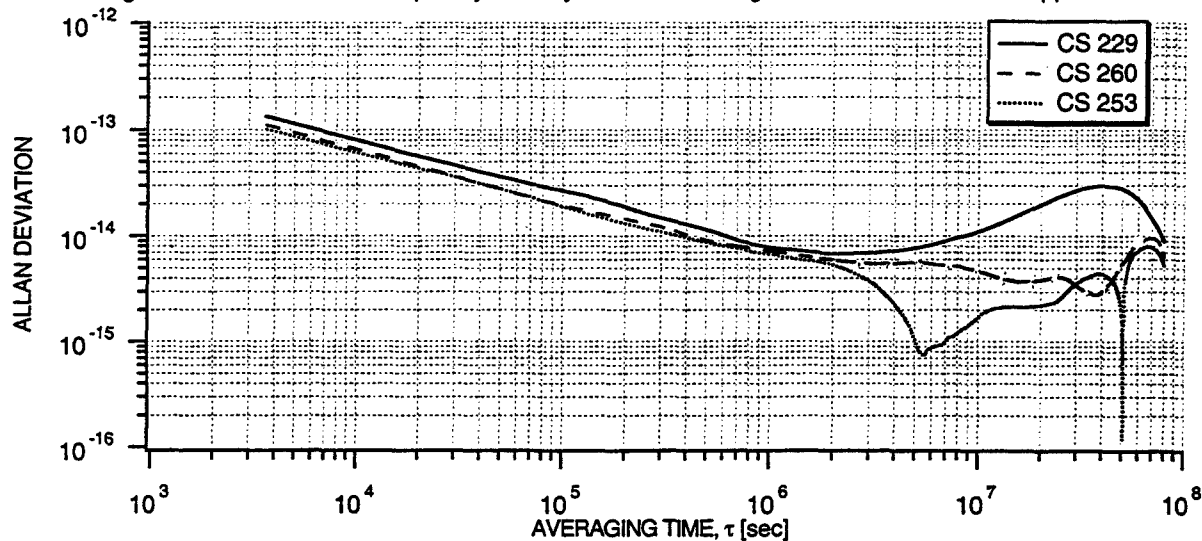
Fig. 1b: Plot of absolute frequency stability using the Tavella-Premoli approach.
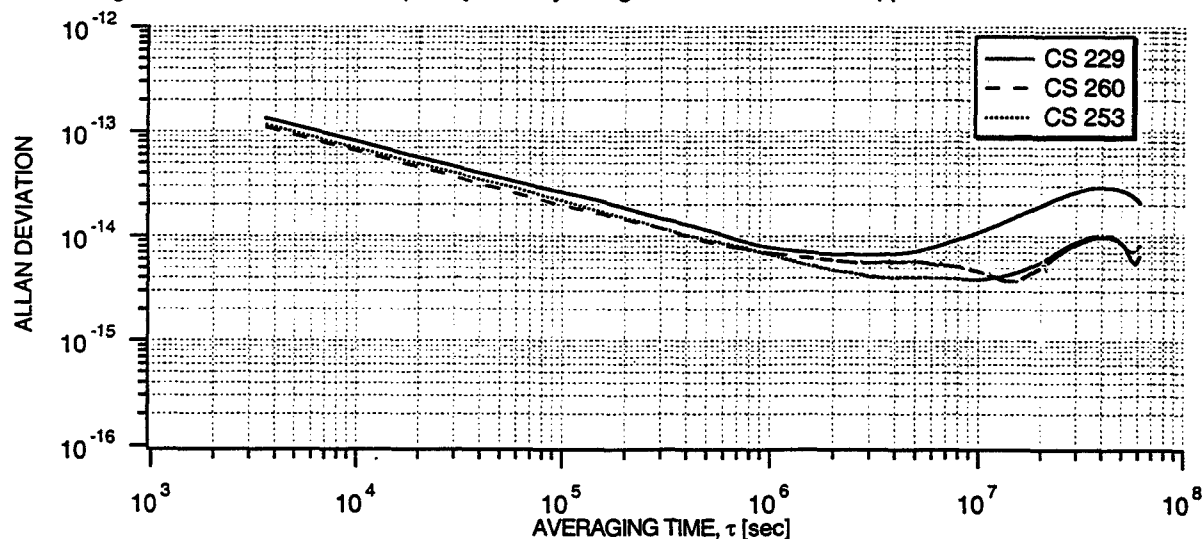
Fig. 2: Plot of absolute frequency stability using the modified approach with a fourth clock (fourth clock's stability not shown).
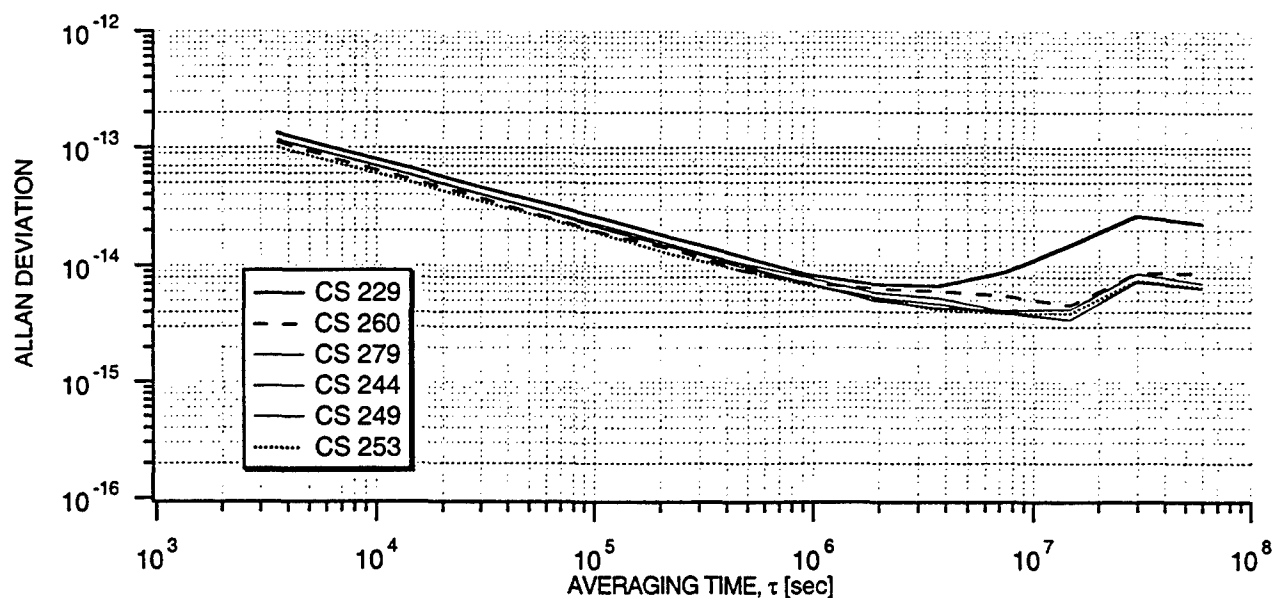
Fig. 3: Plot of absolute frequency stability using modified approach with six clocks - stabilities for all six clocks shown (cf. Fig. 2). The analysis which gave this plot was performed on dyadic averaging times only as opposed to all averaging times shown in Fig. 2.
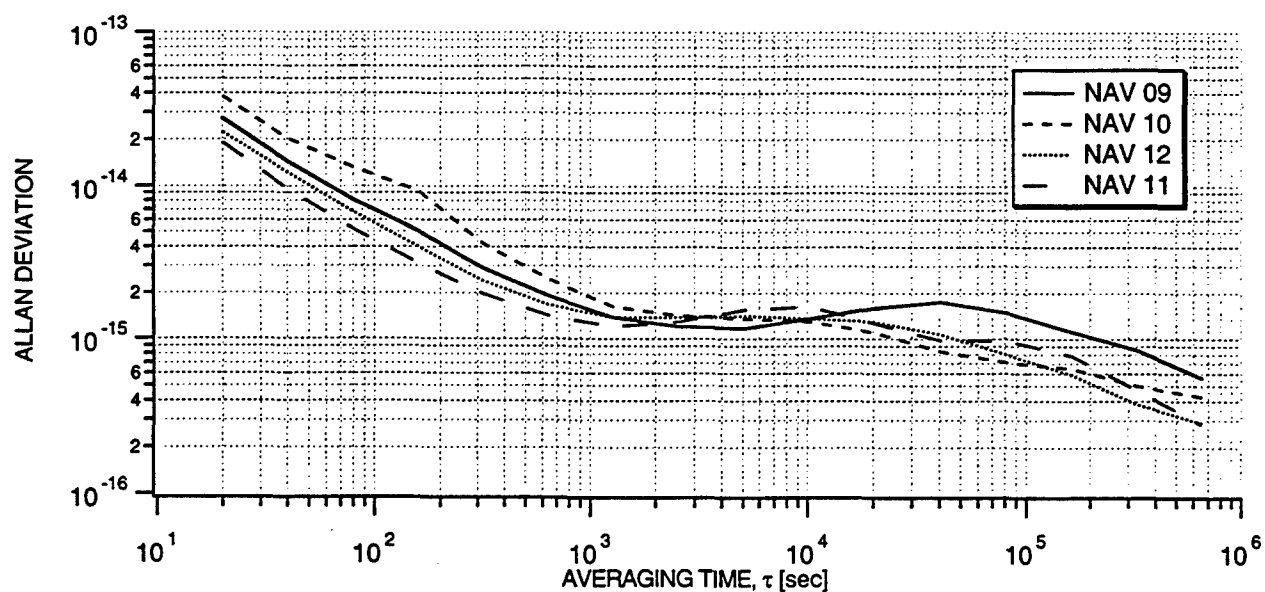
Fig. 4: Plot of absolute frequency stability using modified approach with four active hydrogen masers sampled at 20-second intervals. Analysis performed with dyadic averaging times.

80

Questions and Answers

PATRIZIA TAVELLA (IEN): I am happy that you are continuing with this work and you took the time to read my papers. Thank you for the quotation.

I think that maybe the optimizer function can be different in the short and long term. Maybe the long correlation is reasonable in the short term, but not in the long term. Maybe we could investigate if the possible function to be minimized should be different in long and short term.

I would also like to investigate the effect of the uncertainty of the variance evaluation on the positive definitiveness of the matrix, because since the evaluation, I am uncertain due to the limited number of measurements. Maybe the region can change.

FRED TORCASO (USNO): I think moving in that direction would be trying to get a better understanding of the distribution of the sample Allan variance for exactly those integration times. That is actually a difficult problem. There have been a lot of papers appearing which try to estimate the distribution of the sample Allan variance for integration times of, I think, eight samples. It is something ridiculously hard.

It looks like there is some evidence for large integration times in many sample estimates that a gaussian approximation is probably a good one. Maybe this would be a possible way to go.

MARC WEISS (NIST): Have you thought about how to compute uncertainty for Allan variance when you have the n-cornered-hat technique? In other words, there is an uncertainty for the Allan variance when you look at the distribution just because you have a sample variance.

FRED TORCASO: So you like to put error bars around the absolute values?

MARC WEISS: In the presence of an n-cornered hat where you are estimating a variance through the other clocks, I think there is an additional uncertainty because of that. I think the relative stability of the clocks will come in as well. In other words, if you look at one very good clock and you have ten clocks that are ten times worse, you can not see the good clock – at least in theory you should not be able to.

I do not know how to do it. I am wondering if you have looked at that?

FRED TORCASO: I actually have not looked at ways of obtaining error bars on estimates of absolute stability. I am looking into the possibility of comparing very quiet clocks, for instance, hydrogen masers, over a short time scale compared with the high-performance cesium beam clocks that we have at USNO. A similar approach to the one I described may work if we rescale this co-variance matrix that I introduced, "R", to a correlation matrix. Then all the off-diagonal terms of the matrix are of the same order. That will help in the analysis, but I have not done that.

AUTOMATIC FREQUENCY CALIBRATION USING FUZZY LOGIC CONTROLLER

Ching-Haur Chang, Chia-Shu Liao, and Kun-Yuan Tu
National Standard Time & Frequency Lab.
Telecom Labs. of Chunghwa Telecom Co., Ltd.
12, Lane 551, Min-Tsu Road Sec. 5, Yang-Mei, Taoyuan,
Taiwan 326, ROC
Tel: 886-3-424-4246   Fax: 886-3-424-5178
E-mail: changc@ms.chttl.com.tw

Abstract

A way of frequency calibration using fuzzy logic controller (FLC) is presented in this paper. Generally, atomic clocks tend to drift due to temperature, aging, or some environmental effects. It is sure that one cannot compensate for the drift with a fixed amount of control quantity. As a controller, it has the task to adaptively catch up with the variation. Our approach takes advantage of FLC to determine the control quantity. Three procedures are employed in our approach. Firstly the performance of the device being calibrated is observed continuously. Then the FLC uses the performance data to generate the control quantity. Finally the FLC calibrates the device using the computed control quantity. The FLC can calibrate the device at any time since the performance of the device is continuously being monitored. In the experiment, we use FMAS (Frequency Measurement and Analysis System) as the performance evaluation equipment and the FLC is realized by a PC. In the experiment, a cesium-beam oscillator is chosen as the target. The result validates the effectiveness of our approach. An oscillator with frequency offset of -1.4×10^{-13} can be improved to approximately -1.0×10^{-14} after one week of calibration.

INTRODUCTION

Due to temperature, aging, or some environmental effects, atomic clocks generally tend to drift in an unknown way. This ends up with a difficulty in characterizing the clock. For example, it is not possible to compensate for the drift with a fixed amount of control quantity during frequency calibration [1]. A fuzzy logic controller (FLC) has been deemed to be suitable for use in a time-varying, nonlinear, or hard-to-defined system [2]. In this paper, we use FLC to adaptively determine the control quantity to compensate for the drift.

Three procedures are employed in our approach. First, the performance of the device being calibrated is continuously being monitored. Note that this requires a reference frequency with accuracy much better than that of the device being calibrated. Second, the performance data are connected to the FLC. Upon receiving data from the performance evaluation equipment, the FLC calculates the control quantity according to some fuzzy rules. Finally, the FLC calibrates the device through the command compliant to some particular form. The FLC can calibrate the

device according to some predefined criteria. For example, it can be done at a regular interval or on an on-demand basis.

The performance evaluation equipment used in this work is the FMAS (Frequency Measurement and Analysis System), measurement equipment developed by NIST (National Institute of Standards and Technology). The FLC is realized by a commercial PC. Fig. 1 shows the system configuration. The reference frequency used is the master clock in our laboratory. The accuracy of the reference frequency is better than 5×10^{-14} and hence is sufficient for calibrating most commercial oscillators.

Let $y_{ref-ideal}$ denote the frequency offset of the reference frequency relative to the ideal frequency; i.e., $y_{ref-ideal} = (f_{ref} - f_{ideal})/f_{ideal}$. Similarly, the frequency offset of the user's clock relative to the reference frequency is $y_{usr-ref} = (f_{usr} - f_{ref})/f_{ref}$ and that of the user's clock relative to the ideal clock is $y_{usr-ideal} = (f_{usr} - f_{ideal})/f_{ideal}$. Having these relations, the frequency offset of the user's clock relative to the ideal clock can be expressed as

$$y_{usr-ideal} = y_{ref-ideal} + \frac{f_{ref}}{f_{ideal}} y_{usr-ref} \tag{1}$$

Hence, if $f_{ref} \cong f_{ideal}$, then $y_{usr-ideal}$ can be approximated by

$$y_{usr-ideal} \cong y_{ref-ideal} + y_{usr-ref} \tag{2}$$

It is obvious from (2) that $y_{usr-ref} \cong y_{usr-ideal}$ provided $y_{ref-ideal} \ll y_{usr-ref}$. This means that the frequency offset measured from the user's clock can be treated as that relative to the ideal frequency provided that the reference clock is good enough.

To verify the effectiveness of the proposed method, we choose a cesium-beam oscillator with accuracy of -1.4×10^{-13} as the device being calibrated. Experiment result shows that the accuracy can be improved to approximately -1.0×10^{-14} after one week of calibration.

We have assumed in this paper that the reference frequency is available in the site where calibration is performed. If this is not the case, the techniques of transfer standards or means by which oscillators can be made traceable to some standards must be used. Examples of these are via LORAN-C, GPS, common-view GPS, or the technique of GPS carrier phase.

SYSTEM DESCRIPTION

For convenience in later description, the following symbols are defined: y denotes the frequency offset, Δe denotes the phase offset resulting from the frequency offset at the corresponding interval, φ denotes the control quantity to be applied to the device being calibrated, and the subscript denotes the time index. Note that $\Delta e = yT$ where T is the length of the observation interval. Fig. 2 illustrates the basic idea by which our approach is made possible. In the figure shown, a positive frequency offset is assumed initially, i.e., $y_{n-1} > 0$, and the phase offset at the beginning of each observation interval is assumed to be zero. Note that this is tantamount to balancing the phase offset with an action of single step made at the beginning of each observation interval. Also, we use bold lines to indicate the residual frequency offsets in the corresponding observation interval.

It is intuitively seen that the phase offset resulting from the frequency offset of $y_{n-1} > 0$ (i.e., Δe_{n-1} as shown in the figure) can be balanced by imposing a phase offset with direction opposite to the former; i.e., $\varphi_n = -\Delta e_{n-1}$. However, as mentioned in the last section, oscillators tend to drift in an unknown way. It is therefore not possible to keep residual frequency offset to a minimum with such a fixed amount of control quantity. If the residual is equal to zero (i.e., $y_n = 0$) after the above action is done, then the control quantity is deemed to be temporarily correct. In this case, the controller has the task to keep the same control quantity in the next observation interval; i.e., $\varphi_{n+1} = \varphi_n$ as shown in Fig. 2a. If the residual has a positive slope, i.e., $y_n > 0$, then the controller has the task to increase the controller quantity; i.e., $|\varphi_{n+1}| > |\varphi_n|$ as shown in Fig. 2b. On the contrary, if the residual has a negative slope, i.e., $y_n < 0$, the controller has the task to decrease the control quantity; i.e., $|\varphi_{n+1}| < |\varphi_n|$ as shown in Fig. 2c.

The variation of phase error is generally nonlinear. The one shown in Fig. 2a is but a hypothetical case. It cannot be an easy job to have a proper control quantity for atomic clocks. To overcome this difficulty, the FLC is used to evaluate the control quantity before applying it to the device being calibrated. In this work, the control quantity is made to be adaptive in the way

$$\varphi_{n+1} = \varphi_n + \Delta\varphi_n \tag{3}$$

where $\Delta\varphi_n$ is the updating term and is determined by the FLC. The initial value of φ_n can be chosen arbitrarily.

Fig. 3 shows the basic structure of an FLC. It consists of the following four units: 1) fuzzification unit, 2) fuzzy reasoning unit, 3) fuzzy rule base and fuzzy data base unit, and 4) defuzzification unit. Two variables are used as the input to the fuzzy rule base. One is the frequency offset read from the FMAS (i.e., y_n). The other is the difference of the frequency offsets between two adjacent observation intervals (i.e., $\Delta y_n = y_n - y_{n-1}$). Table 1 gives the fuzzy rule base used in this work. The ranges for the two input variables and the output are divided into five parts. They consist of the following fuzzy sets: NB (Negative Big), NS (Negative Small), ZE (ZEro), PS (Positive Small), and PB (Positive Big). The membership functions chosen for these fuzzy sets are of a triangular form. Fig. 4 shows the membership functions stored in the fuzzy data base. Additionally, the fuzzy reasoning method chosen is the Max-Min method, and the mean of maximum (i.e., modified centroidal) is used as the method of defuzzification [2].

EXPERIMENT RESULTS

In our experiment, a cesium-beam oscillator is chosen as the device being calibrated. The frequency offset of a cesium lies between $y_n \in [-1\times10^{-12}, 1\times10^{-12}]$ and therefore $\Delta y_n \in [-2\times10^{-12}, 2\times10^{-12}]$. Taking these ranges into account, the membership functions shown in Fig. 4 are scaled by 10^{-13} and 2×10^{-13} respectively for y_n and Δy_n. The range for the output is the same as y_n.

The oscillator originally has frequency offset of -1.4×10^{-13}. The result shows that the frequency offset can be improved to -1.0×10^{-14} after about one week. Fig. 5 shows the variation of the frequency offset.

CONCLUSIONS

A way of adaptive frequency calibration using a fuzzy logic controller is presented in this work. Atomic clocks tend to drift due to aging or some environmental effects and generally leads to irregular variation in characteristics. Our

approach takes advantage of fuzzy logic controller (FLC) to determine the control quantity adaptively. Experiment results validate the effectiveness of our approach.

REFERENCES

[1] M.A. Lombardi, *Tutorial on frequency calibrations and time transfer*, NIST Time and Frequency Division, Colorado, USA.

[2] J. Yan, M. Ryan, and J. Power, *Using fuzzy logic*, Prentice Hall International (UK) Limited 1994.
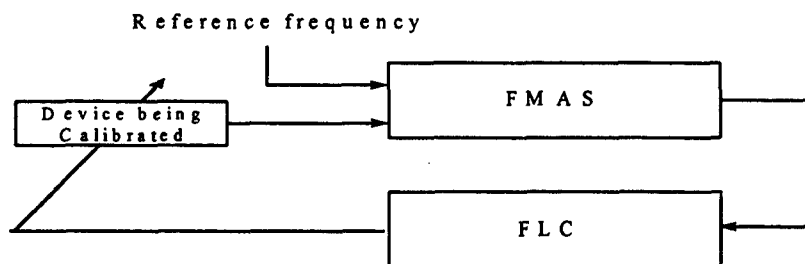
Fig. 1 The proposed frequency calibration method.

(a) $y_n = 0$

(b) $y_n > 0$

(c) $y_n < 0$

86
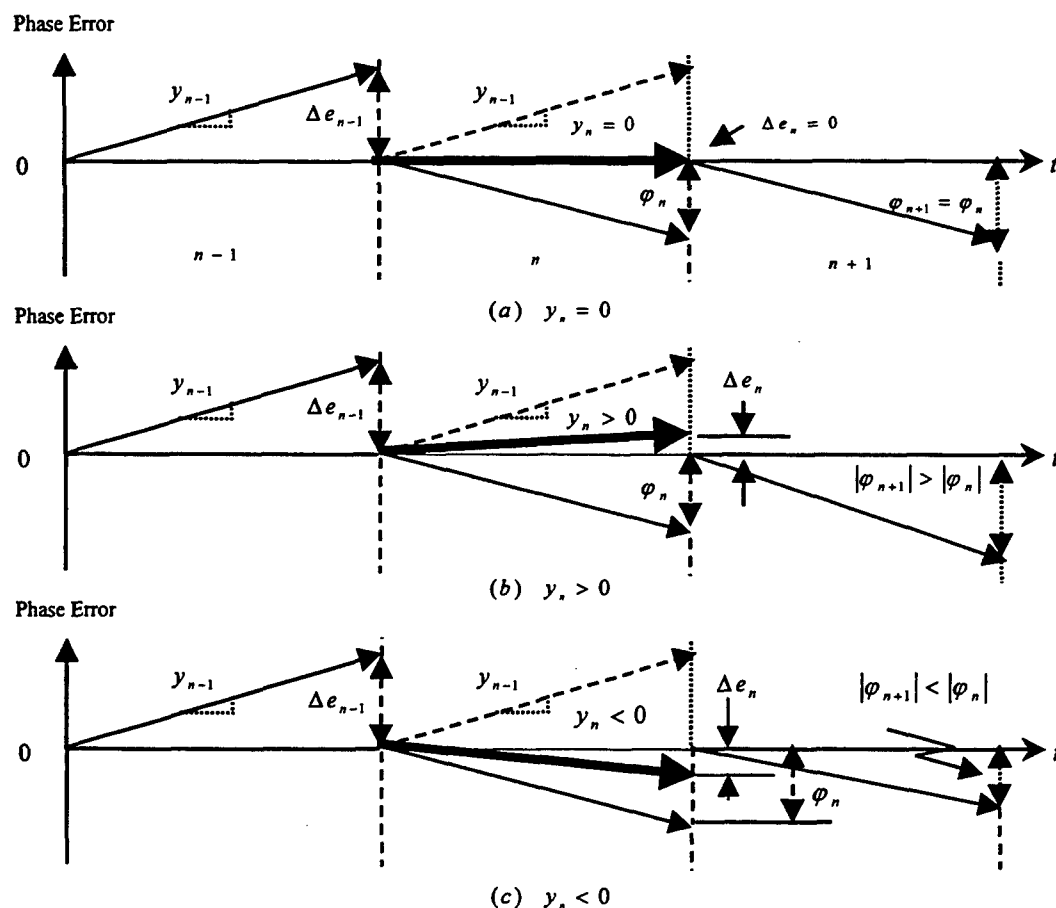
Fig. 2 Basic idea for frequency calibration: (a) $y_n = 0$, (b) $y_n > 0$, and (c) $y_n < 0$.

Fuzzy Rule Base	Fuzzy Data Base

Fuzzy Reasoning Unit

Fuzzification

Defuzzification

Input
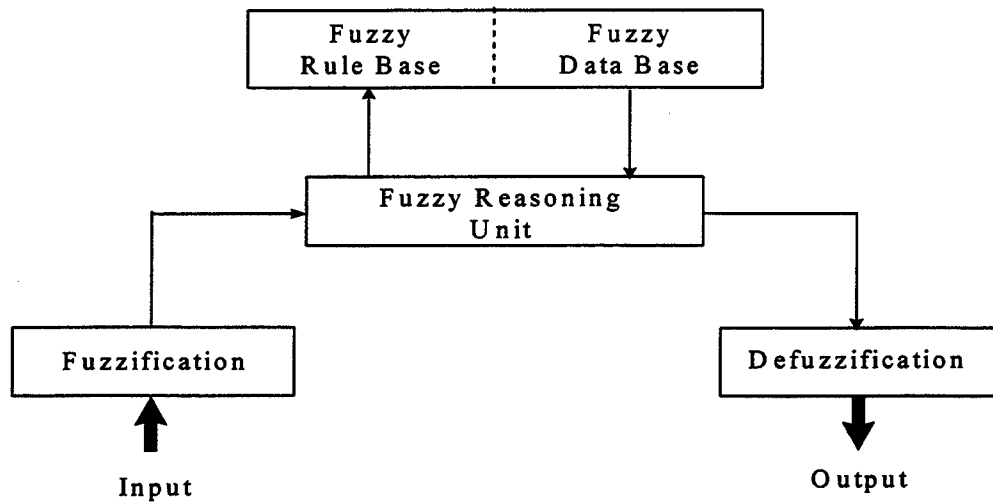
Output

Fig. 3 Basic structure of fuzzy logic controller.

Table 1 Fuzzy rule base.

y_n / Δy_n	NB	NS	ZE	PS	PB
NB	PB	PS	ZE	PS	NB
NS	PB	PS	ZE	PS	NB
ZE	PB	ZE	ZE	ZE	NB
PS	PB	NS	ZE	NS	NB
PB	PB	NS	ZE	NS	NB

87
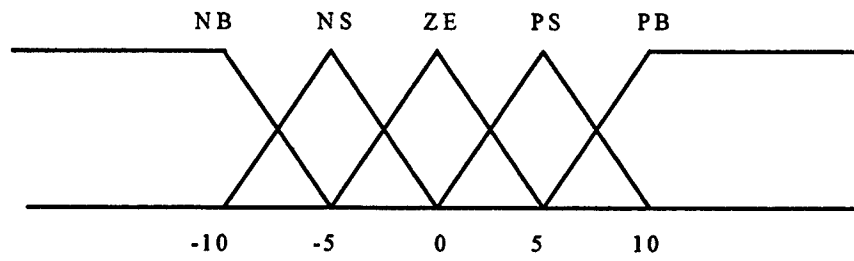
Fig. 4 Membership functions for y_n, Δy_n, and the output.
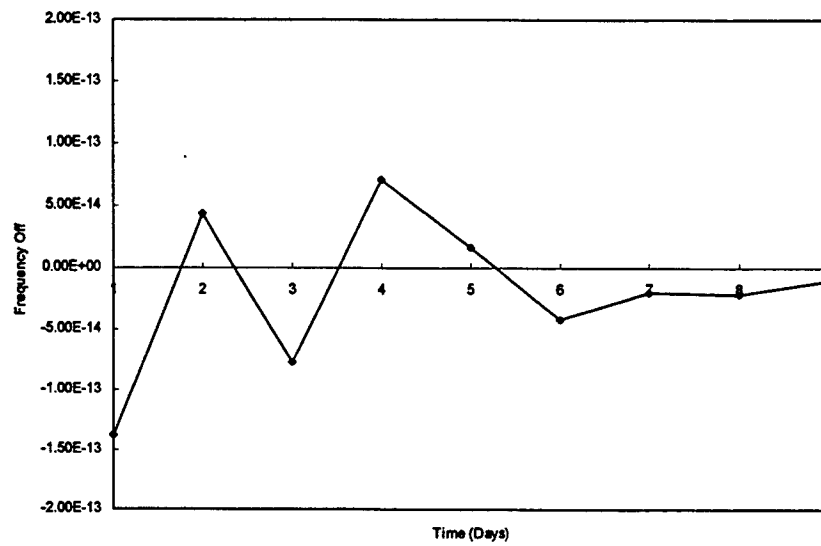
Fig. 5 Frequency offset vs. time.

MILLISECOND PULSAR OBSERVATION AT CRL

Y. Hanado, M. Imae, M. Hosokawa, M. Sekido, A. Kaneko and Y. Shibuya
Communications Research Laboratory
4-2-1, Nukui-kitamachi, Koganei, Tokyo 184 JAPAN

Abstract

Communications Research Laboratory (CRL) has developed a millisecond pulsar observation system which uses an acousto-optic spectrometer (AOS). Even though our 34 m telescope is one of the smallest telescopes used for millisecond pulsar observations, we succeeded in detecting several millisecond pulsars by using our new system which has a wide detection bandwidth. We started regular observations of PSR1937+21 with the 34 m telescope one year ago. The observed pulse phases contain some systematic trends, and we are investigating the data now. We also tested our observation system at the Usuda 64 m telescope of Institute of Space and Astronautical Science (ISAS) and succeeded in detecting two other highly stable millisecond pulsars, PSR1713+07 and PSR1855+09.

INTRODUCTION

Millisecond pulsars which have a millisecond pulse rate, are known to maintain extremely stable pulse timings over a long period of time. For the millisecond pulsar PSR1855+09 with a 5.36 ms pulse period, the fractional frequency stability was reported to be on the order of 10^{-14} over a period of 7 years[1], which is comparable to that of a cesium clock. These characteristics are expected to lead to millisecond pulsars being used in time-keeping metrology, planetary ephemerides, reference frame ties, and so on[2].

Communications Research Laboratory (CRL) serves as the national institute of time and frequency standards in Japan, and we plan to use millisecond pulsars in setting these frequency standards in the long term. We had to develop a highly sensitive observation system because our 34 m telescope at Kashima Space Research Center is not so large for millisecond pulsars that have very weak signals. In 1992, we developed a preliminary filter bank system with 4 MHz detection bandwidth and succeeded in detecting PSR1937+21 [3],which is the brightest millisecond pulsar in the northern sky. Based on this result, we developed an even more sensitive system last year. This system uses an acousto-optic spectrometer (AOS) [4] instead of filter banks, and detection bandwidth of 200 MHz is available. Using this system and 34 m telescope, we started weekly observations of PSR1937+21 in November 1997. Data analysis and system performance checks are now in progress.

We also tested this observation system at the Usuda 64 m telescope of the Institute of Space and Astronautical Science (ISAS), and succeeded in detecting two other weak and highly stable millisecond pulsars, PSR1855+09 and PSR1713+07. The detection of PSR1713+07 was confirmed with the Kashima 34 m telescope.

This paper introduces our new observation system, and presents observations results for PSR1937+21 over a one-year period. The results of preliminary observation for PSR1855+09 and PSR1713+07 at Usuda 64 m telescope are also reported.

OBSERVATION SYSTEM

1. CONCEPT OF SYSTEM DESIGN

In pulsar observation, the precision of pulse arrival time is estimated as follows;

$$\sigma_{rms}(s) \sim \frac{(W)^{3/2} \cdot Tsys}{(B\,t\,P)^{1/2} \cdot <S> \cdot G,} \tag{1}$$

where W is the half-width of the pulse in seconds, P is the pulse period in seconds, Tsys is the system temperature on the source, <S> is the flux density in janskys (Jy), G is the telescope gain in kelvins per jansky (K/Jy), B is the bandwidth in Hz, and t is the integration time in seconds [5]. Because millisecond pulsar signals are very weak, big telescopes such as the 300 m one at Arecibo are usually used for observing their timings. Our 34 m telescope is very small for millisecond pulsar observation and required a system with wide detection bandwidth B and long integration time T.

For a wide-band observation, however, we must note the pulse broadening caused by the dispersion effect caused by interstellar plasma (Fig. 1(a)). In order to suppress this broadening, a wide-band signal must be received as many narrow channels at first and combined after each dispersion delay has been cancelled (Fig. 1(b)). In our new system an acousto-optic spectrometer (AOS) is used for this spectrum analysis instead of a filterbank method. The AOS uses an acousto-optic device such as a single crystal of TeO_2 (Fig. 2). It makes the system simple and compact.

The long integration time is achieved by accumulating many pulses. We developed a high-speed averaging processor which can average up to 2^{24} pulses without any dead time for data transportation. It supplies the averaged data almost in real time.

2. SYSTEM DESCRIPTION

The 34 m telescope has several receivers from 1.5 GHz to 43 GHz with a selective polarizer; we mainly used the right-hand circular polarization in 2 GHz band. An IF signal with 200 MHz bandwidth is divided into four 50 MHz units by the video converter. Each 50 MHz bandwidth unit is divided into 256 200-kHz channels by the AOS, then serially transported to the video averaging processor. This transportation time, which limits the time resolution is at least 12.8 μs (= 50 ns x 256 ch) in minimum. Because the

transportation trigger clock is set to 1/100 of the pulsar period, the time resolution is about 16 μs for PSR1937+21. The video averaging processor works as an 8 bits A/D converter and an averager which allows the addition of 2^{24} pulses (= 7 hours' integration for PSR1937+21) in each channel. At host#1, averaged data for all the channels are combined after a dispersion delay calibration carried out in 1/1000 steps of the pulsar period, and the final pulse profile is defined. From this profile, the peak phase is defined as the arrival pulse timing.

Host#2 calculates the predicted pulse period and supplies it in real time to the synthesizer, which controls the averaging trigger clock of the timing signal generator. This predicted value is obtained from the database calculated by the Tempo program, which is the Princeton pulsar timing analysis package [5]. The reference clock is synchronized with UTC. The observation start time is obtained at a time interval counter by measuring the time difference between the start trigger signal and 1PPS signal of UTC.

OBSERVATION RESULTS

1. PSR1937+21 AT KASHIMA 34 M TELESCOPE

We have been making the weekly observations of PSR1937+21 in the 2 GHz band since November 1997. PSR1937+21 is one of the brightest millisecond pulsars; its flux density is about 3.3 mJy in the 2 GHz band (calculated from [6]) and the pulse period is about 1.5578 ms. One pulse profile is obtained after averaging 1,048,576 pulses (corresponding to about 27 minutes of integration), and 6-8 profiles are obtained in one day. The averaged profile is shown in Fig. 5. From these averaged profiles the peak phases are defined, and their residuals from the predicted phases show the pulse timing noise. Residual $R(t)$ is calculated as

$$R(t) = \phi \, obs(t) - \phi \, calc(t), \tag{2}$$

where $\phi \, obs(t)$ is an observed peak phase, and $\phi \, calc(t)$ is the predicted phase calculated by the Tempo program.

Figure 6 shows the $R(t)$s from Nov. 21, 1997 - Oct. 9, 1998 and Fig. 7 shows the $R(t)$s in each day. This result is made from only the AOS#1 unit for 2150 - 2200 MHz, because other units were out of order during some observation periods. The systematic trend is shown in the long term, and linear trends are shown over a day. These are probably due to an error in the predicted pulse phases or some hardware problems; we are making efforts to eliminate these causes.

In order to estimate the observation precision in hardware, we removed the trends in each day by linear fitting (shown by the solid line in Fig. 7). The standard deviation for all data was 5.4 μs after the fitting, which is comparable to the expected observation precision of 3.2 μs calculated by Equation 1 with W = 80 μs, <S> at 2.2GHz = 3.3 mJy, P = 1.5578 ms, Tsys = 71 K, G = 0.426 K/Jy, B = 50 MHz, and T= 1632 s.

2. PSR1855+09 AND PSR1713+07 AT 64 M TELESCOPE

We carried out a test observation with our new system at the Usuda 64 m telescope. This telescope belongs to the Usuda Deep Space Center of ISAS, and is mainly used for deep space satellite tracking. The system noise temperature is 40 K and the efficiency is 70 % in the 2GHz band. We tried to observe the millisecond pulsars PSR1855+09, which has a 5.36 ms pulse period, and PSR1713+07, which has a 4.57 ms pulse period [7]. Both are weaker than PSR1937+21, but are expected to be more stable.

Figure 8 shows the averaged profiles of PSR1855+09 and PSR1713+07. The observation band was 2275 – 2305 MHz in right-hand circular polarization, and one AOS unit is enough to cover it. Averaging pulses were 131,072 for PSR1855+09 and 262,144 for PSR1713+07, which correspond to the integration of 12 minutes and 20 minutes respectively.

For PSR1713+07, we succeeded in detecting the pulse at the Kashima 34 m telescope afterward. Regular observation of PSR1713+07 at Kashima will start soon.

CONCLUSIONS

We developed a new millisecond pulsar timing observation system for our 34 m telescope at Kashima. This system uses an AOS as a spectral divider instead of filter banks, and we can detect a signal up to 200 MHz bandwidth. We confirmed its performance by detecting PSR1937+21 and PSR1713+07 with the 34 m telescope and PSR1855+09 with the 64 m telescope at Usuda. Using this system, we started weekly observation of PSR1937+21 at Kashima, but the results must be considered carefully because observed peak phases show some systematic trends both in the long term and during one day. Perhaps we misuse the Tempo program; we are now investigating the predicted pulse phases by simulation.

We started VLBI observation for pulsars using the Kashima 34 m telescope and the Kalyazin 64 m telescope in Russia[8]. We intend to contribute to a new reference frame for data of both pulsar timing and VLBI in future.

ACKNOWLEDGMENTS

REFERENCES

[1] V. H. Kaspi, J. H. Taylor, and M. F. Ryba, "High-precision timing of millisecond pulsars. III. Long-term monitoring of PSRs B1855+09 and B1937+21," Astrophys. J., 428, 713-728, 1994.
[2] A.S. Fruchter, M.Tavani, and D.C. Backer, "Millisecond pulsars: A decade of surprise, " Astronomical Society of the Pacific conference series vol.72, pp. 345-356.

[3] Y. Hanado, H. Kiuchi, S. Hama, A. Kaneko, and M. Imae, "Millisecond pulsar observation system at CRL," Proceedings of 23rd Annual Precise Time and Time Interval (PTTI) Application and Planning Meeting, 1991, pp.377-383.

[4] A. P. Goutzoulis and I. J. Abramovitz, "Digital electronics meets its match," IEEE Spectrum, 21-25, August 1988.

[5] R. S. Foster and D. C. Backer, "Constructing a pulsar timing array," Astrophys.J., 361, 300 - 308, 1990.

[6] R. S. Foster, L. Fairhead, and D. C. Backer, "A spectral study of four millisecond pulsars," Astrophys. J., 378, 687-695, 1991.

[7] R. S. Foster, A. Wolszczan, and F. Camilo, "A new binary millisecond pulsar," Astrophys. J., 410, L91-L94, 1993.

[8] M. Sekido, M. Imae, Y. Hanado, Y. Takahashi, Y. Koyama, Y. P. Ilyasov, A. E. Rodin, A. E. Avramenko, V. V. Oreshko, and B. A. Poperechenko, "Pulsar VLBI Experiment with Kashima(Japan)-Kalyazin(Russia) Baseline," A.S.P.Conf.Ser.Vol.105, Proceedings of IAU Colloquium 160 Pulsars: Problems and Progress, pp.117-118, 1996.

Table 1. Specifications

Telescope at Kashima	
Diameter	34 m
Observation frequency	2120 - 2320 MHz
System noise temperature	71 K
Efficiency	65 %
Receiving system	
Total bandwidth	200 MHz (50 MHz x 4 units)
Frequency resolution	~ 200kHz
Time resolution	16 μs
Number of pulse accumulated	2^0 - 2^{24}
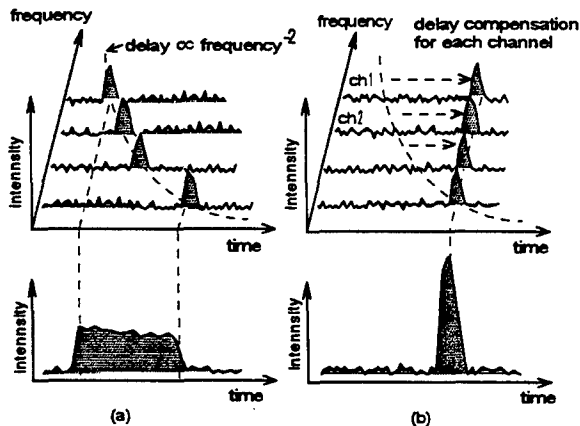
Figure 1. Dispersion effect.

(a) Pulse broadening by dispersion effect for wide band observation.
(b) De-dispersion processing.
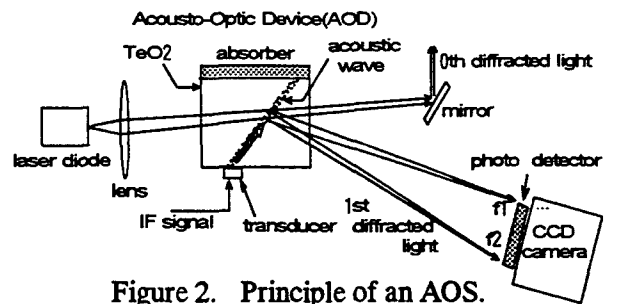
Figure 2. Principle of an AOS.

An electrical input signal is transformed by a transducer into an acoustic wave, which acts as a grating in the acousto-optic device and diffracts an incident laser beam by an angle proportional to the frequency of the electrical input. The first-order diffracted lights are focused onto the photo-detectors of a CCD camera, where they are reconverted into the electrical signals. The intensity of the diffracted light is proportional to the intensity of the electrical input.
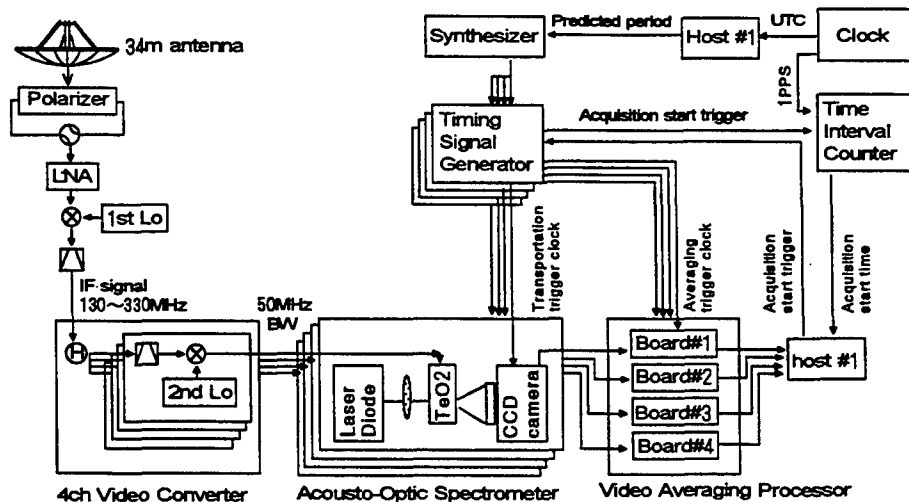
Figure 3. Observation system at CRL
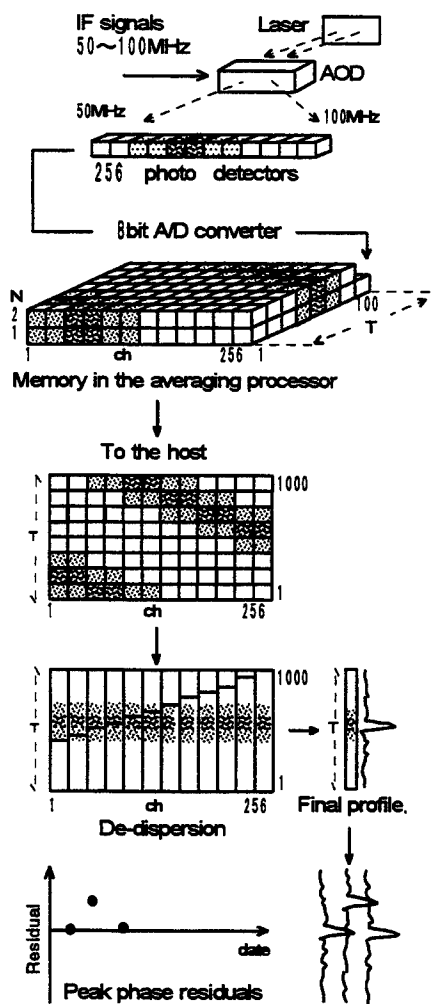
Figure 4. Data flow.
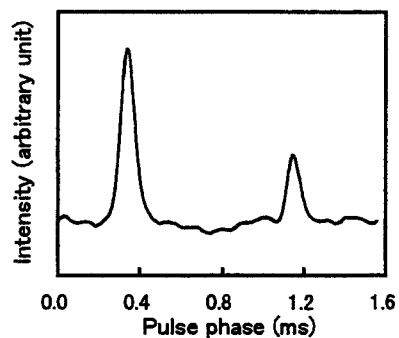
Figure 5. PSR1937+21 profile at Kashima.
Observation bandwidth is 50MHz at 2GHz
and integration time is 27 minutes.
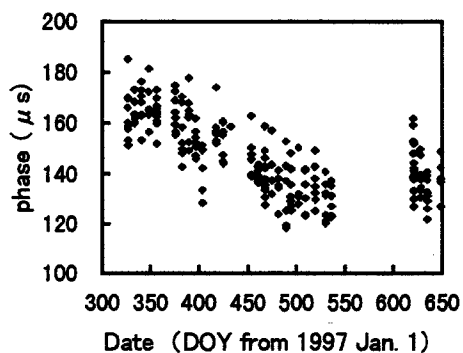
Figure 6. Timing residuals of PSR1937+21.
(Nov. 21,1997~Oct. 9,1998)
Predicted phases are calculated by Tempo program
ver. 10.010.   Each observed phase is obtained from
the observations with 50MHzBW in the 2GHz and
27 minutes integration.
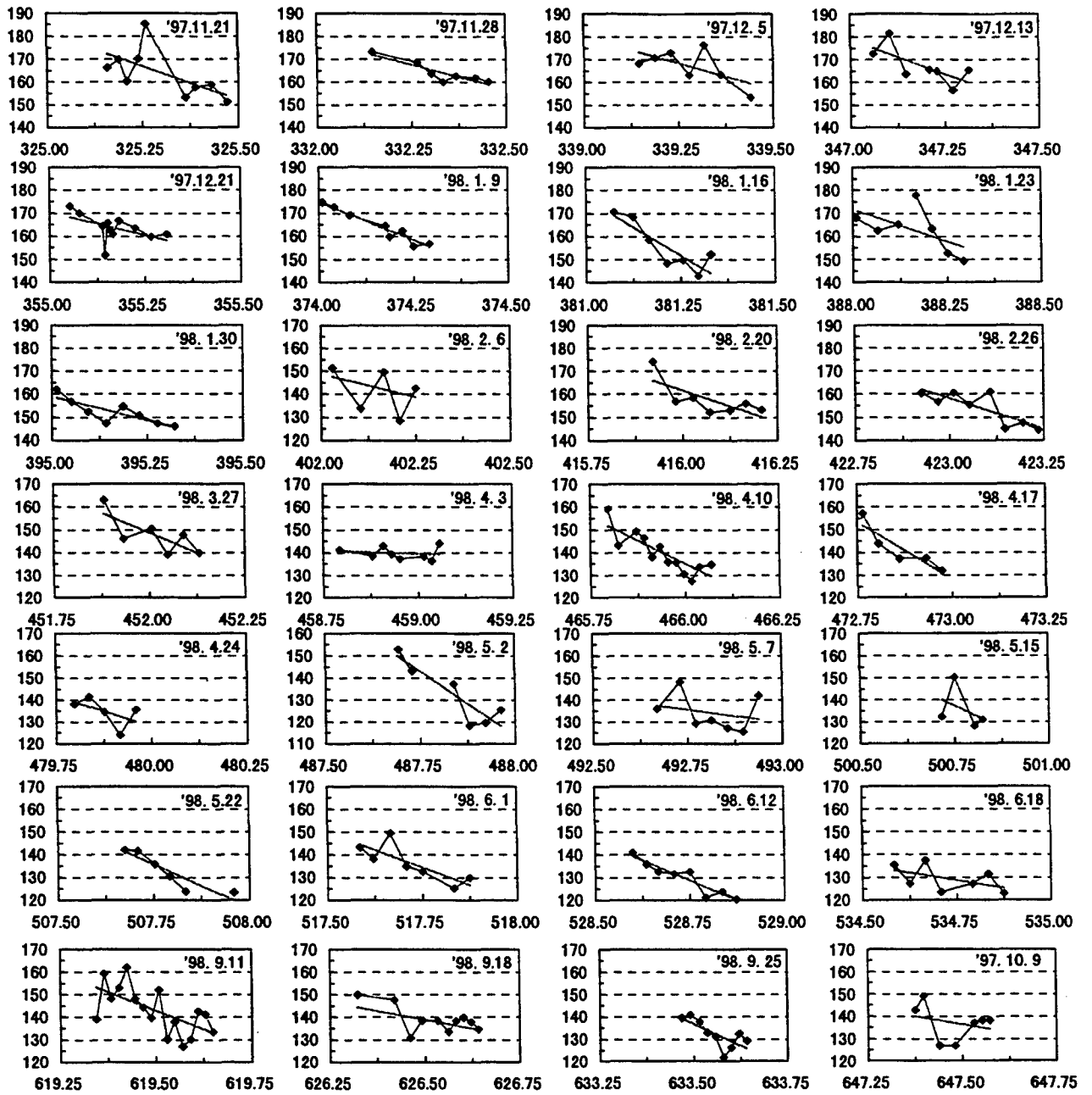
Figure 7. Timing residuals of each observation day for PSR1937+21.
The standard deviation of all data is 5.4 micro second after the linear fitting.
(shown by the straight line in each day.)
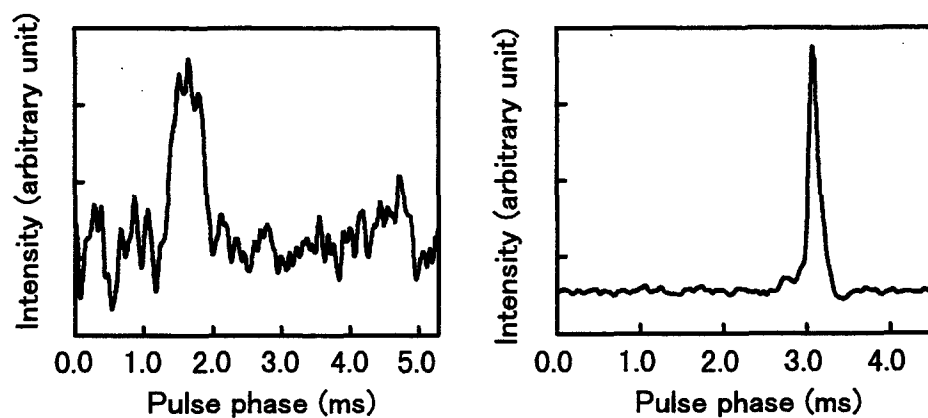
Figure 8.   Pulse profile of PSR1855+09 and PSR 1713+07 at Usuda 64m antenna.
Observation frequency is 2275-2305MHz. (a) PSR1855+09: Pulse period is 5.36ms,
Flux density at 2GHz band is about 2mJy. Integration time is about 12 minutes.
(b) PSR1713+07: Pulse period is 4.57ms, Flux density at 2GHz band is about 4mJy.
Integration time is about 20 minutes.

A BAYESIAN METHOD FOR OSCILLATOR CHARACTERIZATION

F. Vernotte
Observatoire de Besançon
41 bis av. de l'Observatoire, BP 1615, F-25010 Besançon, France
tel +33-3-81.66.69.22 fax +33-3-81.66.69.44
e-mail francois@obs-besancon.fr

G. Zalamansky
Université de Metz
Campus Bridoux, F-57000 Metz, France

Abstract

The power spectral density of frequency fluctuations of an oscillator is generally modeled as a sum of power laws with integer exponents (from -2 to +2). However, a power law with a fractional exponent may exist. We propose a method for measuring such a noise level and determining the probability density of the exponent. This yields a criterion for compatibility with an integer exponent. This method is based upon a Bayesian approach called the reference analysis of Bernardo-Berger. The application to a sequence of frequency measurement from a quartz oscillator illustrates this paper.

INTRODUCTION

It is commonly assumed that $S_y(f)$, the power spectral density (PSD) of frequency deviation of an oscillator, may be modeled as the sum of 5 power laws, defining 5 types of noise:

$$S_y(f) = \sum_{\alpha=-2}^{+2} h_\alpha f^\alpha \qquad (1)$$

where h_α is the level of the f^α noise. But it may be noticed that models with non-integer exponents are occasionally used.

The estimation of the noise levels is mainly achieved by using the Allan variance [1], which is defined versus the integration time τ as:

$$\sigma_y^2(\tau) = \frac{1}{2} \left\langle (\overline{y}_{k+1} - \overline{y}_k)^2 \right\rangle . \qquad (2)$$

In the frequency domain, the Allan variance may be considered as a filter. If the Allan variance versus the integration time τ is plotted, the graph exhibits different slopes, each slope corresponding to a type of noise:

$$\sigma_y^2(\tau) = C_\mu \tau^\mu \qquad \Leftrightarrow \qquad S_y(f) = h_\alpha f^\alpha \qquad \text{and} \qquad \alpha = -\mu - 1. \qquad (3)$$

The estimation of C_μ yields an estimation of the noise level h_α.

However, this curve may exhibit an exponent μ which seems to be non-integer. Does this mean that the corresponding PSD is not compatible with the 5 power law model? In this paper, we propose a method for estimating the most probable value of this exponent in order to solve this ambiguity. This method is applied to an example of stability measurement.

CLASSICAL STABILITY ANALYSIS OF AN OSCILLATOR

Sequence of frequency measures

Figure 1 shows average frequency measures $\overline{\nu}_k$ of a 10 MHz quartz oscillator compared to a cesium clock. The sampling rate is 10 s and the integration time of each frequency measure is also 10 s (sampling without dead time).

In order to obtain dimensionless $\overline{y}_k$ samples, we must subtract the nominal frequency ν_0 (10 MHz) from the frequency measures and normalize by ν_0:

$$\overline{y}_k = \frac{\overline{\nu}_k - \nu_0}{\nu_0}. \qquad (4)$$

Variance analysis

Figure 2 is a log-log plot of the Allan deviation of the quartz $\overline{y}_k$ samples versus the integration time τ. A least squares fit of these variance measures (solid line), weighted by their uncertainties, detects only two types of noise: a white noise and an f^{-2} noise. The corresponding noise level estimations are:

$$h_0 = (2.2 \pm 0.4) \cdot 10^{-5}\text{s} \qquad \text{at } 1\sigma \text{ (68\% confidence)}$$
$$h_{-2} = (2.3 \pm 0.6) \cdot 10^{-12}\text{s}^{-1} \qquad \text{at } 1\sigma \text{ (68\% confidence)}$$

(for the assessment of the h_α noise levels and their uncertainties, we used the multi-variance method described in [2]).

However, for large τ values (corresponding to low frequencies), the variance measures move away from the fitted curve. Two explanations are possible:

- instead of an f^{-2} noise, there is a noise whose non-integer exponent is contained between -2 and -3 ;

- since the uncertainty domains of the variance measures contain the fitted curve, this apparent divergence may be due to a statistical effect.

In order to choose between these two explanations, we decided to estimate the probability density of the exponent with a Bayesian approach.

BAYESIAN APPROACH

Principle

The goal of all measurement is the estimation of an unknown quantity θ from measures ξ, i.e. determining $p(\theta|\xi)$, the density of probability of the quantity θ knowing the measures ξ. The Bayesian theory is based on the following equality [3]:

$$p(\theta|\xi) \propto p(\xi|\theta)\pi(\theta) \tag{5}$$

where $p(\xi|\theta)$ is the distribution of the measures ξ for a fixed value of the quantity θ and $\pi(\theta)$ is the *a priori* density of probability of the quantity θ, i.e. before performing any measurement.

The determination of this a priori density, called the *prior*, is generally one of the main difficulties of this approach (particularly in the case of total lack of knowledge!). In this paper, we use the Jeffrey's prior which ensures properties such as invariance [3].

Spectral density and covariance matrix

Let us define the vector y whose components are the N $\bar{y}_k$ samples. We assume that y is a Gaussian vector. The probability distribution of y is:

$$p(y) = \frac{\exp\left(-\frac{y^t C^{-1} y}{2}\right)}{(2\pi)^{\frac{N}{2}} \sqrt{|C|}} \tag{6}$$

where C is the covariance matrix. Since $S_y(f)$ is the Fourier transform of $\mathcal{R}_y(\tau)$, the autocorrelation function of the frequency deviation, the general term of C is:

$$C_{ij} = 2 \int S_y(f) \cos\left(2\pi f(t_i - t_j)\right) df. \tag{7}$$

Equation (7) reveals the key role played by the spectral density of the noise in the expected fluctuation. We will present a general method for estimating the parameters of the model for $S_y(f)$.

Assumed model for the spectral density

We assume that the sequence of frequency measures is composed of a white noise y_w, whose variance (i.e. the level) is unitary, and of a red noise y_r whose level is unknown, multiplied by the real standard deviation of the white noise σ_w (σ_w is easily estimated from high sampling rate frequency measurement):

$$y = (y_w + y_r)\sigma_w. \tag{8}$$

This yields the following model for $S_y(f)$:

$$S_y(f) = h_0 + h_\alpha \cdot f^\alpha \qquad \text{with } -3 \leq \alpha \leq -1 \tag{9}$$

where $h_0 = 2.2 \cdot 10^{-5}$s, h_α and α are the unknown parameters.

Let us denote y_n, the normalized vector:

$$y_n = y_w + y_r. \tag{10}$$

The corresponding normalized PSD $S_n(f)$ is:

$$S_n(f) = 1 + H \cdot u_\alpha \cdot f^\alpha \tag{11}$$

where u_α is an amplitude factor whose meaning will be explained below (see equation (23)).

Statistical model

The part of the spectral density due to the red noise y_r may be written:

$$S_r(f) = H \cdot u_\alpha \cdot f^\alpha. \tag{12}$$

We used the Bernardo-Berger analysis [3, 4] for estimating the unknown parameter $\theta = (\alpha, H)$.

- Construction of the estimators:

Let us introduce the orthonormal basis of $\Re^N$, $\{p_0, \ldots, p_j, \ldots, p_{N-1}\}$, defined such as the ith component of p_j is:

$$p_{ij} = \widetilde{p}_j(t_i) \tag{13}$$

where t_i is the date of the ith frequency measure and $\widetilde{p}_j(t)$ is a polynomial of degree j, satisfying the orthonormality condition [5]:

$$\sum_{i=0}^{N-1} \widetilde{p}_j(t_i) \cdot \widetilde{p}_k(t_i) = \delta_{jk}. \tag{14}$$

It can be shown than the scalar product of a vector p_j by the noise vector y is an estimate of the noise spectrum for a given frequency f_j [6]. Let us denote ξ_j such an estimate applied to the normalized noise:

$$\xi_j = p_j \cdot y_n. \tag{15}$$

Practically, we limited to 16 the number of estimators p_j (from degrees 0 to 15) for limiting the computation and because the high degrees, estimating the high frequencies, are less informative for a red noise.

Moreover, in order to ensure convergence for very low frequencies (even if the low cut-off frequency tends towards 0), the polynomials must satisfy the moment condition [5, 6]: the minimum degree j_{min} of a polynomial to ensure convergence up to an exponent α is:

$$j_{min} \geq \frac{-\alpha - 1}{2}. \tag{16}$$

Since we have assumed $\alpha \leq -3$, the first 2 estimators (p_0 and p_1) must be removed. Thus we have $n = 14$ estimators $\{p_2, \ldots, p_{15}\}$ and $n = 14$ estimates $\{\xi_2, \ldots, \xi_{15}\}$.

- Construction of the priors:

The covariance matrix defined in relationship (7) is an ensemble average of the different estimate products over an infinite number of realizations of this process:

$$C = \langle \xi \cdot \xi^t \rangle \tag{17}$$
$$C_{ij} = \langle \xi_i \cdot \xi_j \rangle. \tag{18}$$

As for the noise vector y_n, the estimate vector ξ may be split into two terms, according to equations (10) and (15):
$$\xi = \xi_w + \xi_r. \tag{19}$$

The covariance matrix may also be split:
$$C = \langle \xi_w \xi_w^t \rangle + \langle \xi_r \xi_r^t \rangle = I_n + H \cdot u_\alpha \cdot V(\alpha) \tag{20}$$

where I_n is the identity matrix in $\Re^n$ and the general term of the matrix $V(\alpha)$ is:
$$[V(\alpha)]_{ij} = 2 \int_{1/T}^{f_h} f^\alpha \cos(2\pi f(t_i - t_j)) \, df. \tag{21}$$

The high cut-off frequency f_h in (21) is the Nyquist frequency and T is the total duration of the sequence.

Let $e_i(\alpha)$ denote the ith eigenvector of $V(\alpha)$ and $\gamma_i(\alpha)$ its ith eigenvalue ($i \in \{0, \ldots, n-1\}$). The averaged quadratic norm of the estimate vector ξ is:
$$\left\langle \|\xi\|^2 \right\rangle = n + H \cdot u_\alpha \sum_{i=0}^{n-1} \gamma_i(\alpha) = \left\langle \|\xi_w\|^2 \right\rangle + \left\langle \|\xi_r\|^2 \right\rangle. \tag{22}$$

The factor u_α is chosen in such a way that, for $H = 1$, the averaged quadratic norms $\left\langle \|\xi_w\|^2 \right\rangle$ and $\left\langle \|\xi_r\|^2 \right\rangle$ are equal:
$$u_\alpha = \frac{n}{\sum_{i=0}^{n-1} \gamma_i(\alpha)}. \tag{23}$$

The direct problem is now solved since ξ is a vector of $\Re^n$ with a probability distribution given the parameter θ equal to:
$$p(\xi|\theta) = \frac{1}{(2\pi)^{n/2}\sqrt{|C|}} \exp(-\frac{1}{2}\xi^t C^{-1} \xi). \tag{24}$$

Denoting "Tr(M)" the trace of a matrix M and X the matrix defined as:
$$X = u_\alpha \cdot V(\alpha) \tag{25}$$

the Fisher information matrix $I(\theta)$ is (see [4]):
$$I(\theta) = \frac{1}{2} \begin{pmatrix} H^2 \text{Tr}\left(C^{-1}\frac{dX}{d\alpha}C^{-1}\frac{dX}{d\alpha}\right) & H\text{Tr}\left(C^{-1}XC^{-1}\frac{dX}{d\alpha}\right) \\ H\text{Tr}\left(C^{-1}XC^{-1}\frac{dX}{d\alpha}\right) & \text{Tr}\left(C^{-1}XC^{-1}X\right) \end{pmatrix}. \tag{26}$$

The Jeffrey's prior $\pi(\theta)$ is defined as:
$$\pi(\theta) = \sqrt{|I(\theta)|}. \tag{27}$$

The parameter θ is a two-dimensional parameter composed of the exponent parameter α and of the amplitude parameter H. Since we are mostly interested in α, H is called a nuisance parameter.

In presence of nuisance parameter, Bernardo and Berger suggested that α should first be fixed and the conditional prior $\pi(H|\alpha)$ computed for that value. The full prior is then:
$$\pi(\theta) = \pi(H|\alpha) \cdot \pi(\alpha). \tag{28}$$

The conditional prior $\pi(H|\alpha)$ is given by:

$$\pi(H|\alpha) = \sqrt{|[I(\theta)]_{22}|} \qquad (29)$$

where $[I(\theta)]_{11}$, $[I(\theta)]_{12} = [I(\theta)]_{21}$ and $[I(\theta)]_{22}$ are the elements of the Fisher information matrix $I(\theta)$.

The prior for α may be computed as:

$$\pi(\alpha) = c \cdot \exp\left(\int \pi(H|\alpha) \ln |k(\alpha, H)|^{1/2} \, d\lambda\right) \qquad (30)$$

where c is a normalization coefficient ensuring that $\int \pi(\alpha) d\alpha = 1$ and:

$$k(\alpha, H) = [I(\theta)]_{11} - \frac{[I(\theta)]_{12}^2}{[I(\theta)]_{11}}. \qquad (31)$$

This prior is plotted in Figure 3.

- Construction of the posteriors:

According to the Bayes theorem, the posterior probability distribution is given by:

$$p(\theta|\xi) = \frac{p(\xi|\theta)\pi(\theta)}{\int p(\xi|\theta')\pi(\theta')d\theta'}. \qquad (32)$$

The posterior probability distribution for α is then given by:

$$p(\alpha|\xi) = \frac{\int p(\xi|\alpha, H)\pi(H|\alpha)\pi(\alpha)dH}{\int\int p(\xi|\alpha', H')\pi(H'|\alpha')\pi(\alpha')dH'd\alpha'}. \qquad (33)$$

RESULTS AND DISCUSSION

Compatibility with an integer exponent

Figure 4 shows the posterior probability distribution for the exponent α of the red noise using the Bernardo-Berger prior.

The exponent value obtained for the maximum of likelihood, just as for the maximum of the distribution, is $\alpha = -2.2$.

However, $\alpha = -2$ is fully compatible with this prior distribution. Thus, we may conclude that the apparent divergence between the variance measures and the fitted curve in Figure 2 is probably due to a statistical bias of the data. The spectral density $S_y(f)$ is then compatible with the following model:

$$S_y(f) = h_0 + h_{-2}f^{-2}. \qquad (34)$$

Noise level estimation

Selecting an exponent value $\alpha = -2$, we obtained the posterior probability distribution plotted in Figure 5. As in the variance analysis, we chose a confidence interval of 68% (16% probability that h_{-2} is smaller than the low bound and 16% probability that h_{-2} is greater than the high bound):

$$h_{-2} = \left(2.3 \; {}^{+}_{-} \; {}^{2}_{0.8}\right) \cdot 10^{-12}\text{s}^{-1} \qquad \text{at } 1\sigma \text{ (68\% confidence)}$$

The difference between the maximum likelihood value ($h_{-2} = 2.2991 \cdot 10^{-12} \text{s}^{-1}$) and the variance analysis value ($h_{-2} = 2.2949 \cdot 10^{-12} \text{s}^{-1}$) is only 0.18%.

However, the confidence intervals given by these two methods are quiet different. The main difference concerns the symmetry of the variance analysis interval: in this case, we don't take into account the fact that the noise levels are positive, whereas the prior of the Bayesian approach is null for negative values of h_{-2}.

Moreover, the variance analysis interval seems to be a bit underestimated.

CONCLUSION

The variance analysis is an useful tool for a quick estimation of the noise levels in the output signal of an oscillator. However, a negative estimate of a noise level may occur. Generally, in this case, this value is rejected and the corresponding noise level is assumed to be null. On the other hand, although the Bayesian method is a bit heavier, it takes into account properly the a priori information, and gives a more reliable estimation of these noise levels and especially of their confidence intervals.

However, the main advantage of the Bayesian method concerns the verification of the validity of the power law model of spectral density. Each time the model is suspected, such an approach should be used in order to estimate the exponent of the power law. In particular, this method should be very interesting for the study of the f^{-1} and f^{+1} noise, whose origin remains mysterious [7].

REFERENCES

[1] J. A. Barnes, A. R. Chi, L. S. Cutler, D. J. Healey, D. B. Leesson, T. E. McCuningal, J. A. Mullen, W. L. Smith, R. L. Sydnor, R. Vessot, and G. M. R. Winkler, *"Characterization of frequency stability,"* **IEEE Transactions on Instrumentation and Measurement, IM-20**, 105–120.

[2] F. Vernotte, E. Lantz, J. Groslambert, and J. Gagnepain, *"Oscillator noise analysis: multivariance measurement,"* **IEEE Trans. on Inst. and Meas., IM-42**, 342–350.

[3] J. Bernardo and A. Smith, **Bayesian theory**, Wiley & Son, 1993.

[4] G. Zalamansky and C. Robert, *"Bayesian analysis with application to the timing residuals of a pulsar,"* in Proceedings of MaxEnt'98, July 1998, Garching, Germany.

[5] J. E. Deeter and P. E. Boynton, *"Techniques for the estimation of red power spectra. I. context and methodology,"* **The Astrophysical Journal, 261**, 337–350.

[6] F. Vernotte, G. Zalamansky, M. McHugh, and E. Lantz, *"Cut-off frequencies and noise power law model of spectral density: adaptation of the multi-variance method for irregularly spaced timing data using the lowest mode estimator approach.,"* **IEEE Transactions on Ultrasonics, Ferroelectrics, and Frequency Control, 43**, (3), 403–409.

[7] M. Planat, V. Giordano, G. Marianneau, F. Vernotte, M. Mourey, C. Eckert, and J. Miehe, *"Is the frequency noise of an oscillator of deterministic origin ?,"* **IEEE Trans. on U. F. F. C. , 43**, (2), 326–330.
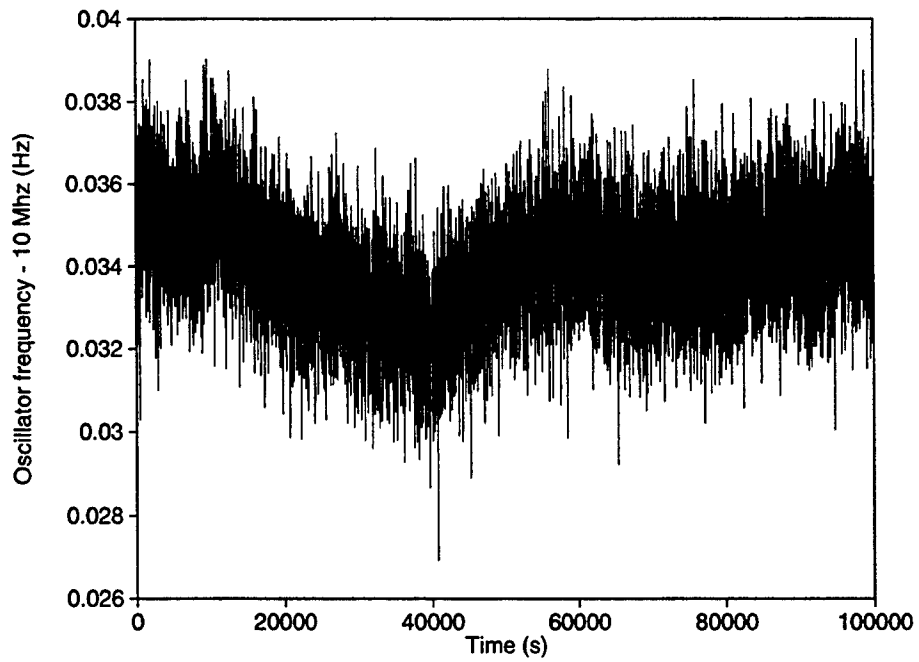
Figure 1: Sequence of frequency measures
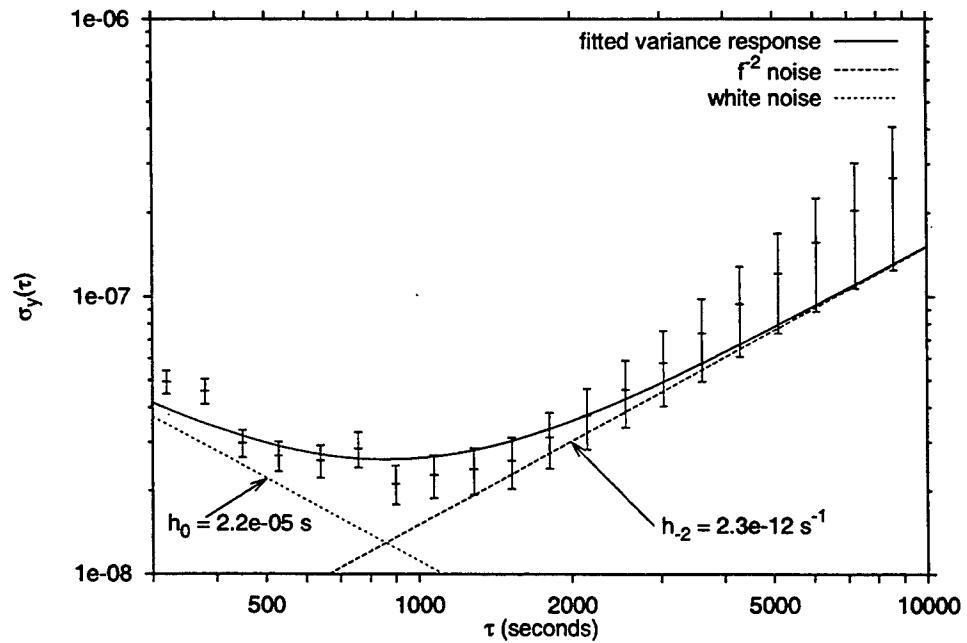
Figure 2: Allan deviation of the sequence of frequency measures

106
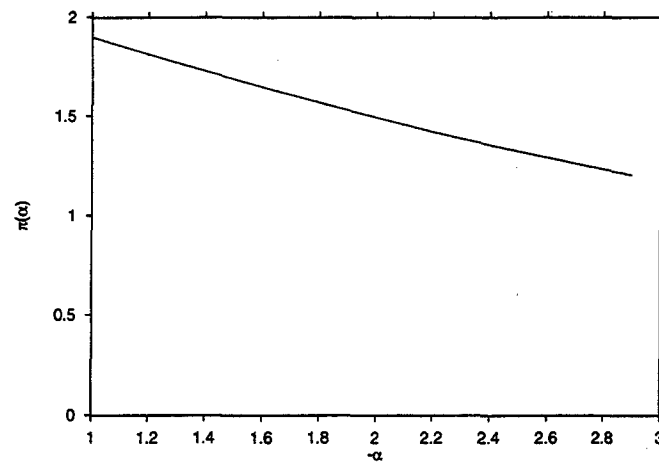
Figure 3: Reference prior for the power α
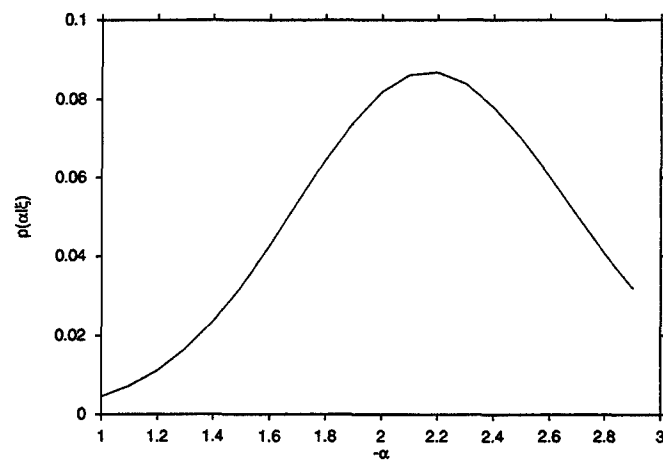
Figure 4: Posterior probability density for the power α
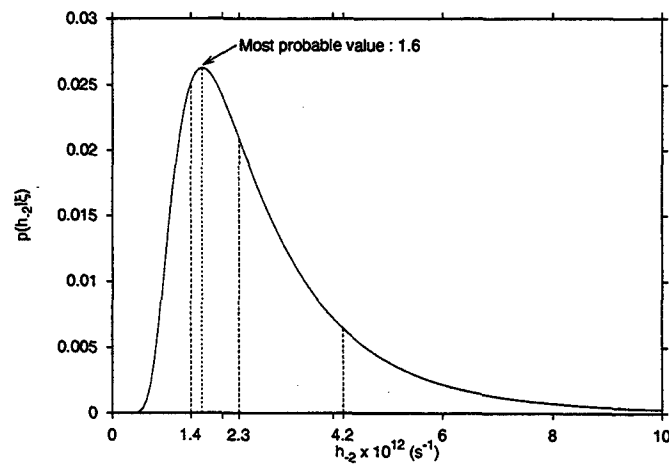
Figure 5: Posterior probability density for the noise level h_{-2}

STABILITY AND ACCURACY OF THE REALIZATION OF TIME SCALE IN SINGAPORE

Dai Zhongning, Chua Hock Ann, and Neo Hoon
Singapore Productivity and Standards Board

Abstract

Singapore Productivity and Standards Board (PSB) maintains the national time scale in Singapore. The time scale has been linked to Coordinated Universal Time (UTC) since October 1997. This paper reports the analysis on the stability and accuracy of the time scale. Time dissemination through GPS is also discussed.

INTRODUCTION

The National Measurement Center (NMC) of PSB is the national metrology institute in Singapore. There are three high performance cesium clocks: Clock I (HP5071A), Clock II (HP5071A), and Clock III (FTS4065). The generation of the UTC(PSB) is based on Clock I selected from the clock ensemble. Clock II is used as backup. Since October 1997, Clock I and Clock II have been linked to UTC through a AUSTRON 2200A GPS receiver, which follows BIPM common-view schedule. It is aligned to UTC within 100 nanosecond.

The dissemination of time scale to users is also very important. GPS common view is a useful method because its high accuracy. A common-view experiment has been done with AUSTRON 2200A and AOA TTR-4P GPS receivers to verify the method.

The aim of this paper is to introduce the setup of the time scale of PSB and the time dissemination through GPS. The first part of the paper mainly introduces maintenance of the time scale. The second part presents the common-view experiment results in PSB.

TIME SCALE OF SINGAPORE

SETUP OF THE TIME SCALE

The setup of the time scale is shown in Figure 4. Clock I is selected from three cesium atomic clocks to realize the national time scale UTC(PSB). AUSTRON 2200A GPS receiver is a single channel NBS type receiver. Its software version is D.32 B.00. The receiver delay is 142 ns. The computer-controlled time interval counter is used to measure the time difference between Clock I and Clock II. The control software is compiled in LabVIEW.

BIPM and other time laboratories have similar setups. These atomic clocks can be compared with each other using the GPS time as reference. These laboratories send data to BIPM every week. The time differences between UTC(PSB) and UTC are computed through the coordination by BIPM. Hence, UTC(PSB) is traceable to UTC. The UTC(PSB) is then aligned to UTC using a microphase stepper adjusted continuously or by step to maintain a long-term agreement.

STABILITY ANALYSIS

Figure 1 (a) shows the difference of UTC and UTC(PSB) from MJD 50674 to MJD 50884 published in BIPM Circular T. Figure 1 (b) shows the difference of UTC and UTC(PSB) from MJD 50899 to MJD 51084. The Allan deviation of UTC(PSB) compared with UTC were computed for different measuring times in Figure 2. For Clock II, its deviation and stability related to UTC(PSB) were also evaluated and analyzed starting with one hour.

The curve in Figure 1 (a) is smoother than the curve in Figure 1 (b). It can be illustrated by calculated Allan deviation. The curve in Figure 2 (b) is not smooth because there are not enough points. But the Allan deviation can be compared for 5 and 10 days. From the figures, the Allan deviation in Figure 2 (a) is 1.23×10^{-14} for five days and the Allan deviation in Figure 2 (b) is 3.11×10^{-14} for five days. The value in first period is better than the value in second period. It implies the stability in the first period is better than that in the second period.

Time difference between Clock I and Clock II was measured at one hour intervals. Then the difference between UTC and Clock II was calculated. The similar curves like Figure 1 was obtained. Allan deviation was also calculated. The Allan deviation for five days in the first period is also smaller than the Allan deviation for five days in the second period. The factors influencing stability are mainly ambient conditions and lifetime of the cesium clocks.

ACCURACY ANALYSIS

The time difference between the reference clock and GPS time also includes the delays in the antenna, cable, and receiver. It also includes propagation time from satellites to antenna and time offset of the reference. Delays in the GPS receiver, antenna, cable between antenna and receiver, as well as cables between receiver and counter, are calibrated or measured. The uncertainty of calibration of GPS receiver is about 8 nanoseconds. The delay of cable can be measured with 2 ns uncertainty. The effect of ionosphere can be compensated. The propagation time from satellites to antenna can be calculated and compensated. There is no significant effect on the common view results if coordinates of antennas can be determined accurately to within centimeters. The coordinates of GPS antennas were determined by precise geodetic survey in our laboratory, with accuracy better than 1 meter. It is estimated the total effect is not more than 20 nanoseconds.

From the figures, the drift of UTC(PSB) is about 6 ns/day. The UTC(PSB) is then aligned to UTC using a microphase stepper. When the drift is large it can be adjusted continuously. When the drift is small it can be adjusted by step. Through this method the time scale can be maintained for a long-term agreement with UTC within 100 nanoseconds.

TIME DISSEMINATION THROUGH GPS

EXPERIMENT SETUP

A common-view experiment has been performed for two months and measurement setup is shown in Figure 4. At one site, AUSTRON 2200A GPS receiver was used and Clock I (HP5071A) is used as reference. At the other site, TTR-4P GPS receiver was used and Clock III (FTS4065) was used as reference. The same time interval measurement between Clock I or Clock III and GPS time was performed.

The TTR-4P GPS receiver was upgraded from firmware version 2.8.2.0 to firmware version 3.0.34.4 in February 1998. Though it is a multichannel receiver, it can be used to follow BIPM schedule as AUSTRON receiver. The difference is that it tracks several satellites at the same time. So it is necessary to choose tracking data according to BIPM schedule. One problem is the tracked satellites according to BIPM schedule may be in different channels. Different channels may have different delays. It will result in some errors. Another problem is that the tracking time is always in 16-minute intervals. It is not the same as the BIPM schedule. The start time of tracking had to be changed daily to track more satellites. The third problem is a software problem. When TTR-4P tracked SV 15, there is an extraordinary offset of several hundred nanoseconds. When SV 15 is enabled and even SV 15 is not tracked, there are also some offset for other satellites in comparing the condition when SV 15 is disabled. Moreover, the offset varied with time. So TTR-4P had to work with SV 15 disabled.

MEASURED SYSTEM DELAYS

The experiment was performed in the same laboratory. In order to determine the relative delay of the TTR-4P GPS receiver to the AUSTRON receiver, Clock I was also used as the reference of the TTR-4P receiver at the beginning. Then comparison was performed about half month. The average relative delay is -49 ns. The standard deviation is 19 ns. The comparison results were scattered. This noise comes mainly from the receiver. Temperature and humidity conditions and multichannel errors also have some effects.

EXPERIMENTAL RESULTS

Next Clock III was used as the reference of the TTR-4P GPS receiver. A common-view experiment was performed from MJD51106 to MJD51127. The common-view results are compared with direct measurement results. The average value was estimated. From Figure 3, the mean results of the common view are agreed well with the direct measurement results. Though noise is high, the effect of noise can be averaged and removed for long term experiment. The difference between average common-view results and direct measurement results is less than 20 ns. It verifies the effectiveness of the method. It is also noted that the drift of Clock III was about 67 ns per day. Through this method, Clock III is also traceable to UTC(PSB). This method allows time standards in various parts of Singapore to be calibrated remotely and accurately.

CONCLUSION

The coordinates of the antenna and time delay shall be measured more accurately. The noise of GPS receiver needs to be reduced to increase common-view accuracy. More time dissemination methods also need to be studied. In order to improve the long-term stability and reliability of UTC(PSB), an ensemble of atomic clocks, including a hydrogen maser, will be used.

REFERENCES

1. D. W. Allan and C. Thomas, "Technical Directives for Standardization of GPS Time Receiver Software", Metrologia, Vol. 31, pp. 69-79, 1994.
2. D. W. Allan and M. Weiss, "Accurate Time and Frequency Transfer during Common-View of a GPS satellite",Proceedingsof the 34th Annual Symposium on Frequency Control, pp. 334-346, 1980.
3. W. Lewandowski and C. Thomas, "GPS Time Transfer",Proceedingsof the IEEE, Vol. 79, No. 7, pp. 991-1000, 1991.
4. F. Cordara, G. Vizio, P. Tavella, V. Pettiti, "An Algorithm for the Italian Atomic Time Scale", Proceedings of 25th Precise Time and Time Interval (PTTI) Applications and Planning Meeting, pp. 389-395, December 1993.
5. F. Cordara and V. Pettiti, "GPS Disciplined Oscillators for Traceability to the Italian Time Standard", Proceedings of 27th Precise Time and Time Interval (PTTI) Applications and Planning Meeting, pp. 113-123, December 1995.
6. Gerrit de Jong and W. Lewandowski, "GLONASS/GPS Time Transfer and the Problem of the Determination of Receiver Delays", Proceedings of 29th Precise Time and Time Interval (PTTI) Applications and Planning Meeting, pp. 229-239, December 1997.
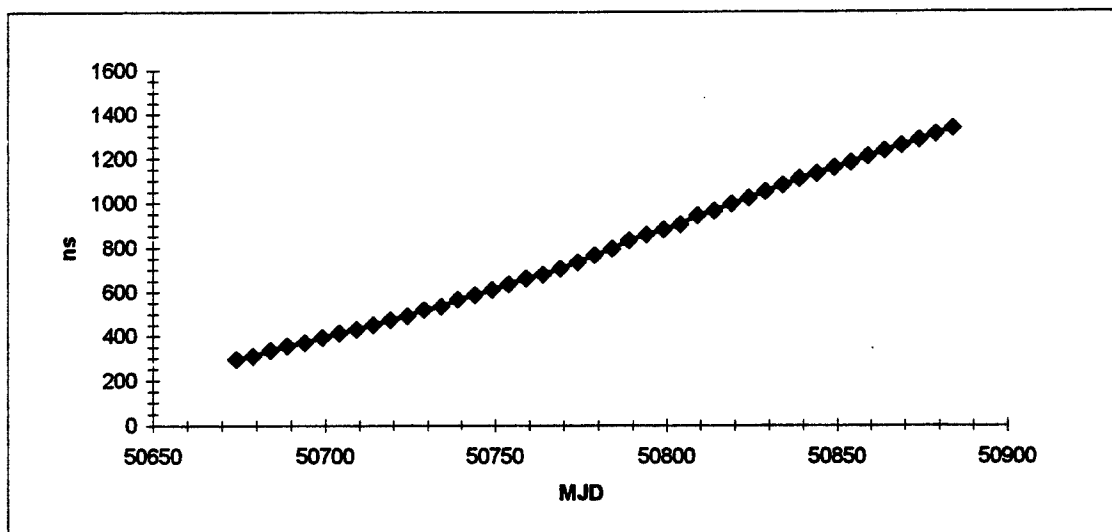
(a)
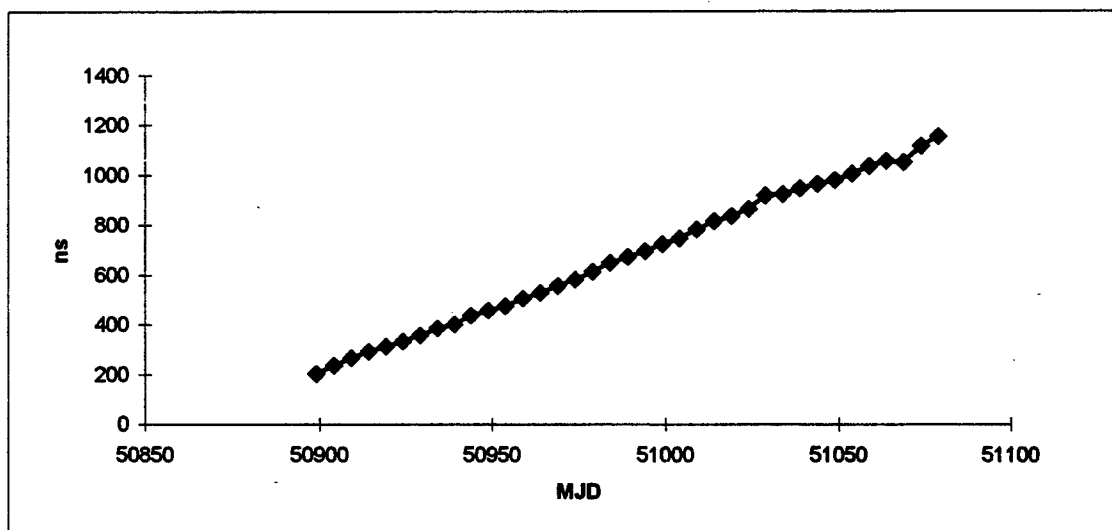
(b)

Figure 1: Difference Between UTC and UTC(PSB). (a) From MJD50674 to MJD 50894. (b) From MJD50899 to MJD51084

FREQUENCY STABILITY
CT123.002

Tau	Sigma
4.32e+05	1.23e−14
8.64e+05	6.03e−15
1.73e+06	5.36e−15
3.46e+06	5.09e−15

Allan Deviation, $\sigma_y(\tau)$

Averaging Time, τ, Seconds

(a)

FREQUENCY STABILITY
CT129.002

Tau	Sigma
4.32e+05	3.11e−14
8.64e+05	2.33e−14
1.73e+06	6.48e−15

Allan Deviation, $\sigma_y(\tau)$

Averaging Time, τ, Seconds
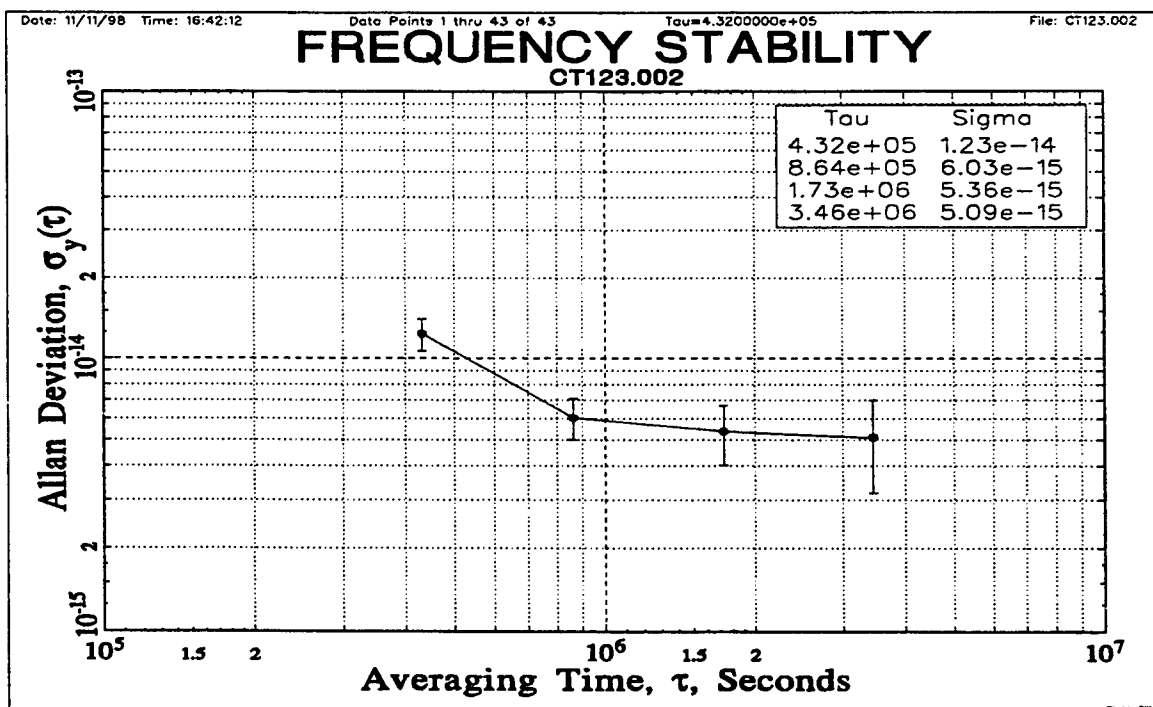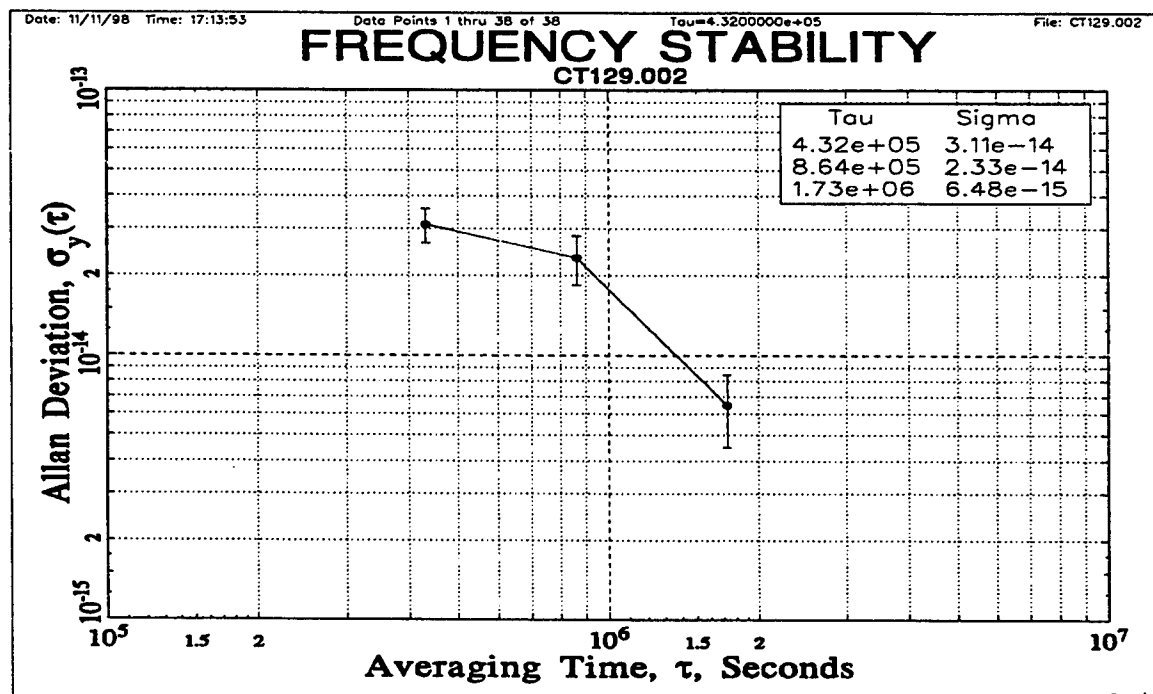
(b)

Figure 2: Allan Deviation of the Time Difference Between UTC and UTC(PSB)
(a) From MJD50674 to MJD50894. (b) From MJD50899 to MJD51084
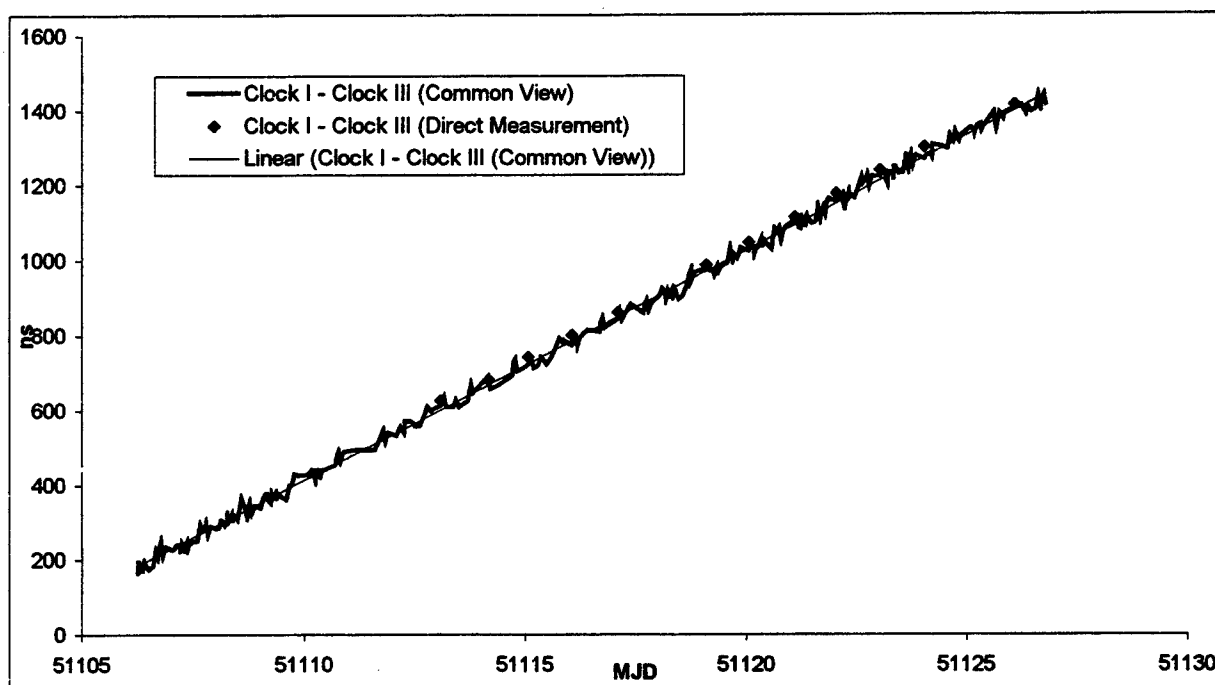
Figure 3: Comparison Between Common-View Results and Direct Measurement
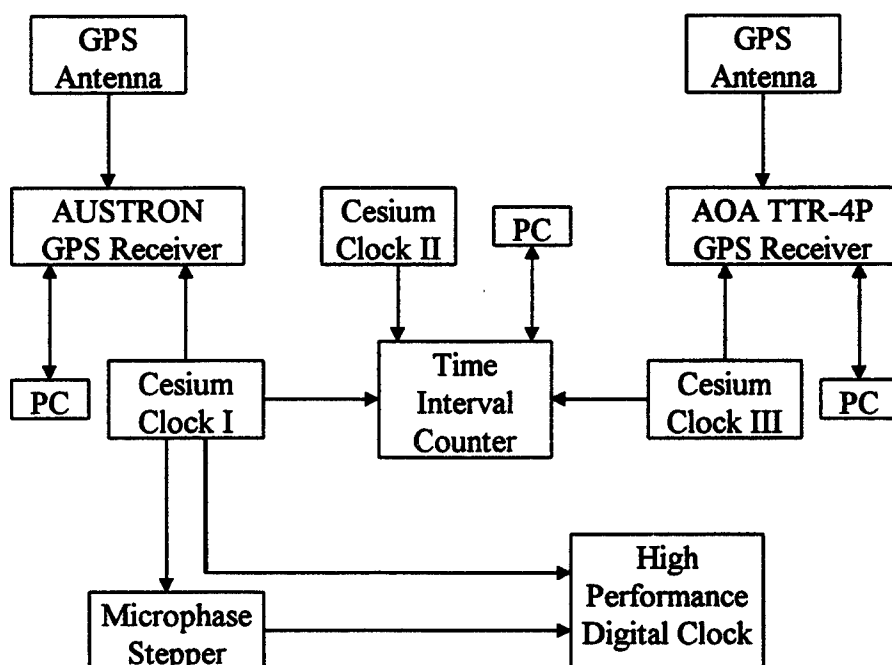
Figure 4: Setup of the Time Scale and Experiment at PSB of Singapore

UNEQUAL-ARMS MICHELSON INTERFEROMETERS

Massimo Tinto and J. W. Armstrong
Jet Propulsion Laboratory, California Institute of Technology
Pasadena, California 91109

Abstract

Michelson interferometers allow phase measurements many orders of magnitude below the phase stability of the laser light injected into their two almost equal-length arms. If, however, the two arms are unequal, the laser fluctuations can not be removed by simply recombining the two beams. This is because the laser jitters experience different time delays in the two arms, and therefore can not cancel at the photo detector. We present here a method for achieving exact laser noise cancellation, even in an unequal-arm interferometer. The method presented in this paper requires a separate readout of the relative phase in each arm, made by interfering the returning beam in each arm with a fraction of the outgoing beam[1]. By linearly combining the two data sets with themselves, after they have been properly time-shifted [2], we show that it is possible to construct a new data set that is free of laser fluctuations.

An application of this technique to future planned space-based laser interferometer detectors of gravitational radiation[3] is discussed.

I. INTRODUCTION

Michelson interferometers, experimental devices used in a large variety of Earth- and space-based, high-precision experiments, rely on a coherent train of electromagnetic waves of nominal frequency ν_0. The injected beam is typically folded into several beams, and at one or more points where these intersect, relative fluctuations of frequency or phase are monitored (homodyne detection). The observed low frequency variations of the fringes are due to frequency fluctuations of the source of the electromagnetic signal about ν_0, to relative motions of the source and the mirrors that do the folding, to temporal variations of the index of refraction along the beams, and to any time-variable field present the experimenter is trying to measure. To perform an experiment in this way it is thus necessary to control, or monitor, the other sources of relative frequency fluctuations, and, in the data analysis, to use optimal algorithms based on the different characteristic interferometer responses to the signal, and to the other sources (the noise). By comparing phases of split beams propagated along equal-length arms, frequency fluctuations of the laser can be removed and signals at levels many orders of magnitude lower can be measured.

A space-based experiment for detecting gravitational radiation, using Michelson interferometry, has been proposed [3]. Since the frequency stability of the lasers it will use will be at best of a few parts in 10^{-13} in the millihertz frequency band, it will be essential for this experiment to be able to remove these fluctuations when searching for gravitational waves of dimensionless amplitudes less than 10^{-20} in the millihertz band[3]. Since the armlengths of this space-based interferometer can be different by several percent, the direct recombination of the two beams at a photo detector will not effectively remove the laser noise. This is because the frequency fluctuations of the laser will be delayed by a different amount of time inside the two different-length arms.

In order to solve this problem, a technique involving heterodyne interferometry with unequal arm lengths and independent phase-difference readouts in each arm has been identified [2], which yields data from which source frequency fluctuations can be removed exactly. This is achieved by taking a suitable linear combination of the two Doppler time series after having time-shifted them properly. This direct method achieves the exact cancellation of the laser frequency fluctuations. An outline of the paper is presented below.

In Sec. II we state the problem, and derive the two Doppler responses, from the two unequal arms of a space-based interferometer, to a gravitational wave signal. The difference between the armlengths implies that the frequency fluctuations of the laser can not be removed by direct differencing of the two data sets. In Sec. III we present our technique for *synthesizing* an unequal-arm interferometer detector of gravitational waves. Our method is implemented in the time domain, and relies on a properly chosen linear combination of the two Doppler data. Our comments and conclusions are finally outlined in Sec. IV.

II. STATEMENT OF THE PROBLEM

Let us consider three spacecraft flying in an equilateral triangle-like formation, each acting as a free falling test particle, and continuously tracking each other via coherent laser light. One spacecraft, which we will refer to as spacecraft a, transmits a laser beam of nominal frequency ν_0 to the other spacecraft (spacecraft b and c at distances L_1 and L_2, respectively). The phase of the light received at spacecraft b and c is used by lasers on board spacecraft b and c for coherent transmission back to spacecraft a. The relative two *two-way* frequency (or phase) changes as functions of time are then independently measured at two photo detectors on board spacecraft a (Figure 1). When a gravitational wave crossing the solar system propagates through these electromagnetic links, it causes small perturbations in frequency (or phase), which are replicated three times in each arm's data[4].

To determine the response of an unequal arm interferometer to a gravitational wave pulse, let us introduce a set of Cartesian orthogonal coordinates (X, Y, Z) centered on spacecraft a (see Figure 2). The X axis is assumed to be oriented along the bisector of the angle enclosed between the two arms, Y is orthogonal to it in the plane containing the three spacecraft, and

the Z axis is chosen in such a way to form with (X, Y) a right-handed, orthogonal triad of axes. In this coordinate system we can write the two two-way Doppler responses, measured by spacecraft a at time t, as follows[5,6] (units in which the speed of light $c = 1$).

$$\left(\frac{\Delta\nu(t)}{\nu_0}\right)_1 \equiv y_1(t) = h_1(t) + C(t - 2L_1(t)) - C(t) + n_1(t) , \qquad (1)$$

$$\left(\frac{\Delta\nu(t)}{\nu_0}\right)_2 \equiv y_2(t) = h_2(t) + C(t - 2L_2(t)) - C(t) + n_2(t) , \qquad (2)$$

where $h_1(t)$, $h_2(t)$ are the gravitational wave signals in the two arms[5,6], and we have denoted by $C(t)$ the random process associated with the frequency fluctuations of the master laser on board spacecraft a; $n_1(t)$, $n_2(t)$ are the remaining noise sources affecting the Doppler responses $y_1(t)$, $y_2(t)$ respectively.

From equations (1, 2) it is important to note the characteristic time signature of the random process $C(t)$ in the Doppler responses y_1, y_2. The time signature of the noise $C(t)$ in $y_1(t)$ for instance, can be understood by observing that the frequency of the signal received at time t contains laser frequency fluctuations transmitted $2L_1$ seconds earlier. By subtracting from the frequency of the received signal the frequency of the signal transmitted at time t, we also subtract the frequency fluctuations $C(t)$ with the net result shown in equation (1).

Among all the noise sources included in equation (1), the frequency fluctuations due to the laser are expected to be by far the largest. A space-qualified single-mode laser, such as a diode-pumped Nd:YAG ring laser of frequency $\nu_0 = 3.0 \times 10^{14}$ Hz and phase-locked to a Fabry-Perot optical cavity, is expected to have a spectral level of frequency fluctuations equal to about $1.0 \times 10^{-13}/\sqrt{Hz}$ in the millihertz band[3]. Laser noise is to be compared with, e.g., the expected secondary noises which will be 10^7 or more times smaller.

If the armlengths are unequal by an amount $\Delta L = L_2 - L_1 \equiv \epsilon L_1$ (with $\epsilon \simeq 3 \times 10^{-2}$ for a space-based interferometer[3]), the simple subtraction of the two Doppler data $y_1(t)$, $y_2(t)$ (which would be appropriate for a conventional equal-arm interferometer) gives a new data set that is still affected by the laser fluctuations by an amount equal to

$$C(t - 2L_1) - C(t - 2L_2) \simeq 2\dot{C}(t - 2L_1)\epsilon L_1 . \qquad (3)$$

As a numerical example of equation (3) we find that, at a frequency of 10^{-3} Hz and by using a laser of frequency stability equal to about $10^{-13}/\sqrt{Hz}$, the residual laser frequency fluctuations are equal to about $10^{-16}/\sqrt{Hz}$. Since the goal of proposed space-based interferometers[3] is to observe gravitational radiation at levels of $10^{-20}/\sqrt{Hz}$ or lower, it is crucial for the success of these missions to cancel laser frequency fluctuations by many more orders of magnitude.

III. UNEQUAL-ARMS INTERFEROMETERS

In what follows we will show that there exists an algorithm in the time domain for removing the frequency fluctuations of the laser from the two Doppler data $y_1(t)$, $y_2(t)$ at any time t. This method relies only on a properly chosen linear combination of the two Doppler data in the time domain. In order to show how this technique works, we will assume the two armlengths L_1, L_2 to be constant and known exactly. The interested reader is referred to [2] for a detailed analysis covering the most general configuration.

From equations (1, 2) we may notice that, by taking the difference of the two Doppler data $y_1(t)$, $y_2(t)$, the frequency fluctuations of the laser now enter into this new data set in the following way

$$
\begin{aligned}
\Lambda_1(t) \equiv y_1(t) - y_2(t) &= h_1(t) - h_2(t) + C(t - 2L_1) - C(t - 2L_2) \\
&+ n_1(t) - n_2(t) .
\end{aligned}
\tag{4}
$$

If we now compare how the laser frequency fluctuations enter into equation (4) against how they appear into equations (1, 2), we can further make the following observation. If we time-shift the data $y_1(t)$ by the round trip light time in arm 2, $y_1(t - 2L_2)$, and subtract from it the data $y_2(t)$ after it has been time-shifted by the round trip light time in arm 1, $y_2(t - 2L_1)$, we obtain the following data set

$$
\begin{aligned}
\Lambda_2(t) \equiv y_1(t - 2L_2) - y_2(t - 2L_1) &= h_1(t - 2L_2) - h_2(t - 2L_1) + C(t - 2L_1) \\
&- C(t - 2L_2) + n_1(t - 2L_2) - n_2(t - 2L_1) .
\end{aligned}
\tag{5}
$$

In other words, the laser frequency fluctuations enter into $\Lambda_1(t)$, and $\Lambda_2(t)$ with the same time-structure. This implies that, by subtracting equation (4) from equation (5), we can generate a new data set that does not contain the laser frequency fluctuations $C(t)$

$$
\begin{aligned}
\Sigma(t) \equiv \Lambda_2(t) - \Lambda_1(t) &= h_1(t - 2L_2) - h_1(t) - h_2(t - 2L_1) + h_2(t) \\
&+ n_1(t - 2L_2) - n_1(t) - n_2(t - 2L_1) + n_2(t) .
\end{aligned}
\tag{6}
$$

From the expression of $\Lambda_2(t)$ given in equation (5), it is easy to see that the new data set $\Sigma(t)$ should be set to zero for the initial $MAX[2L_1, 2L_2]$ seconds. This is because some of the data from y_1 and y_2 entering into $\Lambda_2(t)$ "do not yet exist" during this time interval. Since the typical round trip light time for proposed space-based laser interferometer detectors of gravitational waves will never be greater than about 33 seconds[3], we conclude that the amount of data lost in the implementation of our method is negligible.

We have simulated the procedure (equation 6) using realistic laser and shot noise spectra[3], known arm lengths (differing by about 3 percent), and a simulated monochromatic gravitational wave incident normal to the plane of the interferometer. The results of the simulation are shown in Figure 3. Plotted are spectral densities of the raw laser noise, the raw shot noise, and the canceled time series, $\Sigma(t)$ (equation 6). This illustrates cancellation of the laser noise and modulation of the residual secondary noises[2].

IV. CONCLUSIONS

We presented a time-domain procedure for accurately cancelling laser noise fluctuations in an unequal-arm one-bounce Michelson interferometer relevant to space-borne gravitational wave detectors. The method involves separately measuring the phase of the returning light relative to the phase of the transmitted light in each arm. By suitable offsetting and differencing of these two time series, the common laser noise is cancelled exactly (equation 6).

The technique presented in this paper is rather general, in such that it can be implemented with any (Earth-as well as space-based) unequal-arms Michelson interferometers.

ACKNOWLEDGMENTS

REFERENCES

[1] G. Giampieri, R.W. Hellings, M.Tinto, J.E. Faller, *Optics Communications*, **123**, 669, (1996)

[2] M. Tinto and J.W. Armstrong, *Phys. Rev. D.* Submitted for publication.

[3] LISA: (Laser Interferometer Space Antenna) *An international project in the field of Fundamental Physics in Space*, Pre-Phase A Report, **MPQ 233**, (Max-Planck-Institute für Quantenoptic, Garching bei München, 1998).

[4] F.B. Estabrook and H.D. Wahlquist, *Gen. Relativ. Gravit.* **6**, 439 (1975).

[5] F.B. Estabrook, *Gen. Relativ. Gravit.*, **17**, 719, (1985).

[6] H.D. Wahlquist, *Gen. Relativ. Gravit.*, **19**, 1101 (1987).
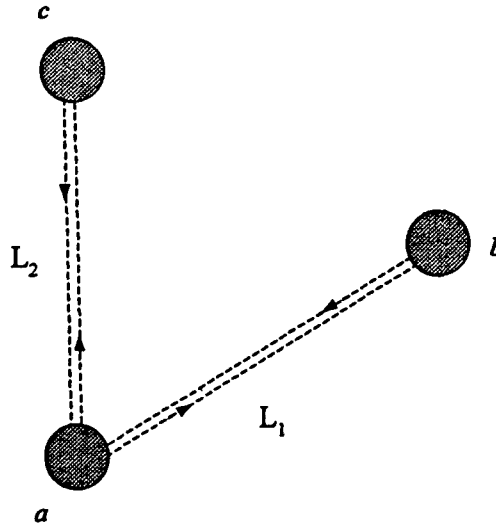
Figure 1. Typical configuration of a space-based, unequal-arm interferometer detector of gravitational waves. The corner spacecraft *a* transmits coherent laser light to the other spacecraft, *b* and *c*. They coherently retransmit back to spacecraft *a* , where coherent two-way phase (or frequency) changes in each arm are then measured. The two arm lengths are denoted with L_1, and L_2.
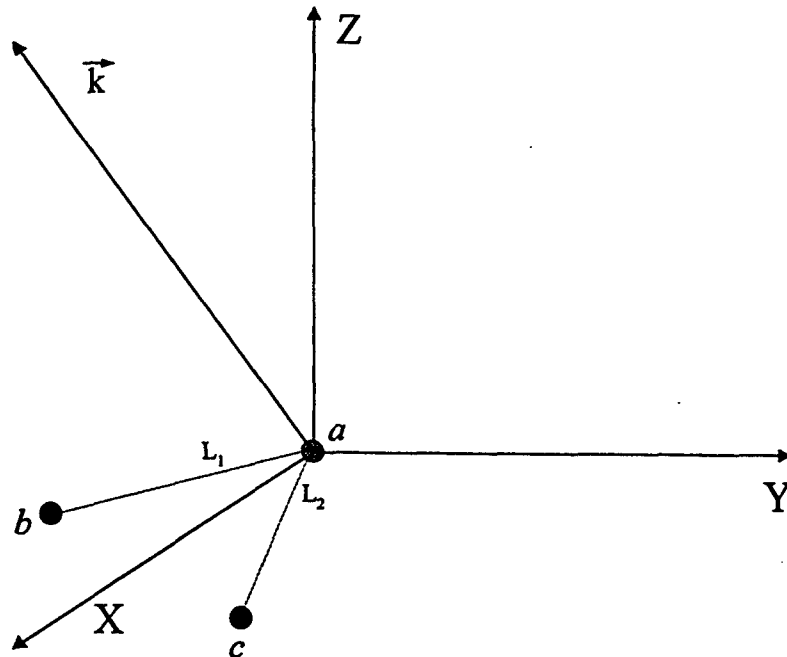
Figure 2. Coherent laser light is transmitted simultaneously from spacecraft *a* to spacecraft *b* and *c*, and coherently transponded back to *a*. The X axis is along the bisector of the angle enclosed between the two arms of the interferometer. The Y axis is orthogonal to the X axis in the plane of the interferometer, and the Z axis is chosen in such a way to form together with (X, Y) a right-handed set of axes. The gravitational wave train propagates along the k direction.
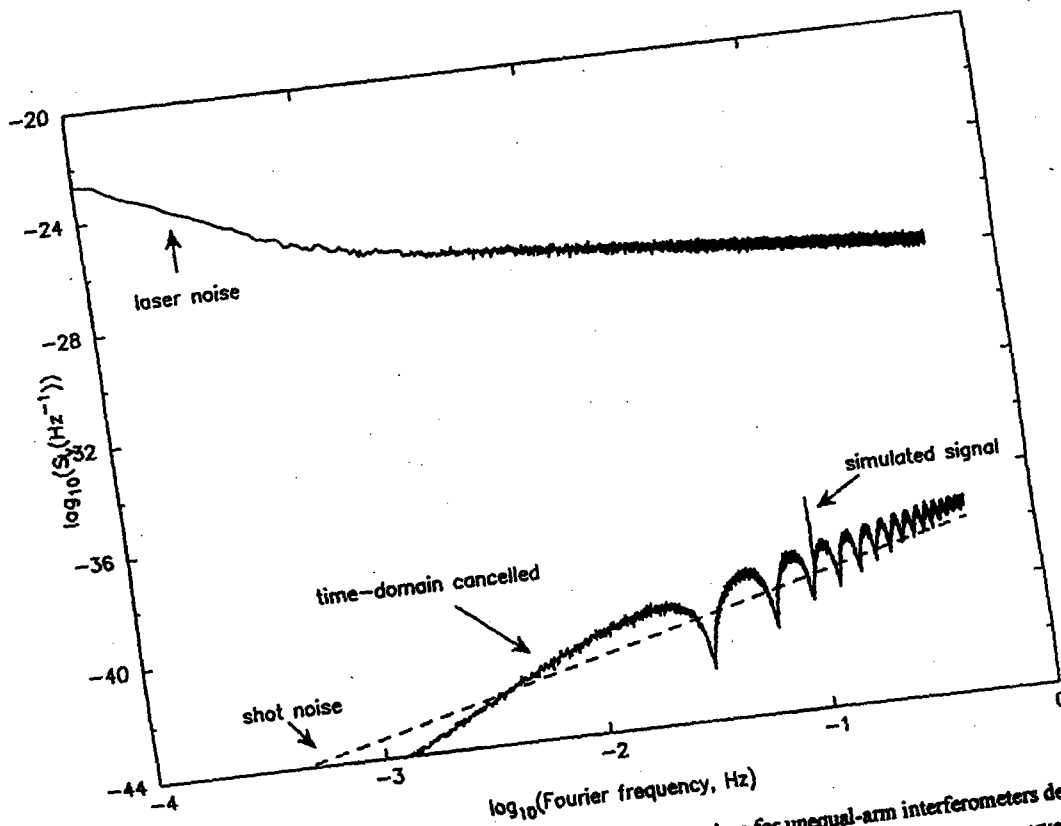
Figure 3. Simulation of the time-domain laser noise cancellation procedure for unequal-arm interferometers described in the text. Fractional frequency fluctuation spectra, $S_y(f)$, are plotted versus Fourier frequency for: (upper curve) raw laser noise having spectral density 10^{-28} $(f/1 \text{ Hz})^{-2/3} + 6.3 \times 10^{-37}$ $(f/1 \text{ Hz})^{-3.4}$ Hz^{-1}, and (lower curve) residual noise after time-domain cancellation procedure. Dashed curve shows the level of shot noise added to each arm (spectral density $\$5.3 \times 10^{-38}$ $(f/1 \text{ Hz})^2$ Hz^{-1}, independent in each arm) and dot-dashed curve showing the predicted modulation of the shot noise spectrum due to our laser noise cancellation is also plotted. Other parameters are $2 L_1 = 32$ sec, $2 L_2 = 31$ sec, and transform length $\$2^{15}$ sec. In addition to shot noise, a simulated sinusoidal gravitational wave with amplitude $h_0 = 10^{-20}$ and $f_0 = 0.1$ Hz incident normal to the plane of the interferometer was added. The time-domain procedure, using the known arm lengths, cancels the laser noise exactly making the simulated signal clearly visible above the (now modulated) shot noise spectrum.

1998 GPS TIME TRANSFER PERFORMANCE

Lt Stacy Jo Huser, USAF
2d Space Operations Squadron
300 O'Malley Avenue, Suite 41
Schriever AFB, CO 80912-3041

Steven T. Hutsell
United States Naval Observatory
Alternate Master Clock

Abstract

Every year more and more government and civilian agencies rely on GPS for accurate timing and navigation. The GPS Operational Control Segment, using information provided by the United States Naval Observatory, maintains the GPS timing signal well within specifications. This paper summarizes 1998 GPS Time Transfer performance for authorized users and relates the results to the mechanics of the GPS time steering algorithm. Data from previous years will also be presented as a means of comparison.

INTRODUCTION

The term "GPS Time Transfer" has historically assumed multiple meanings. Many in the Precise Time and Time Interval community often associate this term with the specific GPS technique used predominantly for international ground laboratory clock comparison, namely, *common-view* GPS time transfer. As we know, common-view GPS time transfer involves the use of multiple (usually paired) ground receivers.

Often forgotten in the PTTI community is the other main GPS time transfer technique, *direct-access* GPS time transfer, which many also dub "standard" GPS time transfer. In the direct-access GPS technique, users can obtain the official Department of Defense (DoD) time reference, UTC(USNO), by employing only one receiver and taking advantage of the available information in the broadcast GPS navigation message [1].

Direct-access GPS time transfer offers advantages that are most useful, primarily, for military or military-related systems. Since direct-access GPS time transfer doesn't require station-to-station communications with other ground receivers, direct-access GPS users can operate autonomously, in anonymity.

The United States Naval Observatory (USNO) performs around-the-clock monitoring of GPS's timing broadcast. USNO monitors three main time signals: 1) individual satellite time, 2) GPS ensemble time (the GPS Composite Clock), and 3) GPS's broadcast of UTC(USNO), which we call UTC(GPS). USNO currently employs Stanford Telecom (STel) 5401C receivers to perform

this monitoring. STel 5401C receivers are dual-channel, keyed sets, and thus, are dual-frequency (L1 and L2) receivers capable of tracking Y-Code and correcting for the effects of Selective Availability (SA). USNO forwards time transfer information, gathered and processed from these receivers, to the GPS control segment, which is operated by the 2d Space Operations Squadron (2 SOPS).

As we know, not all GPS time transfer receivers are key-able, and therefore, not all GPS receivers can correct for SA. These civilian, or "unauthorized," receivers do not realize the same accuracy that keyed, or "authorized," sets benefit from. Therefore, civilian direct-access users often must augment their systems with melting pot schemes, atomic reference clock supplementation, or other techniques. This paper exclusively reviews the recent performance of direct-access GPS time transfer for *authorized* users.

CURRENT TIME TRANSFER PERFORMANCE

Figure 1 shows a plot of the daily UTC(GPS)-UTC(USNO) time transfer root-mean-square (RMS) and average (AVGERR) errors for 1997. The 1997 GPS time transfer RMS was 7.84 ns, significantly lower than previous years. Figure I depicts a visible drop in the RMS in the beginning of the year due, in part, to the Ephemeris Enhancement Endeavor (EEE). After the initial EEE process completed on 28 February 1997 (MJD 97059), the daily RMS value exceeded 10 ns on only eight occasions [2].

Figure 2 shows similar daily time transfer RMS and AVGERR data for 1998. From 1 January 1998 – 23 November 1998, the time transfer RMS was 6.88 ns, a 12% improvement over 1997. This year also saw a new record low of 4.44 ns set on 5 October 1998 (MJD 98278). Looking at both 1997 and 1998 plots reveals that each daily RMS has remained well below the UTC(GPS)-UTC(USNO) specification of 28 ns (RMS), defined in the USNO/2 SOPS interface control document, ICD-GPS-202 [1].

GPS-UTC(USNO) PERFORMANCE

A critical element in the delivery of UTC(GPS) to users is the GPS timescale, called the GPS Composite Clock. Typically, direct-access GPS time transfer users obtain satellite time by locking onto a broadcasting GPS vehicle, subsequently obtain GPS time by correcting for satellite clock offsets, and finally obtain UTC(GPS) by applying GPS-UTC(USNO) corrections [3]. The performance of GPS-UTC(USNO) significantly affects the performance of UTC(GPS)-UTC(USNO), and usually serves as a second indication of how well GPS can deliver time.

The daily GPS-UTC(USNO) offsets for 1997 and 1998 are displayed in Figures 3 and 4, respectively. 2 SOPS remains sufficiently safe from breaking ICD-GPS-202's specification for |GPS-UTC(USNO)|, 1000 ns [1]. In fact, the maximum daily GPS-UTC(USNO) offset in 1997 was –15.2 ns on 16 May (MJD 97136), and 1998's maximum was +8.7 ns, on both 18 and 19 June (MJDs 98169 and 98170).

Obviously, GPS-UTC(USNO) performance has far exceeded specifications; clearly, the GPS time steering algorithm superbly accomplishes the task of meeting the 1000 ns specification. So, how does the GPS time steering algorithm do it?

THE GPS TIME STEERING ALGORITHM

As with many time scales, the stability of the GPS Composite Clock is largely dependent on how effectively its operators discipline it to its assumed "truth" source. Within the timing community exist several different types of steering algorithms, each fulfilling different requirements, and thus serving different purposes. Perhaps no other steering algorithm is more misunderstood than the often (and unfairly) maligned GPS Bang-Bang time steering algorithm.

Many steering algorithms are designed to optimize a cost equation. Usually such a cost equation takes counter-opposing requirements into consideration and provides the user/operator the mathematical vehicle for delicately balancing the given, often conflicting, requirements. Commonly, the conflicting requirements are, specifically, the need to minimize time offsets with respect to a truth source, and the need to ensure sufficient absolute stability.

In GPS, the analogous steering requirements are fairly straightforward. As mentioned earlier, the difference between the GPS time scale and UTC(USNO) must not exceed an absolute value of 1000 ns. Additionally, GPS operators must ensure that the steering doesn't excessively degrade the GPS time scale's stability, essential to GPS's navigation and time transfer missions.

The main reason |GPS-UTC(USNO)| never risks closely approaching tolerance is the impressive stability of the GPS Composite Clock. Ironically, and contrary to popular opinion, however, neither navigation nor time transfer users reap any benefits from tighter GPS-UTC(USNO) time synchronization performance. Many in the timing community have held misperceptions about this subject, usually because many are used to working with systems that offer improved performance as an inverse function of that system's timing offsets with respect to "truth" sources. However, in GPS, navigation users require real-time satellite-to-satellite stability, and not absolute "truth" synchronization, in order to operate optimally.

Likewise, large GPS-UTC(USNO) offsets do *not* degrade service to direct-access GPS time transfer users, either, as long as users appropriately apply the GPS-UTC(USNO) parameters broadcasted in subframe 4, page 18 of the GPS navigation message, to compensate for these offsets [3]. For instance, the GPS time scale could hypothetically be several hundred nanoseconds off from UTC(USNO), but as long as the broadcast corrections are of good quality, users can still obtain UTC(USNO) with excellent results, as indicated earlier.

Therefore, 2 SOPS operators have the freedom to choose time steering parameters designed to place the instability caused by GPS time steering below the noise level of GPS time itself. More importantly, 2 SOPS has the freedom to use a relatively simple steering algorithm to meet its performance objectives [4].

The Mechanics of GPS Time Steering

Perhaps the most common general steering algorithm design involves the use of gain coefficients [or in inverse formulation, damping factors]. Second-order systems generally employ two coefficients, which, in particular, are the phase gain and the frequency gain. Designers usually derive these gain terms from simulations, or from cost equations. Simply stated, these algorithms generally input estimates of time and rate (or, respectively, phase and frequency) offsets, multiply each offset by its corresponding gain term, and add the two results together to calculate a steering value, in a recursive fashion.

Furthermore, many designers choose to impose upper and lower limits to the recursively-calculated steering value. In some systems, the calculated value will more often exceed the imposed limits than not, resulting in the predominant occurrence of "limiter value steers." When a steering system uses limits that are so tight that "limiter value steers" occur almost exclusively, the algorithm essentially behaves as having what is termed as a "bang-bang" characteristic.

GPS uses an *explicit* "Bang-Bang" steering algorithm. The simple mechanics of the GPS Bang-Bang steering algorithm are as follows. These mechanics occur in the GPS Master Control Station (MCS) every 15 minutes:

1. To begin, the algorithm receives MCS-calculated estimates of the time and rate offsets of GPS time with respect to UTC(USNO). These estimates are based on data points downloaded daily from USNO.

2. The algorithm then calculates a so-called "Discriminant," based on the respective time and rate offsets. In layman's terms, the Discriminant is essentially the predicted time (or phase) offset value at which the rate (or frequency) will reach zero, as a result of theoretical steering in the direction opposite to the current rate offset estimate.

3. Finally, the algorithm sets the steer sign to the opposite of the Discriminant sign.

The GPS steering magnitude is a fixed value located in a MCS database file. Currently, the steering magnitude is 1.0 E-19 s/s^2. Over 15 minutes, this translates into a frequency change of only 9 E-17 s/s and a time change of only *40.5 femtoseconds*. Were the algorithm to steer with the same sign for 24 straight hours, this magnitude would translate into a frequency change of 8.64 E-15 s/s, and a time change of only 373 picoseconds. Since GPS users depend on predictions from navigation messages which are typically not older than 24 hours, such small time changes are always insignificant compared to other subcomponents of direct-access GPS time transfer error, which, depending on the subcomponent, can be several nanoseconds. For that matter, 373 picoseconds is actually smaller than the granularity of the broadcast terms for satellite clock offset (465 picoseconds)!

Such changes induced by steering are well into the noise level of GPS [5]. Though 2 SOPS operators will, over time, modify this steering magnitude to appropriately match the ongoing improvements to GPS time performance, currently, the steering magnitude of 1.0 E-19 s/s^2 quite sufficiently meets GPS time steering requirements, with no significant degradation to GPS time stability. A corollary of this conclusion is the assertion that the current GPS time steering algorithm, by itself, tuned properly, is more than sufficient for GPS's steering requirements.

128

Figure 5 shows a visual example of how the GPS Bang-Bang steering algorithm generally works. The example begins with a scenario whereby GPS time is off from UTC(USNO) by -7.0 ns in time, and 0.0 ns/day in rate. The algorithm steers with a positive rate (of 1.0 E-19 s/s^2) until the GPS-UTC(USNO) plot reaches a point of inflection—when the time offset is -3.5 ns, and the rate offset is +2.29 ns/day. At this point of inflection, the Discriminant is zero, and the algorithm therefore begins to steer negatively (at -1.0 E-19 s/s^2) until the GPS-UTC(USNO) time and rate offsets are both near zero. This example shows how the algorithm would remove a -7.0 ns GPS-UTC(USNO) time offset, *in theory*. In reality, however, 2 SOPS receives updates from USNO *daily*, and, therefore, the MCS recalculates its time and rate offset estimates daily, as well. As a result, a theoretical steering strategy projected for, say, six days in the future, will usually change well before the strategy can be fully executed. As in the shown example, the effective "time constant" for steering is usually longer than one day, meaning that one day's worth of steering will usually remove only a *portion* of the estimated GPS-UTC(USNO) error. The result is a day-by-day, continuous drive to *gradually* remove GPS-UTC(USNO) time errors, and, if applicable, rate errors. This strategy proves to work exceptionally well.

GPS TIMESCALE STABILITY

The stability of |GPS-UTC(USNO)| for 1997 and 1998, based on daily GPS-UTC(USNO) data points provided by USNO, is presented in Figure 6. The one-day stability for 1998, 1.61 E-14, is roughly as good as 1997's one-day stability of 1.77 E-14. Perhaps more important to note is the significant improvement in long-term stability for essentially all tau values greater than one day. Several likely factors accounting for the improved GPS timescale stability include the better operational performance of GPS ground [monitor] stations, the inclusion of more rubidium frequency standards in the GPS Composite Clock [6], and, generally stated, an overall improvement in the quality and efficiency of operations at 2 SOPS.

Note how the Allan deviation slope gradually changes to -1 at a tau value of around ten days, indicating the finite bounding of GPS-UTC(USNO). Additionally, note that the effective instability caused by GPS steering, at most, *never* approaches the inherent noise level of GPS-UTC(USNO) for tau = 1 day. Again, one-day stability is especially important, since one day is the nominal GPS navigation upload prediction span. These indicators clearly demonstrate the effectiveness of GPS's Bang-Bang steering algorithm—long-term synchronization at a very small sacrifice to short-term stability.

CONCLUSION

Every year GPS has set new records in direct-access time transfer performance and stability—1998 was no exception. 2 SOPS, USNO, and other agencies will always push to find ways to improve GPS time. Through refinements in the receipt and processing of USNO data, the inclusion of more rubidium frequency standards into the GPS Composite Clock, and the acquisition of better GPS monitor station hardware (and more monitor stations), among other endeavors, GPS can continue its trend of improving stability and time transfer performance for 1999 and beyond.

ACKNOWLEDGMENTS

REFERENCES

[1] ICD-GPS-202, Revision A, 13 December 1996.

[2] Crum, Jeffrey D., Capt.; Hutsell, Steven T.; and Smetek, Ronald T., Jr., *The 2 SOPS Ephemeris Enhancement Endeavor (EEE)*, Proceedings of the 29th Annual Precise Time and Time Interval (PTTI) Applications and Planning Meeting, 2–4 December 1997, Long Beach, CA, USA, pp. 117-130.

[3] ICD-GPS-200, Revision C, 10 October 1993, IRN-200C-002, 25 September 1997.

[4] Hutsell, Steven T., Capt., *Recent MCS Improvements to GPS Timing*, Proceedings of ION-GPS-94, Salt Lake City, UT, USA, 20-23 September 1994, pp. 261-273.

[5] Hutsell, Steven T., Capt., *Ideas for Future GPS Timing Improvements*, Proceedings of the 27th Annual Precise Time and Time Interval (PTTI) Applications and Planning Meeting, 29 November – 1 December 1995, San Diego, CA, USA, (NASA CP-3334), pp. 63-74.

[6] Crater, David T., Lt. and Mobbs, Houston S., Capt., *The Impact of Operating GPS with More Rubidium Frequency Standards*, Proceedings of ION-GPS-98, Nashville, TN, USA, 15-18 September 1998.
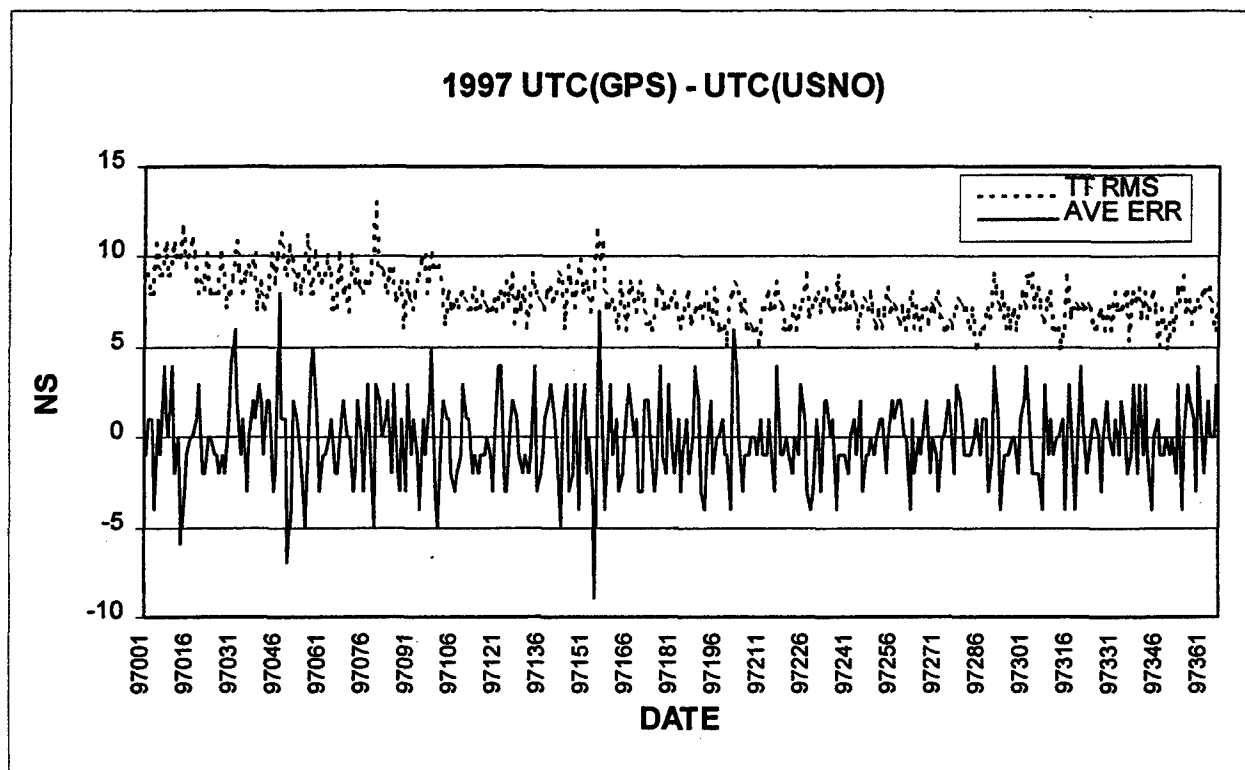
Figure 1. 1997 UTC(GPS) – UTC(USNO) Root-Mean-Square and Average Error
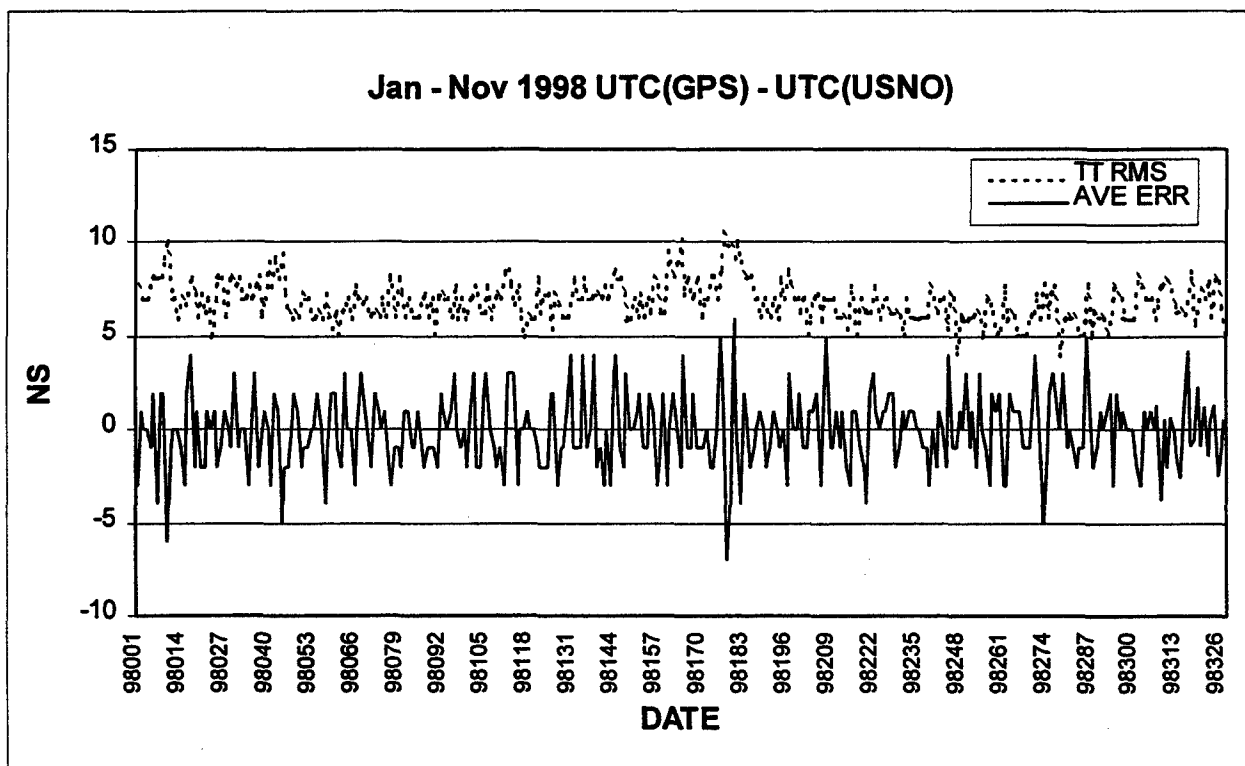
Figure 2. Jan through Nov 1998 UTC(GPS) – UTC(USNO) Root-Mean-Square and Average Error
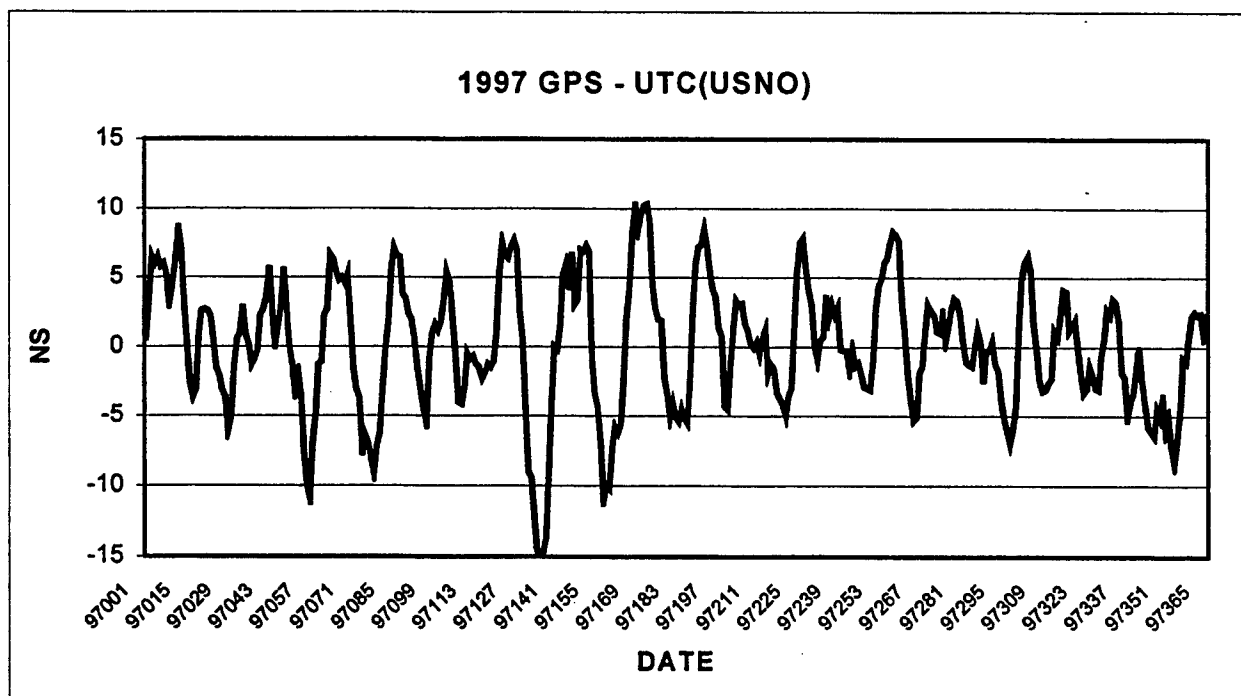
Figure 3. 1997 Daily GPS – UTC(USNO) Offset
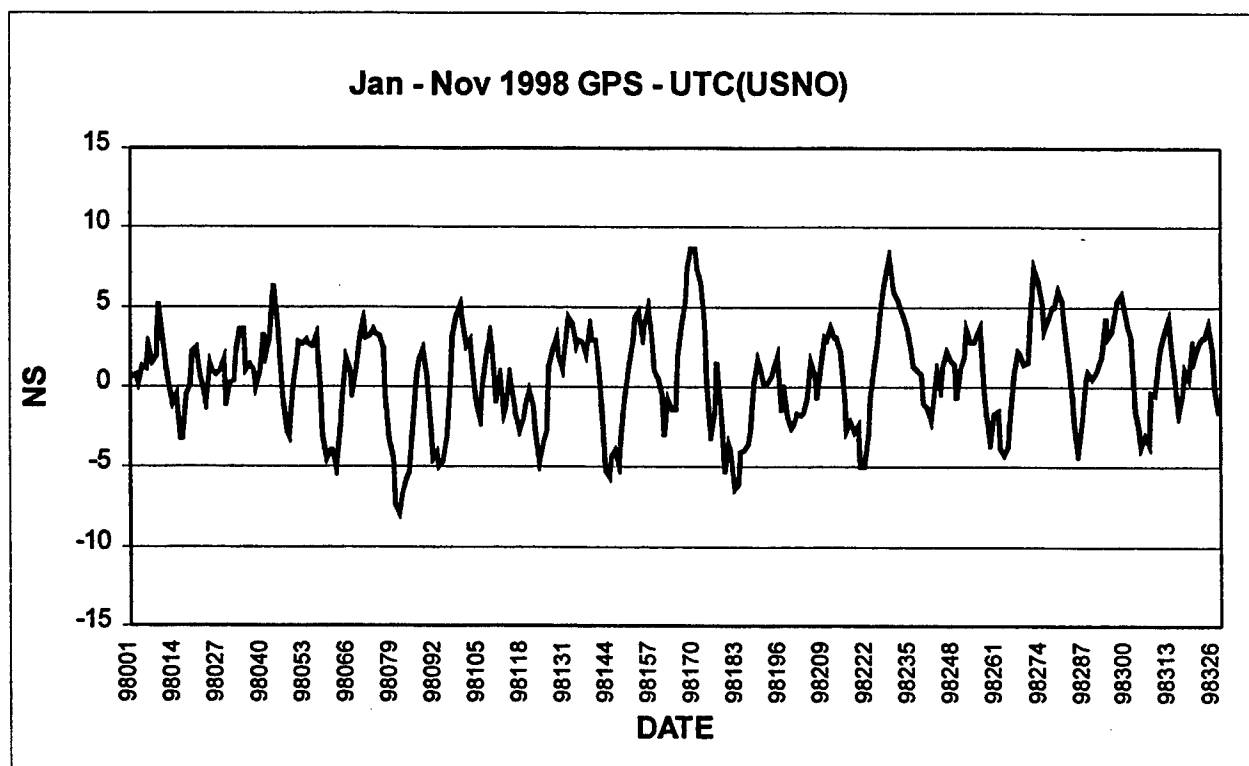
Figure 4. Jan through Nov Daily GPS – UTC(USNO) Offset

132
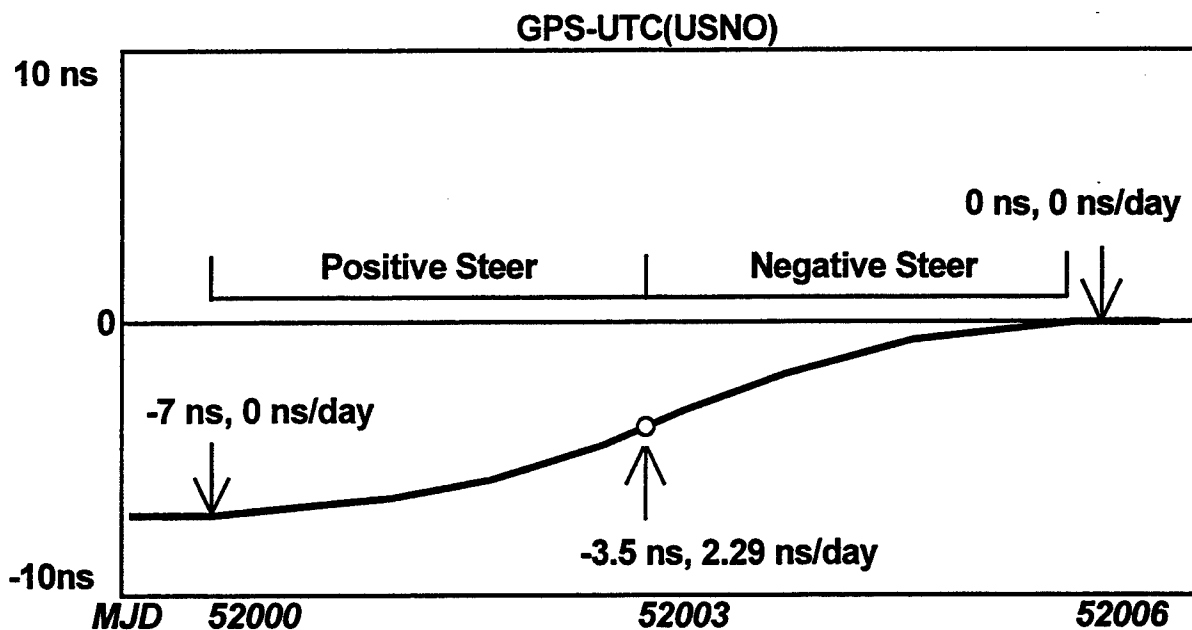
Figure 5. A visual example showing the functionality of the GPS Bang-Bang time steering algorithm.
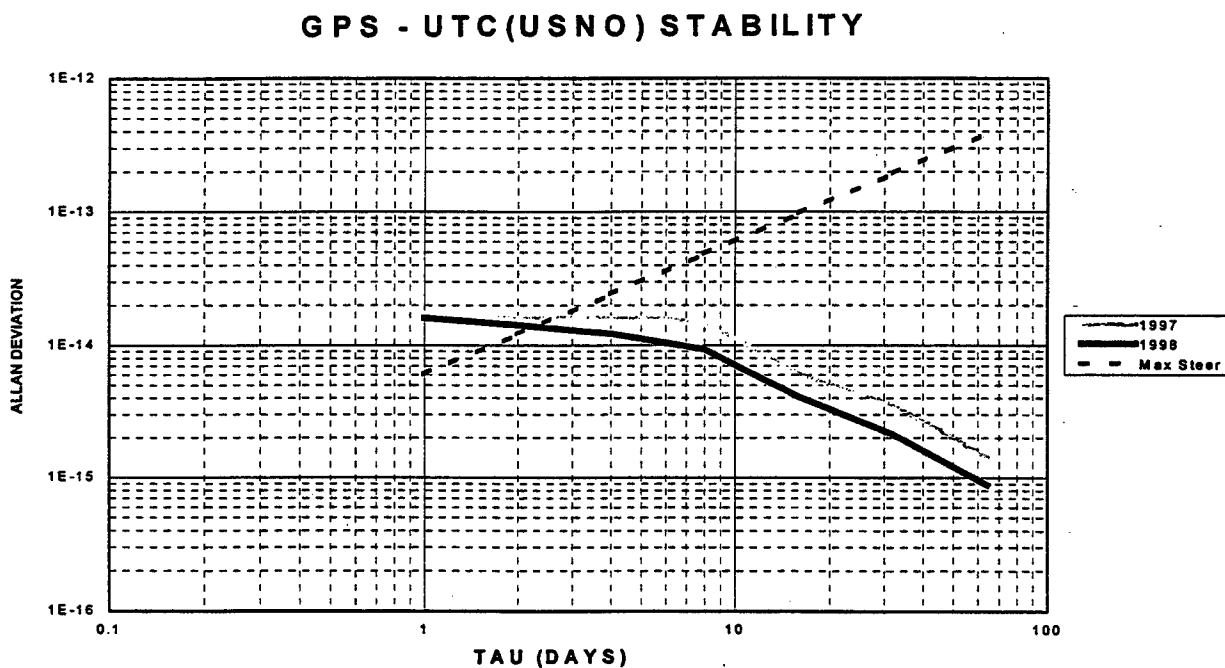
Figure 6. 1997 versus 1998 GPS – UTC(USNO) Stability

Questions and Answers

DIETER KIRCHNER (TUG): In the first part of your talk, you were speaking about UTC GPS, and in the second part, you simply said "GPS" time. Is this identical?

STEVEN HUTSELL (USNO): No. If you want to get as close an approximation to what USNO is providing to DoD users by the GPS direct access signal, you would want this value here. When we are plotting the stability of GPS time versus UTC, we are comparing GPS to UTC - USNO. So, the answer to your question is GPS is sort of a free-wheeling time scale that users use primarily for navigation; and if they want to get as close to UTC - USNO as possible, they apply the Sub-Frame 4, page 18 correction.

PERFORMANCE OF GPS
ON-ORBIT NAVSTAR FREQUENCY STANDARDS AND
MONITOR STATION TIME REFERENCES

Orville Jay Oaks
Thomas B. McCaskill
Marie M. Largay
U.S. Naval Research Laboratory
Washington, D.C.

Wilson G. Reid
SFA, Inc.
Washington, D.C.

James A. Buisson
Antoine Enterprises Inc.
Alexandria, VA

Abstract

The U.S. Naval Research Laboratory (NRL) conducts comprehensive analyses of the Global Positioning System (GPS) atomic frequency standards under the sponsorship of the GPS Joint Program Office (JPO) and in cooperation with the 2nd Space Operations Squadron (2SOPS) at the Master Control Station (MCS) in Colorado Springs, Colorado. Included in the analysis are the on-orbit Navstar space vehicle clocks and the ground reference clocks at each of the five Air Force and seven National Imagery and Mapping Agency (NIMA) GPS monitor stations. A presentation will be made of the performance of the Navstar clocks currently operating in the constellation, which are characterized through the use of phase, frequency, drift and stability histories in addition to frequency stability profiles based on the Allan and Hadamard variances. Clock performance is analyzed using a multi-year database comprised of pseudorange measurements collected by each of the 12 GPS monitor stations. Results of these analyses are routinely used by the MCS in optimizing the q's in the Kalman filter.

Continuous 15-minute measurements of the phase offset of each monitor station time reference from the DoD Master Clock are obtained from Linked Common-View Time Transfer from DoD Master Clock, which is the reference clock at the NIMA Washington, D.C. monitor station. The method is extended to obtain continuous 15-minute measurements of the phase offset of each active Navstar space vehicle clock from the DoD Master Clock. Hence, the performance of all space and control segment clocks is referenced to the DoD Master Clock.

Discontinuities in the phase and frequency of the clocks are removed to yield the unperturbed performance of the clocks. The corrections, together with the probable cause of the discontinuity, are summarized. Examples of the frequency history and the exhaustive calculation, for every multiple of the sample period of 15 minutes from 15 minutes to 18 days, of the frequency stability profile for several Navstar space vehicle clocks and for the time reference at two of the GPS monitor stations will be presented. Analysis of the performance of the first on-orbit Block IIR operational rubidium clock will also be presented.

INTRODUCTION

The pseudorange measurements upon which this analysis is based were collected at the five Air Force and the seven National Imagery and Mapping Agency (NIMA) monitor stations using dual-frequency GPS receivers. *Figure 1* presents the information flow from a single Navstar space vehicle to each of the GPS monitor stations. The use of dual frequencies enabled ionospheric corrections to be based on the measured ionosphere. The pseudorange measurements were collected every six seconds synchronized to GPS time and smoothed to one point every 15 minutes. Clock offsets were computed using the NIMA post-processed ephemerides and observations that were collected at the 12 GPS monitor stations. All monitor station clock performance was computed using Linked Common-View Time Transfer from the NIMA Washington, D.C. site.

A key feature in the NRL Clock Analysis Software System (CLASS) is the capability to detect phase and frequency discontinuities, to solve for the discontinuity, and to correct the clock data. Correction of the data makes possible the analysis of long-term clock, system, and environmental effects[1]. The results of the analysis are included in NRL Quarterly Reports to the GPS Joint Program Office (JPO) and to the Master Control Station (MCS), as well as to other interested members of the scientific community.

Other measures of performance are determined, such as the total operating time for each operational Navstar space vehicle and the operating time for each Navstar clock. Included are histories of the phase, the frequency, and the frequency stability.

CONSTELLATION

The constellation as of 30 September 1998 is shown in *Figure 2*. This table shows by plane and by position in the plane each of the Block II/IIA/IIR Navstar space vehicles in the constellation and the type of clock that was operating. Of the active cesium clocks, Frequency & Time Systems, Inc. manufactured all but the Navstar 30 cesium clock. Kernco, Inc.manufactured the Navstar 30 cesium clock. All Block II/IIA rubidium clocks were manufactured by Rockwell, Inc. The Block IIR rubidium clock on Navstar 43 was manufactured by EG&G. Seven of the 27 clocks operating were rubidium, while twenty were cesium atomic frequency standards. Three of the six planes have four Navstars, while the other three planes contain five Navstar space vehicles (SV) each, although the SVs are not evenly spaced in the planes.

The total operating time for each of the Navstar space vehicles since the space vehicle was inserted into the constellation is presented in *Figure 3*. Thirteen of the space vehicles have been in operation for six years or more, which exceeds the mean mission duration specification.

The number of clocks that have been placed in operation on each space vehicle is presented in *Figure 4*. Eight of the space vehicles are operating the first clock, thirteen are operating the second clock, four are operating the third clock, and two are operating the last clock. Navstar 43 is operating its second clock, but one of the clocks was activated as a test and could be used again when needed.

NAVSTAR CLOCKS

The operating time or length of service, of the clocks that were operating as of 30 September 1998 is presented in *Figure 5*. The shaded bars correspond to the cesium clocks and the unshaded bars to the rubidium clocks. Nine clocks, all cesium frequency standards, have exceeded five years of continuous operation. Two clocks, both cesium frequency standards, have exceeded eight years of continuous operation. Two of the rubidium clocks have attained three years of continuous operation.

The operating times of Block II cesium and rubidium clocks respectively both active and deactivated clocks are presented in *Figures 6* and *7*. The data are presented in order of activation. The shaded bars correspond to the active clocks, while the open bars correspond to the deactivated clocks. The comparison shows that the Block II cesium clocks have an average operating time on-orbit of 3.7 years, while the rubidium clocks have an average operating time on-orbit of 1.3 years.

The one-day frequency offset history for the clocks in plane B of the GPS constellation as of 30 September 1998 is presented in *Figure 8*. NRL analyzes each clock in each plane in the constellation, but only plane B is presented for brevity. The history of the clocks in all planes is included in the NRL quarterly reports.

The two-day frequency drift for each of the clocks in the constellation, presented by *Figure 9*, shows that the rubidium clocks exhibit typically large drift rates, which are characteristic of rubidium frequency standards--the largest being Navstar 38 with a drift of $-5.0\,pp10^{13}$ per day. Six rubidium clocks exhibit negative drift, excluding the rubidium in Navstar 34, which was activated on September 14, 1998 and did not have sufficient data to be included. *Figure 10* is a plot on an expanded scale of the two-day average drift of the cesium clocks. Ten of the cesium clocks exhibit a negative drift, while the other ten exhibit a positive drift. All but one of the cesium clocks exhibit a drift with a magnitude below $5\,pp10^{15}$ per day, which is two orders of magnitude less than the largest drift rate reported for the Block II rubidium clocks.

Figures 11 through *14* are examples of the frequency stability profile for four of the 27 Navstar clocks. *Figure 11* shows the stability of the Navstar 19 rubidium clock, which is typical of the performance of the rubidium clocks manufactured by Rockwell Corporation. *Figure 12* shows the effects of a 10-15 nanosecond oscillation at the orbital period in the phase offset of the Navstar 36 cesium clock manufactured by Frequency and Time Systems. The cause of these oscillations which affected a number of clocks has not been identified. *Figure 13* shows the performance of the best cesium clock in the constellation, the Navstar 30 alternate-source cesium clock manufactured by Kernco. The stability of this clock for a sample time of one day was estimated to be $7\,pp10^{14}$. *Figure 14* shows the performance of the best rubidium clock in the constellation, the Navstar 43 Block IIR clock manufactured by EG&G. The stability of this clock at one day was estimated to be near the noise threshold of the receiver at $2.4\,pp10^{14}$.

The frequency stability profile, made using the precise ephemerides, for the 27 clocks in the constellation that were operational on 30 September 1998 is presented in *Figure 15*. All but seven of the clocks are evenly distributed between $7\,pp10^{14}$ and $1.4\,pp10^{13}$ at one day. *Figures 16* and *17* show the ranking of the estimates of the frequency stability for a sample time of one day using the Allan and Hadamard deviations respectively. In *Figure 16*, three of the six rubidium clocks for which the stability was estimated rank last because of the large drift typical of rubidium clocks. In *Figure 17*, based on the Hadamard deviation which adaptively corrects for the drift [2], all six of the rubidium clocks rank before the cesium clocks with values of stability measured in $pp10^{14}$.

The frequency stability estimates for each of the Navstar clocks for a sample time of one day using the post-fit ephemeris are presented in *Figure 18*. Estimates of the frequency stability were made

using the Allan deviation without any correction for aging. Superimposed on *Figure 18* are dashed lines corresponding to the GPS system specifications of 2 $pp10^{13}$ and 5 $pp10^{13}$ for the one-day stability of the cesium and rubidium clocks respectively. The frequency stability of all Block II space vehicle clocks can be seen to meet the specifications. Eleven of the Block II clocks--nine cesium frequency standards and two rubidium standards--show stability at or below 1 $pp10^{13}$.

TIME TRANSFER

Linked Common-View Time Transfer is a special case of GPS time transfer [3], which uses simultaneous measurements by two users of a Navstar space vehicle clock when the space vehicle is in view of both users. Each of the two users computes his clock offset with respect to the Navstar clock at the same epoch. Then, the difference between their respective clock offsets with respect to the Navstar clock yields the offset between the two user clocks. This procedure results in a measurement which is independent of the Navstar clock, but which retains the difference in the measurement errors.

The precision of a single common-view time transfer measurement was first demonstrated using common-view time transfer measurements taken over a 20-day time span with a single space vehicle. Recently, the precision of the common-view time transfer measurement was definitively determined through the use of multiple common-view measurements taken at the same epoch [4]. This process was made possible with the full constellation of GPS space vehicles. The estimated precision of a single 15-minute interval has been determined to be between 1.4 and 2.7 nanoseconds. Using the measurements from all Navstar space vehicles in common-view during the 15-minute interval, typically 3-7 space vehicles, improves the estimate of the precision of the time transfer measurement to between 0.65 and 1.13 nanoseconds. This level of measurement precision results in the capability to determine the frequency stability of a remote clock (with respect to the DoD Master Clock) anywhere on Earth to within 2 $pp10^{12}$ for a 15-minute sample time and 2 $pp10^{14}$ for a one-day sample time.

A Linked Common-View Time Transfer measurement results by linking two or more remote sites that are in common-view with either the same or another Navstar space vehicle. The precision of the Linked Common-View measurements can be estimated by considering the special case of the sum of stationary random variables with mean zero and standard deviation equal to the precision of a single common-view time transfer measurement. It is expected that the precision of the Linked Common-View Time Transfer will grow as the square root of the number of links multiplied by the precision of a single common-view measurement. However, in the analysis of the stability of a remote clock, it is possible that other factors such as the quality of the receiver and short-term environmental effects could have a greater influence on the precision of the measurements than the effect of multiple links.

MONITOR STATION CLOCKS

Figures 19 and 20 show the one-day average frequency offset six-month history of the ground reference clocks from the DoD Master Clock for the Air Force and NIMA GPS ground tracking stations respectively. These results were obtained using Linked Common-View Time Transfer[4]. The performance of the ground reference clock at the Colorado Springs Monitor Station is superior. It is the Alternate Master Clock #1 which is a hydrogen maser steered to UTC (USNO) by two-way satellite time transfer [5]. The performance of the ground reference clocks at the remaining four Air Force stations, which are equipped with HP5061 cesium beam tubes, has more noise than that of the

ground reference clocks at the NIMA MS, which are equipped with HP5071 high performance cesium-beam tubes. The superior performance of the Colorado Springs monitor station time reference can be seen in the frequency stability profile in *Figure 21*, where its performance is dominated by white phase noise as far out as the profile was estimated, i.e. 18 days. On the other hand, the best NIMA time reference was at the Quito, Ecuador monitor station (Figure 22), which shows a flicker floor of 1 $pp10^{14}$ being achieved at about five days. This station had the lowest short-term noise of all the monitor stations, whereas the Colorado Springs monitor station had the highest. In addition, the time reference for the Colorado Springs monitor station showed a cyclic component at the fourth harmonic of the orbital period (2.99 hours). The cause of this cyclic component has not been determined. The performance of the time reference at each of the ten monitor stations is compared in *Figure 23*, which presents the frequency stability profile for sample times of one to 18 days. The Colorado Springs monitor station is clearly superior, followed by the five NIMA monitor stations, and finally by the remaining four Air Force monitor stations.

CONCLUSIONS

Thirteen of the Block II space vehicles have been in operation for six years or more and have exceeded the expected mean mission duration. An average of two Block II Navstar clocks per space vehicle has been activated. Twenty-one of the space vehicles have at least two spare clocks available to complete the design lifetime. Fourteen Navstar clocks--more than one-half of the operational constellation--are performing with an estimated one-day frequency stability of 1 $pp10^{13}$ using the precise ephemerides and based on the Hadamard deviation. The time reference at each of the GPS monitor stations exhibited a frequency stability for a sample time of one day of between 3 $pp10^{14}$ to 4.2 $pp10^{14}$.

REFERENCES

[1] McCaskill, T. B., Reid, W.G., Oaks, O.J., Beard, R.L., U.S. Naval Research Laboratory, and Buisson, J. A. and Warren, H. E., SFA, ``Performance of Global Positioning System (GPS) On-orbit Navstar Clocks," 1995 IEEE International Frequency Control Symposium}, 31 May--2 June 1995, pp133--139.

[2] Hutsell, Steven H., ``Relating The Hadamard Variance to MCS Kalman Filter Clock Estimation" Proceedings of the 27th Annual Precise Time and Time Interval (PTTI) Applications and Planning Meeting}, 29 November—1 December 1995, pp291--301.

[3] Buisson, J. A., McCaskill, T. B., Smith, H., Morgan, P., and Woodger, J., ``Precise Worldwide Station Synchronization via the Navstar GPS Navigation Technology Satellite (NTS-1)", Proc. 8th Annual Precise Time and Time Interval (PTTI) Applications and Planning Meeting, November 30 -- December 2, 1976, Washington, D.C., pp.55--84.

[4] Reid, W.G., McCaskill, T. B., and Oaks, O.J., U.S. Naval Research Laboratory, and Buisson, J. A. and Warren, H.E., Sachs Freeman Associates Incorporated, ``Common View Time Transfer Using Worldwide GPS and DMA Monitor Stations", Proceedings of the 27th Annual Precise Time and Time Interval (PTTI) Applications and Planning Meeting, November 29---1 December 1995, pp145--158.

[5] Breakiron, Lee A., ``Frequency Steering of Hydrogen Masers", Proceedings of the 50th Frequency Control Symposium, 5 June 1996.
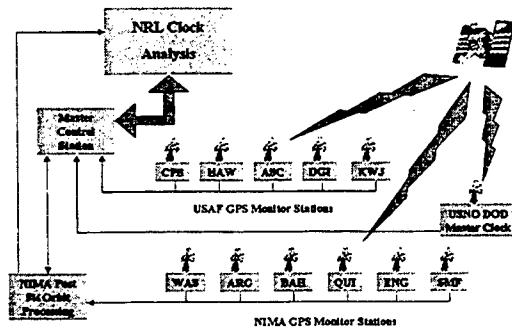
Figure 1. Clock Analysis Data Flow

Plane	Slot 1	Slot 2	Slot 3	Slot 4	Slot 5
A	39	25	27	19	38
B	22	30	13	35	
C	36	33	31	37	
D	24	15	17	34	
E	14	21	16	23	40
F	32	26	18	29	43

☐ Cesium Clock

☐ Rubidium Clock

Figure 2. GPS Constellation Space Vehicle Location
and Clock Type
30 September 1998
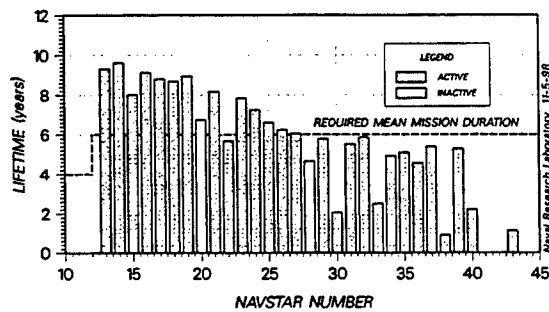
Figure 3. Total Operating Time of Current Navstar
Satellites
30 September 1998
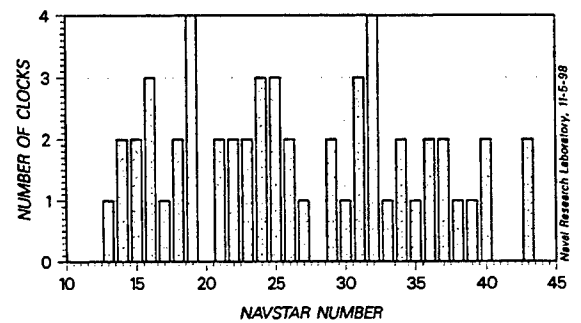
Figure 4. Number of Clocks Operated Since Insertion
30 September 1998
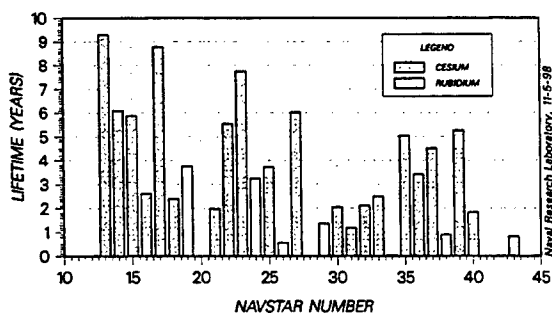
Figure 5. Operating Lifetime of Current Clocks
30 September 1998
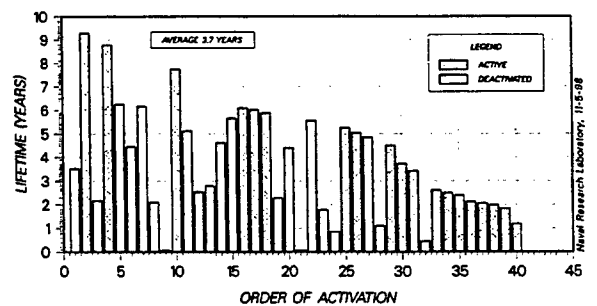
Figure 6. Lifetime of Block II and IIA Cesium Clocks
in Order of Activation
30 September 1998

140
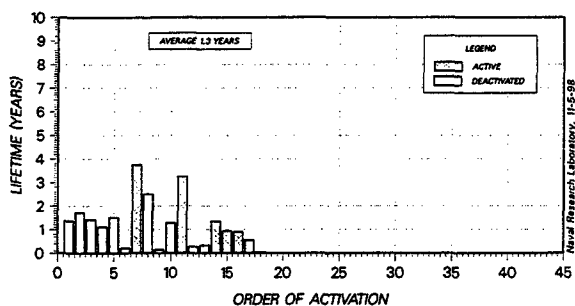
Figure 7. Lifetime of Block II, IIA, and IIR Rubidium
Clocks in Order of Activation
30 September 1998
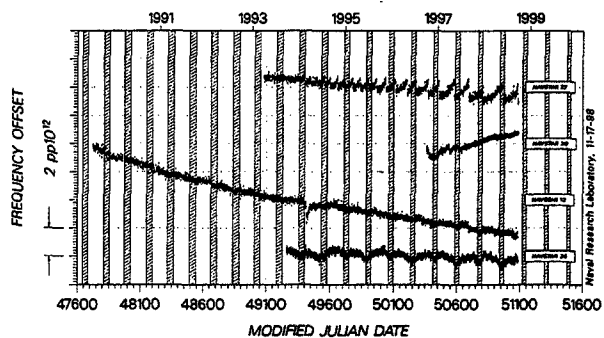
Figure 8. One-Day Frequency Offset History of
Navstar Clocks from DoD Master Clock
Plane B
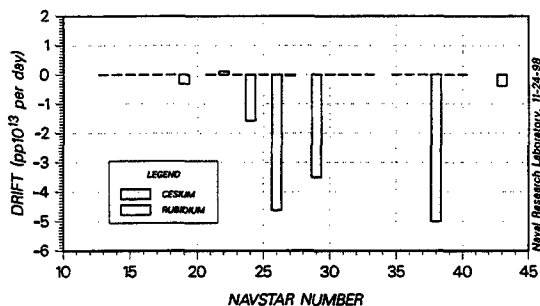
Figure 9. Two-Day Average Frequency Drift of
Current Clocks
1 June 1998 to 30 September 1998
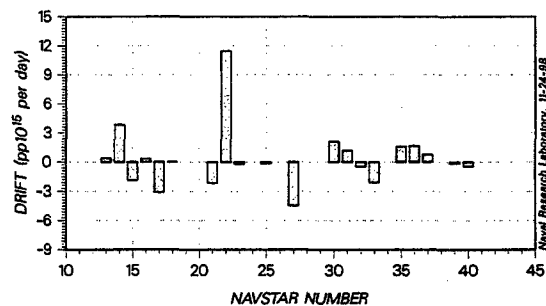
Figure 10. Two-Day Average Frequency Drift of
Cesium Clocks
1 June 1998 to 30 September 1998
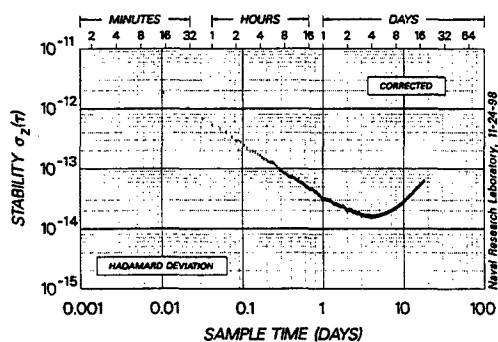
Figure 11. Frequency Stability of Navstar 19
Rubidium Oscillator (No. 53)
1 April 1998 to 1 October 1998
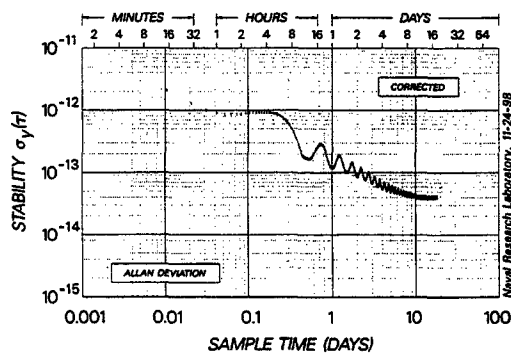
Figure 12. Frequency Stability of Navstar 36
Cesium Oscillator (No. 46)
1 April 1998 to 1 October 1998

141
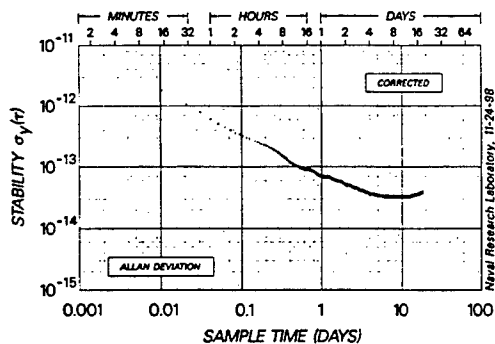
Figure 13. Frequency Stability of Navstar 30
Cesium Oscillator (No. K3)
1 April 1998 to 1 October 1998
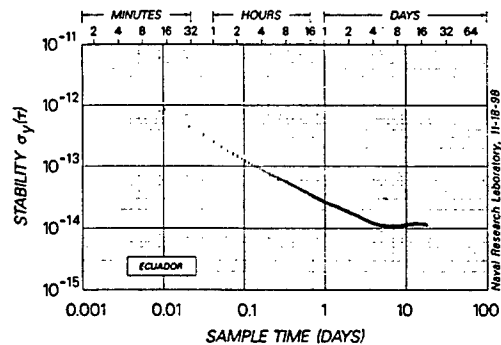
Figure 14. Frequency Stability of Navstar 43
Rubidium Oscillator (No. 06)
1 April 1998 to 1 October 1998
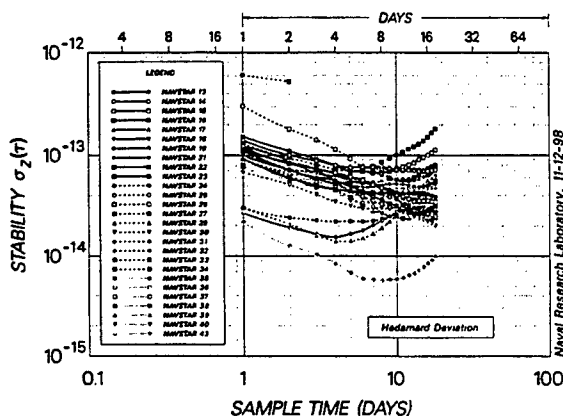
Figure 15. Frequency Stability of Navstar Clocks
1 April 1998 to 30 September 1998
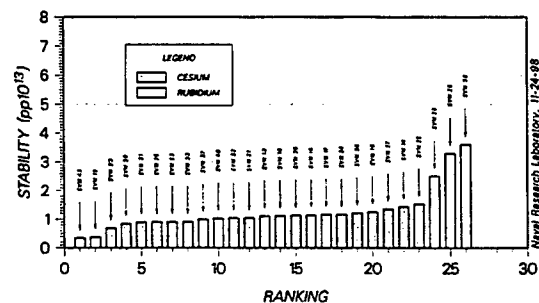
Figure 16. Ranking of One-Day Frequency Stability
Estimates of Navstar Space Vehicle Clocks Using
Allan Deviation
1 June 1998 to 30 September 1998
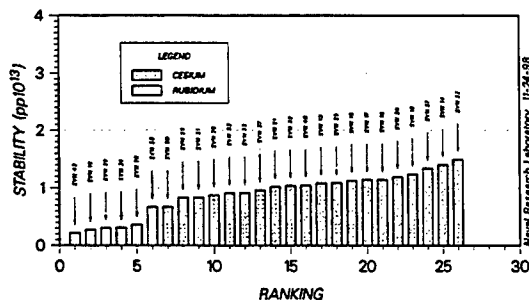
Figure 17. Ranking of One-Day Frequency Stability
Estimates of Navstar Space Vehicle Clocks Using
Hadamard Deviation
1 June 1998 to 30 September 1998
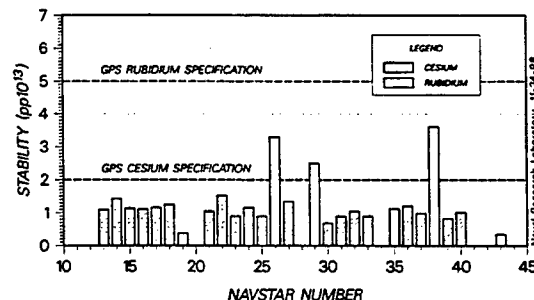
Figure 18. One-Day Frequency Stability Estimates of
Navstar Space Vehicle Clocks Using Allan Deviation
1 June 1998 to 30 September 1998

142
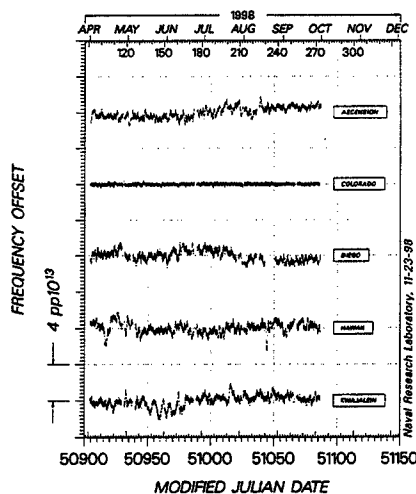
Figure 19. Frequency Offset of Air Force Monitor
Station Time Reference from DoD Master Clock
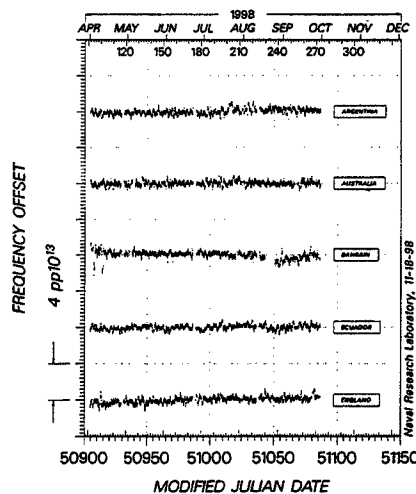
Figure 20. Frequency Offset of NIMA Monitor Station
Time Reference from DoD Master Clock
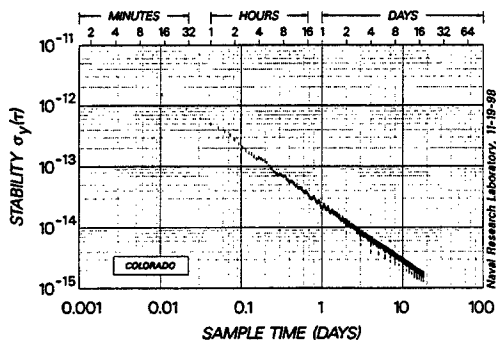
Figure 21. Frequency Stability of Monitor Station Time
Reference with Respect to DoD Master Clock via
Common-View Time Transfer
1 April 1998 to 1 October 1998
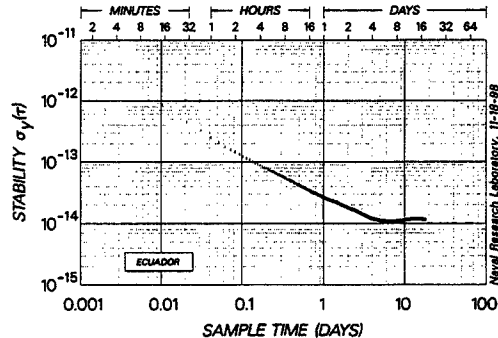
Figure 22. Frequency Stability of Monitor Station Time
Reference with Respect to DoD Master Clock via
Linked Common-View Time Transfer
1 April 1998 to 1 October 1998
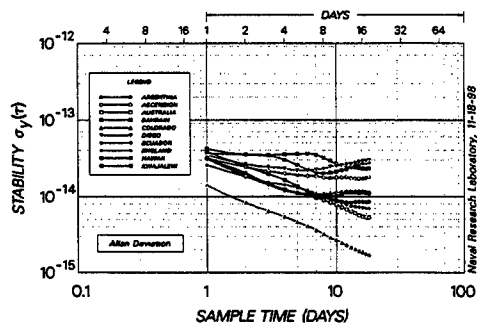
Figure 23. Frequency Stability Profile Comparison of
Time References with Respect to DoD Master Clock via
Linked Common-View Time Transfer
1 April 1998 to 1 October 1998

143

Questions and Answers

DENNIS McCARTHY (USNO): To what extent does the quality of the orbits that you are using affect the analysis of the satellite clocks?

JAY OAKS (NRL): This sounds like a loaded question? Obviously, it plays an important part. That is why we use the NIMA precise orbit, which is reported to be accurate within centimeters. What we see here is mostly dominated by the clock, but there are some anomalies that we investigate, like the orbit where it might be showing up.

SIGFRIDO LESCHIUTTA (IEN): Could you please show us one of the last vugraphs concerning the behavior of the USNO clock monitor station frequency stability profile?

JAY OAKS: Was it the monitor station clock frequency?

SIGFRIDO LESCHIUTTA: Yes.

JAY OAKS: This one? We have one like this for the monitor station frequency stability profile, one for monitor station clocks, and one for the space vehicle clocks.

SIGFRIDO LESCHIUTTA: The one concerning your two-way link.

JAY OAKS: That was this. What I had said is that the Colorado Alternate Master Clock, which is shown here, is a hydrogen maser steered using measurements made once an hour using two-way satellite time transfer measurements between the Naval Observatory and the Colorado Station. That is Steven Hutsell's algorithm and if you have some questions about that, he would probably be happy to answer them. Is that what you were asking?

SIGFRIDO LESCHIUTTA: Yes.

GPS BLOCK IIR RUBIDIUM ATOMIC FREQUENCY STANDARD LIFE TEST

R. Beard, J. White, J. Brad, S. Stebbins, J. Smathers, T. Myers
U.S. Naval Research Laboratory

F. Danzy, A. Frank, W. Reid
SFA, Inc.

J. Buisson
Antoine Enterprises

Abstract

The rubidium clocks in the GPS Block IIR spacecraft have no previous flight experience, and will be the only atomic clocks used on the Block IIR satellites. The U.S. Naval Research Laboratory (NRL), in cooperation with the Global Positioning System Joint Program Office (GPS-JPO), the GPS Control Segment, Lockheed Martin, ITT, and EG&G, is conducting a three year life-test of two flight qualified EG&G Rubidium Atomic Frequency Standards (RAFS) selected from the operational spacecraft inventory. The two RAFS, serial numbers 28 and 30, were selected as representative of the flight configuration build for Block IIR by ITT and provided by the JPO to NRL for this test. The test is intended to build confidence in these units as operational spacecraft clocks and establish a database of fundamental performance characteristics. The two units are being operated in independent thermal vacuum chambers with high resolution monitoring of the clock's frequency compared to the NRL hydrogen maser references. The units' internal monitors that would normally be sent as telemetry and environmental test conditions are monitored and recorded with high resolution.

Output from one of the two units has been used as input to the NRL Time Keeping System Simulator (TKSS). The TKSS was originally built to evaluate the implementation and algorithms used in the Block IIR on-board Time Keeping System (TKS), which determines the satellite's clock signal to the transmitter. Data from the TKSS have been used to evaluate TKS on-orbit performance and serve as an analysis reference. RAFS data from the beginning of the test on 31 March 1997 to August 1998 and representative TKSS data will be presented. Frequency stability results of the RAFS have routinely shown Allan deviation performance in parts in 10^{-14} at one day, much better than initially expected. In addition to the data from the two test units, on-orbit data from the Block IIR clocks is being added to the database for life data analysis as satellites are put into service.

INTRODUCTION

The development of the replacement block of satellites for the Global Positioning System (GPS) known as the Block IIR satellites incorporated a different implementation of the on-board frequency standards. Additionally, new frequency standards were introduced that had no actual flight history on which to base performance and lifetime. The Rubidium Atomic Frequency Standards (RAFS) designed and built by the EG&G Optoelectonics Division of Salem, Massachusetts are the frequency standards being used.

The GPS Joint Program Office (JPO) initiated a special three-year Life Test to attempt to demonstrate the performance and potential of the RAFS units for GPS. The Naval Research Laboratory (NRL) was

chosen as the agency to conduct the test. The prime contractor, Lockheed Martin, was placed under contract by the JPO to supply two flight-qualified RAFS units from the operational build of the Block IIR satellites. Consequently, subcontracts with ITT and EG&G were let to supply materials and support the Life Test. The system operators at the Second Space Operations Squadron (2SOPS) and Aerospace Corporation are also participating in the conduct and analysis of the Life Test data.

PURPOSE OF TEST

A three-year continuous Life Test is to build confidence in the RAFS units for GPS operations and possible follow-on applications [1]. Flight candidate RAFS units from the operational satellites are being evaluated in space-like conditions and environment, designed to be as close to actual operating conditions as possible. Data from this test are to be complemented with on-orbit data from other units launched in the Block IIR satellites to attempt evaluation of the lifetime characteristics of these units as a class of devices. From these data the operating life, probability of failure, and other related mission parameters may be quantified for the RAFS as a class of units[2]. In the development of atomic clocks for GPS, a test of this type had been desired for the different units being used, but launch schedules and availability always precluded the attempts. In this case, the test data and units can also be used as control models for on-orbit performance and possible problem resolution should anything unusual occur in satellites already launched.

TEST CONFIGURATION

RAFS serial numbers 28 and 30 were provided for the test. Two thermal vacuum chambers with independent baseplate temperature controllers are being used to house each of the units. Spacecraft engineers from ITT who are responsible for installation of the RAFS in the satellites installed the test units in the thermal vacuum chambers at NRL using the same procedures and materials as is used in the satellites. Prior to beginning the actual Life Test, a pretest phase for setup and checkout of the equipment and procedures for gathering the data was performed. This pretest period began with the final checkout of the thermal vacuum systems on 26 February 1997 prior to the delivery and installation of the test units on 3 March 1997. A series of tests and analysis of the data collected by the instrumentation was performed to determine the initial operating guidelines and analysis techniques. These initial parameters were used to guide test performance, to verify methods of analyzing and presenting the data and to set the necessary measurement intervals. After the pretest evaluation of the test instrumentation, the Life Test officially began on 31 March 1997.

The equipment configuration is shown in Figure 1. A dedicated data collection computer (RAFS Tester on the diagram) is allocated to the collection of the telemetry from the units. Each unit is capable of sixteen telemetry outputs during ground test, including the factory acceptance test outputs. In the operational telemetry nine outputs are used. The Life Test telemetry data outputs are listed on Figure 1 and read with 16-bit data words. The satellite telemetry is output with a resolution of 8-bit words. The 16-bit word resolution was selected as a convenient over-sampling size to observe the finer structure. Satellite telemetry could then be duplicated for comparison by truncation of the collected data words. The RAFS Tester, shown in Figure 1, also collects data on input power, test equipment operating and environmental conditions in the test area. Environmental conditions in the test room and associated areas could be used to correlate thermal effects in the test equipment or cabling if necessary.

The output 13.4 MHz signals from the units is converted to 5 MHz by a Numerically Controlled Oscillator (NCO) so that they may be input into the dual-mixer phase measurement systems used for clock evaluation. Two systems are used for redundancy, the Short-Term and Long-Term systems. They

are capable of performing high precision phase comparisons between the test units and the NRL reference hydrogen maser. These data are then collected along with the telemetry data on the Test Facility computer, TAGNT. TAGNT is then accessible to the other networked computers for analysis and archiving.

DATA ANALYSIS

The objective of collecting continuous data was interrupted on several occasions by changes required by the experiment or problems with the instrumentation system. These events are listed in Table 1. The events listed created breaks in the continuous data necessitating the stability analysis to be sectioned. The stability analysis sections are shown in Table 2.

Table 1, Life Test Events

MJD /Date	Unit No. 28	Unit No. 30
50581 5/13/97		Baseplate Temperature Change
50601 6/2/97	Baseplate Temperature Change	
50702 9/11/97	Pressure Change	
50862 2/18/98	Lost Power	Lost Power
50869 2/25/98	Powered Up	Powered Up
50888 3/16/98	Vacuum Pump Failure	
50937 5/4/98	UPS Drop Out	UPS Drop Out
50980 6/16/98	UPS Drop Out	UPS Drop Out

Table 2, Stability Analysis Segments

Unit No. 28	Unit No. 30
Weeks 1 - 47	Weeks 1 - 47
Weeks 48 - 51	
Weeks 52 - 70	Weeks 48 - 70

The first adjustments to the configuration was to change the units operating temperatures due to the determination that the temperature of the units was at such a high value that the internal controllers were not functioning properly. The elevated unit temperature was due to the insulating adapter between the unit and the chamber baseplate. This adapter controls conductive heat flow out of the units to the baseplate and was not conducting as anticipated. The adapter conductance was investigated for the Life Test and the flight units by Lockheed Martin and ITT. Corrective action was taken on the flight units. For the Life Test it was decided to operate at a somewhat lower temperature for one unit and the expected lower flight temperature for the other to enable the internal controllers to function properly. Consequently, RAFS unit 28 was lowered to approximately 17° C and RAFS unit 30 to 8° C. Operation was resumed and no further system temperature setting problems occurred.

Instrumentation problems that occurred subsequently were power related. The thermal vacuum and RAFS controller were on the facility's Uninterruptable Power System (UPS) which fed parts of the laboratory which were to operate without dependence on commercial power. Attempting to maintain continuous power and the UPS system failure during the test resulted in the other breaks shown in the

data.

RAFS UNIT 28

In order to present a brief summary of the findings in the test thus far, the majority of the telemetry data will not be presented. For the most part, these data show little out of the ordinary and will be detailed in a future comprehensive report. The figures that follow will focus on the phase performance and will be shown for RAFS unit 28 first. Figure 2 shows linear residuals to the frequency offset of RAFS unit 28 for the first 47 weeks of operation. A number of frequency breaks or discontinuities can be observed. The time and the amount of the discontinuity is indicated in the figure. These small frequency jumps can be readily seen in a higher order residual. Fifth-order residuals are shown in Figure 3 and the frequency changes are obvious. These changes were observed in only two telemetry channels, the Lamp Output Voltage and the Second Harmonic output, shown in Figures 4 and 5 respectively. The cause of these frequency changes is not fully understood, but is certainly associated with the lamp output. RAFS unit 28 was known to exhibit these types of small jumps before it was chosen for the test.

Another important parameter for these units is the frequency drift. All rubidium standards drift, but it is the change in drift that seriously affects the predictability of operation. For GPS the predictability is very important, since the GPS system is a predicted system and relies upon the ability to accurately predict system parameters for at least a day in advance. Consequently, the daily drift was computed for the RAFS Life Test units to provide an estimate of this parameter and is for RAFS unit 28 in Figure 6. These data show that the rate of change of drift is relatively stable and slowly decreasing. The desired or specification daily drift value is 5×10^{-14}/day.

Correcting the frequency jumps, the Hadamard deviation was computed for the span of 1 to 47 weeks. The deviation is shown in Figure 7. The Hadamard deviation is used because it adaptively corrects for frequency drift and is the statistic used by the operators at 2SOPS to tune the system Kalman filter. This filter is used for prediction of satellite performance and generation of the navigation message broadcast to the users.

Figure 8 shows the frequency offset for the span of weeks 48 to 70. The frequency jumps can still be observed with another discontinuity around the end of March associated with a vacuum break. Some vacuum was lost at that time, but determination of the exact disruption was not possible due to the limited range of the vacuum gauge. A brief partial loss of vacuum is believed to have occurred, not a complete loss. The regularity of the frequency jumps changed as a result of the vacuum loss. This can be deduced from the cumulative frequency corrections shown in Figure 9. The regularity of the frequency changes occurring between the pressure changes, resulting in a gradual cumulative increase in frequency offset, is curious. Investigations into the causes of these changes are continuing.

Correcting for the jumps, a comparison of the stability for the first and second spans of data is shown in Figure 10. The stability is quite consistent and is approximately 8×10^{-15} at one day.

RAFS UNIT 30

The phase offset for RAFS unit 30 for weeks 1-47 is shown in Figure 11. Only one of these small frequency shifts was observed over this entire span. This unit has been very well behaved throughout the test. Comparison of stability for the two main periods of continuous data, weeks 1 to 47 and weeks 48 to 80, is shown in Figure 12. These data indicate a possible improvement in the long-term stability between the two periods. Previous tests on the prototypes and engineering models of these units had shown that,

148

with time, these units tend to improve in stability and rate of change of drift. This unit appears to be following that trend.

The stability performance of the two units for the different evaluation periods is summarized in Figure 13. The Allan deviation values given are uncorrected for drift, so they would naturally be higher than drift corrected values, but are used for comparison. The values indicated as "corrected" are corrected for the frequency shifts previously discussed. Overall stability performance of both units has been outstanding.

To evaluate expected on-orbit performance, a hardware simulation of the Block IIR on-board Time Keeping System (TKS)[3] was constructed during the Block IIR development for investigation of satellite performance. This simulation was called the TKS Simulator (TKSS) to distinguish it from the actual on-board equipment. It functions in the same manner as the flight equipment, with the exception that the output VCXO is not the same. A flight equivalent VCXO has not been available for use in the TKSS. However, the TKSS provides comparable performance to that observed from the satellites.

RAFS unit 30 has been used to drive the TKSS. Data from a Life Test unit can then be compared to the Navstar 43 flight units, which are the only ones on-orbit. For the period of 10 July to 5 August 1998 data from the TKSS and Navstar 43 were compared. The stability of RAFS unit 30 over this period is shown in Figure 14. The TKSS phase offset linear residuals over this span are shown in Figure 15. Data taken from Navstar 43, collected as part of the on-orbit evaluation effort on-going at NRL[4], were used to compare relative performance. The comparison is shown in Figure 16. System noise and short-term performance of the on-board VCXO, which was expected to dominate short-term Navstar 43 performance, apparently does so out to a day. Investigation of this unexpected result will continue as further Block IIR satellites are launched.

SUMMARY

The Life Test is over half way through the planned three-year duration. Performance of the two units under test has been outstanding even with the anomalies observed. These observed anomalies would not have created operational problems for the system operators. The overall performance of both units was much better than anticipated. Efforts to create a more comprehensive database on this class of units with on-board telemetry collected along with performance data are continuing. The increased precision of the Life Test telemetry information with the on-board data should prove invaluable in future satellite operations.

REFERENCES

[1] **Rubidium Atomic Frequency Standard (RAFS) GPS Block IIR Life Test Plan,** version 1.1, 24 March 1997, Naval Research Laboratory.

[2] F. Danzy and J. S. P. Smathers 1998, *"Reliability Assessment Test (RAT) Program Life Data Analysis Methods,"* **Naval Research Laboratory Memorandum Report NRL/MR/8150–98–8161, 8 May 1998.**

[3] **Software Requirements Specification, Appendix C, Timekeeping System (TKS)Description, for the Mission Processor CSCI (Operational Baseline) of the NAVSTAR Global Positioning System (GPS) Replenishment Satellites (Block IIR) Phase II, PS23027807, ITT** Aerospace/Communication Division, 100 Kingsland Road, Clifton, NJ 07014, 25 August 1996.

[4] O. J. Oaks, T. B. McCaskill, M. M. Largay, W. G. Reid, and J. A. Buisson 1999, *Performance of GPS On-Orbit Navstar Frequency Standards and Monitor Station Time References,*" these Proceedings.
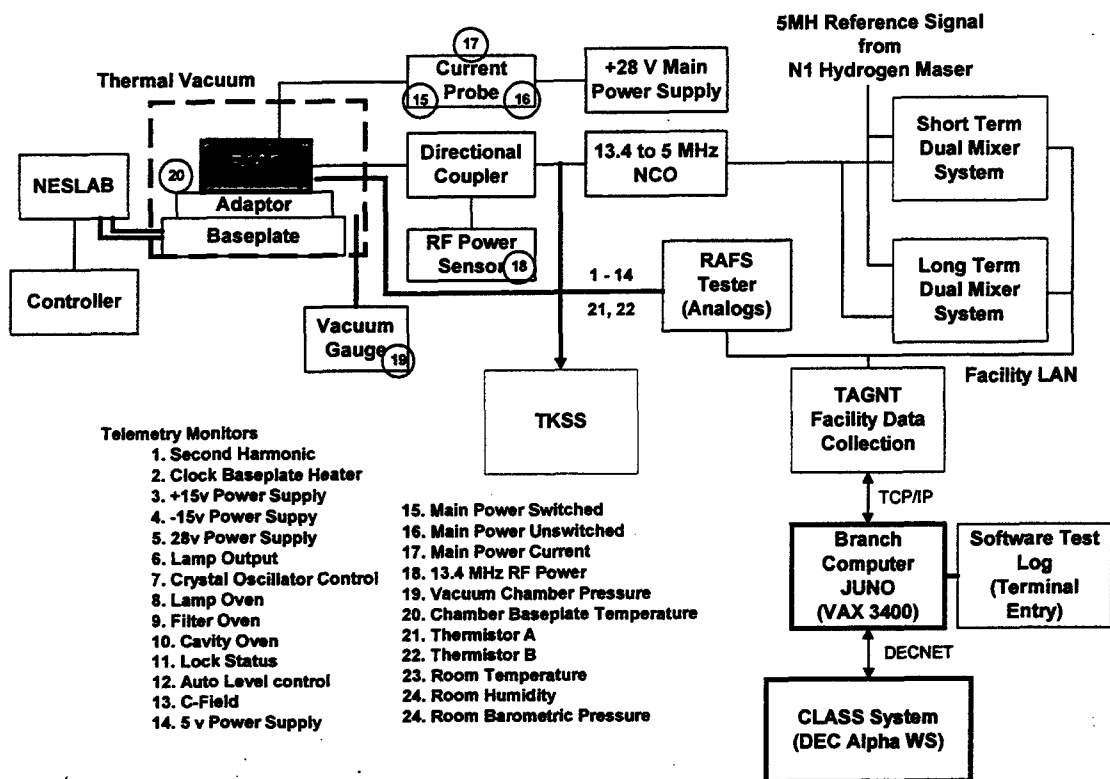
Fig. 1. Life Test Equipment Configuration

Thermal Vacuum

NESLAB

Controller

Adaptor
Baseplate

Current Probe ⑰ ⑮ ⑯

+28 V Main Power Supply

Directional Coupler

13.4 to 5 MHz NCO

RF Power Sensor ⑱

Vacuum Gauge ⑲

5MH Reference Signal from N1 Hydrogen Maser

Short Term Dual Mixer System

Long Term Dual Mixer System

1 - 14

21, 22

RAFS Tester (Analogs)

TKSS

Facility LAN

TAGNT Facility Data Collection

TCP/IP

Branch Computer JUNO (VAX 3400)

Software Test Log (Terminal Entry)

DECNET

CLASS System (DEC Alpha WS)

Telemetry Monitors
1. Second Harmonic
2. Clock Baseplate Heater
3. +15v Power Supply
4. -15v Power Suppy
5. 28v Power Suppy
6. Lamp Output
7. Crystal Oscillator Control
8. Lamp Oven
9. Filter Oven
10. Cavity Oven
11. Lock Status
12. Auto Level control
13. C-Field
14. 5 v Power Supply

15. Main Power Switched
16. Main Power Unswitched
17. Main Power Current
18. 13.4 MHz RF Power
19. Vacuum Chamber Pressure
20. Chamber Baseplate Temperature
21. Thermistor A
22. Thermistor B
23. Room Temperature
24. Room Humidity
24. Room Barometric Pressure

Fig. 2. RAFS No. 28 Frequency Offset, Weeks 1 - 47

151
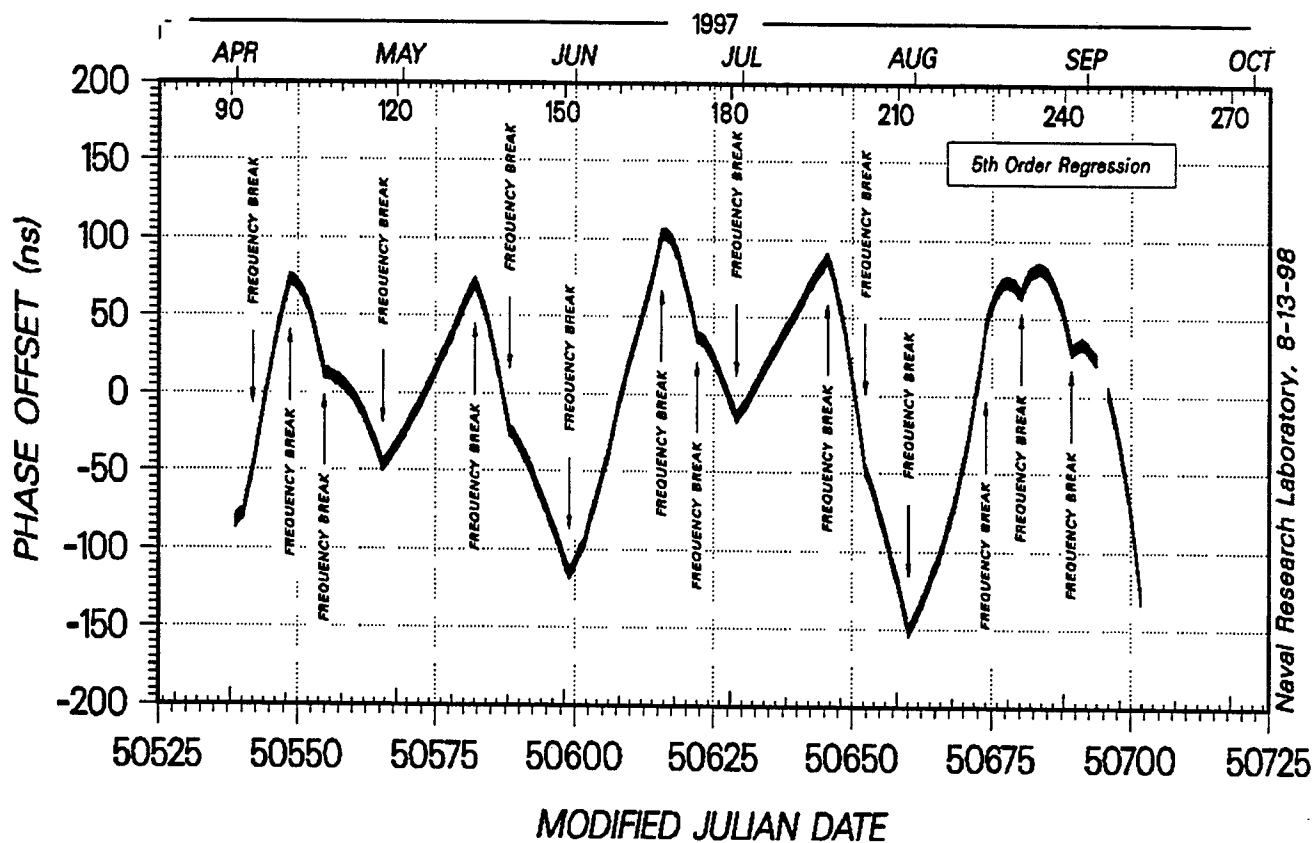
Fig. 3. RAFS No. 28 Phase Offset Residuals Weeks 1 - 24
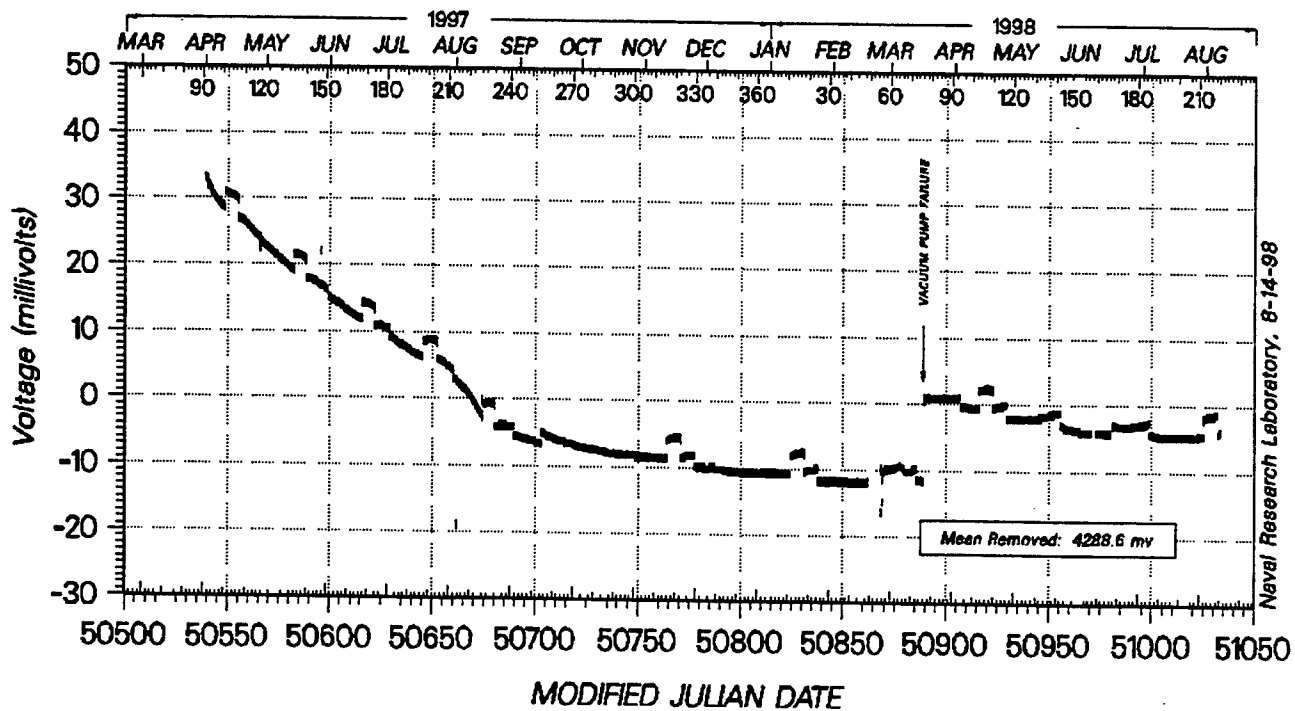
Fig. 4. RAFS No. 28 Lamp Output Voltage
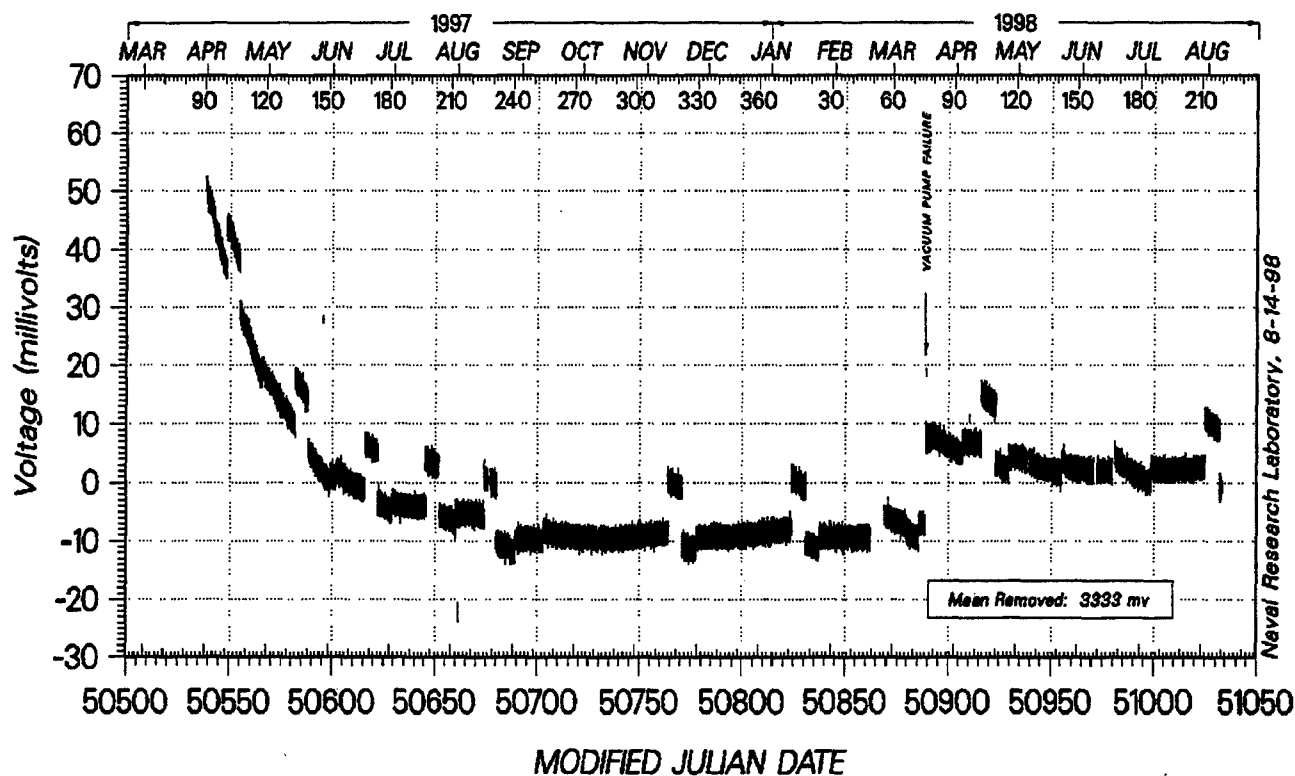
Fig. 5. RAFS No. 28 Second Harmonic Weeks 1 - 70
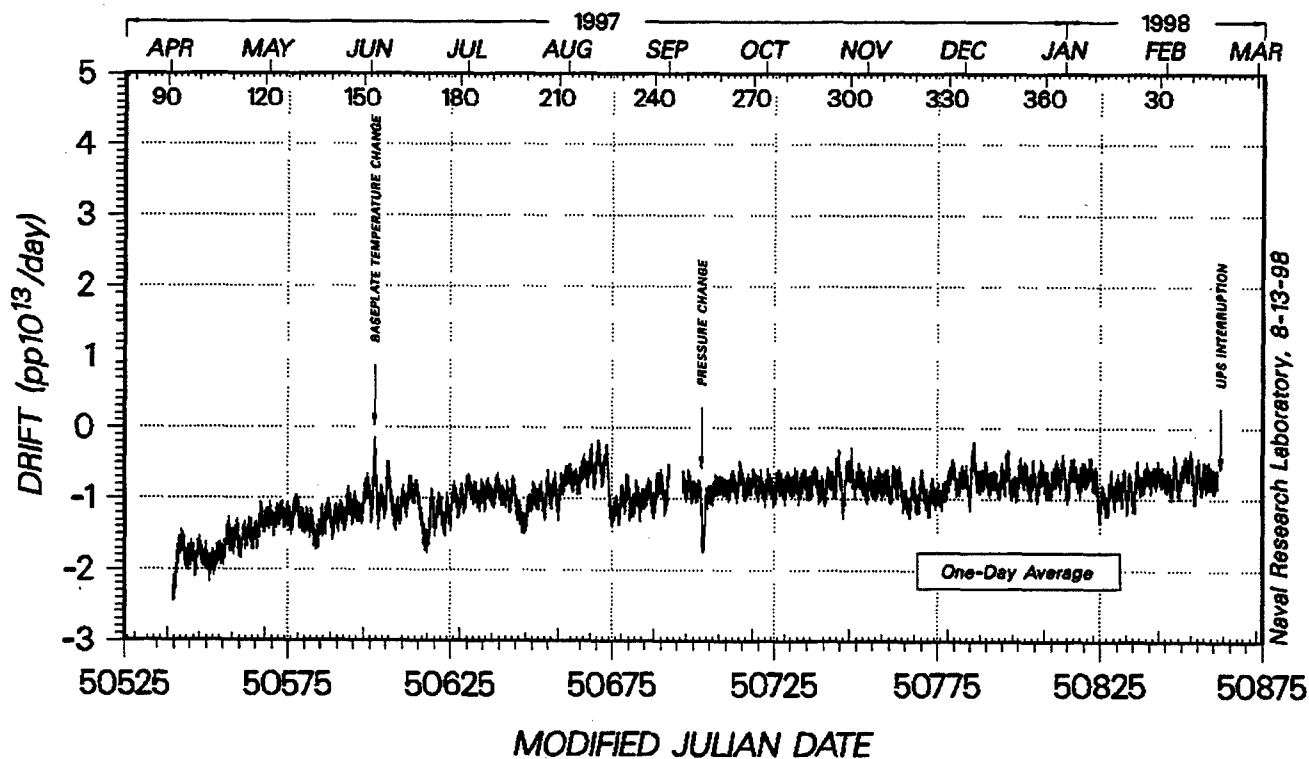
Fig. 6. RAFS No. 28 Daily Frequency Drift Weeks 1 - 47
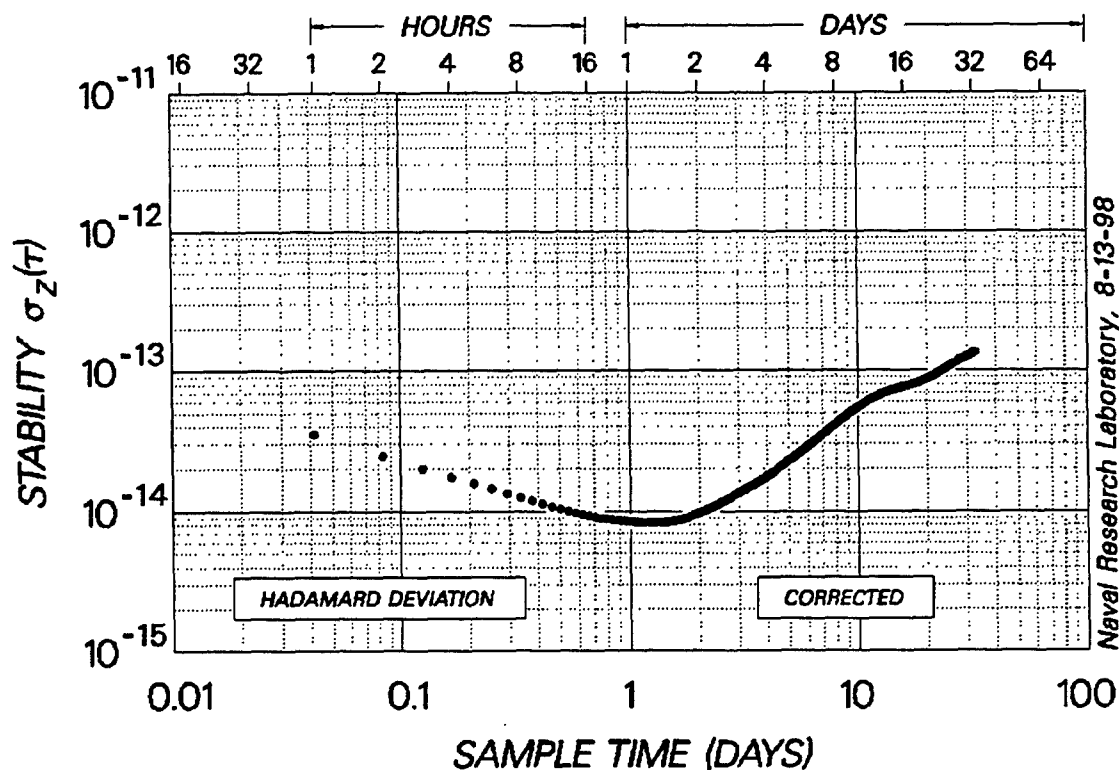
Fig. 7. RAFS No. 28 Stability Weeks 1 - 47
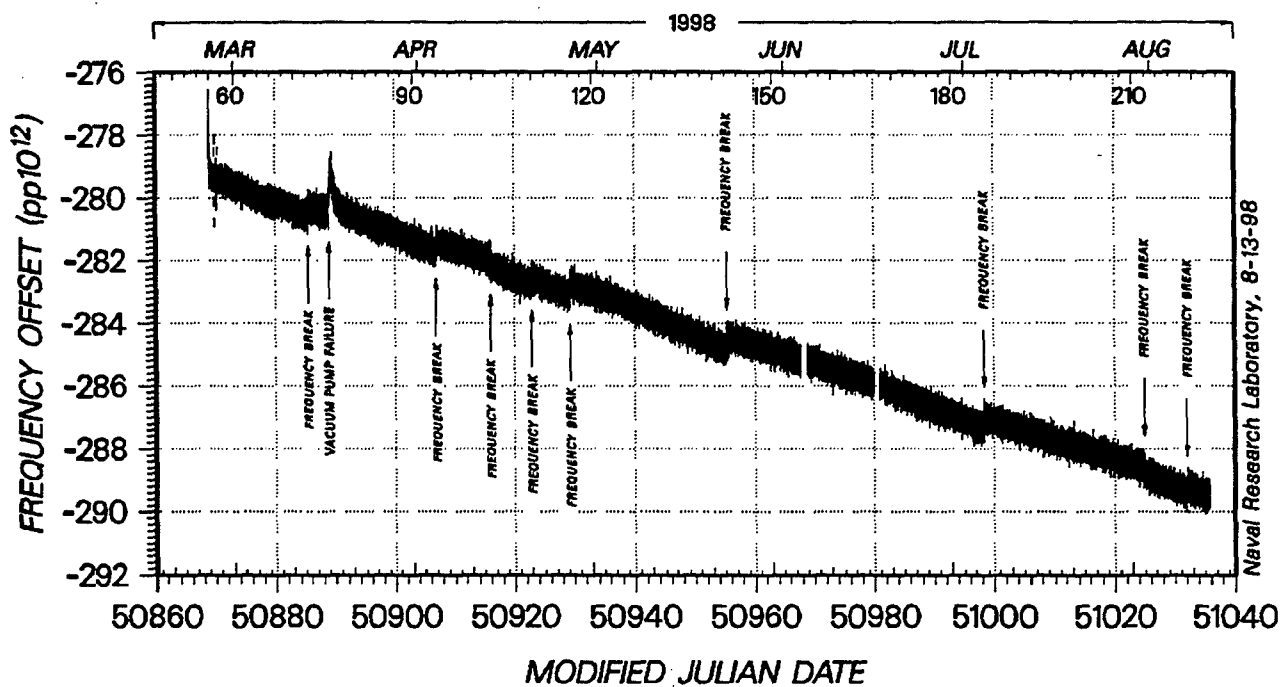
Fig. 8. RAFS No. 28 Frequency Offset Weeks 48 - 70
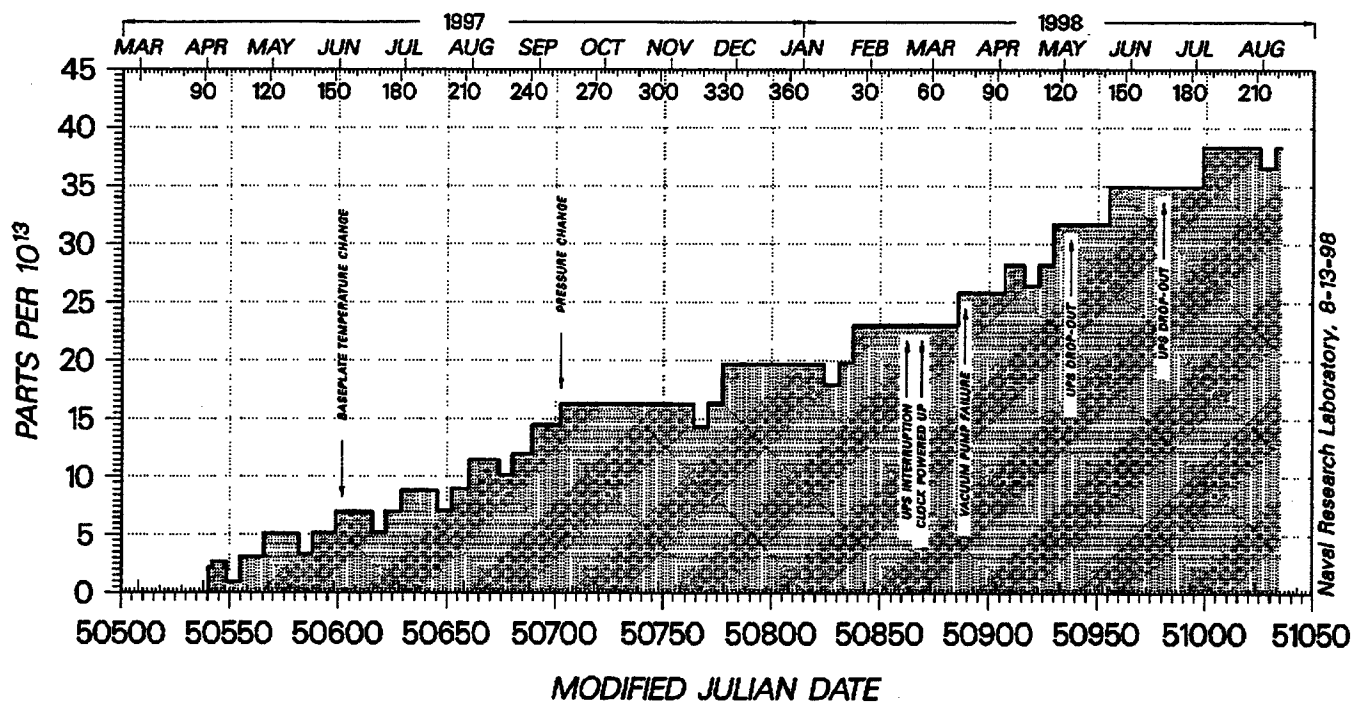
Fig. 9. RAFS No. 28 Cumulative Frequency Corrections Weeks 1 - 70
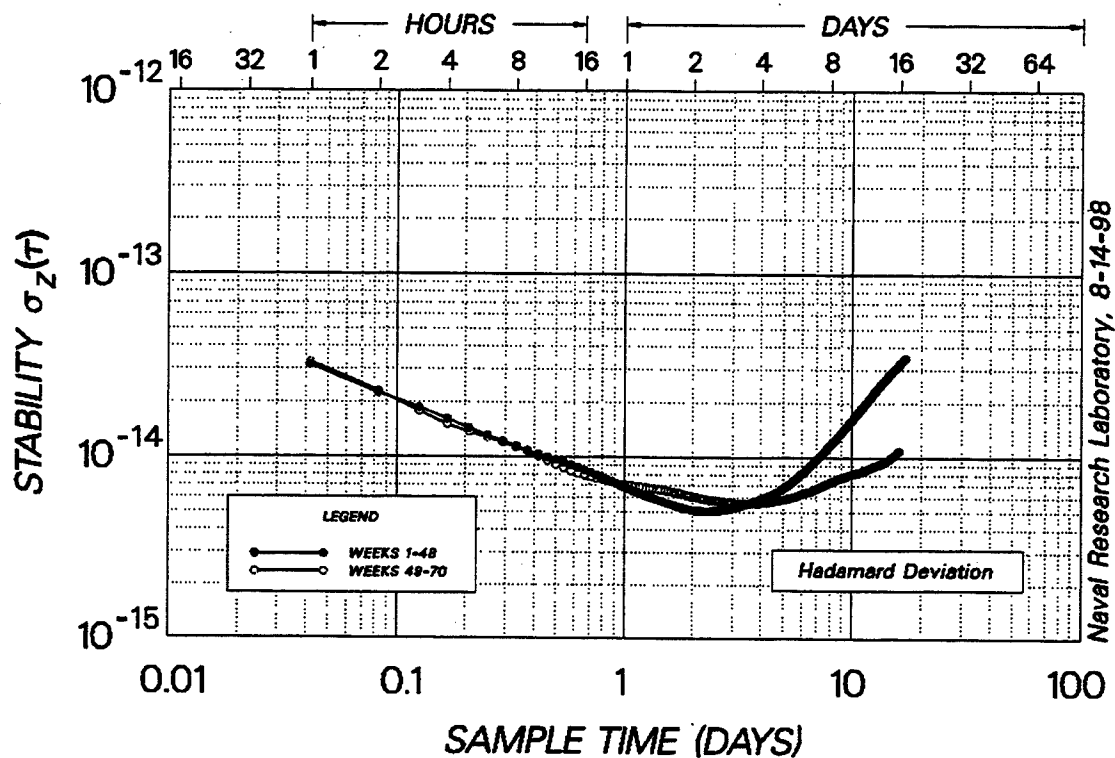
Fig. 10. RAFS No. 28 Stability 31 March 1997 to 11 August 1998
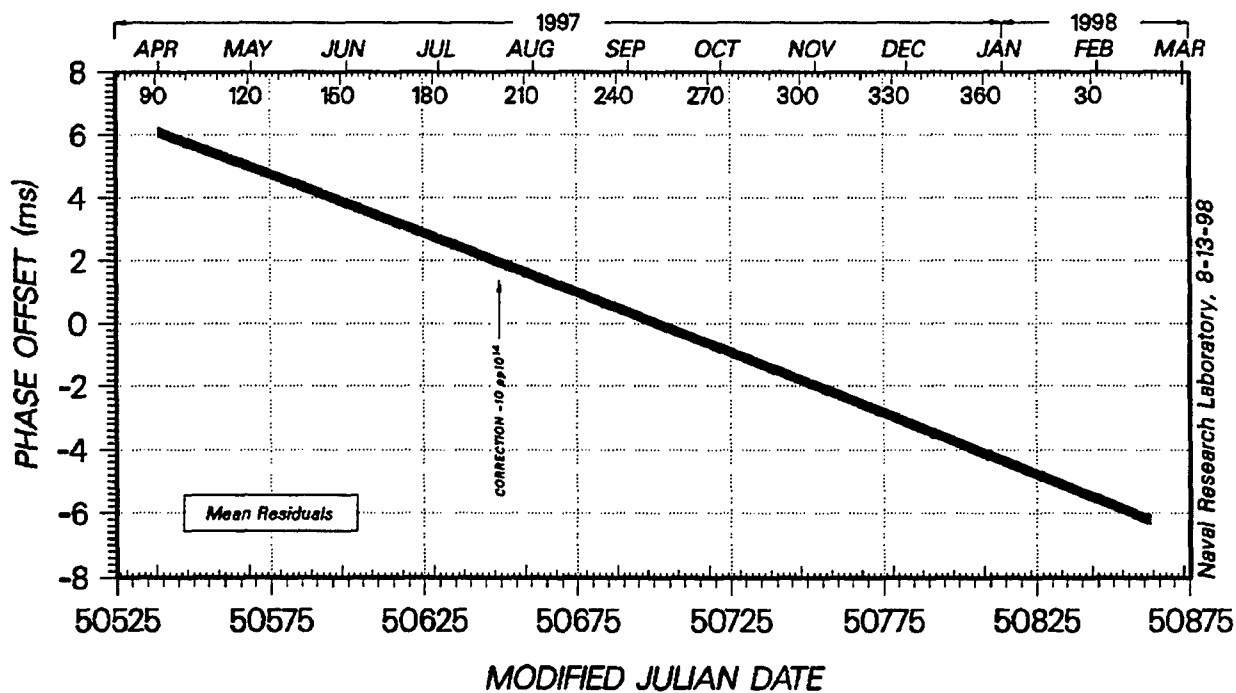
Fig. 11. RAFS No. 30 Corrected Phase Weeks 1 - 47
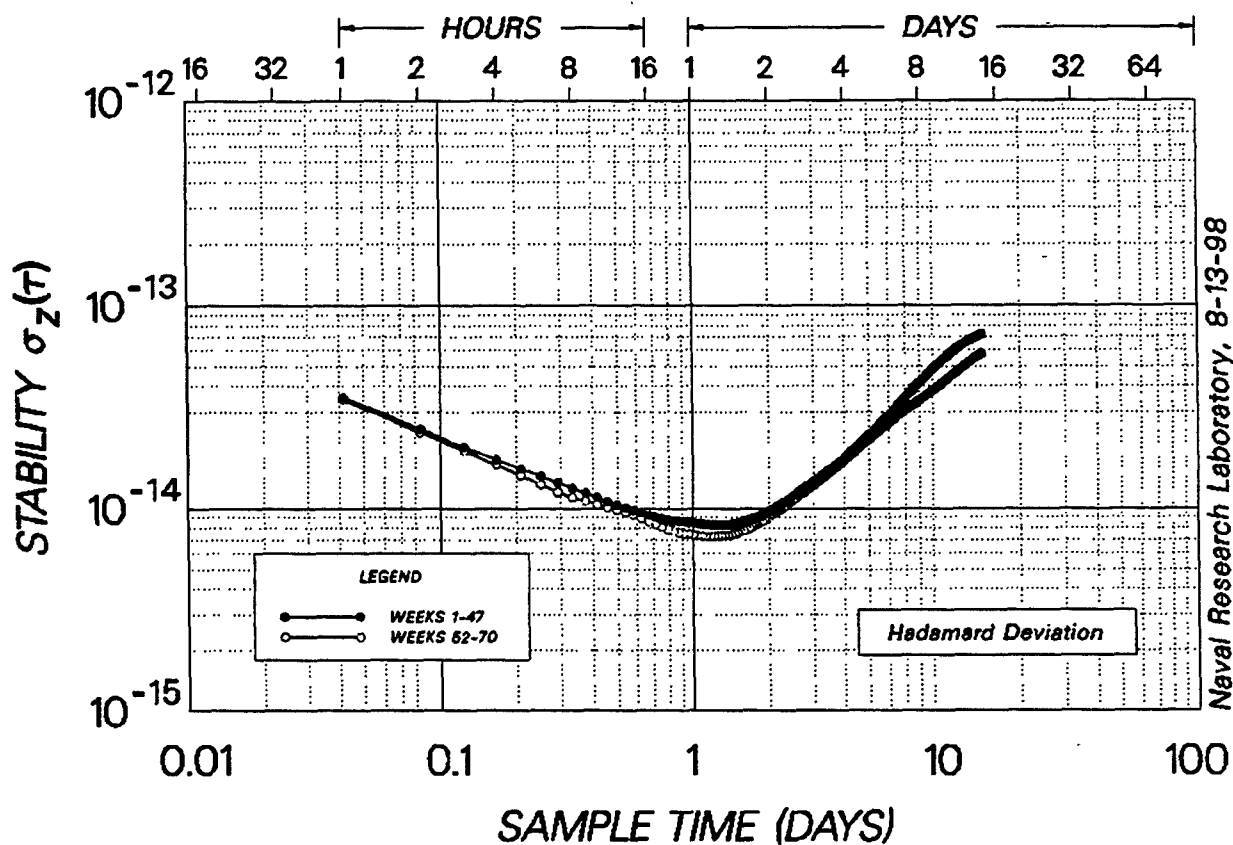
Fig. 12. RAFS No. 30 Frequency Stability 31 March 1997 to 11 August 1998

Unit No.	Data Span (weeks)	Allan Deviation X 10⁻¹⁴	Hadamard Deviation X 10⁻¹⁴
28	1 - 47 uncorrected corrected	7.4 7.2	2.40 0.85
28	52 -70 uncorrected corrected	5.8 5.2	2.60 0.74
30	1 – 47 48 - 70	5.8 3.7	0.68 0.63

Fig. 13. One-Day Stability Summary
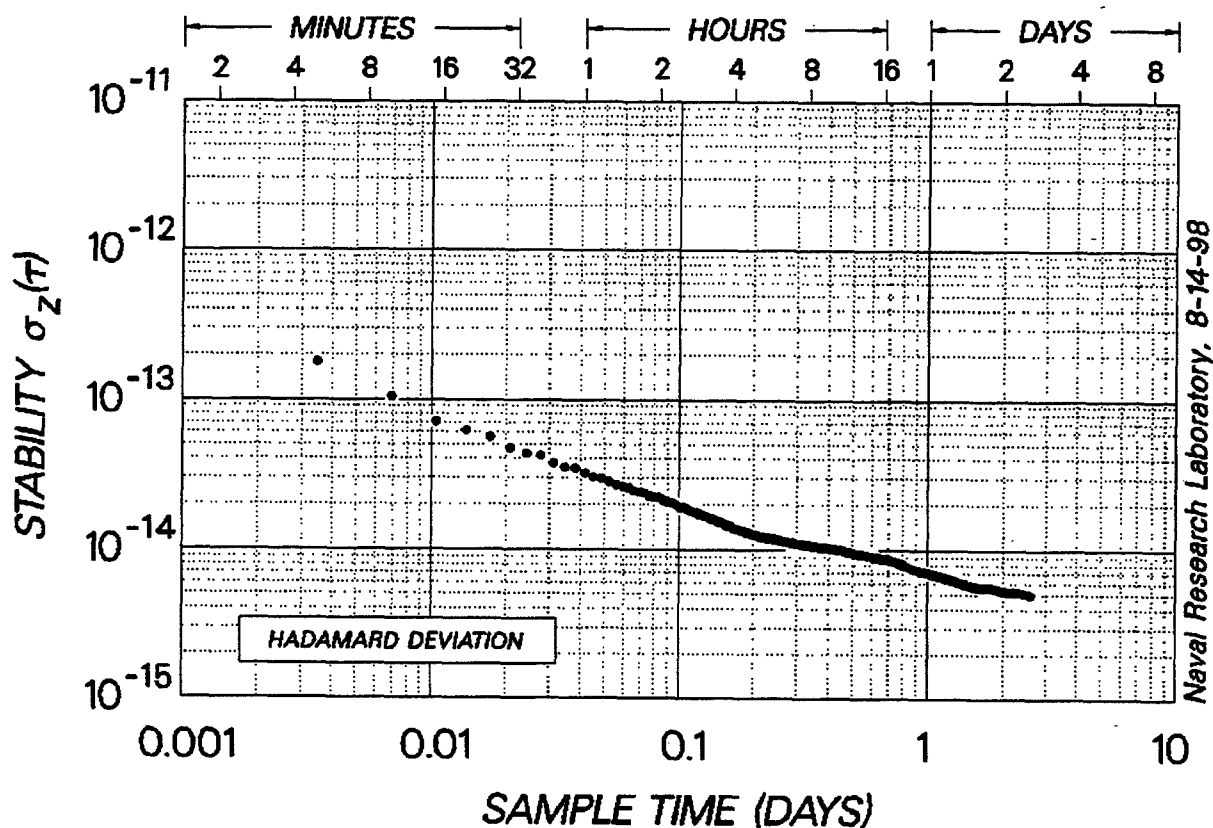
Fig. 14. RAFS No. 30 Frequency Stability 10 July 1998 to 5 August 1998
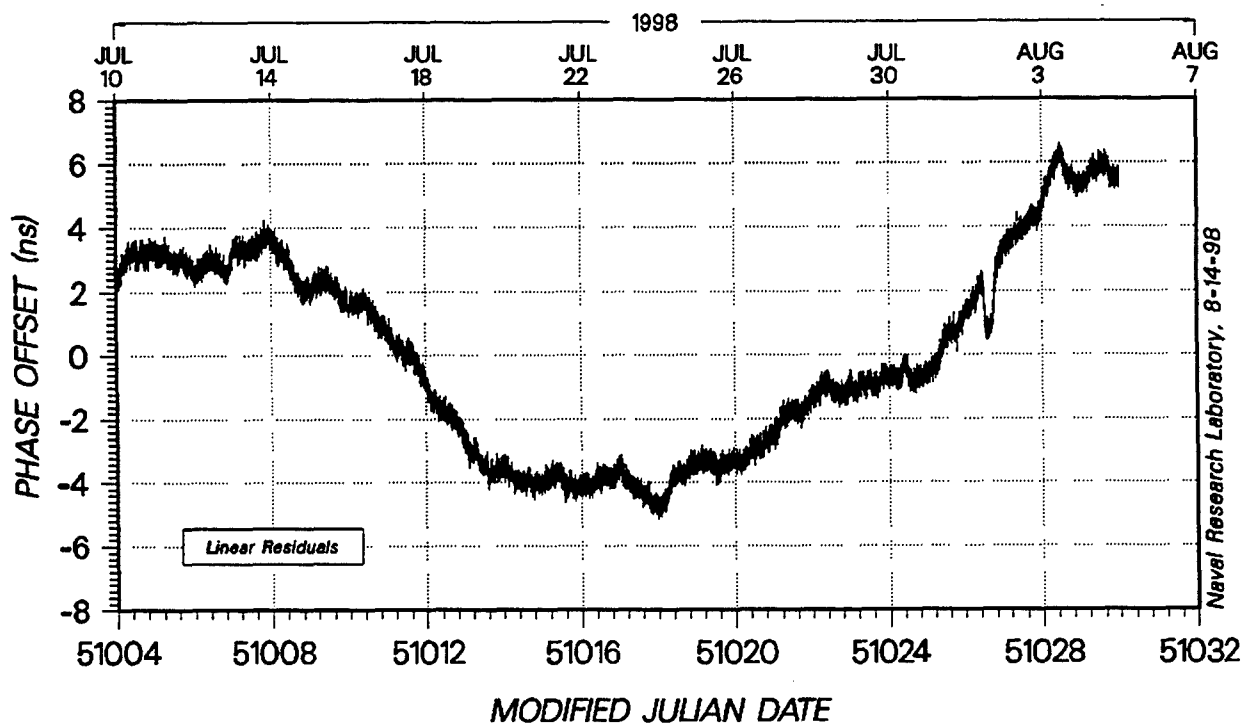
Fig. 15. RAFS No. 30 TKSS Phase Offset
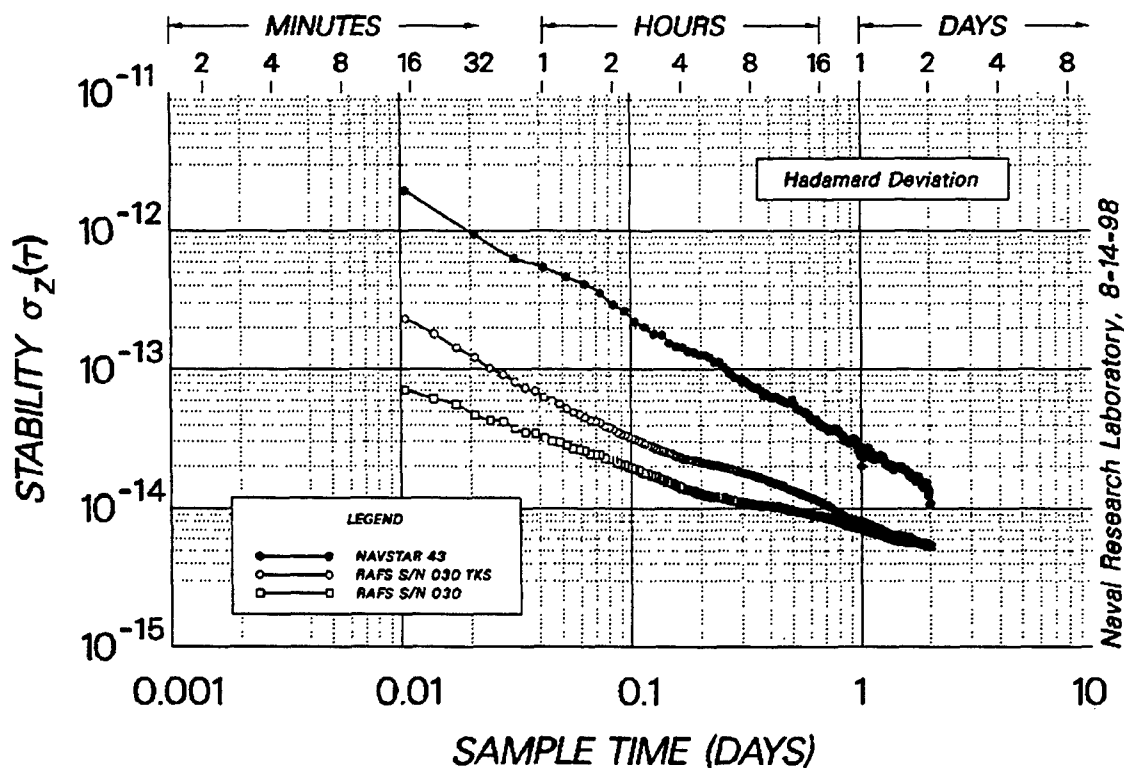
Fig. 16. Frequency Stability Comparison 10 July 1998 to 5 August 1998

Questions and Answers

JIM CAMPARO (The Aerospace Corporation): I think it was RF-28, the first one you showed – it looked like there was a lamp warm-up effect. Did you remove that from the frequency data before you did the Hadamard Variance?

RONALD BEARD (NRL): No. The lamp warm-up does not necessarily show itself in the frequency output. That particular one that I showed was a kind of an anomaly. In the frequency performance, when you look at a longer data span, it does not really make that much significance. In the short term it might.

JIM CAMPARO: I thought I saw a 50-day time constant on the lamp. Was I wrong? Would you please put up the lamp data and the first frequency offset data.

RONALD BEARD: I see. You are talking about this phenomenon here?

JIM CAMPARO: Yes.

RONALD BEARD: Oh, all right. I was thinking of a later one. Yes, that is a warm-up. We do not necessarily remove that from the stability.

JIM CAMPARO: I think if you did, that would probably make the long-term stability look better. It looked like you had an uncorrected drift in that.

RONALD BEARD: Yes, that is probably true.

PATRIZIA TAVELLA (IEN): You spoke of frequency breaks or frequency jumps. Could you comment a bit, please? I think they are not intentional frequency jumps, they are natural. What are they due to? Do we have any statistics on how often they happen and maybe why?

RONALD BEARD: We are still investigating the cause. We think it is probably a lamp phenomenon. We are still trying to determine the frequency of occurrence. It seems to vary in its repeatability, depending on what conditions the unit is involved with. They are very small actual jumps in frequency.

SHORT-TERM CHARACTERIZATION OF GPS-DISCIPLINED OSCILLATORS AND FIELD TRIAL FOR FREQUENCY OF ITALIAN CALIBRATION CENTERS

V. Pettiti, F. Cordara

Istituto Elettrotecnico Nazionale (IEN) G. Ferraris

Strada delle Cacce, 91 - 10135 Torino, Italy

Tel. +39 11 39 19 1, fax +39 11 34 63 84, e-mail: metf@tf.ien.it

Abstract

Quartz and rubidium oscillators disciplined by the signals of the Global Positioning System satellites (GPSDOs) are increasingly used as reference standards in calibration centers and in telecommunication networks, thanks to their cesium-like long-term instability, and several investigations are undergoing in the metrological laboratories of different countries concerning their use for the traceability to the national standards of time. Some of these devices were tested in the past at the Time and Frequency Laboratory of IEN, as regards to their use as frequency and time references in secondary laboratories and their traceability to the Italian standard of time.

In further investigations performed, evidence was found of short-term frequency instabilities, not previously detected, mainly due to temperature effects and to the disciplining algorithms used, that must be taken into account especially in the frequency calibration field. The long and short-term instability results obtained at IEN on some GPSDOs, that show the real uncertainty limits in calibration, are reported in this paper. They are also checked by means of a field-trial on frequency, carried on among some Italian Calibration centers equipped with GPSDOs or other frequency references, using either a free rubidium or a quartz oscillator as travelling standards.

INTRODUCTION

The traceability in Italy to the national time standard UTC(IEN), realized by IEN, of the secondary standards maintained in the calibration centers accredited by the Italian Calibration Service (SIT), can be obtained by means of different synchronization systems, one of the most used now being the GPS in the common-view technique or as a disciplining medium to stabilize the frequency of high quality oscillators [1].

In these disciplined oscillators, the frequency offset and the drift are continuously compensated and therefore a specific approach for the traceability issue has to be followed especially if, as in the case under study, the time signals used in the disciplining process are not originated by the national standard.

The problem of establishing the traceability of the GPSDOs was faced in the past at IEN performing several tests on devices of different manufacturers, leading to a definition of their accuracy and stability limits and of a measurement protocol for their on site calibration [2].

In 1998, the issue of the frequency accuracy and stability of GPSDOs as stand-alone frequency standards, over the observation times involved in the calibration process, has been examined at IEN through an

extensive investigation on eight GPSDOs of different manufacturers, equipped either with a quartz or a rubidium oscillator. The results of these studies and the consequences on the uncertainty budget of the centers accredited for frequency are reported in the following, together with the evaluation of the long-term behavior of some of these devices operating in Italian laboratories, as obtained by implementing the daily measurement protocol agreed upon. Future work envisaged in this field is also outlined.

LONG-TERM CHARACTERIZATION OF GPSDOs

The frequency and time interval measurements performed to estimate the GPSDOs specifications have been referred to UTC(IEN), and the differences between UTC(IEN) and the GPS time scale have been determined with the NBS/GPS receiver used for the international traceability and performing the BIPM common-view (CV) tracking schedule for Europe. The mean frequency deviation between the IEN and the GPS time scales has always been well below $1 \cdot 10^{-13}$ during the instruments testing periods.

The measurement results reported in the following were obtained by means of a Stanford SR620 Time Interval and Frequency Counter, supplying an external 10 MHz derived from UTC(IEN) as a time base. For observation times up to 1000 s, frequency measurements were performed using an additional phase difference multiplier to increase the resolution; meanwhile for longer observation times, time interval measurements were used, started by a 1PPS from UTC(IEN) time scale and closed by a 1PPS supplied by the GPSDO under test.

The indoor equipment and the measurement system was inside the Time and Frequency Laboratory where the temperature has been maintained at $(23 \pm 1,5)$ °C and the AC power stabilized at (220 ± 5) V.

Eight devices from three different manufacturers have been analyzed: two equipped with an ovenized crystal oscillator (OCXO) and labeled in the following as A and B, two with a low drift crystal oscillator (BVA) and labeled as C and D, and four with a rubidium frequency standard (Rb) named E, F, G and H. They have been checked as regards their capability to reproduce GPS time, their short- and long-term instability, their frequency accuracy and the supplying of information useful to establish a traceability to an external reference standard. In some cases the devices have been operated under their default conditions, in others the reference coordinates of the IEN site have been inserted and the receiver forced to operate in "time mode."

The results obtained from daily time measurements and the statistics about the long-term frequency behavior of the GPSDOs under evaluation at the IEN laboratory are reported in Table 1, which clearly shows the effect of the GPS disciplining process, that has compensated for the oscillators frequency offsets and drifts. It can be noticed in fact that the mean relative frequency deviations $\bar{y}$ of the GPSDOs, computed over the whole period from a set of daily averaged frequency deviations, are always negligible in comparison with their uncertainty s_y estimated as the standard deviation of the daily frequency values, and in most cases approach GPS.

Some of these devices have been afterwards remotely tested in the calibration centers where they are operating as reference standards. The measurement protocol for the remote frequency calibration of GPSDOs versus the national time and frequency standard, that requires a calibration center to perform a daily series of 24 time interval measurements between the local 1PPS and the GPS time signals provided by the GPSDO, has been already implemented in six calibration centers that send the results monthly to IEN. Each measurement cycle starts at the beginning of the hour and consists of 60 consecutive time interval measurements; at IEN, 48 daily GPS measurement – lasting 13 minutes each – are performed according to the BIPM CV schedule for Europe. From these two data ensembles, a mean daily time difference between UTC(IEN) and the 1PPS/GPSDO is computed and the daily average frequency deviation of the disciplined oscillator is determined. Plots of Fig. 1, 2 and 3 show samples of the daily

normalized frequency deviations of three GPSDOs computed using the measurement protocol previously described, over a period of three months. Some statistics performed on the data above is summarized in

Table 1 – Long-term frequency behavior of the GPSDOs

GPSDO	A OCXO	B OCXO	C BVA	D BVA	E Rb	F Rb	G Rb	H Rb
days of measurement	98-02-11 98-02-23	98-06-05 98-06-28	98-04-23 98-05-08	98-05-08 98-05-25	98-03-14 98-03-27	98-04-01 98-04-22	98-04-08 98-05-04	98-07-13 98-08-07
y relative freq. deviation	$-0,9 \cdot 10^{-13}$	$0,1 \cdot 10^{-13}$	$-0,6 \cdot 10^{-13}$	$-0,2 \cdot 10^{-13}$	$-0,6 \cdot 10^{-13}$	$0,1 \cdot 10^{-13}$	$3,3 \cdot 10^{-13}$	$0,2 \cdot 10^{-13}$
s_y standard dev. (24 h)	$1,9 \cdot 10^{-12}$	$2,8 \cdot 10^{-13}$	$5,1 \cdot 10^{-13}$	$6,6 \cdot 10^{-13}$	$2,4 \cdot 10^{-13}$	$4,6 \cdot 10^{-13}$	$6,9 \cdot 10^{-13}$	$6,5 \cdot 10^{-13}$
Nr. of samples	12	23	15	17	13	21	26	25

Table 2 that gives the standard deviation of the daily frequency deviations versus UTC(IEN), their upper an lower limits and the number of samples. The mean frequency deviations of the three oscillators, averaged over the same observation time, have not been reported because they are smaller than $1 \cdot 10^{-13}$.

Table 2 – Statistics on remote calibration of GPSDOs

GPSDO	A OCXO	C BVA	E Rb
s_y Standard dev. (24 h)	$0,5 \cdot 10^{-12}$	$1,1 \cdot 10^{-13}$	$1,6 \cdot 10^{-13}$
y_{min}	$-1,7 \cdot 10^{-12}$	$-2,6 \cdot 10^{-13}$	$-3,8 \cdot 10^{-13}$
y_{max}	$1,2 \cdot 10^{-12}$	$2,8 \cdot 10^{-13}$	$4,3 \cdot 10^{-13}$
Nr. of Samples	90	84	79

The fact that the standard deviations computed over 24 hours are smaller than the correspondent ones listed in Table 1, may be due to the smoothing process performed in this case on the data, originated by averaging over the 24 hourly data.

From this long-term analysis of the GPSDOs frequency behavior comes a confirmation that the

measurement protocol adopted is adequate to trace these devices to the national time standard, at least at the level of parts in 10^{-13}, which is perfectly acceptable in most calibration centers.

SHORT-TERM CHARACTERIZATION OF GPSDOs

In the frequency calibration field it is of the utmost importance to characterize the short-term behavior of the oscillator used as a reference in the calibration process. As a sample, in Fig. 4 to 6 have been reported the short-term frequency instabilities of the GPSDOs under test, equipped with different types of oscillators, for averaging times τ of 10 s, 100 s and 1000 s.

The plots show that the instantaneous frequency of the GPSDOs can exceed by orders of magnitude its long-term value, and for $\tau = 1000$ s the frequency deviations values improve significantly over those obtained for $\tau = 10$ s. There is also evidence of periodic variations probably related to the oscillator frequency steering process and to thermal effects.

To get a more complete representation of the short-term behavior of the GPSDOs considered, some statistics over the frequency measurement data has been performed and the results are reported in Table 3.

Table 3 – Short-term frequency behavior of the GPSDOs

GPSDO		A OCXO	B OCXO	C BVA	D BVA	E Rb	F Rb	G Rb	H Rb
$\sigma_y(\tau)$ (ADEV)	1 s	$7,2\cdot10^{-12}$	$4,6\cdot10^{-11}$	$5,9\cdot10^{-12}$	$5,6\cdot10^{-12}$	$6,2\cdot10^{-12}$	$7,9\cdot10^{-12}$	$6,1\cdot10^{-12}$	$7,8\cdot10^{-12}$
	10 s	$4,0\cdot10^{-12}$	$1,0\cdot10^{-10}$	$3,3\cdot10^{-12}$	$3,1\cdot10^{-12}$	$2,7\cdot10^{-12}$	$3,5\cdot10^{-12}$	$3,1\cdot10^{-12}$	$3,6\cdot10^{-12}$
	100 s	$4,2\cdot10^{-12}$	$2,2\cdot10^{-10}$	$1,8\cdot10^{-12}$	$1,7\cdot10^{-12}$	$8,2\cdot10^{-13}$	$8,9\cdot10^{-13}$	$8,8\cdot10^{-13}$	$2,1\cdot10^{-12}$
	1000 s	–	$5,2\cdot10^{-11}$	$2,1\cdot10^{-12}$	$1,9\cdot10^{-12}$	$5,1\cdot10^{-13}$	$9,0\cdot10^{-13}$	$5,6\cdot10^{-13}$	$1,6\cdot10^{-12}$
s_y	1 s	$2,6\cdot10^{-11}$	$3,9\cdot10^{-10}$	$8,3\cdot10^{-12}$	$8,4\cdot10^{-12}$	$7,5\cdot10^{-12}$	$9,2\cdot10^{-12}$	$7,8\cdot10^{-12}$	$9,7\cdot10^{-12}$
	10 s	$1,7\cdot10^{-11}$	$2,8\cdot10^{-10}$	$5,5\cdot10^{-12}$	$6,9\cdot10^{-12}$	$3,0\cdot10^{-12}$	$5,6\cdot10^{-12}$	$3,0\cdot10^{-12}$	$4,9\cdot10^{-12}$
	100 s	$1,6\cdot10^{-11}$	$2,4\cdot10^{-10}$	$5,5\cdot10^{-12}$	$5,6\cdot10^{-12}$	$1,6\cdot10^{-12}$	$3,5\cdot10^{-12}$	$1,0\cdot10^{-12}$	$3,7\cdot10^{-12}$
	1000 s	–	$4,3\cdot10^{-11}$	$4,7\cdot10^{-12}$	$5,7\cdot10^{-12}$	$1,6\cdot10^{-12}$	$3,9\cdot10^{-12}$	$8,6\cdot10^{-13}$	$2,0\cdot10^{-12}$
y_{min}	1 s	$-7,5\cdot10^{-11}$	$-2,1\cdot10^{-9}$	$-4,6\cdot10^{-11}$	$-2,9\cdot10^{-11}$	$-2,2\cdot10^{-11}$	$-2,7\cdot10^{-11}$	$-2,5\cdot10^{-11}$	$-4,3\cdot10^{-11}$
	10 s	$-5,3\cdot10^{-11}$	$-1,2\cdot10^{-9}$	$-1,7\cdot10^{-11}$	$-2,0\cdot10^{-11}$	$-1,1\cdot10^{-11}$	$-1,6\cdot10^{-11}$	$-1,1\cdot10^{-11}$	$-1,5\cdot10^{-11}$
	100 s	$-4,8\cdot10^{-11}$	$-8,2\cdot10^{-10}$	$-2,5\cdot10^{-11}$	$-1,7\cdot10^{-11}$	$-4,9\cdot10^{-12}$	$-1,1\cdot10^{-11}$	$-3,6\cdot10^{-12}$	$-1,3\cdot10^{-11}$
	1000 s	–	$-1,2\cdot10^{-10}$	$-2,4\cdot10^{-11}$	$-2,3\cdot10^{-11}$	$-5,2\cdot10^{-12}$	$-1,2\cdot10^{-11}$	$-4,2\cdot10^{-12}$	$-8,4\cdot10^{-12}$
y_{max}	1 s	$7,2\cdot10^{-11}$	$1,4\cdot10^{-9}$	$1,1\cdot10^{-11}$	$3,8\cdot10^{-11}$	$3,2\cdot10^{-11}$	$3,6\cdot10^{-11}$	$3,9\cdot10^{-11}$	$3,4\cdot10^{-11}$
	10 s	$4,7\cdot10^{-11}$	$1,2\cdot10^{-9}$	$1,9\cdot10^{-11}$	$2,2\cdot10^{-11}$	$1,0\cdot10^{-11}$	$1,7\cdot10^{-11}$	$9,8\cdot10^{-12}$	$1,8\cdot10^{-11}$
	100 s	$4,1\cdot10^{-11}$	$8,3\cdot10^{-10}$	$1,6\cdot10^{-11}$	$2,2\cdot10^{-11}$	$6,7\cdot10^{-12}$	$9,4\cdot10^{-12}$	$2,5\cdot10^{-12}$	$2,0\cdot10^{-11}$
	1000 s	–	$1,2\cdot10^{-10}$	$1,3\cdot10^{-11}$	$2,4\cdot10^{-11}$	$4,3\cdot10^{-12}$	$8,2\cdot10^{-12}$	$5,0\cdot10^{-12}$	$5,6\cdot10^{-12}$
y_β (β=99,7%)	1 s	$5,2\cdot10^{-11}$	$1,3\cdot10^{-9}$	$6,0\cdot10^{-11}$	$3,0\cdot10^{-11}$	$2,6\cdot10^{-11}$	$3,0\cdot10^{-11}$	$2,3\cdot10^{-11}$	$2,6\cdot10^{-11}$
	10 s	$4,2\cdot10^{-11}$	$8,6\cdot10^{-10}$	$1,5\cdot10^{-11}$	$1,7\cdot10^{-11}$	$8,0\cdot10^{-12}$	$1,3\cdot10^{-11}$	$7,8\cdot10^{-12}$	$1,3\cdot10^{-11}$
	100 s	$3,7\cdot10^{-11}$	$6,7\cdot10^{-10}$	$1,5\cdot10^{-11}$	$1,9\cdot10^{-11}$	$4,3\cdot10^{-12}$	$8,2\cdot10^{-12}$	$2,3\cdot10^{-12}$	$1,2\cdot10^{-11}$
	1000 s	–	$1,2\cdot10^{-10}$	$1,2\cdot10^{-11}$	$2,0\cdot10^{-11}$	$3,9\cdot10^{-12}$	$7,4\cdot10^{-12}$	$3,1\cdot10^{-12}$	$5,1\cdot10^{-12}$
Nr. of samples	1 s	4856	4000	3000	4000	3000	3000	4000	4000
	10 s	3000	4000	4000	4000	3000	4000	4000	4000
	100 s	2109	2706	3394	2792	2453	3446	1950	3488
	1000 s	–	689	749	982	694	626	601	851

The frequency supplied by the devices under test has been characterized for averaging times of 1 s, 10 s, 100 s and 1000 s using a frequency difference multiplier and an electronic counter. For each GPSDO has

been reported in the table the following data:

a)   the Allan deviation (ADEV) $\sigma_y(\tau)$,
b)   the standard deviation s_y of the experimental frequency deviations y;
c)   the minimum y_{min} and the maximum y_{max} value of y;
d)   the y_β percentile, that represents the interval including the 99,7% (3σ) of the experimental data;
e) the number of samples.

According to the ISO Guide on Uncertainty in Measurements (GUM) and to Document EAL –R2 of the European cooperation for Accreditation of Laboratories, the calibration centers must declare in their calibration certificates the expanded uncertainty of the results obtained as the standard uncertainty multiplied by the coverage factor $k = 2$, that for a normal distribution corresponds to a coverage probability of about 95%. This means that in our case we have to determine the standard uncertainty of the experimental data, for the observation times commonly used in calibrations, that satisfies the previous requirement.

In all cases, if we compare the ADEV with the y_{min} and y_{max} values, it appears that the first nearly always underestimates the real frequency deviations for every averaging time, and therefore it is not a reliable representation of the uncertainty of the GPSDOs to be used in the computation of the uncertainty budget of a calibration center. The same is also verified if the ADEV values are compared with the y_β ones, that are a more realistic representation of the behavior of the oscillators because they exclude the possible outliers present in the y_{min} and y_{max} values.

On the other hand, also the standard deviation s_y, that in most cases copes better with the range of frequency deviations represented by the y_β values, does not seem to satisfy completely to the criteria of a Gaussian distribution.

Some tests were performed on three sets of experimental data, relative to different observation times, to check their probability density distribution; the corresponding histograms are reported in Fig. 7 to 9, where the continuous line represents the Gaussian fit to each set of data. There is evidence for observation times of 1 s and 10 s that the fit is not representative of the distribution of the experimental data, whereas this works fine for $\tau = 100$ s. But tests performed on the same data sets to check their compliance with a triangular distribution, that in some cases seemed to give a better interpretation of the experimental data, showed that the Gaussian distribution fits better our case.

Coming back to the Allan deviation values, in the frequency stability curve shown in Fig.10 and computed on the experimental data of quartz GPSDO (A) for continuous averaging times τ multiples of $\tau_o = 100$ s, it can be observed that the value of the maximum frequency deviation $\sigma_y(\tau = 4700 \text{ s}) > 3 \cdot \sigma_y(\tau = 100 \text{ s})$ and next to the correspondent s_y value. Therefore the uncertainty estimation given by ADEV versus s_y can be improved by applying the same procedure to all data sets and looking for the maximum ADEV values.

The behavior observable in Fig.10 is typical of disciplined systems that show periodic variations in their output frequencies related to the time constant implemented in the disciplining processes.

FIELD TRIAL FOR FREQUENCY

A first verification of the assumptions of above has been made during an interlaboratory comparison organized in the summer of 1998 among ten calibration centers accredited for frequency by the Italian Calibration Service SIT, to verify the measurement capabilities of these laboratories.

Two kinds of traveling standards with different uncertainty levels were used for this purpose, a rubidium and a high performance quartz oscillator, that have been circulated among the laboratories. The devices

165

have been characterized at the beginning and at the end of the circulation in the reference laboratory, the IEN, as regards to their frequency deviation and frequency drift. Detailed information about the devices specifications, the measurement procedure and the uncertainty evaluation criteria to be followed by the calibration centers were also supplied. Each laboratory was allowed one week time to calibrate the crystal oscillator and two weeks for the rubidium.

The measurement results were reported by the participants in formal calibration certificates that have been evaluated by IEN. Four out of the ten laboratories are equipped with GPSDOs as reference standards; two of them had to characterize the quartz oscillator and the others the rubidium standard. For both devices, the frequency deviations reference values and frequency drift have been determined by IEN, compared with the calibration data received and the compatibility coefficient computed.

This coefficient has been found compliant (<0,5) for both centers involved in the quartz calibration, but only in the case of the rubidium GPSDO the evaluation of the frequency drift was reliable, the short-term frequency deviation of the quartz GPSDO in fact, as previously shown, being at a level that inhibits the evaluation of the quartz daily drift ($2,6 \cdot 10^{-11}$) for the measurement period allowed.

Due to a failure occurred to the circulating rubidium that was replaced afterwards by another device, the data reduction of this loop has not yet been completed, but also in this case we expect that the compatibility of the measurement results is positive in the case of the frequency deviation data, but some problems are foreseen for the drift evaluation.

CONCLUSIONS

The studies, the experiments and the field verifications performed at IEN and in other metrological laboratories [3] on different types of GPSDOs to assess their performances as reliable means of standard frequency and time dissemination and their traceability to a national standard have demonstrated that this goal can be achieved.

To get a reliable uncertainty evaluation on the frequency deviation values that can be reached by a GPSDO in the averaging times from 1 s to 1000 s, commonly used in frequency calibrations, it has been found that the standard deviation or the maximum value of ADEV seem to be the better estimators to be taken into account for the uncertainty budget in calibrations.

A field verification of the assumptions presented in this paper, by means of a circulation of a rubidium oscillator between the calibration centers equipped with GPSDOs, is still ongoing and the first results confirm the assumptions made.

REFERENCES

[1] F. Cordara, V. Pettiti, P. Tavella: *"IEN Time and Frequency metrological activity and support to user needs"*. Proceedings of the 28th Precise Time and Time Interval (PTTI) Applications and Planning Meeting. Reston, Virginia , December 1996, pp. 37-50.

[2] F. Cordara, V. Pettiti: *"GPS Disciplined Oscillators for traceability to the Italian Time Standard"*. Proceedings of the 27th Precise Time and Time Interval (PTTI) Applications and Planning Meeting. San Diego, California , November - December 1995, pp. 113-124.

[3] J.A. Davis, J.M. Furlong: *"A study examining the possibility of obtaining traceability to UK national standards of time and frequency using GPS-disciplined oscillators"*. Proceedings of the 29th Precise Time and Time Interval (PTTI) Applications and Planning Meeting. Long Beach, California , December 1997, pp. 329-343.

Normalized frequency deviation vs. UTC(IEN)
April - June 1998 (April 1 = MJD 50904)
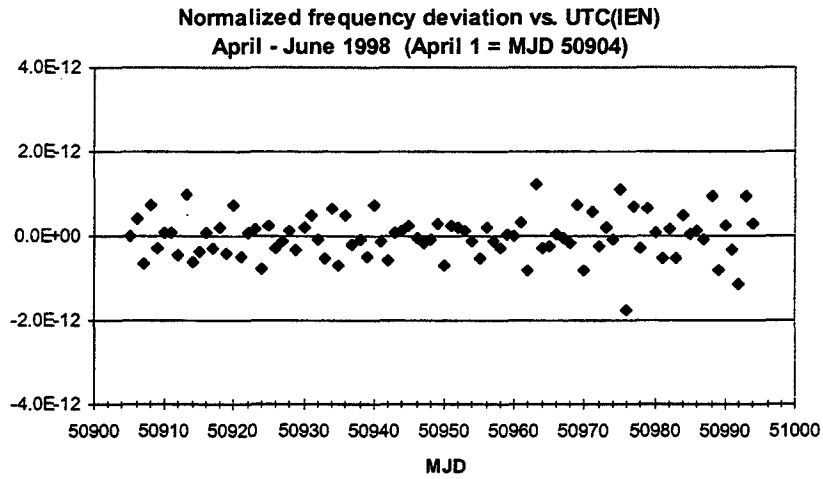
Fig. 1 – Remote calibration of a GPSDO (A) with an OCXO

Normalized frequency deviation vs. UTC(IEN)
April - June 1998 (April 1 = MJD 50904)
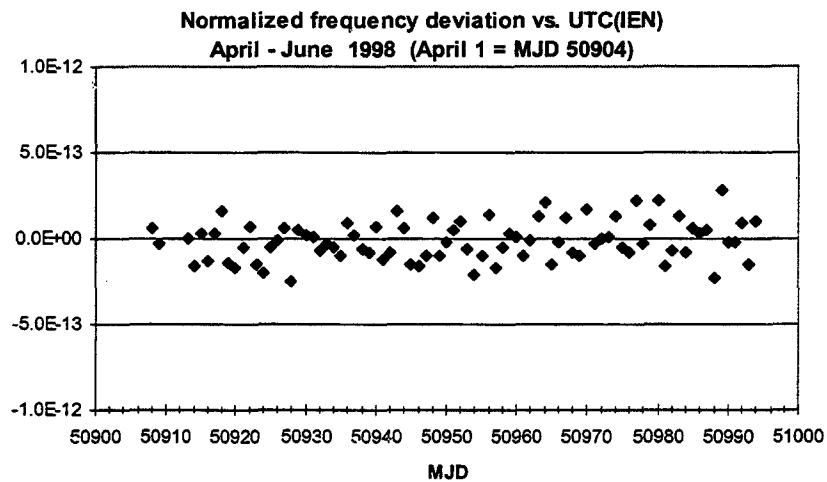
Fig. 2 – Remote calibration of a GPSDO (C) with a BVA

Normalized frequency deviation vs. UTC(IEN)
April - June 1998 (April 1 = MJD 50904)
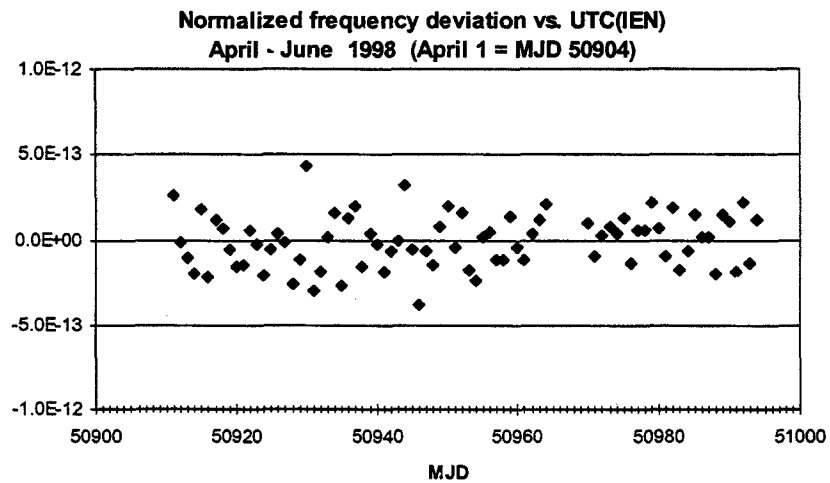
Fig. 3 - Remote calibration of a GPSDO (E) with a Rb

167
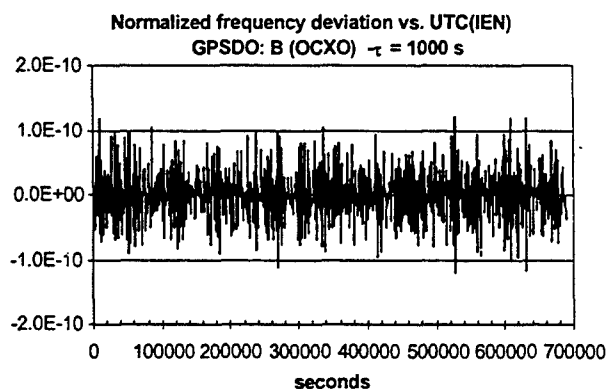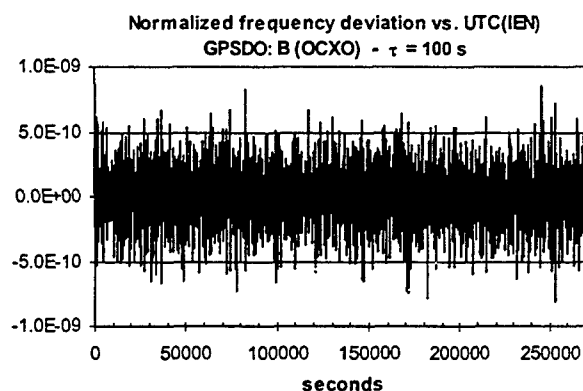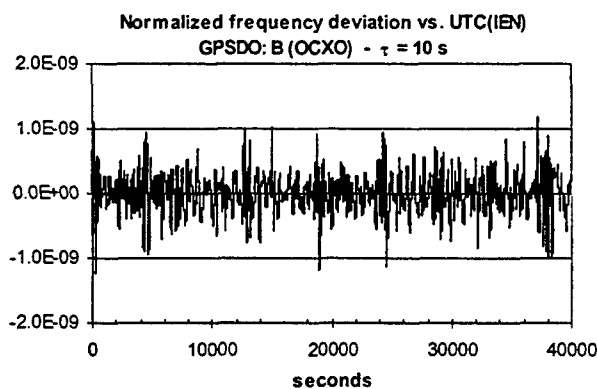
Fig. 4 – GPSDO (B), with an OCXO, for different measuring times
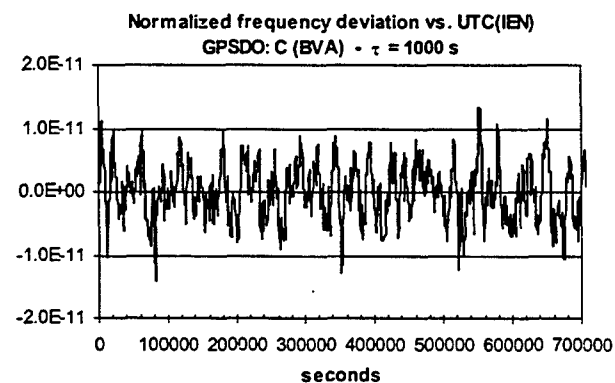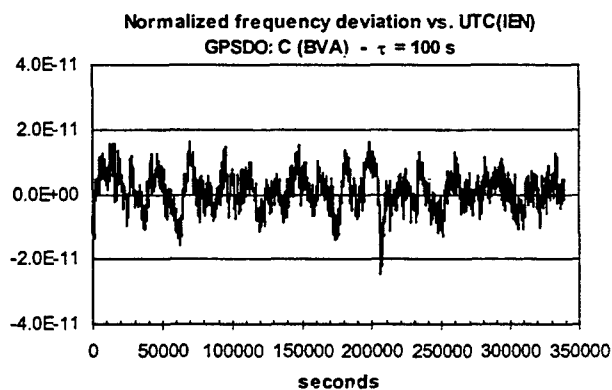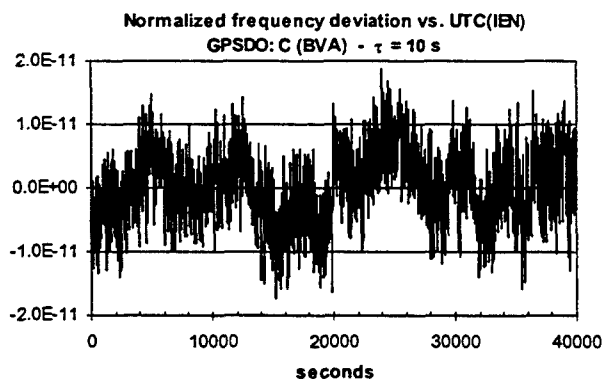
Fig. 5 – GPSDO (C), with a BVA, for different measuring times

168
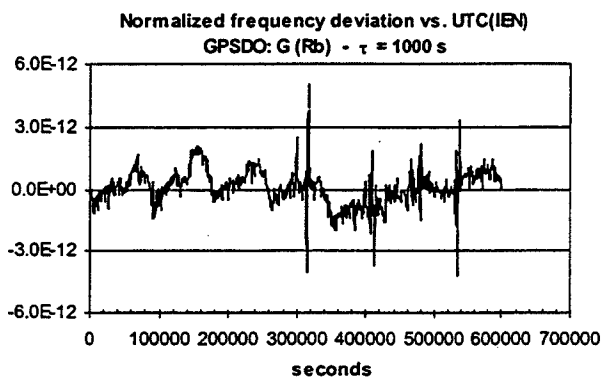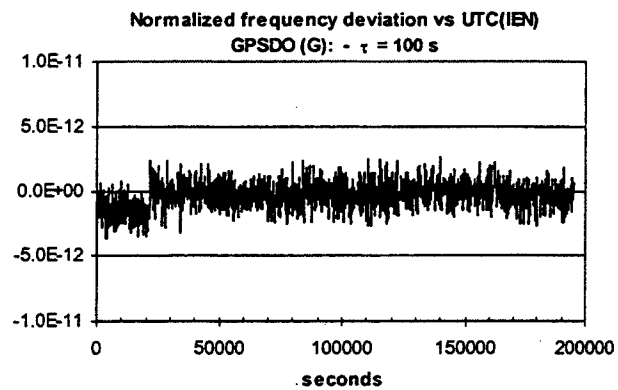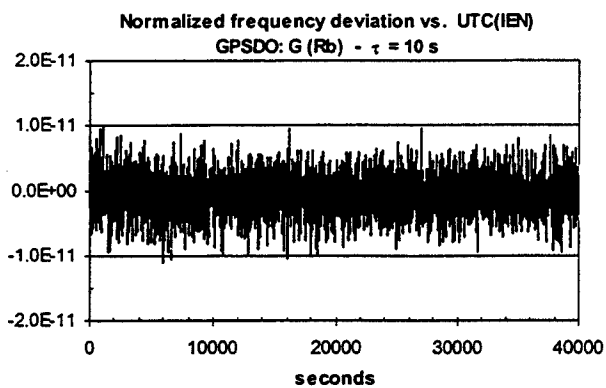
Fig. 6 – GPSDO (G), with a Rb, for different measuring times
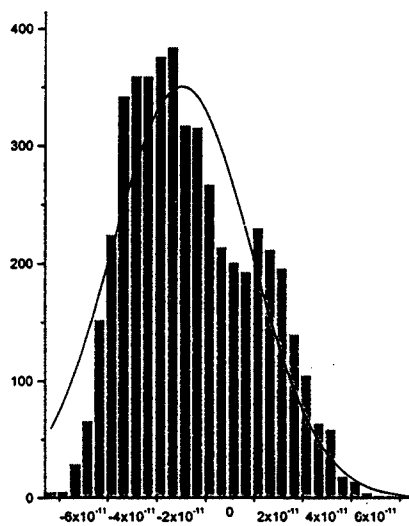
Fig. 7 – Frequency output histogram of GPSDO (A) for measuring time of 1 s
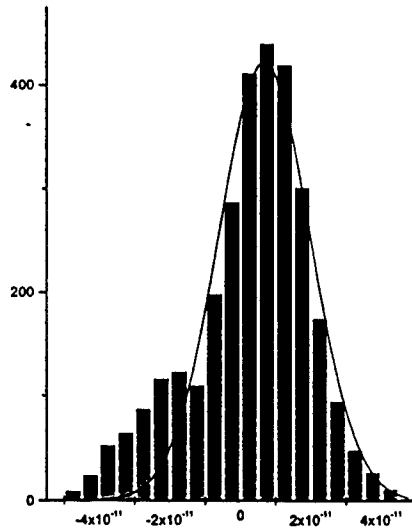
Fig. 8 – Frequency output histogram of GPSDO (A) for measuring time of 10 s
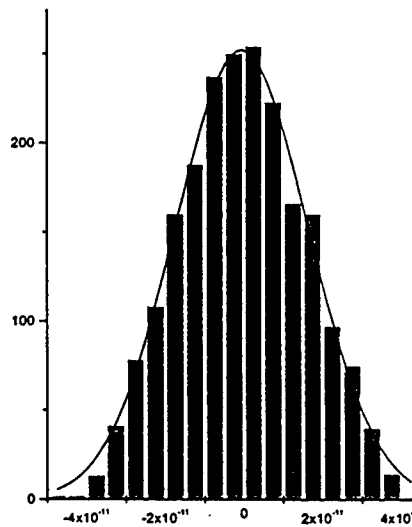
Fig. 9 - Frequency output histogram of GPSDO (A) for measuring time of 100 s
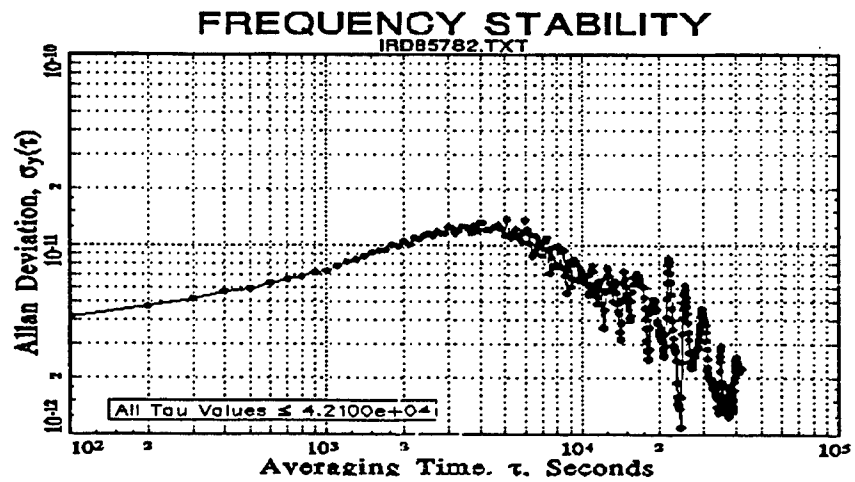
Fig. 10 - ADEV vs. time of GPSDO (A), equipped with an OCXO, for measuring time of 100 s

Questions and Answers

ROBERT DOUGLAS (NRC): That is very beautiful work. I am interested in your feelings about the statistical control of the other variables. Your calibration certificate is something which has evaluated some things, but there is a question of monitoring the stationarity of things like multipath, interference, even spoofing, or the GPS system itself. I am wondering how you integrate your calibration certification with a program for assurance that these elements, are in fact, under statistical control.

FRANCO CORDARA (IEN): Well, of course, what you are saying is something that can be done in the National Lab on each device. But I cannot foresee, in the case of secondary centers, that there are the quality of oscillators to continue this kind of observation to improve what we get. Of course, there are uncertain limitations in the way of evaluating them. I would call it a good compromise to leave these oscillators, after initial calibrations, in the National Laboratory completely free running. So, it is a compromise solution between the optimum and the worst.

I do not know if it has been clear – one thing that is very important to be aware of is not to look in the specifications of this kind of oscillator, only to the long-term accuracy of these devices when they work in the short term. In the short term, you have even two-times worse figures you have to take into account; and to make a proper characterization, at least once for all.

ANALYSIS OF ON-ORBIT BEHAVIOR OF GPS BLOCK II-R TIME KEEPING SYSTEM

Todd Dass, John Petzinger, John Rajan, Harris Rawicz
ITT Industries
Aerospace/Communications Division
100 Kingsland Rd
Clifton, NJ 07014-1993

Abstract

This paper presents three phases of the Time Keeping System analysis (TKS) of the first on-orbit GPS IIR Satellite, SVN 43. The first phase is a comparison of the performance of the SVN 43 Rubidium Atomic Frequency Standard (RAFS) to other GPS satellite clocks. The results indicate that the SVN 43 RAFS is performing better than specification and ranks highly when compared to the other clocks in the constellation. The second phase was to analyze all available data to determine the causes of several transients seen in the SVN 43 TKS. This led to a concentration on the RAFS and associated inputs and outputs, as well as the utilization of TKS simulation tools. The third phase was to examine the entire system to determine how to improve our visibility into the TKS operation. This led to an SV software enhancement whose purpose is to buffer TKS related data in SV memory for subsequent dump and analysis. An example will be presented showing the value of this new TKS buffer capability in the investigation of some TKS events that occurred in August 1998.

INTRODUCTION

The first Block II-R satellite (SVN 43) of the Global Positioning System (GPS) Replenishment constellation built by Lockheed Martin Missiles and Space was made available to users on 31 January 1998. ITT ACD built the Navigation Payload for the Block IIR. The Navigation Payload produces the signals for the GPS users. Block IIR provides an order of magnitude enhancement to the GPS system, including accuracy, simplicity, and low on-orbit maintenance. The SVN 43's primary Rubidium Atomic Frequency Standard (RAFS#1) designed by EG&G has been powered since 13 August 1997. The RAFS stabilized quickly, and until 20 December 1997 no unusual phase or frequency jumps were observed.

RAFS STABILITY

Figure 1 and Figure 2 put into perspective the excellent performance that has been seen with the SVN 43 RAFS. These charts were made with the use of the precise clock data available at the National Imagery and Mapping Agency (NIMA) website[1]. The SVN 43 RAFS is performing better than the GPS Block IIR one-day stability requirement of $5x10^{14}$ parts. The chart depicts

rubidium clocks with a clear bar and cesium clocks with a solid bar. Note that the rubidium clocks, in general, have the best one-day stability.

NAVIGATION PERFORMANCE

The GPS Master Control Station (MCS) computes an estimated range deviation (ERD) which is an estimate of the range error an authorized user would see using the broadcast ephemeris and clock. The daily peak ERDs for the second quarter of 1998 were averaged and the SVs were ranked in order of this averaged peak ERD,[2] as shown in Figure 3. The ranking in this chart correlates very closely with the ranking by the one-day Hadamard deviation. In other words, as one would expect, the clocks with the higher one-day stability are yielding superior Navigation performance.

TKS DESIGN

A simplified block diagram of the TKS is shown in Figure 4. As can be seen from the diagram, the 10.23 MHz VCXO is kept in phase lock with the RAFS. The 10.23 MHz VCXO provides the heartbeat for the GPS P/Y/CA code ranging signal. Software monitors the difference between the expected phase and actual phase and makes VCXO tuning adjustments to maintain lock of the VCXO to the RAFS.

Transients in either the VCXO or the RAFS will show up as larger than expected phase errors. Capturing these phase error measurements is critical to determining the nature of transient in the TKS. Phase error measurements are collected from telemetry whenever the 2SOPS (Second Space Operations Squadron) is in contact with the SV, which is typically less than 1 hour in any 24-hour period. With limited contact time, it is very unlikely that phase error data will have been captured during a TKS transient. This is why the capability to buffer phase error data on board the SV was recently added.

SUMMARY OF SVN 43 TRANSIENTS

The SVN 43 RAFS has exhibited transient behavior in space for short periods of time. The transients occurred between the fourth and sixth months after AFS turn-on. There were five phase transients identified to date and they are summarized in Table 1. In every case, the phase moved in the same direction.

Table 1. Summary of Transients

When	From AFS On	Size
12/20/97	129 Days	~ +16 μs (non-standard codes)
1/19/98	159 Days	+9.8 ns
1/22/98	162 Days	+12.2 ns
1/22/98	162 Days	+6.8 ns
2/9/98	180 Days	+192 ns (non-standard codes)

The TKS has software logic to autonomously protect GPS users from phase transients larger than 15.84 ns. This logic activated in two of the five events listed above and is identified by the words "non-standard codes." The events large enough to cause non-standard codes are evident to the 2SOPS. In these cases, the 2SOPS took action to correct the phase offset via a new Navigation upload and restored standard codes to get the SV back on line.

The other cases are less noticeable to the 2SOPS since they fall into the normal range of errors that are typically seen with GPS satellites over the course of a day. In these more subtle cases, NIMA data were the first place we noticed the transients. After identifying a transient with NIMA data, we went back to the MCS Kalman reports to verify there was a rise in ERD at the time of day the NIMA data showed a transient.

12/20/97 EVENT ANALYSIS

Telemetry indicated on 12/20/97 07:22:30.0, the TKS went to "fast loop/non-standard codes" in response to unexpected large phase errors of greater than 15.84 ns. Six seconds later, the TKS went to "open loop" in response to the RAFS internal frequency-locked loop going out of lock. 2SOPS first made contact with the SV at 08:10 and telemetry from that contact shows the RAFS internal frequency-locked loop in lock and all the RAFS telemetry to be nominal except for a one LSB change of the RAFS VCXO voltage. The phase error from this contact was extrapolated back to the time of the event (07:22:30.0) to determine that a total phase transient of +16μs was present. This phase transient suggests that the RAFS increased frequency over some interval enough to integrate into +16μs of phase.

An SV memory dump performed during this contact revealed several more clues that helped in the investigation. In particular, the last three phase error measurements were saved, and the fourth prior phase error could be inferred. Also, since this 4th previous phase error caused the TKS to go to "fast loop" mode, we determined that the fifth previous phase error must have exceeded 15.84 ns.

In addition, monitor station measurements collected just prior to non-standard codes imply the occurrence of a RAFS transient rather than a VCXO transient. Those measurements reveal a single measurement with a discontinuity of -114.9 ns just prior to non-standard codes. This is exactly what would be expected with the VCXO tuned to its maximum value. A VCXO transient would have caused several measurement outliers, rather than a single outlier, given the characteristics of the control loop design.

175

In summary, having examined all available data for the 12/20/97 event, it is clear that the RAFS frequency standard changed frequency within a 3-second window to a very large relative frequency offset of about 1.92e-6. The TKS went to fast loop, and 6-seconds later saw that the "lock" bit from the RAFS was off, and then went to open loop. It appears that the RAFS spontaneously re-locked within 10 seconds of the frequency jump, resulting in a phase error of 16 μs. The RAFS frequency returned to the pre-event level, as there were no frequency discontinuities present in the NIMA clock data.

Prior to this event, SVN 43's status had been set "unhealthy" for testing purposes. If users had been using SVN 43, their receivers would have measured a pseudorange error of 40m for one epoch before SVN 43 recognized the error and effectively ceased transmission.

2/9/98 EVENT ANALYSIS

From the NIMA clock data, we derived the +192 ns permanent phase change. These data also showed that there was no permanent frequency change. A frequency change to the VCXO could have caused only a temporary phase change. The permanent phase change is not a multiple of the 74.6 ns RAFS cycle period of the reference timing change, ruling out the digital timing chain components.

Again, there was no S-Band contact during the event and thus no phase error telemetry captured. However, significantly, a one LSB change in the RAFS VCXO control voltage was observed across the event.

Telemetry indicates on 2/9/98 22:33:13.5, the TKS went to "fast loop/non-standard codes" in response to unexpected large phase errors of greater than 15.84 ns. Later at 22:36:18.0, the TKS went to "slow loop," indicating the event had run its course and the phase error measurements had stabilized.

Monitor station measurements just before non-standard codes do reveal outliers and from those outliers, inferences can be made about the characteristics of the underlying transient in the RAFS. For example, a 5.74 ns outlier is visible in the last monitor station measurement just prior to non-standard codes. This implies that the measured phase error was 35.2 ns. ± 1.67 ns and that the TKS must have been in "fast loop."

The phase error vs. time curve for the RAFS for the 2/9/98 event is not as easy to nail down as for the 12/20/97 event. To be correct, a RAFS frequency error vs. time curve must meet the following three conditions:
1. Integrated over time, it sums to 192 ns.

2. The first four phase errors (derived from monitor station measurement data) induced in the TKS loop are in the following ranges: < 3.5 ns, 3.5-15 ns., 15-25 ns., 35.2 ± 1.67 ns.
3. The TKS takes about 123 epochs (1 epoch = 1.5 sec) to return to slow loop.

Given the three constraints listed above, Figure 5 shows a possible scenario in which the RAFS frequency error peaks at 8e-9 and then is gradually corrected (epochs 0-75) until it is finally back to its nominal frequency. The integrated frequency error vs. time is exactly 192 ns.

In summary, the 2/9/98 event looks like a less severe version of the 12/20/97 event. Since the maximum frequency offset of the RAFS was ~ 1e-8, the RAFS internal frequency-locked loop stayed locked, or if it ever became unlocked, the unlock condition was not detected by the SV. The TKS protected users from ~ 60m URE errors by generating non-standard codes when the phase error was < 2m (5.74 ns).

SVN 43 DATA CAPTURE ADDITIONS

Capturing phase error data is critical to help characterize the profile of a transient. As an example of the usefulness of phase error data in characterizing a transient, the Control Segment inserted a four-nanosecond phase step in SVN 43 in September 1997 while phase error telemetry data was being recorded. Figure 6 is a plot of the phase error telemetry data overlaid by simulation data for a four-nanosecond phase step. The simulation was used to verify that we have a valid model of the effects of a phase jump in the TKS of SVN 43.

Since the noise and the transients are similar, we are sure that we have a valid model of the effects of the phase jump on the TKS system.

The next step was to examine the difference between a phase step and a frequency step. A frequency step was introduced into the ASIC Test Bed (ATB) during formal qualification testing (FQT) of the software. Figure 7 contains a plot of the phase error data during the ATB frequency step transient. A simulated frequency step was overlaid to show that the TKS simulation provides an accurate representation of a frequency step. Figure 7 also shows a window that represents the new phase error buffering capability described in the next paragraph. A simulated phase jump was added to Figure 7 to show how data in the window will show the difference in the phase error output between a frequency and a phase step.

A modification to the SVN 43 software was made to add three buffers to capture phase error telemetry in a plus/minus 150-second window around a TKS transient. These data will be buffered in SV memory for later dump to the ground for analysis. These buffers will be utilized to characterize the profile of a transient. We will be able to distinguish between a frequency vs. a phase transient, the size of the transient step, and random wander variation. The size of a phase step is obtained directly, while the initial slope of the phase error plot determines the size of the frequency step. Figure 7 shows the window of phase error telemetry that we can expect to capture around a transient.

177

ON BOARD TKS DATA BUFFERING CAPABILITY

On 16-August-1998, the new trace buffer capability paid off by capturing detailed information about some TKS events. This section will show details of the investigation of the events, which include examples of how we used the new capability, as well as other data to aid in the investigation.

DATA CAPTURED IN TKS BUFFERS

There were a few TKS events that occurred during eclipse season in August. Analyses of these events implicate the 10.23 MHz VCXO and not the RAFS. The new TKS Trace Buffer capability worked very well at capturing valuable evidence to help troubleshoot the events.

The first collection of events consisted of two fast to slow loop transitions on 16-August-1998. Telemetry indicated that the TKS entered the first Fast Loop at 01:46:21.0 GPS followed by entry into non-standard codes at 01:46:22.5 GPS. Standard codes were restored by ground command at 05:35:19.5 GPS, which put the SV back on-line for the users. The ERDs remained low through this event and no upload was required prior to bringing the SV back on-line.

The second collection of events occurred toward the end of eclipse from about 23 August 1998 through 31 August 1998. These events were not visible in the ERDs, but were noticed in the NIMA data as uncharacteristic noise in plots of frequency and first difference of phase. Further examination of phase error telemetry uncovered some outliers that indicated noise in the TKS that was likely caused by noise in the 10.23 MHz VCXO frequency.

TKS EVENT EVIDENCE

The following significant telemetry occurred with the 16 August event:
1) Transition to fast loop at 01:46:21.0
2) Transition to non-standard codes at 01:46:22.5
3) Transition to slow loop at 01:48:04.5
4) Transition to fast loop at 01:51:00.0
5) Transition to slow loop at 01:52:42.0
6) Ground command to standard codes at 05:35:19.5.

The TKS trace buffer showed a runoff of phase error that started around 01:30 and peaked at 01:46:21.0, where fast loop was entered when the TKS exceeded the 15.84 ns failure threshold. A plot of the TKS trace buffers with buffer 0 and buffer 1 combined is shown in Figure 8. Fast loop was able to track out the phase error and a transition to slow loop occurred at 01:48:04.5, but whatever was happening with what we believe was VCXO frequency was still present. Fast loop

again was entered at 01:51:00.0, followed by a transition to slow loop at 01:52:42. The TKS remained in slow loop after the last transition.

2SOPS made the first contact with the SV at 02:11. Phase error telemetry from that contact starts with a positive bias of about 4 ns. This is shown in Figure 9.

The most telling evidence of what may have happened is found in the samples of the frequency estimate variable from the TKS trace buffer and TKS dumps. This plot is shown Figure 10. The plot shows that the 10.23 MHz VCXO may have taken a rapid frequency change of -1e-9 parts on 16 August. It appears that the VCXO frequency took a month to return to its original value. The rapid step change in VCXO frequency on 16 August was faster than the slow loop time constant could keep up with and, thus, the transition to fast loop. Once the VCXO frequency stabilized, the TKS slow loop was able to compensate for it and keep it locked to the RAFS.

Another indication of noise in the TKS can be seen in the plot of the clipping count (Figure 11), which is stored in the TKS trace buffer. The clipping count shows the number of times the phase error crossed the 3.548 ns clipping threshold. As can be seen from the plot, the counter began incrementing, beginning with the 16 August event, and didnt stop incrementing until 1 September. For reference, eclipse season ended on 31 August. During this whole period, the noise in the TKS wasnt passed appreciably into the L-band as ERDs remained low and stable and non-standard codes protected the user from the rapid change on 16 August.

The NIMA phase data did indicate some noise in the TKS that prompted us to look closer into the phase error telemetry. In particular, the first difference of NIMA phase plot (Figure 12) shows some noise in the period between 23 August and 31 August.

There were several outliers noted in the phase error telemetry during this period of noise seen in the NIMA data. One plot shown in Figure 13 indicates the phase error grew to about 10 ns within a ½ hour interval.

THE INVESTIGATION PROGRESS

The investigation into the cause is still ongoing. At this point the RAFS has been ruled out, since there was no permanent phase offset present that was present in the other RAFS-related events. This means that the RAFS has been event free since February 9, 1998. The likely source of this activity falls with the 10.23 MHz VCXO and that has been the focus of current investigation effort.

CONCLUSIONS

The GPS Block II-R Rubidium Atomic Frequency Standard in SVN 43 is the best in the constellation based on the one-and ten-day Hadamard deviations and the second quarter ERDs.

RAFS has exhibited transients. It is still unclear whether these are only beginning of life phenomenon.

The TKS data capture capability now available provides an internal analysis capability that complements the external analysis capability provided by NIMA data and Naval Research Lab GPS clock reports.

The combination of the accuracy of SVN 43 and the analysis capabilities of the data sources insure a more accurate GPS constellation in the future. It also provides a foundation for future satellite designs that provides a better a path to extended GPS constellation availability, integrity, and accuracy.

REFERENCES

[1] http://164.214.2.59/geospatial/products/GandG/sathtml/
[2] ERD data compiled by Dave Koster of Lockheed Martin Missiles and Space
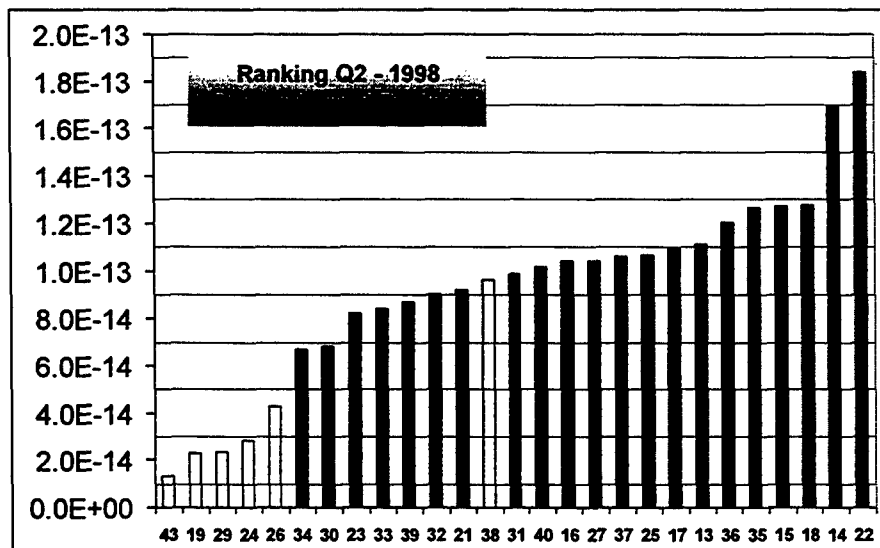
Figure 1. Ranking by 1-Day Hadamard Deviation
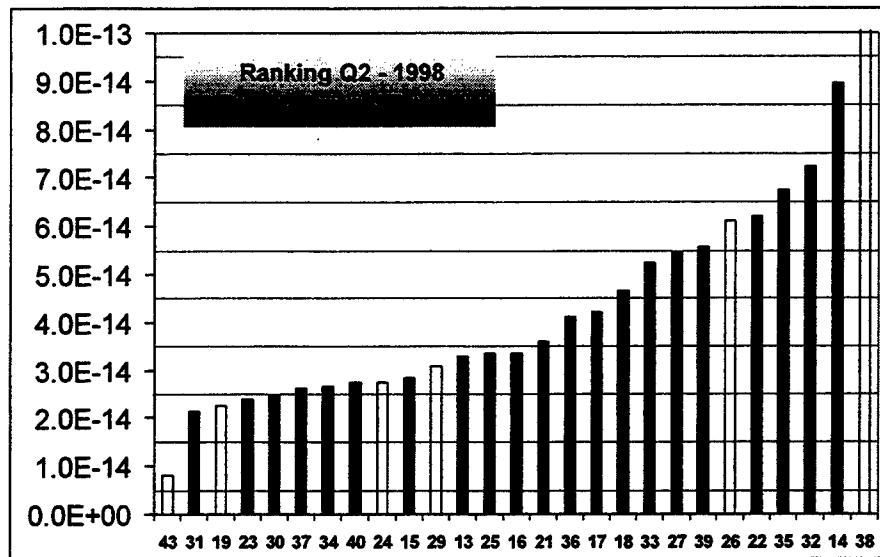
Figure 2. Ranking by 10-Day Hadamard Deviation
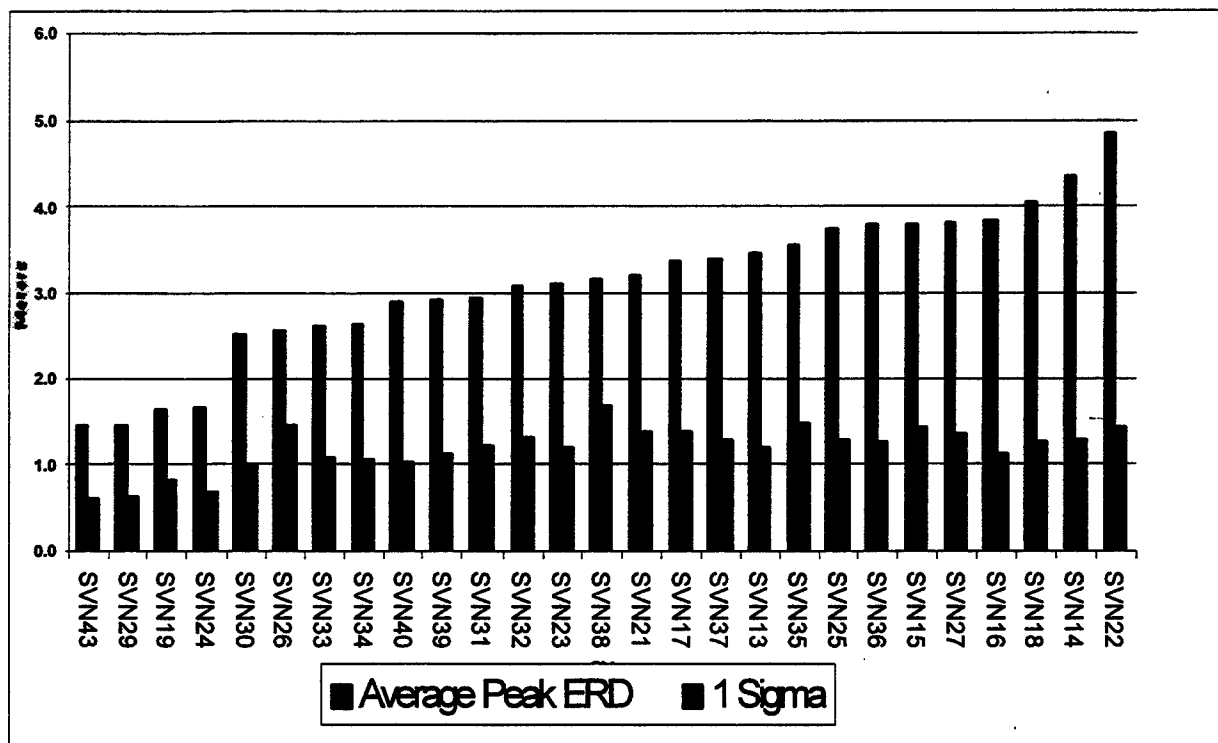
Figure 3. Ranking by ERD
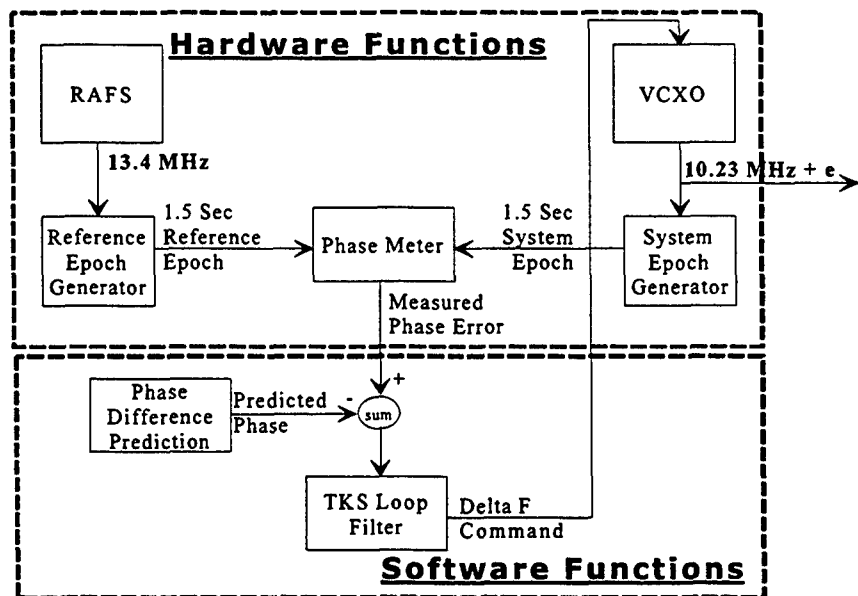
Figure 4. TKS Block Diagram
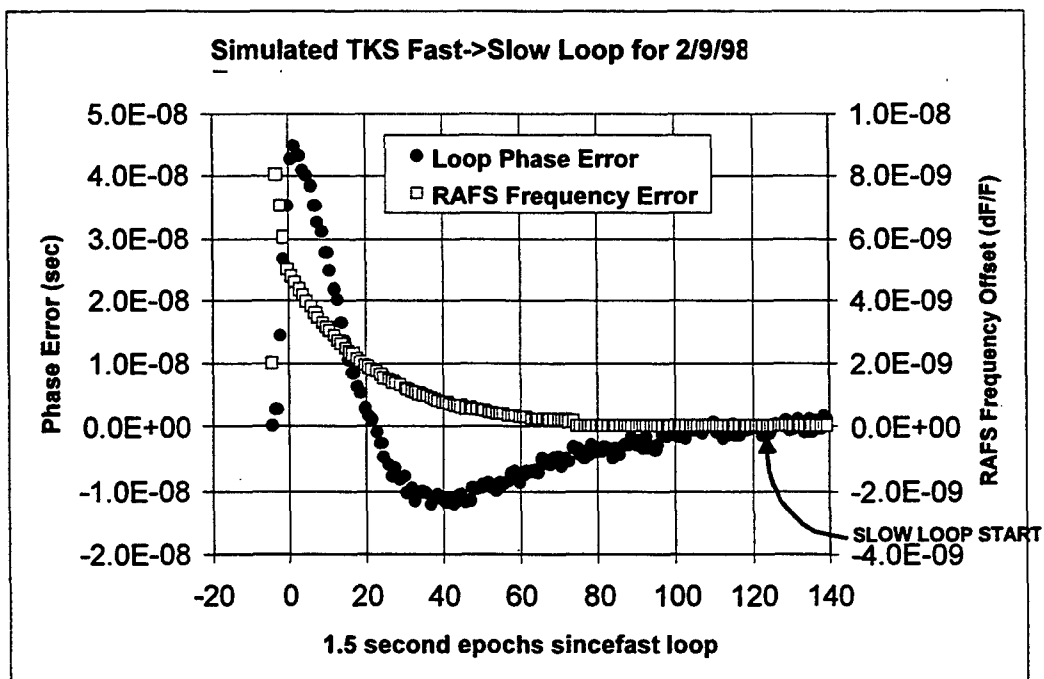
Figure 5. Feb. 9 Event Simulated Transient Profile

PHASE METER ERROR
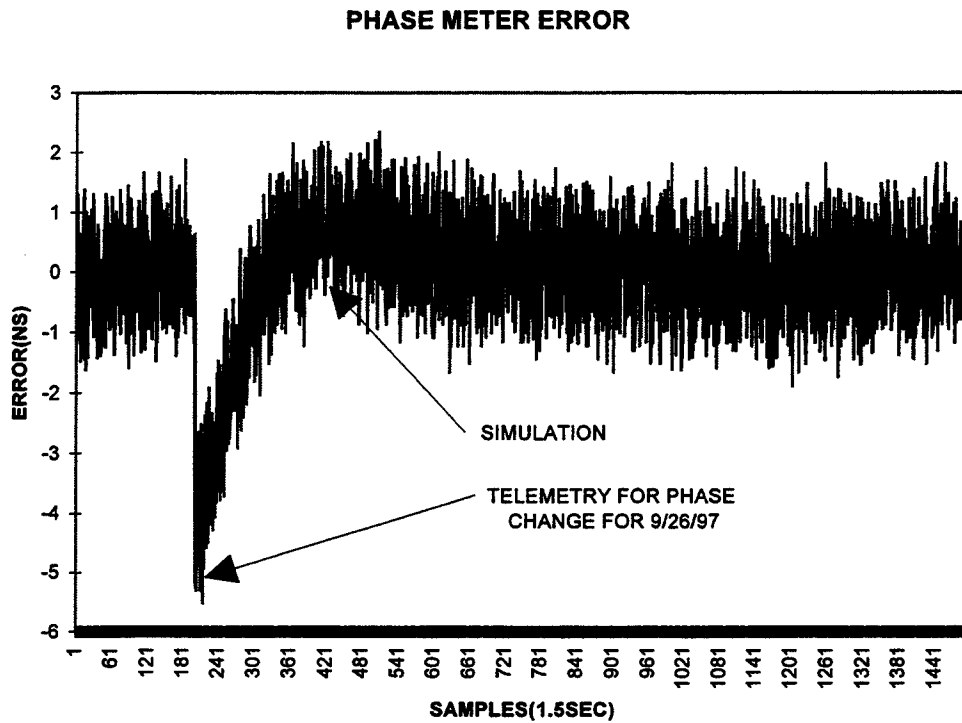
Figure 6. Phase Error Profile for Phase Transient

PHASE METER ERROR TRANSIENTS
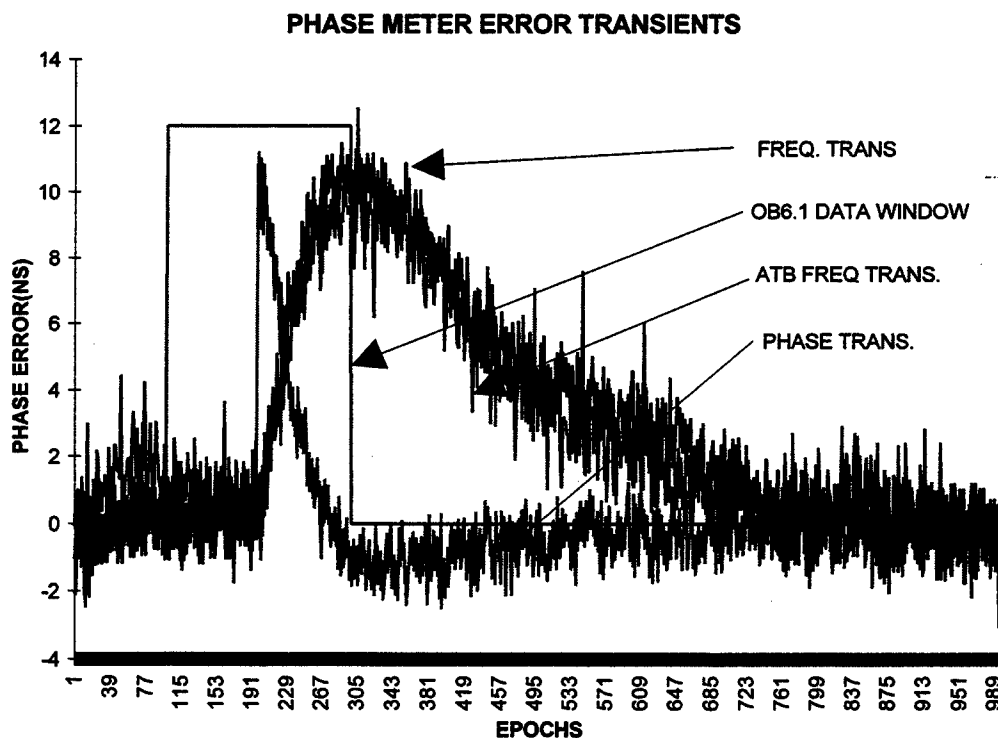
Figure 7. Phase Error Profile for Phase and Frequency Transients

183

8/16/98 Trace Buffer 0 and 1 Combined
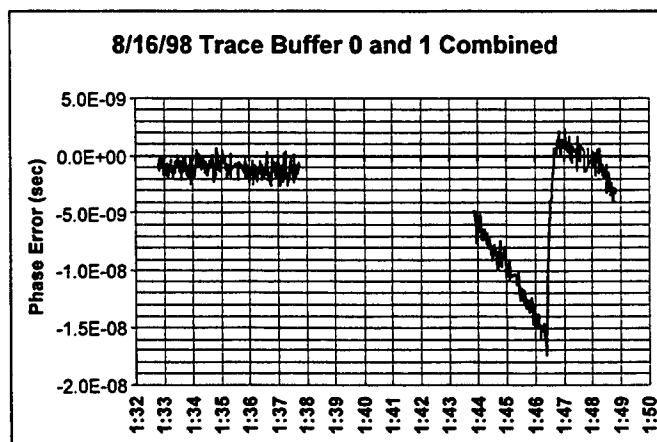
Figure 8. TKS Trace Buffer Plot

Phase Error 8/16/98
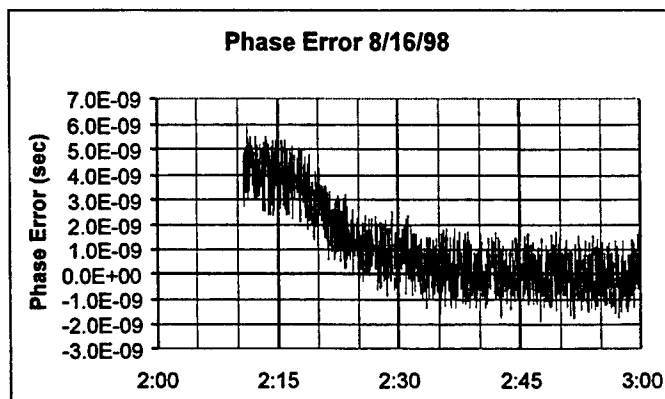
Figure 9. Phase Error Telemetry

Frequency Estimate
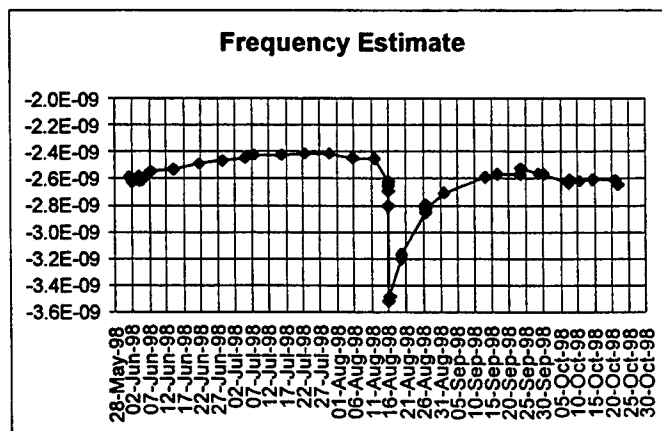
Figure 10. Frequency Estimate Plot

184
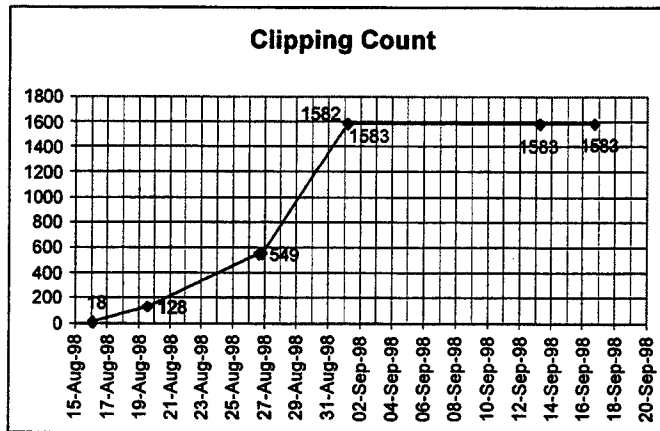
Clipping Count

Figure 11. Plot of Clipping Count

SVN 43 First Difference of Phase (NIMA)
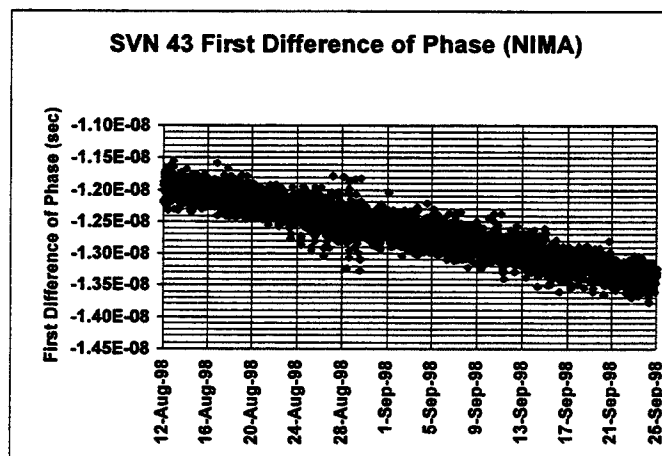
Figure 12. NIMA First Difference of Phase

Phase Error 26-AUG-98
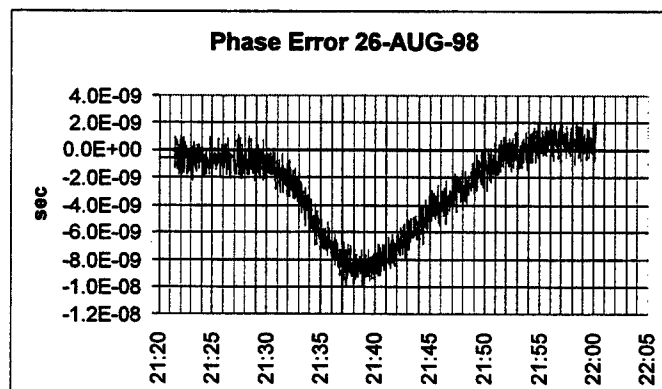
Figure 13. Phase Error Telemetry August 26

Questions and Answers

HUGO FRUEHAUF (Odetics Telecom): Have you considered taking a lot of VCXOs that you have, and checking them in the lab for phase pops to see what their condition is as a possible clue?

THEODORE DASS (ITT): A lot of testing is done on these clocks prior to delivery, and none of the clocks have exhibited any of these phenomena at the EG&G factory or during the RAFs' life test. There was a paper earlier that showed some frequency discontinuities in the RAFs. There has been a lot of testing and more of the RAFs have exhibited this phenomena.

HUGO FRUEHAUF: Yes, but EG&G would only be testing the frequency standard, it would not be testing the external VCXO, right?

THEODORE DASS: In these particular events, we do believe it is not the VCXO, but that it is the RAF. So, we do not suspect the VCXO. Now, we did have another event on August 16th that we do suspect was a VCXO. As my presentation was long, I did not get to it. None of the test data on the VCXOs has shown any of what we saw on August 16th. It should have shown up in the testing if it had exhibited the same thing we saw on-orbit.

REAL-TIME GPS MONITORING OF ATOMIC FREQUENCY STANDARDS IN THE CANADIAN ACTIVE CONTROL SYSTEM (CACS)

F. Lahaye, M. Caissy, J. Popelar
Geodetic Survey Division
Natural Resources Canada (NRCan)

R.J. Douglas
Frequency and Time Standards, Institute for National Measurement Standards
National Research Council of Canada (NRC)

Abstract

Ten Real-Time Active Control Points (RTACP) across Canada continuously monitor all GPS satellites in view and generate wide area GPS corrections with an update rate of 2 s. Dual frequency high precision geodetic GPS receivers using free running atomic frequency standards (masers, Cs and Rb) provide pseudorange and phase measurements at 1 s intervals. Ionosphere-free, carrier-phase-filtered pseudorange data are combined with rapid GPS satellite orbit predictions and RTACP coordinates in a least-squares adjustment to determine satellite and station clock offsets with respect to a virtual reference clock (VRC). The VRC is maintained as a weighted mean of RTACP long-term clock models. The VRC is related to the mean GPS system time using a long-term linear clock model with correlation time of a few days and it is traceable to UTC (NRC). This approach mitigates the effects of instabilities of individual RTACP clocks, eliminates clock discontinuities, and provides VRC stability better than 10^{-14} for time intervals greater than 1 day. The system provides continuous RTACP clock synchronization with RMS residuals in the range of 0.1-0.5 ns and real-time GPS satellite clock corrections with RMS residuals in the range of 0.3-0.8 ns. The quality of the real-time results are presented and discussed.

INTRODUCTION

The Geodetic Survey Division operates the Canadian Active Control System (CACS). It comprises a Master Active Control Station (MACS) and a network of continuously operating GPS data acquisition stations, called Active Control Points (ACPs), which are distributed across the Canadian landmass and track all GPS satellites in view. The GPS data from several ACPs are contributed to the International GPS Service (IGS). The NRCan Analysis Center processes the Canadian and a portion of the global IGS data to generate daily precise GPS satellite ephemerides and clocks, earth orientation parameters (EOP), and ionospheric, tropospheric and terrestrial reference frame information, as well as rapid GPS orbit predictions [1].

Ten of the CACS tracking stations (Fig. 1) have been enhanced to facilitate real-time data communication with the processing center, forming the Canada-wide network of Real-Time ACPs (RTACPs). Data from these RTACPs are available at the Real-Time Master Active Control Station (RTMACS) in less than two seconds for the computation of wide area GPS corrections, which is known

as the Canadian GPS•C service. The system architecture, data communication infrastructure, and the real-time application software are described in [2].

The RTMACS configuration, processes, and GPS•C positioning performance are described in [3] and [4]. A state-space domain algorithm is used to compute real-time corrections to the broadcast satellite orbits and clocks using ionosphere-free, carrier-phase–filtered pseudoranges, predicted GPS satellite ephemerides, and the RTACP station coordinates. The RTACP receiver clock offsets and a grid of vertical ionospheric delays for a single-layer model of the ionosphere are also generated. The GPS•C service facilitates real-time GPS positioning of about half a meter horizontally and a meter vertically, when using geodetic quality receivers. All GPS receiver and satellite clock offsets are determined with respect to a Virtual Reference Clock (VRC), which is maintained as a weighted mean of long-term models of selected RTACP receiver clocks.

A description of the real-time GPS data processing, clock monitoring, and the VRC maintenance is presented below. The real-time station and satellite clock results are compared with the precise geodetic post-processing results produced by the NRCan Analysis Center using the global IGS network data. Allan variances of the de-trended real-time RTACP receiver clocks and the VRC are also presented.

REAL-TIME GPS DATA ACQUISITION, COMMUNICATION, AND PROCESSING

The RTMACS and RTACP network is based on Hewlett-Packard UNIX servers, dedicated frame relay communication facilities, and the Real-Time Application Platform (RTAP) technology [2]. The RTAP has been used to implement a real-time distributed database, which uses a scan system for process control, data acquisition and communication, a calculation engine to automate data processing within the database, and an event manager to handle real-time events, inter-process communication, and run-time priorities. Land and satellite communication links between the RTMACS and the RTACPs support TCP/IP protocol with the maximum communication delays of less than 0.5 and 1.5 seconds respectively. The necessity to use the satellite communication links in order to provide Canada wide coverage is limiting the present GPS•C service update rate to 2 seconds.

The pseudorange and carrier-phase data represent the time delay between the GPS signal transmission from the satellite and its detection at the receiver, as measured by the difference of the corresponding satellite and receiver clocks. This delay can be expressed as the sum of the geometric satellite range delay, the tropospheric delay, and the ionospheric delay; it also includes the satellite and receiver clock misalignment, the Selective Availability (SA), and relativistic effects. In general, the pseudorange measurements show a noise of about 50 cm, whereas the noise of the carrier-phase data is at a centimeter level if its cycle ambiguities can be correctly resolved.

At two-second intervals, RTACP observation history of the latest five epochs is retrieved from the RTMACS database using criteria which minimize latency, maximize coverage, and assure input from RTACP stations with high quality atomic frequency standards. All the GPS data for the selected epoch are corrected to the first order for the ionospheric delay by combining the L1 and L2 measurements to mitigate any long-term ionospheric biases. However, the ionosphere-free combinations show increased short-term noise in comparison with the L1 data. The pseudoranges are then filtered using carrier-phase by averaging the differences between the ionosphere-free pseudorange and the carrier-phase measurements and by integrating the ionosphere-free carrier-phase. At the start of a satellite pass or when a cycle slip is detected, the averaging and integration are restarted. As the average converges to the ionosphere-free carrier-phase ambiguity, the noise of the filtered pseudoranges decreases to about 5

cm. However, the averaging takes some time to converge, mainly due to the increased pseudorange noise for satellites at low elevation angles. The detection of cycle slips is also important for the quality of the filtered data. Only filtered pseudoranges below the noise threshold for the determination of ionosphere-free carrier-phase ambiguities are used in the subsequent processing.

GPS satellite positions, which are interpolated from predicted ephemerides available at 15-minute intervals, and the known RTACP station coordinates are used to compute the geometric satellite ranges in the observation equations. The relativistic corrections are applied to and the tropospheric delays are removed from filtered pseudorange observations using the Hopfield model for the corresponding satellite elevation angles. In this way, only the GPS satellite and the RTACP receiver clock corrections remain as unknowns in the observation equations, which are solved in a least-squares adjustment. The filtered pseudoranges are assigned weights proportional to the satellite elevation angles, and the least-squares adjustment is constrained using *a priori* information obtained by RTACP receiver clock modeling, as described below.

STATION AND SATELLITE CLOCK MODELING

Polynomials of the first and second order are being used to model both the RTACP receiver and the GPS satellite clock offsets with respect to the system reference clock. Real-time clock model parameters are updated using a sequential scheme with clock offsets weighted as a first-order Markov process according to their age and a given correlation time. Two models are maintained for each of the receiver and satellite clocks to follow their short and long-term behavior. The short-term models are used to provide *a priori* estimates of the receiver and satellite clock offsets in the least-squares adjustment.

First-order polynomials have been used for the RTACP receiver clocks with typical correlation times of a few minutes and a few days for the short- and long-term models respectively. Figure 2 shows the least-squares updates to the short-term RTACP receiver clock models, which reflect the short-term performance of the external frequency standards used and the GPS data noise. These updates for RTACPs with H-masers are mostly well within a 0.5 ns range, whereas for the RTACPs with Cs and Rb frequency standards are generally within 1 and 0.8 ns respectively.

Second-order polynomials have been used to model the GPS satellite clocks with correlation times of a few seconds and a few days for the short- and long-term models respectively. The short-term satellite clock models also include the effects of Selective Availability (SA). Figure 3 shows the least-squares updates to the short-term satellite clock models, which are generally within 0.5 ns, but the lack of pseudorange data and their higher noise for low satellite elevations at the beginning and the end of each satellite pass are apparent.

THE VIRTUAL REFERENCE CLOCK

There are two basic approaches to the definition and maintenance of the system reference clock: (1) to use one of the receiver clocks in the network as the system reference clock or (2) to define a Virtual Reference Clock (VRC) as a mean of selected receiver clocks in the network. The first approach is relatively simple to implement, but makes the system completely dependent on a single station and its performance, which is from an operational point of view highly undesirable. The second approach requires an efficient way to deal with sudden changes in individual receiver clock behavior in order to maintain the VRC stability. The VRC stability of the real-time CACS is controlled in two steps:

189

- In the first step, the least-squares estimation of the short-term RTACP receiver clock model updates is controlled using *a priori* weights reflecting the short-term model noise levels. Each RTACP receiver clock weight is limited by a selectable maximum value. RTACP receiver clock discontinuities due to resets are closely monitored and the affected receiver clocks are down-weighted accordingly. No constraints are presently applied for the estimation of short-term satellite clock model updates, although the least-squares adjustment allows for it.

- In the second step, the VRC is generated and updated as a weighted mean using de-trended long-term RTACP receiver clock models. The *a priori* weights here correspond to the departures of individual receiver clocks from their long-term models. The VRC is then referred to the mean GPS system clock by applying the broadcast satellite clock corrections to the satellite clock offsets and using a long-term linear clock model with correlation time of a few days to smooth any undesirable effects of SA and other satellite clock irregularities. "Steering" of the VRC is accomplished by applying the same bias with opposite sign to the appropriate parameters of all the clock models in the system.

The VRC is usually initialized by assigning zero weights to all but one RTACP receiver clock, which uses an H-maser frequency standard. This represents the first step to the realization of the system reference clock as outlined above and the VRC offset and drift with respect to the mean GPS system clock are those of the selected RTACP receiver clock. The VRC is then "steered" in order to be aligned with the mean GPS system clock; this amounts to introducing clock corrections similar to the broadcast clock corrections for all the clocks in the system. Indeed, after this step the long-term satellite clock model parameters show very good agreement with the broadcast satellite clock corrections for all the GPS satellites using Cs clocks and the current PRN13; some modeling enhancements will be required to obtain similar agreement for the older GPS satellites using Rb clocks. The weighting scheme described above can then be introduced with appropriate maximum values with which an RTACP receiver clock is allowed to contribute to the maintenance of the VRC. After a receiver clock reset detection, the RTACP is excluded from the VRC computation for a period corresponding to the long-term model correlation time. The 1 pps from the RTACP receiver at NRC1 is monitored and traceable to the UTC(NRC). Operator intervention and modification of real-time CACS configuration and data processing parameters are efficiently accomplished by means of a graphical user interface to the RTAP database.

The period between November 16 and 22, 1998 has been chosen to show timing results obtained by the present real-time system implementation. From November 16 to 19 the NRC1 receiver clock, which uses the H-4 maser frequency of the Frequency and Time Standards Laboratory of the Institute for National Measurement Standards, was used as the system reference clock. As of November 19, the H-masers at NRC1, ALGO and YELL, the Cs clocks at STJO and ALBH, and the Rb frequency standard at WINN were selected to establish and maintain the VRC. The RTACP receiver clock offsets with respect to their long-term models for the six RTACPs during the entire period are shown in Figure 4. The daily variations of the GPS receiver clocks using H-masers are typically within few nanoseconds, whereas those using Cs clocks show variations of about 10 to 30 ns and those using Rb frequency standards vary in the tens to hundreds of nanoseconds depending mainly on the RTACP environment.

COMPARISONS OF THE REAL-TIME CLOCK RESULTS

The NRCan Analysis Center global GPS products have been using, most of the time, the H-maser-based ALGO receiver clock as the reference clock in daily precise GPS satellite orbit computations, and high quality relative receiver clock offsets are available at 7.5 minute intervals [5]. Comparisons of clock results between independent solutions by the IGS analysis centers and NRCan show agreement at the nanosecond level [6]. The real-time clock offsets were also referred to the ALGO receiver clock to

facilitate direct comparisons. Figure 5 shows the differences between the real-time and the precise relative receiver clock offsets between the stations ALGO and NRC1 and YELL. The biases apparent in the graphs reflect the pseudorange biases explicitly applied to the data from the given stations for the precise NRCan post-processing. The real-time VRC offsets with respect to the mean GPS system time are shown in Figure 6.

Allan variances of the de-trended real-time RTACP receiver clocks for the 3.5 days of data, when the VRC was used, are shown in Figure 7. The stations equipped with H-masers (NRC1, ALGO, and YELL) consistently show the best clock performance. The stations using Cs clocks (ALBH and STJO) have better long-term performance than the stations with Rb frequency standards (WINN, PRDS, and SCHE), which show better short-term stability. The frequency of the Cs clock at CHUR was adjusted on November 21 and as a result the receiver clock shows poor long-term performance. The VRC, which represents the common reference, clearly shows the best of all performance with the stability better than 10^{-14} for time intervals greater than 1 day.

CONCLUSION

The GPS•C service of the Canadian Active Control System has been implemented to facilitate Canada wide real-time positioning and navigation with better than 1-meter accuracy. Ten RTACPs and the RTMACS form a distributed computer network using frame-relay land and satellite communication links. The GPS satellite and the RTACP receiver clock corrections are computed every 2 seconds with a latency of about 3 seconds and maintain real-time synchronization of all the clocks in the system at the nanosecond level with respect to the VRC. The VRC is realized as a weighted mean of selected RTACP receiver clocks and shows better than 10^{-14} stability for time intervals greater than 1 day. Comparisons with precise post-processing clock results produced by the NRCan Analysis Center show agreement at a few-nanosecond level.

ACKNOWLEDGEMENTS

REFERENCES

[1] P. Tétreault, R. Ferland, J. Kouba and J. Popelar, "NRCan (EMR) Analysis Center 1997 Annual Report to the IGS," *1997 Annual Report, Volume II, International GPS Service for Geodynamics*, IGS Central Bureau at Jet Propulsion Laboratory, Pasadena, in preparation, 1998.

[2] M. Caissy P. Héroux, F. Lahaye, K. MacLeod, J. Popelar, J. Blore, D. Decker, R. Fong, "Real-Time GPS Correction Service of the Canadian Active Control System," Proceedings of the 9th International Technical Meeting of The Satellite Division of the Institute of Navigation, ION GPS-96, September 17-20, 1996, pp. 1787-1791.

[3] F. Lahaye, M. Caissy, P. Héroux, K. MacLeod, J. Popelar, "Canadian Active Control System Real-Time GPS Correction Service Performance Review," *Proceedings of the National Technical Meeting of the Institute of Navigation*, Santa Monica, USA, January 14-16, 1997, pp. 695-698.

[4] S. Skone, M.E. Cannon, K. Lochhead, P. Héroux, F. Lahaye, "Performance Evaluation of the NRCan Wide Area System," *Proceedings of the 9th International Technical Meeting of The Satellite Division of the Institute of Navigation,* ION GPS-96, September 17-20, 1996, pp. 1787-1791.

[5] R.J. Douglas and J. Popelar, "PTTI Applications at the Limits of GPS," *Proceedings of the 26th Annual Precise Time And Time Interval Applications and Planning Meeting,* 1994, pp. 141-151.

[6] J. Kouba, "1997 Analysis Coordinator report," in 1997 Annual Report, *Volume I, International GPS Service for Geodynamics,* IGS Central Bureau at Jet Propulsion Laboratory, Pasadena, in preparation, 1998.

Figure 1: Real-Time Canadian Active Control System network.

a)

b)

c)
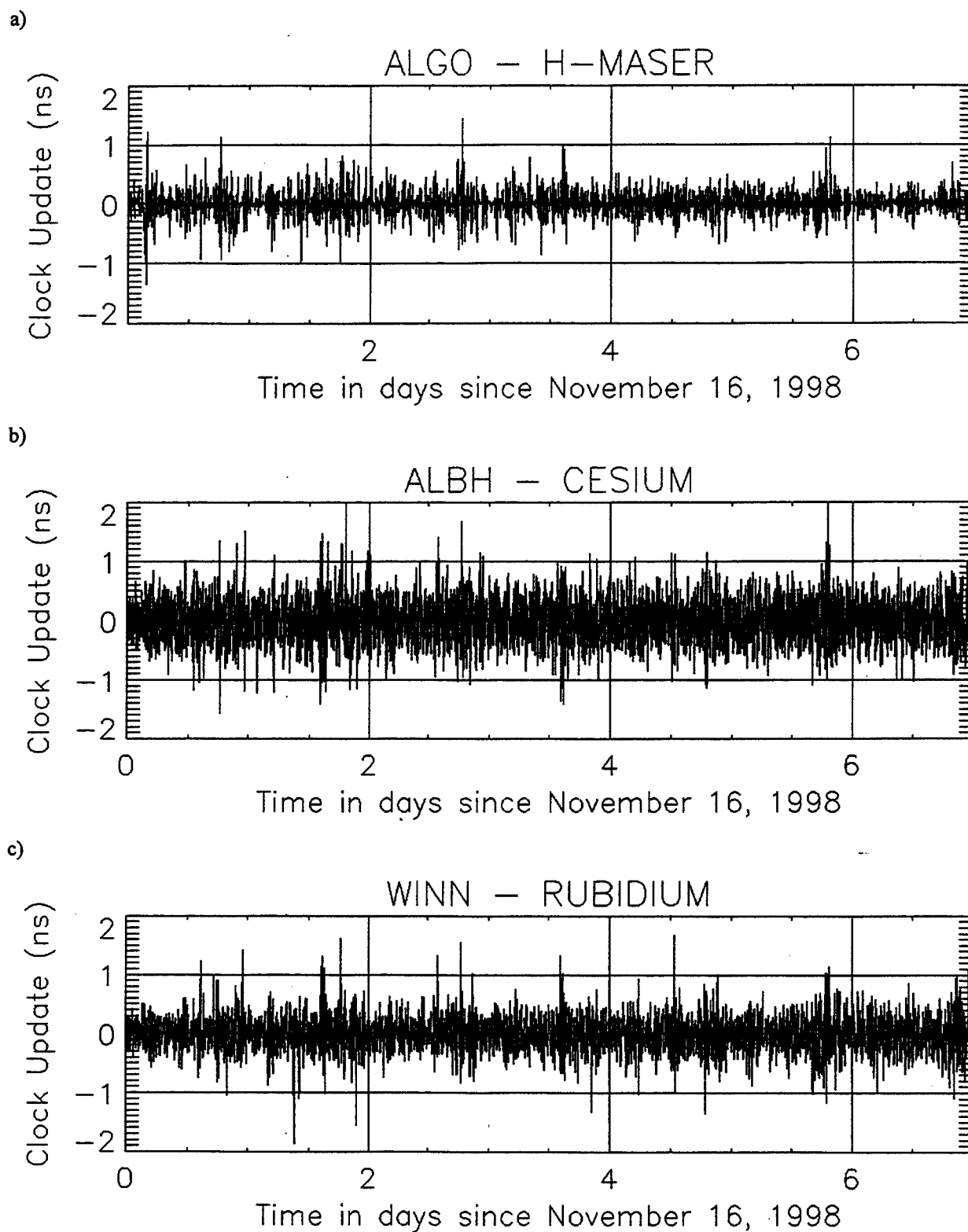
Figure 2: Real-time updates to short-term station clock models for RTACPs equipped with a) H-Maser, b) Cesium and c) Rubidium frequency standards.
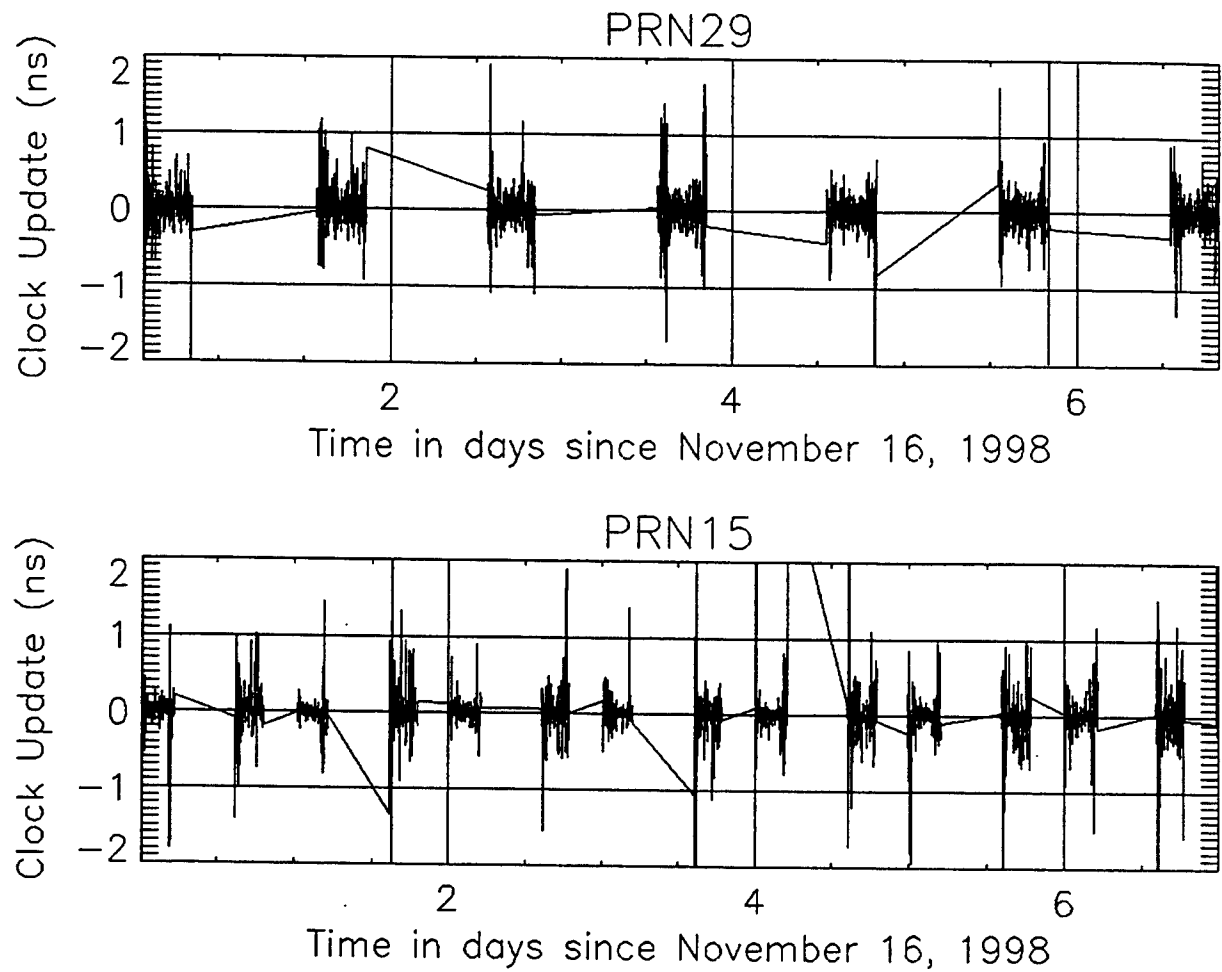
Figure 3: Real-time updates to short-term GPS satellite clock models for a satellite with SA (PRN29) and a satellite without SA (PRN15).
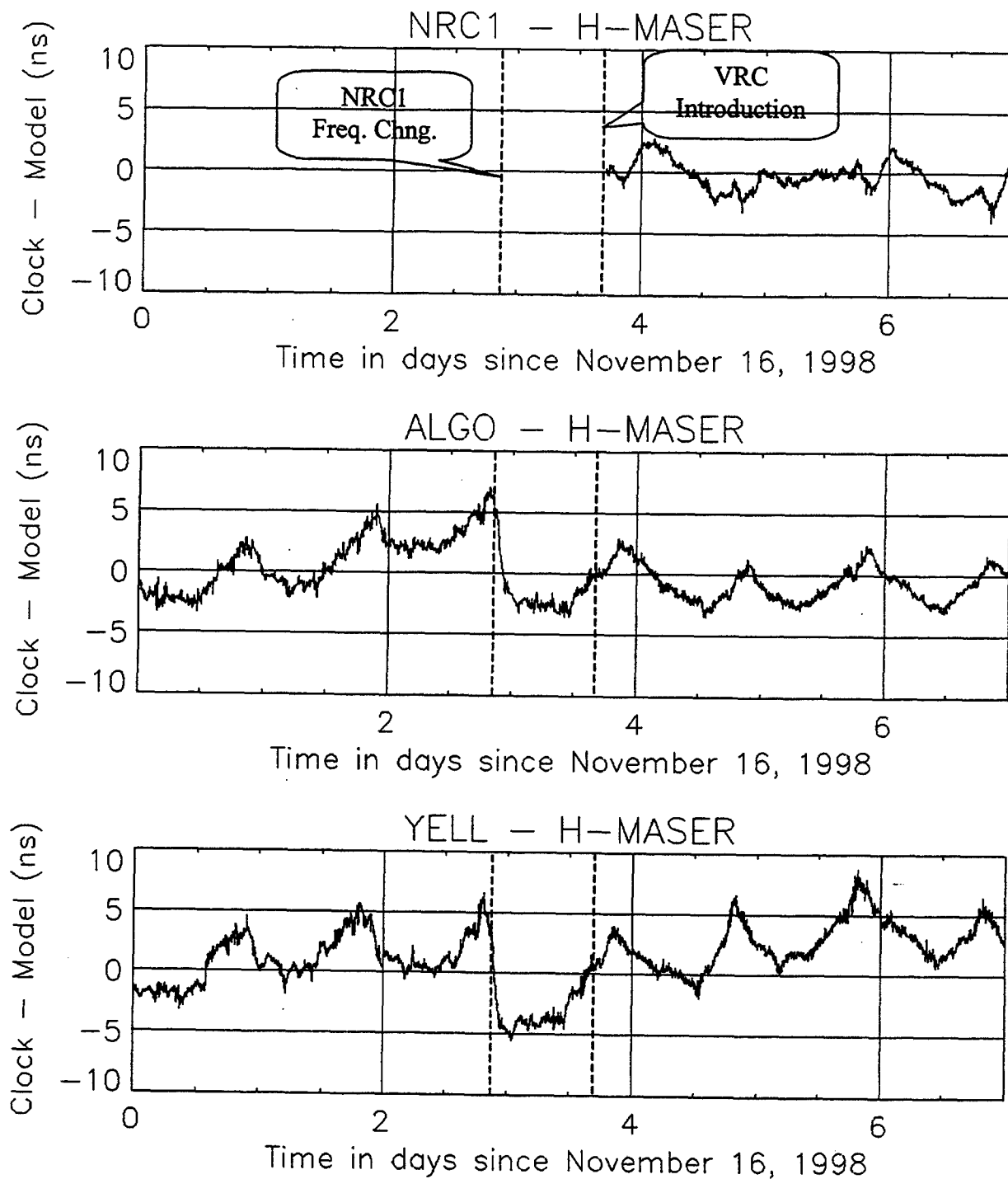
Figure 4a: Real-time RTACP receiver clock offsets for the stations using H-masers with their long-term clock models removed.
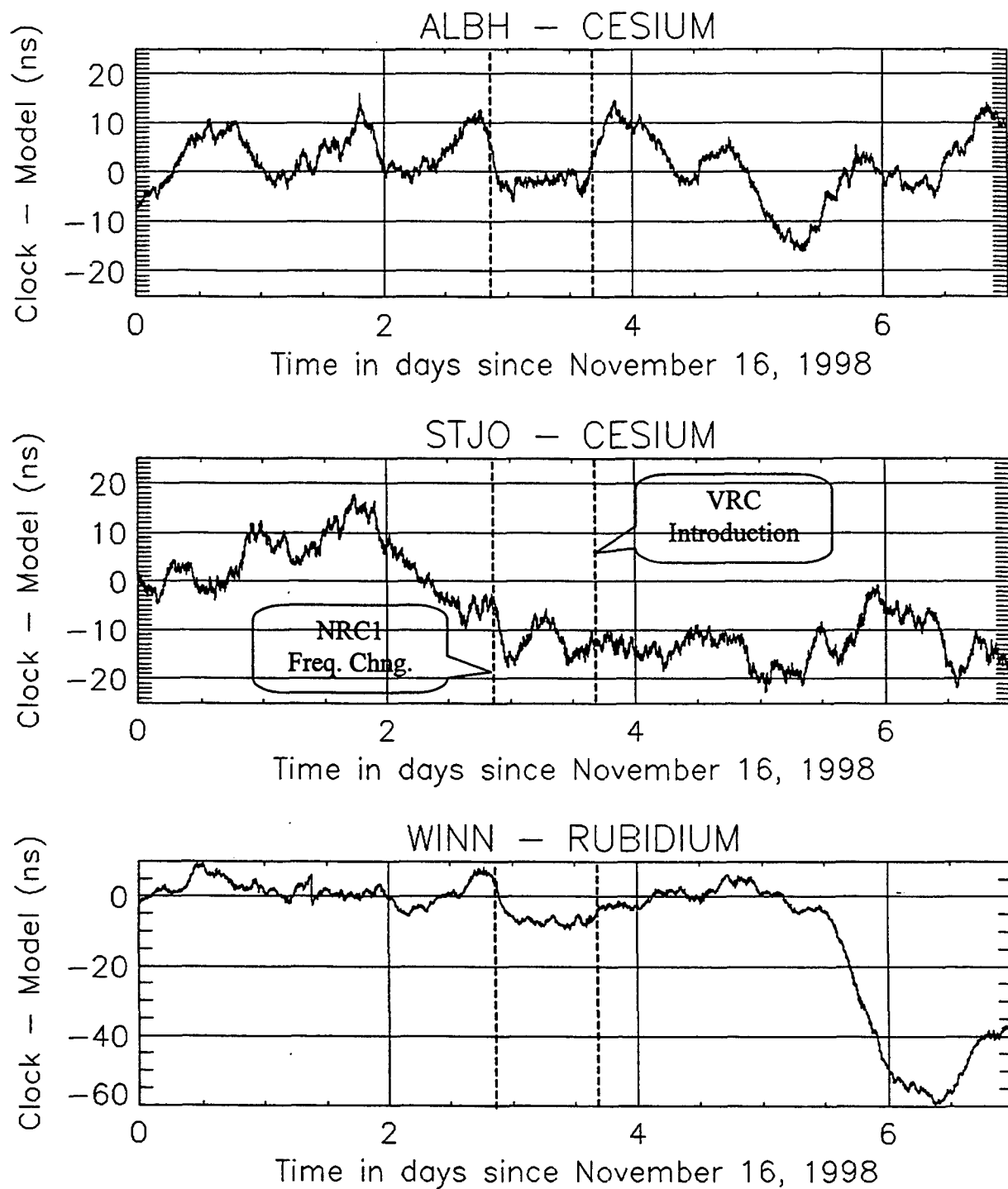
Figure 4b: Real-time RTACP receiver clock offsets for stations using Cs and Rb frequency standards with their long-term clock models removed.
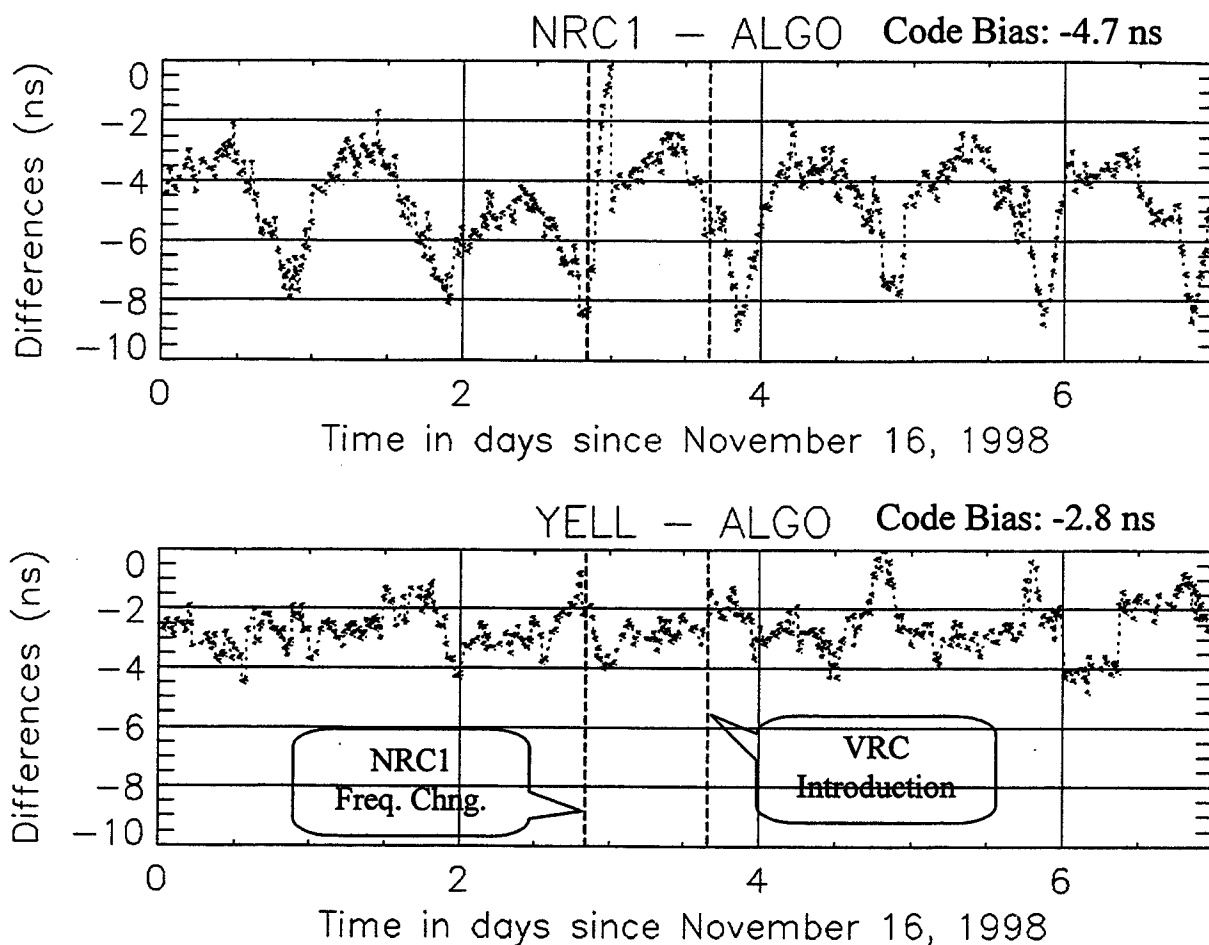
Figure 5: Differences between the real-time and the NRCan precise post-processed relative receiver clock offsets for NRC1, YELL, and ALGO.
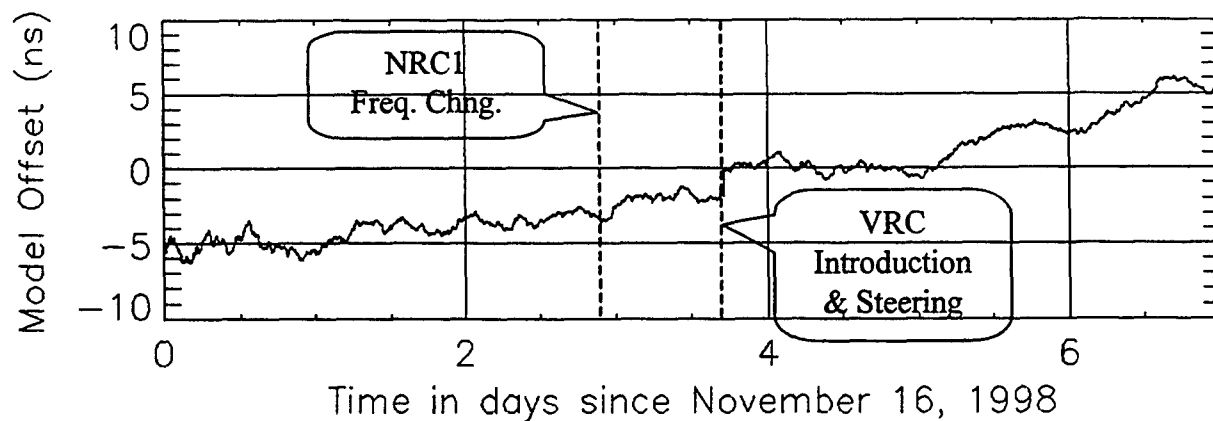
Figure 6: The real-time VRC offset with respect to the mean GPS system time.
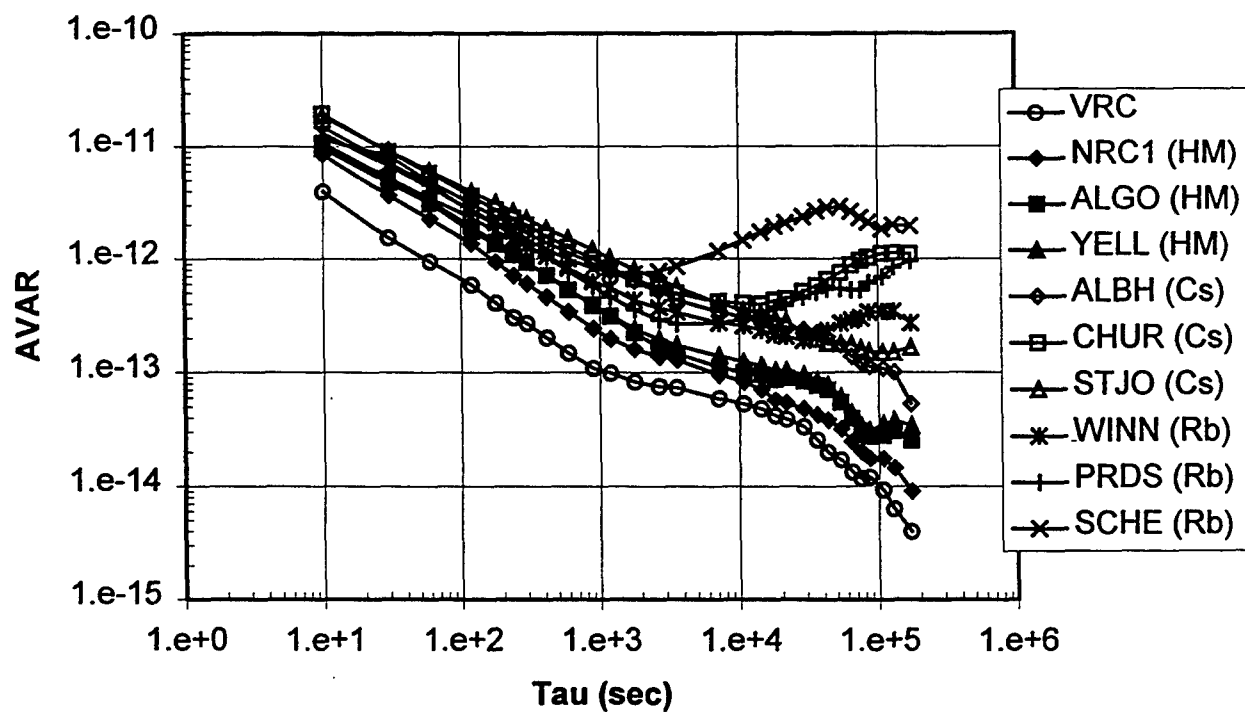
Figure 7: Allan variances of the de-trended real-time RTACP receiver clocks and the VRC.

Questions and Answers

DEMETRIOS MATSAKIS (USNO): I just wanted to point out that the maser that you are referring to at the USNO is a steered maser, and the steering typically varies by a little less than a nanosecond per day. When you do the analysis that you talked about, it might be better to remove all of that. We do have the information to trace the steered maser to an average of our masers, and it is available by anonymous FTP.

By the way we are also looking into changing a bias on it and there could be up to a 40-nanosecond change, gradually introduced, in the near future.

A TEST
OF THE USE OF GLONASS PRECISE CODE
FOR HIGH-PRECISION TIME TRANSFER

J. Azoubib and W. Lewandowski
Bureau International des Poids et Mesures, Sèvres, France

Abstract

In a first attempt to evaluate performance of the GLONASS P-code time transfer, one-site measurements are used to show that single-channel GLONASS precise code, combined with temperature-controlled antennas, reduces the noise experienced by time receiving equipment to a few hundred of picoseconds for a one-day averaging times, thus allowing frequency comparison at a level of a few parts in 10^{15}.

INTRODUCTION

Although not as well known as the GPS, the Russian global satellite navigation system GLONASS possesses comparable capabilities for navigation, precise geodetic positioning, and time-transfer applications [1]. During the last few years studies of time and frequency comparisons of remote atomic standards have seen several interesting developments involving GLONASS: C/A-code single-channel measurements led to similar to GPS performances for continental links; intercontinental links were affected by lack of post-processed GLONASS precise ephemerides [2].

But the performance of single-channel GPS and GLONASS C/A-code common-view time transfer, uncertainty of about 3 ns, is barely sufficient for the comparison of current atomic clocks and needs to be improved rapidly to meet the challenge of the clocks now being designed. For this reason the timing community is engaged in the development of new approaches to time and frequency comparisons. Among them are techniques based on multi-channel GPS and GLONASS C/A-code measurements, GPS carrier-phase measurements, temperature-stabilized antennas, and standardization of receiver software. This paper reports on the first test of GLONASS P-code for time transfer, and on specially protected receiver antennas. A one-site comparison shows that for single-channel GLONASS P-code time and frequency transfer a stability of 2 parts in 10^{15} is obtained over one day (200 picoseconds/day). These results indicate that GLONASS P-code time and frequency transfer in multi-channel mode should reach at least a stability of 1 part in 10^{15} over one day (100 picoseconds/day) for short baselines.

ADVANTAGES OF GLONASS

The Russian Global Navigation Satellite System (GLONASS) was inaugurated in 1982 and is still under development. GLONASS offers the international community in time metrology a useful additional tool for high-accuracy time transfer. The GLONASS constellation broadcasts a C/A-code signal free of Selective Availability (SA) and unencrypted P-code signal, unlike the GPS P-code, which is subject to Anti-Spoofing (AS) encryption.

The GLONASS P-code has two main advantages for precision time synchronization. First, GLONASS P-code has a wavelength that is 1/10th that of GLONASS C/A-code and about 1/5th that of GPS C/A-code. This has the effect that GLONASS P-code pseudo-range measurements are considerably more precise than comparable GPS or GLONASS C/A-code measurements. Second, GLONASS P-code is transmitted on both L1 and L2 frequencies, so it allows high-precision ionospheric delay measurements.

Originally GLONASS signals were broadcast on 48 frequencies (24 frequencies in the future) in contrast to GPS, which is broadcast on 2. This causes some difficulties with the delay biases, which vary with frequency. These, however, can be resolved, so the GLONASS system provides the net advantage that it is less vulnerable to intentional or unintentional jamming.

Until recently no post-processed GLONASS precise ephemerides are available. This, however, has changed as the Scientific Assembly of the International Association of Geodesy decided, on 3-9 September 1997 in Rio de Janeiro, to organize an International GLONASS Experiment (IGEX) in 1998. The IGEX begun on 19 October 1998 with participation of several tens of geodetic and timing institutions, and the first GLONASS precise ephemerides expressed in the ITRF are already available to civil users at the end of 1998. This will make the use of GLONASS more efficient for intercontinental time links. Other improvements will follow, among them rigorous transformation parameters between the WGS 84 reference frame used by GPS and the PZ-90 reference frame used by GLONASS.

ONE-SITE COMPARISON

For the determination of GLONASS frequency biases, described in the paragraph below, and a test of GLONASS P-code time transfer, we use a one-site comparison of time receivers. A one-site comparison calls for the computation of common views for two independent time receivers located at the same site, connected to the same clock, and with antennas separated by no more than several meters. Comparisons at short distances allow the cancellation of common clock errors and certain other systematic errors. If the software

used by the receivers is identical, no error should arise from satellite broadcast ephemerides, antenna coordinates, or imperfect modelling of the ionosphere and troposphere. Any constant bias measured is caused by delay differences of the two time-receiving systems, including the receiver itself, the antenna, and the cables, and any observed noise arises in the hardware and in multipath effects. In fact, the noise ascribed to space factors for the comparison over several hundred kilometers is almost equally well cancelled as that for the one-site comparisons. The particular advantage of a one-site comparison, however, is the elimination of the clock discrepancies, so that only the noise of the receiving equipment is observed. This can serve to characterize the receiving equipment.

GLONASS FREQUENCY BIASES

GLONASS data are subject to a receiver bias which may be different for each GLONASS frequency [3]. The spread of these biases across satellites can reach 15 nanoseconds and, therefore, mask other noise sources.

Based on the data available so far, GLONASS frequency biases appear to be a function of temperature and relate to specific receivers. But once calibrated with respect to a reference receiver, and provided that temperatures are maintained via laboratory air-conditioning together with a TSA antenna set-up, these values remain pretty constant and can therefore be compensated in the software. Figure 2 shows one-site GLONASS P-code common-view values dt_i, for each track i, between two time receivers, for the GLONASS frequencies Nos. 1, 4 and 10. One can see clearly the biases between the values of dt_i resulting from the use of different GLONASS frequencies. For each GLONASS P-code frequency, the dispersion of the mean value of the dt_i over the whole period of computation is of the order of 0.8 ns.

In order to estimate the GLONASS frequency biases, let the mean value of the dt_i over the whole interval of computation for the common views using the frequency f, be written as follows : $<dt_i>_f$. We can arbitrarily choose the frequency No. 10 as a reference frequency and then define a bias for the frequency f as follows :

$$B_f = <dt_i>_{10} - <dt_i>_f$$

The biases so estimated for the two involved receivers are listed in Table 1.

Table 1. GLONASS P-code frequency biases with respect to frequency No 10.

GLONASS Freq. No. f	B_f /ns
1	-7.8
4	-5.4
6	-2.3
9	-0.2
10	0
12	-1.0
13	-1.1
21	-1.3
22	-0.6
24	-1.6

A TEST OF GLONASS P-CODE

In a one-site comparison test we demonstrate the improvement brought about by the use of GLONASS P-code for common-view time transfer by comparing the results with those obtained from GLONASS and GPS C/A-code common-view time transfers. We used a one-site test specifically to analyze the noise of our time receiving equipment: 1) when used with GPS and GLONASS C/A-code in single-channel and multi-channel modes, both with and without a TSA (temperature–stabilized antenna) antenna; and 2) when used with GLONASS P-code in single-channel mode, both with and without a TSA antenna.

Figure 3 shows some examples of one-site comparisons over a period of about eight days using the same pair of receivers equipped with TSA antennas throughout. We observe that C/A code comparisons are affected by some systematic changes. The GLONASS C/A-code data are slightly noisier than GPS C/A-code data, as the delays depend on the frequency. After removing the bias specific to each GLONASS frequency and activating the TSA antennas, the GLONASS P-code comparison shows outstanding performance [4].

Time deviations of one-site comparisons were computed for four cases (Figure 4):

- GPS C/A-code single-channel without TSA antennas,
- GPS C/A-code multi-channel without and with TSA antennas,
- GLONASS P-code single-channel with TSA antennas and biases compensated for different GLONASS frequencies.

Except for GLONASS P-code the level of noise for the all above comparisons is about 3 ns. The gain in stability between GPS C/A-code single-channel and a multi-channel comparison is in line with our expectations according to the considerations reported above.

The multi-channel comparison without TSA antennas is affected by a systematic effect which becomes evident at about 3×10^4 second. This effect is removed when the TSA antennas are activated. However, a smaller systematic effect with a period of several hours persists: this may have its origin in the antenna cables. Recent data from another pair of receivers of the same type equipped with TSA antennas exhibit no systematic effect.

The level of noise for the GLONASS P-code comparison, using TSA antennas and after removing the bias specific to each frequency, is about 600 picoseconds. The reduction in noise level between GPS C/A-code single-channel and GLONASS P-code single-channel comparison is about 5. The use of GLONASS P-code in multi-channel mode should provide an improvement in stability similar to that found for GPS C/A-code. Consequently, the expected time stability with an averaging time of one day should be several tens of picoseconds: this corresponds to a frequency stability of several parts in 10^{16}. Multi-channel GLONASS P-code time transfer will be the object of our next study as suitable receivers are now available.

CONCLUSIONS

As GLONASS P-code, unlike GPS P-code, is available to civilian users, it is in the general interest to take best advantage of it. There are two main reasons for this. First, GLONASS P-code has a wavelength that is 1/10th that of GLONASS C/A-code and about 1/5th that of GPS C/A-code, which has the effect that GLONASS P-code pseudo-range measurements are considerably more precise than comparable GPS or GLONASS C/A-code measurements. Second, GLONASS P-code is transmitted on both L1 and L2 frequencies, so it allows high-precision ionospheric delay measurements.

As now practiced, GPS and GLONASS C/A-code time transfer are limited mainly by hardware instabilities and, over long distances, by uncertainty in the determination of ionospheric delays. The use of GLONASS P-code combined with the use of temperature-stabilized antennas provides an improvement to resolve these two problems. GLONASS post-processed precise ephemerides, necessary for long-distance links, are now available.

GLONASS P-code single-channel data obtained in the course of a one-site comparison shows a noise reduction of 5 relative to GPS C/A-code single-channel data performance. The use of GLONASS P-code in multi-channel mode promises a gain in stability by a factor of about 3. Consequently for short baselines, the expected time stability for an averaging time of one day should be of about 100 picoseconds, which corresponds to a frequency stability of 1 part in 10^{15}.

REFERENCES

[1] J. Gouzhva et al.; July/August 1992, "High-Precision Time and Frequency Dissemination with GLONASS," GPS World, pp. 40-49.

[2] W. Lewandowski, J. Azoubib, G. de Jong, J. Nawrocki, J. Danaher, 1997, "A new approach to International Time and Frequency Comparisons: 'All-in-View' Multi-channel GPS+GLONASS Observations," Proc. ION GPS-97, pp. 1085-1091.

[3] G. de Jong, W. Lewandowski, 1997, "GLONASS/GPS Time Transfer and the Problem of the Determination of Receiver Delays," Proc. PTTI'97, pp. 229-240.

[4] J. Azoubib, W. Lewandowski, G. de Jong, 1998, "A New Approach to International Time Transfer: Multi-channel and Multi-code GPS+GLONASS Common-New Observations," Proc. EFTF'98, pp. 87-93.
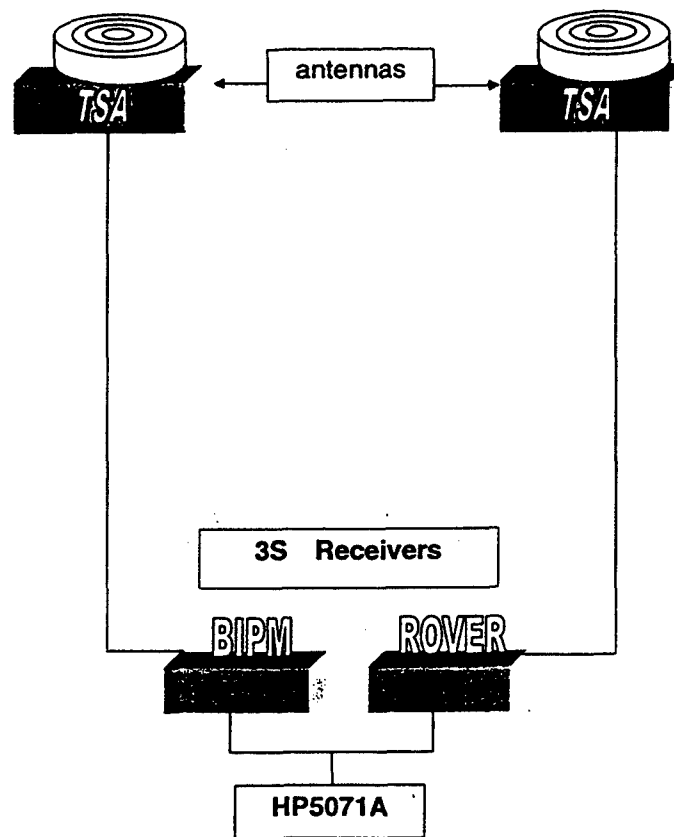
Figure 1. Scheme of one-site comparison with two TSA antennas.
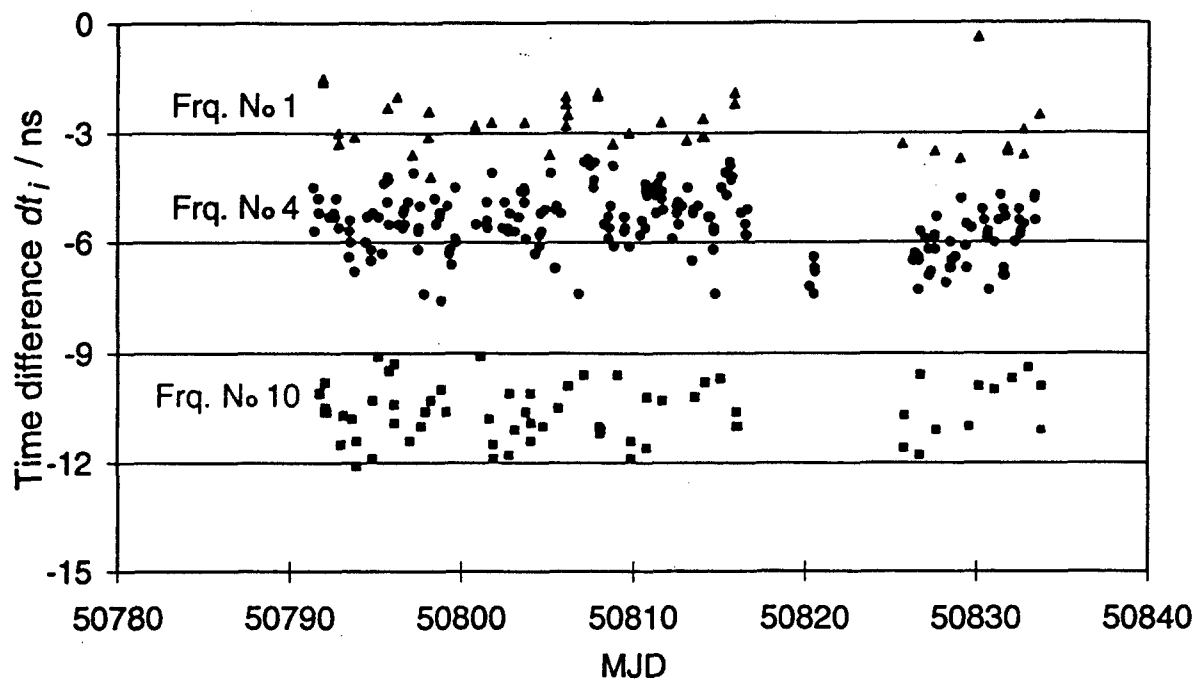
Figure 2. GLONASS P-code frequency biases – one site GLONASS P-code common-view values dt_i.
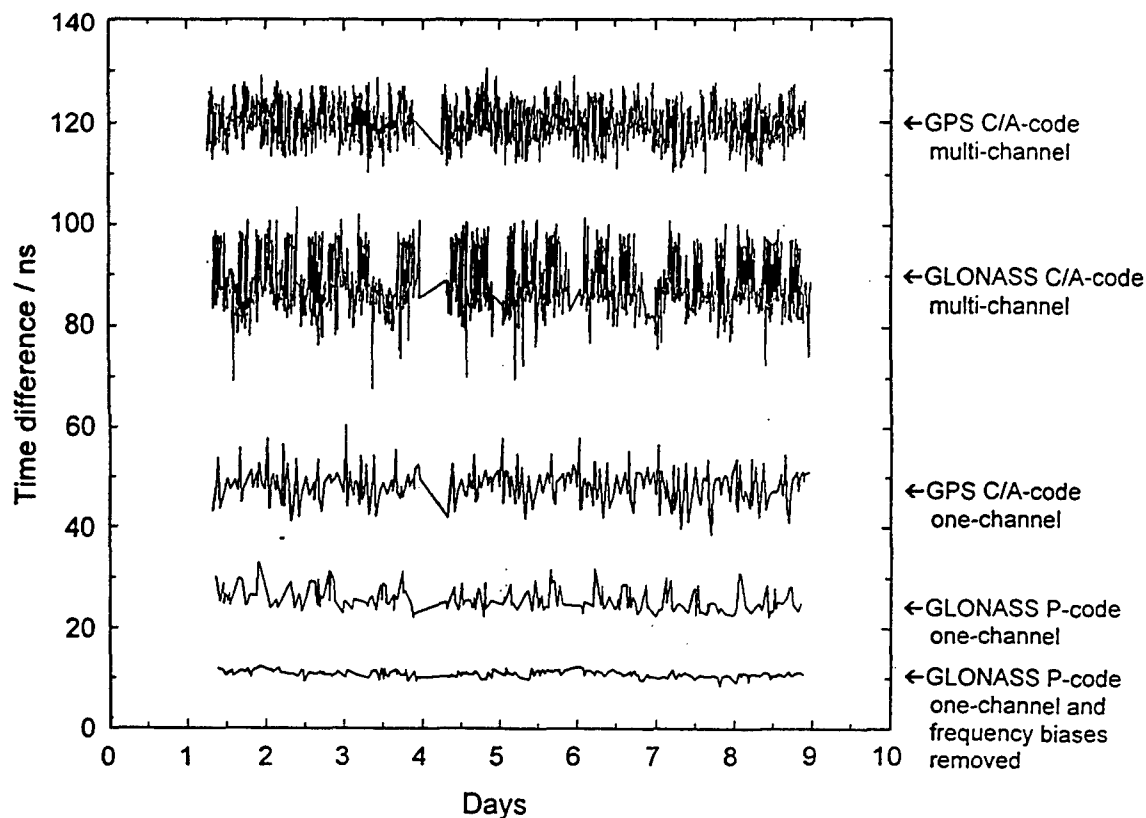
Figure 3. One-site comparisons (two separate TSA antennas on a single site).
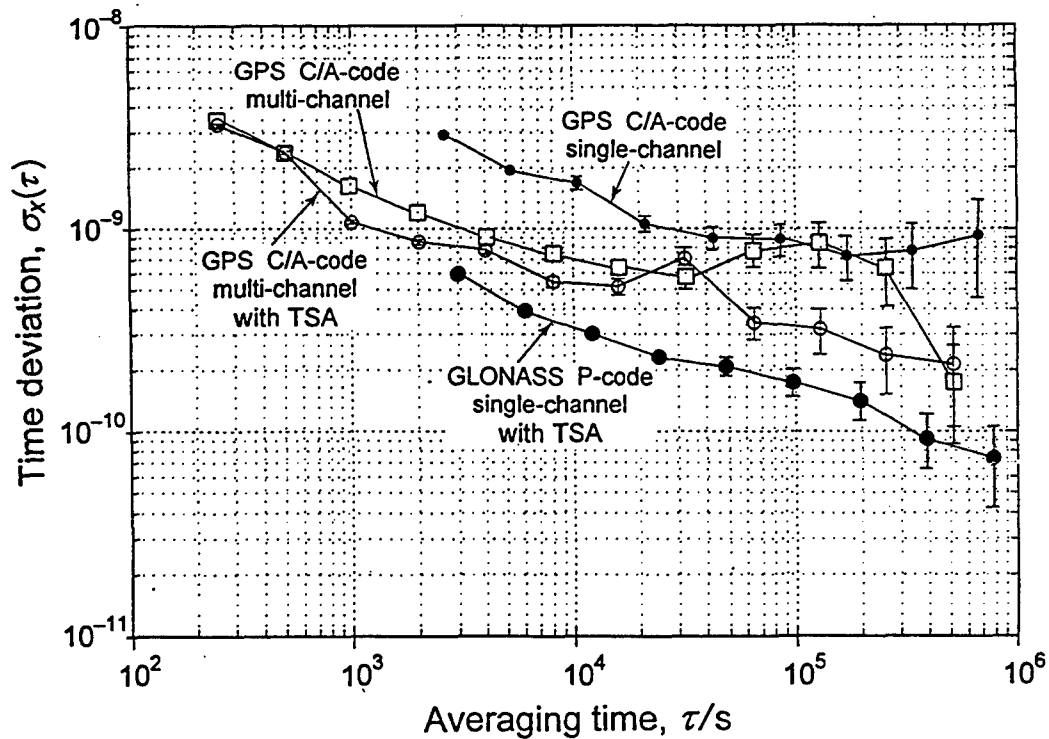
Figure 4. Time Deviation for one-site comparisons (two separate antennas on a single site).

Questions and Answers

GERRIT de JONG (NMi Van Swinden Laboratorium): I have a question about the calibration you made between the channels. You took channel 10 as a reference, and then you determined relative calibration values against that frequency. Did you do the same test with another GLONASS receiver? Is the calibration the same for every receiver or do they have to be calibrated individually?

JACQUES AZOUBIB (BIPM): It is to a specific receiver. The Frequency 10 was arbitrarily chosen. We could have chosen another reference frequency, and it would not have changed anything concerning the stability results we obtained.

We could have also chosen the mean value of the different frequencies and computed the bias as it shifted between this mean value and the different values of dt(i). So the choice of Frequency 10 is completely arbitrary.

GERRIT de JONG: Yes, but my question was not about the choice of that frequency, my question was: is this for two receivers, the BIPM receiver and the Rogue receiver? For instance if you take two receivers, could you get the same calibration factor or not?

JACQUES AZOUBIB: Not at all. I will read from this vugraph: "Once calibrated with respect to the reference receiver, this value remains critical...." Before, I said that it is a function of particular and specific receivers. That means that for each receiver a set of biases should be computed.

DEMETRIOS MATSAKIS (USNO): Did the relative biases change with temperature? You referenced them all to Satellite 10. Do they all go up and down together?

JACQUES AZOUBIB: We have not done any experiments. We got this information from 3S Navigation – that the biases are related to our frequency comparator.

DEMETRIOS MATSAKIS: I wondered if the relative bias was varying with temperature between the biases of the channels?

WLODZIMIERZ LEWANDOWSKI (BIPM): We were informed by 3S Navigation that the biases can be affected by temperature if the receiver antenna is not protected. That is one of the reasons to develop the temperature-stabilized antennas. Colleagues from 3S Navigation who know electronics said that these biases are sensitive to temperature. To take the full advantage of this technology, we have to stabilize the antenna and the receiver. If stabilized, these biases are pretty constant. This is now easy to do; so this is not a problem.

DEMETRIOS MATSAKIS: The other question I have is a little complicated. I think one of the big exciting things that is coming out of your work will be an ability to check for calibration errors in the GPS receivers on a daily basis. You have already talked about how you see the diurnal term in GPS receivers. We also see 100-day or longer-term variations. I wonder if it has gone on long enough that you can see changes that happen between the BIPM traveling GPS calibrations, so that we know that it really is GPS varying on the longer scale and not the GLONASS.

WLODZIMIERZ LEWANDOWSKI: You underlined a very important point. This use of GLONASS P-Code and the way we are doing this leads us to something extremely interesting, because it gives an

excellent reference to calibrate other receivers, GPS, for example. This is just at the beginning. We are on the verge of a series of GLONASS P-Code calibrations. We now have the receiver at the Paris Observatory which will go to our laboratories equipped with GLONASS P-Code receivers. We would like to invite you to also participate in this exercise at several laboratories in Europe. The receiver will also go to South Africa, Australia, and Japan. There are already many laboratories equipped with these receivers. We would like to repeat these calibrations. What we expect – maybe it is too optimistic, but we expect, based on the knowledge of what Jacques has just shown, that we are going to sub-nanosecond calibration of timing equipment. That is very exciting. Because, right now we are at the level of several nanoseconds, even 10 nanoseconds. The receivers delays are changing during the season, up to 10 nanoseconds.

You showed yesterday how well it is behaving. You know, it is within a few nanoseconds of UTC, so we now have to care about one nanosecond or even better calibration. This is something which this study gives us hope to achieve – maybe next year.

JACQUES BESER (3S Navigation): I just wanted to add a clarification. I mentioned yesterday that the antenna pre-amplifier, of course, contains filters. Those filters come from the manufacturer with specifications on them, and you can see that the specification basically indicates delays as a function of frequency, and temperature. So, the manufacturer clearly states that those parabolas, if you want – as temperature changes, not only will the entire "parabola" move up and down, which means an absolute delay will change, also the sides of it will kind of squeeze or enlarge. So, there will be an inter-channel frequency change frequency by frequency, as well as an absolute value. So, that was the answer to your question.

If you saw the data I presented briefly yesterday, you saw that when we turn off one of the TSA antennas and one of the receivers, all of a sudden you see the spreading increasing. That again showed experimentally that the temperature obviously had an effect frequency by frequency.

RESULTS OF RIRT'S COMPARISONS VIA GLONASS SIGNALS

**Dr. Pyotr P.Bogdanov, Prof. Arvid G.Gevorkyan,
Prof. Vadim S.Zholnerov
Russian Institute of Radionavigation and Time (RIRT)
2 Rastrelli Square, St.Petersburg, 193124, Russia**

Abstract

At present using the signals of satellite navigation system for comparisons of remote clocks in common-view mode is the most popular and precise method. But its practical realization in Russia via GLONASS signals was suspended for many years due to lack of automated receiving system. This paper describes the experimental operation of automated system for receiving of GLONASS signals in the Russian Institute of Radionavigation and Time, St.Petersburg. The results of the time scale comparisons are presented for the period from the beginning of 1996 to the end of 1998.

INTRODUCTION

In late 1993 in Russian Institute of Radionavigation and Time (RIRT) timing receiver named ASN-16-02 was developed on the base of its own serial GLONASS ASN-16 receiver. It meets the requirements of Bureau International des Poids and Mesures (BIPM) Time Section [1]. To obtain the execution of measurements and their processing automatically the interface between receiver and personal computer (PC) was held. This set of devices was named as Receiving and Data Processing System (RDPS).

At the same time many platforms of the Russian State Time and Frequency Service (STFS) continue to use for GLONASS time comparisons the serial ASN-16 receiver with additional time interval measurer of the difference between receiver's internal time scale (TS) and user's clock. To provide the execution of measurements and their processing automatically using RDPS in this case, development of the additional interface module and software was required. The developed system is successfully maintained in the structure of the Secondary Time/Frequency Reference of RIRT, providing GLONASS common-view time comparisons and data exchange with other laboratories.

The present paper describes principles of construction and operation of the Receiving and Data Processing System on the basis of ASN-16 type receiver, as well as results of its application.

DESCRIPTION OF RECEIVING AND DATA PROCESSING SYSTEM

Modified Receiving and Data Processing System on the basis of ASN-16 type receiver provides:
- forming the current plan of measurements execution on the basis of schedules received from BIPM and STFS;
- carrying out measurements sessions according to current plan;
- statistical processing of measurements for various variants and conditions;
- forming information for data exchange with other users in the STFS and BIPM format;
- displaying GLONASS state;
- forming an additional information about presence of satellites in visible zone for given user or network of users;
- graphic displaying of measurements processing results and other information; monitoring of receiver operation.

The system consists of GLONASS receiver ASN-16 or ASN-16-02 type, timing intervals measurer (TIM), IBM - compatible PC, interface module (IM1) for connection with the receiver and interface module (IM2) for connection with TIM both installed in PC, and software of the system. Block diagram of the system is given in Figure 1, the view of the system - in Figure 2. Main specifications of the system are given in Table 1.

When ASN-16 unit is used, the value of the offset between the internal TS of the receiver and UTC (SU) - ΔT_{RCVR} is determined in the receiver and then given out to PC. Simultaneously the signal of the receiver's internal TS is sent to start input of TIM, and the signal from the user's clock is sent to stop input of TIM. The value of the offset between the internal TS of the receiver and the user's clock - ΔT_{TIM}, is measured by means of TIM and then transfers to PC. During subsequent processing of results in PC the value of measured offset between the user's clock and UTC(SU) is defined: $\Delta T_{REF} = \Delta T_{RCVR} + \Delta T_{TIM}$.

When ASN-16-02 unit is used the value of the offset between the user's clock and UTC(SU) — $\Delta T_{RCVR} = \Delta T_{REF}$, is determined in the receiver directly and then given out in PC. In this case TIM is used only for monitoring of receiver's internal TS generation and user's clock.

Data exchange with other users provides the reception of BIPM and STFS schedules, measurement results from other laboratories in BIPM or STFS format, as well as forming measurements results in given format.

The software of the system is realized in MS DOS operational system version 5.0 using the computer languages such as Clipper 5.01 and Borland C ++ 3.0

PROCEDURES FOR MEASUREMENTS PLANNING, PERFORMING AND PROCESSING

Forming of current plans of measurement execution is produced on the basis of BIPM schedule, issued two times a year, and STFS schedule, issued two times a month. The BIPM schedule foresees the execution about 89 measurements sessions per day of 13-minute duration of each one. However the number of sessions executing in RIRT decreases to 25-35 per day because of features of ASN-16 receiver's operation. The STFS schedule foresees the execution four sessions per day only.

Planning of measurements sessions for independent operating mode of user is also possible, for example, several sessions for each satellite over each visible zone, for described time instants, etc. In this case forming of plan is executed on the basis of GLONASS almanac. Receiving of almanac is carried out once a week or after getting a message from GLONASS Coordination Scientific Information Center (CSIC) concerning system status change.

Execution of measurement sessions according to the current plan is produced in automatic mode completely. The execution of sessions directly by operator is also possible by set of appropriate mode.

The primary processing of measurements is executed in receiver. As GLONASS navigation message does not include model parameters of ionosphere and troposphere, the ionosphere and troposphere delays are computed using parameters stored autonomously in the receiver. Internal delay is determined by means of calibration of the receiver before each session.

Secondary measurement processing is realized totally by PC and is connected with getting session estimates for time offset of user's clock against UTC(SU) and GLONASS time, as well as estimates averaged over 1 day or for any other time interval. For computation of session estimates an averaging procedure can be chosen from following alternatives: linear approximation, square approximation or combined algorithm given by BIPM (square approximation of pseudorange measurements over 15-second sections with subsequent linear approximation over all session interval). Estimates with averaging over 1 day or over desired time interval are computed using all the session estimates, for the chosen satellite or for certain elevation angle.

RESULTS OF TIME COMPARISONS

List of laboratories, which observe GLONASS according to the STFS and BIPM schedules is given in Table 2.

The results of accuracy estimation of the laboratory's clock comparisons relative UTC(SU) and GLONASS time in the "direct synchronization" mode and the results of accuracy estimation of GLONASS common view comparisons between RIRT and other laboratories are given in Table 3. These results are the minimum and maximum values obtained on the basis of the method of least squares interpolation and linear model for time differences with one month averaging.

The presented data show that the average value of the accuracy determination of the offset between laboratory's clock and UTC(SU) or GLONASS time in the "direct synchronization" mode is 33 ns (discrepancy from 20 to 48 ns). The average values of the clock comparison accuracy in the GLONASS common-view mode are 17 ns (discrepancy from 11 to 28 ns) for Russian laboratories and RIRT and 13 ns (discrepancy from 9 to 19 ns) for foreign laboratories and RIRT. These results correspond to the tentative uncertainty estimations for "direct synchronization" mode and common-view mode well enough [2,3]. They show also that the comparison accuracy for Russian laboratories are worse than the one for foreign laboratories. It can be explained by great ground antenna coordinate uncertainties, as well as using of non-effective models for account of ionosphere and troposphere delays in ASN-16 type receivers.

The increase of time comparison accuracy using this system can be achieved by standardization and subsequent realization of BIPM requirements to GLONASS time receivers and to processing procedures [4]:

- the use of standard formulas and parameters for calculation of ionosphere and troposphere corrections;
- the use of ground antenna coordinates of GLONASS receivers expressed in the International Earth Rotation Service (ITRF) in Cartesian x, y, z form and their transformations in PZ-90 frame system using standard formulas and parameters adopted by all manufactures, or use of transformation of broadcast ephemeredes from PZ-90 into ITRF according to a standardized set of formulas and parameters;
- the stabilization of receiver's antenna temperature.

CONCLUSION

The automated Receiving and Data Processing System on the basis of ASN-16 type receiver developed in RIRT provides GLONASS common-view time comparisons in accordance with BIPM and STFS schedules and data exchange with   other Russian and foreign laboratories.

The results of data processing show that the average value of the accuracy determination of the offset between user's clock relative UTC(SU) and GLONASS time is about 35 ns (rms) in "direct synchronization" mode. The average value of the accuracy of the remote clocks comparisons is about 15 ns (rms).

The increase of time comparison accuracy using this system can be achieved by standardization and subsequent realization of BIPM requirements to GLONASS time receivers and to processing procedures.

ACKNOWLEDGEMENTS

REFERENCES

1. Y.G.Gouzhva, A.G.Gevorkyan, P.P.Bogdanov, V.V.Ovchinnikov.   *Full-Automated System for Receiving and Processing GLONASS Data.*   Proc. of ION GPS-94 7th Intern.Techn. Meeting, 1994.
2. W.Lewandowski, J.Azoubib, A.G.Gevorkyan, P.P.Bogdanov, et al.   *First Results from GLONASS Common-View Time Comparisons Realized According to the BIPM International Schedule.* Proc. of the 28th Annual PTTI Applications and Planning Meeting, 1996.
3. W.Lewandowski, J.Azoubib, A.G.Gevorkyan, P.P.Bogdanov, et al.   *A Contribution to the Standardization of GPS and GLONASS Time Transfer.* Proc. of the 28th Annual PTTI Applications and Planning Meeting, 1996.
4. Y.G.Gouzhva, A.G.Gevorkyan, P.P.Bogdanov. *Comparing Synchronization Accuracy of Users Clock via GPS/GLONASS Signals.* Proc. of ION GPS-93 6th Intern.Techn. Meeting, 1993.
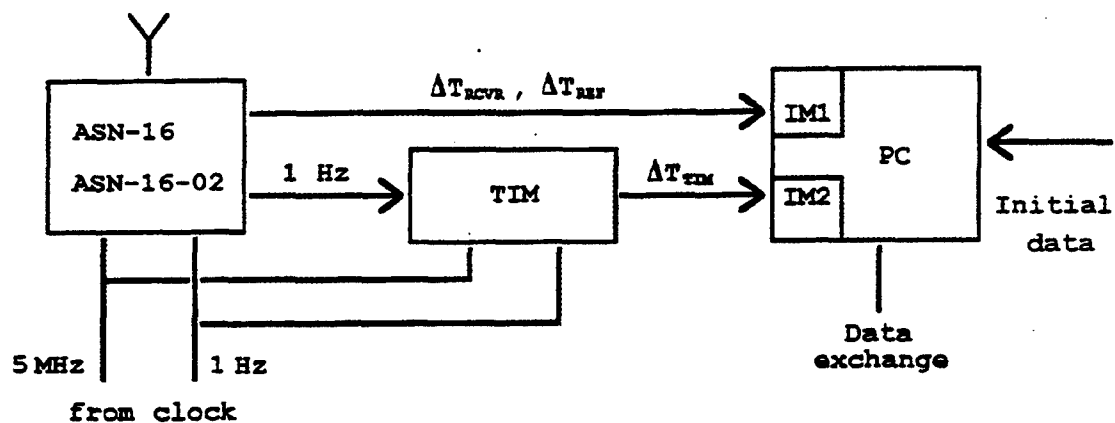
Figure 1. The block diagram of the Receiving and Data Processing System
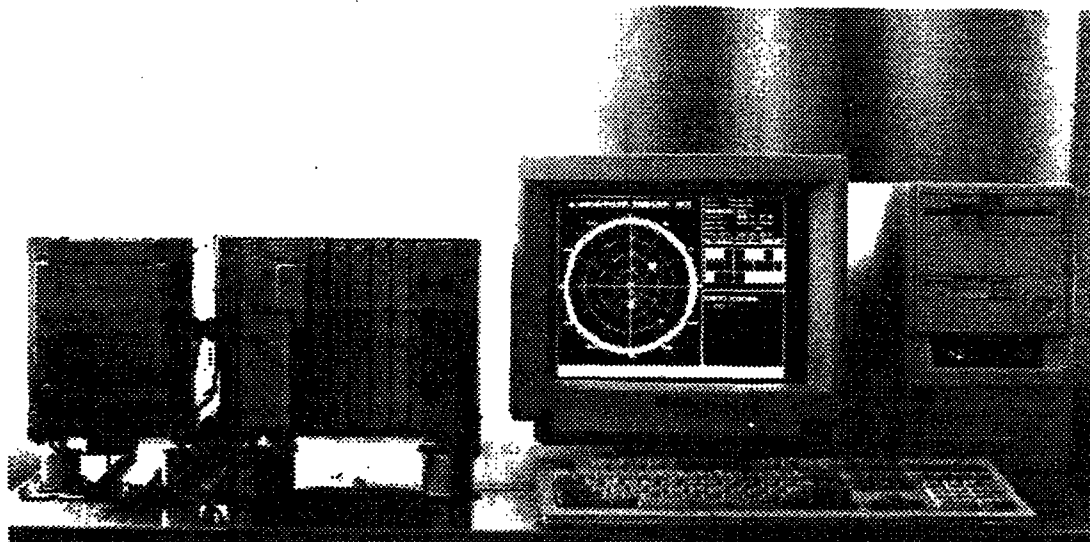
Figure 2. The view   of the Receiving and Data Processing System

Table 1. Specifications for Receiving and Data Processing System
on the basis of ASN-16 type receiver

Parameter	Value
Code operation	C/A
Operation frequency, MHz	1600
Measurements accuracy of pseudorange, m	0,5
Measurement time, s	1
Data output rate, s	2
Error of determination of the offset between user's clock and UTC(SU), ns	50
Error of determination of the offset between remote clocks, ns	20
Continuous operating not less than, hour	24
Power supply of the receiver (DC), V	27
Power consumption, W	150
Weigh, kg	27

Table 2. Laboratories observe GLONASS according to STFS
and BIPM schedules

Laboratory		Equipment
1. Laboratories observe CLONASS, according to STFS schedule:		
SU	(Mendeleevo, Russia)	ASN-16
ACSC	(Moskow region, Russia)	ASN-16
IRK	(Irkutsk, Russia)	ASN-16
KHAB	(Khabarovsk, Russia)	ASN-16
NSK	(Novosibirsk, Russia)	ASN-16
RIRT	(St.Petersburg, Russia)	ASN-16-02
KHAR	(Kharkov, Ukraine)	ASN-16
2. Laboratiries observe CLONASS, according to BIPM schedule:		
VSL	(Delft, Netherlands)	R-100/40T
DLR	(Oberpfaffenhofen, Germany)	R-100/10
RIRT	(St.Petersburg, Russia)	ASN-16-02
BIRM	(Beijing, China)	R-100/30
LDS	(Leeds, UK)	ISN-RX1
NIST	(Boulder, Colorado, USA)	R-100/30

Table 3. Results of accuracy estimation of clock comparisons

Laboratory	Uncertainty (rms), ns		
	UTC(i)-UTC(SU)	UTC(i)-GLONASS	UTC(i)-UTC(RIRT)
SU	21-48	21-33	11-19
ACSC	30-42	28-42	15-26
IRK	20-39	20-34	12-21
KHAB	21-41	20-32	16-28
NSK	25-38	24-34	11-23
RIRT	26-40	25-34	—
KHAR	22-45	21-37	11-24
VSL	27-40	26-33	9-14
DLR	29-43	29-37	11-13
BIRM	28-39	27-35	14-19
LDS	27-44	28-42	20-33
NIST	29-38	27-33	11-17

IEM KVARZ AND QUARTZLOCK'S GPS-DISCIPLINED RUBIDIUM FREQUENCY AND TIME STANDARD

Clive Green
Quartzlock (UK) Ltd., Devon, England, UK
IEM Kvarz, Nizhny Novgorod, Russia

Abstract

IEM Kvarz and Quartzlock have devised a GPS-disciplined rubidium frequency and time standard to 10^{-14} level accuracy. As a result of employing unique carrier phase tracking techniques with algorithmic weighting of "all-in-view" software clock techniques with an excellent OCXO or rubidium oscillator built in, both short-term stability (STS) at 10^{-13} level and long-term stability (LTS) to 10^{-14} is realized. Now IEM Kvarz and Quartzlock have reduced the overall size and most importantly introduced temperature control for both the antenna and the downconverter, receiver, and processor. The original quad helix antenna eliminates multipath errors and the need for a choke plate, while the downconverter at the antenna means that the coax carries only 90 MHz, so it can be very long and thin (not short and fat for 1.5 GHz). Time output accuracy meets GPS time transfer atomic clock comparisons at < 5 ns, while LTS can be little improved, and STS has wander, noise floor, and holdover built to the 10^{-14} level. IEM Kvarz and Quartzlock have now exceeded even high performance commercial cesium stability at only 20% of its cost and the need to employ a hydrogen maser test to maintain 10:1 integrity margin above GPS (and cesium) performance.

INTRODUCTION

IEM Kvarz and Quartzlock have devised a GPS-disciplined rubidium frequency standard with 10^{-14} and time to 5 ns uncertainty.

As a result of employing unique carrier phase tracking techniques with algorithmetic weighting of 'all-in-view' software clock techniques with an OCXO or Rubidium Oscillator built in, both short-term stability (STS) at 10^{-13} level and long-term stability(LTS) to 10^{-14} is realized.

Now it is planned to reduce the overall size and most importantly to temperature control the down converter, receiver, and processor. The original quad helix antenna eliminates multipath errors and the need for a choke plate, while the downconverter at the antenna means that the coax carries only 90 MHz, so it can be very long and thin (not short and fat for 1.5 GHz). Time output accuracy meets GPS time transfer atomic clock comparisons at <5 ns, while LTS can be little improved.

IEM Kvarz and Quartzlock have now exceeded even high performance commercial cesium stability at only 20% of its cost and the need to employ hydrogen masers in test to maintain 10:1 integrity margin above GPS (& cesium) performance.

A special measurement system had to be developed to meet the requirements of precision GPS frequency & time standards. A reference source with stability of parts in E-15, distribution amplifier with only <10ps/°C phase stability, and very low phase noise of -165 dBc/Hz at 100 Hz offset; extraordinary high isolation of 130dB and internal stability of 10^{-15} complement the phase comparator system with 1.5 10^{-15} resolution in a short measurement time 100 seconds.

The complete measurement system and results are described below.

Carrier phase tracking GPS enables this level to be maintained as tests at 5 & 33 days have demonstrated (5 x 10^{14})

Two demonstrations show identical results at locations 2,500 km apart using the best available national references in Germany (PTB) and Russia (IEM) for the carrier phase tracking GPS.

Certification of the 'starting point' passive hydrogen maser in the UK by NPL confirmed that performance to 10^{-14} levels in a stand alone portable unit with required retrace is realised . Measurement capability in a 100 second measurement time was realized at 1.5 10^{-15}.

Using a GPS-disciplined MTI oscillator (the 250 oven version at 1000s control time constant), time (!) error data relative to the PTB standard time were recorded in the PTB once an hour for several weeks. Over a time interval of 33 days, the linear regression of one-day-values (which in turn were derived from the one-hour-values) yielded a slope of (1.008 +/- .007)ns/d.

Now the slope of the time error data is the (averaged) frequency. Thus, from these measurements the frequency error was determined to be a systematic component of 1ns/d or 1$10^{-14}$, which corresponds to the frequency difference between UTC (PTB) and UTC (UNSO) to which GPS time is linked. This result could (within 33 days) be determined with an uncertainty of only 8* 10^{-16} !

Another result from the data was that the one-day-values for the time error (each calculated from 24 one-hour values) has a noise of only 3 or 4 ns. If you use these to estimate the frequency stability as 4 ns/86400s you get 5* 10^{-14} ! Even if you add a square root of 2 for beginning and end of the day, each having their own

uncertainty, you are still clearly better than 10^{-13} for the one-day-average frequency stability.

MEASUREMENT SYSTEM - QUARTZLOCK MODEL A7 FREQUENCY AND PHASE COMPARATOR

The two measurement inputs are called A and B. An input from the reference source at 5 or 10MHz is connected to A and an input from the device under test (DUT) is connected to B. The inputs A and B are actually interchangeable.

Both inputs are multiplied to 100MHz and then mixed down to 1MHz using an internal LO at 99 MHz. As the LO is common to both channels, any phase jitter or drift will eventually be removed when the channels are compared. The LO is actually phase-locked to one of the inputs. The 1MHz signals are multiplied to 10MHz. The 10 MHz from channel B is converted to 9MHz by mixing with 1MHz signal derived from the LO. The 10MHz from channel A is mixed with the 9MHz from channel B to give the 1MHz difference.

The basic 1MHz difference signal is made available at the front panel and is then processed further as follows:
It is filtered by a crystal filter and then multiplied by 5 to give 5MHz. This 5MHz is available at the front panel. The filtered 1MHz difference signal is then mixed down to 100MHz by means of a 900kHz LO-obtained division from the 99MHz LO. This 100kHz signal is then divided by 100000 to give 1Hz pulses, which are output to the front panel. The frequency difference multiplier may be operated in two modes, frequency mode and time difference mode.

THE PASSIVE HYDROGEN MASER FREQUENCY SOURCE

The 5 MHz frequency output of a CH1-76 passive hydrogen maser was measured at the National Physical Laboratory relative to two active hydrogen masers that form part of the UK national time standard. A brief description of the measurements and the results are provided below.

The Phase Measurements

A 5/10 MHz phase comparator (TimetechModel P/Comp 10-001/96) was used to measure the phase differences between the 5 MHz signals from two Sigma Tau active hydrogen masers (one Model MHM-2010, and one Model VLBA-112) and a CH1-76 passive hydrogen maser (serial no. 84065). The phase differences were recorded every second over a seven-day period from 1997 August 26 (MJD 50686)

to 1997 September 2 (MJD 50693). The performance of the phase comparator was monitored by recording common signal inputs. Comparisons of the three hydrogen masers relative to each other showed that the CH1-76 was the dominant source of instabilities for averaging times of 10 seconds or greater.

THE RESULTS - FREQUENCY OFFSET FOR PASSIVE MASER CH1-76

Figure 1 shows the phase differences between the CH1-76 passive hydrogen maser and the Sigma Tau active hydrogen maser (Model VLBA-112) from MJD 50686.5 to MJD 50693.3. The change in rate on MJD 50692 is a result of steering correction applied manually to the CH1-76 passive hydrogen maser. The mean frequency offsets of the CH1-76 maser relative to UTC (NPL), before and after the steer, are listed below.

MJD 50686.5 to MJD 50692.6 (CH1-76 after a cold start) mean relative fractional frequency offset = -44 x 10^{-14}

MJD 50692.7 to MJD 50693.3 (CH1-76 after manual steer) mean relative fractional frequency offset = 3 x 10^{-14}

THE RESULTS - FREQUENCY INSTABILITY FOR CH1-76

Figure 2 shows the phase differences between the CH1 - 76 passive hydrogen maser and the Sigma Tau active hydrogen maser (Model VLBA -112) From MJD 50686.5 to MJD 50692.6, with a frequency offset of 38 ns/day subtracted from the data. Note that data after the manual steer are not included. The instability in the frequency output of the CH1-76 passive hydrogen maser for averaging times from 10 to 10^5 seconds was calculated from the phase measurement data using the standard formula for the Allan variance ($\sigma^2_y(\tau)$):

$$\sigma^2_y(\tau) = (2(N-2)\ \tau^2)^{-1} \sum_{t=1}^{t=N-2} (x_{i+2} - 2x_{i+1} + x_i)^2$$

where the formula is applied to a data set of N evenly spaced points $x_1 \ldots x_N$ spaced an interval τ apart. The results of the calculations are shown in Figure 3. The values for the root Allan variances at averaging times increasing at decade intervals are listed in Table 1, and were determined by interpolating between the calculated results shown in Figure 3.

Table 1
Frequency instability of passive maser CH1-76 expressed as root Allan variances
for averaging times from 10 s to 10^5 s

τ (s)	σ_y
10	3×10^{-13}
10^2	9×10^{-14}
10^3	4×10^{-14}
10^4	2×10^{-14}
10^5	6×10^{-15}

Typical Results

Figure A: Frequency and time transfer stability characteristics of GPSDO at τ = 1,000s averaging time calculated from phase data

σ_y	MODσ_y	σ_x	Mean Fractional Frequency Offset
5.0×10^{-13}	3.5×10^{-13}	2.1×10^{-10}	6.3×10^{-13}

Figure B: Frequency and time transfer stability characteristics of GPSDOs at τ = 1,000s averaging time calculated from 1PPS data

σ_y	MODσ_y	σ_x	Mean Fractional Frequency Offset
1.0×10^{-12}	5.7×10^{-13}	3.6×10^{-10}	1.3×10^{-12}

Fig C: Performance Characteristics of GPSDO H (Quartzlock 8A-Rb)

Characteristics	GPSDO H
Mean Frequency Offset (τ=1,000s)	$5.0\text{x}10^{-13}$
Free Running Oscillator σ_y (τ=1,000s)	$6.0\text{x}10^{-13}$
Free Running Oscillator σ_y (τ=100,000s)	$6.0\text{x}10^{-14}$

REFERENCES

National Physical Laboratory Report, 23 September 1998.

Davis and Furlong, *"Report on the study to determine the suitability of GPS disciplined oscillators as time and frequency standards traceable to the UK national time scale UTC (NPL,"* October 1997.

W. Klische and G. Kramer, *"The GPS carrier as a practical frequency reference,"* European Time and Frequency Forum, 1997.

C. Little 1997/8, private communication.

A. Sheronov 1997/8, private communication.

N. Demidov 1997/8, private communication.
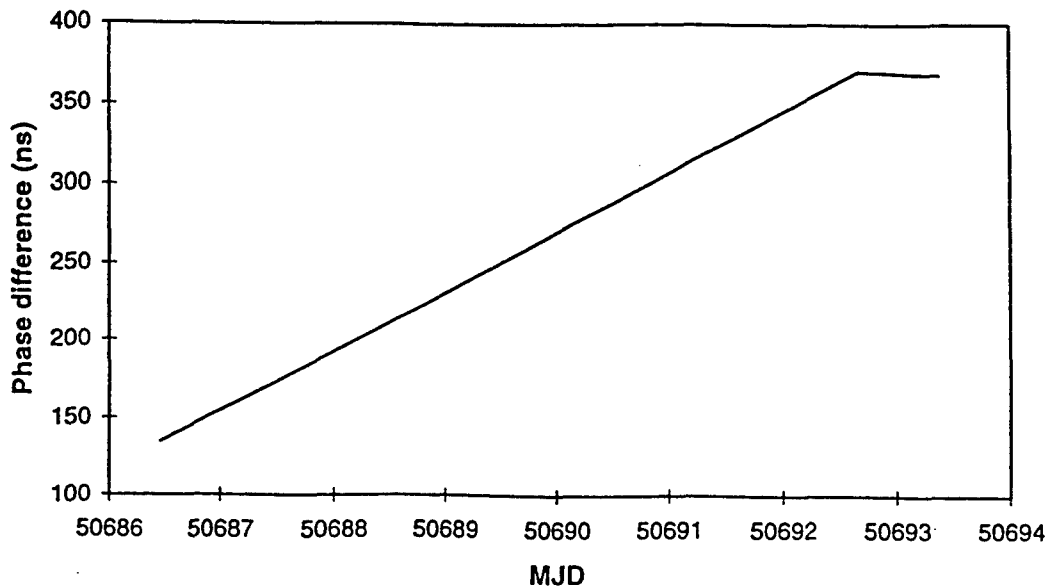
FIGURE 1 : phase difference between 5 MHz outputs of
NPL active hydrogen maser and CH1-76 passive hydrogen maser (serial
no. 84065)
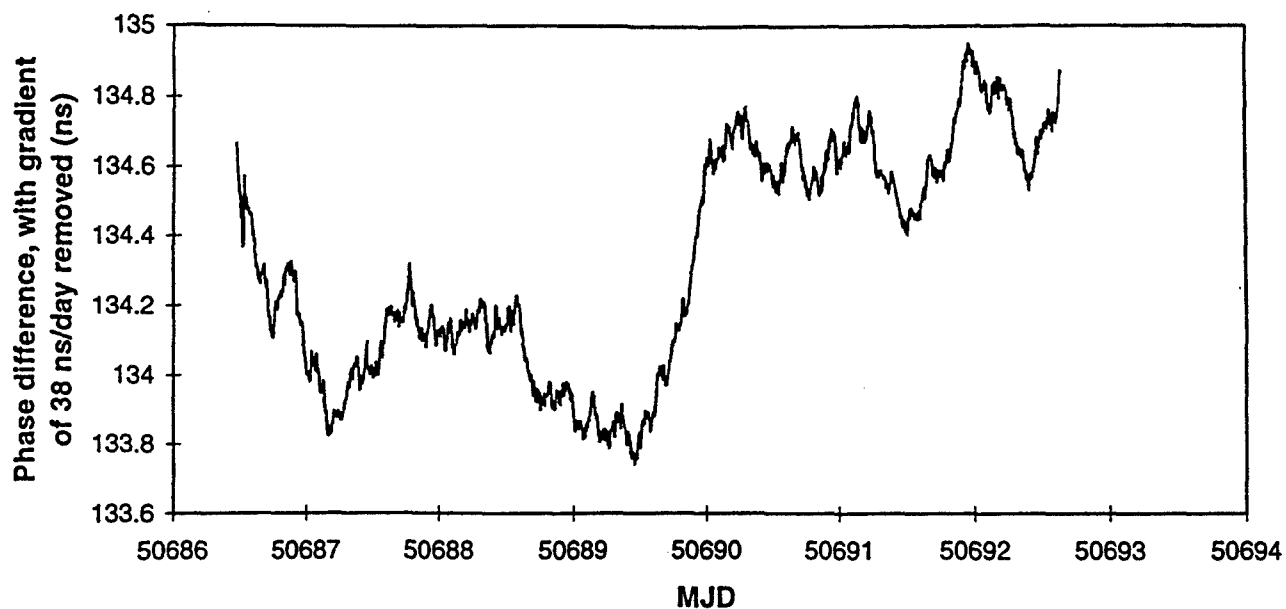
FIGURE 2: phase difference, with 38 ns/day gradient removed, between 5 MHz outputs of NPL active hydrogen maser and CH1-76 passive hydrogen maser (serial no. 84065)
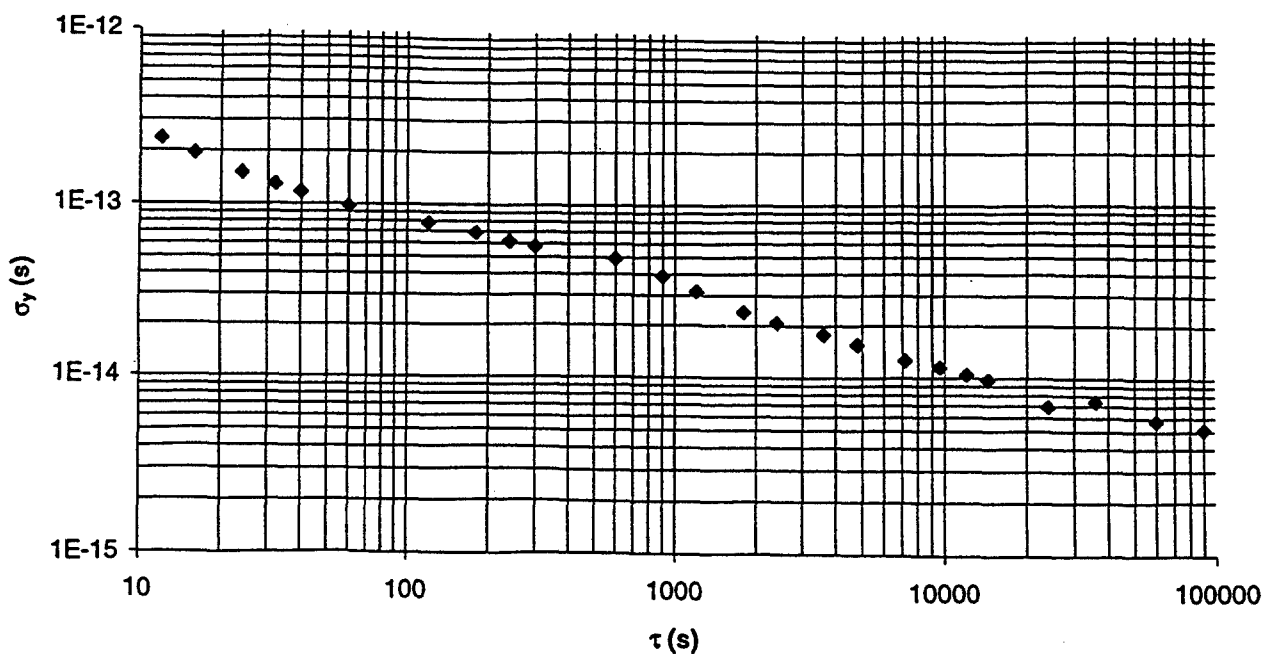
FIGURE 3: frequency stability of CH1-76 passive hydrogen maser (serial no. 84065) expressed in terms of the root Allan variance (σ_y)

PRECISE CLOCK SOLUTIONS USING CARRIER PHASE FROM GPS RECEIVERS IN THE INTERNATIONAL GPS SERVICE

J. F. Zumberge, D. C. Jefferson, D. A. Stowers,
R. L. Tjoelker, and L. E. Young
Jet Propulsion Laboratory, California Institute of Technology
4800 Oak Grove Drive, Pasadena, CA 91109-8099, USA
tel +1 818 3546734 fax +1 818 3934965
e-mail James.F.Zumberge@jpl.nasa.gov

Abstract

As one of its activities as an Analysis Center in the International GPS Service (IGS), the Jet Propulsion Laboratory (JPL) uses data from a globally distributed network of geodetic-quality GPS receivers to estimate precise clock solutions, relative to a chosen reference, for both the GPS satellites and GPS receiver internal clocks, every day. The GPS constellation and ground network provide geometrical strength resulting in formal errors of about 100 psec for these estimates.

Some of the receivers in the global IGS network contain high quality frequency references, such as hydrogen masers. The clock solutions for such receivers are smooth at the 20-psec level on time scales of a few minutes. There are occasional (daily to weekly) shifts at the microsec level, symptomatic of receiver resets, and 200-psec-level discontinuities at midnight due to 1-day processing boundaries.

Relative clock solutions among 22 IGS sites proposed as "fiducials" in the IGS/BIPM pilot project have been examined over a recent 4-week period. This allows a quantitative measure of receiver reset frequency as a function of site. For days and sites without resets, the Allan deviation of the relative clock solutions is also computed for subdaily values of τ.

TWO-STATION EXAMPLE

Figure 1 shows the network of geodetic-quality receivers in the International GPS Service. A number of these use hydrogen maser frequency references, some of which have been proposed as timing fiducials in the IGS/BIPM pilot project (http://maia.usno.navy.mil/gpst.html) to use the phase of the GPS carrier in time transfer (e.g.[1]). These sites are indicated by large circles in Figure 1.

The GPS phase and pseudorange observables are modeled as

$$L_r^x = \rho_r^x + b_r^x + z_r^x + \omega_r^x + C_r - c^x + \nu_r^x \tag{1}$$

and

$$P_r^x = \rho_r^x + z_r^x + C_r - c^x + \eta_r^x, \tag{2}$$

where L_r^x (P_r^x) is the measured phase (pseudorange) between transmitter x and receiver r, ρ_r^x is the range, b_r^x is phase bias, z_r^x is the troposphere delay, ω_r^x is the phase windup, C_r is receiver clock, c^x is transmitter clock, and ν_r^x (η_r^x) is the phase (pseudorange) noise. One receiver clock is chosen as a reference; all clock solutions are relative to the reference. No a priori correlations are assumed among clock solutions.

At JPL's IGS Analysis Center, each day a subset of 37 stations in Figure 1 is selected with good geographic distribution. Data from this subset are used to estimate precise transmitter parameters[2]. Receiver parameters from sites not in the subset can be determined with precise point positioning[3]. The formal error of each estimated clock is about 100 psec (3 cm).

Figure 2 shows the Madrid, Spain (mad2) clock estimate minus the Tidbinbilla, Australia (tid2) clock estimate during April, 1998. The difference is piecewise linear with occasional μsec-level shifts. The shifts represent a change at one of the sites, usually a receiver-induced reset.

For this clock "baseline" the period April 17-30, 1998 is free of resets. The mad2 − tid2 difference has been de-trended for this period (the slope − about 7 nsec/day $\approx 8 \times 10^{-14}$ − is the result of a frequency offset between the two sites) and shown in Figure 3. Except for the 0.2-nsec-level shifts − due to 1-day processing boundaries − the solution is smooth at the 20-psec level.

IGS/BIPM CLOCK SITES, OCTOBER 1998

Information on stations in the IGS can be found at http://igscb.jpl.nasa.gov. The sites with 4-character IDs

```
algo brus drao fair fort gode gol2 hob2 irkt kokb mad2 mate nlib nyal nrc1 onsa piel
tid2 usno wes2 wtzr yell
```

have been proposed as timing fiducials in the IGS/BIPM pilot project. For each day during the 4-week period beginning October 4, 1998, we have computed the relative clock estimates among all clock baselines, and then computed the Allan deviation $\sigma(\tau)$

$$\sigma(\tau) = \sqrt{\frac{\sum_{i=1}^{N-2m}(x_{i+2m} - 2x_{i+m} + x_i)^2}{2(N-2m)\tau^2}}, \tag{3}$$

where $m = \tau/\tau_o = 1, 2, 4, 8, ...64$ and $\tau_o = 300$ sec is the spacing of data used in parameter estimation. In (3), x_i indicates the ith difference in clock estimates between the two sites that form the baseline.

In the event that a given receiver has a sufficiently large discontinuity in its clock during the day, the Allan deviation of that receiver with respect to any other will be

anomalously large. This suggests that, to determine whether a given receiver had a shift during the day, one should look at its Allan deviation with respect to all other receivers, and choose the smallest. If this is sufficiently small, it did not have a shift during that day.

Figure 4 gives an example for October 27, 1998. For each site indicated on the abcissa, the values of $\sigma(\tau)$ for that site with respect to other sites are plotted as ordinates. It is clear that four sites – fort, gode, hob2 and nlib – have variations on that day that are large with respect to the other sites. In Figure 4 we have taken $\tau = 600$ s, although the character of such a plot is the same for other values of τ.

For each receiver, day, and τ, we have computed the smallest $\sigma(\tau)$. The median values over the 4-week period are given in Table 1. (Median is used because it is insensitive to outliers.) On a given day, if a receiver can be paired with no other to achieve $\sigma(\tau) < 10^{-12.9}$ for $\tau = 600$ s, then that receiver is assumed to have a shift during that day. The number of such days are given as the last column in the table. Because it was disconnected from its H maser during most of October (IGS Mail 2034, October 2, 1998, ftp://igscb.jpl.nasa.gov/igscb/mail/igsmail/igsmess.2034) the results for hob2 (Hobart, Tasmania) are indicative of the receiver's internal oscillator.

As an example, the results using this methodology for the clock at Algonquin Park, Canada (algo) are plotted in Figure 5.

CONCLUSIONS

Of 22 sites proposed for use in the IGS/BIPM pilot project, four exhibited no resets during the 4-week period beginning October 4, 1998. For 17 others (excluding 1 which was using its internal oscillator), there were typically 1 to 9 days where the receiver exhibited a reset. Allan deviations are typically $\log_{10} \sigma(\tau) \approx -13.2 \pm 0.1$ at $\tau = 300$ s to $\log_{10} \sigma(\tau) \approx -14.2 \pm 0.3$ at $\tau = 19200$ s.

REFERENCES

[1] Kristine Larson and Judah Levine 1995, *"Time Transfer Using the Phase of the GPS Carrier,"* **IEEE Transactions on Ultrasonics, Ferroelectrics, and Frequency Control**, 45, 3, 539-540.

[2] J. F. Zumberge, M. M. Watkins, and F. H. Webb 1998, *"Characteristics and Applications of Precise GPS Clock Solutions Every 30 Seconds,"* **Navigation** , 44, 4, 449-456.

[3] J. F. Zumberge, M. B. Heflin, D. C. Jefferson, M. M. Watkins, and F. H. Webb 1997, *"Precise point positioning for the efficient and robust analysis of GPS data from large networks,"* **J. Geophys. Res**, 102, B3, 5005-5017.

site	τ 300 s	600 s	1200 s	2400 s	4800 s	9600 s	19200 s	shift days
algo	-13.32	-13.56	-13.78	-13.95	-14.14	-14.28	-14.40	0
brus	-13.21	-13.27	-13.31	-13.43	-13.54	-13.53	-13.75	2
drao	-13.32	-13.54	-13.73	-13.91	-14.06	-14.18	-14.32	1
fair	-13.25	-13.50	-13.73	-13.89	-14.10	-14.23	-14.51	6
fort	-13.02	-13.19	-13.44	-13.64	-13.71	-13.68	-13.60	9
gode	-13.32	-13.49	-13.72	-13.90	-13.98	-14.05	-13.99	6
gol2	-13.25	-13.49	-13.73	-13.94	-14.13	-14.26	-14.41	7
hob2	-9.20	-9.42	-9.70	-9.99	-10.30	-10.60	-10.89	23
irkt	-12.69	-12.96	-13.21	-13.47	-13.66	-13.85	-13.98	10
kokb	-13.20	-13.36	-13.54	-13.75	-13 93	-14.10	-14.25	4
mad2	-13.26	-13.44	-13.61	-13.82	-13.99	-14.15	-14.28	6
mate	-13.25	-13.35	-13.50	-13.68	-13.84	-13.87	-13.85	9
nlib	-13.27	-13.49	-13.66	-13.77	-13.99	-14.11	-14.20	4
nyal	-13.14	-13.36	-13.58	-13.77	-13.93	-14.04	-13.64	8
nrc1	-13.28	-13.48	-13.67	-13.80	-14.00	-14.14	-14.31	3
onsa	-13.28	-13.47	-13.65	-13.83	-13.98	-14.11	-14.24	3
pie1	-13.31	-13.53	-13.74	-13.93	-14.11	-14.32	-14.52	0
tid2	-13.13	-13.35	-13.57	-13.78	-13.92	-14.01	-14.11	0
usno	-13.25	-13.50	-13.75	-13.93	-14.13	-14.33	-14.54	0
wes2	-13.31	-13.51	-13.74	-13.90	-14.04	-14.07	-14.14	1
wtzr	-13.14	-13.32	-13.51	-13.70	-13.93	-14.10	-14.21	1
yell	-13.15	-13.39	-13.60	-13.75	-13.92	-13.98	-14.22	6

Table 1: Allan deviation $\log_{10} \sigma(\tau)$ as a function of site for subdaily values of τ. The *shift days* column counts how many days during the 4-week period beginning October 4, 1998 the receiver clock exhibited a step function. Note that the H maser at hob2 was not connected to the receiver for nearly all of October, so that results for it characterize the receiver's internal oscillator.
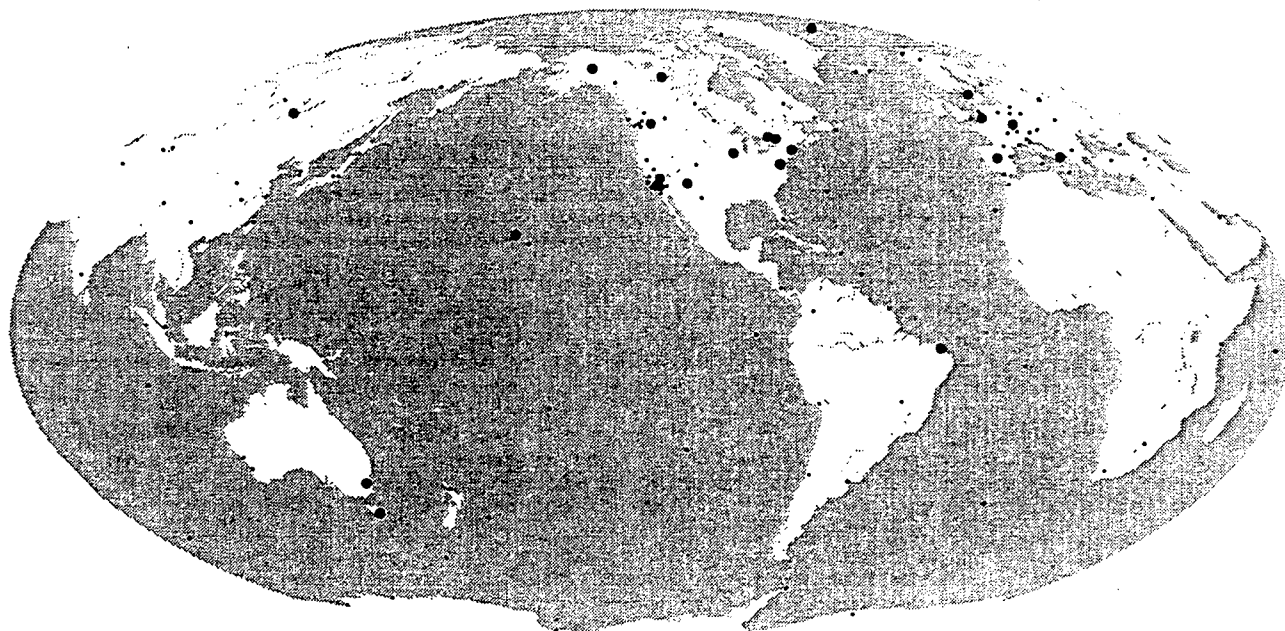
Figure 1: The IGS network as of Oct 15, 1998. The large circles indicate sites proposed as timing fiducials in the IGS/BIPM pilot project.
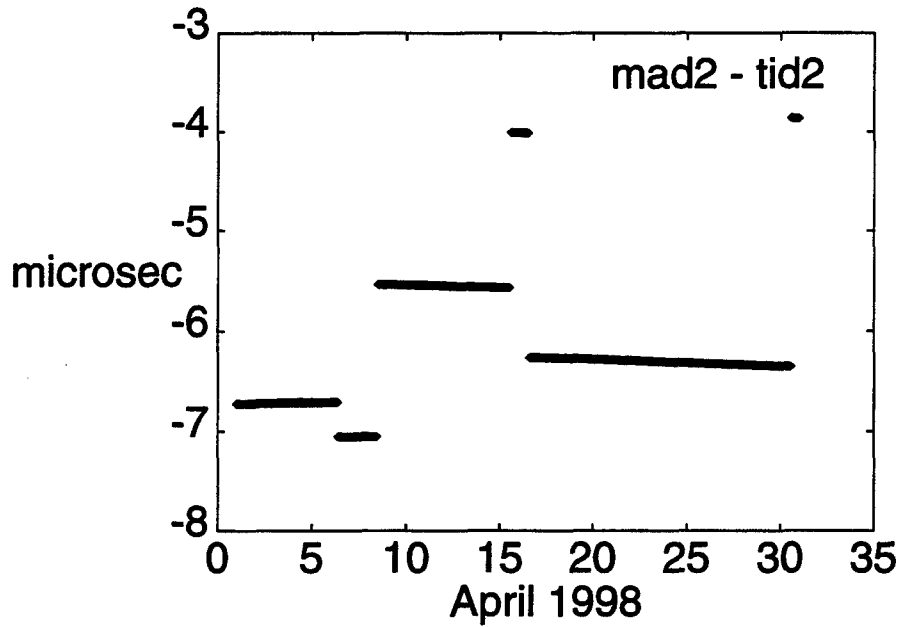
Figure 2: The Madrid, Spain clock solution minus the Tidbinbilla, Australia clock solution, during April, 1998. The difference is piecewise linear with occasional μsec-level shifts. The shifts are presumably symptoms of changes at one or both of the sites.
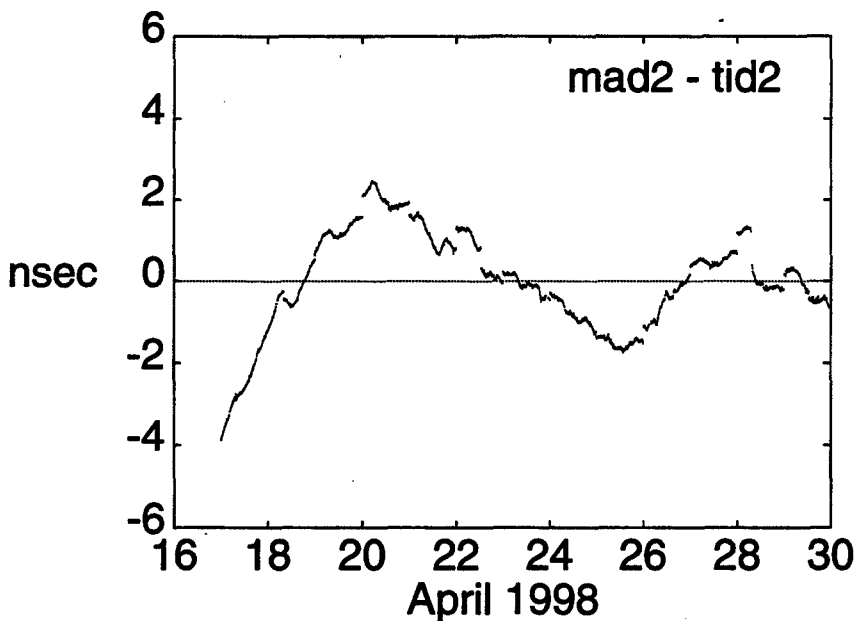
Figure 3: The Madrid, Spain clock solution minus the Tidbinbilla, Australia clock solution, for April 17-30, 1998. The difference has been de-trended (the slope is about 7 nsec/day $\approx 8 \times 10^{-14}$). Except for the 0.2-nsec-level shifts – due to 1-day processing boundaries – the solution is smooth at the 20-psec level.
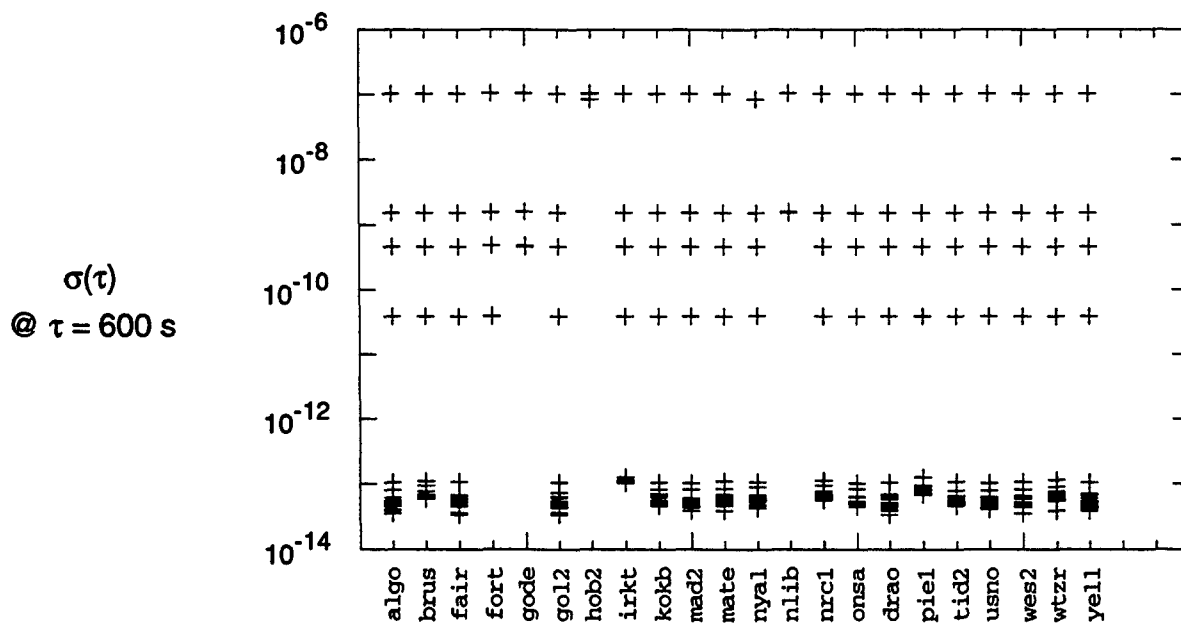
Figure 4: The Allan deviation at $\tau = 600$ s on October 27, 1998, for all baselines among the 22 proposed timing fiducials. The figure indicates that none of the four sites fort, gode, hob2, nlib could be paired with any site to achieve $\log_{10} \sigma(\tau) < -12.9$.
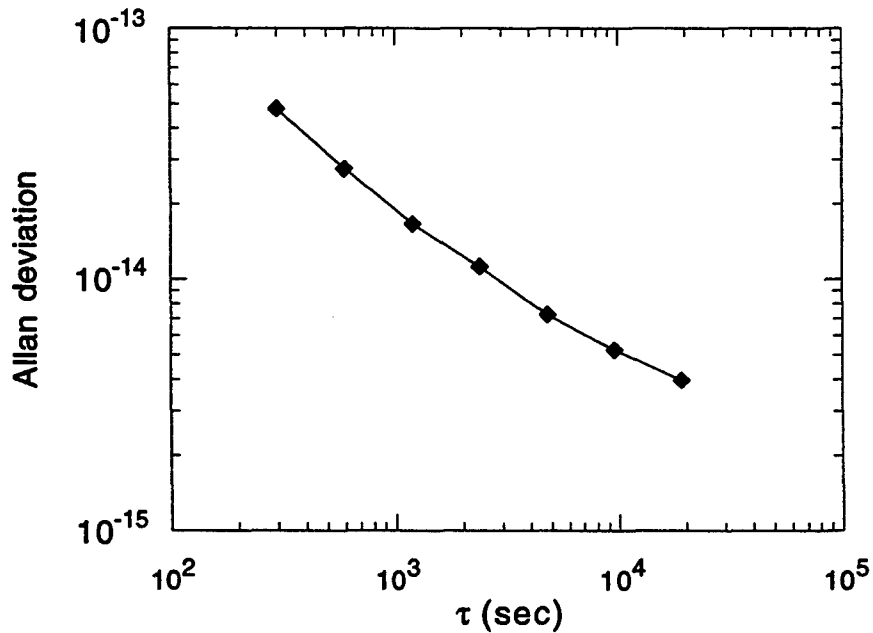
Figure 5: The Allan deviation for Algonquin Park, Canada; see text for methodology. The logarithmic slope is -0.60.

Questions and Answers

JIM RAY (USNO): Jim, will you make this information available once you get it operational?

JIM ZUMBERGE (JPL): Yes, I think we would make it public. We are not quite ready yet.

CALIBRATION CONSIDERATIONS FOR THE IGS/BIPM PILOT TIME TRANSFER PROJECT USING CARRIER PHASE

R. Beard, J. Brad, J. White, and O. J. Oaks
U.S. Naval Research Laboratory
4555 Overlook Ave., SW, Washington, DC 20375, USA

G. P. Landis
SFA, Inc.

Abstract

During the spring of 1998 a pilot project was begun between the Bureau International des Poids at Mesures (BIPM) and the International GPS Service (IGS) to investigate the accuracy of time and frequency comparisons using GPS phase and code measurements. The IGS has established a cooperative network of stations around the world which gather GPS data, analysis centers that provide analysis products from these GPS data and other contributed data. The precision of the data and products has made major contributions to geodynamics and earth sciences and presents the possibility of highly precise time and frequency comparisons.

To compare time information between two sites by whatever means requires the time of propagation of the signal through the equipment, cables, and space to be precisely and accurately known. IGS differential measurements with GPS carrier phase data are highly precise and must be accurately calibrated in order to provide time comparisons. This paper will address the problems and possible techniques for calibration for time comparison. Specialized equipment and GPS system simulators will be described that calibrate from signal reception in the antenna through receiver output.

PURPOSE

During 1998 a pilot project between the International Global Positioning System Service (IGS) and the Bureau International des Poids et Mesures (BIPM) was established to investigate the capability of using GPS carrier phase measurements for time transfer [1]. If this capability can be exploited, the high precision GPS measurements that are providing new dimensions in geophysical research could likewise provide time transfer users with an order of magnitude improvement. Such an increase is highly desirable as a means of comparing the new frequency standards being developed at the various worldwide timing centers. These new frequency standards are requiring a comparison capability far in excess of GPS Common-View capabilities. For the geophysical community, the improved timing capability could be used to relate their measurements to an accurate international time scale reference rather than using GPS Time as the common time.

GPS receivers deployed in the IGS are used to make high precision GPS satellite carrier phase signal measurements between receivers in the network. Careful site and equipment parameters are determined to account for equipment delays and other effects that would degrade the high precision desired. Considerable efforts have already been made in investigating the environmental stability of equipment and

cabling delays that would change during or between the observation times and introduce errors [2]. However, the IGS measurements are based primarily on differential measurements between sites. Common and fixed delays in individual sites or between sites would appear as biases which could be removed without affecting the precise ranging measurements but would leave them ambiguous as to the actual time delay from the satellites through the equipment. Fiducial stations are established to provide a spatial reference within an international earth reference frame. To likewise establish a temporal reference, however, the actual delays and other effects corrupting time propagation through the equipment and between the local time reference or clock are required. This requirement is necessary to determine accurately the time interval from the time scale reference and maintain time epoch. The GPS receivers and associated equipment must be precisely calibrated to permit this kind of precise and accurate, timing measurements to be made at the IGS stations. With this calibration, time can be accurately determined throughout the network. This effort is to examine the ability to perform this calibration and translate this capability for use in IGS stations.

APPROACH

In precise geo-positioning the range to the satellite is described by the pseudorange equation for code phase measurements and by the carrier phase equation for carrier phase measurements [3,4]. The equation for pseudorange (ρ) is

$$\rho = R + c \cdot (b_u - B) + c \cdot (T + I + \upsilon)$$

where R = geometric range, c = speed of light, b_u = site local clock bias, B = satellite clock bias, T = tropospheric propagation error, I = ionospheric propagation error and υ = noise term. The local clock bias in this measurement is a combination of the internal delays in the antenna and antenna cables (Cal $_C$), internal delays in the receiver (Cal$_{Int}$) and the clock offset itself (Clk), as in

$$b_u = Cal_C + Cal_{Int} + Clk.$$

The equation for carrier phase ($\Phi_{u,s}$) is

$$\Phi_{u,s} = R + c \cdot (b_u - B) + c \cdot (T - I + \upsilon_{u,s}^{(\phi)}) + N_{u,s} \cdot \lambda$$

where $\upsilon^{(\phi)}_{u,s}$ is the noise term, which is not necessarily the same as the term in the pseudorange equation, $N_{u,s}$ is the ambiguous number of integer carrier wavelengths difference between the geometric range and measured range at the receiver, and λ is the wavelength of the carrier frequency. The inherent difference between the code and carrier wavelengths and ability of the receiver to measure a fraction of the wavelength that accounts for the carrier phase increased precision. The penalty for this increase is the ambiguous nature of the continuous carrier frequency signal. The precise and accurate determination of the value of Cal$_C$ and Cal$_{Int}$ so that it may be applied to the traceability of time through the observational receiver system is the object of this investigation.

SIMULATION AND RECEIVER INSTRUMENTATION

To precisely and accurately calibrate GPS geodetic receivers the approach of using a GPS satellite simulator was investigated. Previous efforts at NRL in testing the capability of military and civilian GPS Code receivers for timing output through the timing interface resulted in a simulator laboratory being developed. This technique of simulating the satellite constellation signal was used in tests of approximately 25 different types of military and civilian receivers for time dissemination using passive reception in a stand-alone configuration. These tests and others performed in this facility have resulted in GPS time dissemination measurements accurate to approximately two nanoseconds [5]. To be able to

calibrate a GPS receiver to the 10 or 20 picosecond level needed for carrier phase measurements requires the integrity and accuracy of the simulator to similar levels.

The Northern Telecom model STR 2760 simulator is used for this effort [6]. This simulator is capable of providing Clear/Acquisition (C/A), Protected (P), or Secure P(Y) signals from up to 10 GPS satellites simultaneously on both L1 and L2 frequencies. It uses an external hydrogen maser reference signal to avoid frequency changes during the test runs. The simulator and the associated equipment configuration are illustrated in Figure 1. The particular times and coverage of the satellite constellation and control commands for the simulator are provided by the Alpha workstation. In this experiment the accuracy and precision of the simulator signals were also factors in the evaluation so the Secure mode (GPS AntiSpoofing signal) was set to zero in the simulations described below. The other factors in signal propagation, such as ionospheric and tropospheric errors, were also set to zero. An independent examination of the coherent interchannel bias between the carrier and code signals using a wideband digital sampling oscilloscope was undertaken. Each of the 20 RF output channels from the simulator were activated individually with code-only modulation. The phase at a time marker, placed a specified delay from the one-pulse-per-second output, was noted for each channel. The results indicated that all channels kept the same integer and fractional phase values from the 1PPS output. The uncertainty due the RF noise was approximately ±200 ps. Also, each code modulation pattern was inspected to insure that the interchannel bias was less than one nanosecond. This confirmed the simulator's capability to provide coherent phase information to the test receivers.

The local clock used was the in-house hydrogen maser reference for the Precision Clock Evaluation Facility. For these simulations accurate timing was not evaluated. Precision of the simulator and receivers in the different ranging mode required coherence throughout the configuration.

Two geodetic-quality TurboRogue receivers [7] capable of receiving eight satellites on two frequencies simultaneously were used to receive the simulated signals. Short cabling connected the receivers to the simulator to minimize delays or uncertainties. Actual installation cable lengths and antennas would cause greater uncertainty and will ultimately need calibration for operational use. These tests were designed to examine the internal delays and possibility of correlating the code and carrier measurements. If these two parameters may be sufficiently correlated without ambiguity in the calibration process, the calibration values would be more meaningful in operation.

As an independent measure of the delays through the equipment the one-pulse-per-second (1PPS) signals from the simulator and the receivers were collected and compared to the receiver measured values. These data can also be used to correlate the 1PPS generation in the receiver.

SIMULATION AND DATA REDUCTION

Two simulation runs were performed. In each run nine satellite signals were generated and data were collected in the two receivers for approximately 1800 seconds. The 1PPS signals were collected manually by alternately taking readings from the two receivers.

The simulator range data have a resolution of 10.0 mm. A least-squares method is used to fit a polynomial to the simulator range data and the coefficients of the polynomial are used to calculate the simulator filtered range data. The order of the fit is increased until the standard deviation of the fit is consistent with the 10.0 mm resolution. The carrier phase residuals are calculated by taking the difference between the receiver carrier phase measurements and the filtered simulator range data. In an ideal system this value

should be equal to the integer number of wavelengths of the range when the receiver starts tracking the satellite. Starting with the carrier phase residual data expressed in wavelengths, the integer and fractional data are calculated. Changes in the integer part are due to cycle slips. The magnitude of the fractional part adjusted to be less than half. Continuous carrier phase fractional data are generated, adding an integer number of wavelengths to the carrier phase fractional data such that the absolute difference between samples is less than a half wavelength. The integer correction for the first sample is set at zero. This operation is necessary to correct for phase rollovers.

DATA RESULTS

Results from the first simulation run will be presented. The pseudorange residuals derived from the true range determined from the simulation command setup and the first channel in receiver #1 is shown in Figure 2. These residuals are uncorrected for the local clock offset; consequently, larger measured residual values than normal are shown on the ordinate axis. The precision and relationship of the code and phase values are being evaluated. The three pseudorange measured values, Clear/Acquisition (C/A), Precise Code on L1 (P1) and Precise Code on L2 (P2) are shown. The apparent jump in the P2 is relatively common in these receivers. All channels and satellites received are shown in Figure 3. The grouping of the data around the respective values shows good precision. The channel jumps are clearly shown, although not all channels show them.

If the biases and trends are removed and shown with the carrier phase values, the result is shown in Figure 4. A wavelength of L1 is shown for scale to demonstrate the precision capability of the receiver to measure the pseudorange under ideal conditions. The truth data from the simulator are quantized at the 10 mm level.

All pseudorange measurements from receiver two are shown in Figure 4. No jumps are evident and the biases between the C/A, P1, and P2 values are less. The carrier phase values for all simulated satellites from receivers #1 and #2 are shown in Figures 6 and 7 respectively. There is a bias between the pseudorange as shown in Figures 3 and 5. The primary source of the bias is the clock error value in each receiver's solution.

The significance of these data is the relative level of noise evident in the combination of simulator and receiver. Clearly, this setup shows that short-term noise will not be a limiting factor in calibration down to around 10 picoseconds. The other feature on the data is the walk in relative phase between all channels of both receivers and the simulator. Since the excursion is evident in both sets of receiver data, the most likely source of the phase change is in the simulator, the clock signals, or the distribution to the receivers. Such variations will likely be among the limiting factors of any approach to absolute calibration.

The primary concern in calibration, though, will be the absolute truth of the calibration. There must be a way to differentiate between the identical carrier cycles to be able to make a time comparison between simulator and receiver. The TurboRogue receivers provide a one pulse per second (1 PPS) that is derived from the receiver's internal clock. They also provide a correction in the output data stream between the generated time of the 1 PPS signal and the receiver's best estimate of time. All reported time and carrier phase data in the receiver are relative to this receiver clock. In principle, measurement of the 1 PPS against the simulator tick and application of the data correction should provide the necessary link.

It has been reported [8] that the internal factors in the receiver design cause ambiguities in the 1 PPS which are not corrected by the output data. Another critical factor in this approach is the 1 PPS signal itself (Figure 8). The rise time of the signal is much greater than the few picoseconds desired in the calibration

process. Establishment of a specific point on the rising edge of the pulse is helpful, but even so, there is roughly a 100:1 ration between the nanosecond rise time and 10 picosecond measurement.

SUMMARY

These results have demonstrated that the STR 2760 simulator is an exceptionally quiet signal source. It also raises the possibility of wandering of the relative phase in the range of half a wavelength or more. The next step in this process will be to repeat the measurements with receivers of another design to sort out the receiver and simulator contributions to uncertainty in the absolute delay. We will also update the simulator firmware and software to reduce the possibilities of simulator-induced errors.

Once successful calibration of directly connected receivers can be achieved with the upgraded simulator, the next step will be to look at the complete receiving equipment. A special anechoic chamber, developed for this purpose, will be used. The configuration is shown in Figure 9. This chamber will be used to determine a calibration factor for the complete equipment suite from antenna to receiver output.

REFERENCES

[1] J. R. Ray 1998 , "The IGS/BIPM time transfer project," IGS Analysis Center Workshop Proceedings, European Space Operations Centre, Darmstadt, Germany, pp. 65-70.

[2] F. Overney, Th. Schildknecht, and G. Beutler 1997 , "GPS time transfer using geodetic receivers: Middle-term stability and temperature dependence of the signal delays," Proceedings of the 11th European Frequency and Time Forum, Neuchâtel, Switzerland, pp. 504-508.

[3] P. Axelrad and R.G. Brown 1996, "GPS Navigation Algorithms," *Global Positioning System: Theory and Applications, Volume 1*, Parkinson and Spilker, eds., Volume 163 Progress in Astronautics and Aeronautics, American Institute of Aeronautics and Astronautics, Inc., 370 L'Enfant Promenade, SW, Washington, D.C. 20024-2251 8, pp. 409-433.

[4] A. Kleusberg and P.J.G. Teunissen, eds., 1996 , *GPS for Geodesy*, Lecture Notes in Earth Sciences 60, Springer-Verlag, Berlin/Heidelberg.

[5] V. Zhang, M. Weiss, E. Powers, and R. Loiler 1998, "GPS Week Roll-over & Y2K Compliance for NBS-Type Receivers," Proceedings of the 30th Annual PTTI Systems and Planning Conference, 1-3 December 1998, Reston, Virginia, U.S.A.

[6] STR 2760 GPS Simulator Reference Manual, Version 3.08, dated March 1997.

[7] TurboRogue Operators Manual, Allan Osborne Associates, Software Version 3.2.32.1, June 1995.

[8] E. Powers 1998, "Hardware Delay Measurements and Sensitivities in Carrier Phase Time Transfer," Proceedings of the 30th Annual PTTI Systems and Planning Conference, 1-3 December 1998, Reston, Virginia, U.S.A.
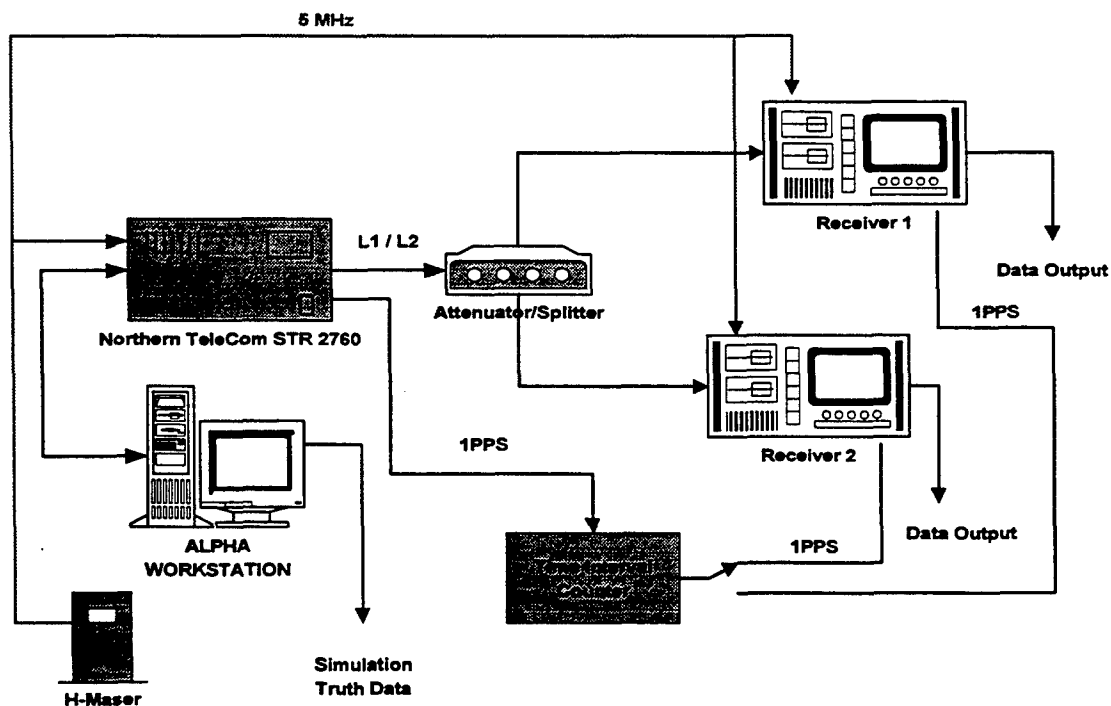
Figure 1. Simulation Configuration
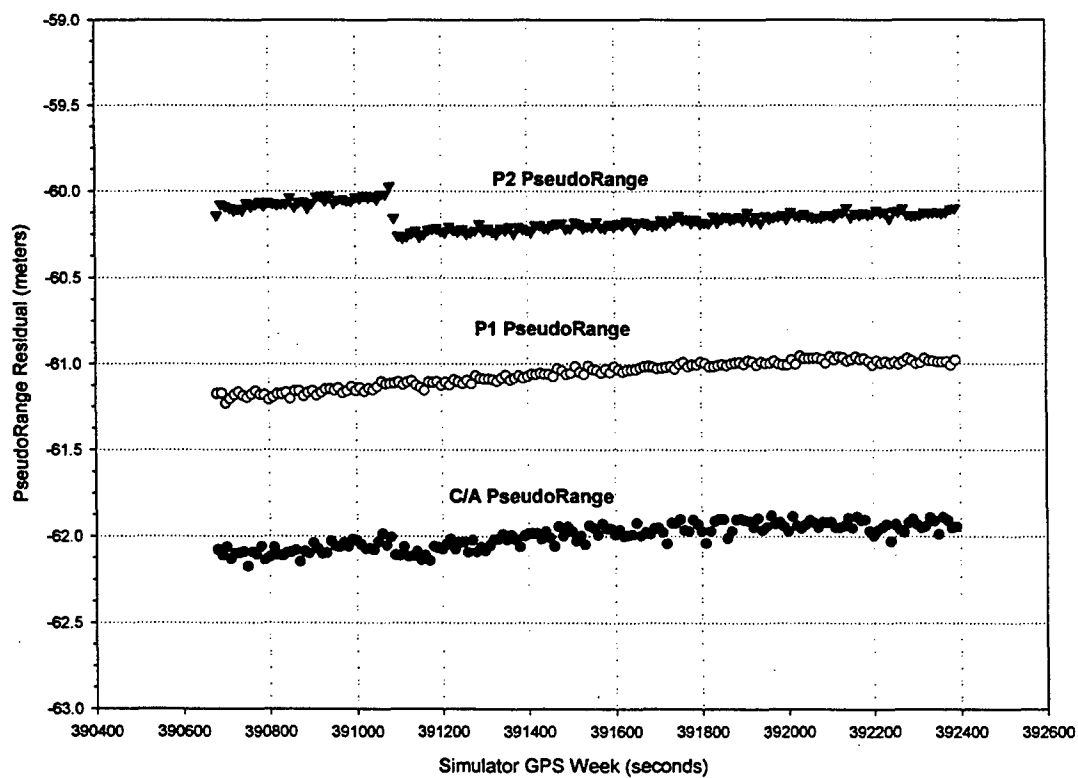
Figure 2. Receiver One PRN 01
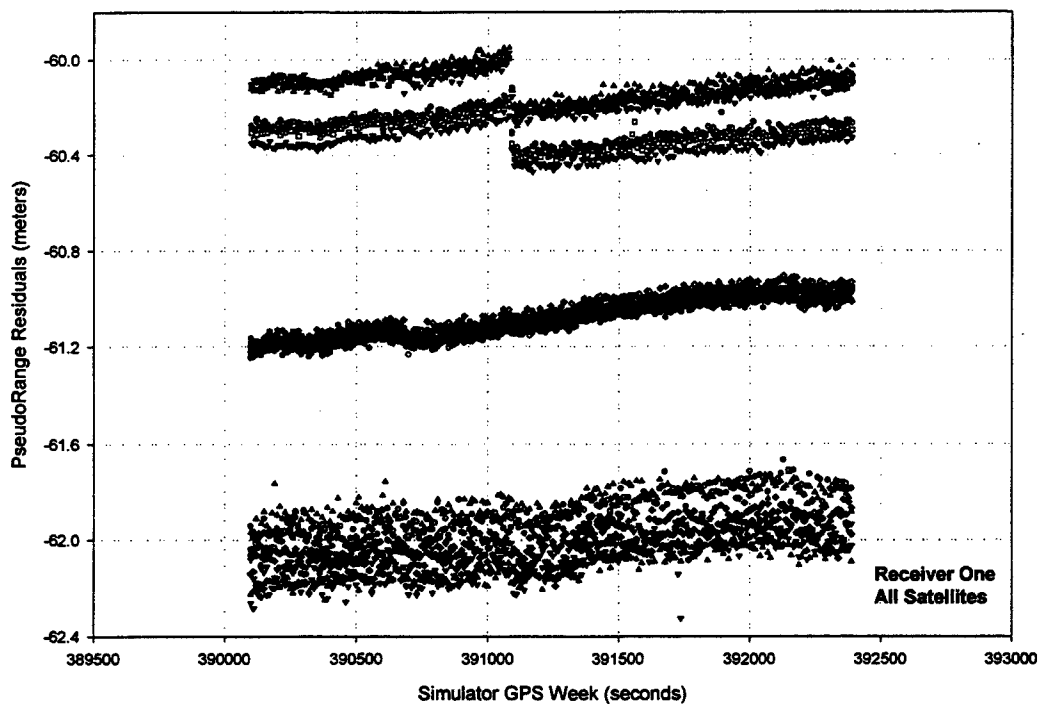
Figure 3. Receiver One All Satellites
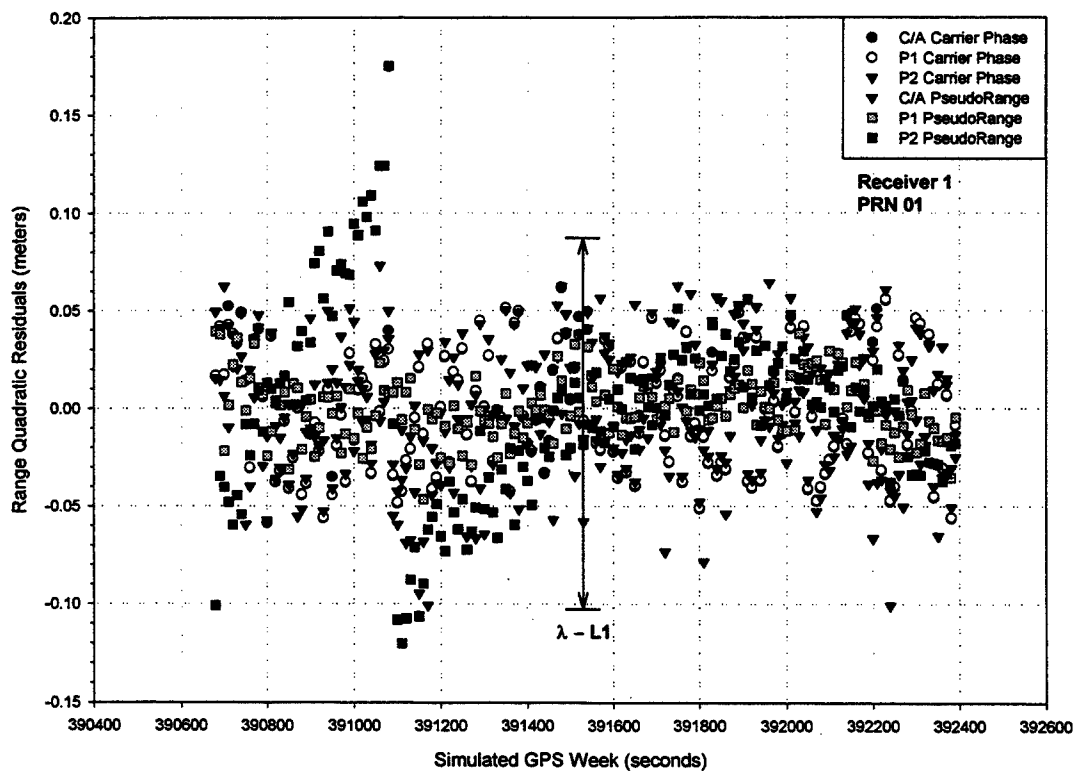
Figure 4. Receiver One, PRN 01 Residuals

241
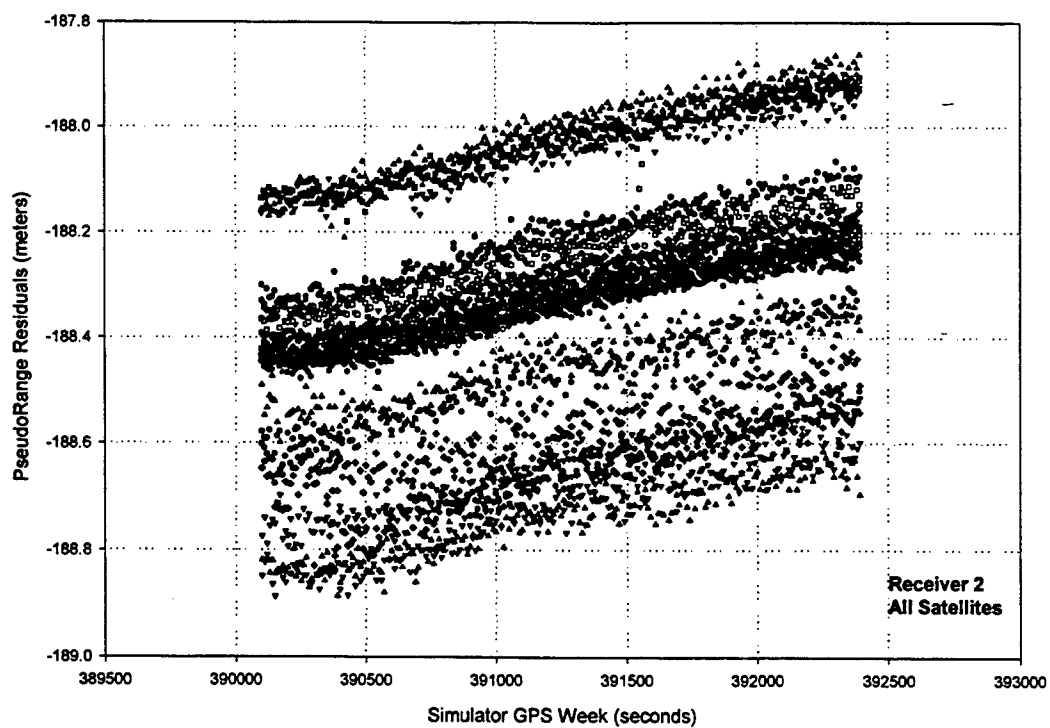
Figure 5. Receiver Two All Satellites
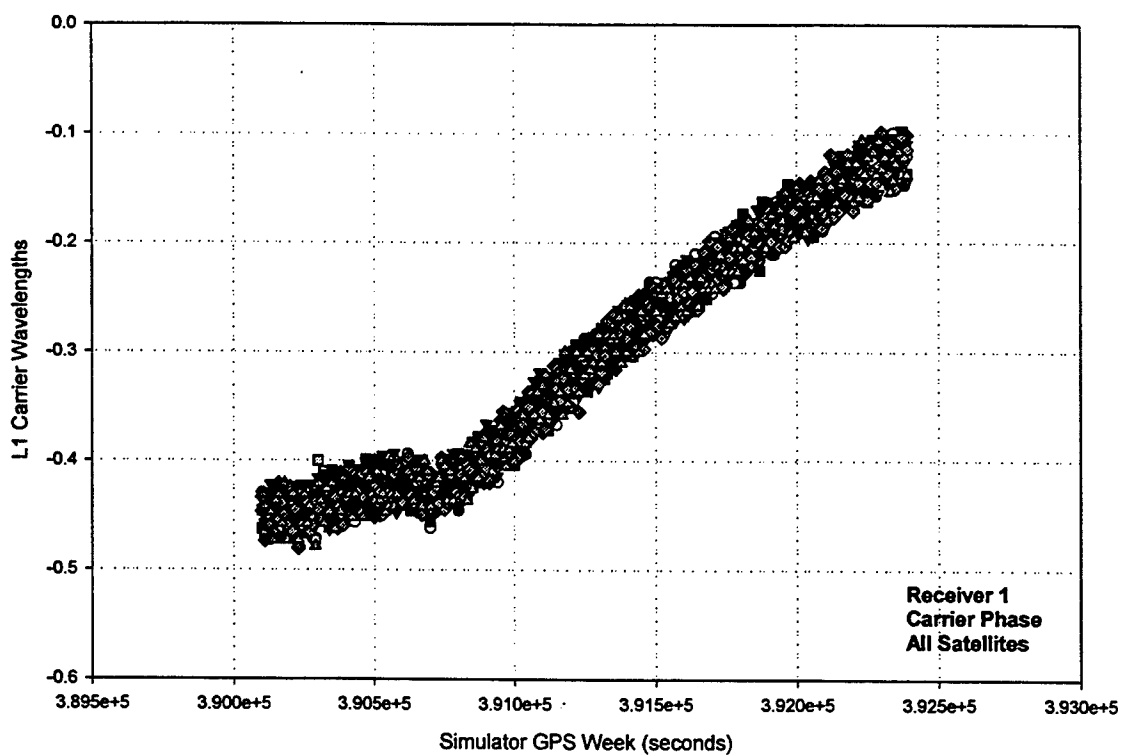
Figure 6. Receiver One Carrier Phase All Satellites
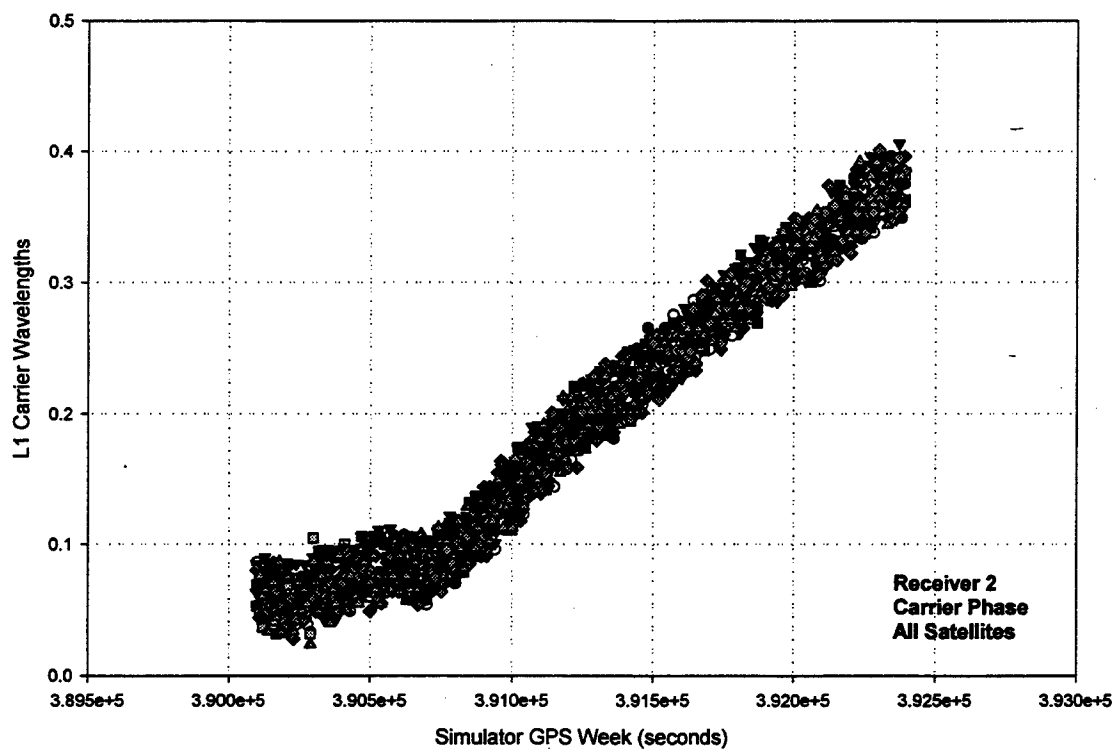
Figure 7. Receiver Two Carrier Phase All Satellites
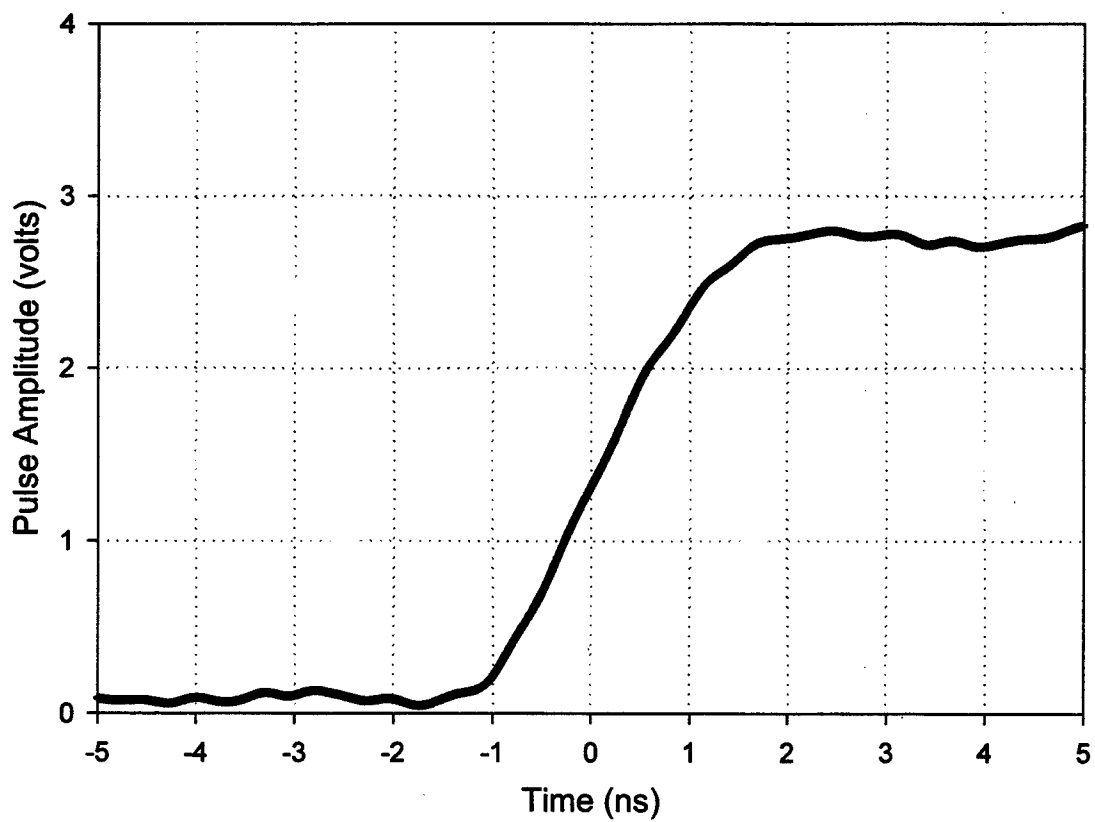
Figure 8. 1PPS Reference from Simulator
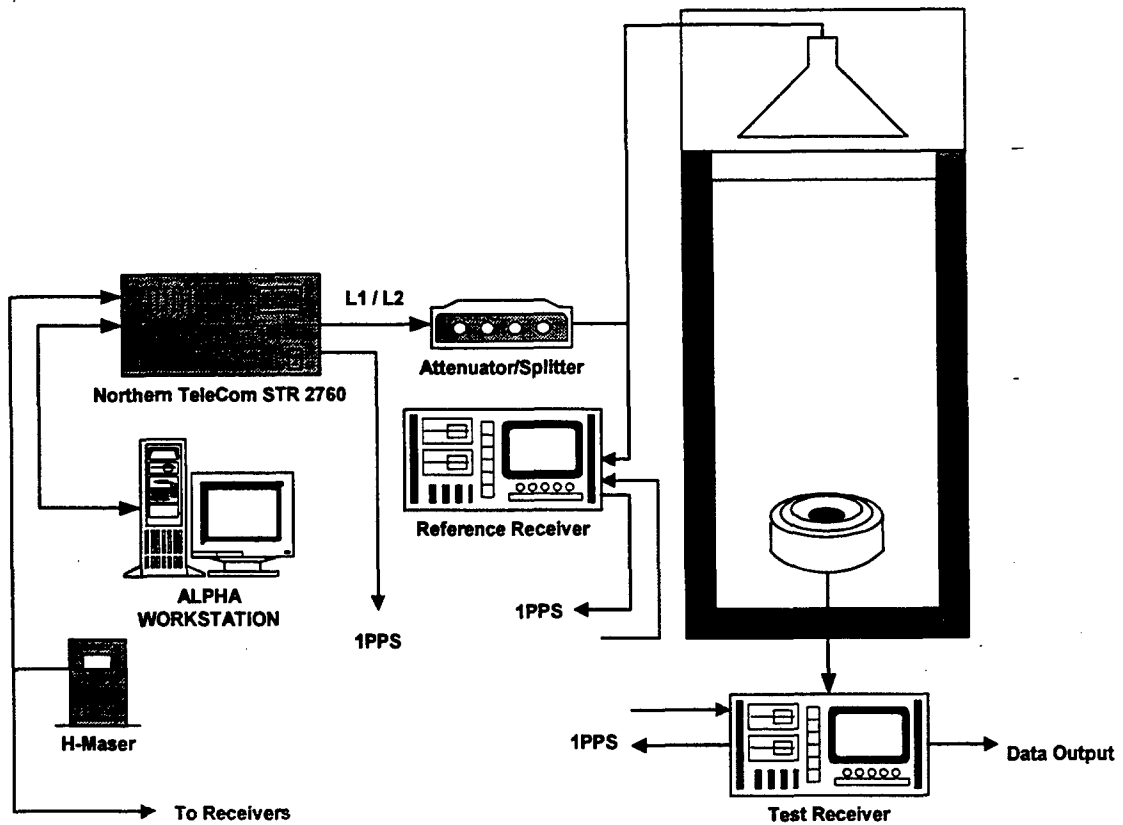
Figure 9. Final Simulation Configuration

Questions and Answers

JIM RAY (USNO): May I ask what you would hazard as a guess for the end-to-end absolute calibration?

JOE WHITE (NRL): I do not think I would really like to hazard one. There are so many variables that we have not looked at thoroughly. I think it would be difficult. I believe that we probably, within our ability to simulate signals, could get to the hundred picosecond level. Whether we can really get everything all together and continue it, and find a receiver that is stable enough is the question. I think that probably everybody who is going to show data today is going to show some receiver hops. We have to decide which side of the hop is truth.

JIM RAY: It looks like great work.

A LONG-TERM COMPARISON BETWEEN GPS CARRIER-PHASE AND TWO-WAY SATELLITE TIME TRANSFER

Kristine Larson
JILA and Department of Aerospace Engineering Sciences
University of Colorado, Boulder
Boulder, CO 80309
tel 303-492-6583 fax 303-492-7881
e-mail kristine.larson@colorado.edu

Lisa Nelson, Judah Levine, and Tom Parker
NIST Time and Frequency Division
Boulder, CO 80303

Edward D. Powers
Time Service Department, USNO
Washington, DC 20392

Abstract

We have conducted GPS carrier-phase time-transfer experiments between the Master Clock at USNO in Washington, DC and the Alternate Master Clock at Schriever Air Force Base near Colorado Springs, Colorado. These clocks are also monitored on an hourly basis with two-way satellite time-transfer (TWSTT) measurements. We compare the performance of the GPS carrier-phase and TWSTT systems over a 167-day period. Apart from an overall constant time offset (due to unknown delays in the GPS hardware at both ends), we find that the systems agree within ± 1 ns, with a drift of 1.9 ± 0.1 ps/d. For averaging times of a day, the carrier-phase and TWSTT systems have a frequency uncertainty of 2.5 and 5.5 parts in 10^{15}, respectively.

INTRODUCTION

Initial analysis of GPS carrier-phase data for time-transfer applications has been extremely promising [1]-[5]. Direct comparisons between carrier-phase and code-based common-view GPS show good agreement at times greater than 1 day [2]. As both systems depend directly on the GPS constellation, this is not a truly independent measure of the accuracy of the two systems. Furthermore, the noise of the common-view technique for periods of less than a day limits the value of comparisons between the common-view and carrier-phase techniques.

Initial comparisons between two-way satellite time-transfer (TWSTT) and GPS carrier-phase on continental-scale baselines have also been encouraging, but have been limited because of the somewhat

irregular TWSTT observing schedule between most timing laboratories [1]-[3]. None of these studies has compared TWSTT and GPS carrier-phase time-transfer for periods of less than several days. In order to evaluate the accuracy of GPS carrier-phase for these periods, more frequent TWSTT measurements are required. In this study we have concentrated on a time-transfer experiment where such measurements are available. Nearly hourly TWSTT measurements are made between the Master Clock at the U.S. Naval Observatory (Washington, D.C.) and the USNO Alternate Master Clock at Schriever Air Force Base (Colorado Springs, Colorado). These data provide an ideal opportunity to assess both the short-term and long-term accuracy of the GPS carrier-phase time-transfer system.

TIME-TRANSFER SYSTEMS

Geodetic quality dual-frequency GPS receivers have been installed at USNO and Schriever Air Force Base. These particular receivers simultaneously track up to 12 satellites and produce both pseudo-range and carrier-phase measurements at 30 s intervals.

The USNO GPS receiver is supplied with an external 5 MHz reference signal from USNO (MC#3). This master clock includes a hydrogen maser and an auxiliary output generator (AOG), see Fig. 1. Its output is steered to a second Master Clock, which is known as USNO(MC#2). This clock is also realized using a hydrogen maser. USNO(MC#2) defines UTC(USNO) and is the reference source for TWSTT. The USNO GPS receiver was installed in April 1997.

The GPS receiver at Schriever Air Force Base (USNO-AMCT during these experiments) also has an external 5 MHz reference supplied by AMC(AMC#1). This alternate master clock also contains a hydrogen maser and an AOG distribution amplifier. It is steered to USNO(MC#2) using the nominally hourly TWSTT data. The USNO-AMCT GPS receiver was installed in March 1998.

In order to compare the carrier-phase and TWSTT estimates between USNO and USNO-AMC, we must know the difference between MC#2 and MC#3 at the USNO in Washington, since the former is the reference for the TWSTT system there, while the latter drives the GPS carrier-phase receiver. This difference is monitored using a switched/multiplexed time-interval counter. The counter is connected to the clocks using a fiber-optic link; the measurement system has an observed diurnal variation of about 100 ps p-p and possible seasonal drifts as large as 1 ns.

The GPS receivers at USNO and Schriever (USNO-AMCT) are part of the IGS network [6], a cooperative, continuously operating global GPS tracking network. The data are freely available over the Internet and can be accessed through anonymous ftp. Descriptions of all IGS sites and data archiving procedures can be located at http://igscb.jpl.nasa.gov.

GPS CARRIER-PHASE DATA ANALYSIS

The GPS carrier-phase observable $\Delta\phi_r^s$ for a given satellite s and receiver r can be written as follows:

$$-\Delta\phi_r^s\lambda = \rho_g + c\delta^s - c\delta_r + N_r^s\lambda + \rho_t - \rho_i + \rho_m + \epsilon, \qquad (1)$$

where individual terms are in units of length. λ is the carrier wavelength, ρ_t and ρ_i are the propagation delays due to the troposphere and ionosphere, ρ_m is the multipath error, and ϵ represents unmodelled errors and receiver noise. N_r^s is the initial number of integer cycles, known as the carrier-phase ambiguity or bias. ρ_g is the geometric range, or $|\vec{X}^s - \vec{X}_r|$, where $\vec{X}^s$ is the satellite position at the time of transmission and $\vec{X}_r$ is the receiver position at reception time. Proper determination of ρ_g requires precise transformation parameters between the inertial and terrestrial reference frames, i.e. models of precession, nutation, polar motion, and UT1-UTC. Finally, δ_r and δ^s are the time of the receiver and satellite clocks, respectively, in seconds.

In order to achieve the highest precision carrier-phase results, we must model or correct all the terms in Equation 1. We used a geodetic software package to analyze the GPS carrier-phase data [7]. Both satellite and receiver clocks are modeled as white noise, so that the estimates are uncorrelated from epoch to epoch. The receiver clock at USNO is treated as the reference clock, and all other clock estimates are reported relative to it. Coordinates of the GPS satellites are taken from the IGS (International GPS Service) [6]. The effect of the ionosphere is removed by using an appropriate linear combination of the $L1$ and $L2$ phase data. Variations in the troposphere, station coordinates, and carrier-phase ambiguities are estimated from the data. In order to minimize multipath errors, carrier-phase data observed below elevation angles of 15 degrees are discarded.

While carrier-phase receivers typically record data at 30 s intervals, we have decimated the data to 6-minute intervals to reduce the computational burden. Although in theory we only require the data from the two receivers located at USNO and Schriever, in practice we have also used data from Algonquin (Ontario, Canada) to help define the terrestrial reference frame and Goddard Space Flight Center (Greenbelt, Maryland) to help resolve carrier-phase ambiguities. The 167-day time series can be analyzed in 24 hours on a dual-processor 200 MHz workstation. A large fraction of that time is spent on ambiguity resolution.

RESULTS

This comparison covers a period of 167 days. There are 39,083 GPS carrier-phase observations, or a loss rate of 2.5% for the 167-day period (an average of 234 measurements per day). The TWSTT measurements are made on nearly an hourly basis, with 3,105 measurements during this period (an average of about 19 measurements per day). The USNO MC#3-MC#2 data are made available as hourly measurements; we use linear interpolation on this data set to compute the correction to the GPS carrier-phase measurements.

SYSTEMATIC ERRORS

Initial analysis of the carrier-phase data demonstrated that there were some difficulties with the carrier-phase time-transfer system. The GPS receiver at Schriever frequently reset its internal clock, at one point doing this as often as once every 5 days. These resets occur in two circumstances: when the internal clock has drifted by more than 0.03 s or when the receiver has recorded a "clock set" command. The first scenario should not be relevant to receivers which are connected to hydrogen masers. The second occurs when power has been turned off or when the receiver has lost track of several satellites, rendering it incapable of determining position. Since position is the primary output of a geodetic receiver, the receiver resets all parameters, including the clock, and searches the sky to re-acquire all visible satellites. Since geodetic GPS receivers were designed to be used by surveyors and geophysicists, it was expected that the units would be used in the field on battery power. Thus, power is frequently turned off. For laboratory use and timing applications, power outages should be eliminated as much as possible.

We still do not fully understand why the Schriever receiver reset its clock so frequently. The Schriever and USNO GPS receivers lost power at least three times during the 167-day period described in this paper. But, this does not explain the remaining 16 resets, all of which occurred at Schriever. A new GPS receiver was installed at Schriever in late October, 1998. We are currently monitoring data from the new receiver to see if this alleviates the problem. It is possible that other factors, such as RF interference, may be responsible for the clock reset problem at Schriever.

Large (peak-to-peak amplitude of ~400 ps) diurnal signals were visible in the carrier-phase clock estimates. Comparisons with records at USNO suggested that these periodic signals were highly

correlated with local air temperature. The antenna cable being used at USNO to connect the GPS antenna to the GPS receiver was 89 m long, and nearly all of it was exposed to full sunlight. The sensitivity of the cable delay to temperature was not known, but was thought to be in range of 0.5 to 1.25 ps/m-°C. A similar cable was tested and was found to have sensitivity of 0.53 ps/m-°C. Assuming that 90% of the cable was exposed to a daily temperature variation of 10°C, a cable with this sensitivity to temperature would have a 420 ps p-p diurnal change in its delay. See [8] for more details.

In Figure 2a) we show typical carrier-phase clock estimates for the Schriever-USNO baseline. Superimposed on the estimates are the hourly TWSTT measurements, which indicate that the long-term behavior of the carrier-phase estimates is in good agreement with TWSTT. Nevertheless, the diurnal variations in the carrier-phase estimates are readily apparent. In Figure 2b) we remove a low-order polynomial from the time series, so that we can more directly compare to temperature records, which are shown in Figure 2c), using a sensitivity of the cable delay to temperature of 40 ps/°C. In Figure 2d) we demonstrate that subtracting a simple correction, which depends solely on temperature, can significantly improve the precision of the GPS carrier-phase clock estimates.

Several days after these data were collected, a new cable was installed at USNO. This cable was expected to a have a temperature sensitivity better than 0.02 ps/m-°C. This new cable was installed mostly in the ceiling of the building instead of on the roof where it was exposed to the elements. In Figure 3 we show carrier-phase clock estimates directly before and after the cable was changed at USNO. This new cable has substantially improved the stability of the carrier-phase GPS clock estimates.

We estimated the change in the receiver delay due to the reset of its internal clock using an average of the observations 30 minutes before and after each reset, and assuming that the local reference oscillator was well-behaved during this period. This method is straightforward, but is obviously not optimum – at the very least it introduces a random-walk into the long-period observations. In a future analysis we plan to compare our current reset estimates with reset calibrations computed using the change in the 1 Hz output pulses from the receiver.

Unlike the clock resets where the data loss is typically small (often less than a few minutes), a lengthy power outage could produce a bias in the clock estimates that would be difficult to remove. In this analysis, we assumed that there was no change in the clocks during power outages, which is adequate only for short periods. In one instance (the day the new cable was installed at USNO) we did adjust the GPS carrier-phase estimates by ~1 ns to bring the carrier-phase time series into agreement with TWSTT. We corrected for the local MC#3 oscillator by using the calibrations provided by USNO. Finally, we applied a 40 ps/°C temperature correction for data collected before the new cable was installed at USNO.

Since the delay through the carrier-phase GPS receivers was not known, these data have an unknown constant time offset with respect to the two-way observations. (This constant delay is in addition to the time steps whenever the internal clock of the receiver is reset). We adjusted the mean of the carrier phase data to compensate for this overall time offset.

STATISTICS

The final carrier-phase clock estimates are shown in Figure 4, along with the hourly TWSTT measurements. Despite the problems we discussed in the previous section, it is clear that the corrected GPS carrier-phase clock estimates agree well in the long-term with the TWSTT measurements.

If we difference the carrier-phase and TWSTT at common epochs (by interpolating to the higher rate of the GPS data), we can see the agreement between the two systems is better than ±1 ns over the

167-day period (Figure 5). The trend of the difference between the systems is 1.9±0.1 ps/d, which is well within the uncertainty of drift in the MC#3-MC#2 measurement system at USNO.

Figure 6 summarizes the TDEV information in the two systems. For periods of less than a day, the carrier-phase estimates are significantly more precise than the TWSTT system, with carrier-phase TDEV of 15 to 88 ps between 6 minutes and 12 hours. At approximately one day, the two systems overlap in TDEV, and agree for longer periods, which is consistent with their long-term agreement in the time domain (Figure 5). The rolloff in TDEV at long time intervals is consistent with the fact that AMC(AMC#1) is steered to USNO(MC#2). If we calculate the TDEV of the difference of TWSTT and GPS carrier-phase, we see that nearly all the noise at periods of less than a day comes from the TWSTT system. The combined noise of TWSTT and carrier-phase is flicker PM in nature beyond 1 day, with a level of about 100 ps. GPS carrier-phase frequency uncertainty at periods of less than a day is significantly better than for TWSTT, with values of 2.5 and 5.5 parts in 10^{15} at one day (Figure 7).

CONCLUSIONS

The carrier-phase data in the USNO-AMC/USNO link (after temperature correction) have exhibited a stability similar to that observed using the NIST/USNO link reported in [2]. For time intervals less than 1 day the stability of carrier phase is well below 100 ps. The high quality TWSTT link between the AMC(AMC#1) and USNO(MC#2) provides a unique opportunity to obtain information about the long-term stability of both links. The combined noise of the two links is at the 100 ps level.

In spite of the new antenna cable at the USNO, the carrier-phase data are undoubtedly still degraded to some extent by thermally induced changes in the hardware delay and by the small residual time steps due to the resets in the receiver clock. We plan to address both of these problems in the near future.

ACKNOWLEDGMENTS

REFERENCES

[1] K. Larson and J. Levine 1998, "Time-transfer using the Phase of the GPS Carrier," **IEEE Trans. on Ultrasonics, Ferroelectronics and Frequency Control**, Vol. 45, No. 3, pp. 539-540.

[2] K. Larson and J. Levine 1998, "Carrier-Phase Time-Transfer," submitted to **IEEE Trans. on Ultrasonics, Ferroelectronics and Frequency Control**.

[3] F. Overney, L. Prost, G. Dudle, Th. Schildknecht, G. Beutler, J. Davis, J. Furlong, and P. Hetzel 1998, "GPS time-transfer using geodetic receivers (GeTT): Results on European baselines," **Proc. 12th European Frequency Time Forum**, in press.

[4] D. Jefferson, S. Lichten, and L. Young 1996, "A test of precision GPS clock synchronization," **Proc. 1996 IEEE Frequency Control Symposium**, 1206-1210.

[5] G. Petit, C. Thomas, and Z. Jiang, "Use of Geodetic GPS Ashtech Z12T Receivers for Accurate Time and Frequency Comparisons," **Proc. 1998 IEEE Frequency Control Symposium**, Pasadena, 306-314.

[6] G. Beutler, I.I. Mueller, and R.E. Neilan 1994, "The International GPS Service for Geodynamics (IGS): Development and start of official service on January 1, 1994," **Bulletin Geodesique, 68(1)**, 39-70.

[7] S. Lichten and J. Border 1987, "Strategies for high-precision Global Positioning System orbit determination," **Journal of Geophysical Research, 92**, 12,751-12,762.

[8] E. Powers 1999, "Hardware delay measurements and sensitivities in carrier phase time transfer," these Proceedings.
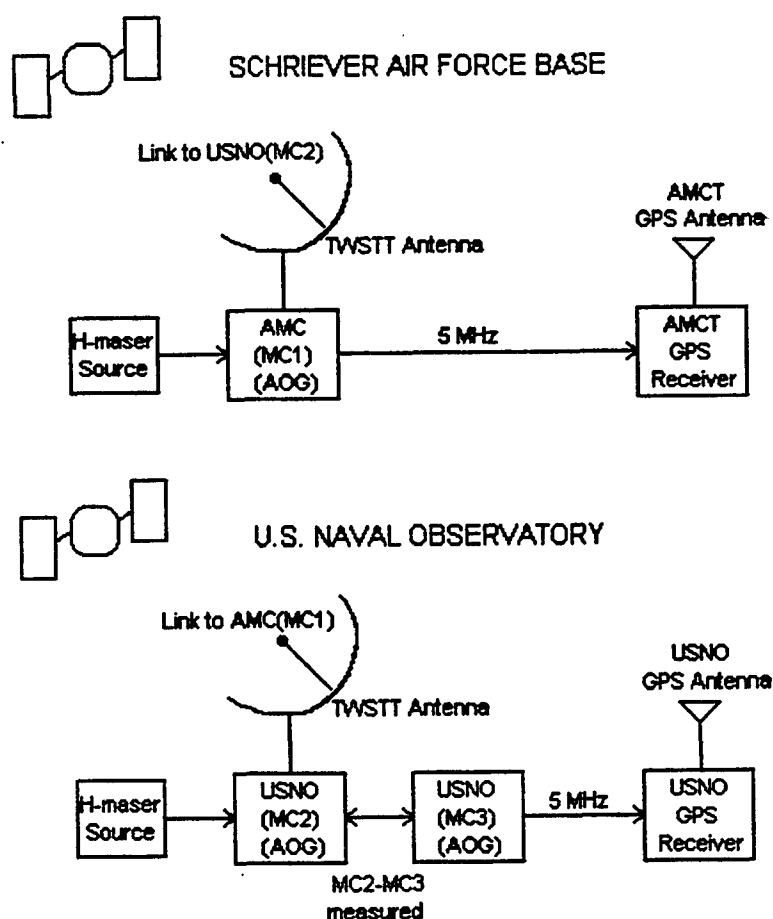
Figure 1: Measurement schematics at the U.S. Naval Observatory and Schriever Air Force Base.
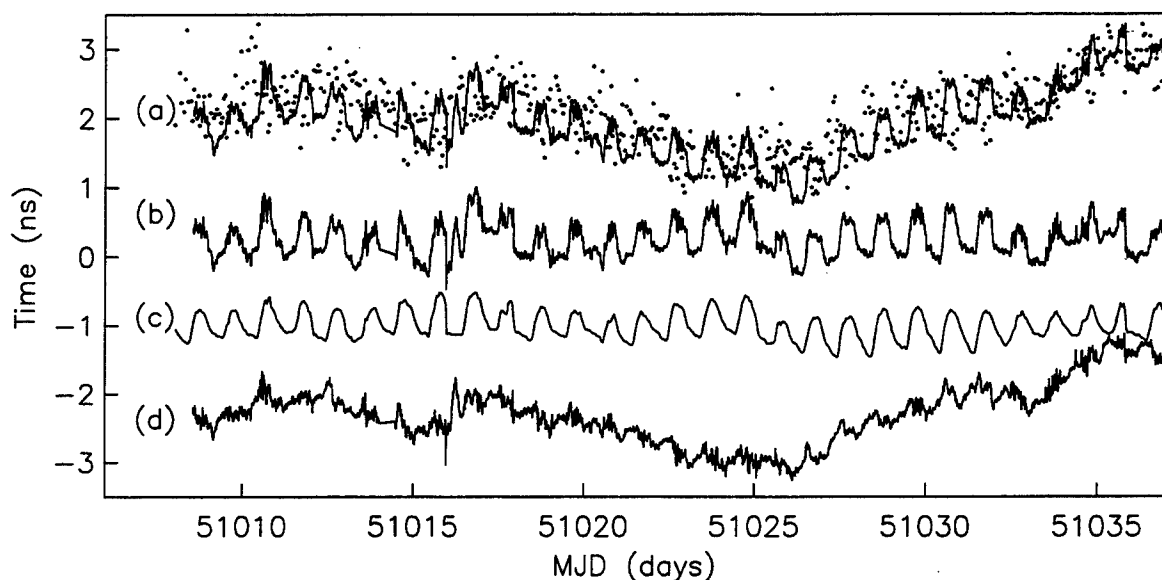
Figure 2: (a) Carrier-phase estimates of USNO-AMC (Schriever) minus MC-USNO plotted with TWSTT measurements; (b) Carrier-phase data from (a) with low order polynominal removed; (c) Local USNO air temperature records, converted using 40 ps/°C; (d) Carrier-phase estimates of USNO-AMC (Schriever) minus MC-USNO with 40 ps/°C temperature correction applied. The time series are offset with respect to each other for display purposes only.
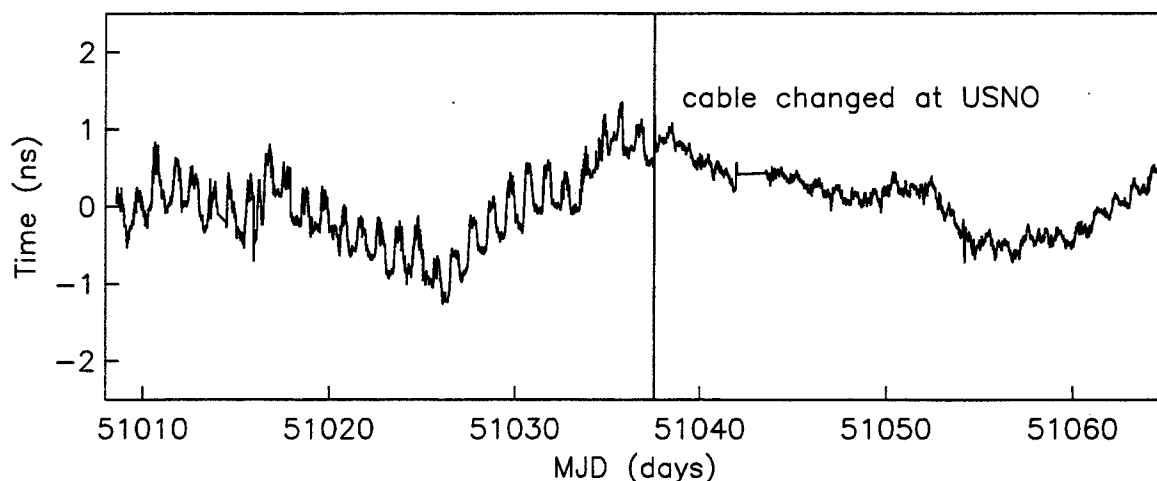
Figure 3: Carrier-phase estimates of USNO-AMCT relative to USNO. Note change in diurnal signal apparent after the cable was changed at USNO.
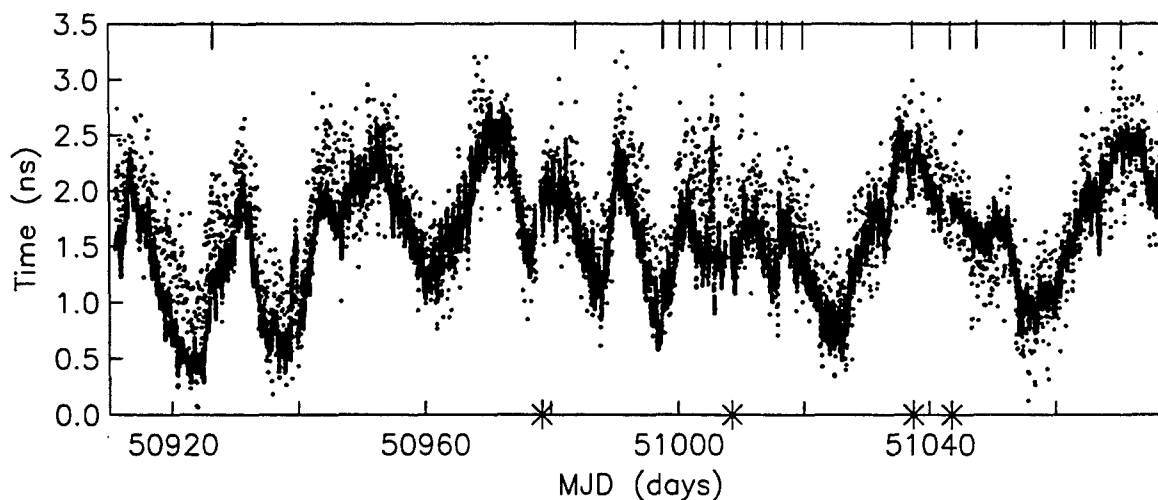
Figure 4: Schriever minus USNO carrier-phase clock estimates, with TWSTT measurements shown as dots. Clock resets are shown as tick marks above. Significant data gaps in the carrier-phase data are shown as asterisks below.
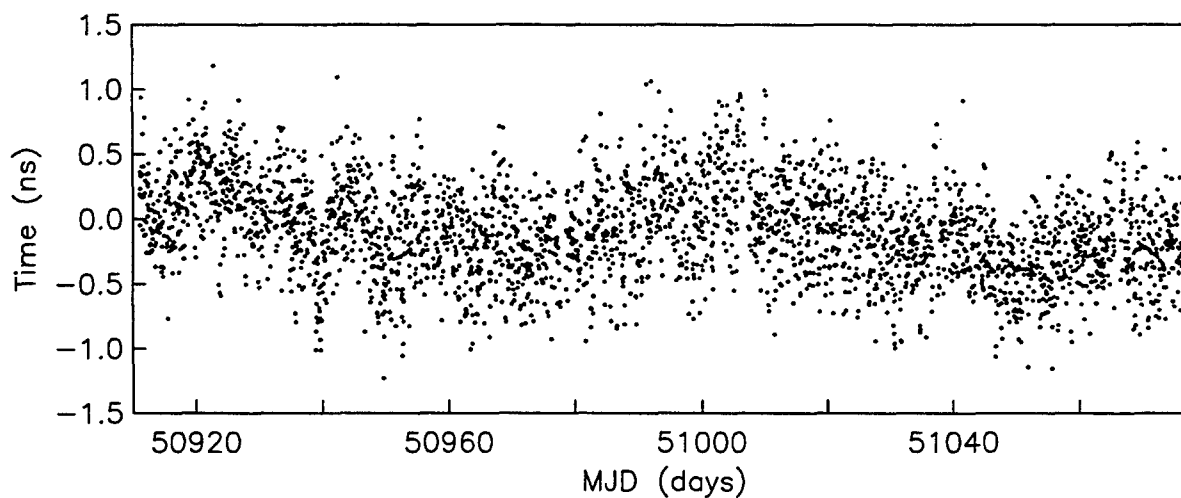
Figure 5: The difference between TWSTT and GPS carrier-phase estimates at common epochs.
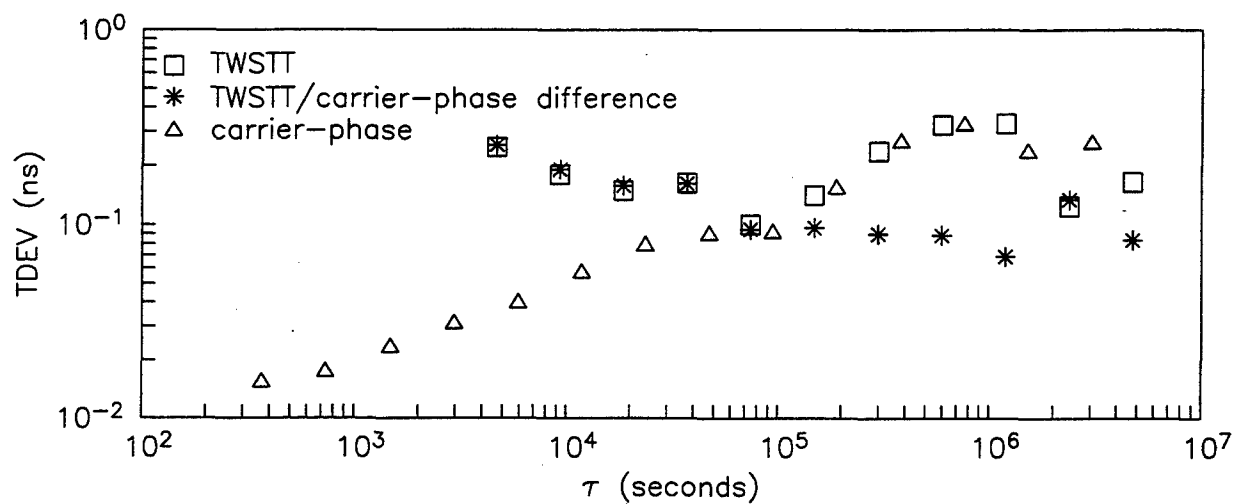
Figure 6: TDEV of GPS carrier-phase, TWSTT, and the difference between GPS carrier-phase and TWSTT.
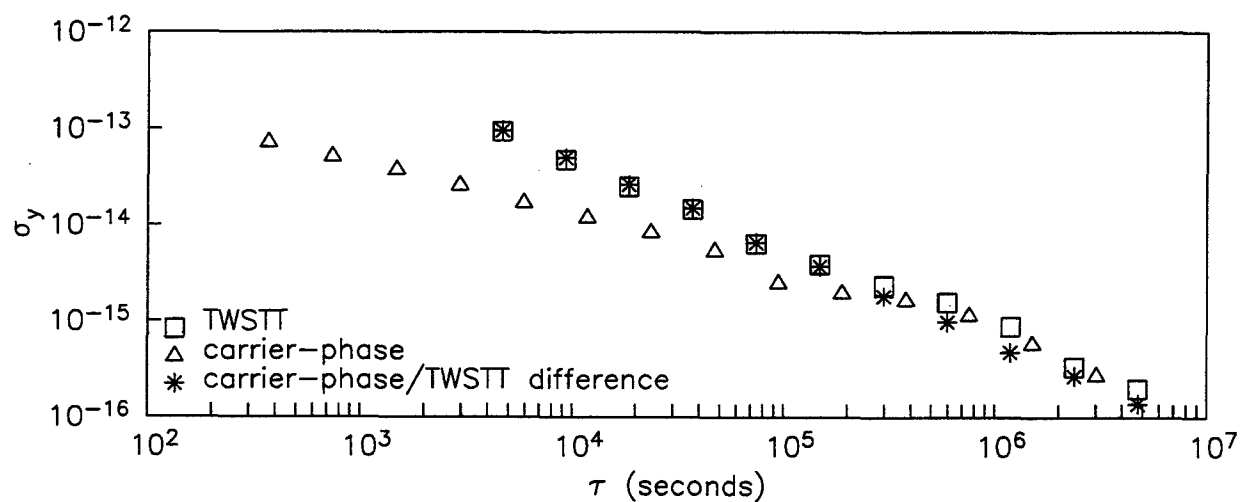
Figure 7: Allan deviation of GPS carrier-phase, TWSTT, and the difference between GPS carrier-phase and TWSTT.

Questions and Answers

JIM RAY (USNO): I just had a comment about automation. Jim Zumberge and I did not go into this in our presentations. It is useful to keep in mind that the IGS rapid product delivery schedule starts with data being delivered in daily batches shortly after midnight each day. That data flow goes automatically through data centers to the analysis centers and results in the analysis centers producing their products, sending them back to the IGS coordinator who then combines them and releases them to the public. The total beginning-to-end schedule – this is everyday, daily – is 16 hours right now. I would say that process is almost completely and totally automated.

From a clock standpoint, while the IGS currently only distributes satellite clocks – conceptually, there is no difficulty in adding, in a relatively minor way, the station clock. So, I do not really regard that as a very significant issue. My main question to you is on the one PBS statement that you made. I went to some considerable detail to write a report – a fairly lengthy report – breaking down one such event that was studied in excruciating detail, concluding that the one PBS monitor for the TurboRogue glitch that we looked at, was good to probably a few picoseconds as well as the geodetic determinations could possibly establish it – and certainly at the hundred picosecond level or better.

I for one have a tremendous interest in anything that indicates that this is not reliable. So if you have that, I think you ought to write it up and distribute it to that larger community. It is extremely relevant.

JUDAH LEVINE (NIST): Let me explain where our comment comes from. We have sites where there are several masers at the same site. An apparent glitch in the carrier-phase data can be estimated two different ways. That is, we can look at what the receiver's 1PPS does, and we can now ask the friends of the maser, say "Hello, what happened?" I do not want to put a hard number on those two numbers what that difference is, but I would say it is not two picoseconds. It is something which we will begin to worry about. I can get numbers for you –Lisa Nelson has the numbers. I do not remember them exactly. They are not precisely the same number. Let me find out exactly what the number really is; but I would guess it is more like 100 picoseconds.

JIM DeYOUNG (USNO): Judah, at some point along the line I was talking to Kristine (Larson), and I suggested that she look at the Kalman filter estimate of the two-way data; because I think sometimes this audience forgets that two-way is a real-time system, that we make those hourly measurements once every hour; we get the time difference and then the hydrogen maser at the AMC is steered based on a Kalman filter (an instantaneous Kalman filter estimate) which matches up actually quite good to the carrier phase. At least, it is behaving normally.

JUDAH LEVINE: Remember that we are measuring – the way we have done it, the intention is to drop out all the clocks. We are trying to compare apples against apples by a real-time measurement against a real-time measurement. Yes, we can certainly do that. I have a feeling that may cloud the issue a bit.

A VERY-SHORT-BASELINE TIME TRANSFER EXPERIMENT USING TWO GEODETIC-QUALITY GPS RECEIVERS AND CARRIER PHASE TECHNIQUES

Jon D. Clarke, John A. Davis, and Andrew Lowe
Centre for Time Metrology, National Physical Laboratory
Queens Road, Teddington, Middlesex TW11 0LW, UK

Abstract

For over 10 years primary timing laboratories have used signals from the Global Positioning System (GPS) to compare atomic timescales. The method used, the common-view of GPS satellites, does not use the GPS system to its full potential. Recently, there has been much interest in using geodetic-quality GPS receivers for time transfer. The result has been a substantial improvement in the precision of the resulting time and frequency transfers.

In this paper, a detailed account is presented of common-clock comparisons made at NPL between a recently purchased Ashtech Z12-T receiver and an older Allen Osborne Associates (AOA) TTR-4P receiver. Data collected from these geodetic-quality GPS receivers were processed using analytical software developed at NPL. Direct comparisons are made between the two receivers using both P1 and P2 coded signals, and L1 and L2 phase measurements. Measured ionospheric delays were obtained from both receivers and compared. Multipath is one of the major causes of errors in the surveying applications of geodetic GPS receivers. Code-phase differences were used to estimate the magnitude of code multipath present in both receivers. The principal sources of error present in the common clock measurements are discussed and possible improvements are considered. The future direction of geodetic time transfer work at NPL is also outlined.

1 INTRODUCTION

The application of geodetic GPS techniques to frequency and time transfer has produced some very impressive results [1],[2]. These results have increased the interest in using geodetic GPS time transfer for international comparisons between primary timing laboratories. One recent development has been the formation of a joint BIPM/IGS pilot project to coordinate studies in the field [3].

The quality of geodetic GPS frequency and time transfers will, however, be limited by the delay stability of both the GPS receiver's instrumentation and that of the associated measurement systems [4]. Other local environmental considerations, for example the susceptibility of the receiver's antenna to multipath, will also limit the receiver's performance.

The post-processing of geodetic GPS data is more complicated than the processing of data collected by other high precision time transfer methods. Only a few primary timing laboratories have the capability to postprocess their own geodetic GPS data, and those who do usually use commercial software.

In this paper the results of a very-short-baseline common-clock experiment between NPL's Ashtech Z12-T and AOA TTR-4P geodetic–quality GPS receivers are presented. NPL's development of analysis software from first principles is described. The relative performance of NPL's GPS receivers is evaluated by using the analysis software to compare both the code and phase data available from both receivers. By combiningthesedata with the broadcast GPS almanac data, a detailed evaluation was possible, including an examination of the physical processes limiting the receivers' performance.

2 GEODETIC GPS HARDWARE AT NPL

NPL possesses two geodetic quality GPS receivers, an Ashtech Z12-T and an AOA TTR-4P. The hardware configuration is shown in Figure 1. The Ashtech Z12-T is a modified version of the Ashtech Z12 receiver, where the internal oscillator is replaced by a 20 MHz external reference signal. The receiver provides 1 PPS input and output signals, which lock the receiver's internal clock. The TTR-4P is an older receiver widely used in primary timing laboratories. The two receivers' antennas are located approximately five meters apart. Standard frequency and 1 PPS reference signals for the two receivers originate from common frequency distribution and 1 PPS generation units. All the receivers' input signals are referenced to NPL's Sigma Tau Active Hydrogen Maser.

3 DATA SETS EXTRACTED FROM THE RECEIVERS

Several data sets were extracted from the receivers. RINEX data were extracted from the Ashtech Z12-T receiver. Although in principle available, similar RINEX data could not be obtained from the TTR-4P receiver; however, code and phase measurements were obtained from the receiver using its "block 015" data. Both data sets were collected with a measurement epoch of 30 seconds synchronized to GPS time. The GPS almanac data were also extracted from the Ashtech Z12-T receiver, which was used in NPL's postprocessing software.

4 POSTPROCESSING SOFTWARE DEVELOPED AT NPL

The baseline between NPL's two geodetic GPS receivers is 5 m. With this limited baseline extensive data postprocessing is still required to compute comparisons between the two receivers with a measurement precision of 10 picoseconds.

Several distinct operations are performed by the analysis software:

1) Each day's data are processed separately. The software's data input included code and phase variables from each receiver, along with the GPS almanac data and approximate receiver coordinates. The data are processed in 30 s blocks, which corresponds to the measurement epoch.

2) The GPS almanac is decoded to obtain satellite coordinates, at each measurement epoch, which were then used to calculate accurate satellite azimuth and elevation values. Satellite azimuth and elevation angles are generated in the Ashtech Z12-T and TTR-4P output data sets, but only with a precision of $1°$, which is not adequate for the comparison of the receivers' clocks with 10-picosecond precision.

3) A first calculation is made of the relative coordinates between the phase centers of the two antennas, using only the code variables P1 and P2, and the satellite azimuth and elevation values calculated in step 2. A separate estimate is made at each measurement epoch by calculating the pseudo-range differences $(P1_{(TTR-4P)}-P1_{(Ashtech\ Z12-T)})$ and $(P2_{(TTr-4P)}-P2_{(Ashtech\ Z12-T)})$ using each satellite. The antennas' relative coordinates are then optimized to minimize the scatter between pseudo-range differences calculated from each satellite in view. This calculation is repeated for each measurement block, and finally a mean value for the relative coordinates is determined.

4) Phase data are now introduced into the analysis. Step (3) is repeated using phase rather than code measurements. Phase ambiguities are corrected by adding integer cycles to the L1 and L2 measurements. With these very short baselines, resolving the phase ambiguities is relatively straightforward. Using a single day's data, the coordinate differences between the two antennas could be determined with sub-centimeter precision. Separate relative coordinates are calculated for the L1 and L2 frequencies to reflect the slightly different phase centers in the antennas.

5) The software is then used to generate a wide range of output parameters using the optimized relative coordinates in the processing. These include: measured code and phase differences between the two receivers, ionospheric delay measurements, and receiver code/phase differences used in the study of code multipath.

5 DIRECT COMPARISONS BETWEEN THE TWO RECEIVERS

P1 code differences, calculated between the two receivers are shown in Figures 2 and 3. P2 code differences were also calculated but are not shown here. Figure 2 shows individual satellite tracks, while the mean value calculated from all satellites simultaneously tracked by both receivers is shown in Figure 3. The P1 and P2 code differences showed no obvious correlations. There is a scatter of several nanoseconds within individual tracks; this decreases to (1-2) nanoseconds (1σ) for the mean value

averaged over all satellites. The scatter in the data appeared asymmetric, with notable outliers. The majority of these were attributed to multipath occurring within the AOA TTR-4P receiver, often when the satellite is at low elevation angles. The data scatter reduces with satellite elevation angle, due in part to the increased gain of the antenna at these angles. There was no obvious correlation between individual satellite tracks. The scatter on the P2 data is approximately twice that on the P1 data. This is consistent with the lower levels of received P2 signals.

The phase differences between the two receivers are shown in Figures 4 and 5. The scatter on the phase data is noticeably lower than that from the code data, typically 10-picosecond scatter between successive measurements on the same satellite track. The long-term variations show no obvious correlation with long-term variations in the code measurements. Individual satellite tracks correlated extremely well (Figure 4), with a typical 20-picosecond RMS scatter (1σ) between all the tracks measured in the same epoch. This shows that the majority of the phase instabilities are correlated between measurements from all of the satellites. The phase differences observed at L1 and L2 frequencies also agreed well (Figures 5), although there were variations of up to 60 picoseconds in the L1-L2 phase differences (Figure 6). The short-term instabilities in the phase differences correlate with temperature cycling in the room containing the receivers; this cycling has a period of approximately 30 minutes (See Figures 4, 5, and 6). The Ashtech Z12-T receiver temperature is included in Figure 5. There was no obvious correlation with outdoor temperature. More detailed studies are planned to isolate the causes of the phase instabilities.

6 IONOSPHERIC DELAY MEASUREMENTS

Over a longer baseline a geodetic GPS time transfer will be limited by the effectiveness of the ionospheric delay correction. Three different methods of measuring the L1 ionospheric correction are shown here: (i) using code α(P1-P2) differences (Figure 7); (ii) using phase α(L2-L1) differences (Figure 8); and (iii) using single frequency code-phase 0.5(P1-L1) differences (Figure 9) calculated at the L1 frequency. ($\alpha = F_2^2/(F_2^2 - F_1^2)$) where F_1 and F_2 are the transmission frequencies of L1 and L2 respectively). Absolute values of the ionospheric delay may be obtained from the code measurements; however, only relative ionospheric delay changes may be obtained using the phase measurements, and the code-phase differences. Good agreement is obtained between all three methods. The phase measurements clearly demonstrated far less noise than on the code measurements; this was in part due to the encryption of the GPS P-code, and in part due to phase measurements being intrinsically less noisy. The noise on the code measurements obtained from the AOA TTR-4P receiver was approximately half the level of noise obtained from the Ashtech Z12-T receiver. There was no obvious bias between code measurements obtained from different receiver channels or from different GPS satellites; however, there was a bias of 30 nanoseconds between the coded ionospheric measurements obtained from the Ashtech Z12-T and AOA TTR-4P receivers. The single frequency code-phase differences are shown to be effective in

determining ionospheric delay changes.

The differences between ionospheric phase measurement obtained from the Ashtech and AOA TTR-4P receivers are shown in Figure 10. Variations in these plots of up to 100 picoseconds were observed which correlate with satellite elevation. This may be due to the different relative phase patterns of the two antennas. A simple alterative explanation is that the height component of the antenna coordinate differences may be slightly in error.

7 MEASUREMENT OF CODE MULTIPATH

A major limitation to the use of geodetic GPS receivers for positioning applications is multipath. Phase multipath is typically a thousand times smaller than code multipath. The quality of the GPS code measurements is vital for the analysis of geodetic GPS data, which may be severely degraded by code multipath. Measuring code-phase differences from individual satellite tracks is an excellent way to identify code multipath. The repeating GPS constellation each sidereal day enables multipath to be observed through the repeating delay changes observed in the code phase differences. Examples are shown in Figure 11 for data obtained from NPL's Ashtech Z12-T receiver. The repeating code phase difference patterns were observed at both L1 and L2 frequencies. The patterns observed were noticeably different at the two frequencies, because multipath effects are frequency-dependent (Figures 11 and 12). The origin of much of this multipath may well be a copper dome on NPL's laboratory roof. The Ashtech Z12-T antenna has recently been moved; the new site will be examined for residual code multipath.

8 FUTURE WORK

NPL has an active program to develop its geodetic GPS installation. NPL intends to purchase another geodetic-quality GPS receiver, enabling "three-cornered-hat" comparisons in future. Also NPL has a 3S Navigation combined GLONASS/GPS receiver from which the L1 CA code GPS channels may be used for direct comparisons with geodetic GPS receivers. Instrumentation delay instabilities may be reduced through temperature control of the GPS receivers, antennas, and connecting cables. Work is underway to improve the frequency distribution system from NPL's Active Hydrogen Maser.

NPL is in the process of upgrading its geodetic GPS installation to meet the requirements of an IGS station. NPL is also playing an active part in comparisons between geodetic GPS and other high precision time transfer methods, including TWSTFT and GLONASS time transfer.

9 CONCLUSIONS

This paper has demonstrated that short–baseline common-clock experiment using geodetic GPS receivers may be analyzed from first principles using relatively straightforward software. This type of analysis may be usefully performed by primary timing laboratories to obtain an insight into the performance of their geodetic GPS timing receivers.

A major source of errors is due to delay instabilities within the receiver instrumentation. The analysis described in this paper has identified the magnitude of both the code and phase instabilities occurring between NPL's geodetic GPS timing receivers. Other physical processes limiting geodetic GPS time transfer, including ionospheric delay determination, code multipath, and antenna phase dispersion, have been examined. Future work is required to optimize the receiver's performance.

10 REFERENCES

[1] K. M. Lawson and J. Levine, "Time transfer using GPS carrier phase methods," Proceedings of the 29 th PTTI meeting, pp. 221-228, December 1997.

[2] F. Overney, L. Prost, G. Dudle, Th. Schildknecht, G. Beutler, J. A. Davis, J. M. Furlong, and P. Hetzel, " GPS time transfer using geodetic receivers (GeTT): Results on European baselines," Proceedings 12 th EFTF, pp. 94-99, March 1998.

[3] J. Ray, " The IGS/BIPM pilot project to study accurate time and frequency comparisons using GPS phase and code measurements," Proceeding of the 30 th PTTI meeting (these Proceedings), December 1998.

[4] F. Overney, Th. Schildknecht, G. Beutler, L. Prost, and U. Feller, "GPS time transfer using geodetic receivers: Middle term stability and temperature dependence of the signal delays," Proceedings of the 11 th EFTF, pp. 504-508, March 1997.
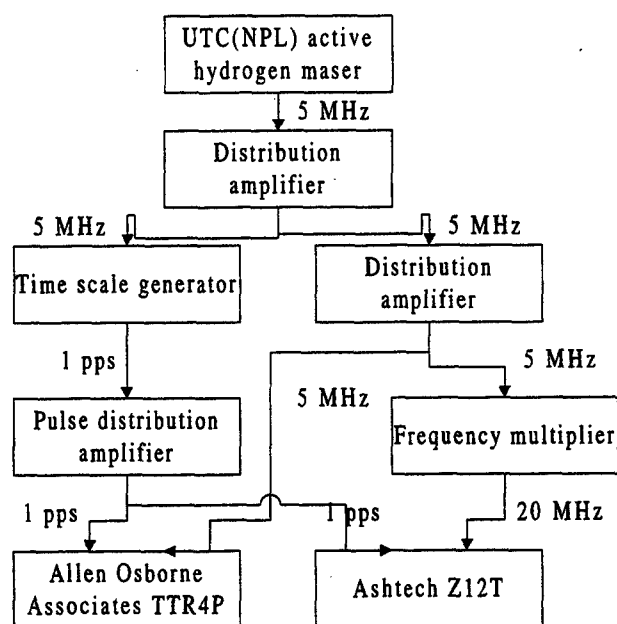
Figure 1: Ashtech Z12-T and AOA TTR-4P receiver hardware configuration.
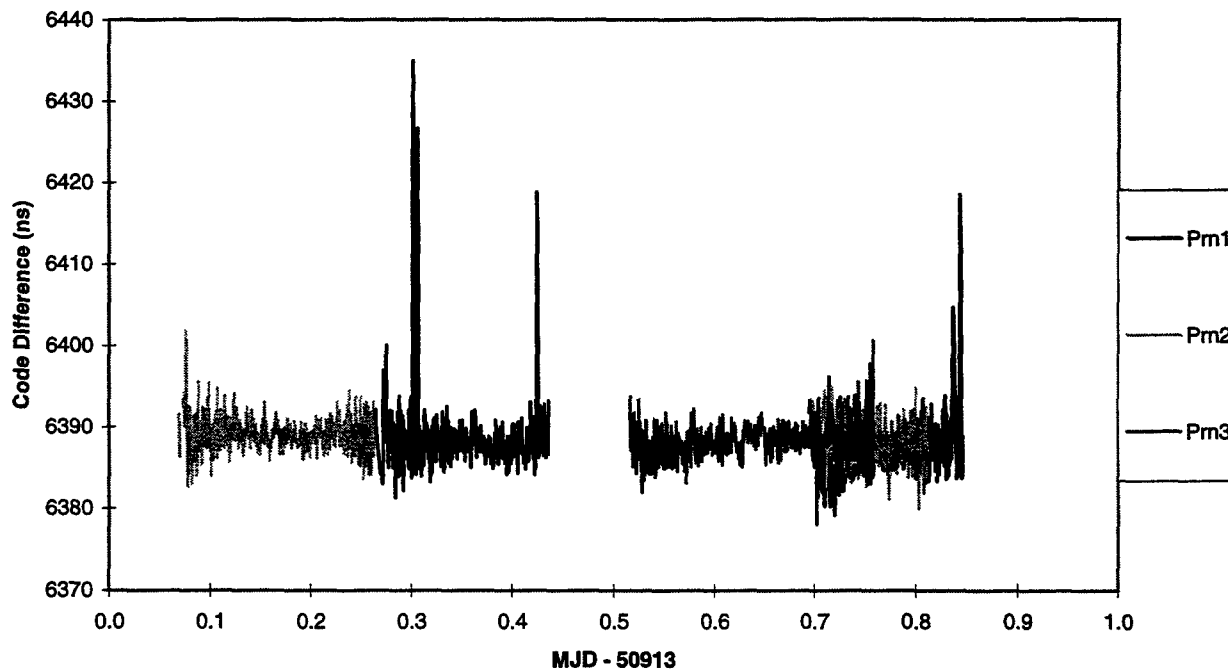
Figure 2: P1 code comparisons (AOA TTR-4P - Ashtech Z12-T), individual satellite tracks.
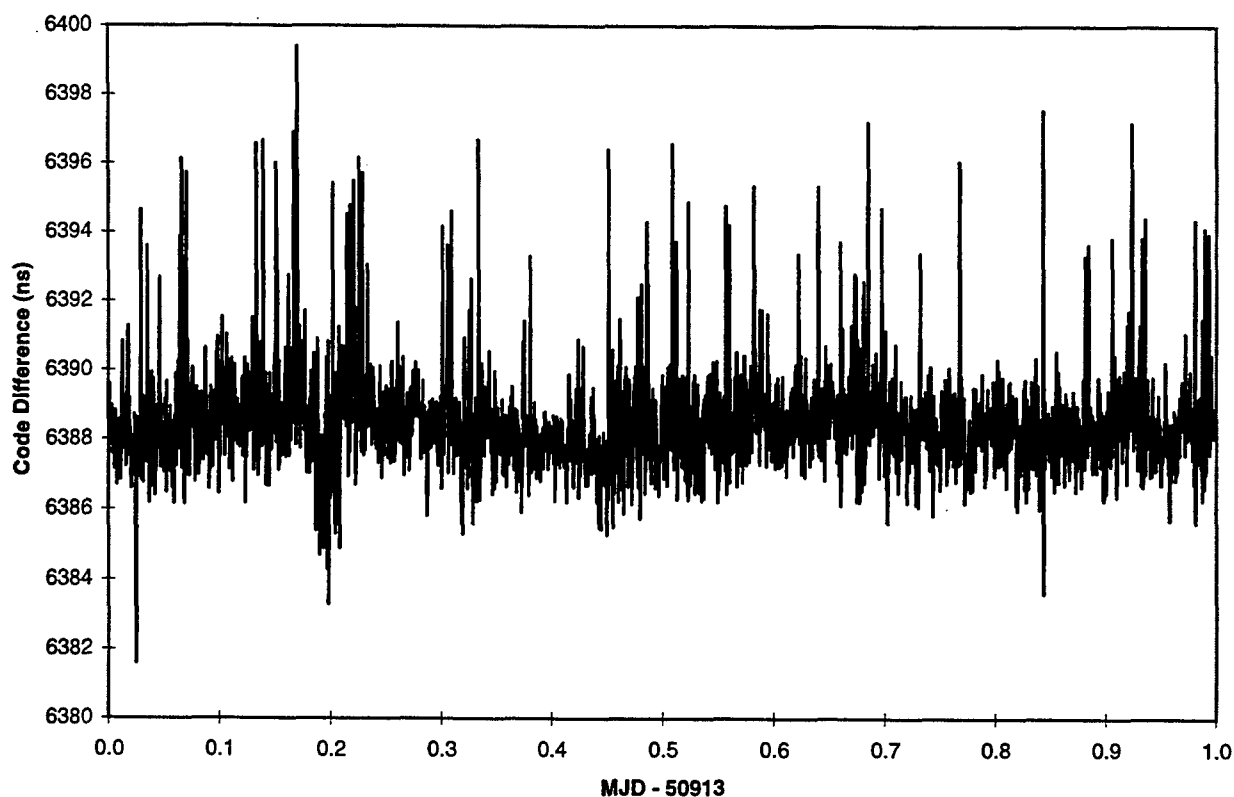
Figure 3: P1 code comparisons (AOA TTR-4P - Ashtech Z12-T), mean values.
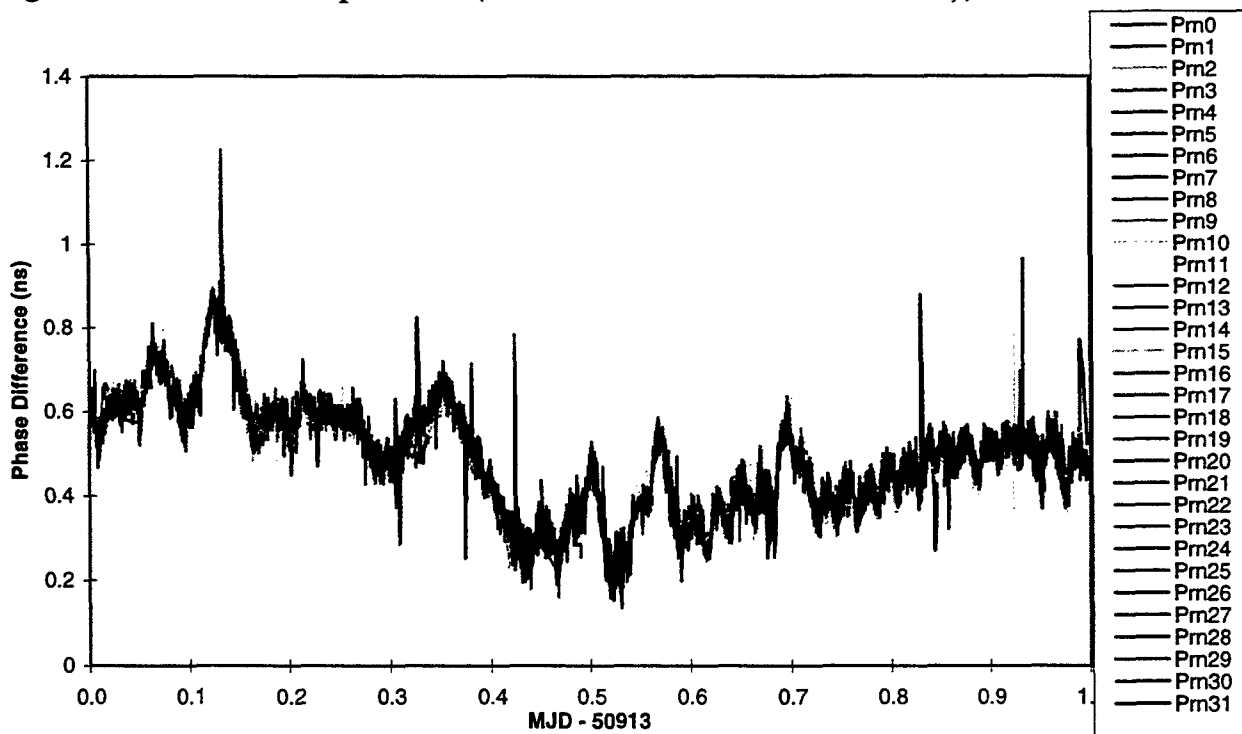
Figure 4: L2 phase comparisons (AOA TTR-4P - Ashtech Z12-T), individual satellite tracks.
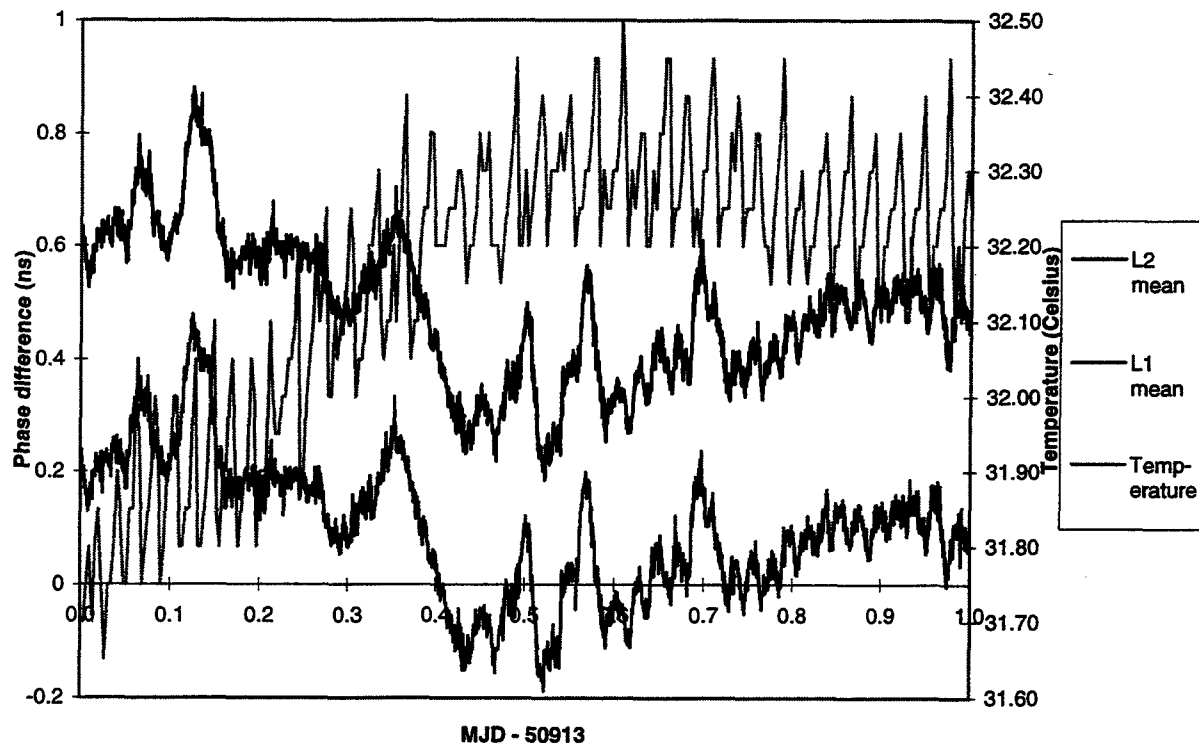
Figure 5: L1 and L2 phase comparisons (AOA TTR-4P - Ashtech Z12-T), mean values.
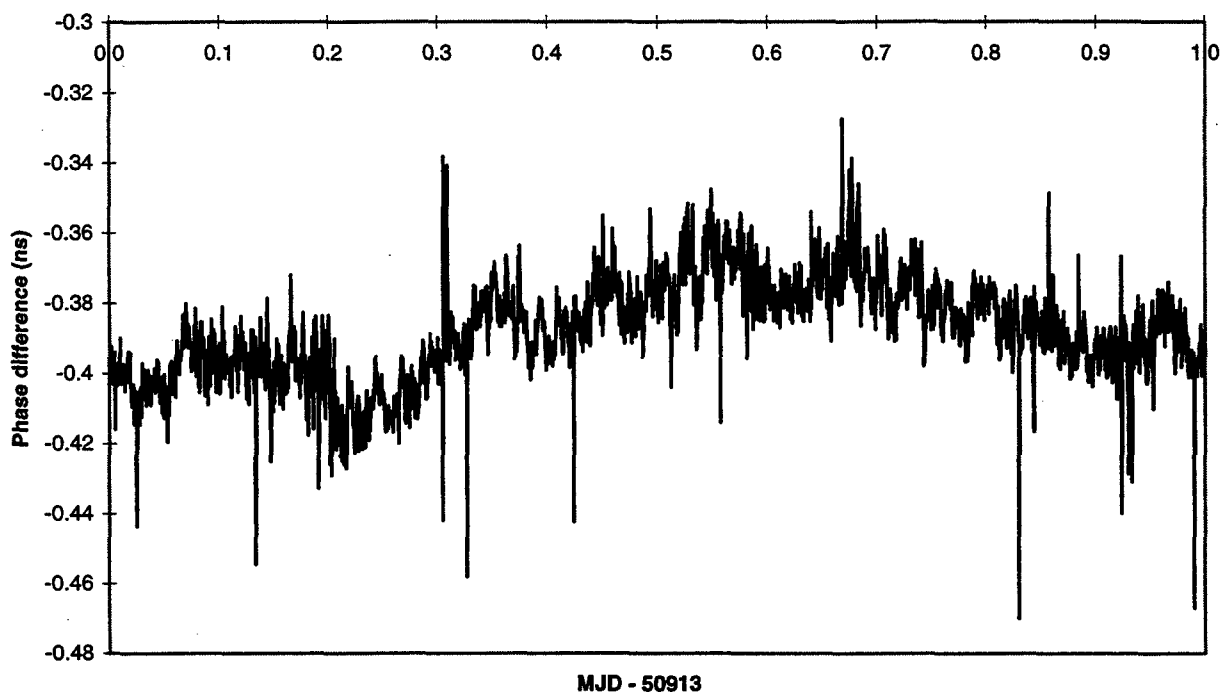
Figure 6: Phase comparisons (AOA TTR-4P - Ashtech Z12-T), L1 - L2 differences.
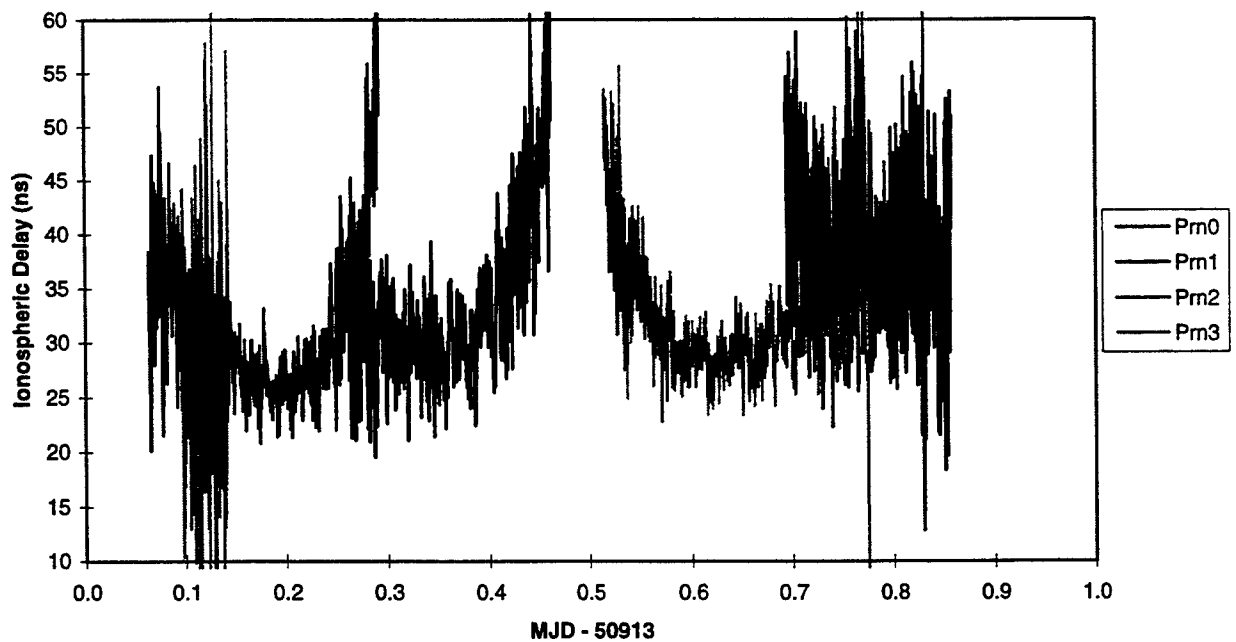
Figure 7: Code ionospheric delay measurements, individual satellite tracks, Ashtech Z12-T receiver.
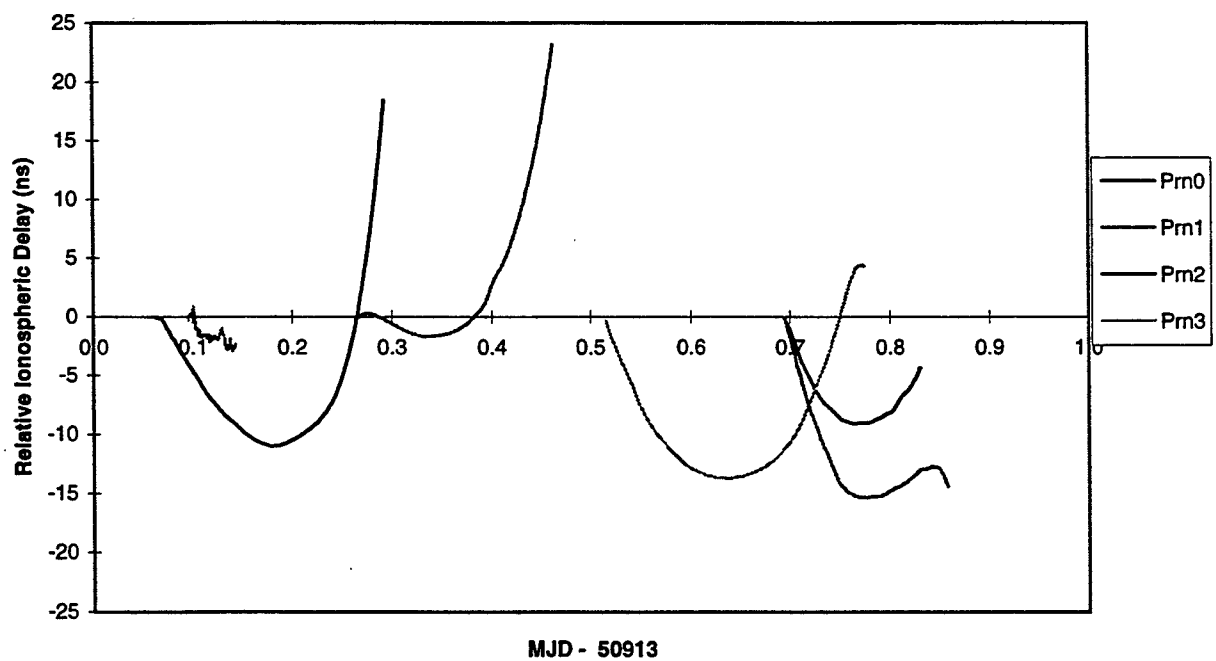
Figure 8: Phase ionospheric delay measurements, individual satellite tracks. Ashtech Z12-T receiver.
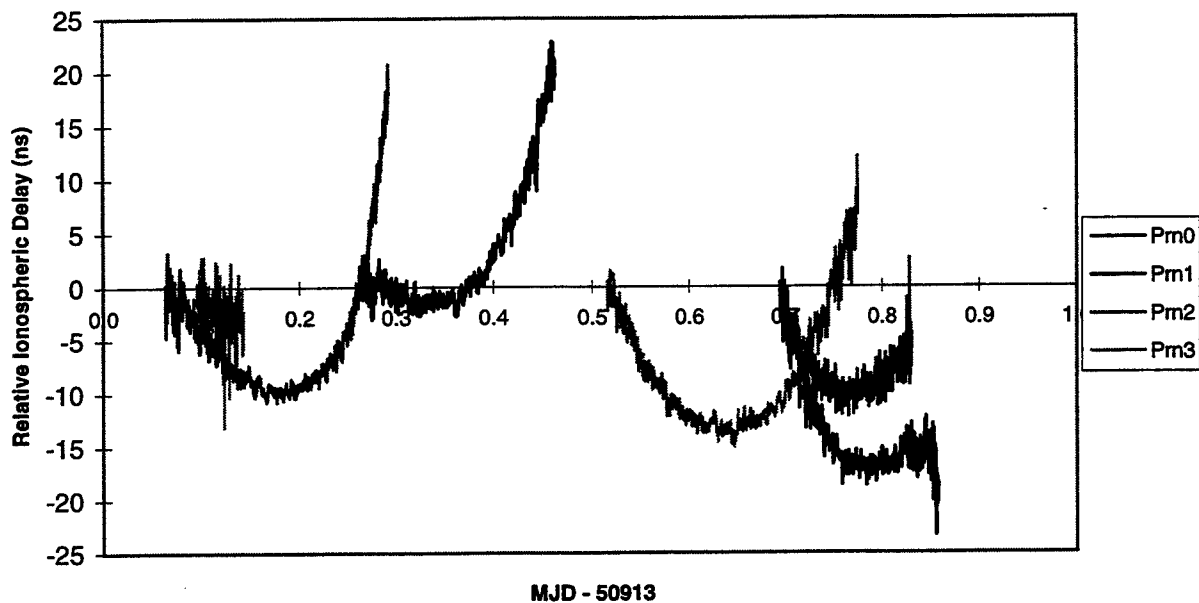
Figure 9: L1 single frequency ionospheric delay measurements, individual satellite tracks. Ashtech Z12-T receiver.
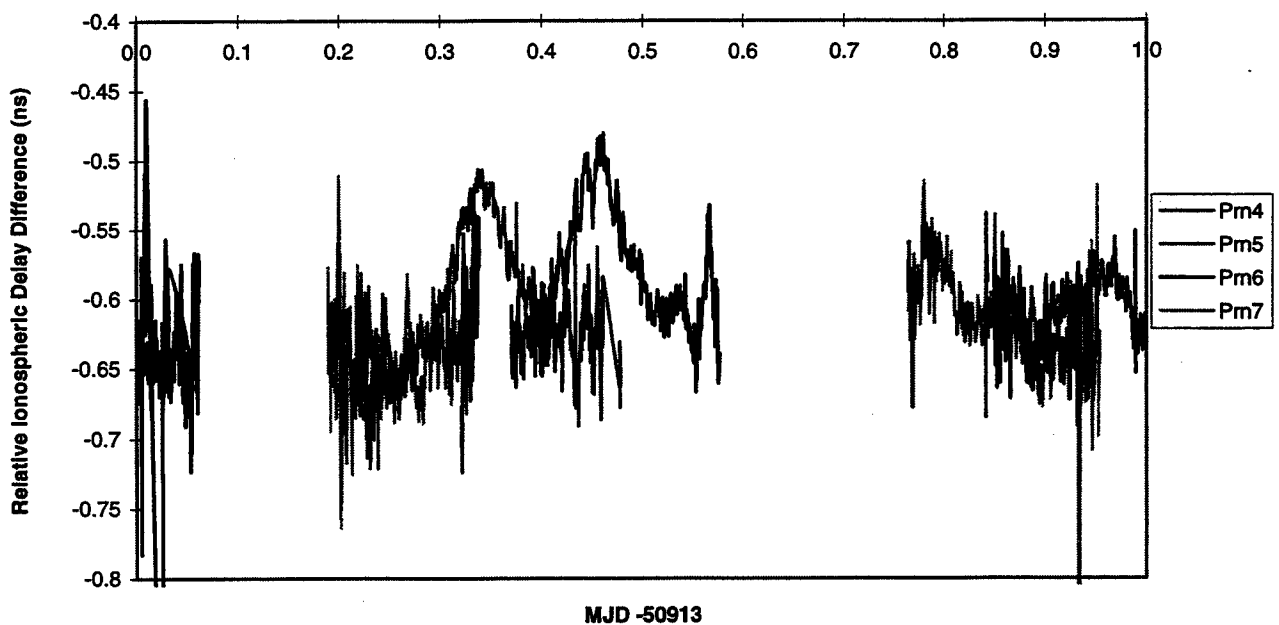
Figure 10: Phase ionospheric delay measurements, individual satellite tracks, (AOA TTR-4P - Ashtech Z12-T) phase differences.
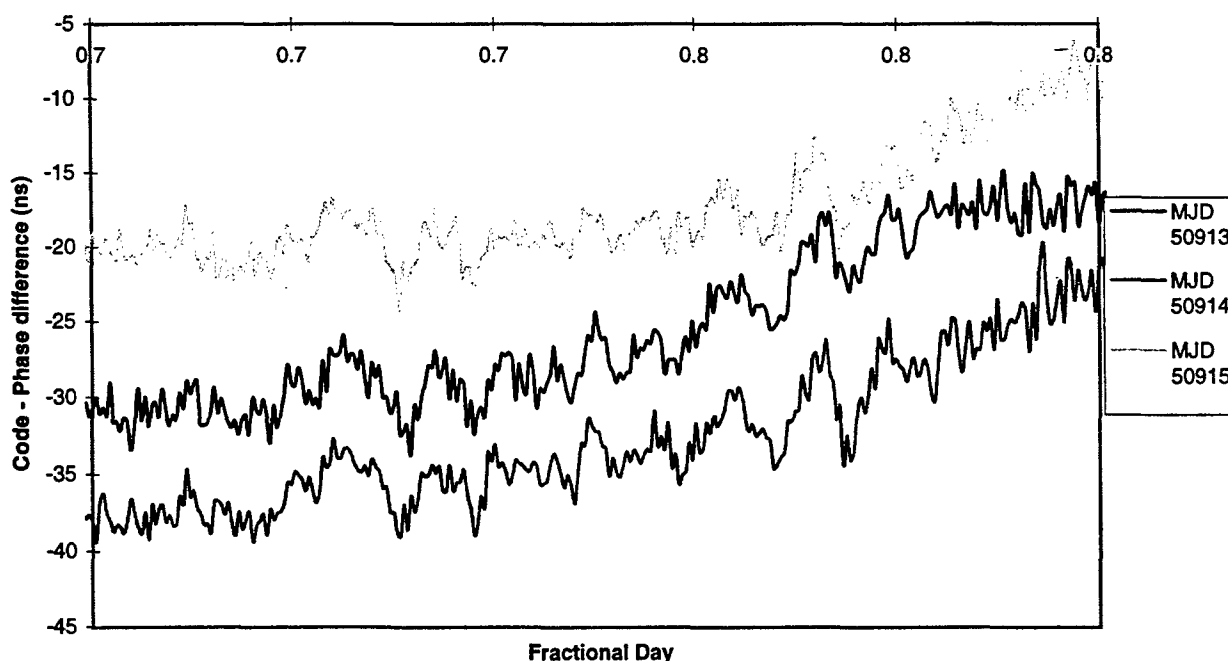
Figure 11: P1-L1 code-phase differences, PRN 31, MJD 50914 and 50195 data offset by four and eight minutes respectively, Ashtech Z12-T receiver.
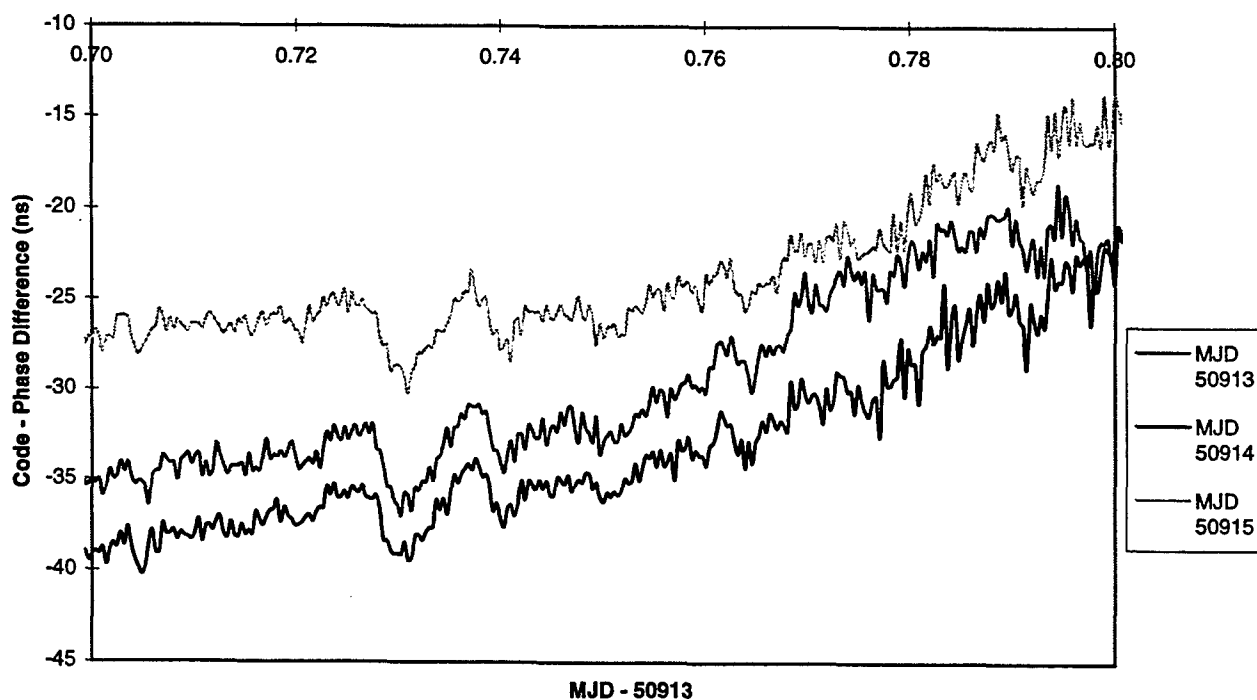
Figure 12: P2-L2 code-phase differences, PRN 31, MJD 50914 and 50195 data offset by four and eight minutes respectively, Ashtech Z12-T receiver.

268

Questions and Answers

MIHRAN MIRANIAN (USNO): On the TTR4-P, were you using any kind of an elevation mask for the ionosphere? Because it is notoriously bad for ionospheric measurements.

JOHN DAVIS (NPL): No, we were not. We were using everything that we could collect from the TTR4-P because the Ashtech had more channels (12); the TTR4-P had eight. Also, we discovered that the TTR4-P found it slightly harder to lock onto satellites. So in reality, everything was used. Where there was a TTR4-P track, there was always an Ashtech. We did not use a mask. In those P-1 measurements, everything has been included, wherein after the average including the low-elevation satellites was measured, we could put a mask on.

MIHRAN MIRANIAN: Yes, we use them at the Observatory, and we found that anything below about 25 degrees is really useless.

FIRST RESULTS ON A TRANSATLANTIC TIME AND FREQUENCY TRANSFER BY GPS CARRIER PHASE

G. Dudle, F. Overney, L. Prost
Swiss Federal Office of Metrology
Lindenweg 50, CH-3003 Bern-Wabern, Switzerland

Th. Schildknecht, T. Springer
Astronomical Institute of the University of Berne
Switzerland

P. Hetzel
Physikalisch Technische Bundesantalt
Braunschweig, Germany

E. Powers
U.S. Naval Observatory, Washington, DC, USA

Abstract

Time and frequency transfer by GPS carrier phase, also referred to as Geodetic Time Transfer (GeTT), has been studied intensively in the frame of a collaboration between the Swiss Federal Office of Metrology (OFMET) and the Astronomical Institute of the University of Berne (AIUB). Two terminals equipped with geodetic GPS receivers have been built and were successfully deployed over European baselines. The study has demonstrated the low instrumental noise of GeTT ($\sigma_y(\tau) = 10^{-13}$ at $\tau = 100$ s) which makes this method an ideal tool for frequency comparisons between high performance clocks since much shorter averaging times are required than with GPS common view.

This new time and frequency transfer method is now to be tested over longer baselines. In this paper we report on a transatlantic campaign between the Physikalisch-Technische Bundesanstalt in Germany (PTB) and the US Naval Observatory, Washington (USNO). Besides the longer baseline the choice of these two sites offers also the possibility to compare frequently GeTT and TWSTFT.

The paper outlines the main parts of a GeTT campaign and summarizes the first results of time and frequency transfer by GPS carrier phase between PTB and USNO.

INTRODUCTION

The GPS Common View (CV) and the Two Way Satellite Time and Frequency Transfer (TWSTFT) are up to now the most used methods for precise time and frequency transfer. In parallel with the development of new types of frequency standards achieving outstanding performances, there is a demand for new tools to compare these devices. Requiring only receiver capabilities on either side of the comparison, the CV method is relatively simple to use. However, an averaging time of at least a few days is needed to compare the new frequency standards at their best levels. On the other hand, the TWSTFT technique allows comparisons with a shorter time but at the prize of heavy sending and receiving equipment on each site.

An interesting alternative to associate simplicity and precision is to use geodetic GPS receivers [1]. Since only code information is processed in the CV technique while carrier phase information is discarded, the GPS is not used to its full potential in time and frequency transfer. The approach to record all GPS observables (Code CA, P1, P2, phase L1, L2) is well established in the geodesy community where these observations are carried out routinely in the framework of the International GPS Service for Geodynamics (IGS) [2]. Powerful tools have been developed to deal with the problem of phase ambiguity, ionospheric and tropospheric delays and satellite orbits. It is thus natural to seek for improvement of the time and frequency transfer by GPS in a collaboration between the geodesy and the time and frequency communities. The recent IGS - BIPM pilot project [3] is a perfect example of a joint effort in this direction.

As a precursor to the IGS-BIPM project, a collaboration between the Astronomical Institute of the University of Berne (AIUB) and the Swiss Federal Office of Metrology (OFMET) has led to the development and construction of two terminals and the processing software for geodetic time transfer (GeTT).

CAMPAIGN SETUP

A typical configuration of a GeTT campaign is shown in Figure 1. A GeTT terminal is placed on each site participating in the campaign. For simplicity, only two sites are drawn in Figure 1 but more stations could be included and treated simultaneously. The local clocks to be compared provide a 5 MHz signal and a 1 PPS. Each station acquires all 5 GPS observables every 30 s and sends the results daily to the processing center via FTP. A detailed description of a GeTT terminal can be found *e.g.* in [4]. Taking into account the precise orbits of the satellites and information on ionospheric and tropospheric delays, the processing center computes for each observation the delay between an arbitrarily chosen reference station and all other participants. The final GeTT results are computed 5 days after the observations when the IGS products become available.

For the study of this paper, a first GeTT station has been placed at the PTB in Braunschweig, D. It will be labeled PTBA throughout the paper. A second is installed at the USNO, Washington, USA, and is referred to as USNB. The baseline between the two receivers measures 6'275 km. At the PTB, the local clock connected to the station is a hydrogen maser (Kvarz CH1-75, labeled H2), the same clock that is used for the TWSTFT measurement. This maser is free running and not steered to follow the local timescale. However, a local comparison every 30 minutes between the maser H2 and UTC(PTB) allows to perform time transfer experiments. The local clock at the USNO is also a hydrogen maser (MC2), but in contrast to the PTB

configuration this maser is corrected once a day to follow UTC(Mean), which is a steered time-scale [7]. Local comparisons at the USNO to connect UTC(USNO) to other stations are, therefore, not necessary. Both stations were installed around MJD 51014 and the campaign will probably last beyond the end of 1998.

FREQUENCY TRANSFER

Let us first assess the frequency transfer capabilities of GeTT over the transatlantic baseline. Since only relative frequency is of interest here, the local comparisons at the PTB between the maser H2 and UTC(PTB) are not taken into account. Figure 2 summarizes the main results of this part of the study in the form of an Allan variance diagram. The black triangles give the comparison of H2 at PTB and MC2 at USNO by GeTT. Typical individual performances of the participating clocks are represented by diamonds (H2 at PTB) [6] and triangles (MC2 at USNO) [7]. The circles, finally, indicate a comparison between PTB and USNO by means of GPS CV. For this purpose, out of the set of unequally spaced CV observations, one value was computed every 6 hours.

Several important features have to be emphasized on this graph. First, for averaging times of 10^4 s up to 10^5 s, both local clocks, the masers at the PTB and at the USNO, have a relative frequency stability in the 10^{-15} range and, thus, do not represent a limiting factor for the experiment. Secondly, it has to be noted that GeTT performs, as expected, better than classical GPS CV for all averaging times displayed. For short τ (< 10^5 s), the improvement gained by GeTT is at least one order of magnitude. This result is of great practical importance. If 2 clocks at the 10^{-14} level are to be compared, averaging times of up to 10^6 s (> 10 d) are required with GPS CV, while $3 \cdot 10^4$ s (< 1 d) are sufficient with GeTT. This makes this tool suitable for the comparison of clocks of the upcoming generation of primary frequency standards. Another important and surprising point is the observed slope on the $\sigma_y(\tau)$ plot for GeTT. The instrumental noise of CV averages with τ^{-1} indicating phase noise. For GeTT, however, the $\sigma_y(\tau)$ decreases with $\tau^{-1/2}$, a signature for white FM. Since both clocks are significantly below the noise level computed with GeTT, the slope -1/2 must be ascribed to the method. While the mechanism leading to this behavior is not fully understood yet, some elements of explanation can nevertheless be pointed out. In order to verify if the excessive noise is due to the long baseline between PTB and USNO, a comparison with another station was undertaken. This third station, also located at the USNO, is not a dedicated GeTT terminal but part of the IGS network [2] in which it is labelled USNO. It is steered by a different maser than USNB. Figure 3 shows the delay between the stations USNO and USNB as measured with GPS carrier phase. In fact, since all delays in the present setup are given against PTBA, the difference USNB -USNO is obtained by evaluating (PTBA - USNO) - (PTBA - USNB). Discontinuities in the delay are clearly visible in the graph at the transition between consecutive days. These jumps are the consequence of a discrete offset correction which is calculated every day to bring the average phase solution in agreement with the average of the code. Odd behavior of the code on a given day induces large differences between the offset of two consecutive days and causes the observed discontinuities. A good example of such a behavior is Day of Year (DoY) 280. If the Allan variance is calculated for a set of delays between USNO and USNB as displayed in Figure 3, the level of noise for short τ is identical for this short baseline to the $\sigma_y(\tau)$ observed for PTBA - USNB. To make the influence of these jumps on the Allan variance even clearer, especially for $\tau < 10^4$ s, data of a single day were used, thus avoiding entirely the discontinuities.

The resulting Allan variance is displayed in Figure 4. Since no jumps are present in this subset of data, it is not surprising that the noise level of the Allan variance is lower. But in addition to the lower noise, the slope for $\tau < 5 \cdot 10^3$ s is also steeper than previously. It is also interesting to note that even though the comparison USNB - USNO is obtained over the detour of PTBA the noise is similar to the one measured in a common clock experiment over a zero-baseline campaign (long dashes in Figure 4).

For longer baselines, however, more elements seem to be of importance. This becomes apparent in Figure 4 where the Allan variances for other comparisons with different baselines are shown as well. As before, two IGS stations (USNO and NRC1 at the NRC in Canada) have been used for this study. These are not dedicated stations for time and frequency transfer but rather permanent receivers of the IGS network. Both stations are steered by hydrogen masers. The table below gives an overview of the baselines between USNB and the other stations.

Location	Name of station	Baseline with USNB (km)
Washington, USA	USNO	~ 0
Ottawa, Canada	NRC1	735
Braunschweig, D	PTBA	6'275

Again, data of one day only are used to avoid the jumps described above. The lowest curve in Figure 4 is again the comparison over the near-zero-baseline USNO-USNB. Slightly higher is the comparison between USNB and NRC1. For the largest baseline between USNB and PTBA, the Allan variance shows again the $\tau^{-1/2}$ dependence even though there are no discontinuities present in the data set. It has to be noted, however, that only one single day of data has been processed and that the behavior could vary from day to day. Systematic measurements will be necessary to answer this question definitely.

A last striking feature in Figure 2 is the excessive noise for 10^5 s $< \tau < 10^6$ s. The contour of the $\sigma_y(\tau)$ of the comparison for $\tau > 3 \cdot 10^5$ s can be reproduced perfectly by the Allan variance of a sine wave with a period of $1.45 \cdot 10^6$ s (16.8 d). Since this is an uncommon period for GPS measurements, it is unlikely that this behavior is due to the GeTT method itself. Individual performances of the participating clocks, however, do not show any evidence for an oscillation either. More investigations are required to explain the observed excess noise, including a comparison with other stations.

TIME TRANSFER

A second important part of the study is the time transfer experiment. Besides the fact that both institutions, PTB and USNO, maintain an excellent timescale, the choice of these sites offers the further advantage that a TW time transfer is routinely carried out between both parties. Observations take place 3 times a week, on Monday, Wednesday and Friday. The goal of this part is to demonstrate the time transfer capabilities of GeTT. As already mentioned above, the GeTT terminal at the PTB is not steered by UTC(PTB),but by a free running maser. To be able to correct for the delay UTC(PTB) - H2, a local measurement is performed every 30 minutes. The same clock H2 is also used in the TWSTFT experiment at the PTB. At the USNO, local comparisons are not required, since the maser steering TWSTFT and GeTT is corrected to follow UTC(USNO).

The results of the comparison of the two timescales are represented in Figure 5. The white circles stand for the data obtained by TWSTFT [9]. Over the displayed period of 80 d, 24 successful TWSTFT sessions were carried out between PTB and USNO (out of a scheduled maximum of 34). Each data point represents the average of the data collected over one TWSTFT session lasting 120 s. The black curve gives the GeTT results of which 2880 are taken per day. To speed up the processing time, the delays are calculated every 300 s only, reducing the amount of data by a factor of 10. Uncalibrated internal delays of the GeTT terminal have made it necessary to shift the raw data by a fixed amount of -112.9 ns to fit the GeTT results to the TWSTFT. The third curve in gray is added to the graph to visualize the difference of transfer by GeTT and by GPS CV. On average, 15 CV observations per day are possible between PTB and USNO. These data have again been shifted to match the TWSTFT results (shifted data = raw data - 24.4 ns). It is easiest to analyze the time transfer capabilities if the difference between the transfer by TWSTFT and the transfer by the alternative method is built. The two curves of Figure 6 correspond to transfer$_{GeTT}$ - transfer$_{TW}$ (black triangles, connected by a solid curve to guide the eye) and to transfer$_{CV}$ - transfer$_{TW}$ (white squares, connected by a dotted line). For this graph, no averaging has been performed on the GeTT data. Displayed are simply the differences between the GeTT result corresponding to the epoch for which a TWSTFT result exists and the TWSTFT result itself. For the difference CV against TWSTFT, a linear interpolation was used to compute the delay measured by CV at the epoch for which a TWSTFT result is available.

Having shifted CV and GeTT data, the absolute value in Figure 6 can not be of interest. What is more important is the constancy of the difference and, thus, the internal delays. The delays in the GeTT terminals seem to be insensitive to an interruption of the acquisition. On two occasions (DoY 238 and DoY 258) over the period of interest, the method failed to acquire data continuously. The delays seem not to have changed after the restart since no discontinuity can be observed on these days. Let us point out that the spread of the result GeTT - TWSTFT is significantly smaller than that of the difference CV - TWSTFT. As expected, GeTT outperforms GPS CV as a time transfer tool.

However, the difference between the time transfers by GeTT and TWSTFT respectively is drifting with an average slope of +43 ps/d. The origin of this slope is not known. Since Figure 6 displays differences of comparisons by two distinct methods which are steered by the same clocks, the only possible explanation for the slope is a drift of a delay in one or the other time transfer system. Delays in the antenna and the cables are known to change with temperature, but the coefficients for GeTT [8] are not large enough to explain the observed slope. It is also difficult to draw conclusions from the difference CV - TWSTFT, mainly due to the large spread of the data. More work is needed to explain the origin of the drift between GeTT and TWSTFT.

CONCLUSION

The possibility of time and frequency transfer by GPS carrier phase between the PTB, Braunschweig, D and the USNO, Washington, USA has now been studied over a period of 4 months. The study has proven the feasibility of this technique over transatlantic distances and shown a good reliability throughout the campaign. The hardware of GeTT is only slightly more complicated than classical GPS CV, but for short

averaging times GeTT outperforms GPS CV by at least one order of magnitude. The price to pay is a more sophisticated processing of the data. However, the required tools exist and have already proven their adequacy to handle the large amount of data in a network of over 10 stations. A frequency transfer at the level of 10^{-13} for $\tau = 300$ s was possible over the 6'275 km long baseline of this study. At present, this limit seems to be imposed by the data processing. As for the time transfer the results look very promising as well. The main goal of this part of the study was to check the constancy of the different local delays. The difference of the time transfer by GeTT and the time transfer by TWSTFT has drifted with a slope of 43 ps/d over the period of 80 observed days. It remains unclear whether this slope must be ascribed entirely to GeTT or if the involved TWSTFT contributes also to this difference. More work needs to be done on this topic. It is also important to note that in the present setup not all local delays are known and that, therefore, it is impossible to carry out absolute time transfer. In spite of this, GeTT is certainly an interesting additional tool for time and frequency transfer, especially due to its quasi-continuous acquisition of data which makes an uninterrupted comparison between remote timescales possible.

ACKNOWLEDGMENTS

REFERENCES

[1] Th. Schildknecht, G. Beutler, W. Gurtner, M. Rothacher, "Towards sub-nanosecond GPS time Transfer using Geodetic Processing Technique", Proc. 4th EFTF, pp. 335-346, 1990.

[2] G. Beutler, I. I. Mueller, R. E. Neilan, "The International GPS Service for Geodynamics (IGS): the Story", IAGS Syposium No 115, pp. 3-13, 1995.

[3] J. R. Ray, "The IGS/BIPM Time Transfer Project", IGS Analysis Center Workshop Proceedings, in press 1998

[4] F. Overney, et. al, "GPS Time Transfer Using GeodeticReceivers(GeTT): Results on a European Baseline", Proc 12th EFTF, pp. 94-99, 1998.

[5] Th. Schildknecht et al., these proceedings

[6] A. Bauch, private communication

[7] J. Deyoung, private communication, for the data cf also http://tycho.usno.navy.mil/gpscp_dd.html and links there

[8] F. Overney, Th. Schildknecht, G. Beutler, L. Prost, U. Feller, "GPS Time Transfer using Geodetic Receivers: Middle-Term Stability and Temperature Dependence of the Signal Delays", Proc 11th EFTF, pp, 504 - 508, 1997.

[9] The TWSTFT data used for this graph are available in standard format from FTP sites at the PTB and the USNO.
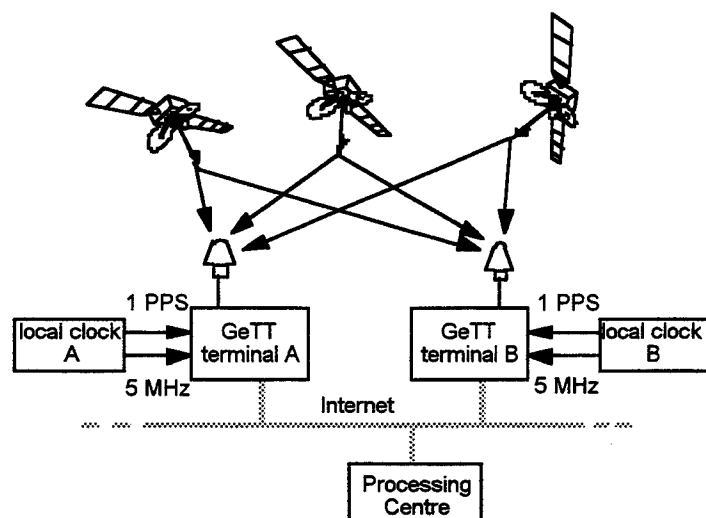
Figure 1: A typical configuration of a GeTT campaign. On each site, a GeTT terminal is installed and connected to the local clock to be compared. Acquired data are sent daily via FTP to the processing center which delivers the delay between the arbitrarily chosen reference station and all other participants 5 days after the observations.
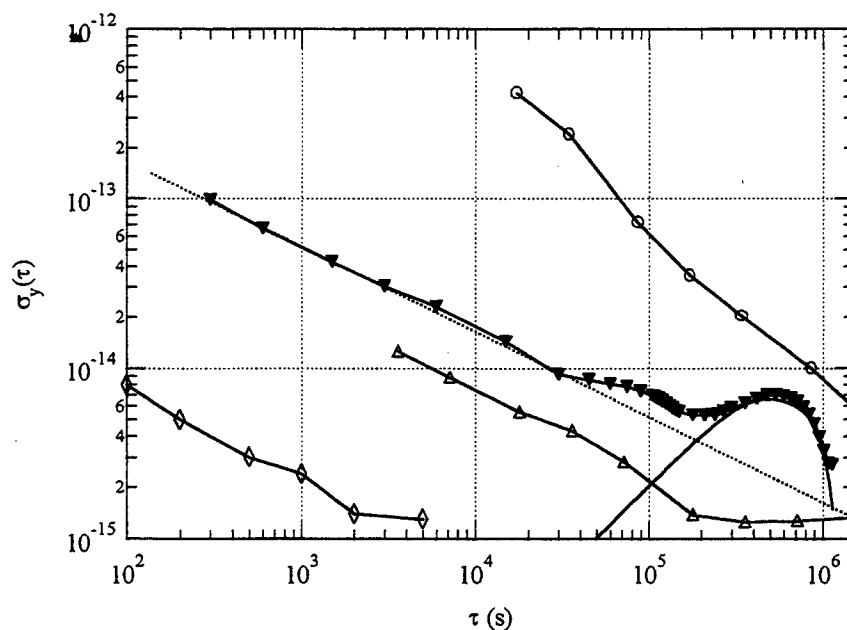
Figure 2: Allan variance for the comparison H2 - MC2 by GeTT (black triangles), the local clocks H2 at PTB (diamonds) and MC2 at the USNO (white triangles). The white circles represent the Allan variance for a comparison between PTB and USNO by GPS CV (not with the same clock sources). The plain line without symbols shows the $\sigma_y(\tau)$ for a sine wave with amplitude 2.2 ns and a period of $1.45 \cdot 10^6$ s.
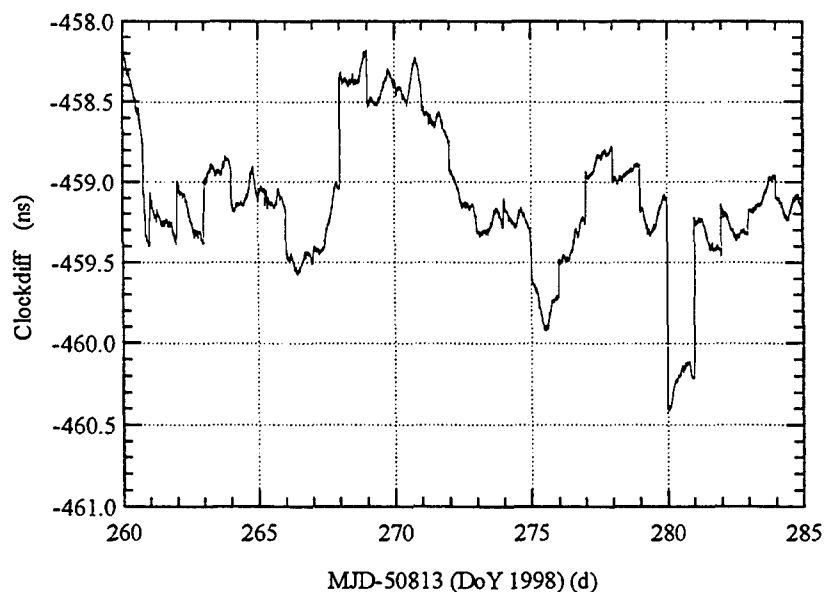
Figure 3: Delay between USNB and USNO as measured by GeTT. Discontinuities discussed in the text are clearly visible
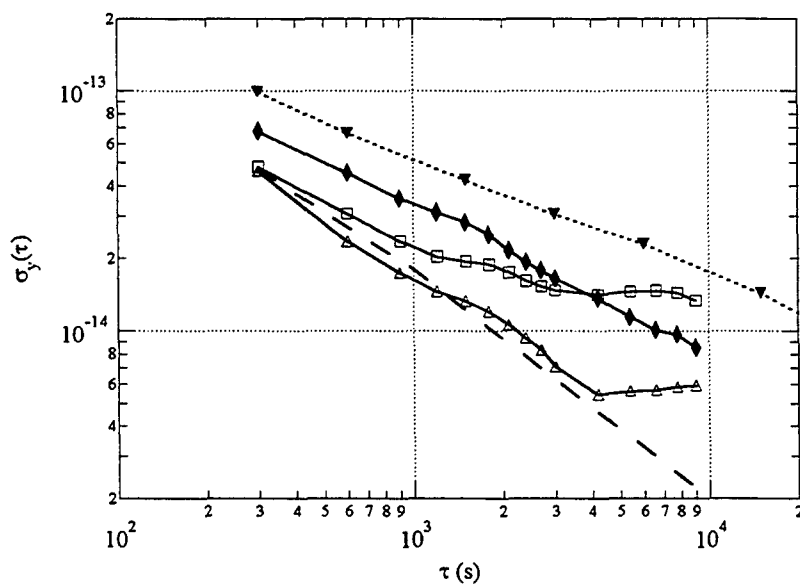
Figure 4: Allan variance computed with only one day of data for different comparisons: USNB-USNO: white triangles; USNB -NRC1: white squares; PTBA - USNB: black diamonds. For purpose of comparison the Allan variance for the complete set of data PTBA - USNB is also indicated (short dashes, inverted black triangles). The instrumental noise of GeTT, as measured over a zero baseline in a common clock experiment, is indicated by the long dashed line.

278
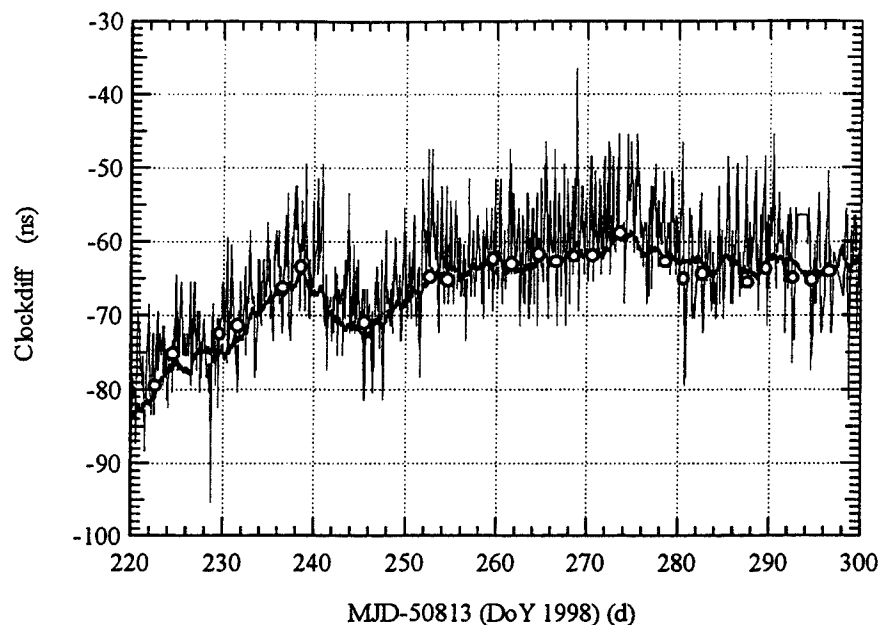
Figure 5: Difference of the timescales at PTB and USNO by a) TWSTFT in white circles, b) GeTT, black curve, c) GPS CV in gray. The result of GeTT has been shifted by -112.9 ns, those of CV by -24.4 ns, both to match the result of TWSTFT.
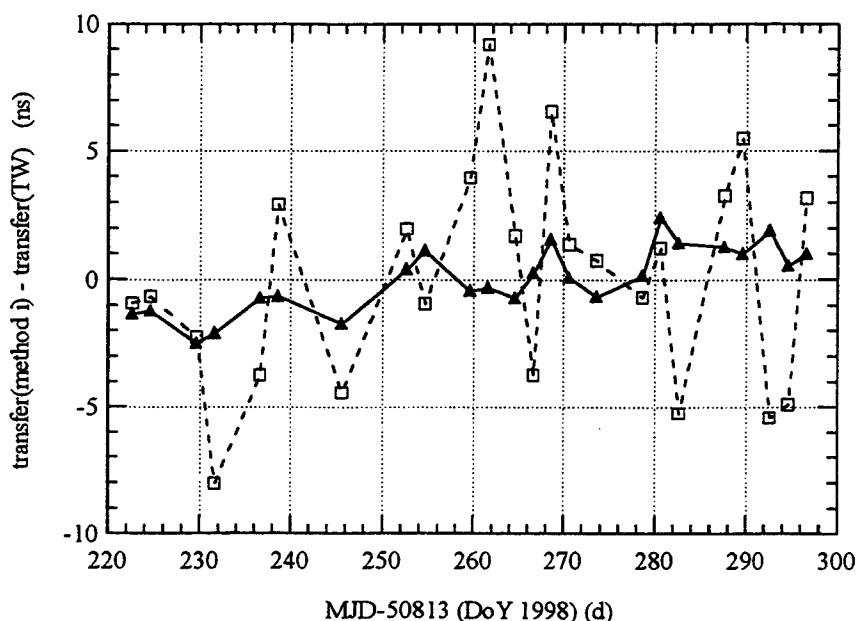
Figure 6: Black triangles: Difference between the time transfer by GeTT and the time transfer by TWSTFT
White squares: Difference between the time transfer by CV and the time transfer by TWSTFT.

Questions and Answers

JIM DeYOUNG (USNO): Perhaps I missed it, but at PTB the distance between the two-way antenna and the clock hall is quite a long distance, 100 meters to 150 meters, or perhaps more. Can you tell me the location of where the Ashtech – or whatever antenna you use, what is the location of it? Is it on the clock hall?

GREGOR DUDLE (Swiss Federal Office of Metrology): It is almost in the clock hall. We use approximately 40 meters of cable, so it is not very far away.

DIETER KIRCHNER (TUG): When you say you have carrier phase measurements every 30 seconds, is this an average over 30 seconds?

GREGOR DUDLE: No, no. This is just the 30-second observations. We have an observation every 30 seconds.

DIETER KIRCHNER: So, there is no averaging.

GREGOR DUDLE: No.

ROBERT DOUGLAS (NRC): When you say that it is an independent measure; what is the initial point for the integration? Because, you are integrating the carrier phase ---

GREGOR DUDLE: I am not the expert on the data processing. Maybe we can discuss the data processing problem after this session.

HIGH PRECISION TIME AND FREQUENCY TRANSFER USING GPS PHASE MEASUREMENTS

T. Schildknecht, T. Springer
Astronomical Institute
University of Bern
Sidlerstr. 5
3012 Bern, Switzerland
tel +41-31-6318594 fax +41-31-6313869
e-mail schild@aiub.unibe.ch

Abstract

The use of GPS C/A code measurements for time transfer by means of the so-called common view method is a widely accepted technique. The full potential of the GPS system for time and frequency transfer is, however, only exploited by using all phase and code observables from all satellites in view. Geodetic processing techniques, adapted to the specific requirements to process data from specially modified geodetic receivers, will be presented. We will also discuss the requirements for the receivers, and the control as well as the calibration of instrumental delays. The potential of the technique will be illustrated by laboratory experiments and measurement campaigns on continental and intercontinental baselines.

INTRODUCTION

The GPS has been used for many years by the time and frequency community to compare clocks over long baselines. The predominant technique in this field is the so-called common-view method. This technique uses C/A code pseudorange measurements in order to estimate the receiver clock offset with respect to GPS time at each station. To compare clocks of two timing laboratories the corresponding clock offsets registered at the two stations are then simply differenced a posteriori. The term "common-view" reflects the fact that the observation scenarios are arranged in a way that the two stations of a baseline observe the same satellite simultaneously. In this configuration the predominant errors, namely the satellite orbit and the satellite clock error, are to a great extent "common" to both stations and thus reduced considerably.

Results from single-frequency, single-channel receivers show routinely an accuracy of several nanoseconds over a 13-minute pass and a frequency stability of a few parts in 10^{-14} over one day [1].

Many extensions of the common-view technique have been conceived over the past years. They all try to overcome one or several basic limitations of the classical common-view approach by using:

- multichannel receivers to observe several satellites simultaneously,

- P-code receivers to reduce the intrinsic measurement noise,

- dual-frequency receivers to measure the ionospheric delays.

In the early days of GPS, the geodetic community recognized that the system offers a much more precise observable than the code pseudoranges, namely the reconstructed carrier phases. Geodetic GPS receivers therefore record C/A-, and P-code on both frequencies as well as the carrier phases on both frequencies. In contrast to the common-view technique the raw data are stored at each station, and then collected and processed in a central processing center. The position uncertainties obtained for global networks of stations are of the order of 1 cm [2]. Since receiver clock errors are closely related to position errors, the use of geodetic GPS techniques for precise frequency and time transfer has been suggested a long time ago [3]. During the last years several groups started to publish results (see e.g. [4], [5]).

Recent progress in the field stipulated the setup of the IGS/BIPM Pilot Project to Study Accurate Time and Frequency Comparisons in December 1997 [6]. This joint project of the International GPS Service (IGS) and the Bureau International de Poids et Mesures (BIPM) wants to exploit the potential of the IGS network and analysis centers by a) using the precise orbit and position information from the IGS and by b) including geodetic-type GPS receivers at timing laboratories into the IGS processing schemes.

In this paper we describe the principles of the geodetic GPS processing for time and frequency transfer. We also discuss the problem of tying the receiver internal clock to the external clock, and emphasize the necessity to monitor and control all types of delays. Finally, for time transfer results on long baselines we refer to a separate communication of these proceedings [7].

GEODETIC GPS PROCESSING FOR TIME AND FREQUENCY TRANSFER

The C/A- and/or the P- or Y-code, as registered by receiver i at time t_i from satellite j, is defined as follows:

$$p_i^j = c \cdot (t_i - \tau^j)$$

where

t_i is the arrival time, or observation time, of a signal as measured by the clock of receiver i.

τ^j is the transmission time of the same signal, measured in the time frame of satellite j.

The pseudorange p_i^j may be related to the slant range ρ_i^j at time t_i and to the delays due to the Earth's atmosphere. The slant range is the geometrical distance between receiver at observation time t_i and the position of the satellite at time τ^j:

$$p_i^j = \rho_i^j - c \cdot \Delta\tau^j + c \cdot \Delta t_i + \Delta\rho_{i,ion}^j + \Delta\rho_{i,trop}^j \qquad (1)$$

where

c is the speed of light,

$\rho_i^j \doteq |\vec{r}(\tau^j) - \bar{R}(t_i)|$, $\vec{r}(\tau^j)$ being the satellite position at transmission time, $\bar{R}(t_i)$ being the position of receiver i at time t_i,

$\Delta\tau^j$ is the error of the satellite clock w.r.t. a theoretical GPS-time,

Δt_i is the error of the receiver clock w.r.t. GPS-time.

$\Delta\rho_{i,trop}^j$ is the delay of the signal due to the neutral atmosphere (tropospheric refraction), and

$\Delta\rho_{i,ion}^j$ is the delay of the signal due to the ionosphere (ionospheric refraction).

Geodetic receivers also record the reconstructed carrier phase ϕ_i^j of the received signal. The essential difference of phase vs. code is (a) a much higher precision (rms error of about one millimeter compared to an rms of about one centimeter for the P-code), and (b) an unknown number N_i^j of entire cycles of carrier phase.

As the receiver keeps track of the integer number of cycles as a function of time, only one initial phase ambiguity number N_i^j is needed per satellite pass. An additional difference between code and phase concerns the sign of ionospheric refraction: a signal delay corresponds to a phase advance. This leads us to the following phase observation equation:

$$\lambda \cdot \phi_i^j = \rho_i^j - \Delta\rho_{i,ion}^j + \Delta\rho_{i,trop}^j - c \cdot \Delta\tau^j + c \cdot \Delta t_i + \lambda \cdot N_i^j \qquad (2)$$

where N_i^j is the initial phase ambiguity parameter for satellite j and receiver i.

Eqns.(2) and (1) immediately reveal that the receiver clock errors (w.r.t. to GPS-time) can be determined under the provision that all remaining terms can either be accurately determined from the data or may be inferred from an independent source. In order to compare two receiver clocks the difference of two quasi-simultaneous observations of the same satellite by two receivers i and k may be formed. This difference will no longer contain the satellite clock error.

It is essential that each receiver makes measurements to several satellites (ideally to all in view) quasi-simultaneously ("quasi" says that simultaneity can only be achieved apart from (small) receiver and satellite clock errors).

Given the much higher precision of the phase observable we would like to directly use Eqn. (2) to derive the receiver clock error Δt_i. It is, however, impossible to solve for the initial phase ambiguities N_i^j at this point. The phase measurements alone thus provide information about the behavior of the receiver clock (w.r.t. to GPS-time or in the case of single differences w.r.t. to a second receiver clock), but there remains an unknown "calibration" constant. However, the phase measurements provide all information we need to perform frequency transfer!

For time transfer the code observations are mandatory in order to determine the phase ambiguity. We note, however, that the low precision code measurements are used to determine a few parameters only. In other words we could also say that all code observations of an uninterrupted measurement series (which may last weeks) are used to estimate a single clock offset parameter for the beginning of the series.

In the actual processing we take advantage of the IGS network by taking all the geometrical information from the IGS products.

Figure (1) shows a short interval of a clock comparison between two hydrogen masers at USNO as estimated from P-code measurements (P3) and from carrier phase measurements (L3). The

Figure illustrates the dramatic difference in the intrinsic precision of the two observables. This is also reflected in the Allan deviation for the same data given in Figure (2).

ACCESSING THE RECEIVER CLOCK

There is one fundamental question common to all GPS techniques trying to compare clocks:

How can we relate the receiver internal time tags to the external signals of the clock to be compared?

It is important to notice that the epochs used in the GPS data processing are receiver internal epochs which are related (via software) to a receiver internal hardware clock. This hardware clock is not directly accessible in most geodetic GPS receivers! Clock estimates from geodetic GPS receivers are therefore first of all estimates of (virtual) internal clocks only!

There are in principle two possibilities to tie this internal clock to the laboratory clock to be compared: a) by forcing the receiver clock to operate synchronously with the laboratory clock, or b) by measuring clock signals from the internal clock with respect to the external clock.

Many geodetic GPS receivers possess an option to syntonize their internal time base with an external time base by means of a frequency input. Technically this syntonization has to be performed very carefully in order not to compromise the phase stability of the external time base (e.g by the phase noise of phase locked loops). The use of this external frequency input thus allows one to compare frequencies of laboratory clocks.

In order to compare time we must, in addition to the syntonization, either synchronize the receiver internal clock and the laboratory clock, or measure the phase of the receiver clock with respect to the external clock. Currently geodetic receivers are generally not fitted with either a 1 PPS synchronization input or a 1 PPS output. (The steered 1 PPS 'GPS time' output of some receivers should not be confused with a 1 PPS output of the internal clock!)

For our experiments we decided to fully synchronize the receiver clock with the external clock. This approach eliminates the necessity of an external time interval counter and the associated data logging hard- and software. We built two geodetic time transfer terminals (GeTT terminals) around custom modified Ashtech Z12 receivers. The receivers have a 20 MHz and a 1 PPS input, allowing complete replacement of the internal clock by the external laboratory clock. For details see [8]. The modified receivers were marketed as Ashtech Z12-T and an upgraded version will soon be available under the name Z12-Metronom.

CONTROLLING LOCAL RECEIVER DELAYS

When using zero- or single-difference GPS observations for time transfer, each single delay from the receiver antenna phase center to the point where the observables are measured has to be taken into account. This is different for the standard geodetic techniques where the so-called double-differencing eliminates all receiver internal delays in the processing.

Local delays are not critical as long as they are stable over time. In the case of frequency comparison constant delays are of no influence at all. For time comparison between laboratory clocks the receiver internal as well as the external delays (e.g. cable delays) have to be calibrated. The simplest approach is to calibrate an ensemble of GeTT terminals by mutually comparing them with their 1 PPS input connectors as reference points. This is performed by driving two or more terminals by the same clock on a short baseline of a few meters.

The crucial point, especially for time transfers, is the long-term stability of the local delays. For most delays it is very difficult to measure them in a direct way during the observations. We may therefore try to either stabilize them by some means, or correct for the variations in the processing by means of a calibrated model of their dependency on environmental parameters. We use a mixture of both approaches, depending on the type of delay.

Three major delays may be distinguished: a) the delay through the antenna and the associated preamplifier, b) the delay through the cable from the antenna to the receiver, and c) the receiver internal delays. The variation of these delays depends, to the first order, on the variation of the ambient temperature only. Figure (3) shows the measured temperature dependency of two antennas of the same type (Dorne Margolin) for code and phase observations. Measurements for the standard RG213 antenna cables have shown variations of up to 1.44 ps/°C/m. For the Z12 receiver internal delays we measured variations of up to 165 ps/°C. For details see [8]; extensive measurements may also be found in [9].

Antenna delay variations may be minimized by thermally stabilizing the preamplifier. Commercial versions of stabilized antennas are available, e.g. from 3S Navigation. We decided to measure the antenna temperature continuously and to apply corresponding corrections in the processing on the basis of a calibrated model.

In many cases the antenna cable is the most critical element. This may be surprising, but unprotected cables on rooftops can easily exhibit seasonal delay variations of up to 0.1 ns per meter of cable! There are simple remedies like using so-called "phase-stabilized" cables, minimizing the length of cable submitted to the outside environment, and protecting the cables from direct sunlight.

The variations of the receiver internal delays may be very different for different types of receivers. In the case of the Ashtech Z12 we simply stabilize the temperature of the receiver to about 0.1°C by means of a small thermal chamber. The same chamber also serves to stabilize all clock signal distribution electronics.

RESULTS

There are two types of results to report on: a) results from a time transfer experiment on an intercontinental baseline, and b) results from clock comparisons within the existing global IGS network.

Since July 1998 two GeTT terminals have been continuously operating on a transatlantic baseline between the US Naval Observatory (USNO), Washington, and the Physikalisch Technische Bundesanstalt (PTB) in Germany. The hydrogen masers driving the terminals at both sites are simultaneously compared via GPS common-view, and TWSTFT. The campaign is a collaboration between the Astronomical Institute of the University of Bern (AIUB) and the Swiss Federal Office of Metrology (OFMET). First results are reported in a separate communication of these proceedings [7].

The Center for Orbit Determination in Europe (CODE), an IGS analysis center located at the AIUB, has been routinely determining precise satellite and receiver clocks in the IGS network. Since July 1998 a dedicated time and frequency comparison subnet is processed separately. It contains sites of the IGS net, as well as a series of stations of dedicated campaigns (e.g. the USNO-PTB campaign). Figure (4) indicates the locations of the stations of this subnet. The processing scheme is arranged in a way that only station clock parameters are estimated while using CODE final IGS products for all remaining parameters. The results are accessible on

the CODE anonymous FTP, and shall soon be available as official products in the framework of the IGS/BIPM Pilot Project.

Figure (5) shows Allan deviations for a set of clocks in the mentioned subnet. The maser at PTB was (arbitrarily) chosen as a reference. The results clearly demonstrate that a frequency comparison at the 10^{-14} level on global baselines is achievable after a few hours. On the other hand the slopes of the Allan deviations show that the frequency transfer process is not dominated by pure phase noise (the slopes are roughly -0.5 instead of -1.0). This may indicate correlations between the clock estimates and other parameters like tropospheric delays. Although the slopes for very short baselines are close to -1 (see Figure 2), there is no obvious dependency from the baseline length on long baselines. Further investigations are necessary to identify the potential correlations, and to improve the models.

CONCLUSIONS

A dedicated time and frequency comparison subnet is processed at the IGS CODE analysis center. Carrier phase and pseudorange observations are processed with geodetic techniques using the precise orbit and position information from the IGS. Frequency comparisons of H-masers on global baselines at the level of 10^{-14} over a few hours are routinely achieved.

For time transfer two terminals were developed, and their internal delay variations carefully analyzed. Since July 1998 these terminals are continuously operating on a transatlantic baseline between USNO, Washington, and the PTB in Germany. The comparison with TWSTFT is very promising.

REFERENCES

[1] N. Ashby, and M. Weiss 1980, *"Accurate Time Transfer Using Common-view of a GPS Satellite,"* **Proceedings of the 34th Annual Symposium on Frequency Control,** 28-30 May 1980, Philadelphia, Pennsylvania, pp. 334-346.

[2] IGS Report, 1997, in press.

[3] T. Schildknecht, G. Beutler, W. Gurtner, and M. Rothacher 1990, *" Towards Sub-nanosecond GPS Time Transfer Using Geodectic Processing Technique,"* **Proceedings of the 4th European Frequency and Time Forum,** pp. 335-346.

[4] K. M. Larson, and J. Levine 1998, *"Carrier-phase Time Transfer"*, **IEEE Transactions on Ultrasonics, Ferroelectrics, and Frequency Control,** submitted.

[5] D. C. Jefferson, S. M. Lichten, and L. E. Young 1996, *"A Test of Precision GPS Clock Synchronization,* **Proceedings of the 1996 IEEE International Frequency Control Symposium,** 5-7 June 1996, Honolulu, Hawaii, pp. 1206-1210.

[6] J. Ray and C. Thomas 1999, *" The IGS/BIPM Pilot Project to Study Accurate Time and Frequency Comparisons using GPS Phase and Code Measurements"*, these Proceedings.

[7] G. Dudle, F. Overney, L. Prost, T. Schildknecht, and T. Springer 1999, *" First Results on a Transatlantic Time and Frequency Transfer by GPS Carrier Phase,"* these Proceedings.

[8] F. Overney, L. Prost, U. Feller, T. Schildknecht, and G. Beutler 1997, *"GPS Time Transfer using Geodetic Receivers: Middle Term Stability and Temperature Dependence of the Signal Delays,"* **Proceedings of the 11th European Frequency and Time Forum,** 4-7 March 1997, pp. 504-508.

[9] G. Petit, C. Thomas, Z. Jiang, P. Uhrich, and F. Taris 1998, *"Use of GPS Ashtech Z12T Receivers for accurate Time and Frequency Comparisons,"* **Proceedings of the 1998 IEEE International Frequency Control Symposium,** 27-29 May 1998, Pasadena, California, in press.
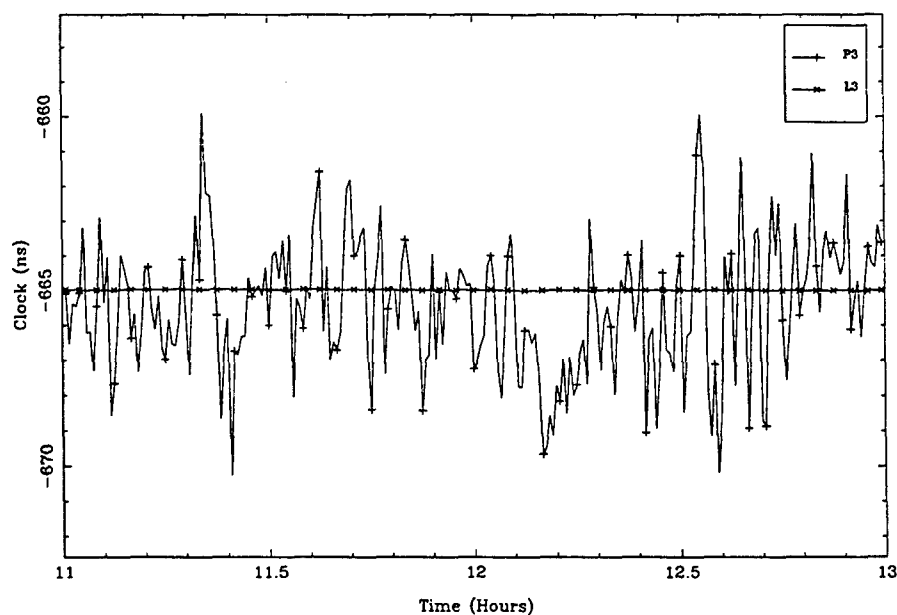
Figure 1: Comparison between 2 hydrogen masers at USNO, as estimated from P-code (P3) and carrier phase (L3) measurements.
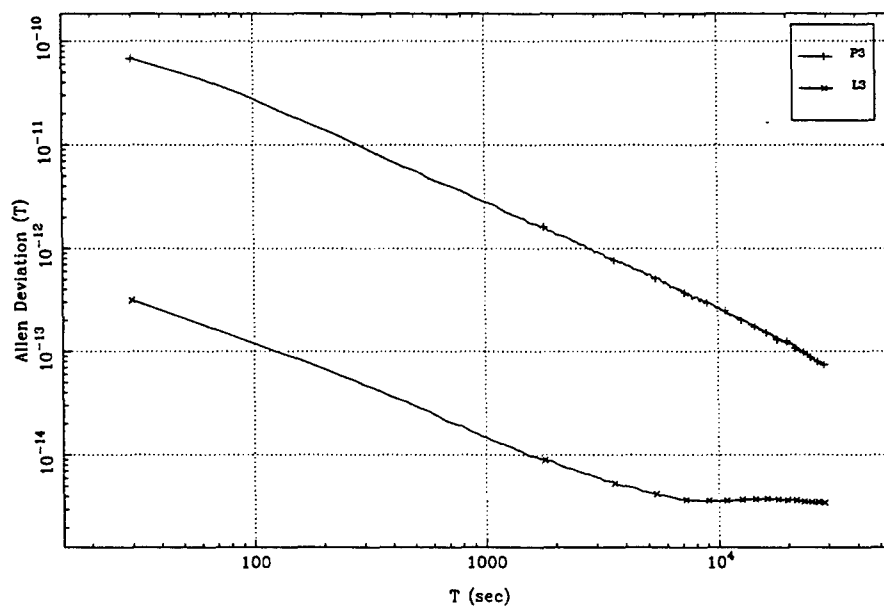
Figure 2: Allan deviation for the data given in Figure (1) using 24 hrs of data. Both Figures (1) and (2) reflect the difference in the intrinsic precision of the two observables.
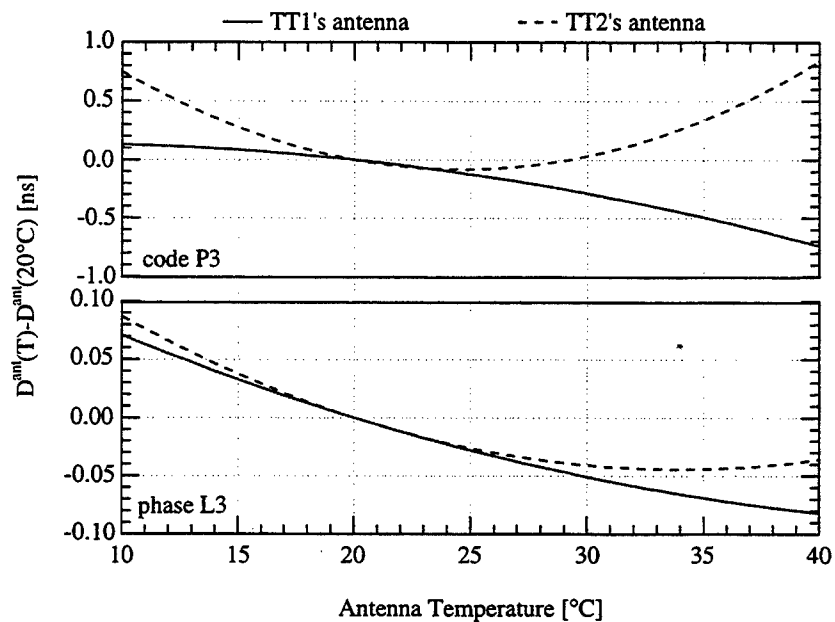
Figure 3: Measured temperature dependency of two antennas of the same type (Dorne Margolin) for code (P3) and phase (L3) observations.
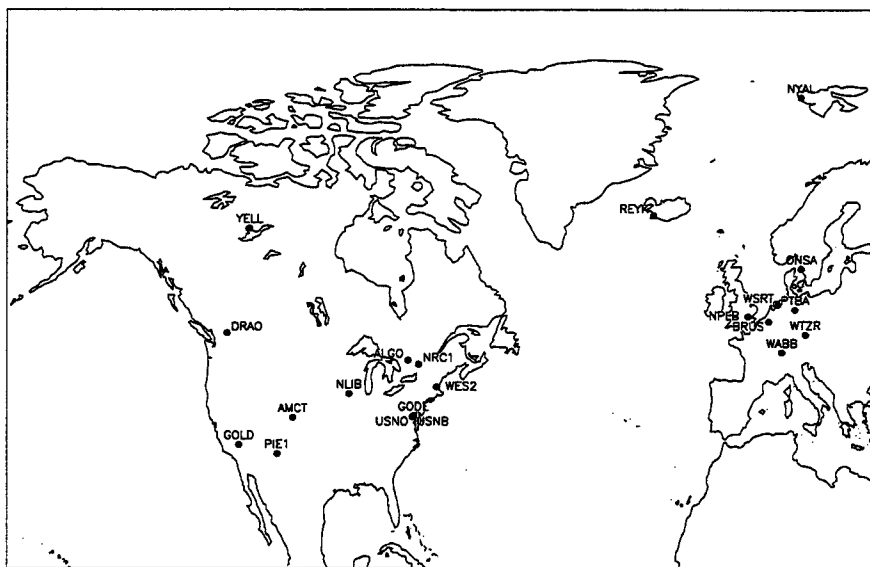
Figure 4: Locations of stations used in the time and frequency comparison subnet since July 1998, comprising IGS sites and stations from dedicated campaigns.
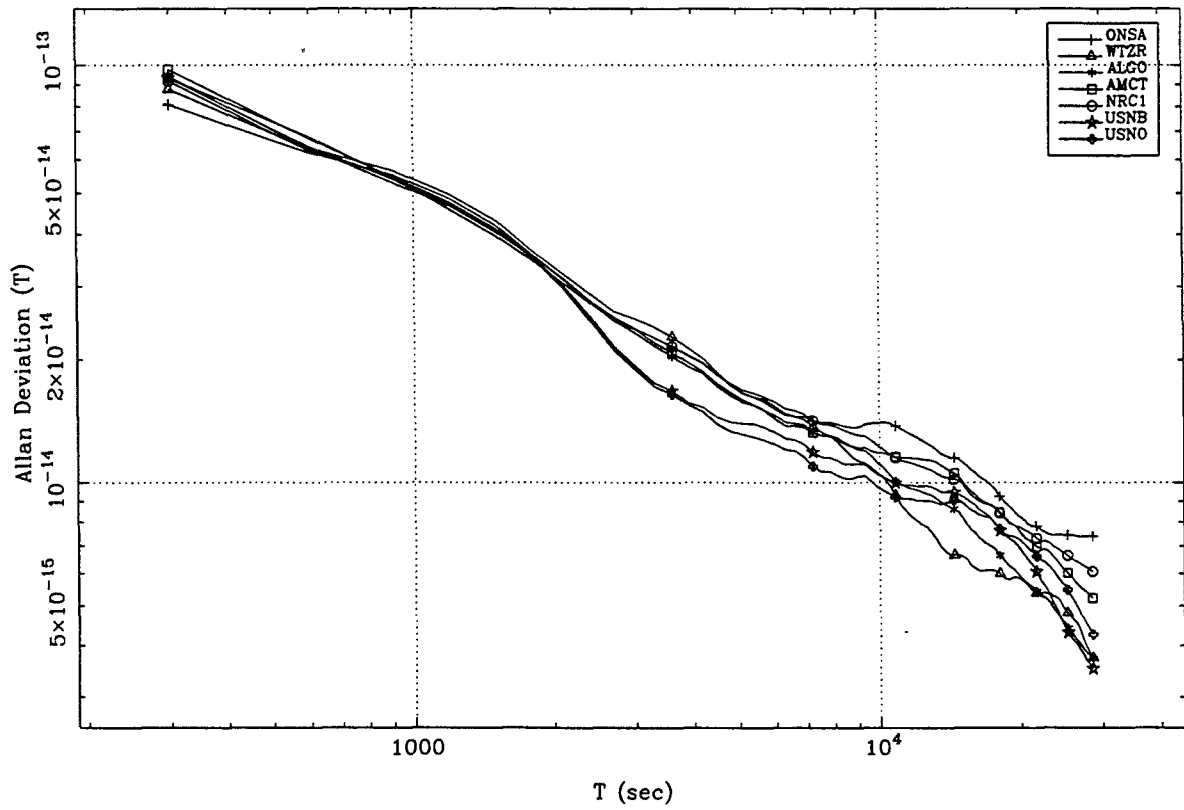
Figure 5: Allan deviations for a set of clocks in the mentioned subnet. The maser at PTB was (arbitrarily) chosen as a reference.

Questions and Answers

GERARD PETIT (BIPM): I have one comment. You looked pessimistic when you plotted limitation on the Allan Deviation plot. If you used the Modified Allan Deviation it would look much lower.

THOMAS SCHILDKNECHT (University of Bern): That is true, yes.

GERARD PETIT: You should really use a Modified Allan Deviation so that it looks like you have a much larger margin relative to the instrumental measurements.

THOMAS SCHILDKNECHT: You are referring to that one or to the last one? You mean this one?

GERARD PETIT: Yes. Actually, if you plot it in the Modified Allan Deviation you have a much larger margin.

THOMAS SCHILDKNECHT: Yes, that is true. I agree. We should have plotted that in Modified Allan Deviation.

DIETER KIRCHNER (TUG): I think it would only look better in the Modified Allan Deviation plot if you have white PM. It seems not to be a white PM. It slopes a bit. Maybe you would not gain too much.

THOMAS SCHILDKNECHT: It is not really a slope of minus 1 in this diagram, I agree. But, it is close to minus 1. There is a big difference between this 750 kilometer baseline; it is not minus one, but also it is not minus a half. On the long baseline, it is minus a half. So, that is something we have to look into. There is certainly a correlation between the clock errors we estimate on the long baselines and other parameters in the processing link to troposphere modeling and other ones; we know that. We have to do our homework to look at these correlations.

Until now, nobody within the geodetic community was interested in looking at these correlations because they just wanted to get rid of the clocks, and get rid of the troposphere because they were interested in the geometry.

MARC WEISS (NIST): If the code lock moves because of delay changes over long periods of time, say days, weeks, or months, will that pull the carrier phase transfer as well?

THOMAS SCHILDKNECHT: Yes, it will. Because, if we have, let us say, a power failure or a complete reset on one of the receivers, we have to reinitialize the ambiguities; so we can not just connect everything at the phase level. This reinitialization of the phase ambiguity – I mean, for that, we definitely need the code. If the code is wrong or has a jump, or whatever, an offset, it will fully go into the time or clock error estimates.

MARC WEISS: For generating TAI, the thing that really matters is the five-day measurements and longer.

THOMAS SCHILDKNECHT: Yes.

MARC WEISS: So, if it is no better than the code in the long term, is there an advantage?

THOMAS SCHILDKNECHT: It is really crucial that there are no ambiguities in this tie of the internal clock to the external one. I mean, you are probably referring to these jumps or ambiguities in the one PPS output, for example. I mean, this is crucial that we can really be sure that at the 50-picosecond level or whatever we want, this delay is stable, even after receiver resets.

HARDWARE DELAY MEASUREMENTS AND SENSITIVITES IN CARRIER PHASE TIME TRANSFER

Edward Powers, Paul Wheeler, David Judge, Demetrios Matsakis

U.S. Naval Observatory

Washington, D.C.

Abstract

Precise time and frequency transfer experiments using GPS carrier phase with time stability less than one hundred picoseconds are now being reported. Strong daily variations in some of the data reported indicate temperature sensitivity in the measurement hardware. The environmental dependence of the instrumental delays of a commonly used carrier phase GPS receiver, its antenna, and several types of antenna cable are reported in this paper.

INTRODUCTION

Carrier phase GPS time and frequency transfer experiments are now showing the potential for 100 picosecond time transfer [1, 2] and frequency transfer to 1E-15 for one-day integration time. To gain a better understanding of the error contributions of the GPS measurement hardware, we performed a series of experiments to determine their stability over a range of temperatures and through receiver resets and power cycles. Zero-baseline stability analysis of the receiving hardware will also be discussed in this paper, as briefly will absolute calibration issues and plans for future testing.

GPS ANTENNA AND ASSOCIATED ELECTRONICS

GPS antennas were not studied, but we note that many geodetic antennas are based on a Dorne & Margolin DM C146 broadband antenna. This antenna has a bandwidth of 425 MHz (1200 MHz – 1625 MHz) with a characteristic impedance of 50 ohms and a VSWR rating of 1.5:1. The wide bandwidth implies that the delay through the antenna is small (< 500 ps), and thus any change in delay due to temperature would also be small. In contrast, the electronics package within and immediately after the GPS antenna contain 20-MHz-wide filters so as to remove unwanted near-band interfering signals, and their delay is around 25 to 50 ns.

For this experiment we tested the antenna electronics of an Allen Osborne Associates (AOA) choke ring antenna, which is widely used in the geodetic community. We separated the antenna from its associated electronics and used a network analyzer to measure the delay through the electronics portion at both 1575.42 MHz (L1) and 1226.6 MHz (L2). We found a delay variation of tens of nanoseconds (ns) across the 20 MHz wide P-code bandwidth. The net delay at both L1 and L2 frequencies was measured to be approximately 30 ns +/- 5 ns. Because the entire GPS C/A and P-code spectrum must pass through these non-symmetrical filters, it may be incorrect to assume the net delays through these filters are the same as measured at precisely the L1 and L2 center frequencies. This effect should cause a smaller bias for the C/A code delay, because it occupies a smaller bandwidth over which the filter response is flatter.

We heated the antenna electronics assembly and observed a variation in the delay on the order of 4 to 16 ps/°C and also noted a slight change in the center frequency of the filter response. The test data also indicate that an L1, L2 bias may exist in this set of electronics, which will cause the receiver's ionosphere corrections estimates to be biased. Since the L1 and L2 filters may respond differently to temperature changes, this ionosphere bias may change slightly with temperature.

Additional experiments were also performed using an older AOA antenna electronics design that contained only a wide-band 600 MHz low noise amplifier with no filters. The variation in delay across the GPS L1 and L2 spectrum was only a few ns and the change in delay due to temperature was small. No measurable L1, L2 bias was observed.

GPS ANTENNA CABLE

As reported in [3, 4], the net changes in electrical delay due to temperature fluctuations in the GPS antenna cable can have a significant impact on the time and frequency transfer performance when using carrier phase to compare remote clocks. Measurements made the Astronomical Institute, University of Berne and the Swiss Federal Office of Metrology[4] of RG-213/U and RG-58 type cable showed a net electrical delay variation of about –0.42 ps/C/m between temperatures of –20 °C to +40 C. At higher temperatures (+40 C to +70 C) the electrical delay changed by an even greater amount, –1.38 ps/C/m. For a GPS receiver installation with 200 feet (60 meters) of exposed antenna cable, this error could amount to as much as 1 ns over the course of a 15 °C diurnal cycle, and seasonal fluctuations of several ns could be expected.

Several cable types typically used as GPS antenna cables were studied. Thirty-meter lengths of RG-214/U, RG-217, RG-8A, and Andrew's FSJ1-50A cables were placed in a thermal chamber and their delay characteristics were measured over a range of temperatures. The thermal chamber was stepped in temperature by 20 °C from 5 °C to 45 °C and then back to 5 °C. Delay measurements were made using a network analyzer around both of the GPS frequencies of 1575 MHz and 1226 MHz, by sending a 1 PPS signal through the cables to a SRS620 time-interval counter and with a time-domain reflectometer. Close agreement between the time–interval counter 1 PPS measurements and the network analyzer measurements were obtained. As can be seen in Figures 1 and again summarized in Table 1, the Andrews FSJ1-50A phase stable HELIAX™ cables proved to be 15 to 30 times more thermally stable than the cables previously used at USNO. The FSJ1-50A cable is low loss and much lighter than solid dielectric cables. The main disadvantage of the FSJ1-50A cable is that it is more rigid and somewhat more fragile than standard coax cables.

GPS Antenna Cable Delay vs. Temperature
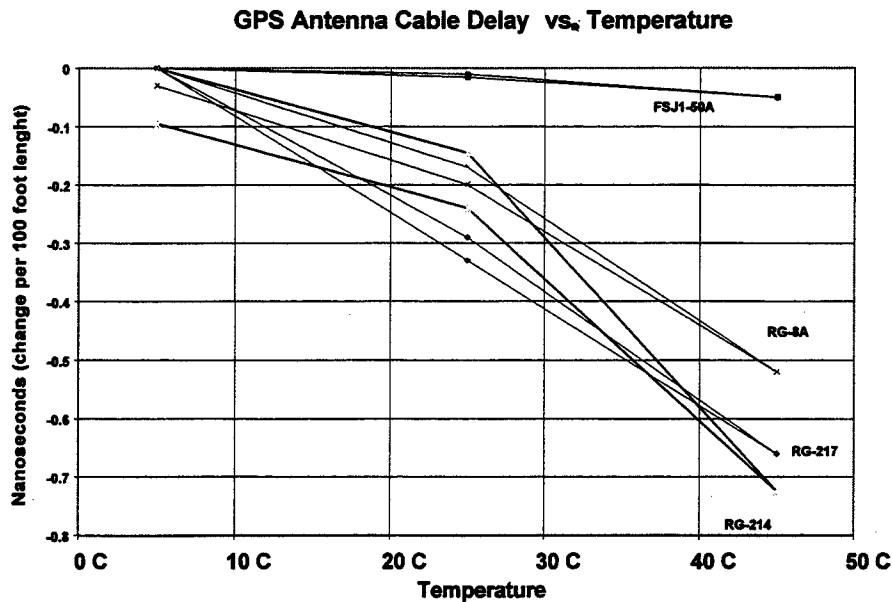
Figure 1 GPS Antenna Cable Delay versus Temperature

Table 1. GPS Antenna Cable Measured Properties

Cable Type	RG-217	FSJ1-50A	RG-214	RG-8A
Loss at L1/100 ft.	7.5 dB	7.5 dB	14 dB	11 dB
Loss at L2/100 ft.	6.5 dB	6.75 dB	12 dB	9 dB
Temp Coefficient	0.54 ps/C/m	0.03 ps/C/m	0.54 ps/C/m	0.45 ps/C/m
Velocity Factor	0.66	0.84	0.66	0.66

The low-loss foam dielectric used in Andrew's HELIAX™ cable has a dielectric constant that decreases with increasing temperature [5]. This causes an increase in the velocity of propagation within cable, which results in a decrease in electrical delay. For the Andrew's HELIAX™ cables the delay change due to thermal expansion and the change in dielectric constant are very similar in magnitude but of opposite signs, which allow these two effects to tend to cancel. In contrast, a typical solid dielectric cable experiences a greater delay change from dielectric constant variation than from the physical length change. Delay hysteresis is another problem that plagues most cable types. When solid or foam dielectric cables are subjected to thermal changes, their physical length and dielectric constant will change, and when the cable is returned to its original temperature the cable may not return to its original electrical length. Andrew uses a temperature cycling process to reduce the hysteresis effect.

GPS RECEIVER STABILITY

The temperature stability of two 12-channel AOA TurboRogue™ GPS receivers was measured in a zero-baseline experiment, during which two GPS receivers were operated from the same GPS antenna and shared a common clock. When data from the two receivers are differenced, the only error contribution that remains is from the GPS receiver.
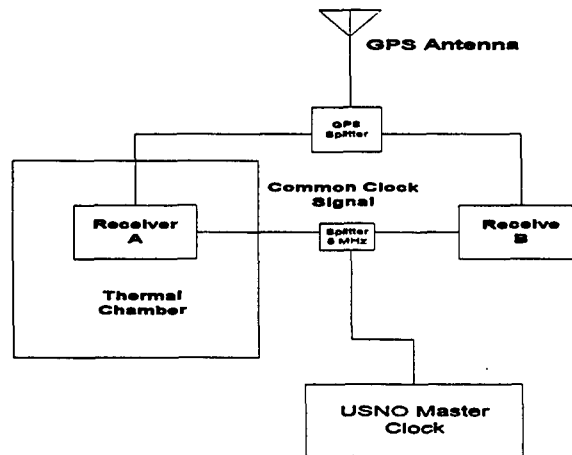
Figure 2 Zero-Baseline Experiment

As shown in Figure 2, one receiver was placed in a thermal chamber and subjected to temperature steps of 5 °C over a range from 20 to 35 °C. The second receiver was held at room temperature, which through most of the experiment was constant to about 1 °C. Later the experiment was repeated after exchanging the two receivers. The measurements were terminated prematurely when one of the receivers was needed operationally. The L1 CA code and L1 and L2 carrier measurements from each of the receivers were differenced and analyzed. We found that the code measurements tended to be approximately ten times more sensitive to the temperature than the carrier phase measurements. Tables 2 and 3 show the results of typical measurements for both GPS receivers, and Figure 3 shows the L1 carrier phase measurements.

Table 2 TurboRogue Temperature Sensitivity Receiver 245 (Uncertainty)

Receiver 245 Temperature	L1 CA Code	L1 Carrier Phase	L2 Carrier Phase	PPS Time Output
20 °C	0 ps (100 ps)	0 ps (50 ps)	0 ps (50 ps)	0 ps (50 ps)
25 °C	450 ps (100 ps)	25 ps (50 ps)	45 ps (50 ps)	250 ps (50 ps)
30 °C	1250 ps (100 ps)	115 ps (50 ps)	165 ps (50 ps)	540 ps (50 ps)
35 °C	1800 ps (100 ps)	200 ps (50 ps)	275 ps (50 ps)	900 ps

Table 3 TurboRogue Temperature Sensitivity Receiver 202 (Uncertainty)

Receiver 202 Temperature	L1 CA Code	L1 Carrier Phase	L2 Carrier Phase	PPS Time Output
20 °C	0 ps (100 ps)	0 ps (50 ps)	0 ps (50 ps)	0 ps (50 ps)
25 °C	200 ps (100 ps)	- 30 ps (50 ps)	- 40 ps (50 ps)	190 ps (50 ps)
30 °C	1200 ps (100 ps)	20 ps (50 ps)	25 ps (50 ps)	500 ps (50 ps)
35 °C	1700 ps (100 ps)	70 ps (50 ps)	120 ps (50 ps)	725 ps (50 ps)

At temperatures between (20 – 25) °C , receiver 202 exhibited the smallest thermal sensitivity with relative L1/L2 carrier phase measurement delays changing inversely to the code measurements, but

receiver 245's code and carrier phase measurements tended to change delays proportionally. It is not yet understood why the GPS code measurements tended to be ten times more sensitive to thermal changes than the carrier phase measurements.

GPS RECEIVER TEMPERATURE TEST
L1 CARRIER PHASE MEASUREMENT
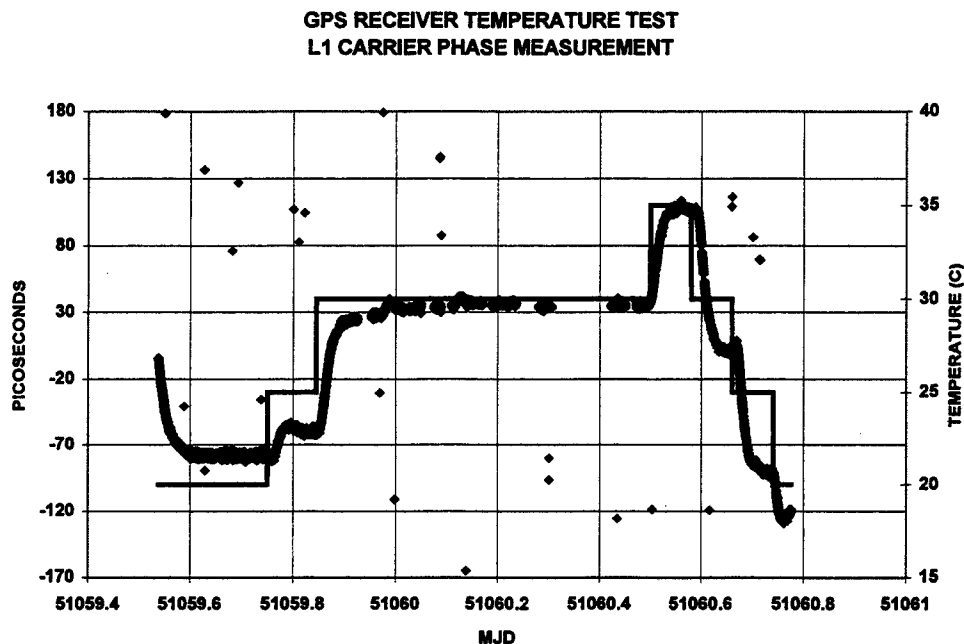
Figure 3 Zero-Baseline L1 Carrier Phase Temperature Testing

USING AN EXTERNAL CLOCK WITH THE TURBOROGUE™

In this section we will discuss the errors associated with locking the TurboRogue™ internal clock to an external frequency and time standard and how to correct for some of the errors that occur during this process.

All of the receiver's internal measurements are referenced to a common internal clock running at 20.456 MHz. This internal clock is phase-locked to an external 5 MHz frequency standard by dividing the external 5 MHz frequency reference (N) and the internal 20.456 MHz clock (M) down to common sub-multiples in the range of a few tens of kilohertz. These two sub-multiple frequencies are mixed and the resulting error signal is used to phase-lock the internal 20.456 MHz clock to the external frequency reference. The two N/M divider circuits used in the receiver's frequency synthesis chain are not synchronous. A receiver power cycle will reset this divider chain and the phase relationship between the internal frequency reference and the external frequency reference will be lost. This relationship is preserved in the event of software resets. Figure 4 shows a block diagram of the receiver's frequency synthesis chain and time base. The receiver outputs a one-pulse-per-second (1PPS) time output that is

297

divided down from the internal 20.456 MHz frequency reference. This 1 PPS is approximately synchronized to GPS time during the receiver's initial startup and is used internally by the receiver as a time mark for its GPS measurements. The jitter on this receiver's 1PPS is typically 125 ps, with one standard deviation being 45 picoseconds per 10 seconds average. As shown earlier in Tables 4 and 5, the 1 PPS output is sensitive to temperature changes at the level of 50 ps/C.

A TurboRogue™ can be used as a time transfer receiver if the 1PPS output from the receiver is measured against the local time reference. The internal receiver measurement of a GPS space vehicle's (SV) clock offset is referenced to the internal receiver's clock which is internally referenced to the receiver 1PPS, so the internal receiver clock can be subtracted out by subtracting the GPS SV clock offset measurements from the external time interval measurements (see Equations 1-3 below).
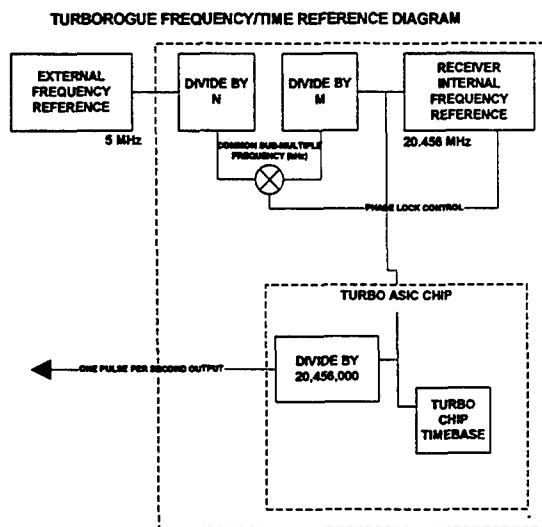
Figure 4 Block Diagram of TurboRogue™ Timing Architecture

A = GPS SV clock offset + Receiver calibration bias − Receiver clock offset   (1)

B = User Local clock − Receiver clock offset   (2)

A − B = GPS SV clock offset + calibration bias − User Local clock offset   (3)

This ability to subtract out the receiver internal clock allows the user to correct for jumps or resets in the internal receiver time base caused by either a power cycle or software reset.

Using the zero-baseline experimental setup described above, we periodically reset and power-cycled one of the two receivers used in the experiment. We found that the 1 PPS difference between these two receivers equaled the CA code measurement jumps to within a 200 ps measurement uncertainty (see Table 4).

Table 4 Results from Six Power Cycle Experiments

	CA Code Difference (NS)	One PPS Difference (NS)	Re-Calibration Difference (NS)
Power Cycle #1	-317.3	-317.5	0.2
Power Cycle #2	163.1	163.07	0.03
Power Cycle #3	-147.8	-147.6	-0.2
Power Cycle #4	-62.5	-62.62	0.12
Power Cycle #5	9.7	9.53	0.17
Power Cycle #6	-155.4	-155.54	0.14

We have also found that, after a receiver software reset and subsequent time re-synchronization the bias in the code range measurement will change by multiplies of 24.4427 ns. This 24.4427 ns step size is one half the period of the receiver internal frequency reference (20.456 MHz). Substituting the closest multiple of this step seems to work in all cases except for power interruptions.

Working with Allen Osborne Associates, we developed a modified frequency synthesis chain has been developed that will accept an external 1PPS timing signal from the local clock to force the synthesis chain to return to its previous state after a power interruption. This could allow a TurboRogue™ receiver to be used as a timing receiver without the use of an external time-interval counter, but further investigation is needed. The additional data processing techniques that will be needed to resolve this 24.4427-ns ambiguity should be simple to develop if the external time reference is stable.

Table 5 Receiver Reset Correction Values for USNO(AMC) to USNO(DC)

MJD	GPS – Clock (ns)	Type of Reset	Number of 24.443 (ns) Cycles	Cycle Error (ns)	1 PPS – Clock (ns)	1 PPS Error (ns)
51020.0	782.35	Soft	32.008	0.17	782.23	0.1
51042.0	-1173.0	Soft	47.99	0.24	-1173.35	0.35
51047.6	1026.75	Soft	42.006	0.15	1026.39	0.36
51052.6	195.5	Soft	7.998	0.05	195.45	0.05
51061.6	-195.35	Soft	7.992	0.2	-195.63	0.28
51065.9	162.45	Power	6.646	8.65	161.98	0.47
51066.5	179.3	Power	7.336	8.06	179.67	-.375
51070.6	-31	Power	1.268	6.35	-30.47	-.53
51082.6	-97.3	Soft	3.981	0.45	-97.63	0.33

USNO operates two IGS reference stations, one at USNO Washington DC (IGS designation: USNO) and the other at the USNO Alternate Master Clock at the GPS Master Control Station in Colorado Springs (IGS designation: AMCT or AMC2). USNO also continuously measures each station's TurboRogue™ receiver's 1PPS error signals relative to the Master Clock at both locations. Using reduced data publicly available by the CODE [7], we have examined a series of nine resets of AMCT receiver and found that

the internal clock error after resets can be corrected to within the measurement noise of a few hundred picoseconds. Most of this uncertainty can be attributed to data processing errors in the geodetic software used. Table 5 shows the size of these nine jumps, the cause of each jump, and information on measured correction factors.

STABILITY OF CODE AND CARRIER PHASE MEASUREMENTS

The relative stabilizes of two TurboRogue™ receivers are analyzed in this section. Figure 5 shows zero-baseline L1 CA code difference measurements from two receivers measuring PRN 26 from horizon to horizon. At low elevation angles the differential measurement noise approaches 1 ns, and at elevation angles above 25 degrees the noise drops to only a few hundred picoseconds. This is due to the much higher signal strength received at higher elevations due in large part to the antenna gain pattern. Zero-baseline L1-code measurements were typically 100 times noisier than the L1-carrier phase measurements. The L2 code-less carrier phase measurements were about five times noisier than the L1 carrier phase measurements. Figure 6 shows the relative frequency stability of these three observables.

FUTURE PLANS

Additional and more thorough testing is planned to better understand the delays in the antenna electronics and to design new antenna electronics. Further studies of the receiver's sensitivity to changes in RF power level, temperature changes, use of different antenna electronics and filters, power supply fluctuations, and multi-path are planned.

We also plan to investigate a more direct approach to eliminating many of the GPS receivers' sensitivities by use of a calibrated signal generator. Our approach would be to design an elementary L1 and L2 CA/P code signal generator (calibrator) that could work cooperatively with the GPS receiver. This calibrator would be clocked from the user's time reference in a well-controlled and calibrated manner. The signal from this calibrator would be injected directly after the first stage low noise amplifier but before any filters. This injection point would be calibrated such that the code transitions have known offsets from the local time reference [6]. The L1 and L2 carrier phases would be generated so that coherence would be preserved on restart after power cycles or through other hardware resets.

The GPS receiver firmware would need to be modified so that the receiver can track this calibration pseudolite signal. With the advent of WAAS and other pseudolite-based systems, these modifications may already be in the works. A PRN sequence would be chosen that is compatible with existing pseudolite signal structures. It would be important to try to replicate the present GPS signal structure shape so that the receiver's tracking loops would not be biased. The calibrator signal would be tracked continuously on one of the receiver's unused channels or the receiver could sequence through each channel to calibrate any receiver inter-channel and L1, L2 biases.

The main advantage to this approach is that the calibrator signal would travel through the same path as the normal GPS measurements, and any delay fluctuations due to thermal changes would cancel. The normal GPS receiver measurement would be referenced to the receiver clock, as will the calibrator measurements. Each of the GPS measurements would be subtracted from the calibrator measurements, thus re-referencing the measurements to the local time reference with zero calibration delay.

During the initial proof of concept stage we plan to use a STel Model 7200 calibrator as our signal generator. This signal generator is capable of transmitting a zero Doppler L1/L2 C/A and P-code signal that can be calibrated to 1 ns [7].

CONCLUSIONS

Carrier phase measurements have been shown to be very stable and useful for frequency comparisons, but questions still remain as to the absolute calibration of the carrier phase measurement and how accurately it can be related to the user clock.

To approach 100 picosecond long-term stability in a carrier phase time/frequency transfer system, minimizing the thermal sensitivities in the GPS receiver and associated hardware is required. Use of phase-stable antenna cable will be needed if more than a few meters are exposed to the extremes of outdoor temperature changes. Either thermally controlled antenna enclosures or antenna electronics designed to be thermally stable over wide temperature range will be needed. Thermally controlled enclosures, like those used for the Geodetic Time Transfer Terminal (GeTT) [4], will also be required for the GPS receiver.

Receivers like the TurboRogue™ and the Ashtech Z12-T have been shown to be capable of making very stable GPS code and carrier phase measurement with stability better than 100 picoseconds. Great care must be taken in relating the internal receiver clock to the external frequency reference. For the TurboRogue™, a time-interval counter can be used to relate the receiver's internal clock to an external frequency/time standard. Modifications to the TurboRogue™ frequency synthesis design have been made to simplify relating the internal clock to an external reference.
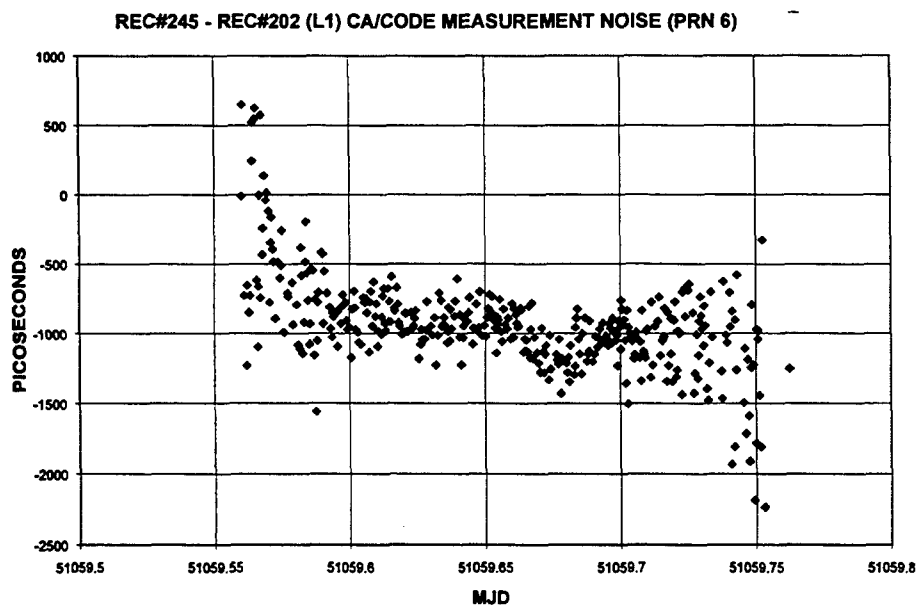
Figure 5 Zero-Baseline L1 CA-Code Measurement for a Complete Satellite Track
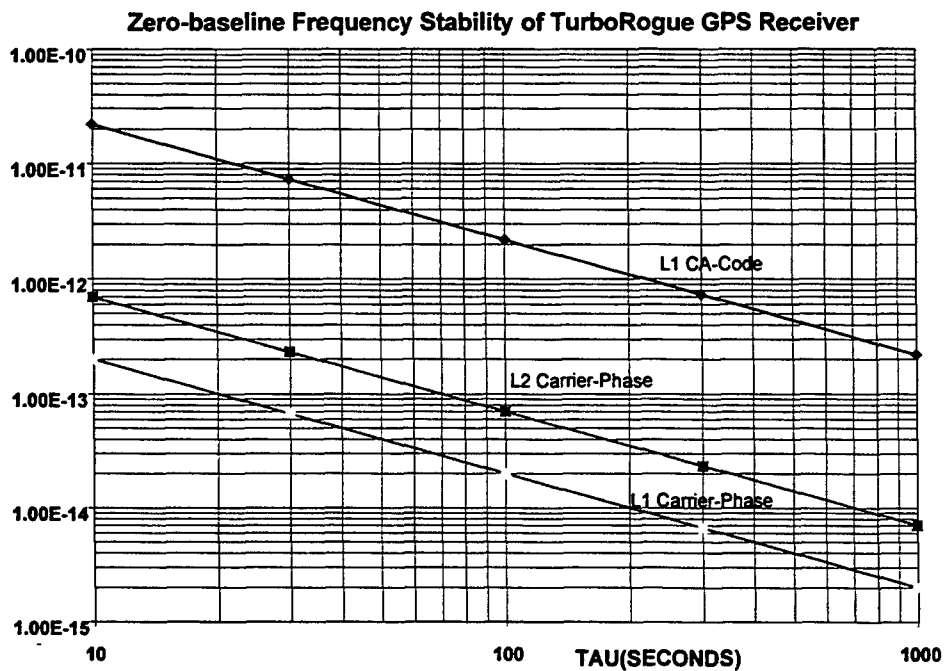
Figure 6 Stability of Receiver Measurement Noise

ACKNOWLEDGMENTS

REFERENCES

[1] K. M. Larson and J. Levine, 1998, *"Time Transfer Using GPS Carrier Phase Methods,"* Proceedings 29th Annual Precise Time and Time Interval (PTTI) Systems and Applications Meeting, 2-4 December 1997, Long Beach, California, USA, pp. 221-228

[2] G. Petit and C. Thomas, 1996, *"GPS Frequency Transfer Using Carrier Phase Measurements,"* IEEE International Frequency Control Symposium, 5-7 June 1996, Honolulu, Hawaii, pp. 1151-1158

[3] K. Larson, L. Nelson, J. Levine, and T. Parker, 1999 *"A Long-Term Comparison Between GPS Carrier-Phase and TWSTT,"* these Proceedings

[4] F. Overney, Th. Schildknecht, G. Beutler, L. Prost, and U. Feller, 1997, *"GPS Time Transfer Using Geodetic Receivers: Middle-Term Stability And Temperature Dependence Of The Signal Delays,"* Proceedings 11th European Frequency and Time Forum, 4-7 March 1997, Neuchâtel, Switzerland

[5] Andrew Inc., technical information retrieved from commercial Website,
http://www.andrew.com/products/heliax/catalog37.asp

[6] E.D. Powers, M. Miranian, J.D. White, and J. Brad 1998, *"Absolute Time Error Calibration Of GPS Receivers Using Advanced GPS Simulators,"* Proceedings 29th Annual Precise Time and Time Interval (PTTI) Systems and Applications Meeting, 2-4 December, Long Beach, California, USA, pp. 193-198

[7] G. Duddle, F. Overney, L. Prost, Th. Schildknecht, T. Springer, P. Hetzel, and E. Powers 1999, *"First Results on a Transatlantic Time and Frequency Transfer by GPS Carrier Phase,"* these Proceedings

Questions and Answers

JIM DeYOUNG (USNO): Ed, in the temperature plots that you were showing, the square waves – was that actually just showing the impulse time of the temperature change?

ED POWERS (USNO): It is just the impulse time. They actually look pretty close to a square wave. The response time in the chamber was pretty fast. You could see the slope, though, it did have a little corner. For simplicity's sake I just rounded it off.

JIM DeYOUNG: So, was there any evidence from the time of the impulse – in other words, was there a lag time in the reaction?

ED POWERS: Yes, I did see some in the first receiver I tested. If you shocked the receiver too hard, you might actually get a little impulse and a little overshoot.

THOMAS SCHILDNECHT (University of Berne): Am I correct that one of your conclusions is that the one PPS output of the TurboRogues can be used down to a level of 100 picoseconds to reconstruct the offsets during the power cycles resets?

ED POWERS: It does appear that way. I did not mention this, I meant to, but Demetrios has done some analysis of the data that you provided him, where he was able to correct them down to below the nanosecond level. I think the NIST group had similar results where they were able to eliminate the jumps below the nanosecond level. But the zero-baseline test allows me to do it without any noise, so it is much clearer to see.

THOMAS SCHILDKNECHT: Yes, because it is really the crucial point in the whole line. To be sure that this one PPS output is really traceable to the internal clock.

ED POWERS: When I say 100 picoseconds, that is in a controlled environment. You can see that the differential temperature coefficient between the one PPS and the code are going to give you maybe a 50-picosecond per degree Celsius sensitivity right there. So, if you are going to just run an open laboratory that goes up three or four degrees Celsius, you are not going to do it. If you change your temperature more than that amount, you certainly will not do it. So, stabilizing the hardware may be critical, like you have already found.

DEMETRIOS MATSAKIS (USNO): I know that these comments are going to appear at the end of the Proceedings. We want to put in our paper a table of the jumps that we have seen with co-data and just how well the PPS took it out. I would like to pass this discussion to Judah, who is analyzing some of data from the TurboRogues. Try to put that in your printed version too.

JUDAH LEVINE (NIST): All of our jump data is your data.

DEMETRIOS MATSAKIS: It is processed through GIPSY, so there is a processing noise in there.

JUDAH LEVINE: I understand. But the one PPS jump stuff is on your Web site.

ED POWERS: I think what Demetrios is looking for is just the plot or the difference between the jump-corrected data and the fit-corrected data.

SIGFRIDO LESCHIUTTA (IEN): I would like not to raise a question, but to make a couple of very general remarks concerning the very interesting sessions we had this afternoon. I think that we who work in the time and frequency community should congratulate the PTTI Executive Committee for offering us very interesting sessions in which 12 papers of this new technology was opened to some extent. That also brings to mind similar sessions we had in the past years concerning Loran-C and the first use of GPS codes.

I would like to make two statements, and the second one is just a matter of wording. Inside scientific unions, such as the International Union of Radio Science, the International Astronomical Union and similar bodies such as CCIR by tradition, for the word "time comparison" is meant as a comparison between two clocks. These are the reading of the clocks or clock against the time scale. So, I think we should be a bit cautious in speaking of a frequency comparison, phase comparison and, finally, time comparisons.

FREQUENCY TRANSFER USING GPS: A COMPARATIVE STUDY OF CODE AND CARRIER PHASE ANALYSIS RESULTS

C. Bruyninx, P. Defraigne, J.-M. Sleewaegen, and P. Pâquet
Royal Observatory of Belgium
Avenue Circulaire 3, B-1180 Brussels, Belgium

Abstract

This paper investigates the use of GPS codes and carrier phases for frequency transfer applications. Three types of baselines have been studied. First, the noise of the code and phase methods has been evaluated using a zero-baseline with two geodetic GPS receivers driven by the same H-Maser clock, or by a cesium and an H-Maser clock respectively. From the common frequency reference we were able to derive a frequency stability of 6.10^{-16} for averaging times of one day.
The different response of the hardware of the two receivers to small identical temperature variations is emphasized; the differential effect is about 30 ps/°C. The difference between the L_1 and L_2 carrier phase delays is shown too.

Secondly, on-site tests over a 95-m baseline allowed checking the influence of combining two antennae/receivers in different environments. In this case, the effect of the varying temperature on the hardware delays of the receivers and cables is shown; this effect limits the frequency stability to 6.10^{-15} for an averaging time of one day. The possibility to obtain frequency stabilities of a few parts in 10^{16} is shown; this can be reached if all the instruments are located in temperature-stabilized rooms.

Finally, the frequency stability obtained with different code methods is compared on a longer baseline (640 km) between Brussels and Wettzell. In particular, the influence of using IGS satellite ephemerides instead of broadcast ephemerides is shown to be very small. The "all-in-view" methods based on the code, as well as on the carrier phases, are compared to the classic frequency transfer by common view. Preliminary results, using carrier phases, lead to a frequency stability of a few parts in 10^{15} for averaging times of one day. Again, the main limitations are the hardware delay variations due to the changes in ambient conditions.

INTRODUCTION

The Royal Observatory of Belgium (ROB) is one of the few Time Laboratories which is also actively involved within IGS. On one hand, the ROB time laboratory participates in the realization of TAI and on the other hand, the ROB GPS station belongs to the IGS network. Moreover, GPS analysis is done routinely within the frame of the IGS Regional Densification Pilot Project as one of the EUREF local analysis centers [1].

We have taken advantage of this rather unique collocation to study the use of multi-channel geodetic GPS receivers for time transfer applications. These receivers acquire phase and code observations from all satellites in view, and at both L_1 and L_2 frequencies. Our second goal was the evaluation of the critical aspects of the present setup of the IGS receiver BRUS, driven by a hydrogen maser, to contribute to the BIPM/IGS Pilot Project [5].

It is known that the carrier phases cannot provide an absolute time comparison between the internal clocks of the two receivers; this is due to the unknown phase ambiguity which is inherent to all phase observations. However, a combined use of the code and phase observations can provide the necessary information about the absolute time difference, with a typical precision of 50 ps for 1 day observation [2]. In this paper, we investigated only the frequency transfer results obtained using either the codes or the carrier phases. As a consequence, a constant time offset has been subtracted from the computed time differences.

We have set up a test network at the ROB to perform zero- and short-baseline analyses (see Figure 1). In a first laboratory, two receivers named BRUS (ROGUE SNR-12 RM) and BRUR (ROGUE SNR-8000) were installed. The laboratory is not perfectly air-conditioned. The 12-channel GPS receiver (BRUS) belongs to the IGS network. The two receivers are connected to the same antenna (Dome Margolin T), which allows performing the zero–baseline experiments. In a first test, both receivers use a common frequency reference from a passive H-Maser clock, and in a second test, the receiver BRUR uses the frequency provided by a cesium clock (HP5071A) rather than from the H-maser clock.

In order to perform short-baseline experiments, a third GPS receiver (ROGUE SNR-8000) is located in another laboratory, where the temperature is not controlled and varies together with the outside temperature. This receiver, called BRUE, is fed by the same H-maser clock as BRUS, and is connected to a Dome Margolin T antenna located at a distance of 95 meters from the first one.

The longer baseline experiments are performed using the GPS observations of two IGS stations: Brussels (with the receiver BRUS fed by an H-maser clock) and Wettzell (where the receiver is a ROGUE SNR-8000 also fed by an H-maser clock); the distance between the two stations is about 640 km.

In the present paper, we use this setup to investigate which environmental effects influence the signal delays within each type of analyses. The differential delay fluctuations on L_1 and L_2 signal paths, caused by temperature variations in the laboratory where the receivers are located, are also evaluated.

Note that in each case, we computed the synchronization errors between the clocks, as seen from the receivers themselves. These synchronization errors do not correspond to the difference between the external clocks only, but include also the effects of the antenna, receiver, cable, and amplifier delays. The external clocks can only be compared if the relation between the internal receiver clock and the external clock is known.
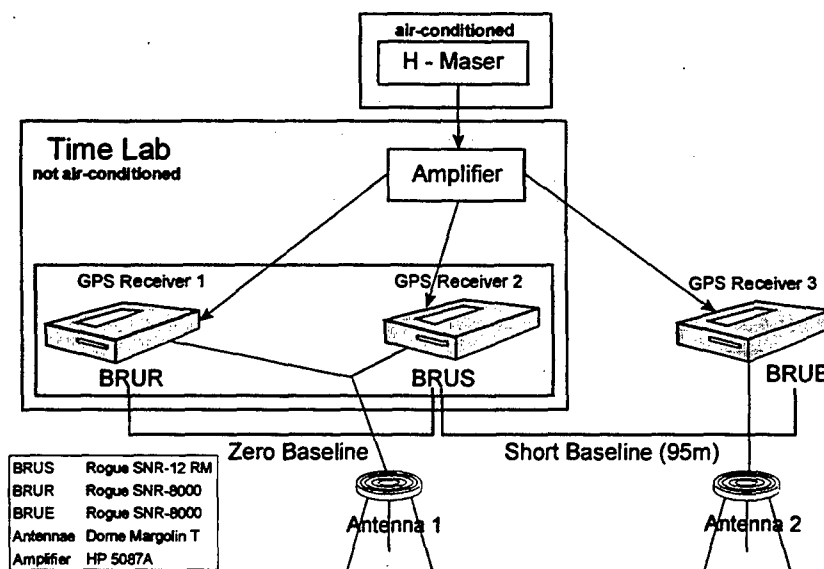
Figure 1: Set-up used for the on-site tests (zero baseline and 95-m baseline).

All computations with GPS code and carrier phase observations have been partially done with the Bernese 4.0 geodetic analysis software [6]. However, since the present version of this software does not comprise a time and frequency transfer module, we made the necessary modifications to the Bernese source code and developed some additional programs which allowed us to obtain the results described in this paper.

ZERO-BASELINE EXPERIMENT

The zero-baseline setup, with the same H-maser clock feeding both receivers (BRUS and BRUR), isolates the effect of receiver hardware delay variations on the results. Figure 2 compares the clock differences obtained with the C/A-code (Fig 2.a) and L_1 carrier phases (Fig 2.b).

Figure 2: Time differences (H-maser - H-maser) and frequency stability analysis for a zero-baseline experiment where both receivers are driven by the same H-maser clock frequency.

The noise of time differences computed from the carrier phases (a few ps) is about 100 times smaller than the noise of the code analysis. We observe a significant correlation between the phase single differences and the temperature variations in the laboratory (Fig. 2.c).

Thanks to the setup of the experiment, the main component responsible for this correlation could be identified as the different sensitivity of both receivers to ambient temperature variations; this leads to an approximate differential temperature coefficient of about 30 ps/°C for the carrier phase signal path. It is interesting to note that for the C/A-code signal path, the variations of the signal delay seem to be anti-correlated in the beginning of the test and correlated with the temperature at the end of the test. At the time of the writing, the cause of this is not yet clear.

The results emphasize the need to locate the receivers in temperature-controlled rooms, as already pointed out by different authors ([2], [3], [4]).

In a second step, the H-maser frequency driving BRUR was replaced by a cesium clock (HP5071A) frequency. The results for the time differences between both local clocks, deduced from GPS code and phase analyses, are shown in Figure 3. They are also compared with the time differences measured directly from a time-interval meter.

It is clearly demonstrated that the carrier phase analysis does not improve the results obtained with codes, because we are limited by the frequency stability of the cesium clock (given by the curve obtained for mod $\sigma_y(\tau)$). Furthermore, the effect of temperature variations on the delay of different hardware components are not visible in this case, again due to the noise of the cesium clock for averaging times shorter than one day.
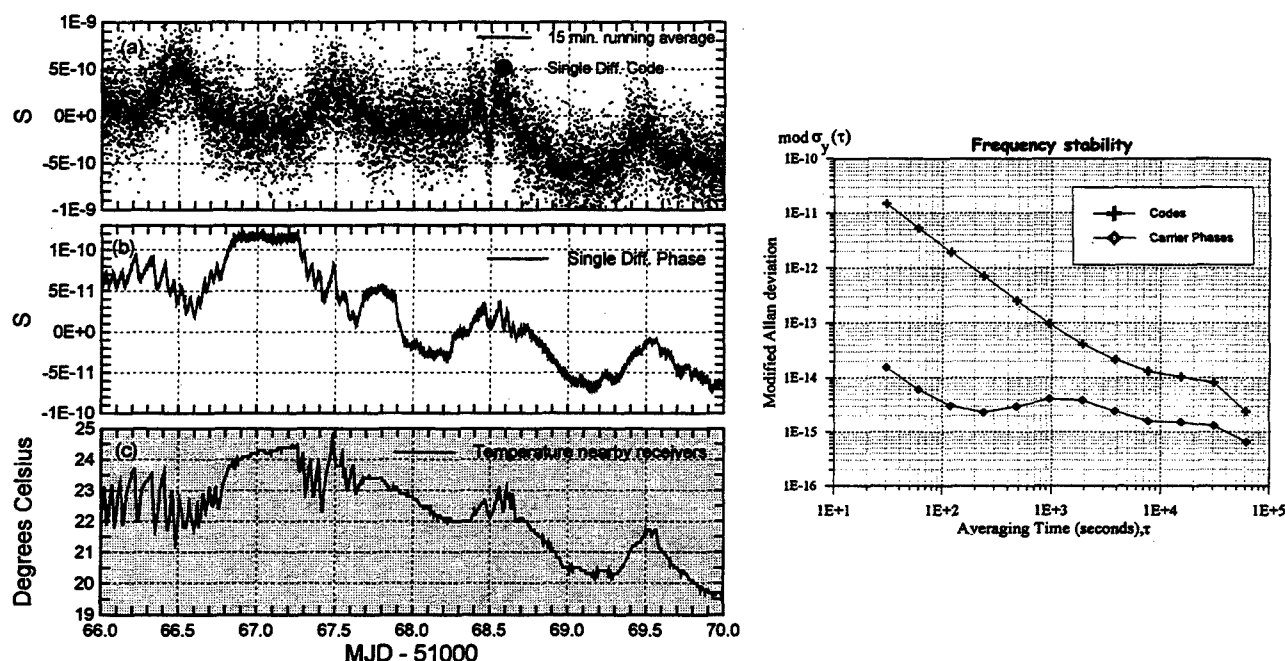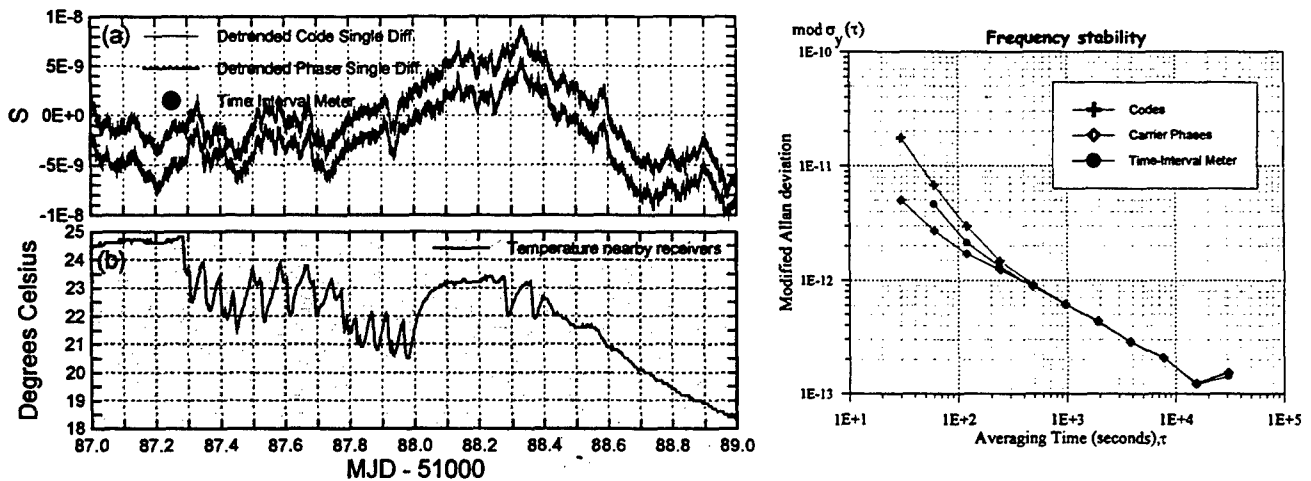

Figure 3: Time differences (H-maser - HP5071A cesium clock) and frequency stability analysis for a zero baseline experiment where one receiver is driven by the H-maser clock frequency and the other one is driven by the cesium clock frequency.

DIFFERENTIAL L1/L2 EFFECT

To compare the effect of temperature variations on the L_1 and L_2 signal path delays, we have used a zero-baseline configuration where one of the two receivers (namely BRUR) was placed in a well climatized room, where the temperature variations were kept smaller than 0.2°C. We considered the hardware delays of this receiver constant. The other receiver (BRUS) was subject to temperature variations as shown in Figure 4.c, resulting in variations of its L_1 and L_2 carrier phase delays. The delay variations are not identical for both carriers. This is due to the fact that the L_1 and L_2 components travel through different paths in the receiver front end. Also shown in Figure 4 is the fact that the L_1 and L_2 delays tend to increase at the end of the day, although the temperature is stable at this time. This indicates that other causes may affect the delays. At the time of the writing, more experiments are conducted to find out the origin of this variation.

ON-SITE BASELINE EXPERIMENT

The synchronization errors obtained from the analysis of the code and phase observations over the 95-m baseline with common time reference are shown in Figure 5. As was the case for the zero baseline, the use of the carrier phase observations (Fig. 5.b) rather than codes (Fig. 5.a) shows a clear improvement (note that the larger noise on the carrier phases with respect to the zero-baseline test is due to multipath). Nevertheless, as seen from the frequency stabilities, the carrier phases and code analyses have similar efficiencies at the averaging time of one day. This is due to the long period fluctuations of the signal, which are perfectly correlated with the temperature variations nearby the receiver BRUE (Fig. 5.c). This large temperature effect (about 0.15 ns/°C) is partly due to the receiver BRUE and partly due to the cable driving the H-maser frequency to the receiver (about 90 meter in open air). The results in Figure 5 show that

310
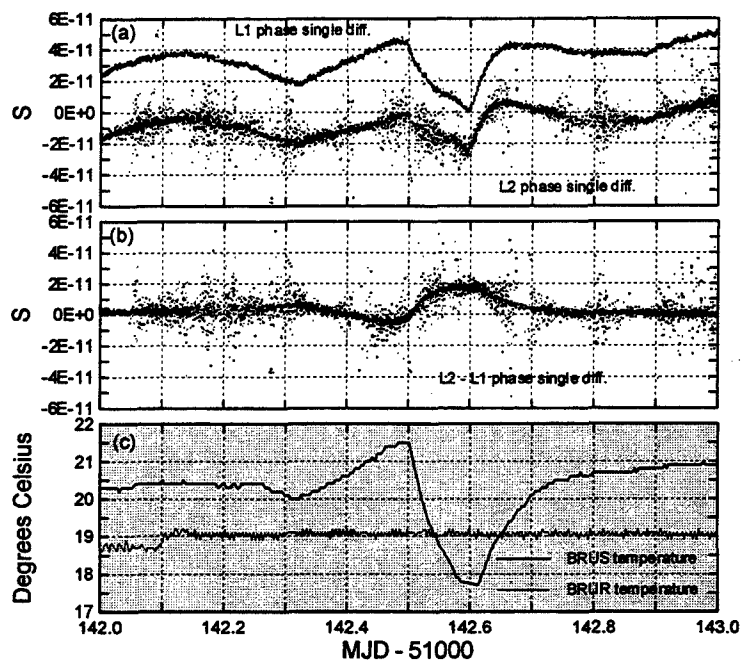
Figure 4: L_1-L_2 differential response to receiver temperature variations, deduced from the frequency transfer for a zero-baseline experiment where both receivers are driven by a same H-maser clock frequency, but one receiver (BRUR) is located in an air-conditioned room.

a frequency stability of a few parts in 10^{16} for averaging times of one day can be reached if all the instruments are located in temperature-stabilized rooms.
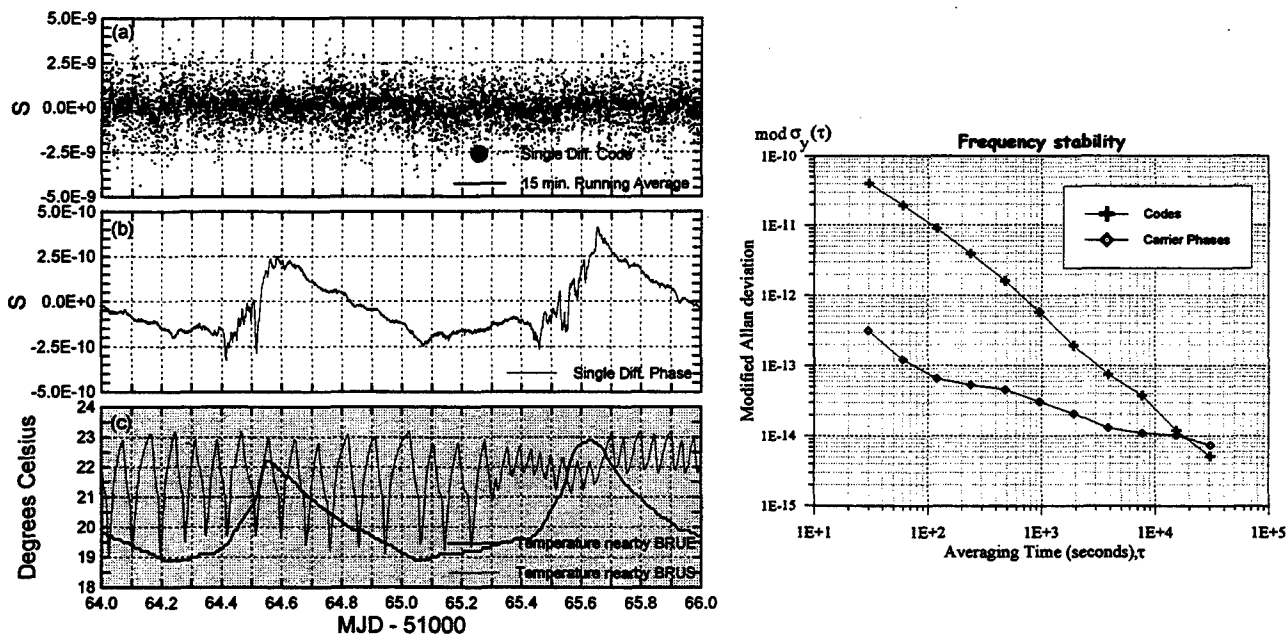
Figure 5: Time differences (H-Maser - H-Maser) and frequency stability analysis for a 95-meter-baseline experiment where both receivers are driven by the same H-maser clock frequency.

MEDIUM-LENGTH-BASELINE EXPERIMENT

Using Code Measurements

The stability of the frequency transfer between two remote H-maser clocks has was investigated on the 640-km-baseline Brussels-Wettzell. Figure 6 compares the frequency stabilities obtained with the classic common-view method (C/A-code on one channel) and with several multi-channel code processing schemes: using broadcast or precise (IGS) ephemerides, and using C/A-code or the ionospheric-free P_3-code.

We can see that all multi-channel results provide the same frequency stability. From this, we can conclude that the IGS precise orbits do not improve the frequency transfer compared to broadcast ephemerides, and that the ionospheric-free P_3 code does not improve the frequency transfer compared to the C/A-code. The optimal method would be to use the C/A-code with an ionospheric model. Figure 6 also compares the "multi-channel" frequency stabilities with the classical common view; the improvement is clear.
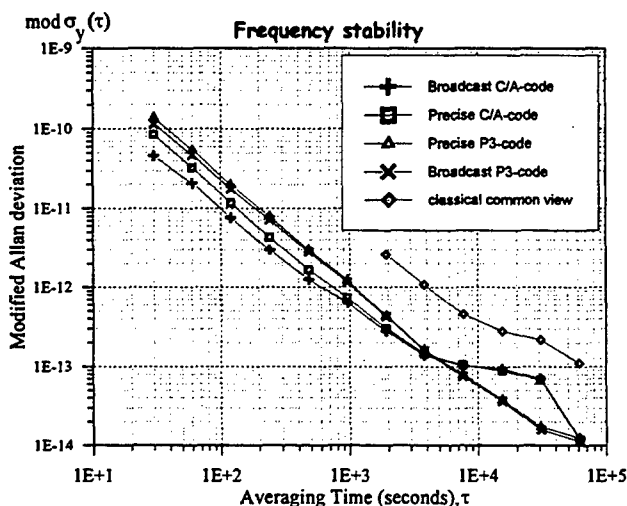
Figure 6: Frequency stability of the frequency transfer using different code data for the medium-length (640 km) baseline experiment where both receivers are driven by H-maser clock frequency.

Using Carrier Phase Measurements

The frequency transfer performed with codes can also be compared with the frequency transfer analysis performed with carrier phases. This is shown in Figure 7; the use of carrier phases shows a clear improvement.

Moreover, the analysis of phases allows again to identify some temperature effects in the frequency transfer, which are perfectly correlated with the temperature variations in the laboratory of BRUS. The amplitude of the effect is quite larger than what was deduced from the zero-baseline experiments, it reaches here about 0.5 ns/°C. Furthermore, from the study of the L_1-L_2 differential response of the receiver BRUS (see Figure 4), it appears clearly that the sensitivity of BRUS to temperature variations was only of about 10 ps/°K. We, thus, attribute the correlation of the temporal

312
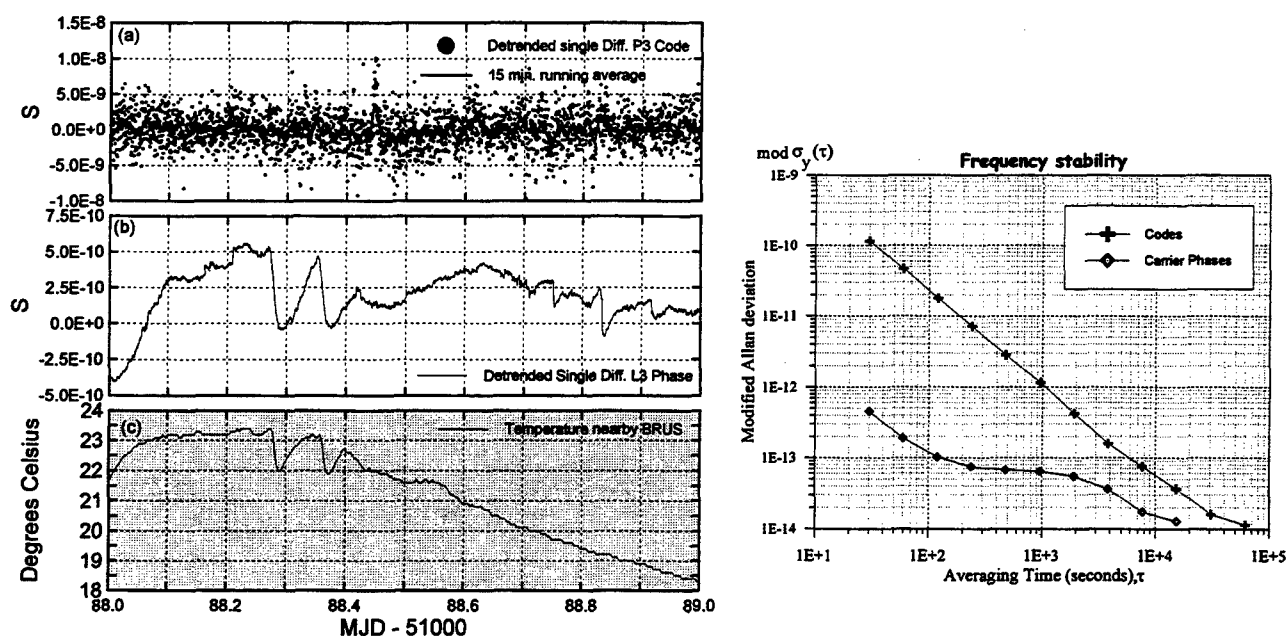
Figure 7: Time differences (H-maser BRUSSEL - H-Maser WETTZELL) and frequency stability analysis for a medium-length (640 km) baseline experiment.

variations with the computed synchronization errors to the amplifier of the H-Maser frequency, which is located in the same laboratory as BRUS and subject to identical temperature conditions.

This has also been confirmed by the direct comparison of the 1pps signal from the H-Maser clock with the 1pps signal output from the receiver BRUR when this one was in an air-conditioned room. From this, we can conclude that the frequency stability of the frequency transfer with carrier phase is limited, due to the influence of temperature variations on the amplifier (not in an air-conditioned room) of the H-maser frequency.

CONCLUSION

We have tested the stabilities of frequency transfer over three types of baselines : a zero, short and medium-length. The computations were done independently on using first the GPS code observables and later the carrier phases. We have demonstrated that in the present situation (where the instruments are not in temperature-stabilized laboratories), the frequency stability for averaging times of one day are 6×10^{-16} for the zero baseline, 6×10^{-15} for the on-site tests with a 95 m baseline between both antennae, and 10^{-14} for a medium-length baseline between Brussel and Wettzell (640 km).The main limitations of our analyses are presently the response of the different hardware components to ambient temperature changes. For some of the components we have derived temperature coefficients : the responses of the receivers is of about 30 ps/°C (depending on the receiver type), the response of the amplifier of the H-Maser frequency is of about 0.5 ns/°C.

The frequency stabilities obtained here can be largely improved if the temperature effects on the instruments are suppressed, i.e. if the instruments are all located in temperature-stabilized rooms. In that case, the frequency transfer using carrier phases for longer baselines should gain more and more interest, and the combined use of code observations could allow to estimate the "absolute" time offset between the receiver internal clocks, and hence between the local clocks connected to the receivers.

313

REFERENCES

[1] Bruyninx, C., Dousa, J., Ehrnsperger, W., Fachbach, N., Stangl, G., Ferraro, C., Fermi, M., Nardi, A., Sciarretta, C., Vespe, F., Figurski, M., Piraszewski, M., Rogowski, J., Johansson, J., Springer, T.A., Beutler, G., Brockmann, E., Gurtner, W., Rothacher, M., Schaer, S., Weber, G., Wiget, A., and Wild U., *"The EUREF Associate Analysis Center,"* 1996 Annual Report of the International GPS Service for Geodynamics, Eds. J.F. Zumberge, D.E. Fulton and R.E. Neilan, pp. 271-309.

[2] Overney, F., Prost, L., Dudle, G., Schildknecht, Th., Beutler, G., Davis, J.A., Furlong, J.M., and Hetzel, P., *"GPS Time Transfer using Geodetic Receivers (GeTT): Results on European Baselines,"* Proc. of the 12ᵗʰ EFTF 98, pp. 94-99.

[3] Overney, F., Schildknecht, Th., and Beutler, G., *"GPS Time Transfer using Geodetic Receivers: Middle-term Stability and Temperature Dependence of the Signal Delays,"* Proc. of the 11ᵗʰ EFTF 97, pp. 504-508.

[4] Petit, G., Thomas, C., Jiang, Z., Ulrich, P., and Taris, F., *"Use of GPS Ashtech Z12T Receivers for Accurate Time and Frequency Comparison,"* Proc. of FCS 98.

[5] Ray, J., *"The IGS/BIPM Time Transfer Project,"* Proc. of IGS Analysis Center Workshop", Darmstadt, 1998, pp. 65-70.

[6] Rothacher, M., and Mervart L. (Eds.), *"Bernese GPS Software 4.0,"* Astronomical Institute, University of Berne, 1996.

TWO-WAY SATELLITE TIME TRANSFER (TWSTT): USNO OPERATIONS AND CALIBRATION SERVICES

James A. DeYoung
U.S. Naval Observatory
3450 Massachusetts Avenue, NW
Washington, DC 20392, USA
dey@herschel.usno.navy.mil

Abstract

The U.S. Naval Observatory maintains a large number of dedicated antennas, modems, and related hardware worldwide in support of high-precision DoD and non-DoD TWSTT time and frequency transfer users. This paper will present a small portion of our operations as an example. Recent TWSTT measured time and frequency comparison results, how we monitor the transmit and receive paths, some recent work done on evaluation of X-band high-power-amplifiers and effects on TWSTT, basics of calibration of high-precision time and frequency systems using TWSTT, and an estimate (~1.1 ns) for a recent co-located Ku-band TWSTT calibration are given.

INTRODUCTION

The U.S. Naval Observatory has been involved in two-way satellite time transfer (TWSTT) since the early 1960s [1]. The expansion of TWSTT at USNO over the last few years has been very rapid. At USNO alone we maintain approximately a dozen fixed and portable very small aperture terminals (VSATs) dedicated to operational world-wide TWSTT experiments linking in real-time remote timing centers to the USNO Master Clock (USNO MC).

The USNO now has two remote centers being compared to the USNO MC via nominal hourly TWSTT experiments. One is the U.S. Naval Observatory Alternate Master Clock (USNO AMC) (2374km, Ku-band) and the other is in the Persian Gulf region country of Bahrain (10,983km, X-band). The usefulness of the high-sampling-rate of TWSTT for these two centers confirms the viability and quality of both Ku-band and X-band TWSTT over worldwide distances. The USNO has developed a method of monitoring signal levels in both the transmit and receive paths that allow monitoring of each stage of the process and allows easy routine monitoring and optimization of signal levels at all times. Recent experiments at X-band allow the study of the effects of optimal and non-optimal signal level insertion into some components along the transmit and receive paths.

The basics of the USNO method of calibration of TWSTT and other timing links will be shown and the first estimate of TWSTT calibration accuracy is developed.

315

RECENT USNO - USNO AMC HIGH-SAMPLING RATE TWSTT

The performance of the USNO(MC2) - USNO AMC(MC1) Ku-band TWSTT link continues to be very good. The nominal sampling rate is @1h. On average we have about 19 to 20 successful TWSTT experiments during the day, out of 24 (79% to 83%). This number includes failed and numerically filtered experiments. In several months the USNO AMC will receive a software and modem upgrade which should allow close to 100% of the experiments to occur. Improvements include a more recent improved modem version, improved automated control and error detection software, remote autoreset, and tweaking of other related TWSTT systems. Figure 1 shows approximately the last 430 days of TWSTT. The rms is 0.536 nanoseconds.

Since the TWSTT is not yet exactly equally spaced, a simple one day time average is generated for each MJD. The simple one-day average data is then used to form fractional frequencies. The rms over the last 430 days is 2.09 parts in ten to the 15th. The precision in time and frequency given above are not the limit of the TWSTT method, since both these clocks are being steered. USNO(MC2) is steered to our USNO(Mean) real-time estimate of UTC(BIPM) once per day, while USNO AMC(MC1) is steered hourly to USNO(MC2). Figure 2 shows the daily fractional frequency performance estimated from the 1-day averaged data.

USNO maintains local atomic times at both USNO and USNO AMC. USNO(A.1) is made up of an ensemble of approximately 35 to 40 Cs and 10 H-maser clocks, while USNO AMC (A.1) is made up of an ensemble of approximately 10 Cs and 2 H-maser clocks. Using TWSTT we may compare the two free-running scales at high precision and accuracy. Figure 3 shows USNO AMC(A.1) - USNO(A.1) compared via TWSTT over about 400 days after removal of a rate of -62060.306 ps/d and a drift of 2.006 ps/d/d. The residual rms is 2985 picoseconds.

RECENT USNO - BAHRAIN HIGH SAMPLING RATE TWSTT

During 1998 a new X-band TWSTT station was installed in the Persian Gulf country of Bahrain. Improvements in hardware and software during October and November 1998 made it possible to sample this remote Cs at a nominal hourly sampling rate. The distance of 10,983km is the longest single-hop

TWSTT experiment ever performed. Figure 4 shows some recent time difference data.

TRANSMIT AND RECEIVE PATH MONITORING

For many years we have kept detailed log books on each antenna system, each timing link, and for each calibration trip. There is a wealth of information in these books that allow us to know what was done, what changes were made, what problems were encountered, how they were fixed, what the results were, etc.

The basic method of monitoring used is to generate baseline measurements when a system is first installed. Input signals are optimized at each stage along the transmit and receive paths.

Figure 5 shows the the transmit path. First from an on-time point a 5MHz and 1-PPS signal is sent to the modem for use in the formation of the transmitted 1-PPS. An oscilloscope is used to measure the clean peak-to-peak signal which is optimized to voltages that are optimal for the modem.

Next the 70MHz output of the modem is monitored with a spectrum analyzer just before insertion into the up converter in order to allow for all losses along the path. The signal into the up converter is optimized to manufacturer's specifications by adding or removing of attenuation pads, usually at the modem output.

The output of the up converter (GHz) is then sent to a high-power amplifier (HPA) or to a solid-state power amplifier (SSPA). The signal into the power amplifier is optimized again to manufacturer's specifications and is sampled at a test port and/or by using a power splitter and power meter system. More on this in a following section.

The receive path is monitored similarly (see Figure 6), except the satellite beacon is used as a signal reference for the baseline and subsequent monitoring measurements. The received signal may be sampled at the output of a low-noise amplifier (LNA) or in the case of a low-noise block amplifier (LNB) at any of the available intermediate frequencies.

The 70MHz output of the down converter is routinely monitored in day-to-day operations by use of a dedicated spectrum analyzer. Antennas are peaked periodically for fixed antennas, while steerable antennas are peaked either

automatically by tracking the beacon or at the time of the TWSTT experiment by the operator.

TWSTT Calibration of High-Precision Time and Frequency Systems

The first fully calibrated TWSTT link was performed by USNO in December of 1992 at the U.S. Naval Observatory Time Service Sub-station (NOTSS)[2]. USNO has since calibrated many remote centers using the co-located TWSTT method. A great deal of experience has been gained during our remote field work. USNO has developed standard calibration methodologies, standard forms and spread-sheet forms to make processing of the data easy and accurate. The method gives a single "calibration value" to be applied to TWSTT experiments which is the sum of all the delay differences in the TWSTT (see Figure 7). The goal is to obtain a single value that describes accurately the sum of the delays between the two on-time points. The solid lines in Figure 7 show the delays at each station from the on-time point to the modem where the actual 1-PPS comparisons are made in the TWSTT modem and the dashed lines show the "RF delays".

The calibration process begins by making measurements with the portable antenna using matched and measured cables. The experiments at USNO are designed to precisely and accurately measure the time time difference between the on-time point of the USNO MC2 to operational USNO modem. The portable/calibration antenna/modem is then shipped to the remote center. Once the portable/calibration system is set up at the remote center and optimized after the method mentioned in the section above, experiments are obtained to isolate the local on-time point to the modem and the field modem to USNO modem. Typically experiments are made over several days to have full confidence that the calibration system is working well. Upon return of the equipment closure experiments are made and the experiment means compared for closure errors--typically 0.5 to 1.0 ns overlaps and better than the 1-sigma level.

The calibration data are then averaged and the sum of the delays is computed and a single calibration time is applied in the routine processing of the operational TWSTT. The details of the mathematics depends on each unique setup.

Once the first system is calibrated it is a simple matter to calibrate backup modems and antenna combinations. if a failure of a component requires it. In critical operational links information is passed in the data files, which allows automatic delay determination with each calibrated antenna/modem combination when the data are processed. Figure 8 shows the basic TWSTT link calibration showing the sequence of events.

TWSTT CALIBRATION OF GPS TIMING SYSTEMS

If a remote station has additional high precision equipment for time and frequency, such as GPS Carrier-Phase (GPS CP) in addition to TWSTT, it is rather easy to use the TWSTT calibration to calibrate a co-located GPS system to be calibrated at the same level of accuracy as TWSTT. A single bias value may be determined to put the uncalibrated GPS on-time with TWSTT. This assumes that the same on time source is used at each timing center (see Figure 9).

FIRST TWSTT CALIBRATION ACCURACY ESTIMATE

A recent, summer 1998, Ku-band syntonization and single-shot synchronization was made at Naval Command, Control, and Ocean Surveillance Research and Development Center (NRaD), San Diego, CA, USA. The data from all the USNO and in the field TWSTT experiments were combined to give an estimate of the accuracy reached. No closure experiments were made for this calibration. The combined error estimate gives an rms of 1.057ns for this calibration (Figure 10). Several methods were employed to obtain intermediate data for the calibration and all seem to give similar results. No experiments were filtered to determine this calibration error. The results are quite good especially those in the field. Improvements in the measurement schemes should allow sub-nanosecond calibrations to be achieved in some cases.

X-BAND TRANSMIT POWER OPTIMIZATION AND CHARACTERIZATION

Recent work allowed us to characterize the performance of a 40-watt high-power amplifier (HPA) for optimization for X-band work. Power meter measurements were made using a power splitter (attn: 50db) in the wave-guide path after the HPA. We inserted various signal levels into the HPA to find the optimum input level in order to reach the full 40-watt output of the HPA. We varied the attenuation in the up converter from 0db to 30db and measured the output power of the HPA through the power splitter. Figure 11 shows the power meter measurements. The optimum up converter attenuation was found to be 10db. When the HPA was over-driven the power dropped, since more power was put into side-bands (dashed lines indicating side-bands in top diagram of Figure 5). When under-driven the full output power of 40 watts was not reached. Figure 12 shows the conversion of the power meter readings to actual power in watts.

This work allowed us to see the effects of over-driving and under-driving an HPA by monitoring TWSTT experiment means and scatter changes in the 1-PPS measurements. Figure 13 shows the variation of the rms scatter of the experiment means with HPA output as the input signal to the HPA was being varied by changing the attenuation in the up converter. The scatter goes up when over-driving the HPA, since nonlinear distortion is introduced. When under-driving the HPA the scatter is increased due to low S/N on the receive side. Figure 14 shows that the mean of the TWSTT experiments varies fairly linearly from the over-driven case to the under-driven case. The approximate relationship is a change of 650 ps per db attenuation change. Most samples were performed at the optimal settings with only a few measurements made in the non-optimal regions.

CONCLUSIONS

TWSTT continues to be a fascinating and useful high precision time and frequency transfer method. The high sampling rate (@1h) experiments continue to prove their worth over distances reaching nearly 11,000 km. Experiments show that TWSTT is stable and able to be calibrated routinely to the 1ns level. New hardware components have been characterized which allow optimal set up and routine monitoring of the TWSTT system in order to reach and maintain the best possible TWSTT precision and accuracy.

ACKNOWLEDGMENTS

REFERENCES

[1] http://tycho.usno.navy.mil/twstt.html

[2] J. DeYoung and R. J. Andrukitis, 1994, "Remote Clocks Linked by a Fully Calibrated Two-Way Timing Link," Proceedings of the 25th Annual Precise Time and Time Interval (PTTI) Applications and Planning Meeting, November 29-December 2, 1993, pp. 285-292.

USNO(MC2) - USNO AMC(MC1) Via Nearly Hourly TWSTT

Fig.1

RMS = 0.536
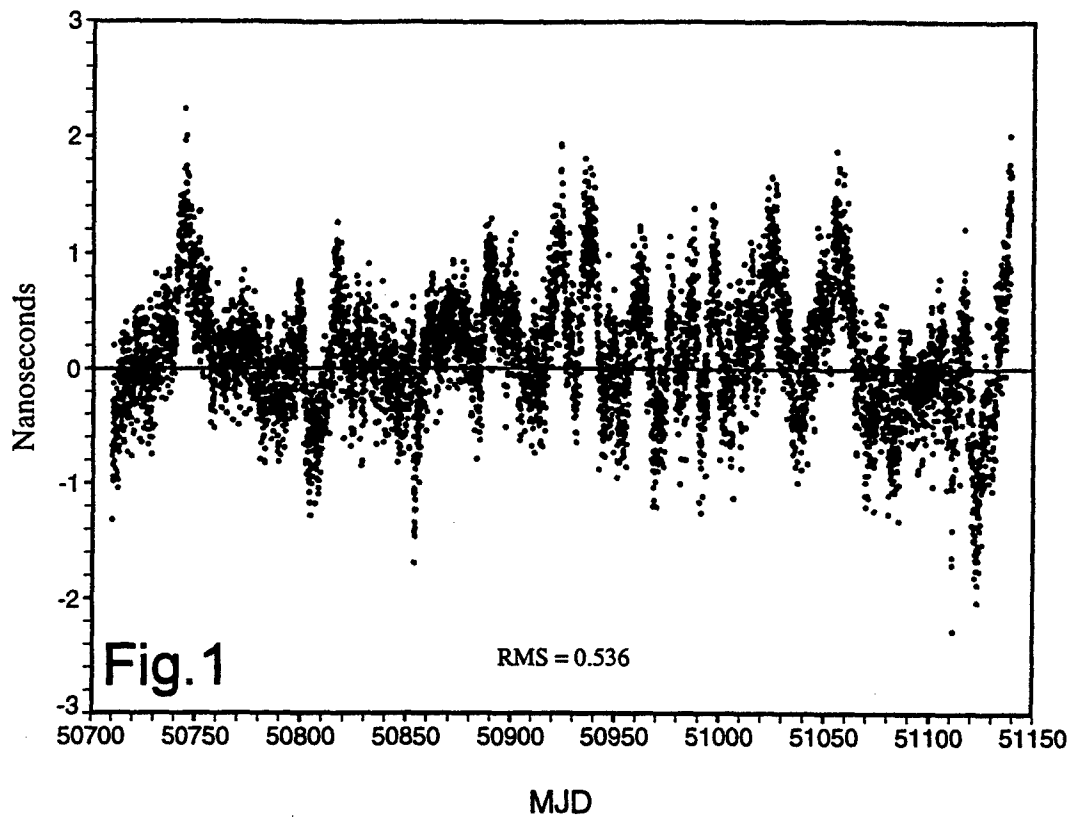
USNO(MC2) - USNO AMC(MC1) Via TWSTT

Frequency @1d from Simple 1d Time Averages

Fig. 2

RMS = 2.092

321
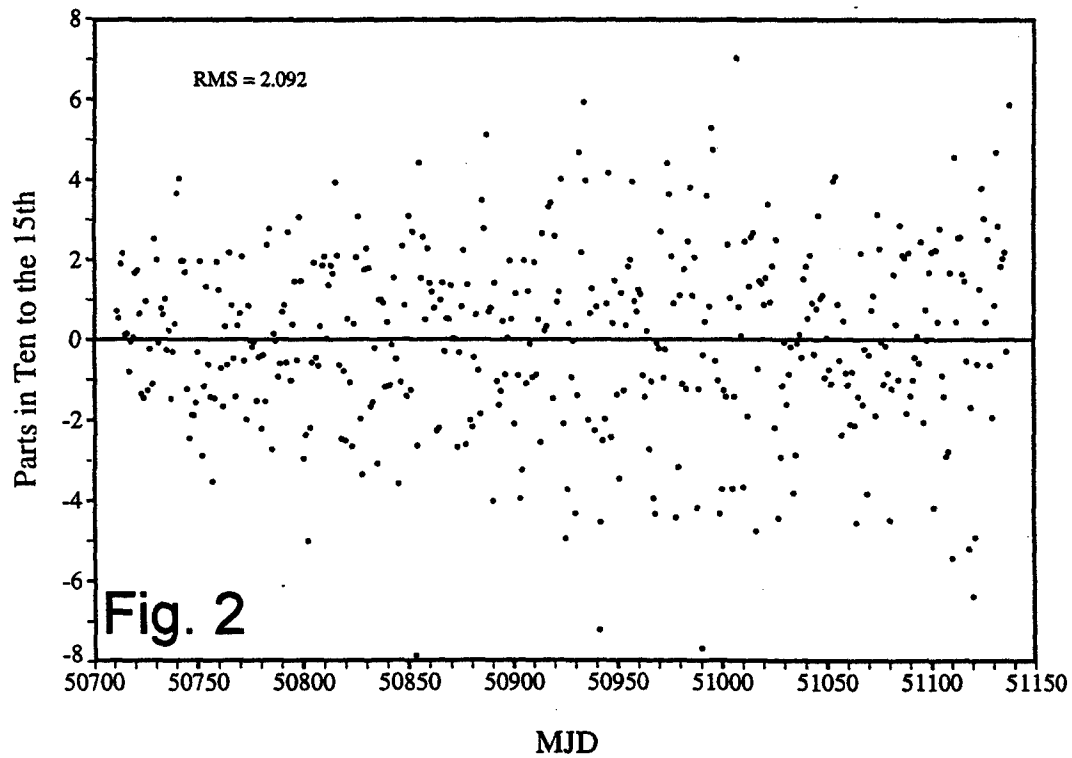
USNO AMC(A.1) - USNO (A.1) via TWSTT

USNO AMC ---> 10Cs + 2 H-maser

USNO ---> 35Cs + 10 H-maser

Fig. 3

RMS = 2985

MJD
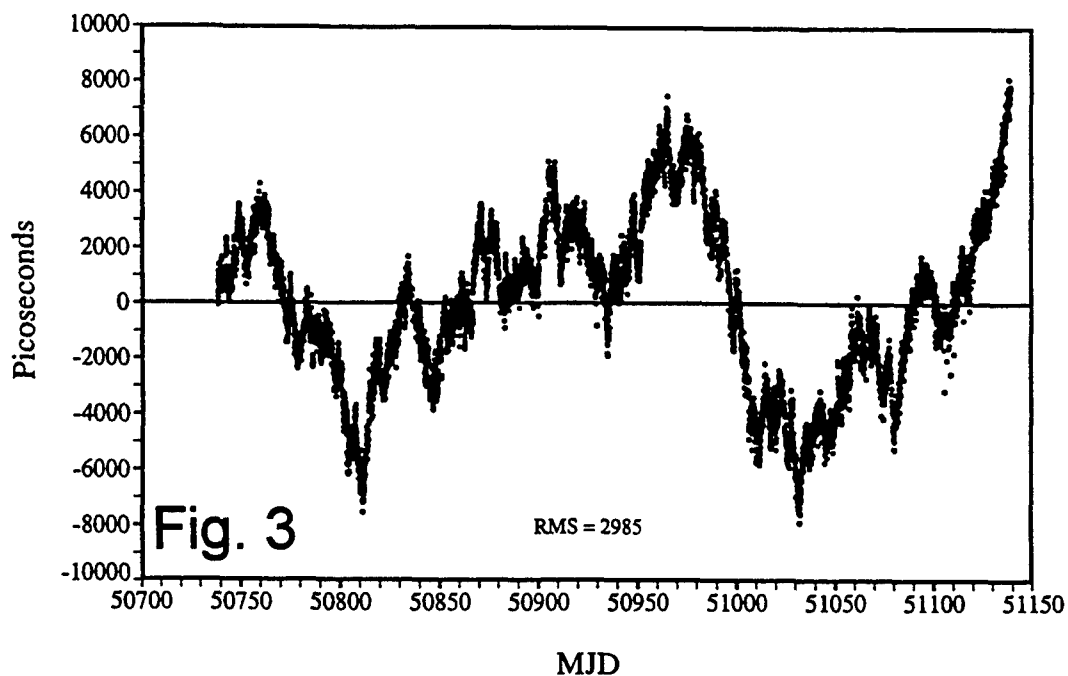
Removed: 1st Order -62060.306 ps/d, 2nd Order 2.006 ps/d/d

USNO(MC2) - BAH(Cs) via TWSTT

10,983km Single Hop X-band

Rate of +9.847 ns/d Removed

Fig. 4

RMS = 1.553

MJD
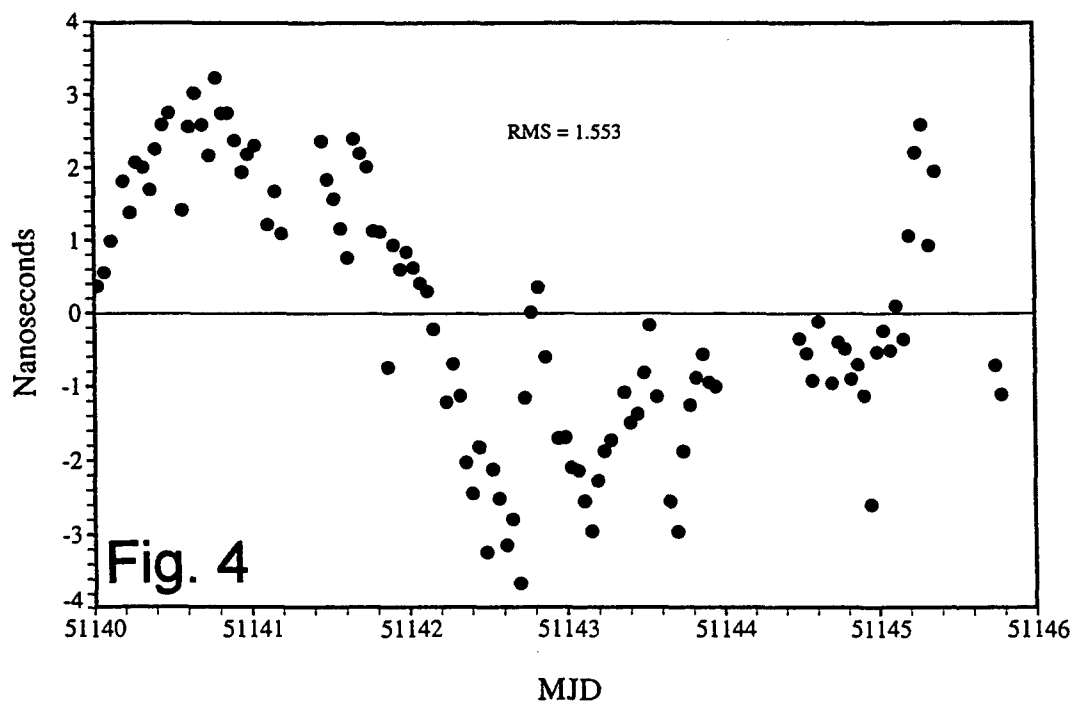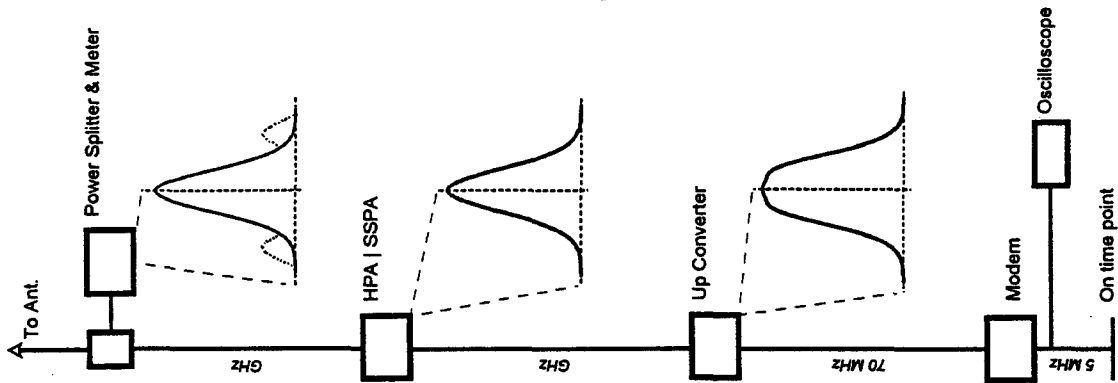
Transmit

Fig. 5
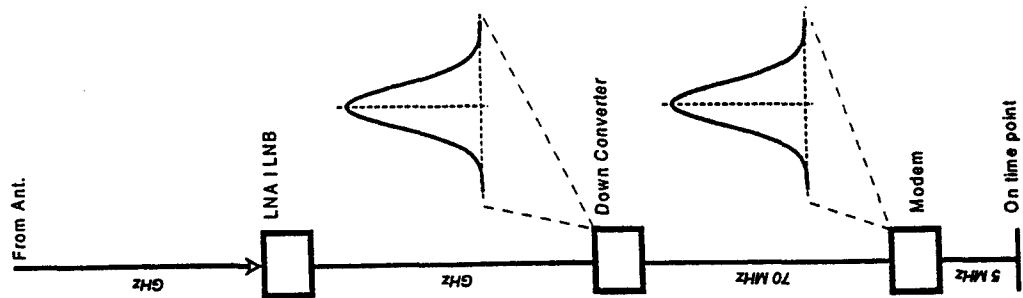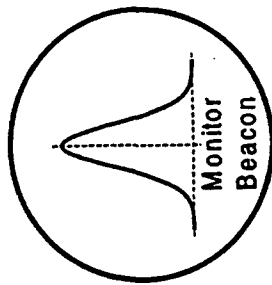
Receive

Fig. 6

Fig. 7

Detail of Portion of Calibration by Co-Located TWSTT Method

Sum delays =   modem(field)
to modem(USNO)
delay difference

+

on time
to modem
delay differences

TWSTT
Cal. Ant

Matched and
Measured cables

Field
TWSTT

TX-RX

TX-RX

USNO
TWSTT

Common On-Time Point
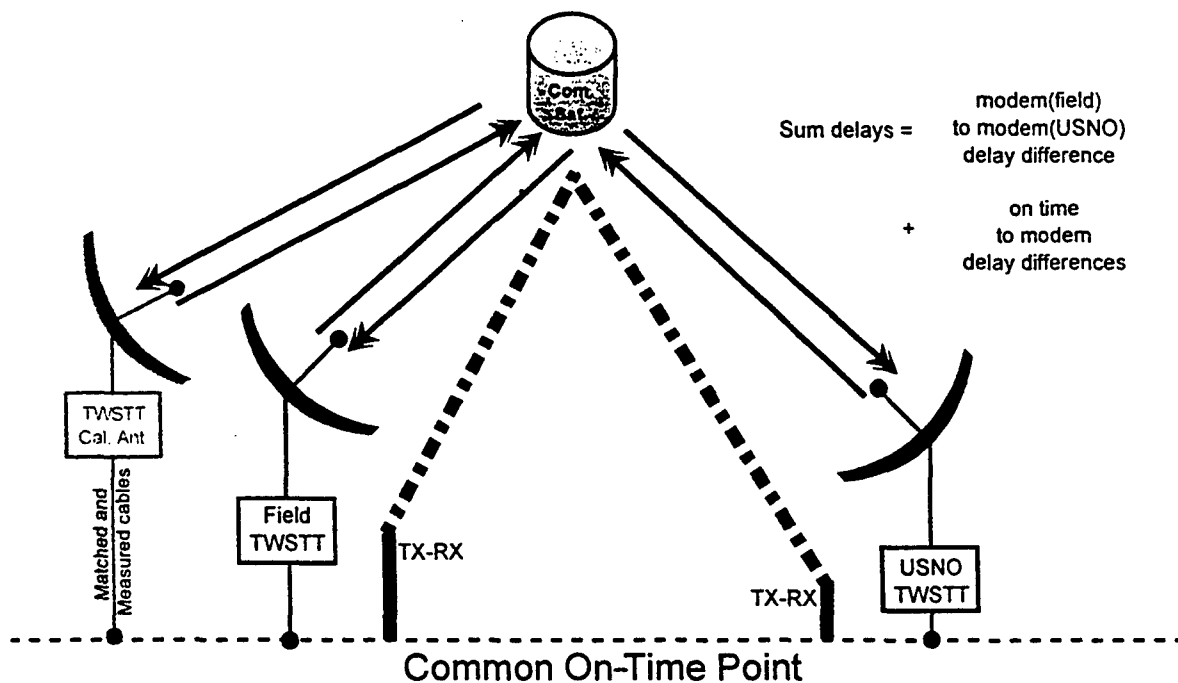
Fig. 8

TWSTT Link Calibrated by Co-Located TWSTT Method

TWSTT
Cal. Ant

TWSTT

TWSTT
Cal. Ant

TWSTT

Common On-Time Point

1,3   **Process Sequence**   **2**
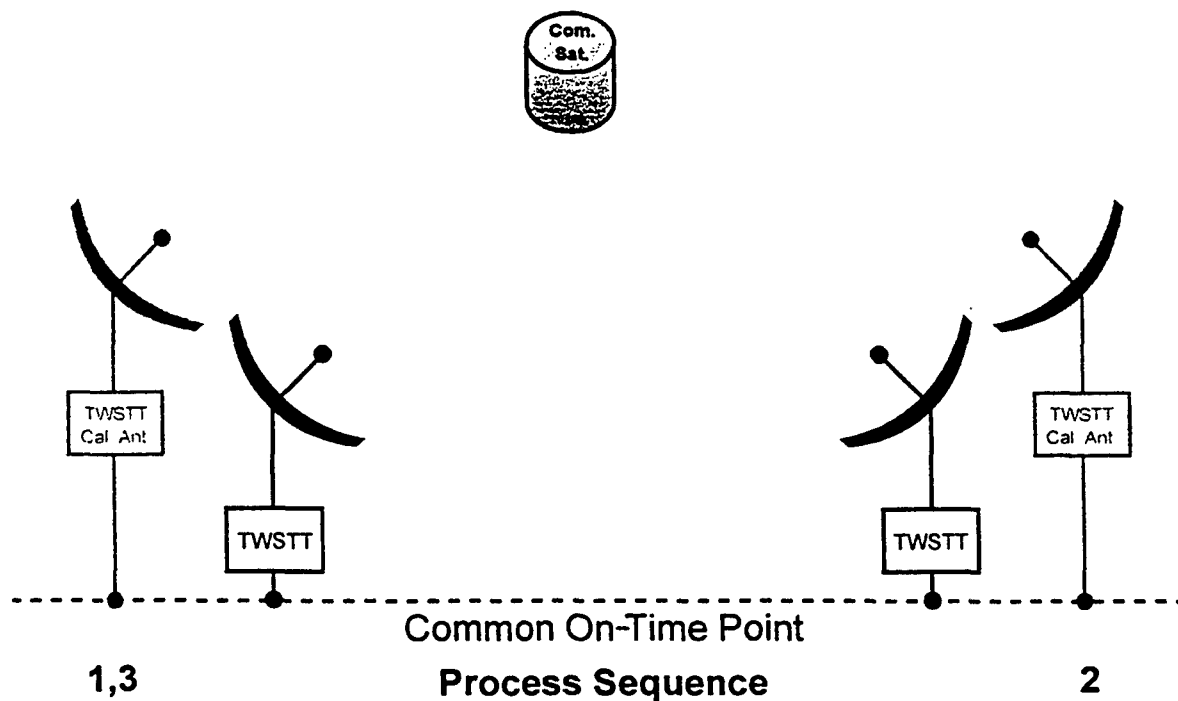
Fig. 9   GPS Receiver Link Calibrated by Co-Located TWSTT Method

Common On-Time Point

1,3   **Process Sequence**   **2**
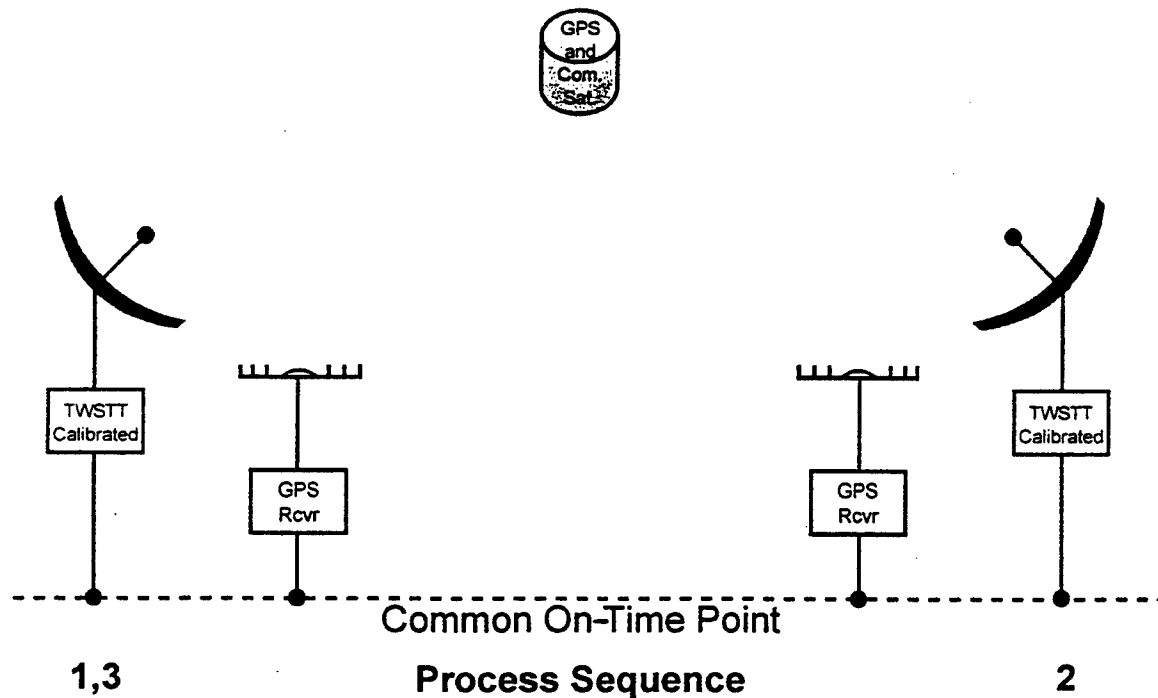
Fig. 10   USNO - NRaD Syntonization and Single-Shot Synchronization

Estimate of Calibration Errors from Experiment Means

Combined Error: 1.057ns

325
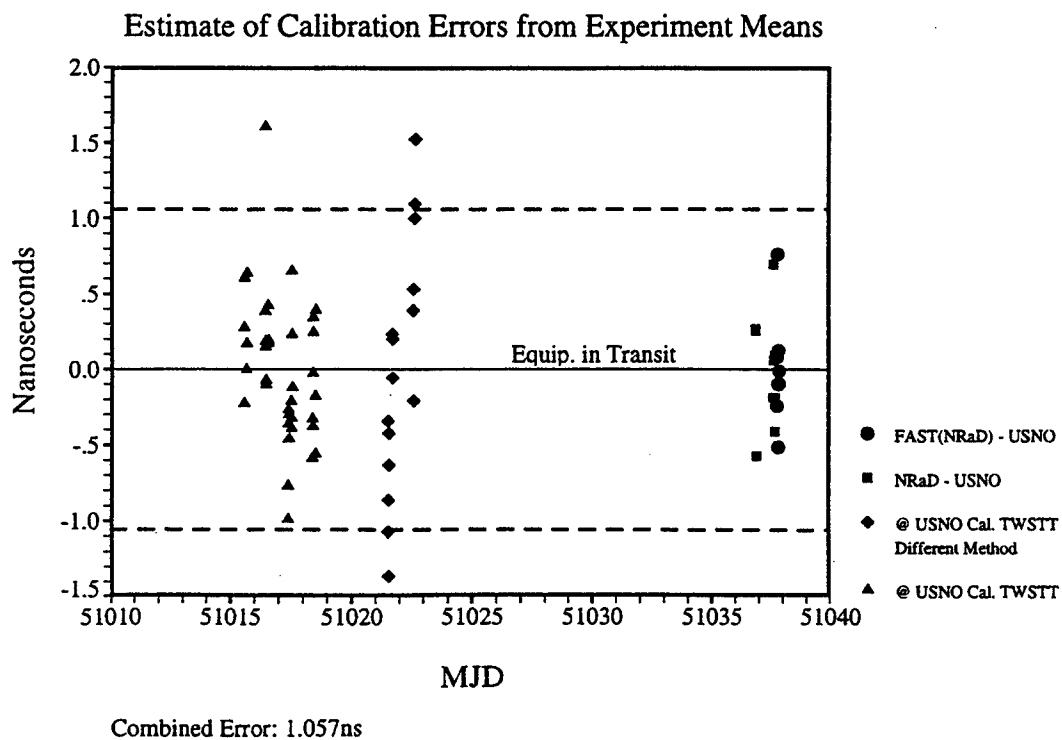
Fig. 11

Power Meter Measurements
Finding the Optimum Input for HPA

Power Splitter Attn: 50db

Over-Driven HPA Optimum Signal Under Driven

Power (dbm) vs Upconverter Attenuation (dbm)
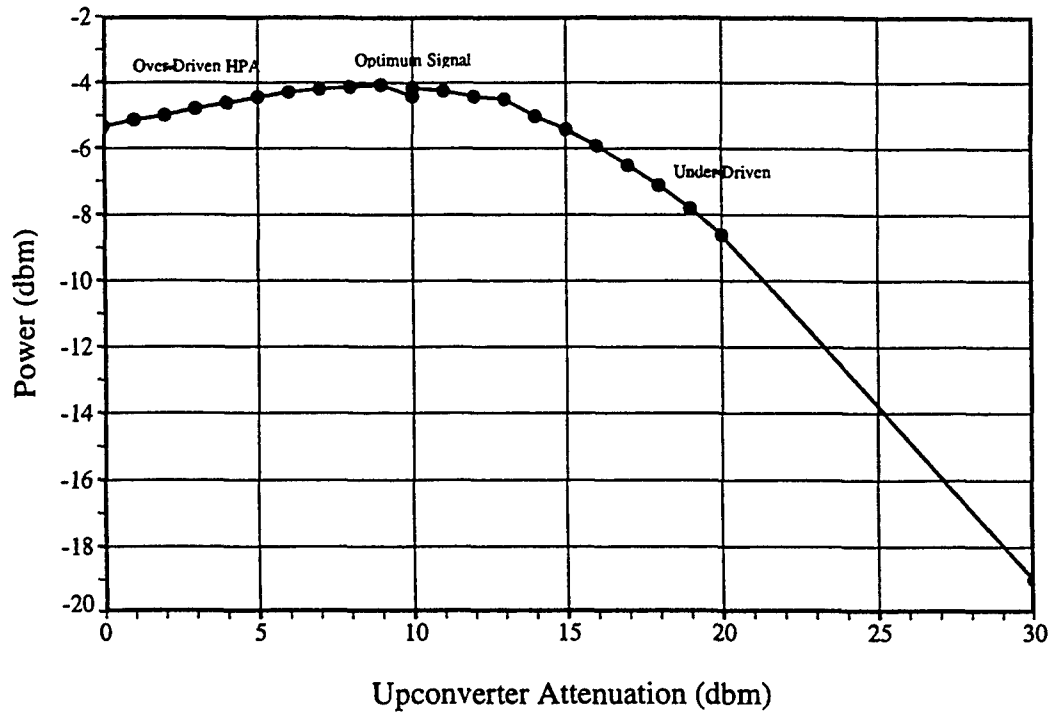
Fig. 12

Power Meter Measurements

Power Splitter Attn: 50db

Watts vs Power Meter Readings (dbm)

326
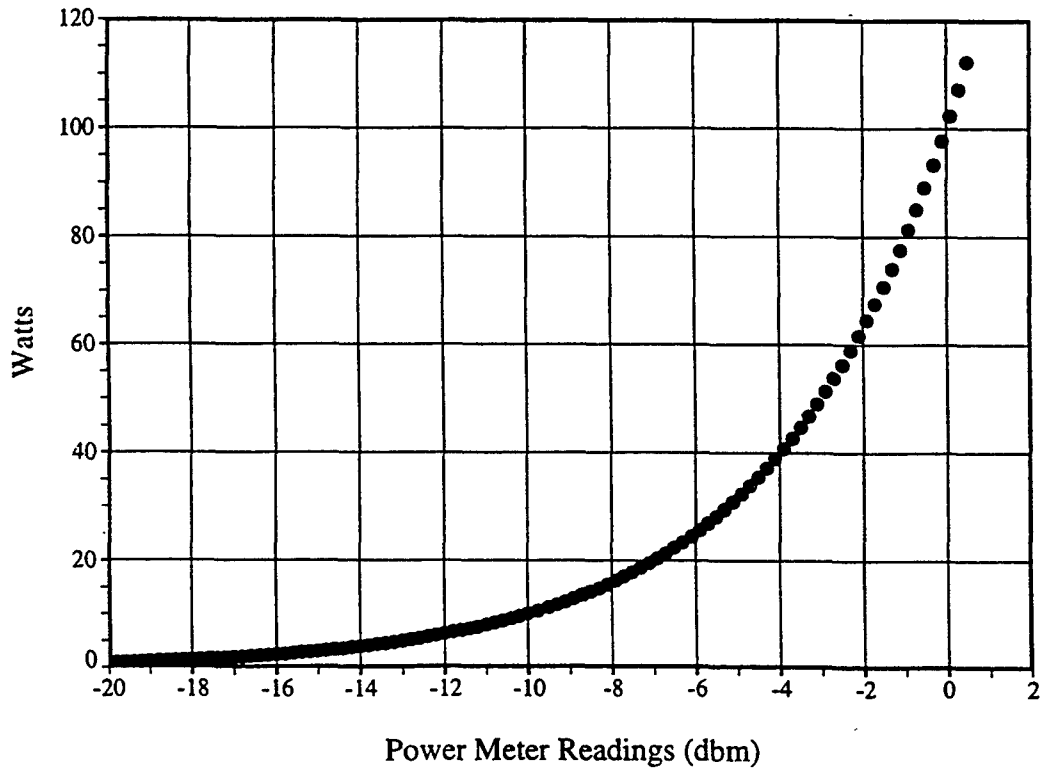
Fig. 13

X-Band (FX2) Baseline TWSTT
Experiment RMS Behaviour w/Signal Varied into HPA

X-Band (FX2) Baseline TWSTT

Fig. 14

Experiment Mean Behaviour w/Signal Varied into HPA
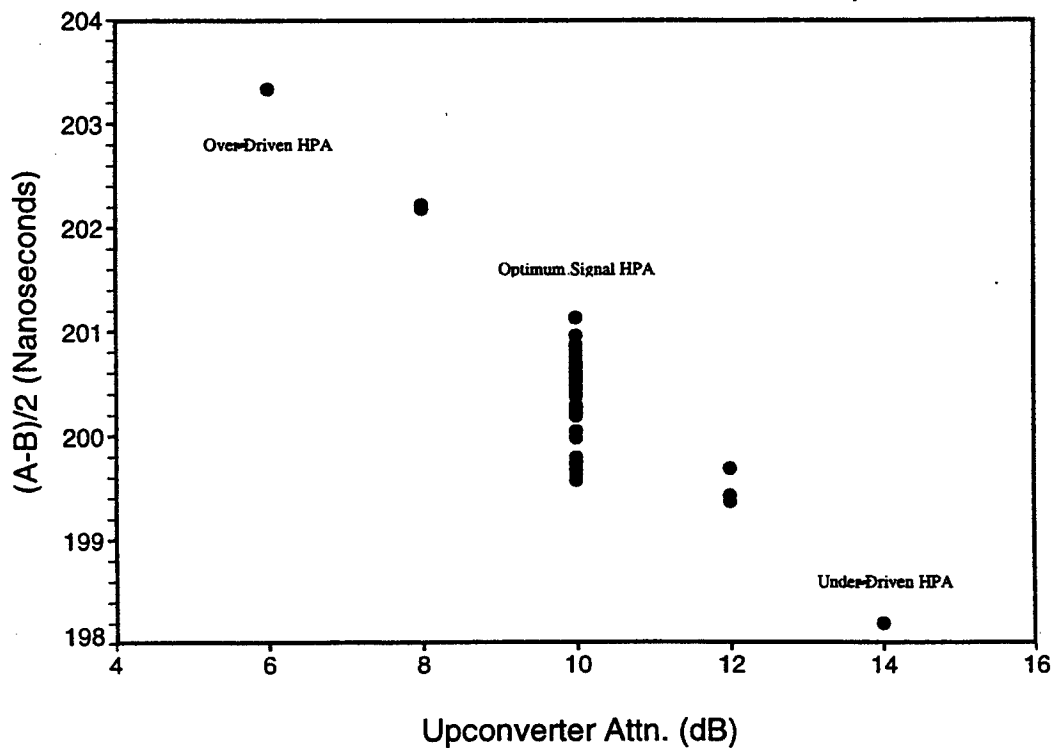
IMPROVING THE DELAY STABILITY OF A TWO-WAY SATELLITE TIME AND FREQUENCY TRANSFER EARTH STATION

Setnam L. Shemar and John A. Davis
Centre for Time Metrology, National Physical Laboratory
Queens Road, Teddington, Middlesex TW11 0LW, England, UK

Abstract

Two-Way Satellite Time and Frequency (TWSTFT) is increasingly used for the routine intercomparison of time scales at primary timing laboratories. The performance of a two-way time transfer link is, however, limited by delay instabilities in the earth station hardware. Several European laboratories have been operating near field satellite simulators to measure the delay instabilities of their TWSTFT earth stations. At the National Physical Laboratory (NPL) we have adopted a different characterization configuration, where two independent characterization loops are used to measure the TWSTFT earth station uplink and downlink delay instabilities separately. This allows an assessment of the performance of the difference loops in the measurement of the delay instabilities. The cables connecting the earth station hardware have also been investigated. Direct comparisons are made between PTFE coaxial cable propagating Ku-band and L-band signals. Furthermore, the performance of a higher chip rate code has been investigated. Finally, the results presented in this paper are used to discuss future improvements in TWSTFT at NPL.

1 INTRODUCTION

High precision time-transfer using the Two-Way Satellite Time and Frequency Transfer method involves an exchange of time-signals between two earth stations via a geostationary satellite [1]. The advantage of this method over a one-way method (such as GPS common-view) is that accurate determination of the satellite and earth station co-ordinates are not required. This is because the free space and atmospheric propagation delays of the signals travelling in opposite directions cancel out almost entirely. However, the present limitations of this method result from delay instabilities within the earth station hardware. These have to be taken into account and require calibration [2, 3]. Furthermore, it is important that hardware delays are stabilized as far as possible in order to reduce uncertainties after calibration.

This paper presents a series of tests that have been used to characterize NPL's

TWSTFT earth station to gain a better understanding of its delay instabilities. The performance of the earth station uplink and downlink characterisation tests is assessed and the origin of delay instabilities demonstrated. Tests have also been carried out on cables to investigate the variation of signal propagation delays with temperature. The earth station delay stability has also been investigated using a spread spectrum signal with a higher chip rate code than is used in the routine TWSTFT measurements.

2 EARTH STATION CHARACTERIZATION

(I) Downlink Tests

Downlink characterization tests were carried out using the configuration shown in Figure 1. The signals output by the Satre and Mitrex modems were input into one of two downlink characterization loops. The characterization test hardware in each loop consisted of the components between the output of each modem and the earth station feed. These included directional couplers, a switch box, Ku-band mixers, a 12.6 GHz phase-locked local oscillator, attenuators, cables, and horns. Apart from two cables and two horns, all of this hardware was located within a laboratory which is temperature-controlled to within 3°. In each loop the 70 MHz output signals from the two modems were combined using a directional coupler and mixed up to 12.67 GHz using a mixer and the 12.6 GHz local oscillator. The resulting signal was attenuated before being transmitted by a horn towards the earth station feed.

Measurements were taken using both the Satre and Mitrex modems for each loop. The switch box was used to switch between the two loops once per minute. The use of two loops allowed an independent check of the hardware. To allow for measurements to settle down after switching between the loops, measurements corresponding only to the final 30 s of each one minute interval were processed. A mean of these data was taken to provide a representative measurement of the loop delay. The resulting measurements of the Mitrex and Satre modems for each of the two loops (Loops 1 and 2) are presented in Figures 3 and 4 respectively. Indoor and outdoor temperature measurements are also shown for comparison. The tests demonstrate an inverse correlation between the loop delay and the outdoor temperature with a temperature coefficient of -0.1 ns/°C. Previous tests have shown that there can sometimes be a good direct correlation [4].

(II) Uplink Tests

Uplink characterization tests were carried out using the configuration presented in

Figure 2. The characterization test hardware in each loop consisted of the components between the Satre modem input and the earth station feed. These included a switch box, a directional coupler, Ku-band mixers, a 14.1 GHz phase-locked local oscillator, attenuators, cables,and horns. An uplink signal of frequency 14.03 GHz was generated by the earth station and transmitted into the horns of two sets of test hardware. The signals received by the two horns were mixed down to 70 MHz using a mixer in each loop and the 14.1 GHz local oscillator. The output from each mixer provided an input for the Satre modem via a switch box.

Measurements were taken for each loop using the Satre modem. The switch box was used to switch between the two loops once per minute. The use of two loops allowed an independent check of the hardware. To allow for measurements to settle down after switching between the loops, measurements corresponding only to the final 30 s of each one minute interval were processed. A mean of these data was taken to provide a representative measurement of the loop delay. The resulting measurements of the Satre modem for each of the two loops (Loops 1 and 2) are shown in Figure 6. The tests show a good correlation between the measurements of Loop 1 and the outdoor temperature with a temperature coefficient of 0.15 ns/°C. The measurements of Loop 2 show a similar but weaker correlation.

(III) Performance of Tests

It is not clear from the measurements for downlink and uplink tests, shown in Figures 3 and 6, what proportion of delay instabilities originate within the test hardware rather than within the earth station. Instabilities within the test hardware could limit the performance of the tests to characterize the earth station. These instabilities can be assessed by subtracting the measurements of one loop from the other. This allows the common contribution of the earth station delay to be removed in order to observe instabilities occurring only within the test hardware.

Figure 5 shows the differences between the two sets of loop measurements taken by the Satre modem in the downlink tests. Indoor and outdoor temperature data are also shown for comparison. It is found that the differences correlate inversely with outdoor temperature. Figure 7 shows the differences between the two sets of loop measurements taken by the Satre modem in the uplink tests. In this case it is found that there is a good direct correlation between the difference in loop measurements and outdoor temperature. These correlations with outdoor temperature indicate that the temperature coefficients of the test hardware in each of the two loops are different. Furthermore, they suggest that the origin of the instabilities are outdoor components. Apart from the horns, which are not expected to show a significant temperature coefficient, the only test hardware located outdoors are cables. We therefore conclude that the cables within the test hardware are the origin of a substantial proportion of the delay instabilities observed using such characterization tests.

3 CABLE CHARACTERIZATION TESTS

Several coaxial cables are used to transmit signals within the earth station, characterization test hardware, and associated time-transfer hardware within the laboratory. As discussed in Section 2, a significant proportion of delay instabilities are found to originate within such cables, particularly those exposed to the large outdoor temperature changes. Consequently, an investigation was carried out on the effect of environmental temperature changes on the signal delays in coaxial cables.

The delay variations within 50 Ω PTFE coaxial cables (Rhophase Microwave Ltd, part number SPS-1751-10000-SPS) have been investigated at Ku-band and L-band using the configurations shown in Figures 8 and 9 respectively. Two 10 m length cables were connected by an attenuator and placed outdoors in order to expose them to relatively large temperature changes. The first test involved propagating Ku-band signals through these cables. The resulting delay and outdoor temperature changes are shown in Figure 10. There is a strong inverse correlation observed between the delay measurements and outdoor temperature, demonstrating that there is a strong dependence of cable delays with temperature. The temperature coefficient is measured to be -0.15 ns/°C. A similar test was carried out by propagating L-band signals through the cables and the resulting measurements are shown in Figure 11. These data also demonstrate a dependence of cable delay with outdoor temperature and the measured temperature coefficient is -0.007 ns/°C.

4 TESTS USING DIFFERENT CODES

The present method of time-transfer employs 2.5 MChip rate coded signals which are available on both the Mitrex and Satre modems. However, a 20 MChip rate code is also available on the Satre modem. The higher bandwidth of this code may offer more stable hardware delays. A comparison has been carried out between the two codes by taking simultaneous measurements using the downlink test configuration shown in Figure 1. The Mitrex and Satre modems were used with 2.5 and 20 MChip rate codes respectively. The results shown in Figures 12 and 13 suggest that an improvement in delay stability is obtained using the 20 MChip rate code. The cause of the large difference in the loop delays (~ 60 ns) is not clear.

5 DISCUSSION

The tests presented in this paper and in previous papers [3, 4] were carried out to investigate the signal delay behaviors of the earth station and characterization hardware in order to realize methods for improving their performance. In Section 2 it was found that the downlink and uplink tests are affected by delay instabilities within the outdoor cables of the test hardware. This limits the performance of the

characterization tests. To improve this it is necessary to reduce the instabilities within the cables.

Results presented in Section 3 demonstrate that PTFE coaxial cables show significant delay instabilities and that cables propagating Ku-band signals show much greater temperature coefficients (by a factor of 20) than cables propagating L-band signals. Cables within the downlink and uplink test hardware are used to transmit Ku-band signals to and from the horns located outdoors. It is clear that these cables could be the origin of the delay instabilities observed within the test hardware in Section 2. This is consistent with the conclusion drawn in Section 2. The instabilities would be greatest for these outdoor cables which are exposed to larger temperature changes.

It is proposed that the delay instabilities within the cables of the characterization hardware could be significantly reduced by transmitting through them at L-band, or possibly at 70 MHz, rather than at Ku-band. This would require a modified characterization configuration involving a Ku-band local oscillator or upconverter located at the antenna.

There are also cables that transmit Ku-band signals between the earth station hardware. These are expected to be the origin of significant delay instabilities within the earth station. By modifying the configuration of the earth station it would be possible to avoid transmitting Ku-band signals through long lengths of cable. The results from Section 3 suggest that the delay instabilities in such cables could be reduced by about an order of magnitude. This would lead to a significant improvement in the time-transfer performance of the earth station.

The increased stability of the 20 MChip rate coded signal described in Section 4 can be explained in terms of its much narrower correlation function. This results in any reflected signals within the earth station having a smaller perturbing effect due to less overlap of the correlation functions generated from the main and reflected signals. Consequently, any changes in the reflected signals will result in smaller changes in the earth station delay and lead to a greater stability.

6 CONCLUSIONS

The results presented in this paper lead us to the following conclusions.

- The delay instabilities of separate characterization loops as well as the differences between them are found to correlate with temperature. The performance of NPL's downlink and uplink characterization tests is presently limited by delay instabilities within the outdoor cables of the test hardware.

- Tests carried out on PTFE coaxial cables demonstrate that they can have significant temperature coefficients. The tests have also shown that PTFE coaxial cables propagating L-band signals have much lower temperature coefficients than cables propagating Ku-band signals.

- PTFE coaxial cables transmitting Ku-band signals between different hardware are the origin of delay instabilities within NPL's characterization and earth station hardware. It is proposed that the instabilities could be reduced by transmitting signals at L-band, or possibly at 70 MHz, through the cables.

- The use of 20 MChip rate coded signals lead to more stable earth station delay
- measurements than using 2.5 MChip rate coded signals.

7 REFERENCES

[1] D. Kirchner, "Two-way time transfer via communication satellites," in Proceedings of the IEEE, Special Issue on Time and Frequency, July 1991, vol 79, no 7, pp. 983-990.

[2] G. de Jong 1989, "Accurate delay calibration of satellite ground stations for two-way time transfer," Proceedings of the 3rd European Frequency and Time Forum (EFTF), 21-23 March 1989, pp. 198-203.

[3] J. A. Davis and P. R. Pearce, "Characterisation of the signal delays in a ground station designed for two-way time transfer," Proceedings of the 7th European Frequency and Time Forum (EFTF), 16-18 March 1993, pp. 113-118.

[4] J. A. Davis, J. M. Furlong and J. D. Clarke, "The performance and characteristics of a two-way time transfer earth station incorporating a new Satre modem," Proceedings of the 12th European Frequency and Time Forum (EFTF), 10-12 March 1998, pp. 169-174.
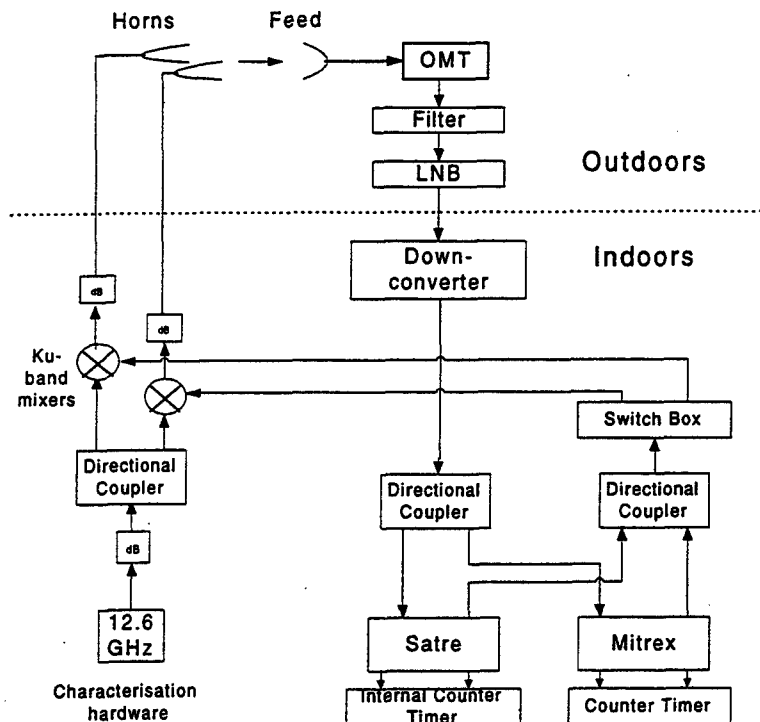
Figure 1. Downlink characterization test configuration.
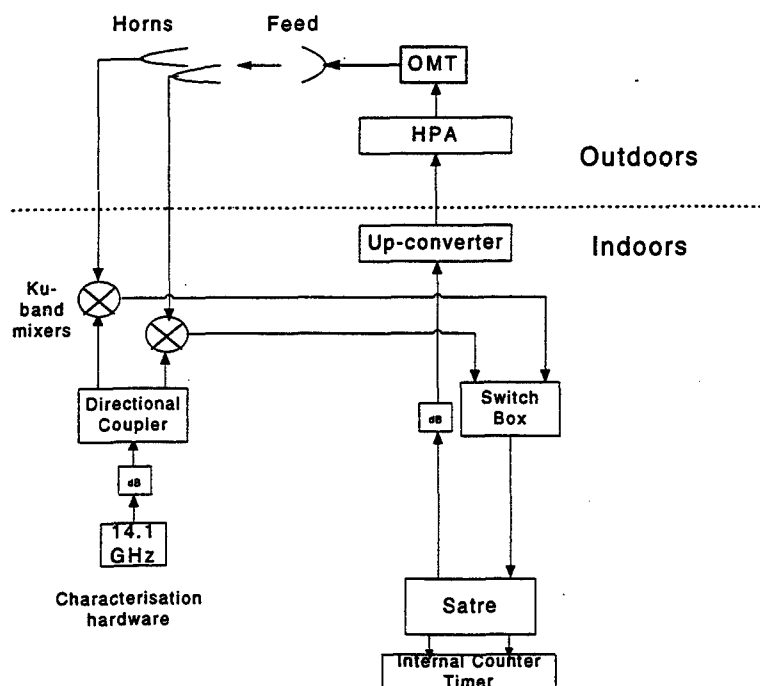
Figure 2. Uplink characterization test configuration.
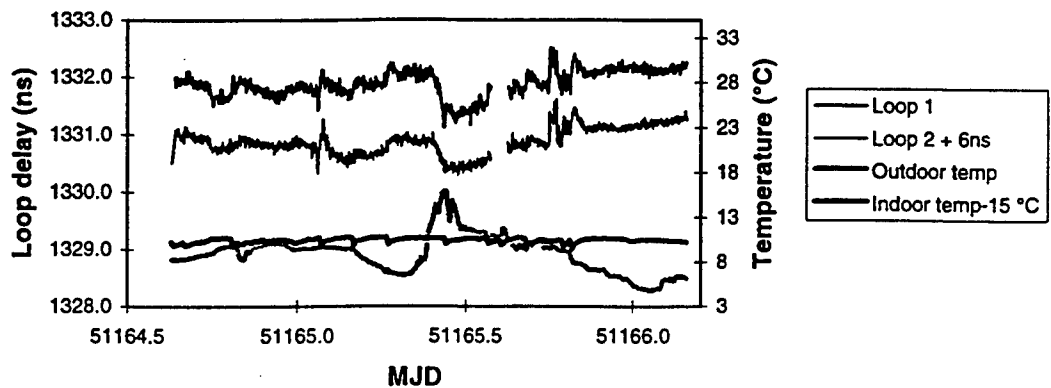
Figure 3. Measurements for two downlink characterization loops taken using the Mitrex modem. Indoor and outdoor remperature data are also shown.
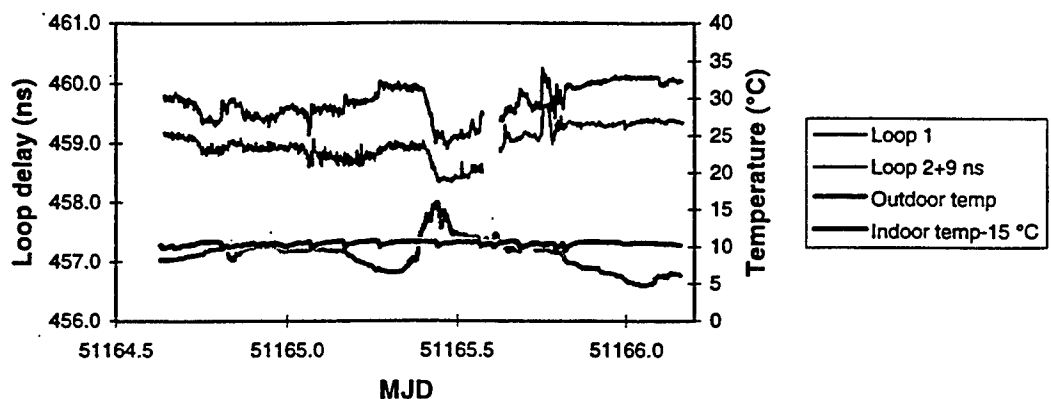
Figure 4. Measurements for two downlink characterization loops taken using the Satre modem. Indoor and outdoor temperature data are also shown.
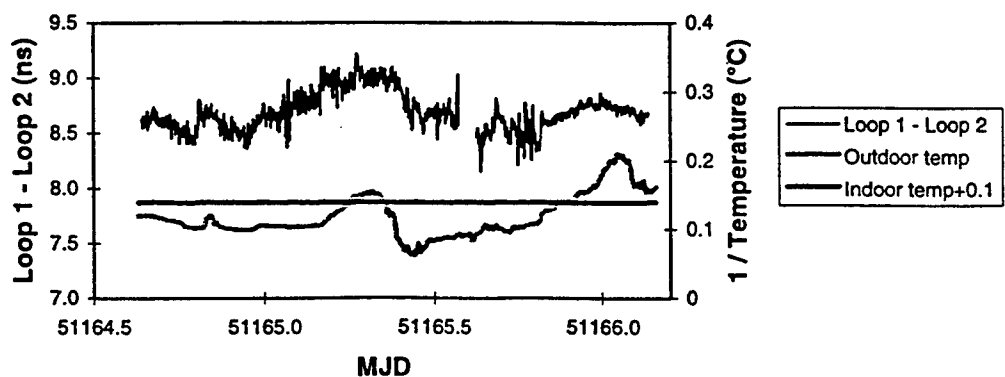
Figure 5. Difference between downlink characterization loop measurements of the Satre modem. Indoor and outdoor temperature data are also shown.
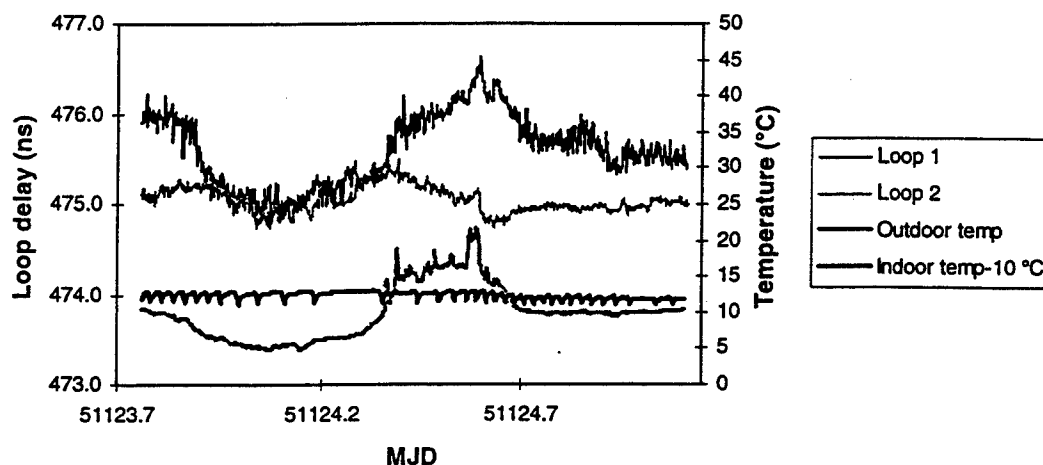
Figure 6. Measurements for two uplink characterization loops taken using the Satre modem. Indoor and outdoor temperature data are also shown.
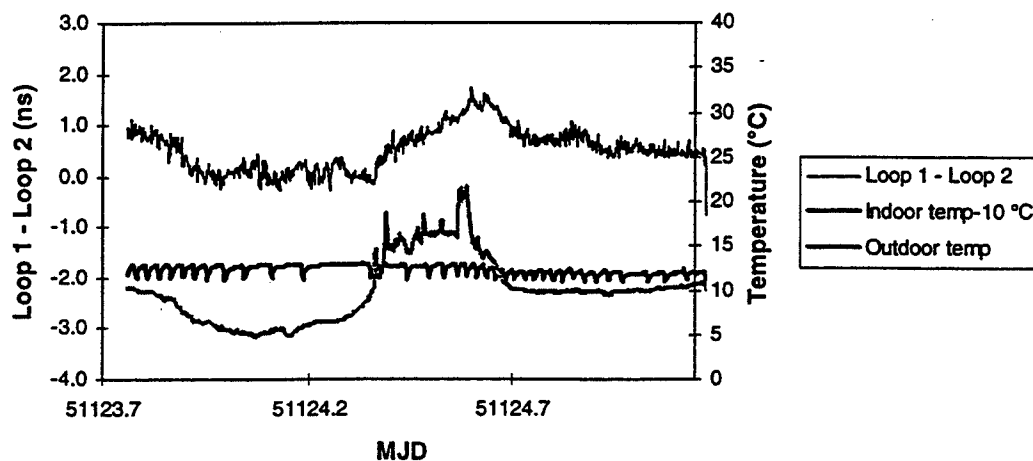
Figure 7. Difference between uplink characterization loop measurements of the Satre modem. Indoor and outdoor temperature data are also shown.
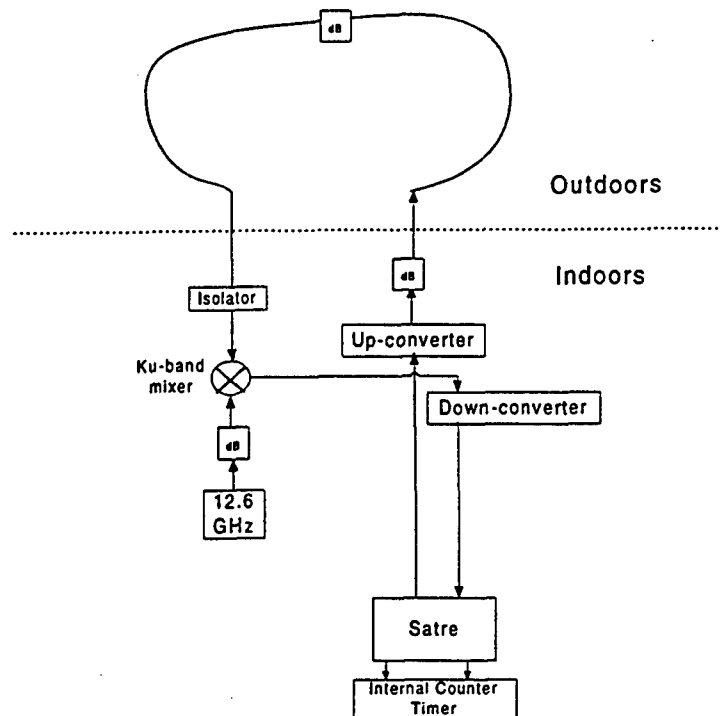
Figure 8. Configuration used to investigate Ku-band signal delay variations in PTFE cables.
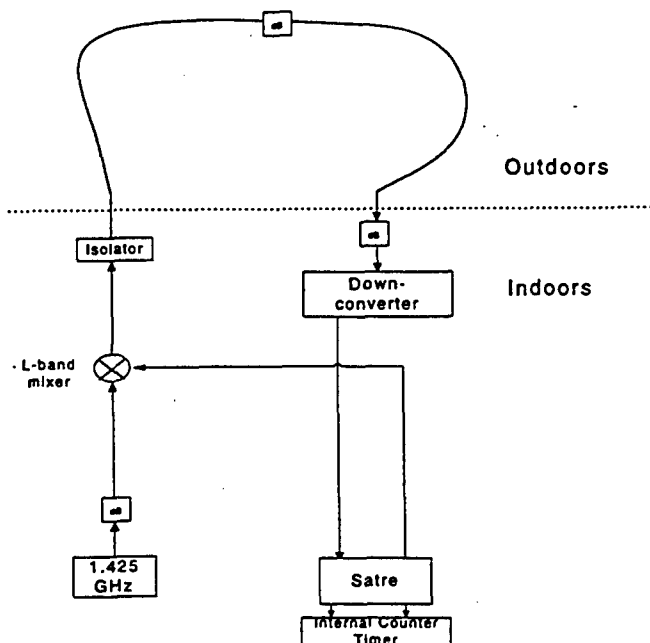
Figure 9. Configuration to investigate L-band signal delay variations in PTFE cable.
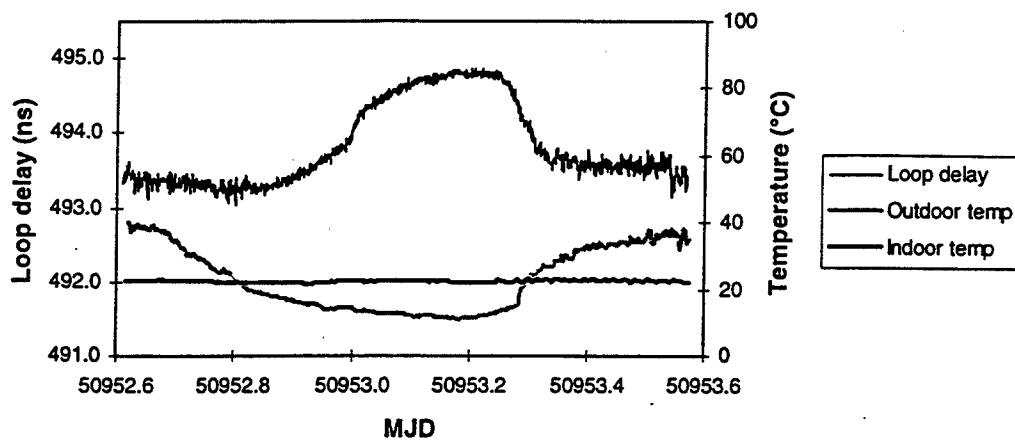
Figure 10. Measurements taken for Ku-band cable tests. Loop delay measurements have been taken with the Satre modem. Temperature data also shown.
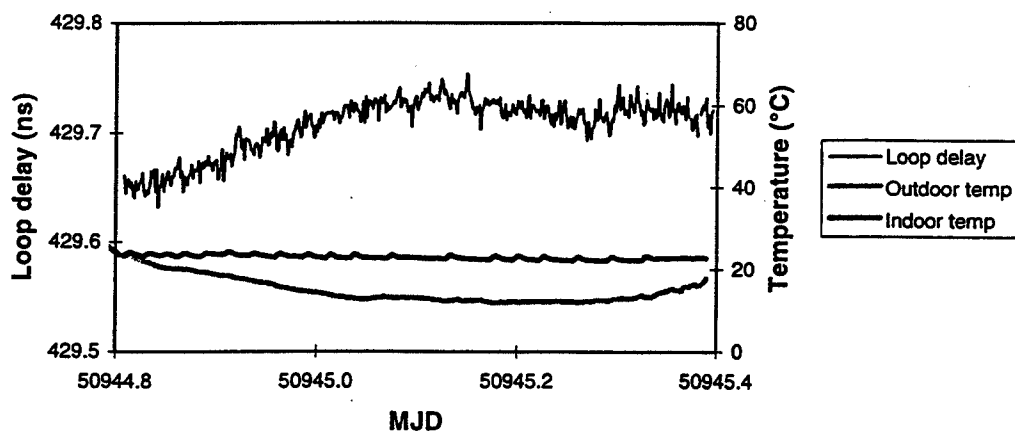
Figure 11. Measurements taken for L-band signal cable tests. Loop delay measurements have been taken with the Satre modem. Temperature data are also shown.
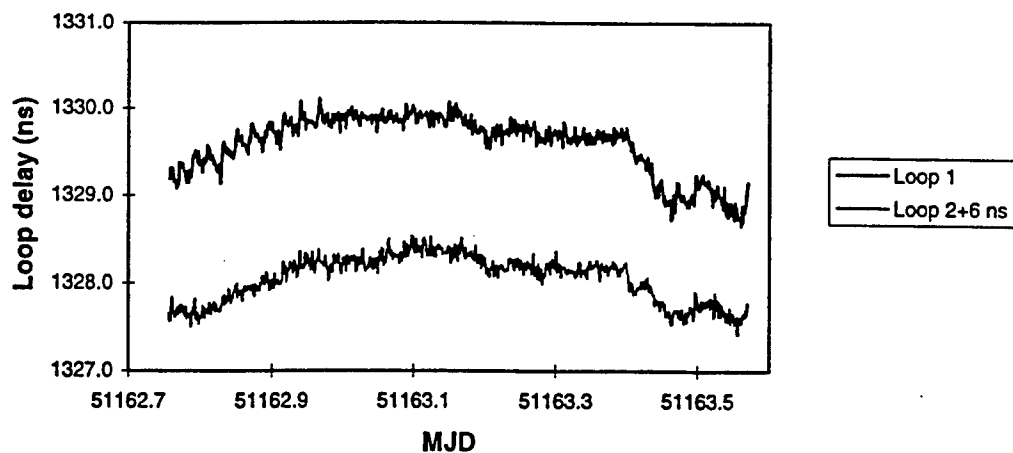
Figure 12. Measurements for two downlink characterization loops taken using the Mitrex modem.
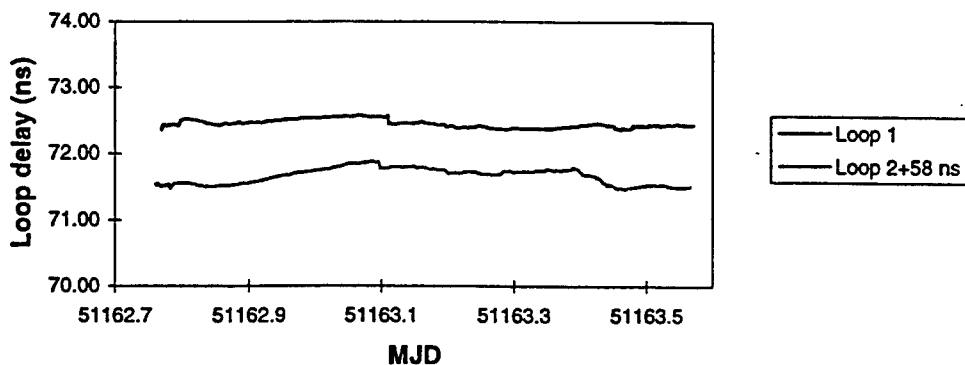
Figure 13. Measurements for two downlink characterization loops taken using the Satre modem.

340

TWO-WAY SATELLITE TIME TRANSFER (TWSTT) APPLICATIONS WITH THE EASTERN RANGE

I. Galysh, D. Koch, R. Beard
U.S. Naval Research Laboratory
4555 Overlook Ave., SW, Washington, DC 20375, USA

W. Reid
SFA, Inc.

J. Buisson
Antoine Enterprises

Abstract

The Eastern Range at Cape Canaveral, as part of the Range Modernization program, is incorporating Two-Way Satellite Time Transfer (TWSTT) systems into their stations. A detailed study of the mechanization of TWSTT into their systems had been performed and an experiment into different satellite links has been reported before. A design implementation has been completed. Acceptance testing was successfully performed at the Naval Research Laboratory (NRL), including over-the-air testing prior to the first installation at the Range Operation Control Center (ROCC), Cape Canaveral. The first phase of ROCC installation was completed in July 1998.

The results of acceptance testing at NRL indicated a sub-nanosecond time transfer capability. Data from those tests will be presented and discussed. Installation test data from the initial phase will be presented. Calibration of these units for absolute time comparison was difficult, but will support a nanosecond-level capability. The calibration methods and results will be described.

INTRODUCTION

The TWSTT System being installed at the Eastern Range will include its own time transfer network, where the Range Operations Control Center (ROCC) will be the master site and the down range sites will be targets. The network will operate in C-band using an Intelsat global transponder. The ROCC will also operate as a target site and perform time transfers with the DoD Master Clock at USNO over a Ku-band satellite link.

In April of 1998 a factory acceptance test was performed at NRL for the Air Force to demonstrate the operation and performance of the TWSTT modems. In July of 1998, the first phase of the network installation was completed by the installation of a TWSTT modem at the ROCC with a Ku-band Very Small Aperture Terminal (VSAT). A site acceptance test was performed and the equipment was accepted. The link to the DoD Master Clock was established. Operational time transfers began in November 1998.

TWSTT CONFIGURATION AND OPERATION

Figure 1 shows a diagram of the hardware configuration of the TWSTT system. Each site within the TWSTT system contains a TWSTT Modem, and a VSAT coupled to a 1.4-meter parabolic antenna to

enable synchronization measurements via a leased geostationary communication satellite transponder. Two-way time transfer communications require approximately 4 MHz of transponder bandwidth and up to three time transfers can be performed in 30 minutes.

Two-way time transfer between two time standards is accomplished by having each of the standards send their 1 Pulse Per Second (1-PPS) signal to the other over a communications circuit. The TWSTT modem sends the 1-PPS using a Pseudo-Random Noise (PRN) code modulation. The transmission medium and the satellite electronics introduce delays, but by sending both directions the delays will be nearly reciprocal. Each site measures the time interval between the transmission of its local 1-PPS and the time it receives the remote site's 1-PPS signal. This exchange continues for 300 seconds to complete a time transfer. The time offsets of the two standards during the exchange can be measured very precisely (0.2 nanoseconds) and accurately (1.0 nanoseconds). By performing time transfers over a period of time, the long-term behavior of the time standard, i.e. frequency changes, rates, jumps, drifts, etc., that affect the accuracy and stability, and, thus, the operational usefulness of a clock may be accurately characterized. Improved confidence in decision making is a key benefit. The day-to-day stability of two-way time transfers can very nearly reach the performance of the best reference clocks.

There are two different satellite links to be used for the Eastern Range TWSTT System. The first link is between the DoD Master Clock and ROCC via G-STAR I in the Ku-band. The second link is between ROCC and the three downrange sites on an Intelsat satellite via a global coverage C-band transponder. The ROCC TWSTT system has a radio frequency switch to the antenna connections for selection between the Ku-band antenna and C-band antenna.

The configuration of the TWSTT modem has changed from that previously reported [1]. The TWSTT modem being deployed in this project is the fourth revision of the NRL-designed modem. Generation four of the TWSTT modem is a repackaging of generation three. The third generation TWSTT modem used previously consists of two Electronic Industries Association standard 19-inch rack-mountable chassis. One chassis contains the TWSTT Modem's computer, and the other contains the VSAT interface and the frequency source. The fourth generation computer chassis is now a single standard rack mount personal computer chassis with all connections in the rear, unlike the PCXI chassis previously used. This change was made because the PCXI chassis has been discontinued. The VSAT Interface has some circuit redesign to improve stability and reliability. More of the hardware is now digital. A color LCD display has been added to eliminate the need for an external monitor and a flip-up keyboard was also added.

The operating system is LINUX, using kernel version 2.0.34. This change was due to the need to update the CPU to Pentium II motherboards, since older motherboards are being phased out of production. The newest version of the operating system supports the newer motherboard chipsets. The TWSTT modem software has gone through maintenance updates and a few improvements. The user interface was updated to add keyboard control in addition to the mouse operations. These changes simplify the software installation. Originally the software was installed in the root directory and operated from there. The software was relocated to another directory and now allows multiple separate user accounts in operation of the TWSTT system.

FACTORY ACCEPTANCE TEST

Before deployment and installation of the TWSTT system to the ROCC, an Acceptance Test was conducted at NRL. The Test was setup as shown in Figure 2. Both TWSTT systems were located at NRL and a Ku-band satellite link was used as the communication medium. The Time Interval Counter (TIC) between the

two frequency standards was used as the comparison reference. The performance was demonstrated during a ten-day test period where three time transfers were performed per day.

Thirty-two time transfer measurements were performed with three measurements per day, as shown in Figure 3. The extra two measurements were performed because of extra satellite time. Four significant outliers can be readily seen in the data, the largest being 18 milliseconds. These outliers have been attributed to transponder interference resulting from the user of the previous communication satellite time slot not completing transmission by the end of their assigned time slot. This type of interference can be operationally avoidable to prevent corruption of the time transfer measurements. The fourth outlier was one of the extra measurements performed. With the outliers and the other extra measurement taken deleted, the remaining 27 measurements were used to demonstrate performance. The phase offset between the two standards was determined with an RMS deviation about a linear least-squares fit to 2.6 nanoseconds. The offset of the two clocks determined by the TIC is shown for the same period in Figure 4. These measurements have an RMS deviation about linear least-squares fit of 3.0 nanoseconds. The larger different in the TIC measurement has been attributed to the 100 sec averaging time for the counter providing a short-term measure on the HP 5071. Differencing the offsets between the two clocks provides a measure of the performance of the TWSTT and associated equipment and the result is shown in Figure 5. The data have an RMS deviation about a linear least-squares fit of 1.8 nanoseconds. Removal of one data point, from MJD 50927 which has a phase offset of 8 nanoseconds, would result in an RMS deviation of less than 1 nanosecond.

CALIBRATION

An important element in the installation of the TWSTT system at the ROCC was the method to calibrate it for accurate over-the-air operation. Pre-calibration was not possible due to possible configuration differences at the installation site. The TWSTT modem was calibrated by taking a portable atomic clock, HP5071A Opt 001, to USNO and synchronizing it with the Master Clock. The time difference of the 1-PPS between the portable atomic clock and the Master Clock and drift were recorded along with the time of measurement. The portable atomic clock was then transported to the ROCC. After connecting the atomic clock 5 MHz and 1-PPS signals to the appropriate ports on the TWSTT modem, the modem was configured to operate as a target site. The time transfer tests performed during the site acceptance with TWSTT relative to USNO were performed using the portable atomic clock. The portable atomic clock was transported back to USNO after the site acceptance testing and the time difference between the atomic clock 1-PPS and the Master Clock 1-PPS was measured. By using the portable atomic clock as the reference at the ROCC the capability of the TWSTT link was compared to an independent precise clock synchronized to USNO. The resulting difference in time as measured at the ROCC and the portable clock was the composite uncalibrated delays in the TWSTT system. As a result the calibration factor was determined to be 81.3 nanoseconds.

SITE ACCEPTANCE TEST

After the physical installation of the TWSTT equipment at the ROCC, an acceptance test was performed to verify the operational capabilities of the TWSTT system at the site. This includes interoperability with the facility, expected operating procedures, and system performance. The system performance portion of the acceptance test consisted of three time transfers at Ku-band twice per day for five days. Each time transfer consisted of 300 one-second measurements. Three time transfers were taken during a half-hour period. Figure 6 shows the equipment configuration. Simultaneously measurements were made using a keyed GPS

receiver at the ROCC operating on a common-view time transfer schedule with USNO. The portable clock discussed above was also used as the local clock for the GPS common-view measurements.

Thirty-one TWSTT measurements were made over a period of eight days and are presented in Figure 7. The measurements plotted show phase offsets between the two clocks of -170.7 nanoseconds at the mid-point of the data interval. These measurements are shown in Figure 8 to have an RMS deviation about a linear least squares fit of 1.2 nanoseconds.

The phase and frequency offset of the two clocks determined by GPS receiver are shown in Figure 9 to be -80.1 nanoseconds and -8.7 pp 10^{14} at the midpoint of the data interval. These measurements are shown in Figure 10 to have an RMS deviation about a linear least squares fit of 10.2 nanoseconds. This less precise result was expected; however, the results confirm the range and trend of the TWSTT data. The phase and frequency offsets between the portable atomic clock and the DoD Master Clock before and after the acceptance test period can be seen from Figure 11 to be -89.4 nanoseconds. Although the data from the portable clock is not continuous and limited, it was believed that based on the performance of the HP 5071 that interpolation between the data points was a reasonable method of estimating performance during the test.

In Figure 12, the data from the three time comparison methods between the ground reference clock at the ROCC from the DoD Master Clock are shown relative to each other. The TWSTT and the portable clock measurements were differenced to obtain the calibration of the TWSTT and the associated equipment. The result of adding the calibration factor of 81.3 nanoseconds to the TWSTT measurements is shown in Figure 13, where it can now be seen that the TWSTT measurements closely agree with the portable clock measurements.

CONCLUSIONS

The factory acceptance test results performed at NRL had overall phase offset variations of up to 7 nanoseconds, but the individual time transfer sessions demonstrated sub-nanosecond phase offset performance on a day-to-day basis when compared with the TIC as seen in Figure 5. The technique of performing three consecutive time transfers for a half-hour measurement session was confirmed as a good operational practice, as witnessed during the first half of this test. The satellite interference observed during the factory test never lasted for the entire 30 minutes of test time and, thus, gave an indication of the quality of the time transfer session.

The site acceptance test results demonstrated overall phase offset variations of up to 6 nanoseconds, but once again the individual time transfer sessions demonstrated sub-nanosecond phase offset on a day-to-day basis. Performing the portable clock trip for calibration was the best method for this site because of the dynamic configurations that were occurring at the time. This site acceptance test would have benefited from more portable clock measurements during the test period, but this was not logistically possible at the time. The small difference in the slope or frequency offset may be attributed to the uncertainty in the portable clock measurements. With multiple portable clock measurements the RMS deviation and resulting uncertainty could be better determined.

Overall the results were quite satisfactory. The methods and techniques used in these tests will form the basis of further testing and calibration in the extension of the TWSTT network to the down range stations of the Eastern Range.

REFERENCES

1. I. J. Gaylsh, D. M. Craig, W. Reid, and J. A. Buisson *"Performance Analysis of the GPS Monitor Station Subsystem Enhancement Program at the Naval Research Laboratory,"* Proceedings of the 1996 Annual Precise Time and Time Interval (PTTI) Applications and Planning Meeting, 3-5 December 1996, Reston, Virginia, U.S.A., pp. 417-428.
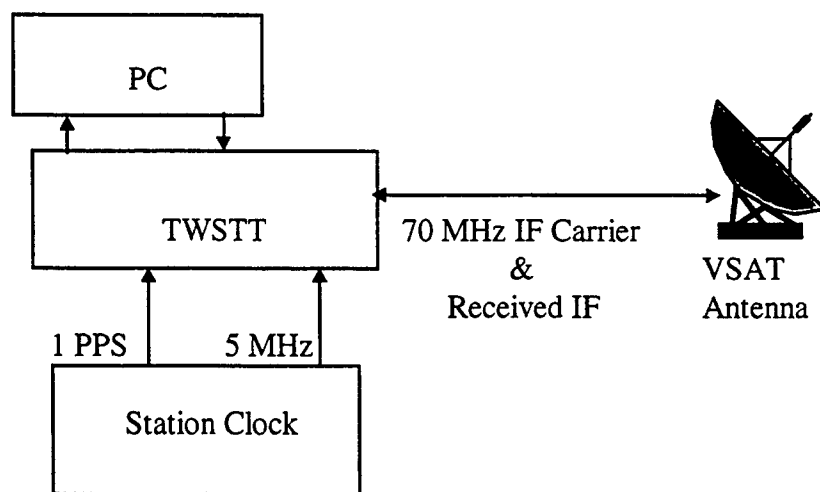
Figure 1. TWSTT Hardware Block Diagram
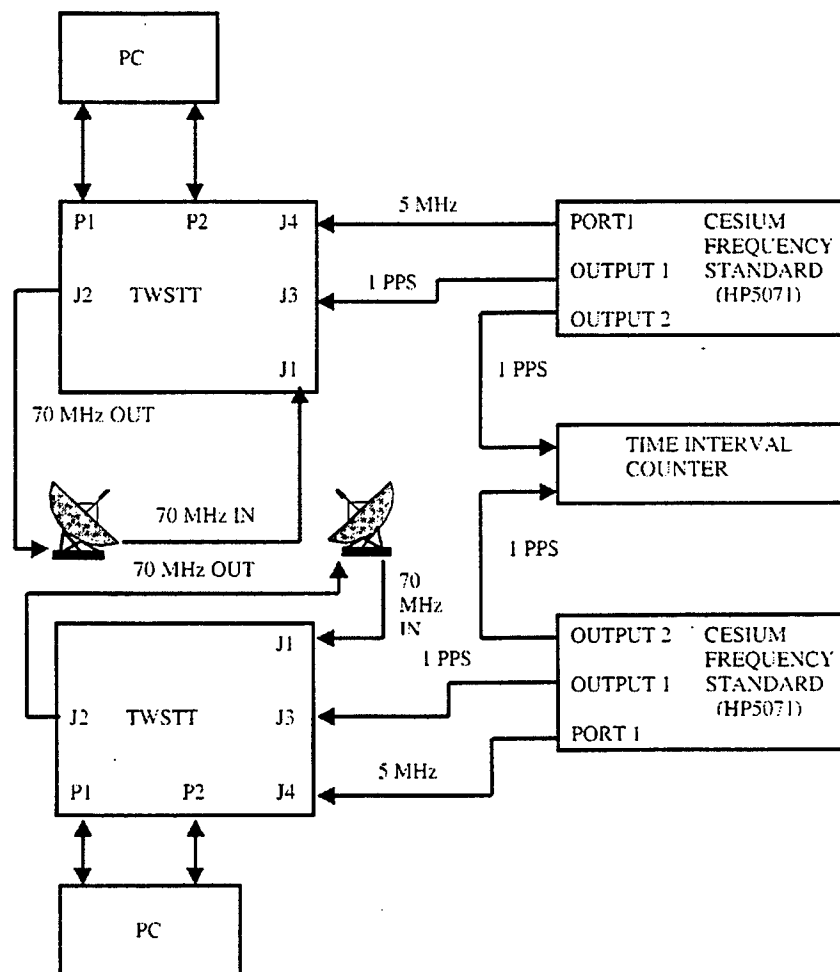
Figure 2. Factory Acceptance Test Hardware Block Diagram
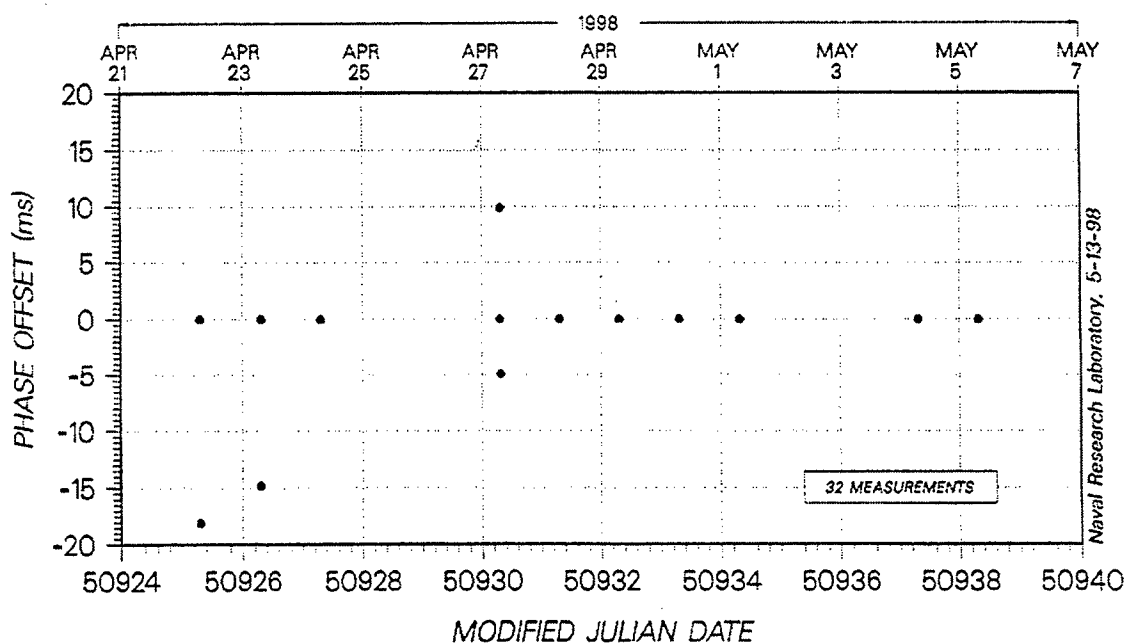
Figure 3. Factory Acceptance Test Results
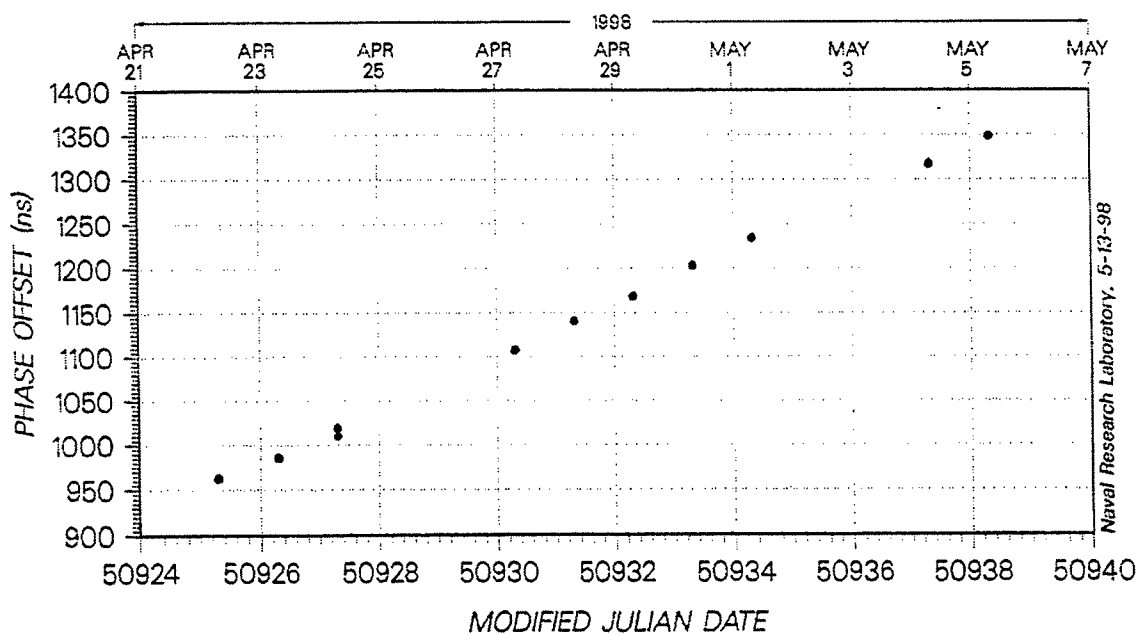
Figure 4. Factory Acceptance Test TIC Measurements

347
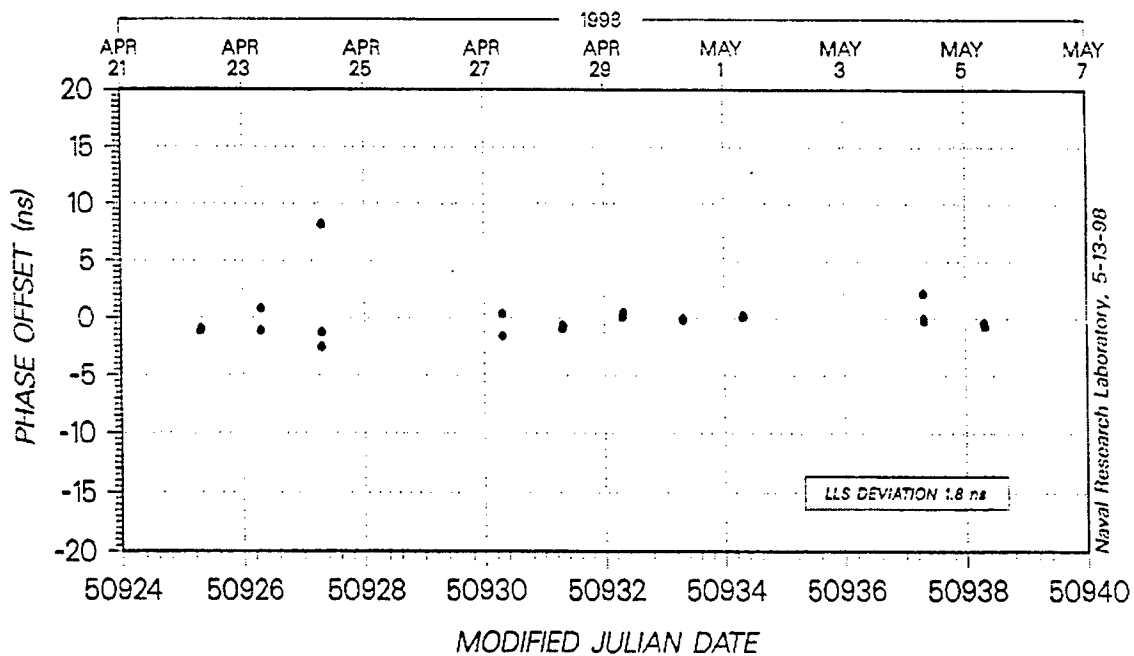
Figure 5. Factory Acceptance Test (TWSTT - TIC) Measurements
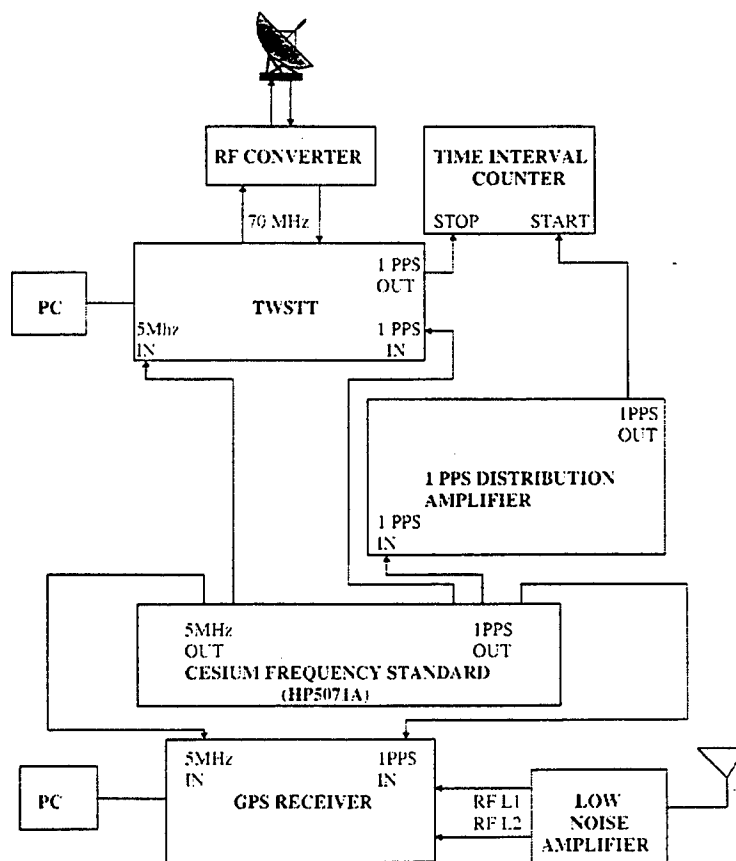
Figure 6. Site Acceptance Test Hardware Block Diagram
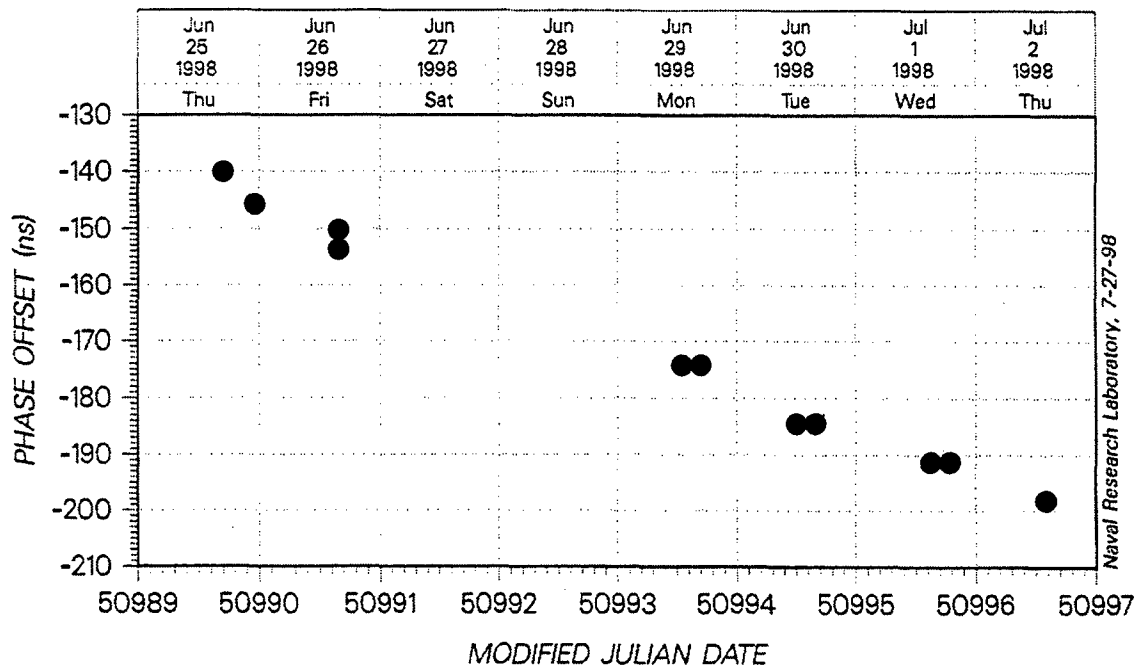
Figure 7. Site Acceptance Test Results
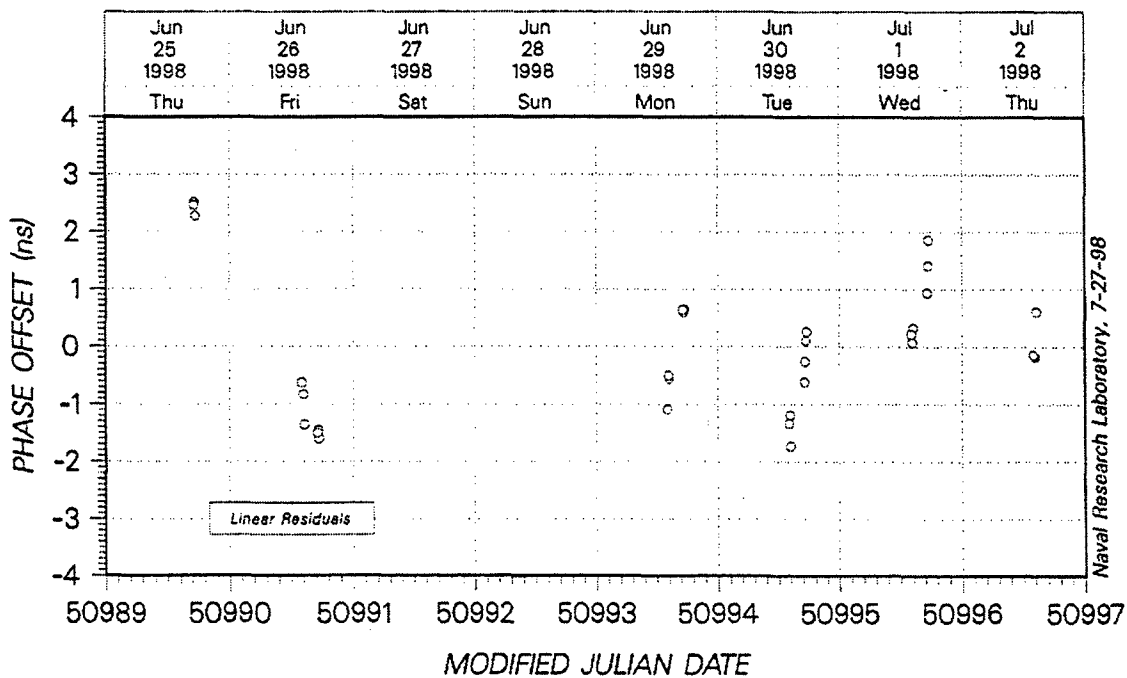
Figure 8. Linear Residuals of Site Acceptance Test Measurements
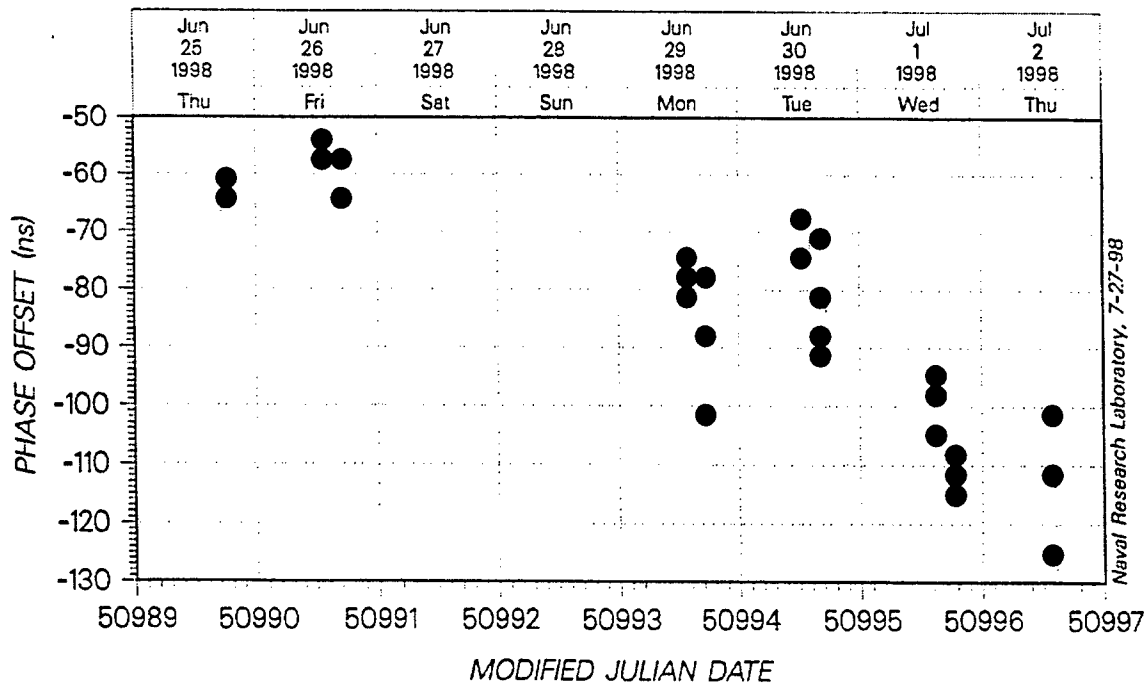
Figure 9. Site Acceptance Test Comparison Results by GPS Common View
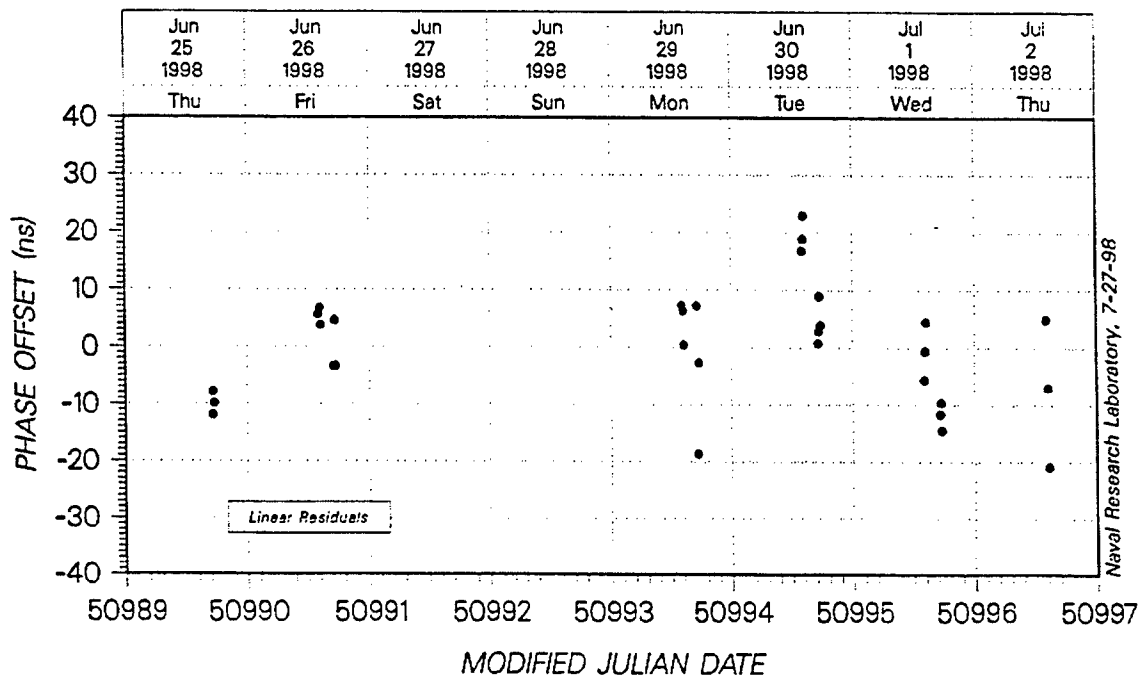
Figure 10. Linear Residuals for Site Acceptance Test GPS Common View

350
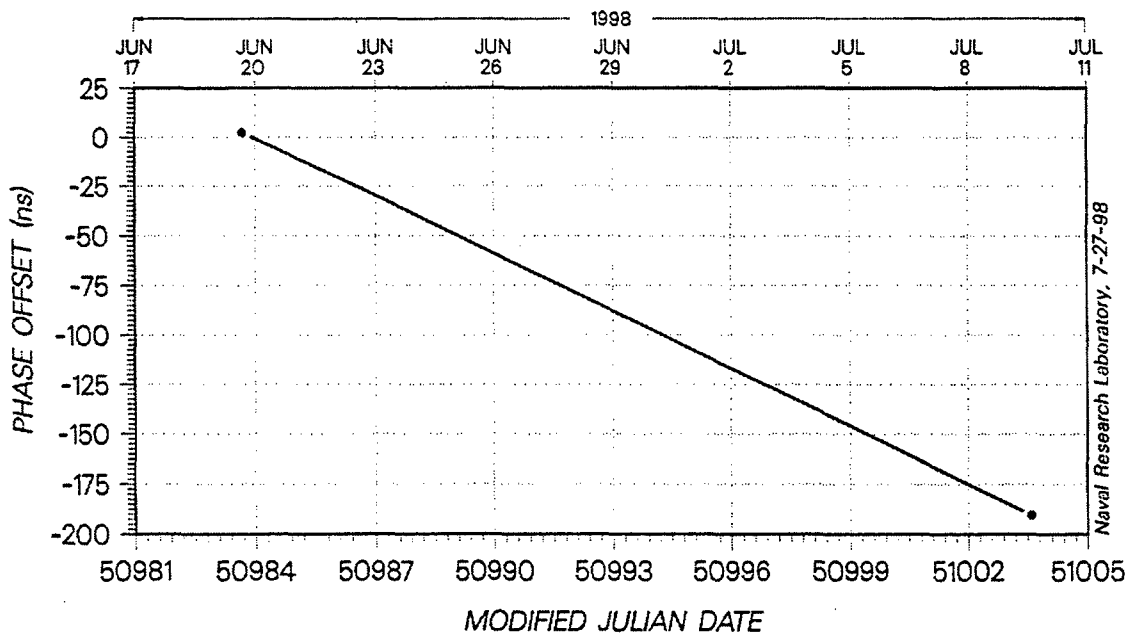
Figure 11. Site Acceptance Test Portable Clock Comparison

Figure 12. Site Acceptance Test Combined Results of Time Transfer Methods
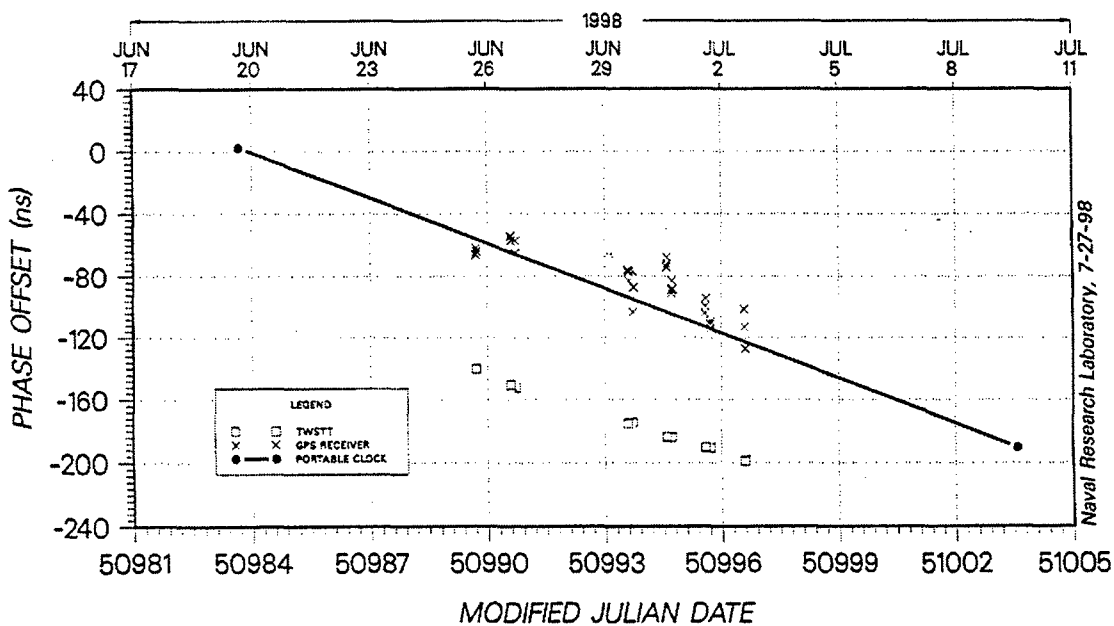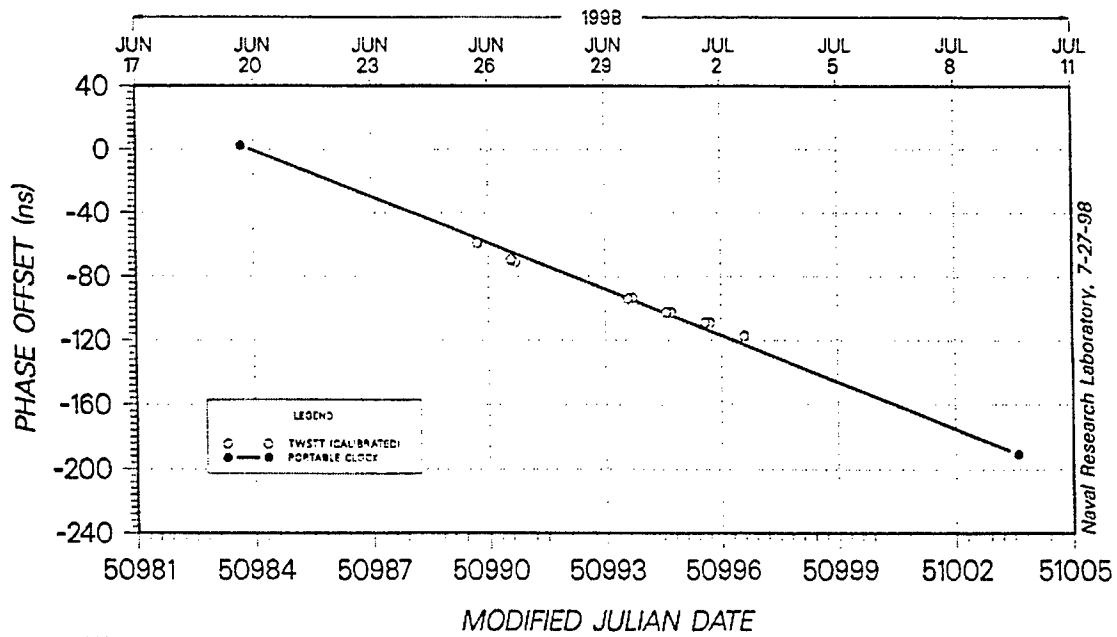
Figure 13. Site Acceptance Test Comparison of TWSTT with Calibration Factor

Questions and Answers

JIM DeYOUNG (USNO): Are there any plans for ongoing or continuous monitoring of the calibration to see how it is going to change over time? Or is this just going to be a one-shot calibration?

DOUGLAS KOCH (NRL): I guess they will look at the data, but this is a one-shot calibration for this initial installation. They follow one installation at the down range sites; each one will be calibrated very much the same way.

MIHRAN MIRANIAN (USNO): I know what GPS receiver you use, and that has a notoriously bad time-interval counter built into it. That is probably why you got your 10 nanoseconds --. If you use an external counter, you could probably do a lot better than that.

TWO-WAY SATELLITE TIME TRANSFER ACTIVITIES IN ASIAN-PACIFIC REGION

Michito Imae, Mizuhiko Hosokawa, Kuniyasu Imamura, Hirotaka Yukawa, Yasuhisa Shibuya
Communications Research Laboratory
4-2-1, Nukuikita-machi, Koganei-shi, Tokyo, 184-8795 Japan

Peter T. H. Fisk, Steve Quigg, Malcolm A. Lawn, John S. Thorn, Michael J. Wouters, Colin T. Coles
National Measurement Laboratory, Australia
PO Box 218, Lindfield NSW 2070, Sydney, Australia

Li Zhang
Shaanxi Astronomical Observatory
P. O. BOX 18, Lintong, Xian, China

Kazuhiro Nakadan
National Research Laboratory of Metrology, Japan
1-1-4, Umezono, Tsukuba-Shi, Ibaraki-Ken 305-8563, Japan

Abstract

Two-Way Satellite Time Transfer (TWSTT) is one of the most precise time transfer techniques, and time transfer using this method has been used between European and North American Time and Frequency laboratories on a regular bases. In the Asia-Pacific Region four Time and Frequency laboratories have been involved in establishing a precise time transfer network using the TWSTT technique.

After several continuous 24-hour TWSTT experiments between Communications Research Laboratory(CRL) in Japan and National Measurement Laboratory(NML) in Australia, a regular, twice weekly TWSTT link has been established since April 1998 using a Ku-band transponder on INTELSAT satellite 702 located at 177 deg. E.

CRL and Shaanxi Astronomical Observatory of Chinese Academy of Science(CSAO) have just established a precise time transfer link using the TWSTT technique from October, 1998. For this time transfer link we are using a Ku-band transponder on the JCSAT-3 satellite, which is owned by Japanese satellite communication company and is located at 128 deg. E. National Research Laboratory of Metrology(NRLM) in Japan is also planning to join the TWSTT link network with a link to CRL also using JCSAT-3 from March1999.

For the next step toward a global TWSTT network we are planning to connect the Asia-Pacific TWSTT link to European and North American time and frequency laboratories. Such a

network of precise time transfer links will not only by itself be useful in contributing to TAI and UTC but also provide an accurate time transfer reference for other precise time transfer techniques such as the GPS carrier phase method.

INTRODUCTION

The basic research on Two-Way Satellite Time Transfer(TWSTT) has been started from the 1960's[1-2] and remarkable progress was made in the 1970's and 1980's[3]. Due to its high potential for accuracy and precision, the TWSTT technique is expected to be one of the highly accurate time transfer methods for the next generation, and to investigate and to realize TWSTT network, the working group on TWSTT(presently TWSTFT) has been organized under the CCDS(present CCTF). Depending on this working group activities, Time and Frequency institutes in Europe and USA are making great efforts to realize this method as a practical tool to contribute to TAI[4-5,8-9].

In the Asian-Pacific region, the history of the research work in the field of TWSTT is also very long; several significant works were performed[3,6-8], but they could not be realized as a practical one.

Recently several Asian-Pacific Time and Frequency institutes are making an effort to establish a TWSTT network in this region and some links are already established and the time transfer using TWSTT have been performing on a regular basis. They are also planning to expand this network.

SITUATION OF T&F INSTITUTES IN ASIAN-PACIFIC REGION

In Asian-Pacific region more than ten Time and Frequency institutes which are contributing to TAI are distributed. Figure 1 shows their locations in this region. The numbers of atomic clocks for TAI in this region are about 40, and it corresponds to 15-20 % of all the clocks in the world. Also these institutes are making studies of construction of primary frequency standards, such as optically pumped Cs beam standards, atomic fountain type Cs standards and ion storage type frequency standards. Some institutes in this region recently started the uncertainty evaluation of primary frequency standards and they attained a stability at the level of $2\text{-}3 \times 10^{-14}$. Therefore it can be said that this region is one of most significant areas for the construction of TAI and UTC.

PRESENT TIME TRANSFER NETWORK FOR TAI

Figure 2 shows the GPS common-view time transfer network for the TAI organized by BIPM using GPS L1 single channel time transfer receivers. There are three node stations in the world for each area, and CRL is the node station for Asian-Oceania region. The delay calibration work of GPS receivers in this region which was organized by BIPM was performed in 1996, among

OP, NML, MSL and CRL. It is difficult to say the GPS time transfer link in this region is well enough calibrated, because it was only for three institutes and done only once. In addition this region is quite wide and the performance of GPS common-view method is not good enough for precise time transfer; therefore a new time transfer method should be considered.

TWSTT NETWORK AROUND ASIAN-PACIFIC REGION

The Major T&F institutes in Asian-Pacific Region are constructing a TWSTT network in this region under mutual cooperation. Main tools for this TWSTT network are the following:

Time transfer modem: TWT-100 "Atlantis Modem",
Earth station: 1.8 m dish Ku-band station which has 4 W of transmission power,
Satellite: INTELSAT 702 for CRL-NML link,
                        JCSAT-3 for links except for CRL-NML link.

JCSAT-3 satellite is owned by Japanese satellite communication company and located at 128 deg. E.

CRL-NML LINK

CRL(Communications Research Laboratory) and NML(National Measurement Laboratory) is conducting TWSTT using INTELSAT 702 satellite on 177 deg. E. The first TWSTT experiment between CRL and NML was performed in October 1997. CRL and NML have been performing TWSTT twice weekly on a regular basis. Figure 3 shows the time transfer results from June 1998 to November 1998. Two institutes are using a hydrogen maser as the reference clock for TWSTT to evaluate the performance of the system.

CRL-CSAO LINK

TWSTT link between CRL and CSAO(Shaanxi Astronomical Observatory in China) has been just started the end of October, 1998 on a regular basis using JCSAT-3 satellite with Ku-band. Figure 3 shows the preliminary results of this link. CSAO uses UTC(CSAO) and CRL uses a hydrogen maser as the reference clock for TWSTT.

NRLM

The National Research Laboratory of Metrology(NRLM) in Japan is preparing a TWSTT equipment, a TWSTT modem and a Ku-band earth station, to conduct a TWSTT between CRL using JCSAT-3. NRLM and CRL will make TWSTT starting from March, 1999.

TL and KRIS

The TWSTT experiments were performed between CRL and TL(Telecommunications Laboratory of Chaunghwa Telecom in Taiwan) and also between CRL and KRIS(Korean

Research Institute of Standard in Korea) in 1992[7-8]. But they were not continuous ones. TL and KRIS are planning to join the TWSTT Asian-Pacific network in near future. TL and KRIS are discussing with CRL to prepare the equipment for the TWSTT.

PROBLEMS TO BE SOLVED FOR HIGHER ACCURACY

TWSTT method has high potential for accurate time transfer in principle, but there also exists several problems to be solved to improve its accuracy and precision. They are :
1) Technical one
Calibration of internal delay change of the equipment including delays of earth stations.
 To compensate this problem CRL is designing to develop a new modem which has a self-calibration function.

2) Operational one
It is difficult to make time transfer by full automatic mode due to the reason that one should transmit a signal to the satellite and it needs to confirm to the satellite operation center just before the signal transmission.

3) Satellite link fee
To perform the TWSTT requires payment for the satellite link and it is not cheap at present. This problem limits the frequency and duration of time transfer, which are one of the reason for the degradation of the total performance of TWSTT. There needs to be further efforts to realize TWSTT as an economical time transfer method. But one should remember that GPS is free to the users in fact, but the construction cost and operation cost exceeds more than 10 billion US$.

4) Existence of suitable communication satellite for TWSTT.

CONCLUSION ABOUT REALIZATION OF A GLOBAL TWSTT NETWORK

The TWSTT network among four major time and frequency institutes, CRL, NML, CSAO, and NRLM, in Asian-Pacific region will be constructed by March, 1999. To expand this network in this region TL in Taiwan and KRIS in Korea will join to this network in near future.

As a next step to realize a real global TWSTT network, we should connect this Asian-Pacific network to European and American ones.

Such a TWSTT network is useful not only for improvement of accuracy and stability of TAI, but also for comparison of another precise time transfer method, such as GPS carrier phase method.

REFERENCES

[1] J. M. Steele, W. Markowitz, and C. A. Lidback, "Telstar Time Synchronization," IEEE Trans. Instrum. Meas., Vol. 13, 1964.

[2] W. Markowitz, C. A. Lidback, H. Uyeda, and K. Muramatsu,"Clock Synchronization via Relay II Satellite," IEEE Trans. Instrum. Meas., Vol. 16, 1966.

[3] Y. Saburi, M. Yamamoto, and K. Harada, "High-Precision Time Comparison via Satellite and Observed Discrepancy of Synchronization," IEEE Trans. Instrum. Meas., Vol. 25, 1976.

[4] J. A. DeYoung, W. J. Klepczynski, A. D. McKinley, W. Powell, P. Mai, P. Hetzel, A. Bauch, J.A. Davis, P. R. Pearce, F. Baumont, P. Claudon, P. Grudler, G. de Jong, D. Kirchner, H. Ressler, A. Soring, C. Hackman, and L. Veenstra, "The 1994 International Transatlantic Two-Way Satellite Time and Frequency Transfer Experiment: Preliminary Results," Proc. of 26th PTTI, 1994.

[5] J. A. DeYoung, A. McKinley, J. A. Davis, P. Hetzel, and A. Bauch, "Some Operational Aspects of the International Two-Way Satellite Time and Frequency Transfer (TWSTFT) Experiment using INTELSAT Satellites at 307 Degrees East," Proc. of 27th PTTI, 1995.

[6] M. Imae, H. Okazawa, T. Sato, M. Uratsuka, K. Yoshimura, and Y. Yasuda,"Time comparison experiments with small K-band antenna and SSRA equipments via domestic geostationary satellite," IEEE Trans. Instrum. Meas., Vol. 32, 1983.

[7] F. Takahashi, K. Imamura, E. Kawai, C. B. Lee, D. D. Lee et al., "Two-way time transfer experiments using an INTELSAT satellite in an inclined geostationary orbit," IEEE Trans. Instrum. Meas., vol. 42, 1993.

[8] B.S.Engelkemier, K. Imamura, F. Takahashi, T. Yoshino, N. S. Chung, and C. S. Liao,"INTELSAT Two-Way Time Transfer Experiments Among Japan, Korea, and Taiwan," IEEE trans. Instrum. Meas. Vol.44, 1995.

[9] J. A. DeYoung, F. Vannicola, and A. D. McKinley,"A Comparison of the Highest Precision Commonly Available Time Transfer Method: TWSTT and GPS CV," Proc. of 28th PTTI, 1996.

[10] H. Ressler, D. Kirchner, and R. Robnik,"Satellite Earth Stations for Two-Way Satellite Time Transfer at the Technical University of Graz," Proc. of 11th EFTF, 1997.
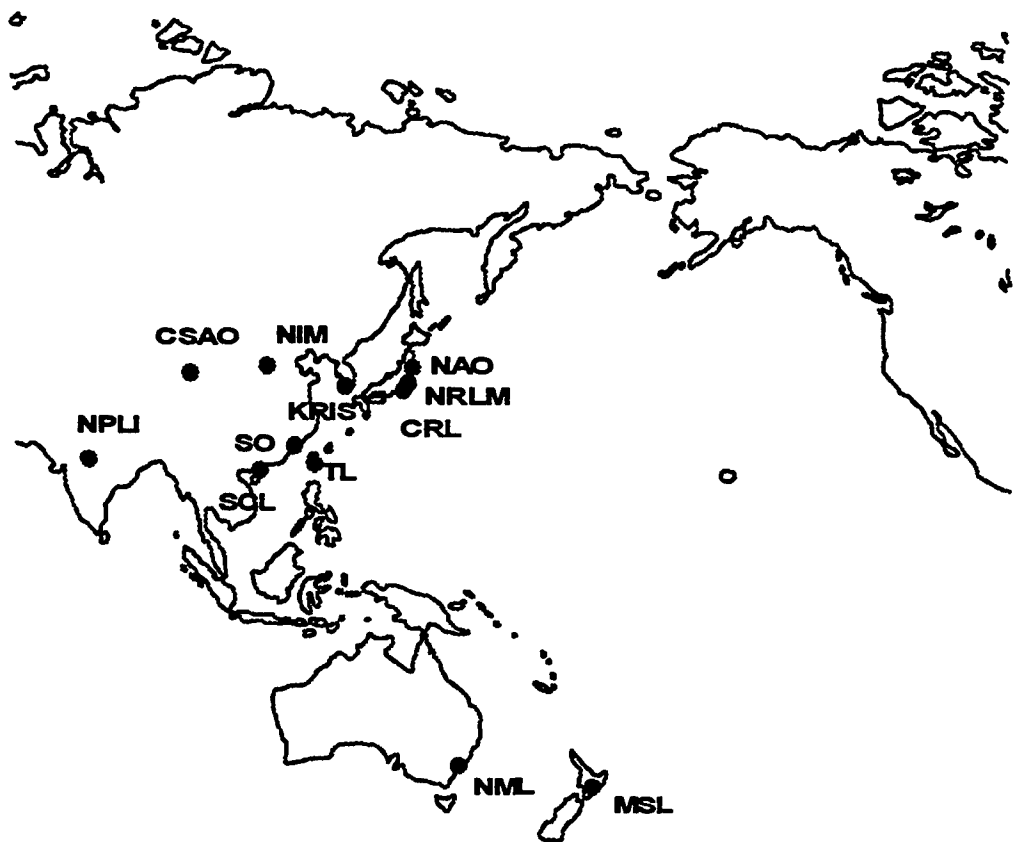
Figure 1. Locations of T&F institute in Asian-Pacific region
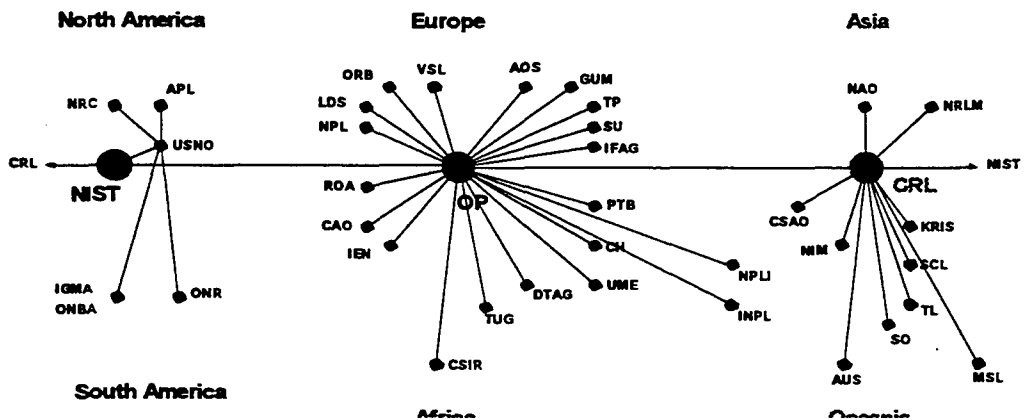
Figure 2. GPS common-view time transfer network
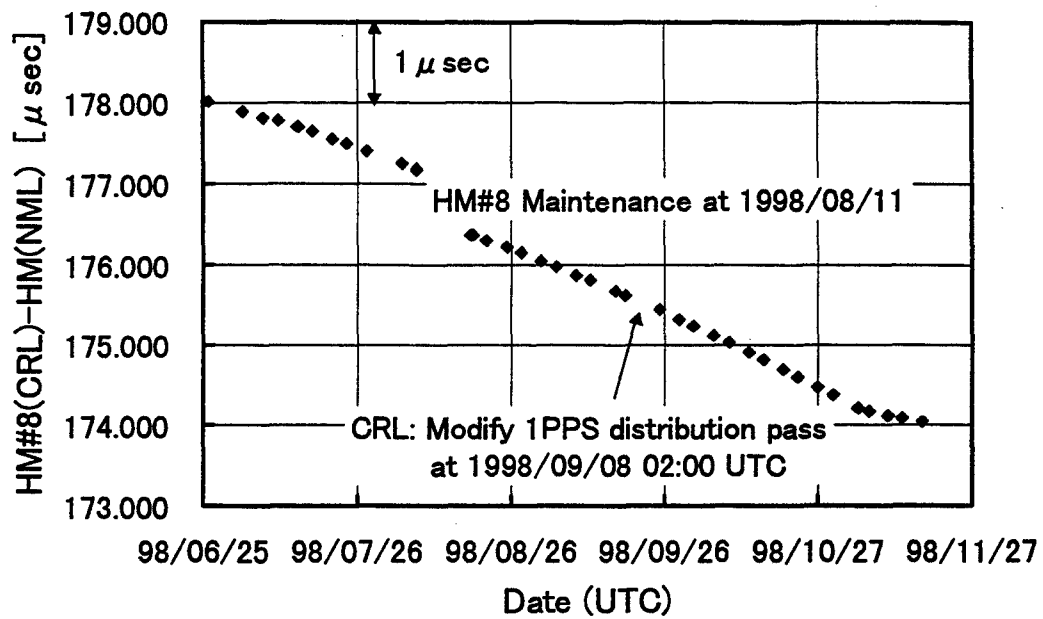
Figure 3. TWSTT results between CRL and NML
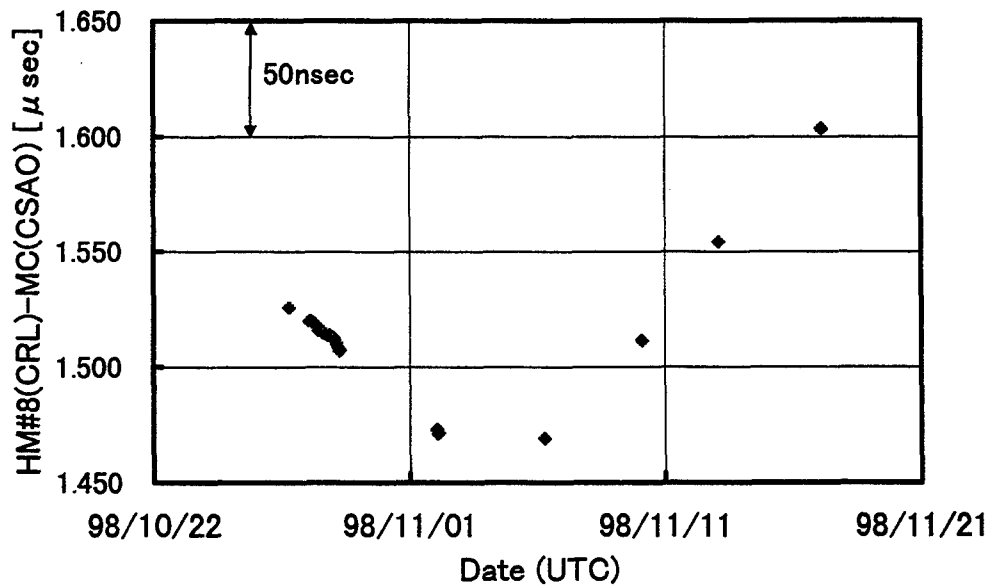
Figure 4. Preliminary TWSTT results between CRL and CSAO
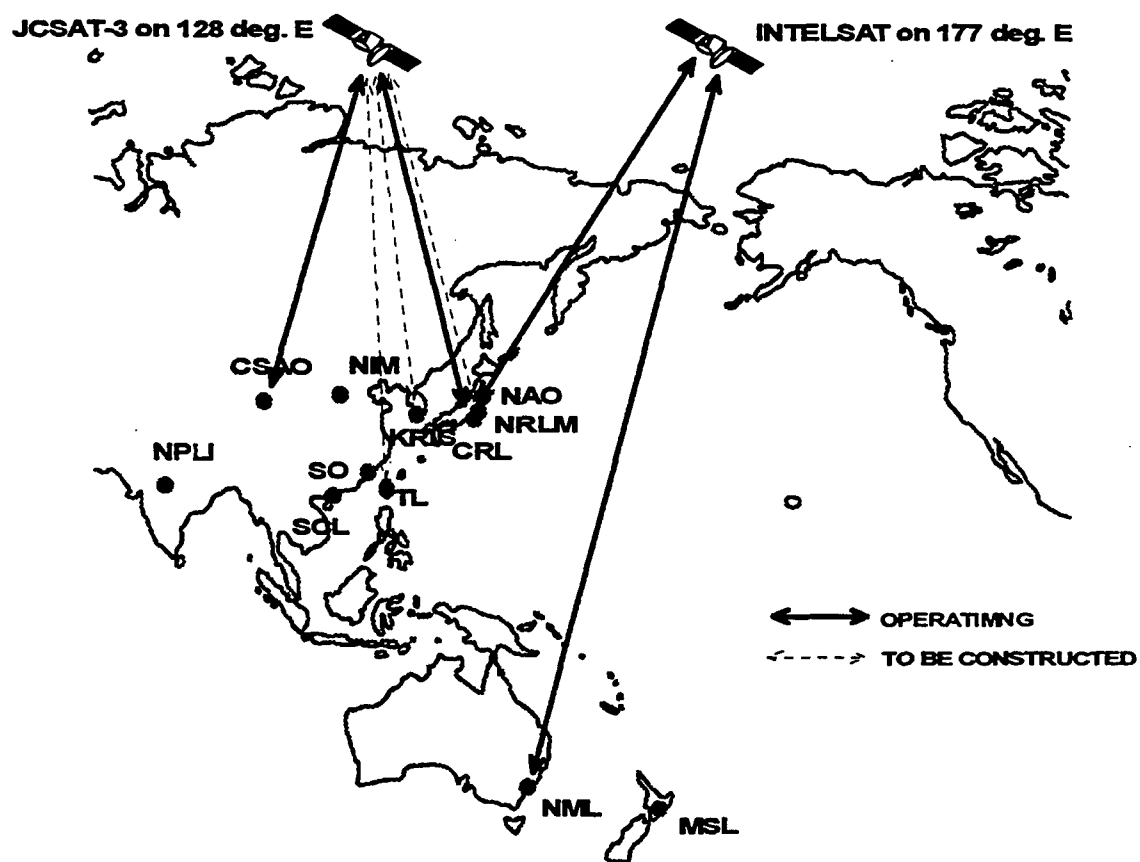
Figure 5. TWSTT network in near future

Questions and Answers

DEMETRIOS MATSAKIS (USNO): The link between Shaanxi and Europe that you are talking about is an important one because it has a possibility of contributing to TAI. I am very concerned about the initial data. I wonder if there are plans to upgrade that. Does Shaanxi have masers or a large ensemble of cesiums that could be a better flywheel?

MICHITO IMAE (CRL): At present they only have a HP-5071A. But they are now making an investigation for a primary frequency standard of the fountain type, under cooperation with Beijing University. So if they complete such a primary standard, we can use this. But unfortunately at present, they do not have a hydrogen maser.

DEMETRIOS MATSAKIS: And just one HP-5071.

MICHITO IMAE: No. They have maybe four or six.

WILLIAM KLEPCZYNSKI (ISI): I think they have six HP-5071s.

MICHITO IMAE: Yes.

WILLIAM KLEPCZYNSKI: Do you have INTELSAT-702? Will that have a spot beam coverage over North America?

MICHITO IMAE: You mean this one?

WILLIAM KLEPCZYNSKI: Yes.

MICHITO IMAE: Yes, this one has a North America spot beam.

WILLIAM KLEPCZYNSKI: Do you have a satellite that you think might be going from Asia to Europe?

MICHITO IMAE: It is difficult to keep the INTELSAT satellite above the Indian Sea, but we will try to keep the satellite.

CALIBRATION OF THREE EUROPEAN TWSTFT STATIONS USING A PORTABLE STATION AND COMPARISON OF TWSTFT AND GPS COMMON-VIEW MEASUREMENT RESULTS

D. Kirchner[1], H.Ressler[2], P. Hetzel[3], A. Söring[4] and W. Lewandowski[5]

[1]Technical University Graz, Inffeldgasse 12, A-8010 Graz, Austria
[2]Space Research Institute, Graz, Austria
[3]Physikalisch-Technische Bundesanstalt, Braunschweig, Germany
[4]Deutsche Telekom AG, Darmstadt, Germany
[5]Bureau International des Poids et Mesures, Sèvres, France

Abstract

After a brief introduction and description of the portable station and a discussion of different approaches to use it for station calibration, the calibration trip is described and the results are presented. The calibrated TWSTFT measurements are compared with the GPS measurements calibrated by a GPS receiver trip carried out at the same time as the TWSTFT calibration and by previous GPS receiver trips. The findings are discussed and some envisaged activities using the portable station are mentioned.

INTRODUCTION

Since 1997 two-way satellite time and frequency transfer (TWSTFT) links are operated on a regular basis between six European laboratories and also between the European laboratories and two laboratories in the USA [1]. All links employ Ku-band channels of the same INTELSAT satellite positioned at 307° E and the measurement data are available in a format published in a draft revision of recommendation ITU-R TF.1153 [2]. This format minimizes the amount of data to be exchanged and allows easy computation of the results. The laboratories contribute to the international atomic time scale and carry out GPS observations according to the BIPM common-view schedules. Initially some of the TWSTFT links were calibrated using the difference between the respective time scales as published by the Bureau International des Poids et Mesures (BIPM) in Circular T. In order to obtain actual GPS calibrations which could also be used to calibrate the TWSTFT measurements, a series of GPS receiver transportations were organized by the BIPM, starting summer 1997. In June 1998 a calibration trip using a portable TWSTFT station developed at the Technical University Graz (TUG) was carried out between the Deutsche Telekom AG (DTAG), Darmstadt, the Physikalisch-Technische Bundesanstalt (PTB), Braunschweig, and the TUG to provide a calibration of the TWSTFT links independent of the GPS calibration. At the same time in the course of one of the GPS receiver trips, GPS calibrations were carried out between these laboratories, allowing a direct comparison of the performance of both techniques.

PORTABLE TWSTFT STATION

At the TUG in addition to the existing TWSTFT system, a second TWSTFT system has been developed to carry out common-clock experiments and for calibration purposes [3,4]. The system comprises a specially adapted VSAT-terminal (1.8 m antenna diameter, maximum EIRP of about 52 dBW, and a G/T of about 22 dB/K), a small 19" rack containing the measurement system designed to be operated with a SATRE-modem providing full frequency agility for the up- and down-link, a spectrum analyzer, a PC controlling the complete system including the spectrum analyzer, an uninterruptible power supply, and a cable drum containing the necessary cables to connect the satellite terminal and the measurement system allowing a maximum separation of 50 m. The system is designed for automated operation using a measurement software developed at the TUG, which allows, apart from other features, on-line monitoring of the measurements. Also available is the necessary software to get the results in both ITU-formats and to process the data [4]. The visited station has to provide a one pulse per second with known relationship to the local time reference and a 10 MHz signal to be connected to the measurement system. Figure 1 shows the satellite terminal. All necessary cable connections are done inside the cabinet at the right hand side providing protection from the environment. The complete measurement system is shown in Figure 2. Figure 3 provides a view into the interior of the trailer used for transportation of the complete TWSTFT system and Figure 4 shows the trailer with the antenna on top of it and the towing car ready to start the trip.

TWSTFT CALIBRATION TRIP

The calibration trip was arranged in a way to be able to make the calibration measurements during the satellite time available for the regular European TWSTFT measurements, trying to omit as few regular measurements as possible. To fit the adhered regular schedule also, the calibration measurements were done over two-minute intervals. The route of the calibration trip can be seen in Figure 5. The underlined dates indicate the days during which the measurements were performed. Depending on the location, two to three hours were needed to set up the station and to be ready for the measurements. In addition to the regular measurements most important with respect to the evaluation of the calibration, in all locations measurements were done between the transported and the local stations and the respective two other remote stations, allowing calculation of the calibration results in different ways. The usual approach is to carry out common-clock time transfer measurements at all sites between the transported station and the local station to get the differential delay between the portable station and the respective local station. Using this approach different signals are employed for the delay calibration and the actual time transfer and, therefore, for signal delays; depending on the received signal, the measured delay and the actual delay can differ from one another. Another approach is to perform a common-clock time transfer between the portable station and the local station at site A and after transporting the portable station to site B to perform a successive time transfer between the transported station and the station at site A and the local station and the station at site A. From the two time transfer results the differential delay of the local stations of site A and B can be calculated. In this case the actual delays are measured, but the stability of the clocks have to be considered, because the measurements are not performed at the same time.

GPS CALIBRATION TRIPS

The GPS calibrations were carried out by means of a GPS receiver provided by the BIPM according to a schedule prepared by the BIPM and also the processing of the data was done at the BIPM. The fourth trip was arranged in a way that the TWSTFT calibrations and the GPS calibrations at DTAG, PTB, and TUG were performed at the same time. Unfortunately, this trip could not be finished as planned, because the receiver got lost and could only be recovered after one year. The detailed calibration results are given in reports published by the BIPM [5-8].

MEASUREMENT RESULTS

The results of the TWSTFT calibration trip are listed in Table 1 and plotted in Figure 6. The results of the TWSTFT calibrations are plotted after having subtracted the individual mean values for each laboratory in order to be able to show the results in one plot. For TUG the mean and standard deviation before the trip are 4.146 ns and 148 ps, after the trip 4.304 ns and 261 ps, and the overall figures are 4.209 ns and 204 ps. For DTAG and PTB the mean value and standard deviation are -277.974 ns and 28 ps, and -174.679 ns and 114 ps, respectively. An assessment of

LAB	CALIBRATION TIME		0.5*CALR	MEAN	STD.DEV.
	MJD	TIME	/ ns	/ ns	/ ps
TUG (1)	50958	141100	4.052		
	50958	141400	4.033		
	50958	141716	4.093	4.146	148
	50958	142900	4.029		
	50960	141100	4.318		
	50960	141400	4.352		
DTAG	50967	141100	-277.955	-277.974	28
	50967	141400	-277.994		
PTB	50969	142329	-174.567		
	50969	142900	-174.529		
	50972	141100	-174.659	-174.679	114
	50972	141400	-174.727		
	50972	141700	-174.783		
	50972	142900	-174.807		
TUG (2)	50976	141100	3.961		
	50979	141100	4.465	4.304	261
	50979	141400	4.544		
	50981	141100	4.245		
TUG (1+2)				4.209	204

Table 1. Results of the TWSTFT calibration trip.

the calibration uncertainty by an error budget results in about 400 ps for the calibration at the TUG and at the PTB and about 1.7 ns at the DTAG. The greater uncertainty at DTAG is due to the greater uncertainty in the determination of the relationship between UTC(DTAG) and the time references used for the local and portable TWSTFT systems.

A summary of the relevant measurement results of the four GPS calibration trips is given in Table 2. The estimated uncertainty with respect to the receiver at the Paris Observatory (OP) given in the respective report is 3 ns for the first trip and 2 ns for the second and third trip. The standard deviations of the daily means range from 0.2 ns to 1.1 ns . For DTAG because of building construction work, no relevant data exist for the third trip [7]. Also for PTB, the results of the third trip have a higher uncertainty due to particularly poor measurement conditions [7].

TRIP No	CALIBRATION PERIOD	LAB	MEAN OFFSET BIPM3-LAB / ns
	50624 - 50629	DTAG	-0.2
1	50631 - 50635	PTB	-1.0
	50638 - 50643	TUG	-12.8
	50757 - 50762	DTAG	+5.0
2	50763 - 50769	PTB	+3.7
	50779 - 50783	TUG	-5.1
	50878 - 50881	DTAG	-
3	50884 - 50888	PTB	-7.5
	50891 - 50895	TUG	-7.6
	50963 - 50966	DTAG	+64.48
4	50967 - 50973	PTB	+2.55
	50974 - 50979	TUG	-5.99

Table 2. Results of the four GPS calibration trips.

Figure 7 shows for TUG - PTB the differences between the TWSTFT results and GPS results after having calibrated the TWSTFT data by the outcome of the TWSTFT calibration trip and after having calibrated the GPS data by the results of the individual GPS calibration trips. To calculate the differences for the GPS data, the result of a linear regression over one day centered at the TWSTFT measurements were used. Figure 8 shows the same for TUG - DTAG, apart from the fact that there are no DTAG data for the third GPS calibration trip. The corresponding numerical data are listed in Tables 3 and 4 using averages over the respective GPS calibration periods to calculate the differences between TWSTFT and GPS. Figures 7 and 8 and Tables 3 and 4 give the results using the first approach for the TWSTFT calibration (see Ch. TWSTFT CALIBRATION TRIP). Using the second approach for TUG - PTB, the results differ only by about 100 ps, but for TUG - DTAG the differences between TWSTFT and GPS become smaller by about 2 ns.

TUG-PTB: TW-GPS			GPS CALIBRATED BY			
	TRIP No	CALIBRATION PERIOD	1st TRIP	2nd TRIP	3rd TRIP	4th TRIP
TW-GPS / ns	1	50631 – 50643	+0.563	-2.437	-11.137	-2.737
	2	50763 – 50783	+2.497	-0.503	-9.203	-0.803
	3	50884 – 50895	+3.976	+0.976	-7.724	+0.676
	4	50967 – 50979	+2.383	-0.617	-9.317	-0.917

Table 3. Differences between the independently calibrated TWSTFT and GPS measurements for TUG - PTB. (Lines give TWSTFT - GPS for the date of a specific trip; columns give TWSTFT - GPS for the dates of the different trips.)

TUG-DTAG: TW-GPS			GPS CALIBRATED BY			
	TRIP No	CALIBRATION PERIOD	1st TRIP	2nd TRIP	3rd TRIP	4th TRIP
TW-GPS / ns	1	50624 – 50643	-3.858	-5.858	–	+53.142
	2	50757 – 50783	-6.227	-8.227	–	+50.773
	3	50878 – 50895	+82.931	+80.931	–	+139.93
	4	50963 – 50979	+14.991	+12.991	–	+71.991

Table 4. Differences between the independently calibrated TWSTFT and GPS measurements for TUG - DTAG. (Lines give TWSTFT - GPS for the date of a specific trip; columns give TWSTFT - GPS for the dates of the different trips.)

DISCUSSION

The differences between TWSTFT and GPS for TUG - PTB show a kind of seasonal effect especially pronounced in the first part (see Figure 7). A closer investigation revealed that this effect was partly caused by the gradually breaking internal power supply of the GPS receiver used at the TUG, being replaced by an external one at MJD 50689. Apart from the third GPS trip, the differences between TWSTFT and GPS for the dates of the respective GPS calibrations making use of the different GPS calibration results, are below 1 ns. This agrees very well with the estimated TWSTFT and GPS calibration uncertainty (see Ch. MEASUREMENT RESULTS). The peak-to-peak difference is about 11 ns and can be assumed to be mainly due to delay variations of the GPS receivers at TUG and PTB. In addition, it should be mentioned that changing the TWSTFT calibration from the value obtained via the Circular T (see Ch. INTRODUCTION) to the one obtained by the TWSTFT calibration trip gives a step of about 18 ns and the average difference between TWSTFT calibrated by the TWSTFT calibration trip

and the uncalibrated GPS data is about -9 ns (cf. [1]). The average correction for the GPS data calculated from the recent GPS calibration trips to be applied to get UTC(TUG) and UTC(PTB) is about -6 ns and 4 ns, respectively, and the corrections used to calculate Circular T are 12 ns and 0 ns, respectively [9].

The differences between TWSTFT and GPS for TUG - DTAG (see Figure 8) show a step after the second GPS calibration trip and another one after the third GPS calibration trip. These steps result from a problem with the GPS reference which is obtained by a divider chain separate from that providing the TWSTFT reference. Therefore, the TWSTFT measurements are not affected. The differences between the TWSTFT measurements calibrated by the TWSTFT calibration trip and the GPS measurements calibrated by the first and second GPS calibration trip are about -4 ns and -8 ns, respectively. Using the second approach for the TWSTFT calibration this becomes about -2 ns and -6 ns, respectively. An explanation for these larger values is the higher uncertainty (see Ch. MEASUREMENT RESULTS) in establishing the relationship between the different time references and UTC(DTAG).

It should also be mentioned that at the time of the TWSTFT calibration at TUG and at PTB SATRE-modems were used and at DTAG a MITREX 2500A modem was employed.

CONCLUSION AND ENVISAGED ACTIVITIES

The portable TWSTFT system worked without problems and is ready for further calibration trips. One problem occurred two weeks after the trip which turned out to originate from a poor soldering at one of the terminals of the switch used to switch between the internal and an external reference frequency. For TUG - PTB the average differences between the calibrated TWSTFT measurements and the GPS measurements for the dates of GPS calibrations were well below 1 ns. One can assume that the variation of the differences between the TWSTFT and GPS time transfer measurements is mainly caused by delay variations of the GPS receiving systems. To get more information about delay variations of TWSTFT systems, repeated TWSTFT calibration trips would be of interest.

Extensive common-clock experiments between the local TWSTFT station and the portable one are planned to investigate the stability of the signal delays of the stations and the possible improvements by using corrections derived from satellite simulator measurements. The portable station may also be used for extended common-clock experiments at remote sites (comparisons with TWSTFT systems or other time transfer systems). Operating two TWSTFT stations at the TUG allows the simultaneous use of two different satellites and, therefore, would enable the TUG to perform simultaneous TWSTFT measurements with stations in the eastern and western parts of the world.

ACKNOWLEDGMENTS

REFERENCES

[1] J. Azoubib et al., "Two-Way Satellite Time Transfer using INTELSAT 706 on a Regular Basis: Status and Data Evaluation," these Proceedings.

[2] ITU-R, "The operational Use of Two-Way Satellite Time and Frequency Transfer Employing PN Codes," Draft Revision of Recommendation ITU-R TF.1153, Geneva: ITU, 1997.

[3] H. Ressler et al., "Satellite Earth Stations for Two-Way Time Transfer at the Technical University Graz," Proc. 11th European Frequency and time Forum, pp. 509-513, 1997.

[4] D. Kirchner et al., "Recent Work in the Field of Two-Way Satellite Time Transfer Carried Out at the TUG," Proc. 11th European Frequency and time Forum, pp. 205-208, 1997.

[5] W. Lewandowski and P. Moussay, "Determination of Differential Time Corrections Between GPS Time Equipment Located at the OP, NPL, VSL, DTAG, PTB, TUG, IEN and OCA," Rapport BIPM-97/5, October, 1997.

[6] W. Lewandowski and P. Moussay, "Determination of Differential Time Corrections Between GPS Time Equipment Located at the OP, CH, SP, VSL, DTAG, PTB, NPL, TUG, IEN and OCA: 2nd Evaluation," Rapport BIPM-98/1, February, 1998.

[7] W. Lewandowski and P. Moussay, "Differential Time Corrections for GPS Time Equipment Located at the OP, VSL, NPL, DTAG, PTB, TUG, IEN, ROA, IPQ and OCA: 3rd Evaluation," Rapport-BIPM-98/7, June, 1998.

[8] W. Lewandowski and H.Konate, "Differential Time Corrections for GPS Time Equipment Located at the OP, VSL, NPL, DTAG, PTB, TUG, ...: 4th Evaluation," Rapport-BIPM, in preparation.

[9] Letter-BIPM, "Differential time corrections used in TAI computations," Ref:CT/TA.373, Sèvres, 19 January, 1998.
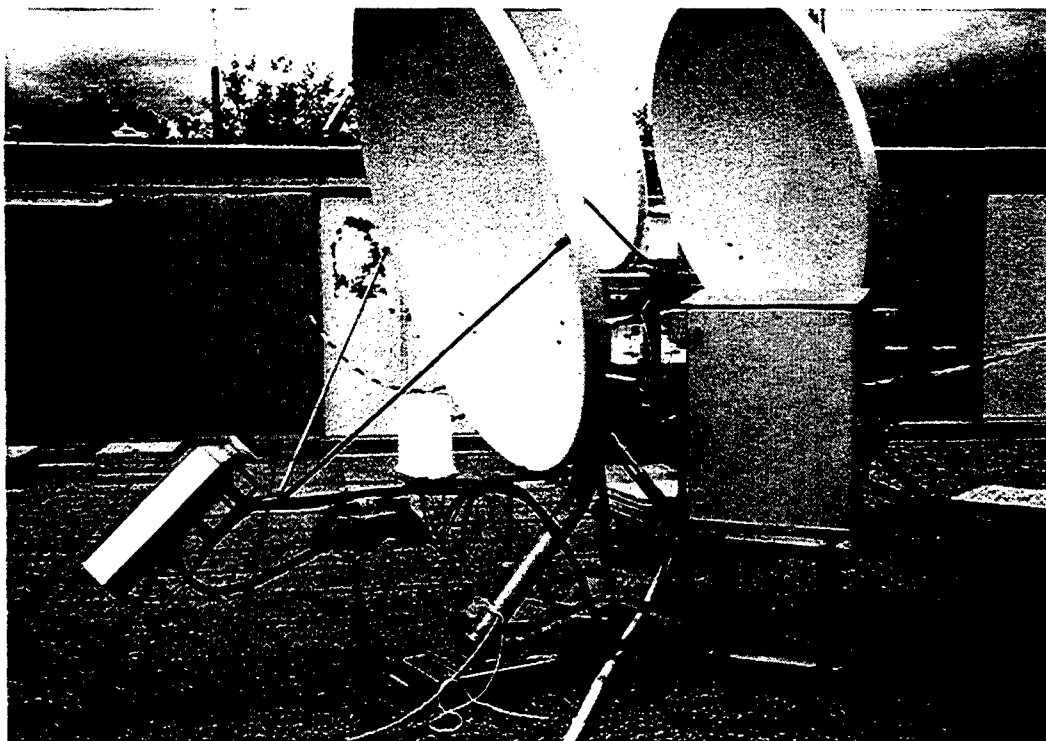
Figure 1. Satellite terminal of the portable TWSTFT station.
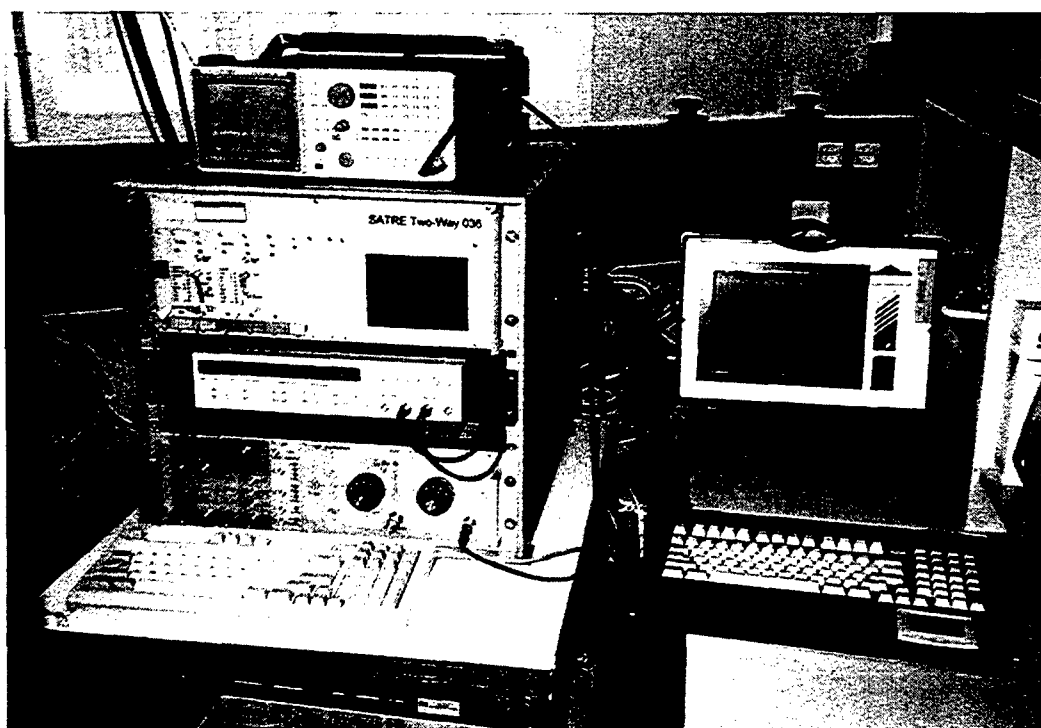
Figure 2. Measurement system of the portable TWSTFT station.
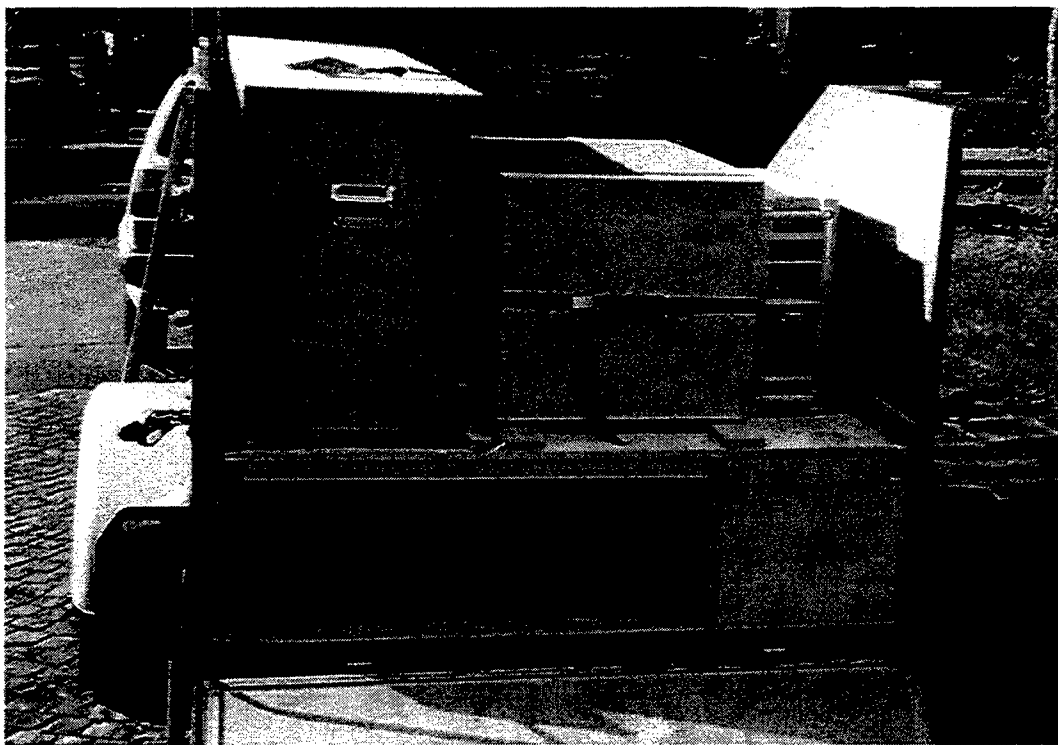
Figure 3. View into the interior of the trailer used to transport the TWSTFT system.
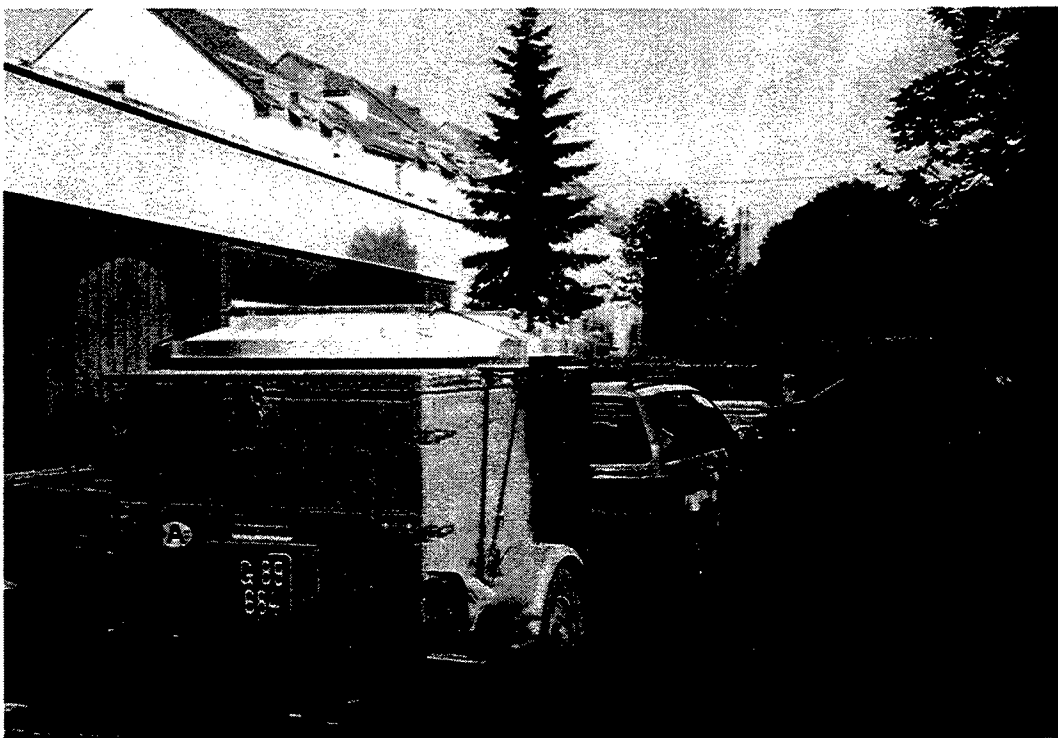
Figure 4. Trailer with the antenna on top of it and the towing car.
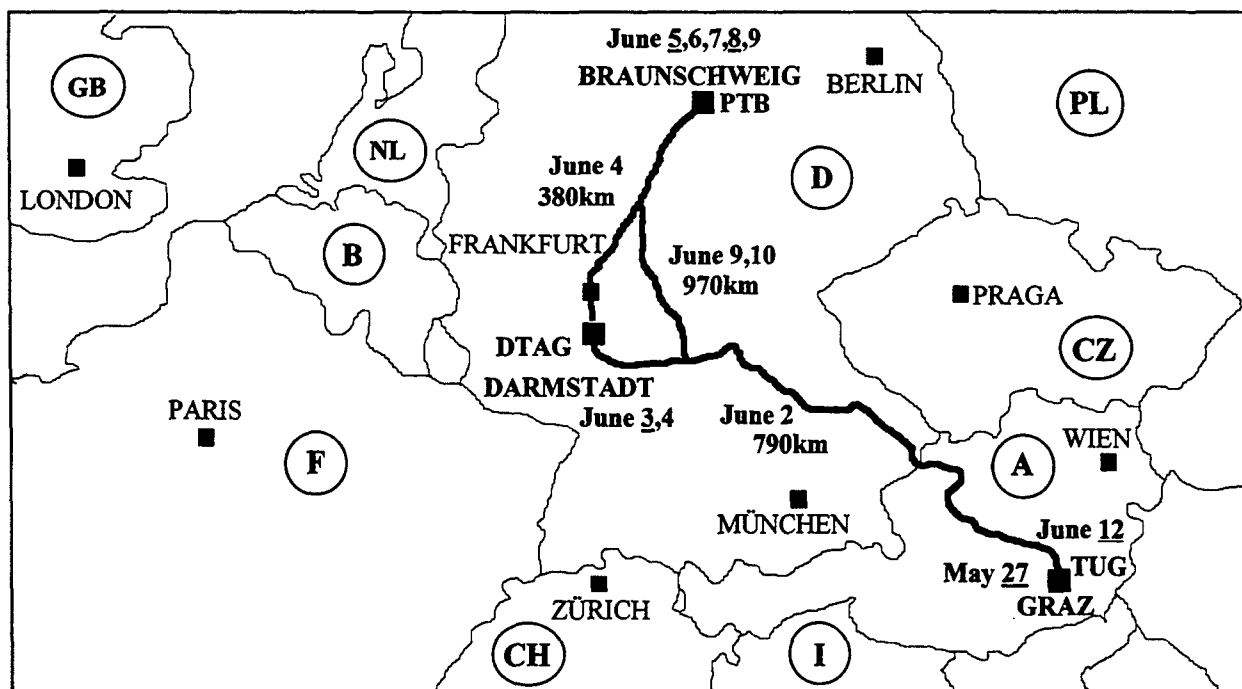
Figure 5. Route of the TWSTFT calibration trip.
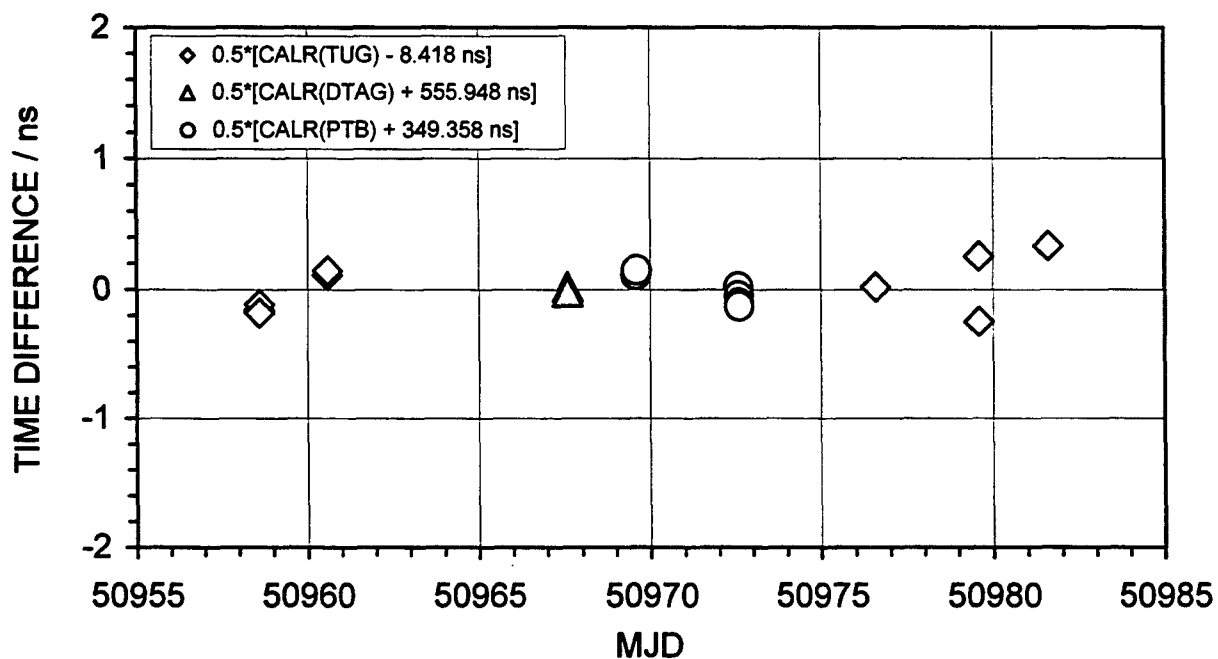
Figure 6. Results of the TWSTFT calibrations.

374
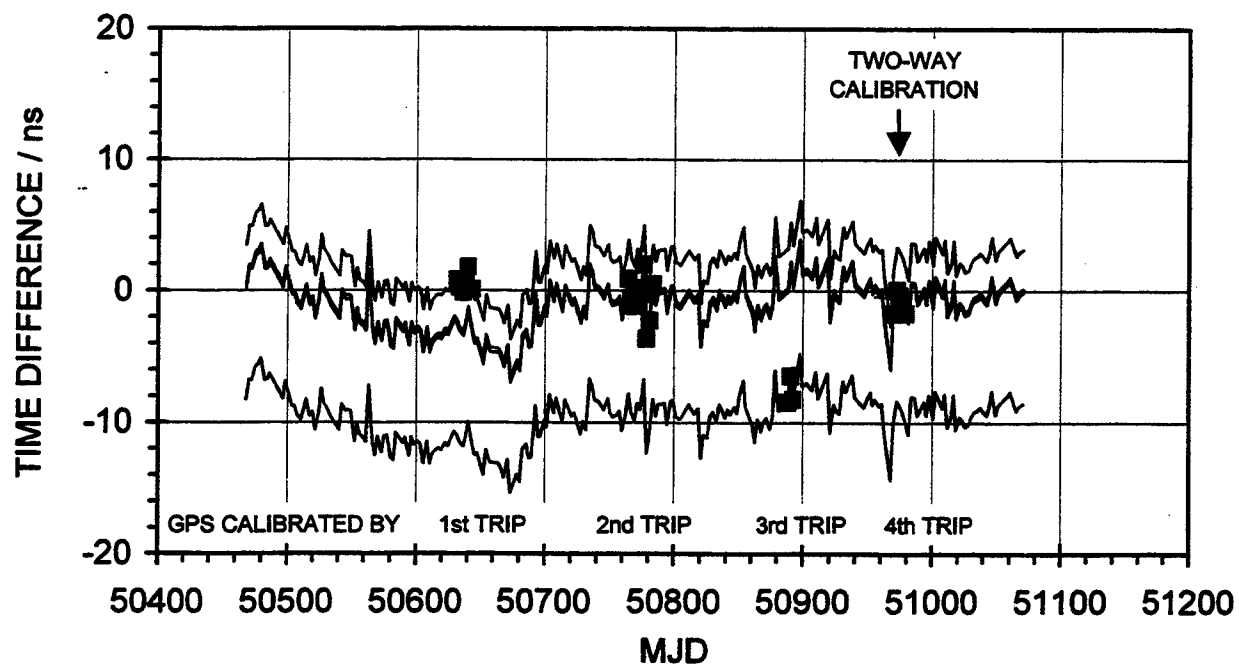
Figure 7. Differences between the independently calibrated TWSTFT and GPS measurements for TUG - PTB.
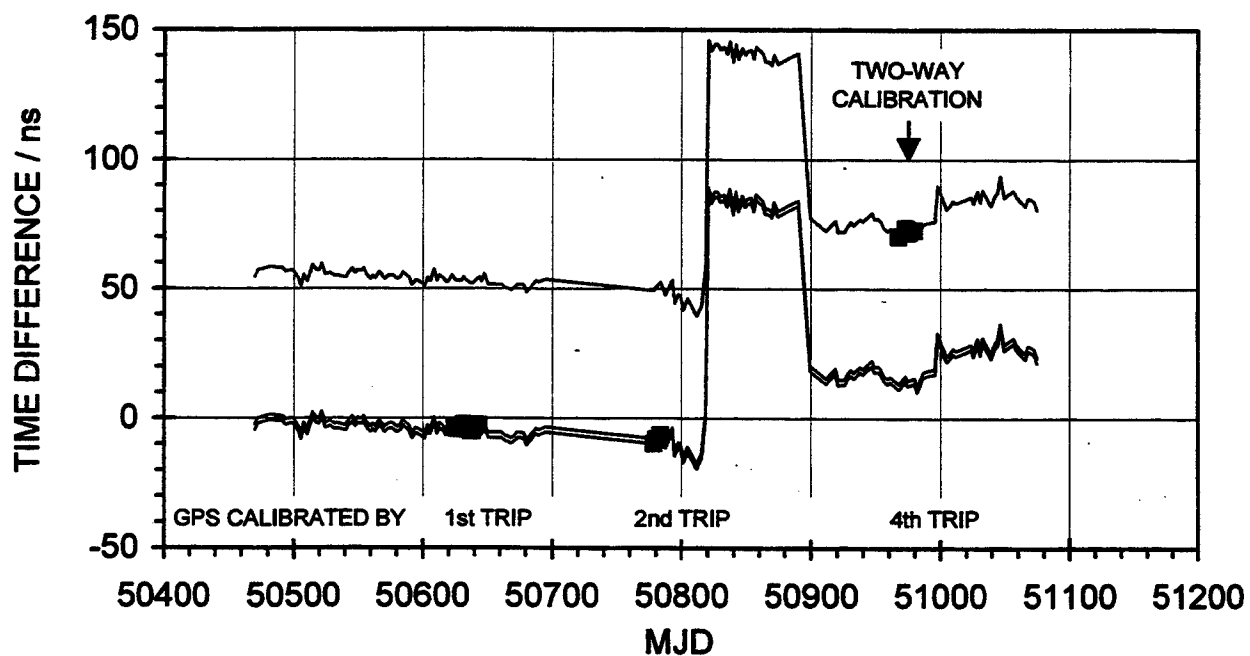
Figure 8. Differences between the independently calibrated TWSTFT and GPS measurements for TUG - DTAG.

375

Questions and Answers

DEMETRIOS MATSAKIS (USNO): Dieter, I think that your talk is an excellent case for using two-way on the basis of the fact that common-view GPS is not, in the end, for one reason or another, calibrated correctly in the short run. I am very curious about the fact that you had a slowly dying GPS receiver. I wonder if there was some indication that people should be looking for in their own receivers.

DIETER KIRCHNER (TUG): Yes, I can tell you the real problem. It was an eight-volt power supply in a NBS GPS receiver, and the voltage slowly decreased. It took weeks before it really failed. The GPS receiver was still working with eight volts, decreasing to 7.5 and so on, until reaching six volts, then it really stalled. You can only detect this by comparing your data with another GPS receiver. I have plotted it down here. You can see it here. This is a comparison between our two on-site GPS receivers. This extra effect here is coming from the slowly dying power supply. After replacing the power supply, you have a change here of three nanoseconds, back to nearly the old figure.

It is dangerous to simply correlate things with temperature because, if it had not really failed, we would say it is a large seasonal effect.

DEMETRIOS MATSAKIS: There is a health or status indicator or some way that you could watch the decay happen?

DIETER KIRCHNER: No. Now we are using an external power supply. We are already experienced in substituting an extra power supply to NBS receivers. So it takes only half an hour to do it. It is easily done.

To give the difference between two-way and the GPS receiver delay variation – this is the delay variation of our on-site two-way station measured by a satellite simulator. There are some problems with these measurements. You see a rapid change here – the scatter is higher and the number changed. This was because we are also receiving using our satellite simulator. We are also receiving the signal back from the satellite. If you have interfering signals from the satellite at the same frequency band, you can have problems.

So, we have to look for a gap in the band. This will not be the case with your simulator.

NEW WAYS TO VISUALIZE TIME AND FREQUENCY DATA

James A. DeYoung
U.S. Naval Observatory
3450 Massachusetts Avenue, NW
Washington, DC 20392-5420, USA
dey@herschel.usno.navy.mil

Abstract

Some of the standards of numerical analysis in time and frequency are the formation of the various square roots of variances, such as Time Deviation (TDEV), Allan Deviation (ADEV), and Total Deviation (TotDev), among others. As time and frequency measurements and transfer becomes better and better, especially at smaller sampling intervals, transient disturbances from such things as environmental perturbations become more and more important to characterize, locate, and understand. While developing software tools to more fully analyze, visualize, and model time and frequency data, especially time transfer data, several "new" ways of looking at the data were tested for usefulness. One new way of looking at time-series data was first reported in 1987 and is called visual recurrence plots or analysis (VRA) [1]. VRA, the auto-correlation function (ACF), power spectral density by the Barnes' Digital Spectrum Analyzer method [2] (PSD), periodogram using phase-dispersion-minimization techniques (Jurkevich[7]), phase plane visualization (PPV), time-frequency analysis (TFA), and even 1-D wavelet decomposition of a time-series signal are being tested. This paper will show some recent results that show that all these numerical tools are useful. Tests will be run on both real and synthetic data.

INTRODUCTION

Over the years the author has been developing and locating useful software tools which lend themselves to useful analysis and visualization of time-series data, both equally spaced and non-equally spaced data, both in real-time and after the fact, and are generally platform—independent. Recent data obtained between USNO(MC2) and USNO AMC(MC1) via TWSTT and a recent article on real-time data analysis [3] brought this subject back to the author's attention. The goal of this paper is to encourage researchers and anyone with time-series data to fully investigate their data and not just stop with the standard TDEV, ADEV, or TotDev variance analysis.

VISUAL RECURRENCE ANALYSIS (VRA)

The author was surfing the Web recently looking for software to compute a Henon mapping [4], phase-plane visualization, and other chaos analysis tools for analysis of the output of his Burlirsch-Stoer method of integrating the solar-system and minor planets. One of the search engine hits produced an interesting link to Visual Recurrence Analysis (VRA) software [5] which was apparently developed for analysis and prediction of the stock markets! The software was downloaded and found to be quite useful and fully functional in that it allows the user to import his/her own data files.

It was learned under the VRA help pages that a new method of visualizing equally spaced time series data called recurrence plots was reported in 1987 and was developed to aid researchers in analysis of dynamical systems [1]. The method produces 2-D plots or images which show large scale structure the authors call typology and small-scale structure they call texture.

The formulation to make a 2-D recurrence image (plot) from a time series [5] is

$$y(i) = (x(i), x(i+d), x(i+2d), ..., x(i+(m-1)d) \qquad 1)$$

where

i is the time index of the original signal $X(t)$,
m is the embedding dimension and,
d is the time delay.

A series of vectors are produced [5]

$$Y=\{y(1), y(2), y(3), ..., y(N-(m-1)d)), \qquad 2)$$

where

N is the length of the original time series.

The result may be a color-coded matrix (image) of the Euclidean distances between all pairs of vectors.

For random signals a uniform pattern over the entire image is seen, while the more deterministic the input signal, the more structure is seen in the image [5].

Also available in the VRA software is a single value estimate of the structure in the VRA image called the Spatial-Temporal Entropy (STE) [5], but no details are given as to how it is computed. 100% entropy indicates pure randomness (unpredictability) in the VRA, while 0% entropy indicates perfect structure (predictability).

PHASE-PLANE VISUALIZATION (PPV)

Phase-plane views of time series are produced from the original time-series by plotting y from the original (x,y) pairs with the first difference of the original y pairs to form essentially (y, y'). In our examples below this will be a time difference between clocks and their rates.

EXAMPLES OF VRA VIEWS OF WHITE NOISE

One of the common power-law noise processes seen in time and frequency keeping is white PM. A synthetic White PM time series was constructed containing 1,000 samples. The time series looks white and normally distributed (Figure 1). The AC shows no correlation at any lag (Figure 2). The PSD is flat (Figure 3). The TDEV shows a slope of -1/2 a characteristic of white PM (Figure 4). The PPV shows a symmetrical distribution along the diagonal (Figure 5). The VRA of white PM shows an overall flat and uniform distribution with little if any significant structure (Figure 6). The STE for this data set is 95%.

EXAMPLES OF VIEWS OF WHITE FM IN THE TIME DOMAIN

Another common power-law noise process often seen is white FM in the time domain. A synthetic time series was again produced and contains 1,000 samples. The times series looks standard for this noise process (Figure 7). The AC shows correlation with lag (Figure 8). The PSD is well behaved and shows a slope of –1.752 (Figure 9). The TDEV shows an overall slope of +½ which is a characteristic of white FM in the time domain (Figure 10). The PPV shows a nearly white frequency distribution across the y-coordinate (frequency) coordinate, but an extension in the x-coordinate (time) which comes from the slight overall slope as seen in the original times series (Figure 11). The VRA image starts to show typological, large-scale structure and shows the small slope as a gradient towards the upper-left and lower-right corners (Figure 12). The STE is 89%.

USNO(MC2) - USNO AMC(MC1) 1-DAY AVERAGES VIA TWSTT

USNO(MC2) is an auxiliary output generator (AOG) whose source is a hydrogen maser. USNO(MC2) is steered once per day using classical methods towards a steered version of our USNO(A.1), which is called USNO(Mean). USNO(Mean) is an on-time and on-rate real-time estimate of UTC(BIPM). The USNO AMC(MC1) is also an AOG with a hydrogen maser source. The USNO AMC(MC1) output is steered nominally once per hour to USNO(MC2) via a Kalman filter.

The time series shows similar structure to white FM in the time domain with some amplitude dampening after about MJD 50750 (Figure 13). The AC shows slight correlation with very small lags (Figure 14). The PSD has a shallow minimum or flattening between frequency 0.001 and 0.03, but otherwise looks much like the

PSD of White FM in the time domain (Figure 15). The spectrum slope is -1.599. The TDEV shows a strong, but small amplitude periodic component with a peak deviation at about 15 days (Figure 16). The TDEV plot should show a peak deviation at 1/2P, which should be one-half of ~30d if it is likely related to the monthly rate changes in the USNO(Mean) as we steer it and the USNO(MCs) to UTC(BIPM). This peak might be related to our steering of this system towards UTC(BIPM), which is updated monthly. The PPV is fairly symmetrical in both coordinates and shows a nearly optimally controlled system in both time and frequency (Figure 17). The VRA (Figure 18) shows a fairly flat image with an intermediate structure between the white PM and white FM examples given above. A strong sharp-edged peak around 420 is a known short-term environmental perturbation in this system which is not easily seen in the original time series. This is an example of a detection of a short-term transient behavior in the system, which shows one of the uses of visualizing data with the VRA. The STE is 93% and is intermediate between the white PM and white FM examples.

A ONE-DAY PERIODIC IN UNEQUALLY SPACED TWSTT DATA

Several tools are available from the astronomical community to generate periodograms from unequally spaced data. The methods for unequally spaced data analysis are typically brute force methods. For example, to generate a periodogram the time series is phase-folded using trial periods and then a statistic is generated to estimate the correlation of data across the phased data that has been sub-binned and a scatter estimate formed for each bin. Phase-folded data that contains no structure has variance statistics that are uniform and large across the phased and sub-binned data. If the data contain structure in phase across the phased and sub-binned data, then the variance statistic is small for each bin and the overall statistic for that trial period is small, often near zero, indicating correlation.

Plotting the overall variance statistic with each trial period generates the periodogram. The method used here is a modified Jurkevich method [7], which gives as the statistic the square of the ½ amplitude of the variation. As an example, a sample unequally spaced data set was generated by the convolution of a 1 cycle per day and 3.754 cycle per day sine waves using the exact same sampling rate as the real TWSTT data to be shown below, i.e. unequally spaced, but well sampled. Periodograms were generated for every month from March 1996 to March 1998. The individual periodograms were then combined to form a 2-dimensional image (Figure 19). The time-series periodogram shows the two signals very well with both showing low-amplitude variation in the 1/2P locations. When data are missing the noise floor is increased, but the synthetic period always have very high signal-to-noise ratios.

In the real nominally hourly sampled TWSTT data at certain times of the year, a small amplitude periodic was seen in the measured time differences with a period of 1 day. It was decided that the data could be broken up into monthly sections

and a periodogram generated for each month using the modified Jurkevich method [7] ι and the unequally spaced data. A 2-D digital image was then generated by merging each monthly periodogram into a matrix and displayed in the form of an image (Figure 20). The strongest signal indicated is the peak at 1 day and it can be easily seen that its amplitude varies over the course of a year. The highest signal level was at the 250 to 300 ps level maximum amplitudes and was seen in the summer. No signal is seen during the winter months. This would imply a seasonal temperature related periodic signal contribution. Several sources could be contributing to this variation in the time-transfer link that will be isolated in the near future.

CONCLUSIONS

All of these methods of analysis including routine inspections of ACFs, PSDs, and all the standard variances have become integral parts of the authors software tool chest. Phase-plane views (PPVs) are easy to produce and provide a quick and useful visualization of the state of a controlled clock in both the time and frequency. PPVs also allow a quick view of how well a controlled system is behaving and so are quite useful in monitoring of steered time and frequency systems. VRA is a useful tool, among others, in visualizing and detecting uncharacteristic short-time-scale impulse behavior in time and frequency systems.

REFERENCES

[1] J.-P. Eckmann, S. O. Kamphorst, and D. Ruelle, 1987, "Recurrence Plots of Dynamical Systems," Europhys. Lett., 4, 973-977.

[2] J. A. Barnes, 1993, "A Digital Equivalent of an Analog Spectrum Analyzer," Proceedings of the 1993 IEEE International Frequency Control Symposium, 2-4 June 1993, Salt Lake City, Utah, USA, pp.270-281.

[3] S. Schneider, "Visualizing Real-Time Data," Performance Computing, December 1998, pp. 33-41.

[4] M. Henon,1969, "Numerical Study of Quadratic Area-Preserving Mappings," Quarterly of Applied Mathematics, 27, 291-312.

[5] E. Kononov, Software VRA Ver. 2.5, June 1998, http://pw1.netcom.com/newugenek/index.html and attached Web pages.

[6] Stable 32 Software Version 1.0, Hamilton Technical services, 195 Woodbury Street, S. Hamilton, MA 01982 USA.

[7] S. Morris and D. L. DuPuy, 1980, "A Photoelectric Study of Three Southern Delta Scuti Stars," Publ. Astron. Soc. Pacific, 92, 303-314.

Time-Domain White PM

Fig.1
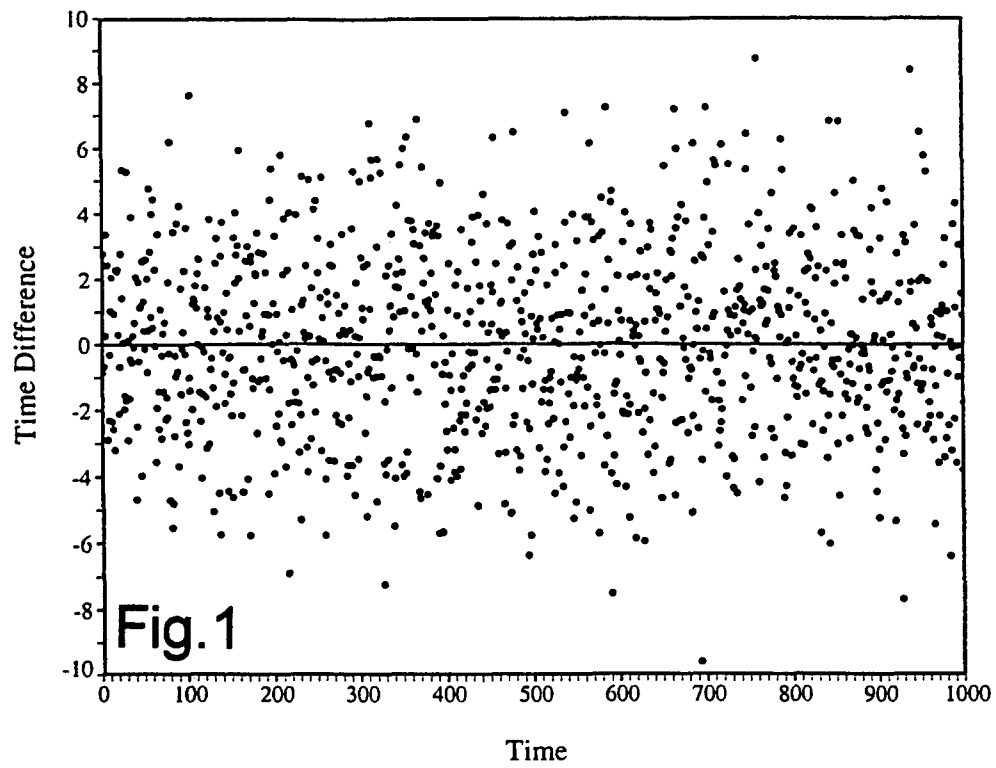
Auto-correlation Function of White PM

Fig. 2
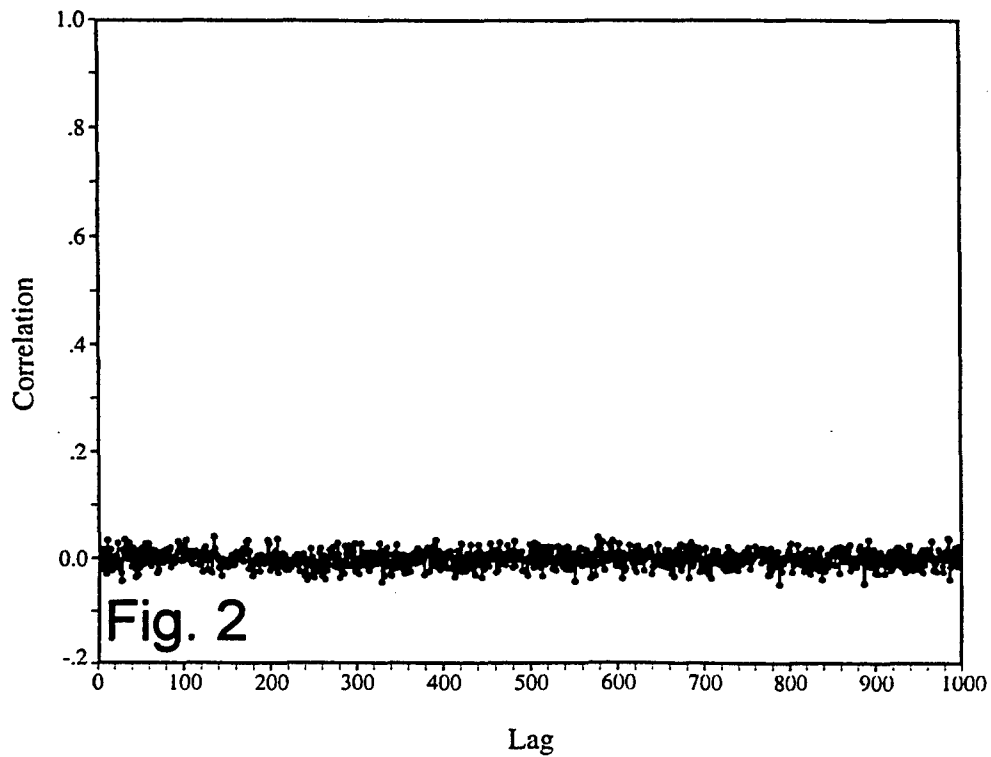
Power Spectral Density of White PM

from the Digital-Spectrum-Analyzer Method

Fig. 3
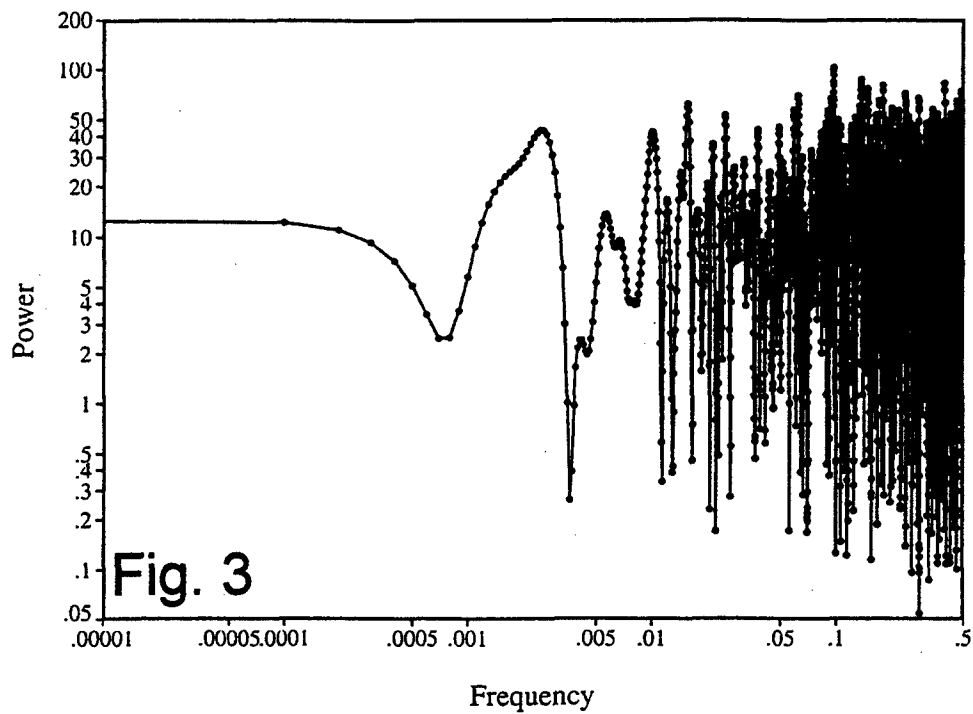
Time Deviation (TDEV) of White PM

For All Tau from Stable Software

Fig. 4

Phase-Plane View of White PM

Fig. 5

Time Difference

Fig. 6
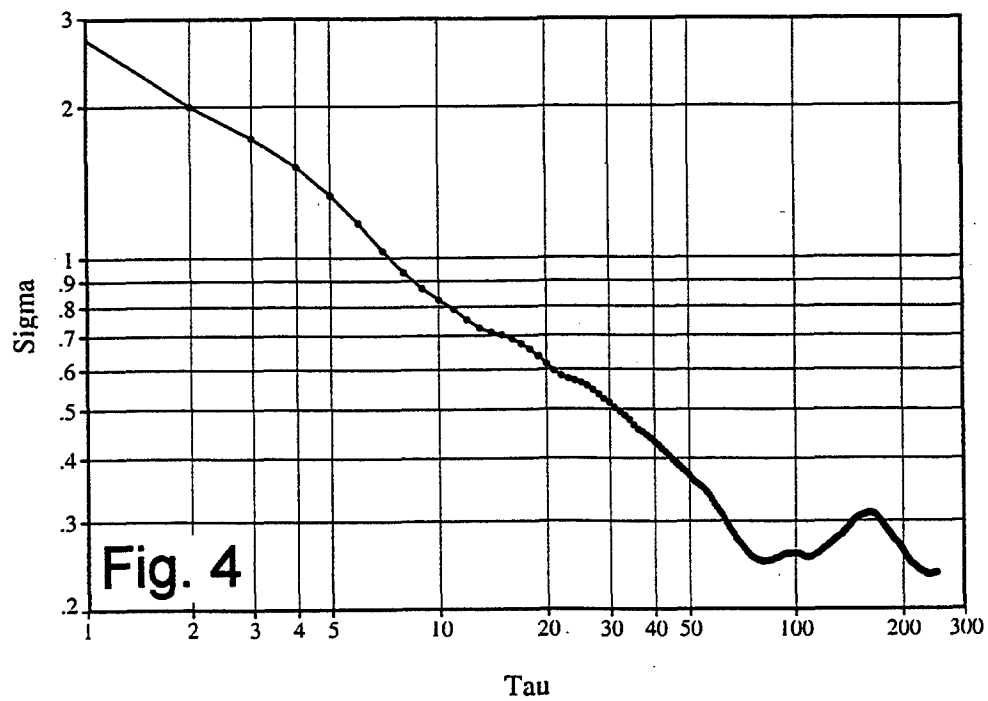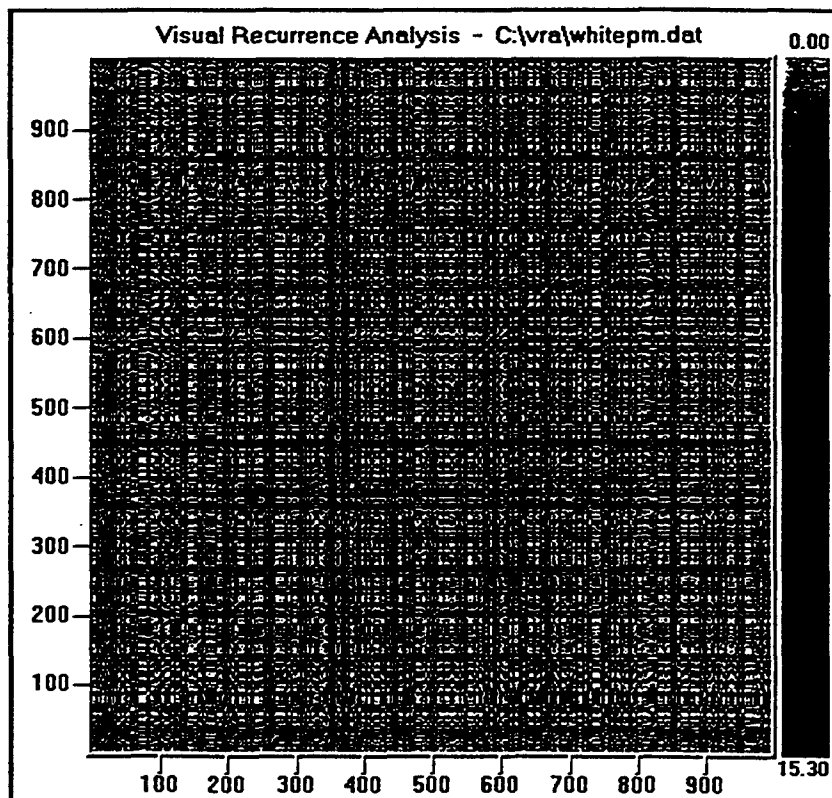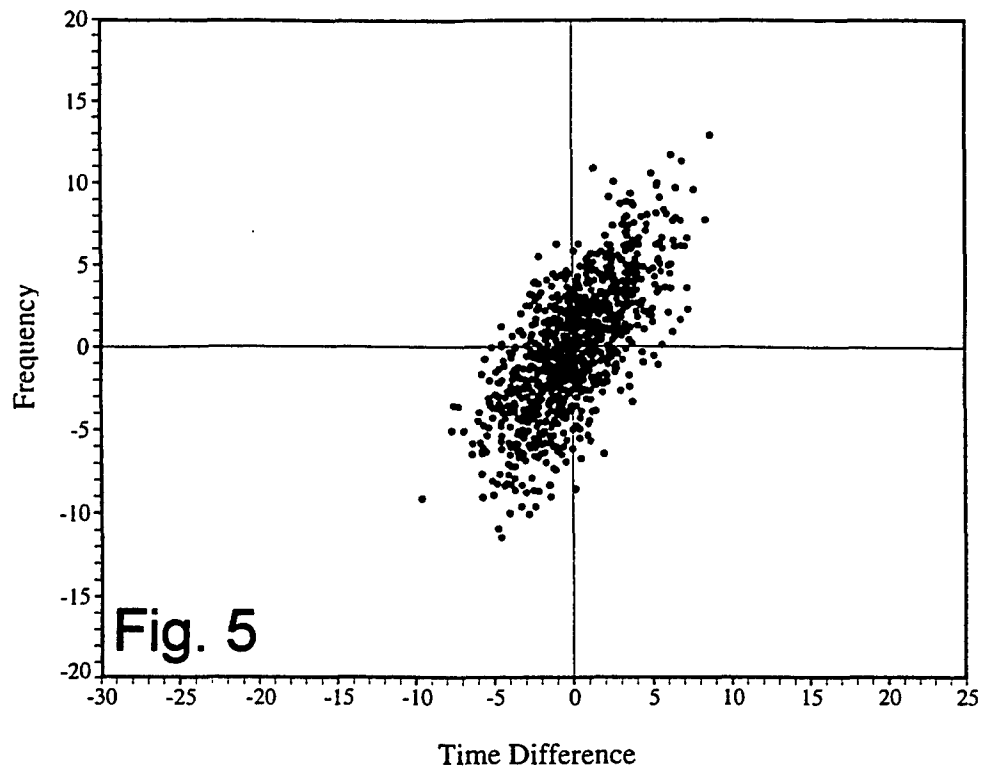
Time-Domain White FM

Fig. 7
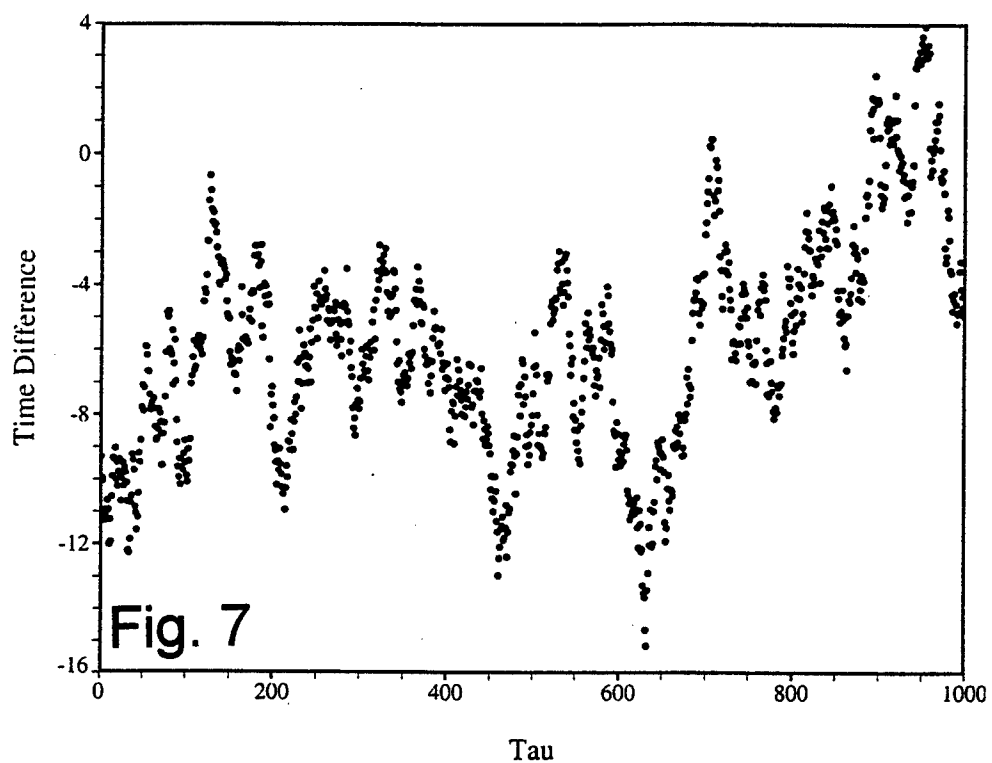
Autocorrelation Function of White FM

Fig. 8
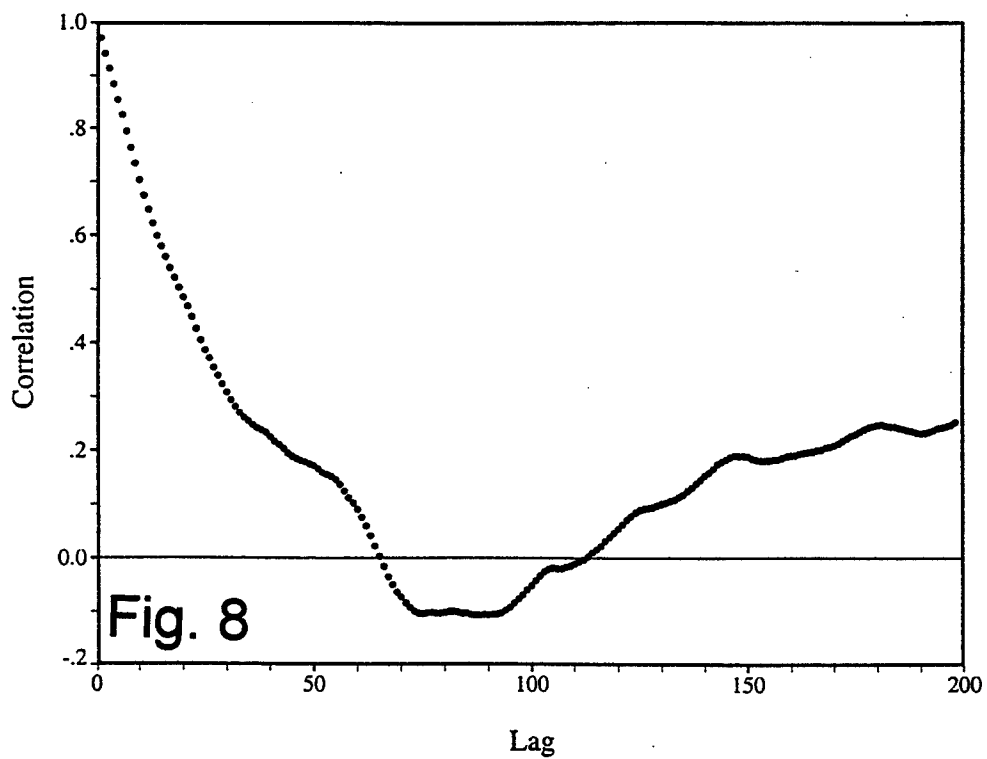
Power Spectral Density of White FM

from the Digital-Spectrum-Analyzer Method

Fig. 9
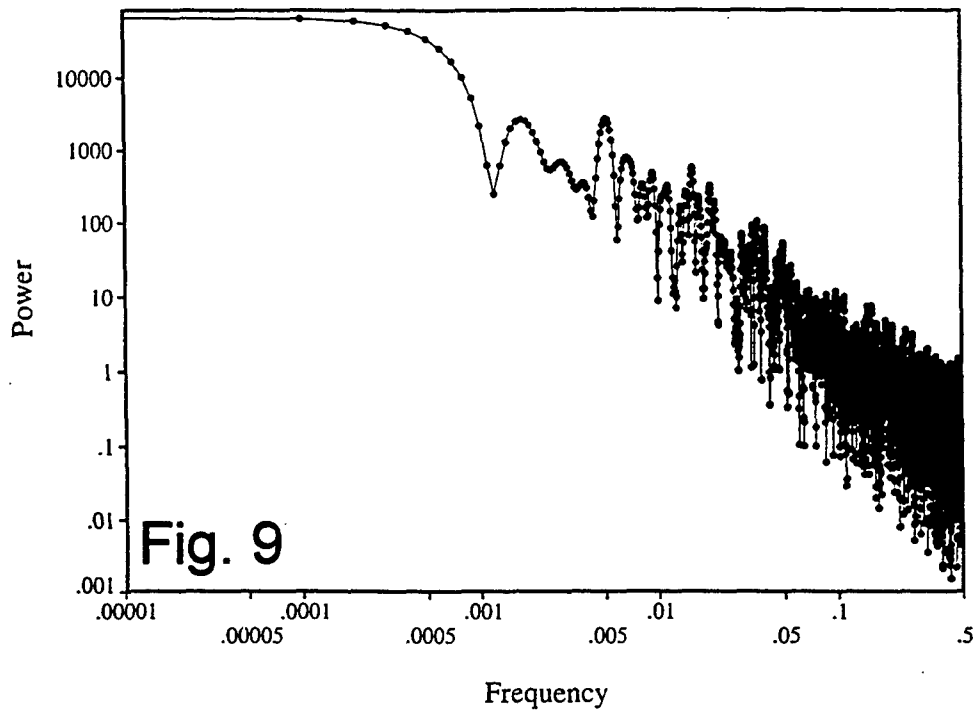
Time Deviation (TDEV) of White FM

For All Tau from Stable Software

Fig. 10

Phase-Plane View of White FM

Fig. 11

Fig. 12

387
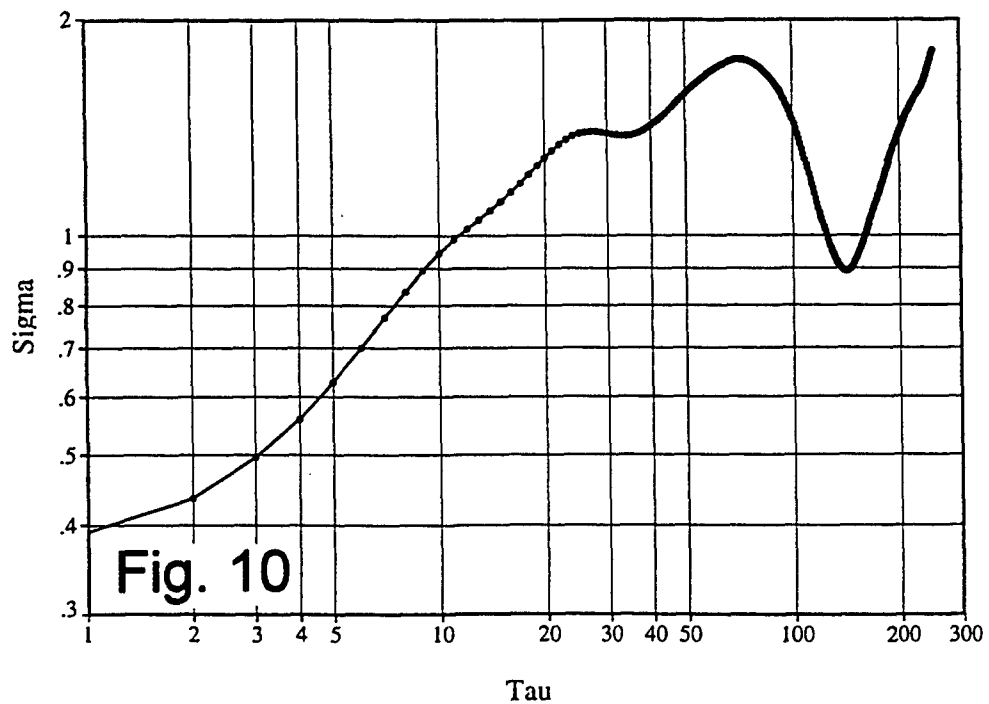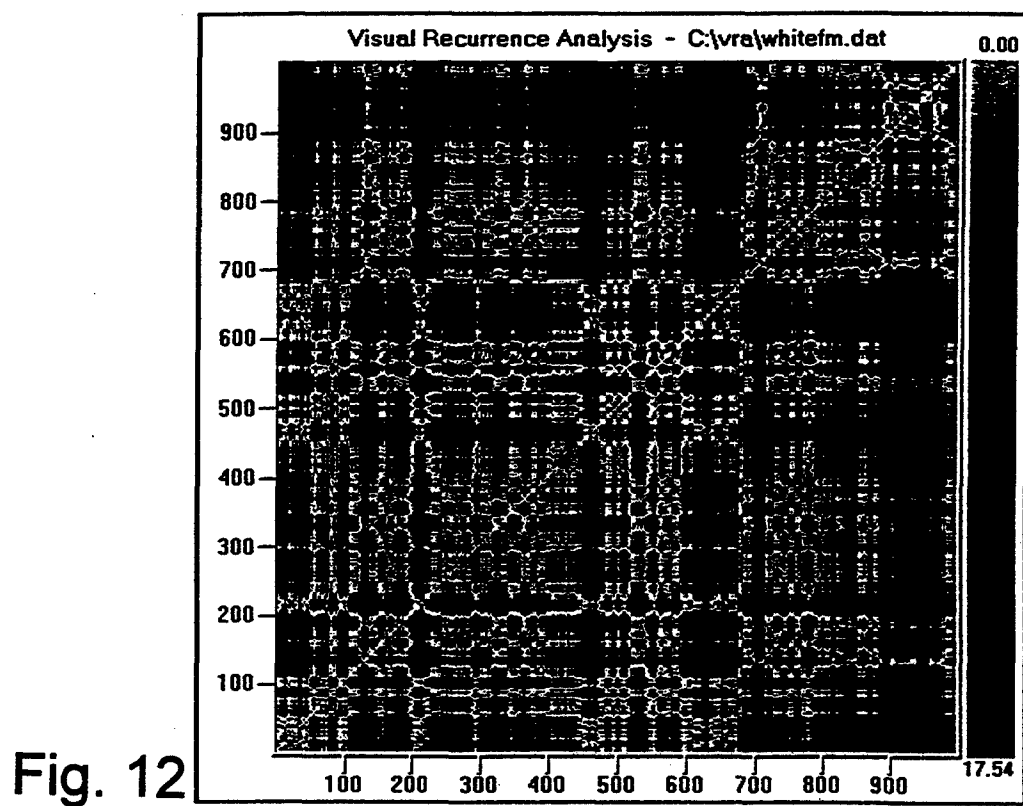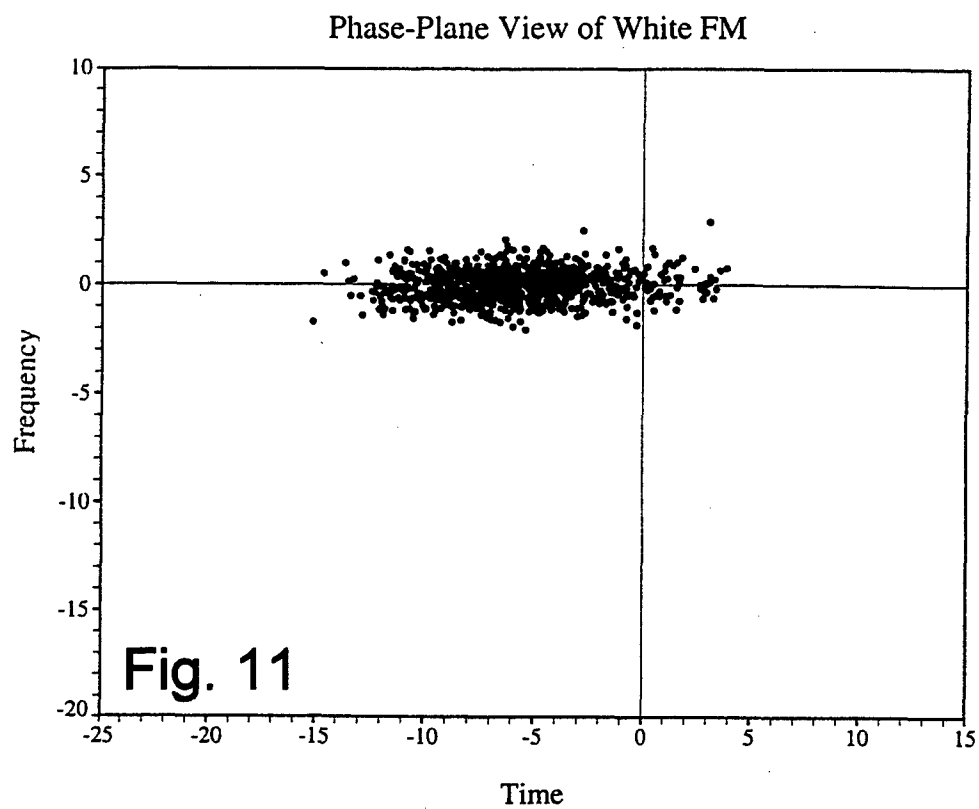
USNO(MC2) - USNO AMC(MC1) via TWSTT

Both are Steered Systems

Fig. 13
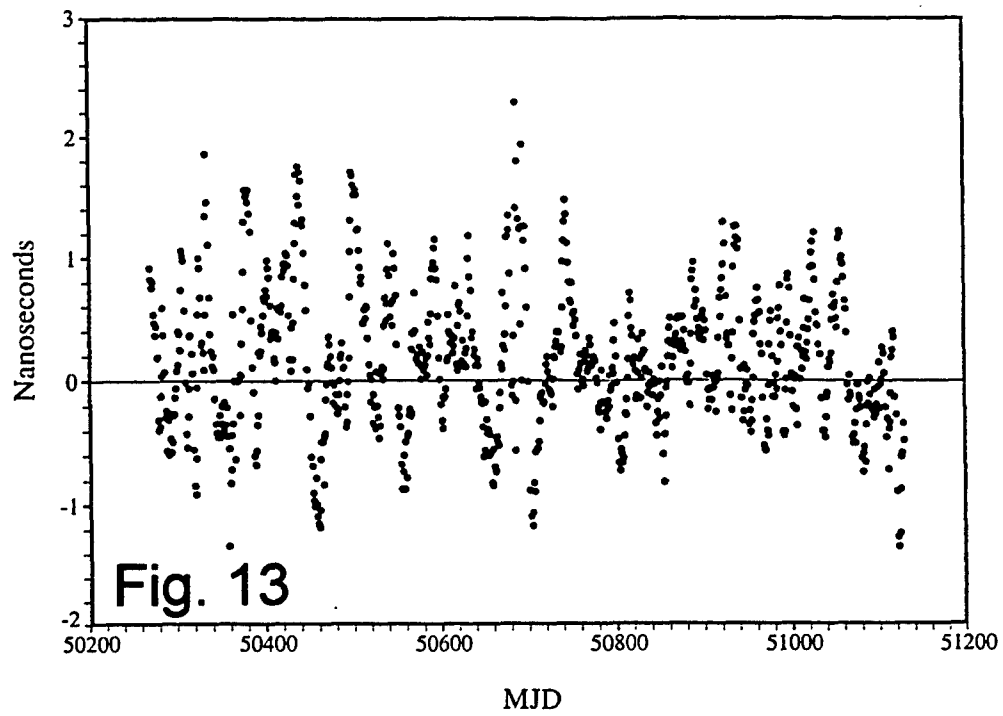
Autocorrelation Function of

USNO(MC2) - USNO AMC(MC1) via TWSTT

Fig. 14
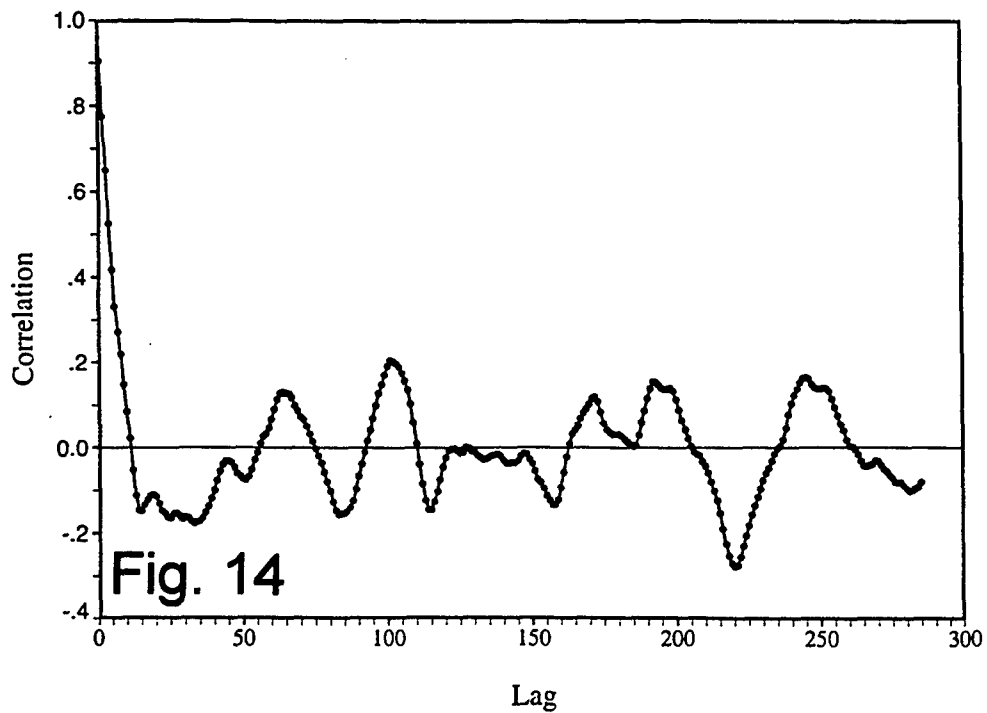
Power Spectral Density of TWSTT
from the Digital-Spectrum-Analyzer Method

Fig. 15
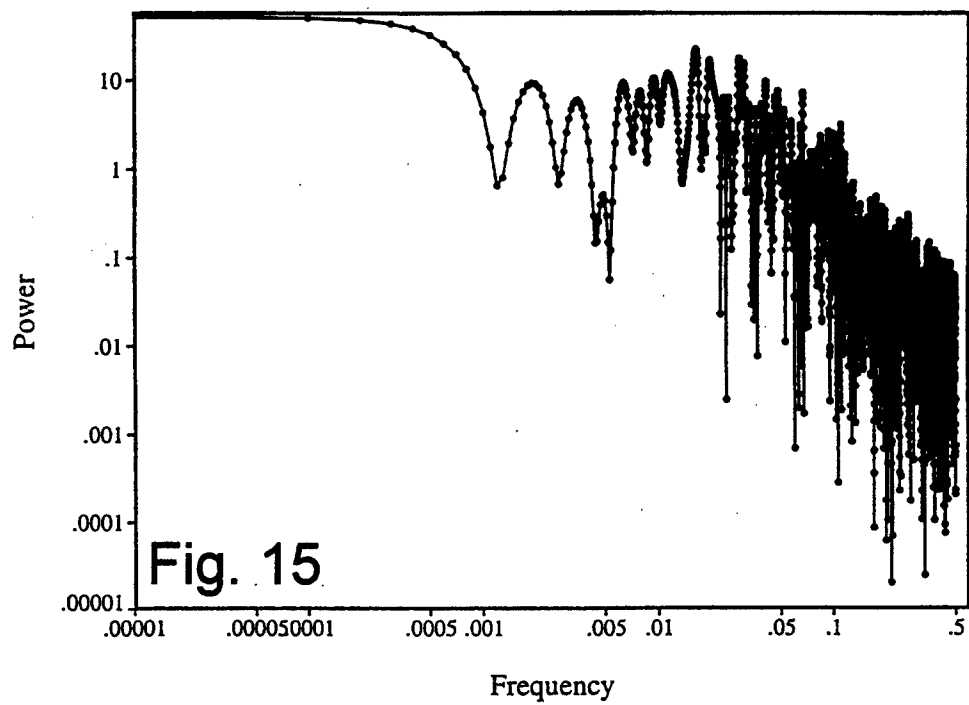
Frequency

Time Deviation (TDEV) of TWSTT

Fig. 16

Days
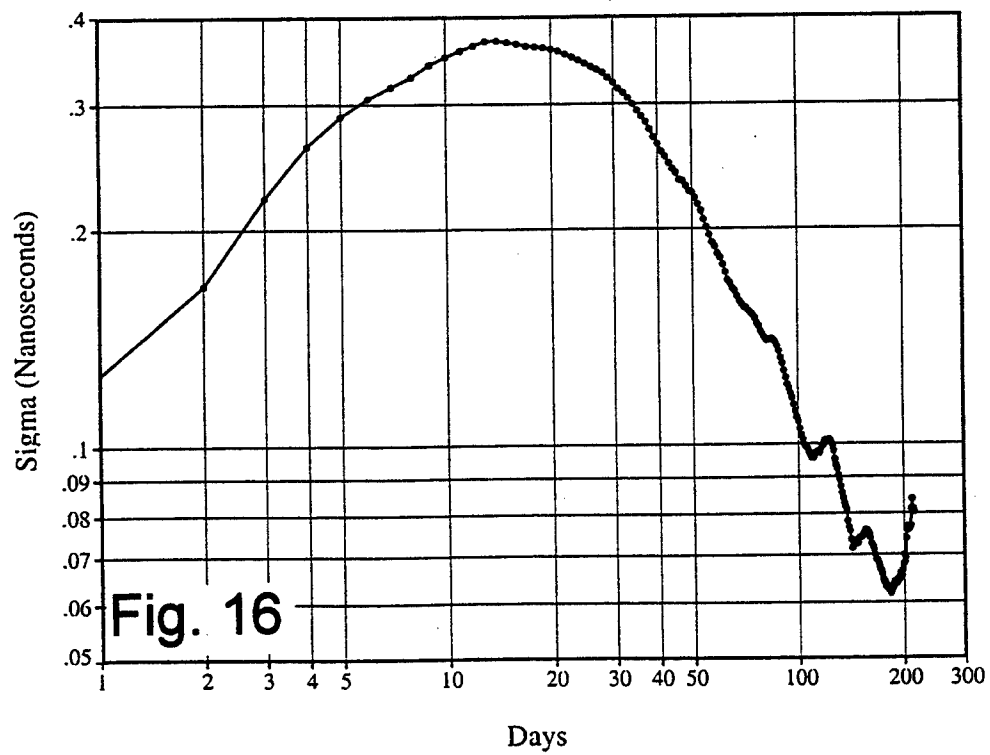
Phase-Plane View of TWSTT

Fig. 17
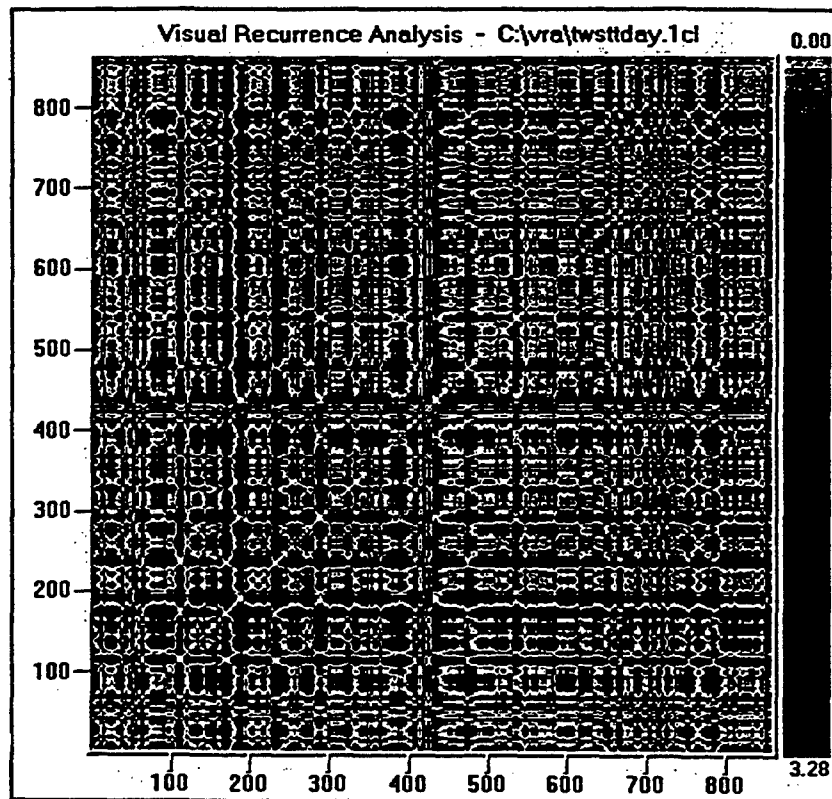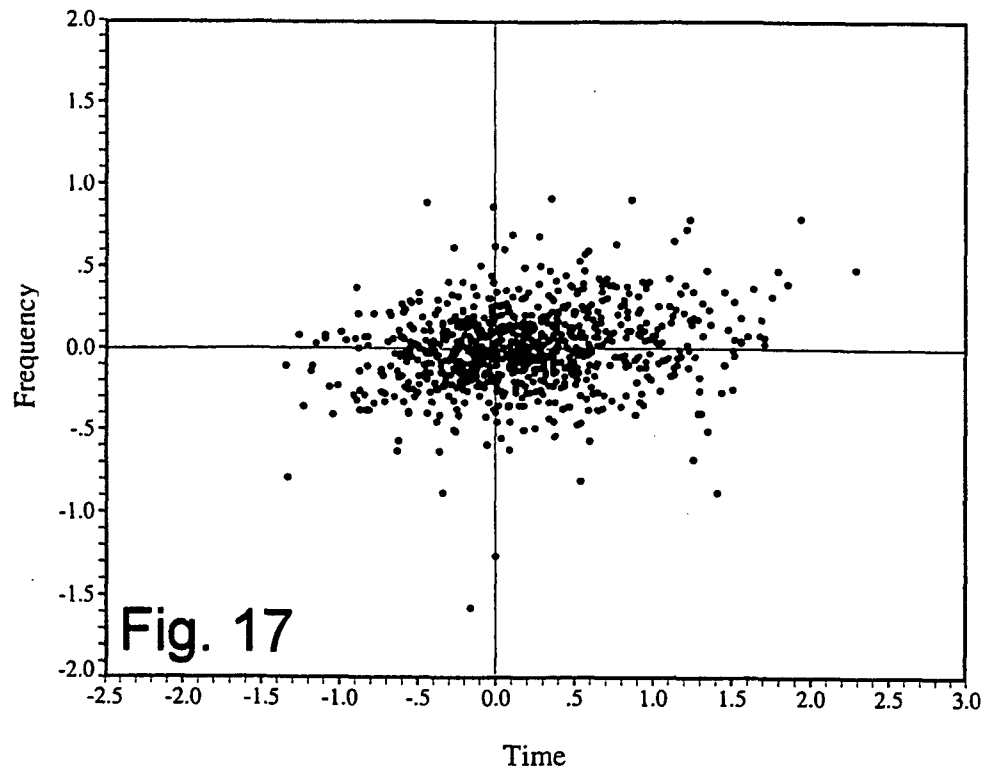
Fig. 18

Time-Frequency Analysis
Synthetic Unequally Spaced Data
Two Signals @ 1cpd & 3.754cpd
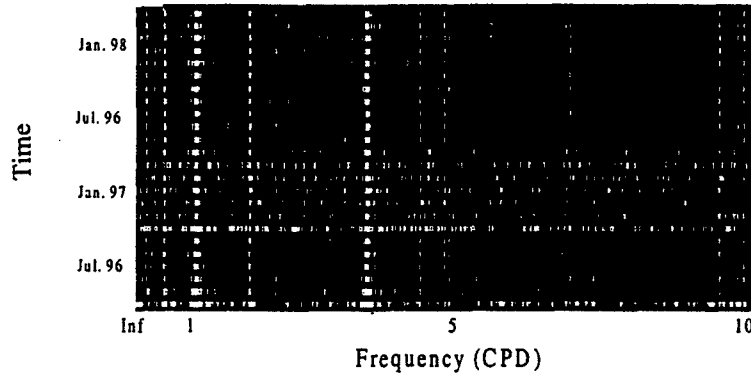
Fig. 19

Scale: Dark Red ---> Red ---> Yellow ---> White
Low signal ---------------------> High Signal

Time-Frequency Analysis
of USNO-AMC TWSTT
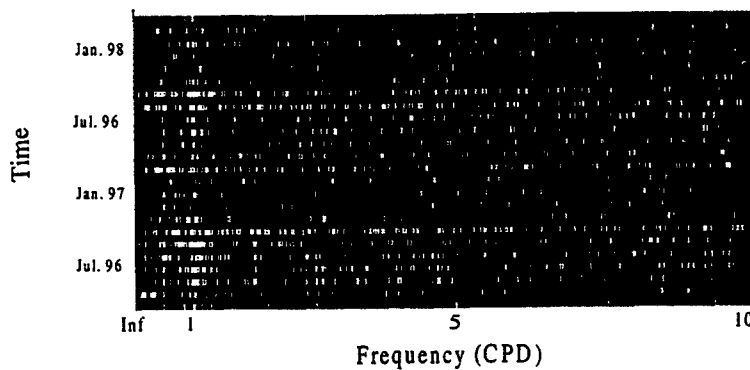
Fig. 20

Scale: Blue ---> Red ---> Yellow ---> White
Low signal --------------> High Signal

TWO-WAY SATELLITE TIME TRANSFER USING INTELSAT 706 ON A REGULAR BASIS: STATUS AND DATA EVALUATION

J. Azoubib[1], D. Kirchner[2], W. Lewandowski[1],
P. Hetzel[3], W.J. Klepczynski[4], D. Matsakis[5], T. Parker[6], H. Ressler[7], A. Soering[8],
G. de Jong[9], F. Baumont[10], J. Davis[11]

[1] Bureau International des Poids et Mesures (BIPM), Sèvres, France
[2] Technische Universität (TUG), Graz, Austria
[3] Physikalisch-Technische Bundesastalt (PTB), Braunschweig, Germany
[4] Innovative Solutions International (ISI), Vienna, Virginia
[5] U.S. Naval Observatory (USNO), Washington D.C.
[6] National Institute of Standards and Technology (NIST), Boulder, Colorado
[7] Space Research Institute, Graz, Austria
[8] Deutsche Telekom AG (DTAG), Darmstadt, Germany
[9] NMi Van Swinden Laboratorium (VSL), Delft, the Netherlands
[10] Observatoire de la Côte d'Azur (OCA), Grasse, France
[11] National Physical Laboratory (NPL), Teddington, United Kingdom

Abstract

TWSTT (Two-Way Satellite Time Transfer) observations in Europe and between Europe and the United States resumed on 20 January 1997, using the INTELSAT 706 satellite on a regular basis. Six European and two US stations observe regularly. Two other European stations are about to become operational. The paper first describes the activities of the CCTF (Consultative Committee for Time and Frequency) Working Group on TWSTT. The use of INTELSAT 706 satellite and status of participating stations is then discussed together with related data. Evaluation of the TWSTT data reported in this paper includes its comparison with GPS common-view time transfer data for selected continental and intercontinental links over a period of one-and-a-half years.

INTRODUCTION

TWSTT (Two-Way Satellite Time Transfer) observations in Europe and between Europe and the United States resumed on 20 January 1997 (MJD = 50468) using the INTELSAT 706 satellite on a regular basis. Three one-hour observation windows, on Monday, Wednesday and Friday, have been purchased from INTELSAT. Within these windows two-minute TWSTT measurements are performed between participating stations according to a schedule. Six

European and two US stations observe regularly. Two other European stations are about to become operational. No significant problems concerning the satellite have been encountered. An ITU standard format is used for the exchange of data. The exchange and storage of dataareeasy, as the files are small. Data are available within two days.

First, a résumé is given of the activities of the CCTF (Consultative Committee for Time and Frequency) Working Group on TWSTT. The use of INTELSAT 706 satellite is then described, as well as the status of participating stations and related data. Evaluation of the TWSTT data reported in this paper includes its comparison with GPS common-view time transfer data for selected continental and intercontinental links over a period of one-and-a-half years. The goal of this study is to compare the stability of GPS common-view and TWSTT techniques, not accuracy.

CCTF WORKING GROUP ON TWSTT

The 11th CCDS (now CCTF) meeting of 1989 issued a declaration 1989/1 encouraging the use of TWSTT and suggesting the creation by the BIPM of an *ad hoc* Working Group on TWSTT. The *ad hoc* Group met twice in 1989 and 1992. Following the decision of the 12th CCDS meeting in 1993, the *ad hoc* Group was converted into a permanent CCDS Working Group with the task of helping the BIPM to elaborate the TWSTT technique for its possible use in the construction of TAI [1]. Since 1993 there has usually been one annual meeting of the full WG and two technical annual meetings of the participating stations. The main achievements of the WG are: development of a standard format; organization of TWSTT time links (choice of modems, schedule of observations, duration of observation, data exchange, ...); negotiation of the best conditions for the use of INTELSAT satellite; and the evaluation of TWSTT links by comparison with other available time transfer techniques.

USE OF INTELSAT 706 ON A REGULAR BASIS

As mentioned in the introduction, the TWSTT system has access to three one-hour observation periods from INTELSAT. In each window, beginning at 14 h UTC, 30 minutes are dedicated to links within Europe, and another 30 minutes to links between the United States and Europe. Within each 30-minute window, sessions are scheduled to last for 2 minutes with a 1-minute break to switch the codes [2].

The participating stations, namely the DTAG, NIST, NPL, PTB, TUG, USNO, and VSL, continue to perform observations on a regular basis, and the data from the present project are currently under evaluation. At the OCA, TWSTT equipment is presently undergoing tests before going into regular operation.

Each session between stations A and B consists of two-minute periods during which second-to-second measurements are carried out simultaneously at both stations. The time transfer measurement for each station is then obtained from a quadratic fit over the 1-second measurement interval. A specific data format has been developed to allow the exchange of two-minute tracks between partner stations. A provisional description of this format is given in the Report of the 3rd Meeting of the CCTF Working Group on TWSTT, held in Braunschweig (Germany) on 28-29 September 1995 [3]. A draft revision of Recommendation ITU-R TF.1153, recommending the use of this format, is presently under study.

Table 1. Availability of TWSTT data.

Laboratory	Continuous observations since ...
TUG	20 January 1997
USNO	22 January 1997
VSL	22 January 1997
DTAG	7 February 1997
PTB	17 February 1997
NIST	21 February 1997
NPL	20 April 1998
OCA	Temporarily interrupted

It is of considerable interest to note that all TWSTT data files listed above use the ITU-R format. This greatly simplifies the computation of time links. It should be emphasized that TWSTT data are available quickly, usually one or two days after a session and, in the case of TUG, one hour after.

COMPARISON OF GPS AND TWSTT MEASUREMENTS

The goal of this study is to compare the stability of GPS common-view and TWSTT techniques, not accuracy. However, some indications on the constant biases between these two techniques are provided. A detailed study of the accuracy of the two techniques is provided elsewhere in these Proceedings in "Calibration of Three European TWSTFT Stations Using A Portable Stations and Comparison of TWSTFT and GPS Common-View Measurement Result" by D. Kirchner et al.

Aside from other differences, the TWSTT and GPS common-view data differ in their density: TWSTT measurements are performed every two or three days during 120 s intervals; GPS measurements are performed every day and there are about thirty 780 s tracks per day, which corresponds to 23400 s GPS observations per day.

It will be shown that very short interval TWSTT data give comparable or sometimes better results when compared with GPS. For the needs of the present comparison a choice was made to smooth and interpolate GPS data to the midpoints of the TWSTT sessions. As a result we obtained differences between the two techniques at intervals of two or three days. This comparison was performed for two types of time link:

• short-distance time link, over 700 km, between the PTB and the TUG,
• long-distance time link, over 8000 km, between the PTB, and the NIST.

The Figure 1 shows the differences between UTC(TUG) and UTC(PTB) obtained by TWSTT and GPS common-view for a period of about fourteen months. One can observe an apparent agreement between the two methods with a shift of several nanoseconds. We observe also a large drift between the two time scales, which complicates somewhat the statistical analysis. Figure 2 indicates the differences between the two methods at the times of the TWSTT observations, as well as the outside temperature at the TUG. The scatter of the differences between the TWSTT and GPS data for this short-baseline is about 12 ns. These differences exhibit an apparent systematic variation correlated with the external temperature. The seasonal effect has always been attributed to the environmental sensitivity of the GPS time equipment [4]. The stronger seasonal effect in 1997 stems from a problem with the power supply to the GPS time receiver at the TUG, which has amplified the temperature dependence of TUG GPS equipment. One should note that clocks are not entirely removed in these differences because of the different nature of the TWSTT and GPS data already mentioned: for GPS we have over 20000 s of observations per day, while for TWSTT we have 120 s of observations every two or three days. Concerning the bias of several nanoseconds between the two methods it should be pointed out that a differential correction issued from a TWSTT equipment calibration was applied to the TWSTT data considered here, but GPS data were not corrected for calibration during this study. Once GPS calibration corrections provided by a series of GPS calibration trips [5] are applied, the observed shift between the two methods disappears (see D. Kirchner et al. in these Proceedings).

Figure 3 shows the time deviation of [*UTC(TUG) – UTC(PTB)*] for the TWSTT and GPS common-view data. We see the same behavior for the two methods. The small differences are not significant. In fact from the beginning we see the behavior of the two clocks used in the comparison. The plot is not a property of the time transfer measurement, but an indication of the performance of the two cesium clocks. A comparison involving two masers would produce a different curve.

The long-distance comparison over 8000 km was performed between UTC(PTB) and UTC(NIST) for a period of about fourteen months (see Figure 4). We also observe for this long-baseline an apparent agreement between the two methods with a shift of several nanoseconds. The scatter of the differences between the TWSTT and GPS data reported on Figure 5 is about 20 ns. If we remove two outliers, this scatter reduces to about 12 ns. No seasonal effect is noticeable. The bias of several nanoseconds observed between the two methods is due to the

way in which the TWSTT data were calibrated. As no independent TWSTT calibration was available for this link, the TWSTT link was calibrated using a GPS link provided by the BIPM Circular T. All transatlantic GPS links in Circular T are corrected for precise satellite ephemerides and ionospheric measurements. No such corrections were applied to the GPS link computed for this study. The GPS link was computed with broadcast ephemerides and modelled ionospheric delay. This is because no reliable ionospheric measurements were available. Differences between the measured and modelled ionospheric delays for the period covered by this study are roughly equal to −10 ns. So the bias we observe here arises from the differences in the computation of GPS links, and not from the differences between the two methods. As was mentioned earlier, this study is not about the comparison of accuracy between TWSTT and GPS methods,but about their stability. To realize a comparison of the accuracy of the two methods an independent calibration of TWSTT and GPS equipment should be organized.

Figure 6 shows the time deviation of [*UTC(PTB) − UTC(NIST)*] for TWSTT and GPS common-view data. For averaging times up to 10 days, the TWSTT link seems to be more stable than the GPS link. This GPS behavior is probably linked to the poor quality of broadcast ephemerides and modelled ionospheric delay which were used for this study.

CONCLUSIONS

• The CCTF WG on TWSTT has been very active for the past five years and has successfully moved the TWSTT method to an operational phase.

• Presently there are six operational and two pre-operational TWSTT stations in Europe and two operational stations in the USA using the INTELSAT 706 satellite. Preparations are also under way to operate several other TWSTT stations in the Asia-Pacific region. They are using INTELSAT 702 and JCSAT-3 satellites. Future connection between Asia-Pacific and Europe-North America TWSTT networks is already under consideration (see M. Imae et al. in these Proceedings).

• The INTELSAT 706 satellite was used for the past twenty-two months on a commercial basis. For this period we observed smooth, uninterrupted, routine operations of a network of TWSTT stations.

• Comparison of the stability of TWSTT and GPS common-view methods during this study can be summarized roughly as follows:

   - for the short-baseline comparison a seasonal effect correlated with outside
     temperature was observed; difference in the stability of the two methods could not
     be determined, as their performance from the beginning is covered by the noise of
     the two cesium clocks being compared;

- for the long-baseline comparison the TWSTT method is more stable than GPS for up to 10 days (GPS was not corrected for precise ephemerides and ionospheric measurements);

- the performance of TWSTT appears to be at least as good as the performance of GPS common view.

• The progress accomplished until now allows us already to look toward possible consideration of the TWSTT method for TAI needs.

REFERENCES

[1] Report of the 12th CCDS Meeting, BIPM, 1993.
[2] The CCDS Working Group on Two-Way Satellite Time Transfer, *Report of the 4thMeeting*, Turin, October 1996.
[3] The CCDS Working Group on Two-Way Satellite Time Transfer, *Report of the 3rdMeeting*, Braunschweig, September 1995.
[4] D. Kirchner et al.,"Comparison of GPS Common-View and Two-Way Satellite Time Transfer Over a Baseline of 800 km," *Metrologia* **30**, pp. 183-192, 1993.
[5] W. Lewandowski and H. Konate, " Differential Time Corrections for GPS Time Equipment Located at the OP, VSL, NPL, DTAG, PTB, TUG, IEN, USNO and NIST: 4th Evaluation," Rapport BIPM, 1998 (in preparation).
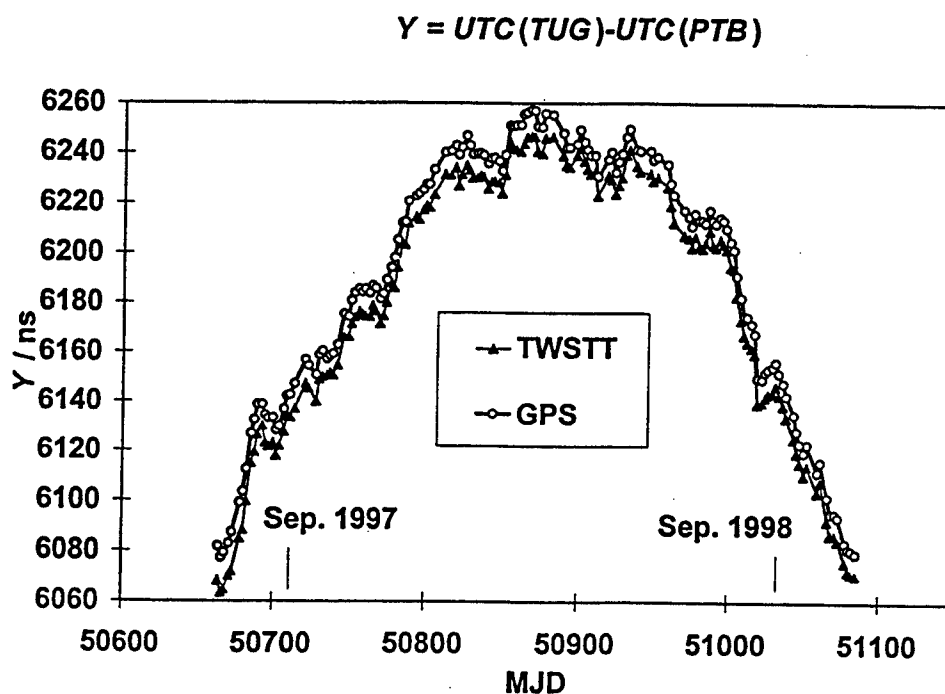
$$Y = UTC(TUG)\text{-}UTC(PTB)$$

Figure 1. Differences between UTC(TUG) and UTC(PTB) obtained by TWSTT and GPS common-view for a period of about fourteen months (after slope removal).

$$Y = [UTC(TUG)\text{-}UTC(PTB)]\ twstt\ \text{-}\ gps$$
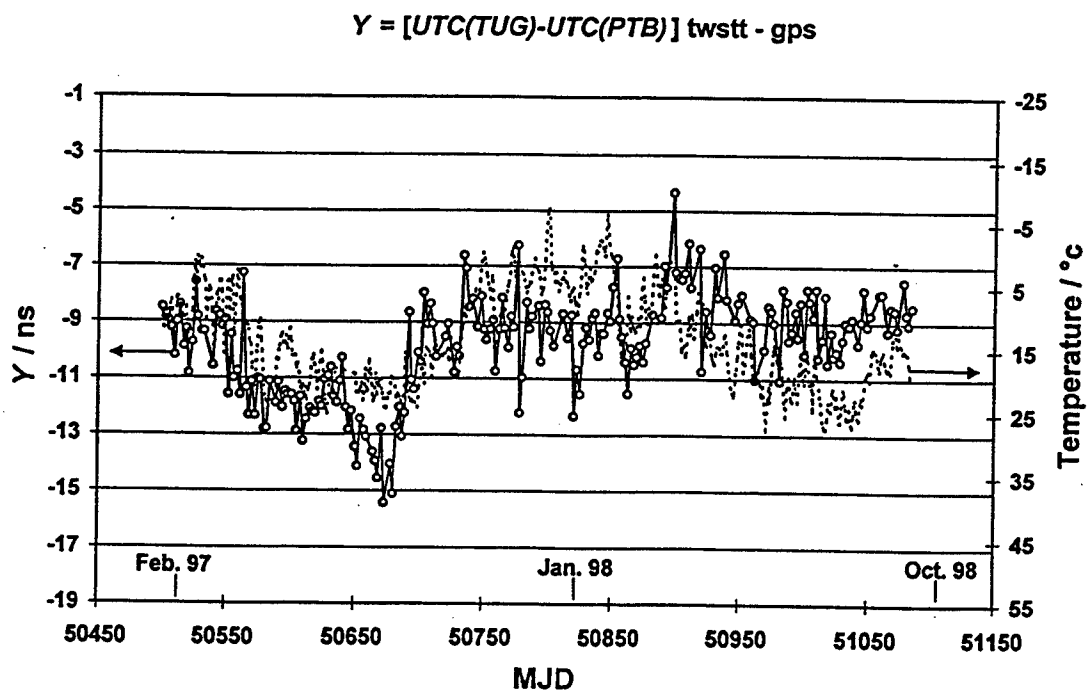
Figure 2. Differences between TWSTT and GPS common-view methods at the times of TWSTT observations, and the outside temperature at the TUG.

399

TIME STABILITY
UTC(TUG)-UTC(PTB) (by TWSTT and by GPS)

Tau	Sigma
2.36e+05	2.57e-09
4.71e+05	3.07e-09
9.43e+05	4.18e-09
1.89e+06	5.69e-09
3.77e+06	5.35e-09
7.54e+06	2.57e-09

o TWSTT

Tau	Sigma
2.36e+05	2.27e-09
4.71e+05	2.92e-09
9.43e+05	4.18e-09
1.89e+06	5.73e-09
3.77e+06	5.67e-09
7.54e+06	2.65e-09

□ GPS

50664-51084 (04/08/97 - 28/09/98)
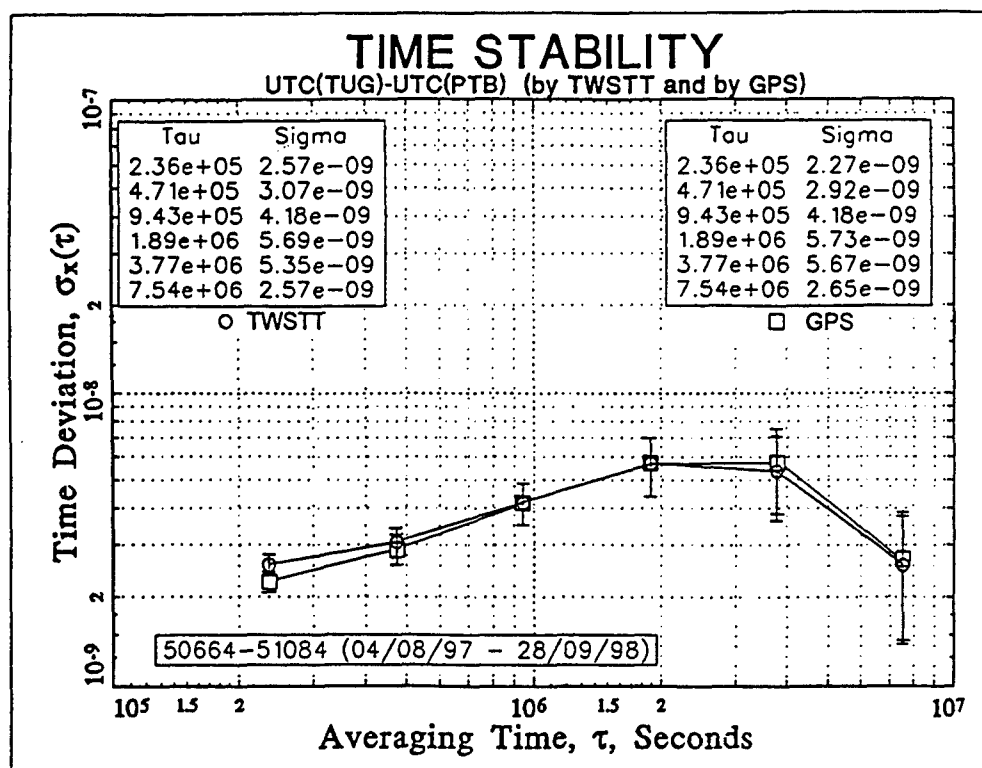
Figure 3. Time deviation of [*UTC(TUG)* – *UTC(PTB)*] for TWSTT and GPS common-view.
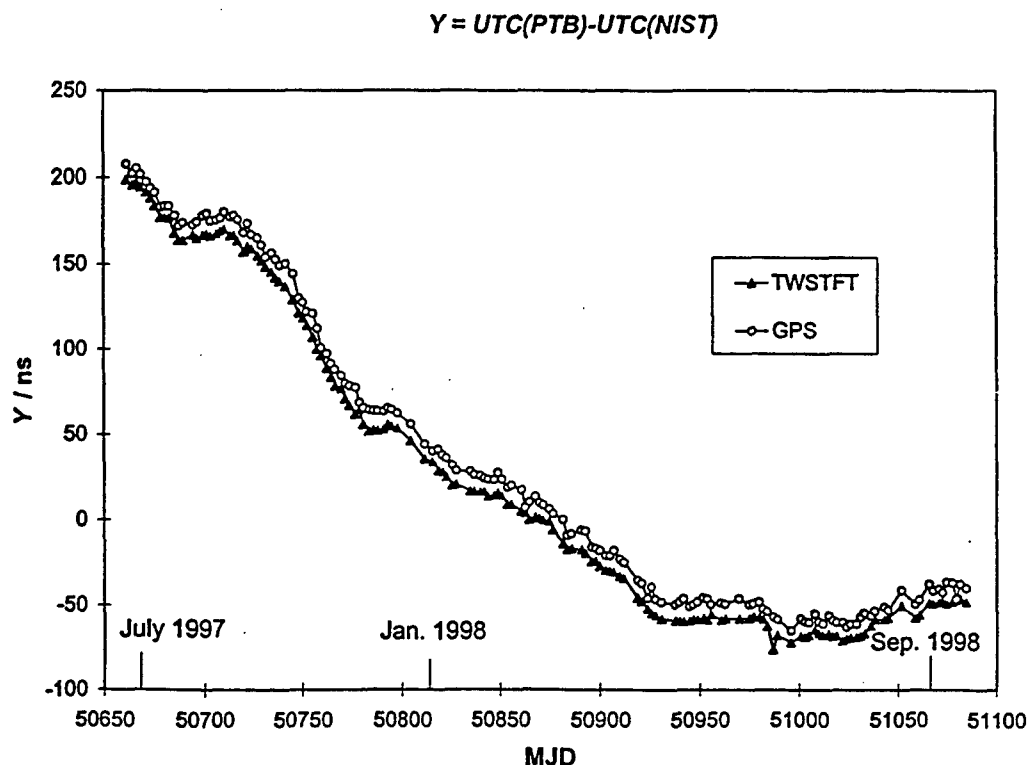
Y = UTC(PTB)-UTC(NIST)

Figure 4. Differences between UTC(PTB) and UTC(NIST) obtained by TWSTT and GPS common-view for a period of about fourteen months.
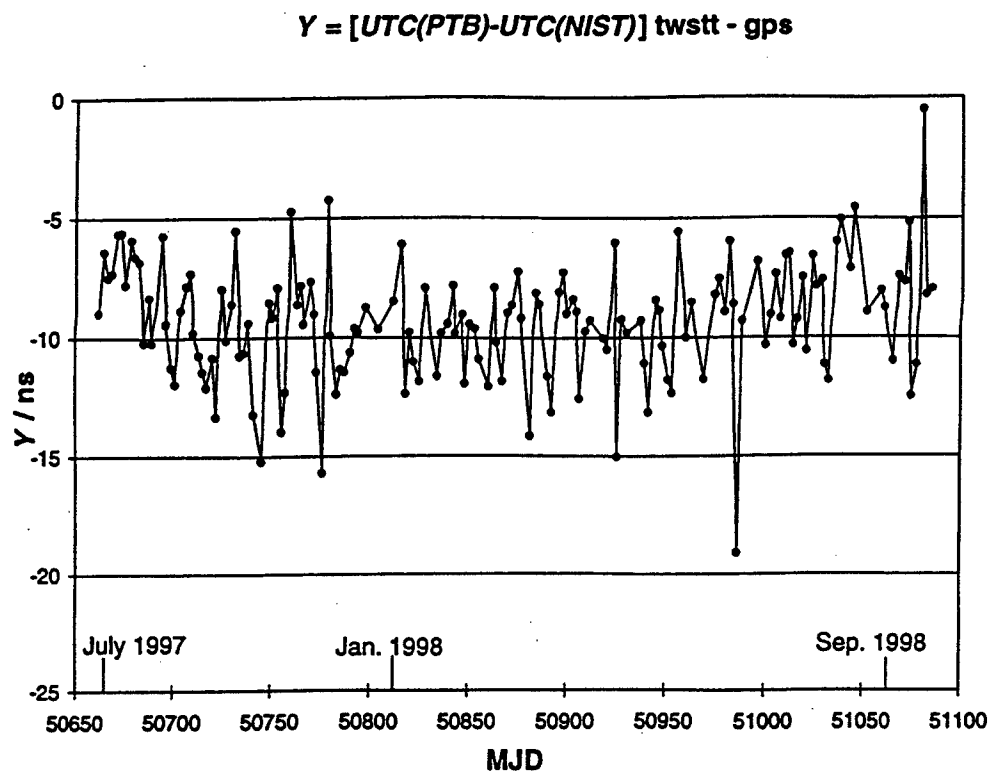
400

Y = [UTC(PTB)-UTC(NIST)] twstt - gps

Figure 5. Differences between TWSTT and GPS common-view methods at the times of TWSTT observations.
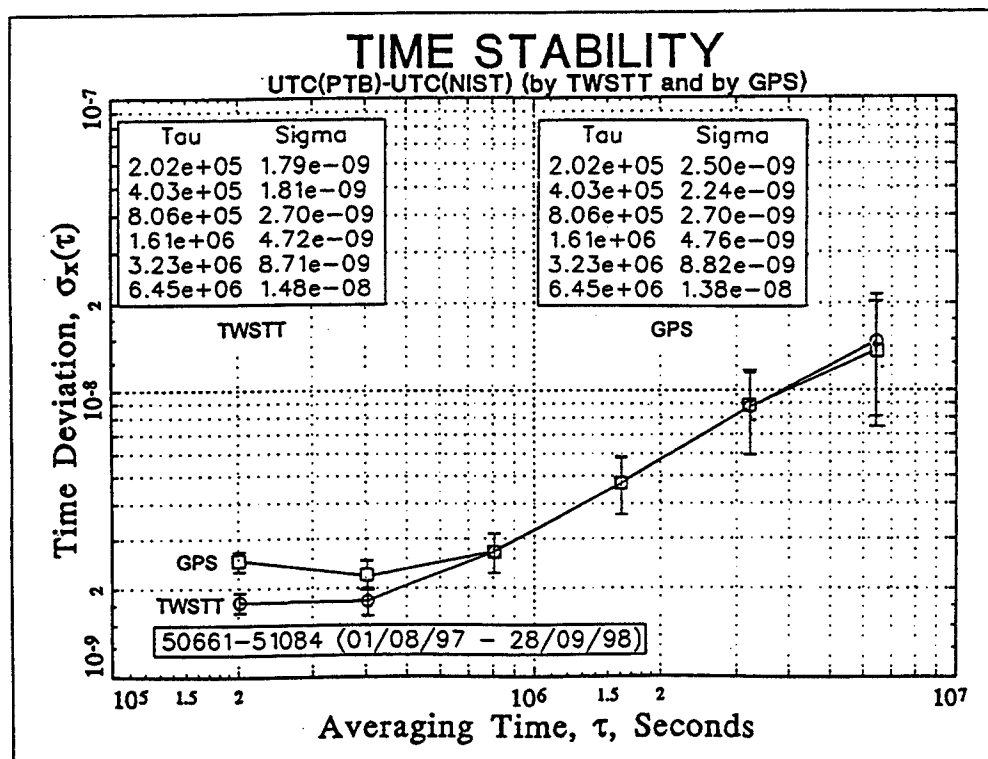
Figure 6. Time deviation of [*UTC(PTB) – UTC(NIST)*] for TWSTT and GPS common-view.

401

Questions and Answers

DEMETRIOS MATSAKIS (USNO): I just wanted to point out that the two-way data that you are talking about is two-way as done in this experiment, which is three times a week. It is actually much more accurate than GPS as is proven at the AMC. The plots that Jim DeYoung showed of free-running time scales between the USNO at Washington and the USNO at the Alternate Master Clock show increased improvement out to well past a month. If you look at unsteered maser-only time scales, that improvement seems to go all the way out to many, many months. But, there is problems there due to the correlation between parabolas and drift, which Marc Weiss was talking about. Certainly, the two-way technique, if it is done repeatedly, like every hour, is even more stable.

JACQUES AZOUBIB (BIPM): I forgot to mention that the data here is not equally spaced. When I computed the time variation, I took an average. So the values of TVAR shown in my vugraphs are a bit biased.

JUDAH LEVINE (NIST): I noticed in the TUG-PTB data that you showed that there was a bias between the two-way data and the GPS data of about 10 or 11 nanoseconds. I was wondering how that is consistent with Dr. Kirchner's calibrations.

JACQUES AZOUBIB: With Dr. Kirchner?

JUDAH LEVINE: Dr. Kirchner reported on a number of calibrations in which you went around measuring the delays of the various stations. I was wondering how, if the delays are understood. You have a bias of about 10 nanoseconds.

JACQUES AZOUBIB: I do not understand your question. Here?

JUDAH LEVINE: No, no. The average of that curve is about 10 nanoseconds off of zero.

JACQUES AZOUBIB: No, I do not agree with you. Because one cannot average here because it is not white phase noise. It is only white noise to 40 days. So if you want to average, you have to average over 40 days, 40 days, 40 days, and 40 days.

JUDAH LEVINE: Every one of those points is more negative than minus seven nanoseconds except one. That curve does not have a mean of zero. Your whole curve is biased down by about 10 nanoseconds.

DIETER KIRCHNER (TUG): Yes, it is true.

JIM DeYOUNG (USNO): The obvious answer that the numbers which BIPM is using are not Dr. Kirchner's answers? So, there is obviously a great deal of improvement there.

JACQUES AZOUBIB: Yes, you are right. If you want, we can make Dr. Kirchner's values in agreement if we add 12 nanoseconds. Because while computing these values, we applied a time constant of 12 nanoseconds, and it was used in order to take GPS calibrations into account.

DIETER KIRCHNER: May I explain it briefly? It is a long story, and I avoided going into this story. BIPM applies corrections to the GPS data and then they calculate the Circular T. After doing the first

GPS calibration trip the next one and the next one showed that there is a bias in the Circular T data. There was a total difference between the Circular T data and the two-way data by about 20 nanoseconds. The correct number was 18.3 nanoseconds. After calibrating the two-way data, with location of the station, and the GPS data, with the results from the GPS receiver trips, the difference is about zero, as we have shown.

These 10 nanoseconds are coming from applying a wrong correction to the GPS data by BIPM. I always had some suspicion about this correction, and in my opinion when this correction was calculated, they simply used a wrong sign. Ten nanoseconds in one direction, in the wrong direction, you have a bias of 20 nanoseconds.

I did not want to explain all this. I can show you the different steps going from Circular T, GPS data, difference between Circular T GPS data, and two-way data, after applying the correction for the two-way data using the transportable station, you have about 20 nanoseconds. Then you apply to the original GPS data the correction found by the GPS receiver trips and you have no difference. You have the zero offset that you want to see. I agree with you here, you see, about the minus ten nanoseconds.

JUDAH LEVINE: And are you saying that the PTB NIST link has the same error in it? Because the number is about the same.

DIETER KIRCHNER: No.

JACQUES AZOUBIB: No, this is a special case for –

JUDAH LEVINE: Please put up the PTB NIST same plot? It also has a mean of about seven, eight, nine, or ten or some number like that. Is that a coincidence or is there another mistake?

JACQUES AZOUBIB: No, for this link, no time constant has been applied.

JUDAH LEVINE: But that number has a mean of about, I do not know, seven maybe, or eight or nine. It is not zero either.

WLODZIMIERZ LEWANDOWSKI (BIPM): I would like to clarify the difference in the delays. First, for the previous graph, we cannot call this a mistake. This is a practice – we are using all the corrections for GPS calibration. That does not mean it is always wrong. These values are changing with time, as shown during the Dr. Kirchner's talk. So Jacques Azoubib was using the current differential calibration for GPS. What he was showing, he was not applying the most recent calibrations. There is a separate talk on this issue. This explains why we have about 10 nanoseconds. It is because we are using several old years' GPS corrections.

This vugraph, this difference comes from something else because here, the two-way link is not calibrated. So just value does not matter, the difference – because there is no calibration for two-way. GPS is calibrated, but two-way link is not. Okay? GPS is calibrated at the level which we can do, several nanoseconds uncertainty. But we do not have a differential calibration for PTB NIST.

DIETER KIRCHNER: I am sorry, I have to make a correction. Also, the two-way link here is calibrated using the Circular T data. So, I think that all this stuff demonstrates that we have to be a bit cautious using the Circular T as an absolute difference between time scales. We already know from USNO that

there were similar problems, 29 nanoseconds or something like that.

WLODZIMIERZ LEWANDOWSKI: Yes, you are right. But what I wanted to say was that there is no independent calibration for two-way.

JUDAH LEVINE: I guess I am a little unclear, under these circumstances, of how we are going to combine GPS data and two-way data into TAI when the calibrations do not seem to agree, for whatever reason. I mean, I am not suggesting that one of them is right or one of them is wrong; but if one has these sorts of differences, then the difference between two laboratories calculated using one method and using another method, it is going to have a difference of something like 10 nanoseconds in it.

WLODZIMIERZ LEWANDOWSKI: I do not agree with this because of Dr. Kirchner's paper. He has shown an excellent argument between GPS calibration and two-way calibration. This is the story of all calibrations which were used from the past GPS calibration trips. But GPS delays are changing. Dr. Kirchner has shown that in fact we have to apply the seasonal GPS calibration results.

DIETER KIRCHNER: Really, it is simple to explain and there is no mystery about it. One has to distinguish between different data sets. So Laboratory "A" and Laboratory "B" are doing GPS measurements. These are the data which are coming out of the GPS receivers. These data are sent to BIPM. BIPM applies corrections to this data according to past GPS receiver trips and one should not use these old calibrations. One should simply use GPS data as relayed from the laboratories and apply the most recent corrections, and we try to do it.

DEMETRIOS MATSAKIS: Can I make a comment here? I had asked Claudine Thomas in June and received a very positive response from her about having the BIPM create a product which would be post-processed corrections for all of these things, which we could all refer to when we are comparing different time scales.

WLODZIMIERZ LEWANDOWSKI: Very quick comment. At the BIPM, because of the changes in the GPS delays, we have decided not to apply calibration results which give values of differential delays lower than 10 nanoseconds. Because we think it does not matter if we apply them because in several months there will be a several nanosecond offset from this value. So, the values of calibration lower than 10 nanoseconds are no longer applied to our GPS links.

GERARD PETIT (BIPM): The whole question of the delay was reviewed more than one year ago, but clearly, it should be reviewed again. It is a moving process and the uncertainties in calibrations are increasing, so we will review it again.

I would like to remind you that for the long-distance links that are used in TAI, GPS links, precise ephemeris on the ionosphere measurements are used for the situation of the GPS links in TAI, are not bad compared to what has been shown here where no corrections have been applied.

DIETER KIRCHNER: I know it is late, but on the other hand, this discussion is so important. I think it is possible to clear up these mistakes. Maybe we can find time in the afternoon to proceed with this discussion. There are action items and discussions right before the closing session. So, I think we should really proceed. I would be sorry if we would go from here without having explained these discrepancies.

A FREQUENCY TRANSFER AND CLEANUP SYSTEM FOR ULTRA-HIGH STABILITY AT BOTH LONG AND SHORT TIMES FOR THE CASSINI Ka-BAND EXPERIMENT

M. D. Calhoun, G. J. Dick, and R. T. Wang
California Institute of Technology, Jet Propulsion Laboratory
4800 Oak Grove Drive, Pasadena, CA 91109, USA

Abstract

New radio science experiments, including a gravitational wave search and several atmospheric occultation studies, are planned for the Cassini Ka-band experiment. These experiments are made possible by reduced solar-induced phase fluctuations at the high frequency (32 GHz) of the radio link between the earth and the spacecraft. In order to match the improved link performance, a significant upgrade is under way to improve the frequency stability capabilities of NASA's Deep Space Network (DSN). Significant improvements are being undertaken in many areas, including antenna vibration and (wet) tropospheric calibration, in addition to frequency generation and distribution.

We describe here the design and development of a system to provide a reference signal with the highest possible frequency stability for both long-term, short-term, and phase noise, at an antenna (DSS 25) that is remote from the frequency standards room at SPC-10 at the Goldstone site. The new technologies were developed in order to meet the very tight requirements. They are: (1) a Stabilized Fiber-Optic Distribution Assembly (SFODA) that includes active compensation of thermal variations to transfer long-term stability over 16 km of ordinary fiber-optic cable, and (2) a Compensated Sapphire Oscillator (CSO) that provides short-term performance in a cryocooled sapphire oscillator with ultra-high short-term stability and low phase noise.

INTRODUCTION

The Cassini spacecraft was launched from Cape Canaveral in October 1997 for a mission to Saturn. Several gravity wave experiments are scheduled, beginning in November 2001, during the cruise phase of the spacecraft. Orbit insertion at Saturn is scheduled for July 2004. After orbit insertion, radio science occultation experiments will be conducted. These experiments require reference signals with the highest stability and the lowest phase noise imposed to date in the Deep Space Network. In order to meet the frequency standards requirements for these Cassini experiments, a new frequency generation device, the Compensated Sapphire Oscillator (CSO), has been developed at JPL and will be implemented in the DSN. The CSO has ultra-high short-term stability and very low phase noise. A hydrogen maser or a Linear Ion Trap standard (LITS) will provide the necessary long-term stability.

A problem arises in maintaining long-term stability because of the distance between the frequency standard, located at SPC 10, and the remote antenna, located 16 km away. The reference frequency transfer is via optical fibers which are subject to temperature variations, which in turn produce phase variations of the reference signal. To mitigate the effect of temperature variations on the long run of fiber cable, an active fiber compensator, the Stabilized Fiber Optic Distribution Assembly (SFODA), has been developed at JPL and will be implemented in the DSN to support the Cassini experiments at DSS 25. We present in this paper the system concept of the CSO and the SFODA. Figure 1 depicts the configuration of the CSO and the SFODA at Goldstone Tracking Station to support the Cassini experiments.

STABILIZED FIBER OPTIC DISTRIBUTION ASSEMBLY

Fiber-optic cable is the preferred medium for distributing RF signals from frequency standards to users located in tracking antennas in the Deep Space Network. A hydrogen maser or LITS is used as the source of a highly stable signal, typically 100 MHz, which is impressed on an optical carrier by intensity modulation of a laser diode. Subsequently, the signal is transmitted via buried optical cable and distributed at a remote location. The optical cable is buried at a depth of 1.5 meters, which isolates it from large temperature variations at the ground surface [1]. The same optical cable passes through three different plenums as well as splice vaults distributed over the 16 km fiber run. Cable exposure to various temperature variations results in degraded stability of the reference signal at the remote user location.

The SFODA utilizes active feedback to correct for phase variations in the reference signal. Figure 2 is a block diagram of the SFODA. A 100 MHz reference signal from a hydrogen maser or LITS frequency standard is the input to the SFODA transmitter. The 100 MHz is multiplied to 1 GHz for transmission to the remote facility. At the receiving end, the SFODA 1 GHz output is fed to the CSO for steering for long-term stability.

At the remote antenna site, the SFODA receiver houses a low noise 100 MHz VCO which is phase-locked to the stabilized 1 GHz. The 100MHz signal is mixed with the 1 GHz reference signal to produce 900 MHZ and 1100 MHz to feedback over the fiber-optic link for phase correction at the source end of the fiber. At the source end, the returned 900 MHz and 1100 MHz are mixed with the reference 1 GHz and translated to 100 MHz. This 100 MHz is phase-compared with the 100 MHz reference from the source frequency standard to produce an error signal for driving the fiber compensator to correct phase variations over the long fiber link.

The fiber link from SPC 10 to DSS 25 is approximately 16 km in length. The compensator reel has 4 km of the same type fiber wound on a heat-conducting cylinder. Ground temperature variations at the burial depth of the optical fiber can be as much as 10°C seasonally; thus, the compensator reel temperature must be capable of a 40°C variation . The peltier devices which drive the compensating fiber have the ability to swing 50°, thus are capable of tracking the worst-case phase variation.

A prototype engineering model of the SFODA has been built and tested at JPL. Laboratory tests indicate that the SFODA can improve long-term stability of the fiber-optic link by approximately three orders of magnitude. This capability allows the reference frequency distribution at the remote antenna pedestal to meet the requirements levied by the Cassini radio science investigators. The scheduled delivery date for the SFODA is December 1999, at which time in-situ testing will be conducted.

COMPENSATED SAPPHIRE OSCILLATOR

Stability and phase noise performance of quartz and atomic frequency sources available to the DSN cannot meet the phase noise requirements and short-term stability goals of the Cassini Ka-band Experiment for offset frequencies below 10Hz – 30Hz. In addition to meeting *this* requirement, the Allan deviation for the CSO is better than that which is possible with hydrogen maser frequency sources for measuring times below 100 to 300 seconds. This indicates a range of at least ×1000 (from 10 Hz to ≈0.01 Hz) over which DSN performance can be improved by the capability of the CSO.

Application to the DSN requires uninterrupted operation for periods of a year or more, a requirement that could not be met using the liquid helium cooling required by previous superconducting and sapphire technologies. While long-life 2-stage Giffard-McMahon cryocoolers are available with ultimate cooling capabilities to about 4K, this temperature is not low enough to provide high-Q operation of superconducting resonators (which require T < 1.5K) or even conventional sapphire resonators, with their somewhat variable turnover temperatures of typically 4K – 6K. Thermal losses associated with vibration isolation, multiple stages of thermal regulation, and with cryocooler aging must all be taken into account, indicating a minimum achievable design temperature of 7K-8K. Fortunately, the quality factor or Q of the sapphire does not degrade below a value of 10^9 until temperatures are raised above 10K, giving a design operation range of 8K-10K. We have developed a compensated resonator design procedure that allows construction of a whispering gallery resonator with turn-over temperatures in this range with typical Q's of 10^9. For the first time it is possible to provide ultra-high short-term stability of a few parts in 10^{15} in a frequency standard that can operate continuously for a year or more.

Design details have been presented previously [2]. General features can be seen in Figure 3, which shows a schematic diagram and photo of the resonator itself, together with a plot of resonator RF fields, calculated using the CYRES-2 finite element program. As is shown in the figure, a small amount of the RF energy extends from the main sapphire resonator into the ruby compensating element, giving rise to a temperature tuning effect which can be seen in Figure 4. Here, the observable change from uncompensated to compensated performance is due to the addition of a ruby element.

Figure 5 shows a block diagram of the frequency-lock circuitry for the 10K-CSO. An 800MHz cavity stabilized oscillator provides the primary signal from which other frequencies are derived. The 100MHz and 1GHz output frequencies as specified by our requirements will also be derived from this signal.

The low 10^{-13} daily variation of the CSO allows easy application as a VCO. Configured as L.O. for the LITS trapped ion frequency standard, a frequency pulling range of more than $\delta v/v/ = 10^{-11}$ was found to be possible by injecting a dc voltage to the Pound frequency lock circuitry. The '

combined LITS/CSO frequency standard was used to demonstrate the lowest statistical variation for any passive frequency standard to date, $3 \times 10^{-14}/\sqrt{\tau}$ [3].

While extremely effective for lower frequencies, vibrations of the cryocooler give rise to observable bright line phase fluctuations from the CSO at offset frequencies above about 50Hz. Thus, matching the capabilities of the CSO, the SFODA transfer system, and the primary standard at SPC-10 means that the CSO must follow the SFODA signal for times longer than about 300 seconds, and must also preserve the excellent phase noise of the quartz cleanup loop for frequencies above about 50Hz.

CSO stability, measured against a "hot" hydrogen maser with excellent short-term stability, is shown in Figure 6. Even with this reference, the short-term stability of the CSO cannot be seen for measuring times shorter than about $\tau = 300$ seconds. A second unit has been constructed and will soon be available for testing, and will provide an appropriate way to measure short-term stability and close-in phase noise for the first time.

ACKNOWLEDGMENT

REFERENCES

[1]   M. Calhoun, P. Kuhnle, and J. Law,   "Environmental Effects on the Stability of Optical Fibers   Used for Reference Frequency Distribution," *Proc. 1993 Institute of Environmental Sciences Applications Meeting,* Las Vegas, NV, May 1993.

[2]   J. Dick and R.T. Wang, "Cryocooled sapphire oscillator for the CASSINI Ka-band Experiment," *Proc. 1997 International IEEE Frequency Control Symposium,* pp. 1009-1014, 1997.

[3] G. John Dick, Rabi T. Wang, and Robert L. Tjoelker, "Cryocooled Sapphire Oscillator with Ultra-High Stability," *Proc. 1998 International IEEE Frequency Control Symposium,* pp. 528-533, 1998.

Figure 1. Reference Frequency Distribution for Cassini Ka-Band Experiment at DSS 25

Figure 2. Phase-Stabilized Fiber-Optic Reference Frequency Distribution (SFODA)
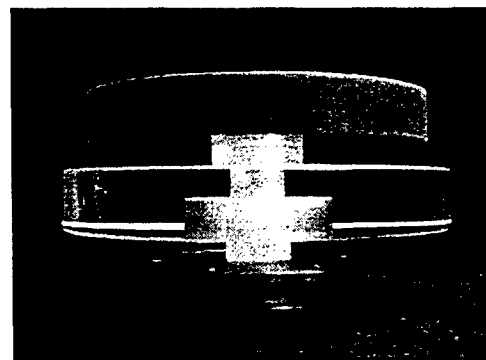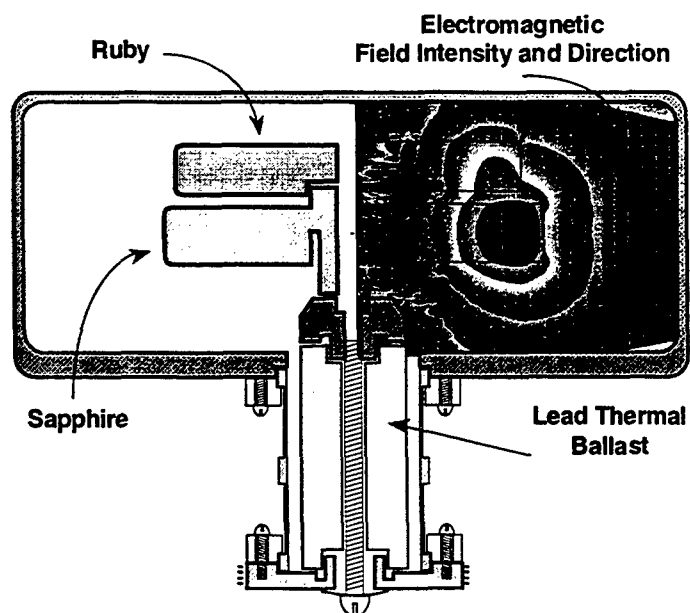
Figure 3. Compensated Sapphire Resonator. Thermally induced variations in the frequency of the sapphire resonator are canceled by paramagnetic spins in a weakly coupled ruby element.
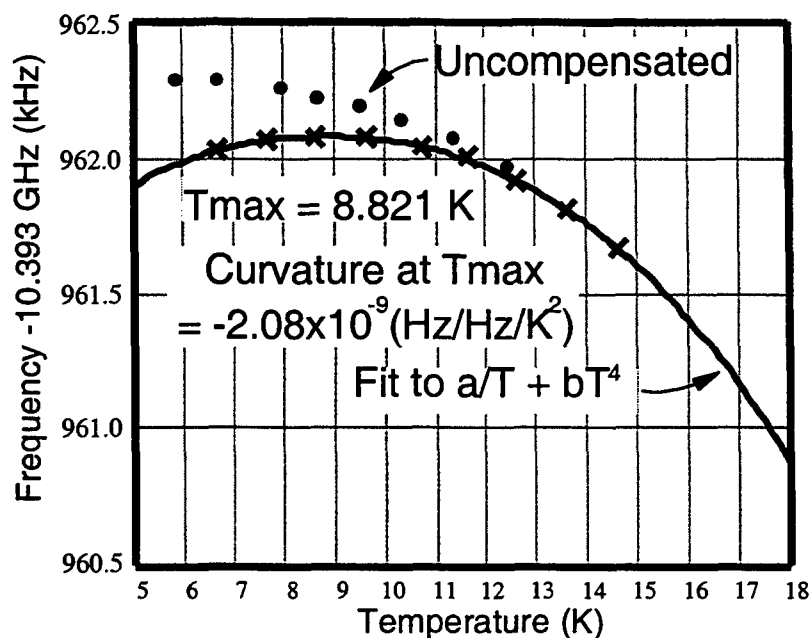
Figure 4. Measured temperature dependence of the compensated resonator with a 4mm spacing between sapphire and ruby elements.   Uncompensated temperature dependence is also shown.
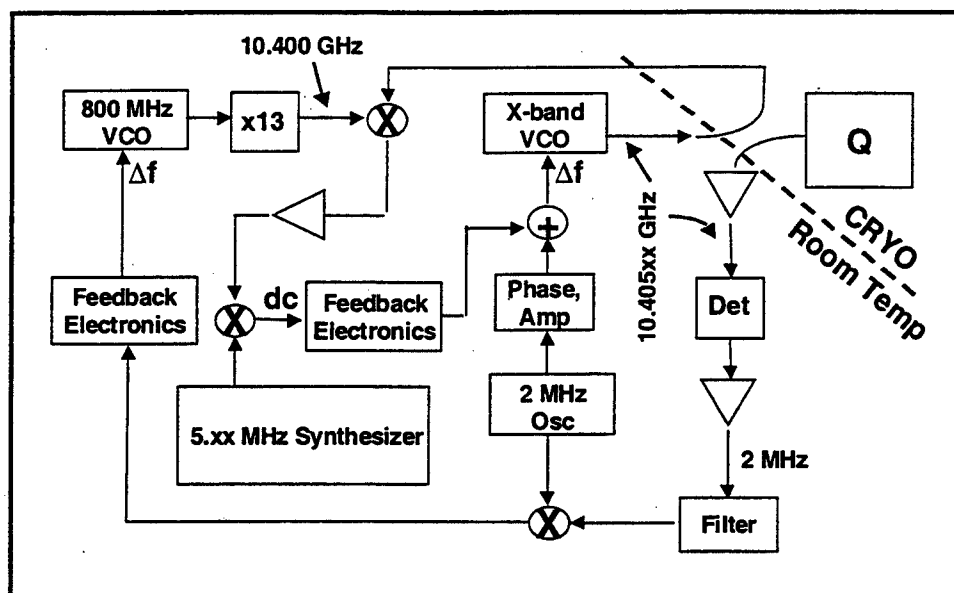
Figure 5. Block diagram of Pound circuit frequency feedback system for 10K CSO. Individual resonator frequencies vary up to + or – 20MHz from the 10.400GHz nominal operating frequency. Proper loop operation requires at least 5MHz difference, as show in this example.
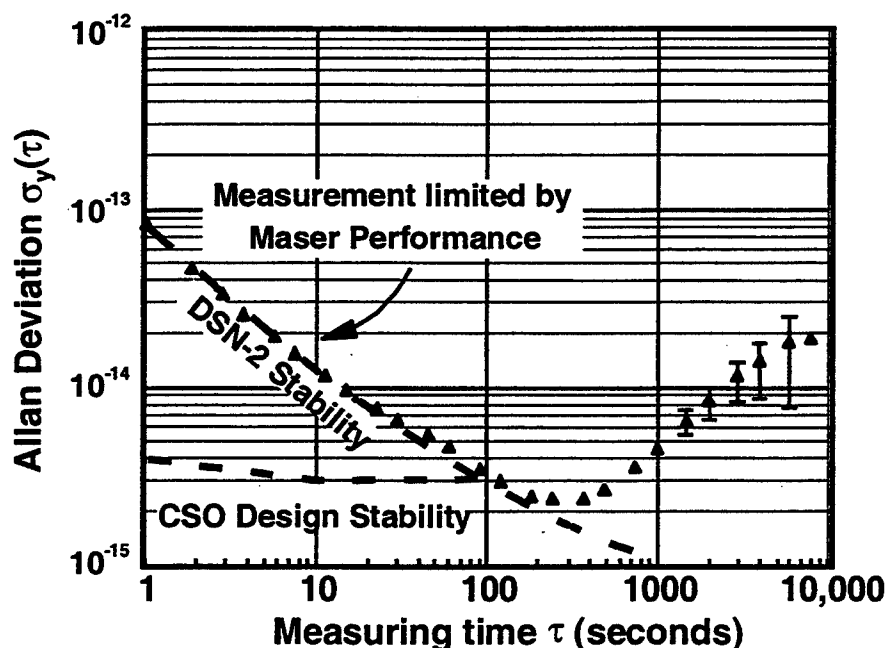
Figure 6. Measured frequency stability for the 10K CSO against a DSN-2 hydrogen maser tuned for best short-term stability. Even this "hot" H-maser reference dominates the observed short-term variation. The long-term turn-up is due to the CSO, and is likely caused by sensitivity of the rf electronics to room temperature variations.

Questions and Answers

DEMETRIOS MATSAKIS (USNO): I wonder if you have done an error budget on your old inadequate fiberoptics system and know where your errors are coming from.

MALCOLM CALHOUN (JPL): Yes we do. We have characterized the entire system and we know very well where the errors are coming from.

DEMETRIOS MATSAKIS: Can you tell us the big ones?

MALCOLM CALHOUN: The big ones are still the cables.

DEMETRIOS MATSAKIS: Expansion?

MALCOLM CALHOUN: Yes, these are approximately seven parts per million per degree C; roughly 30 picoseconds per kilometer per degree C. Very large contributors to these phase variations.

In the 70-meter net and then the 34 meter HEF-network, we have installed a passively compensated fiber that has very nearly a zero temperature coefficient. The cost is prohibitive in a 16-kilometer link and would cost $1 million just for the cable alone. The last time we priced this cable, it was $54 per meter for a six-fiber cable. That is 16 kilometers, or almost $1 million. Then it is not direct burial cable, it is duct- or plenum-type cable, so we would have to build a duct all the way from the processing center to the remote location. This is not feasible. We can build an atomic frequency standard and install at the antenna for less cost than installing the passively compensated fiber.

WOLFGANG SCHAEFER (Time Tech): Have you considered the two-way links or having two fibers?

MALCOLM CALHOUN: Yes, we have looked at two-way links, and it works very well. The problem that I had was that the (WDM) Wave Division Multiplexer devices and the splitters cause an optical loss that degrades the signal-to-noise ratio. So, the method that I ended up with was the single wave link method. I get an improved single noise ratio, which helps the phase noise performance, which works very well. Also, the reflection method worked, but with the same problem again. I had a 50 percent reflector in line at the remote end; it sent the same signal back and the loss at my receiving end was too high.

EFFECT OF CLOCK NOISE ON THE SYNCHRONIZATION PERFORMANCE OF CONSTANT BIT RATE (CBR) TRAFFIC IN AN ATM NETWORK

T. Jayawardena and C. Olszewski
AT&T Labs
101 Crawford Corner Rd.
Holmdel, NJ 07733

Abstract

When Constant Bit Rate (CBR) traffic with an associated frequency is carried over an ATM network, the frequency needs to be reconstructed at the exit node of the ATM network. One method for reconstructing this frequency is the Synchronous Residual Time Stamp (SRTS) method. This method relies on two synchronized clocks, one at the entrance and the other at the exit of the ATM network.

This paper quantifies the synchronization performance of the signal leaving the ATM network when different levels of noise are present in the signal source clock, the clock at the entrance to the ATM network, or the clock at the exit of the ATM network. Simulations were performed to study the effects of these noise sources separately and in combination. The SRTS scheme itself generates noise with a characteristic time deviation (TDEV) signature. The noise on the signal leaving the ATM network is determined by both the SRTS signature noise and the noise of clocks in the entrance and exit nodes of the ATM network. As the noise of the clocks rise above certain levels, the noise on the signal tends to be determined more by the clock noise than the inherent noise from the SRTS scheme.

INTRODUCTION

A key advantage of Asynchronous Transfer Mode (ATM) networks from a telecommunications carrier's perspective is the ability to carry voice, video, and data traffic on a single network. This is achieved by segmenting the voice, video, or data traffic stream into small units and sending them across the ATM network in 53-byte ATM cells. User information, i.e. voice, video, or data, is converted into ATM cells at the entrance to the ATM network and reconverted to the original format at the exit of the ATM network.

The small constant size of ATM cells makes it possible to achieve the desired Quality of Service (QoS) for different types of traffic carried over an ATM network. QoS is a term used to characterize the transmission characteristic requirements of different types of ATM traffic. The most stringent QoS is needed to carry Constant Bit Rate (CBR) user information. CBR traffic has a frequency associated with the bit rate of the signal which needs to be reconstructed at the exit node of the ATM network. There are two popular

methods for achieving this: The adaptive method and the Synchronous Residual Time Stamp (SRTS) method.

In the adaptive method, the cell inter-arrival times are averaged at the exit node of the network to reconstruct the original bit rate. Although at the entrance of the ATM network cells carrying the CBR traffic are generated periodically, their transit times through the network are not constant due to Cell Delay Variation (CDV) encountered within the network. When the adaptive method is used, low frequency CDV, which cannot be removed by averaging, will degrade the synchronization performance of the exiting signal.

The SRTS method relies on two synchronized clocks, that is, two clocks having the same average frequency, one at the entrance and the other at the exit of the ATM network. (Strictly speaking, the clocks are only "syntonized," i.e. have the same frequency. Keeping with telecommunications' parlance we shall use "synchronization" to mean "syntonization.") Bits of the incoming CBR traffic are periodically assigned a time stamp upon entrance to the ATM network. This time stamp is sent along with the information bits to the exit node of the ATM network. There, the time stamp and exit clock are used to recreate the frequency of the signal leaving the ATM network. This scheme is illustrated in Figure 1. An important advantage of the SRTS scheme is that the synchronization performance of the signal exiting the ATM network is largely insensitive to CDV. However, the synchronization performance of the signal is affected by the behavior of the clocks at the entrance and exit nodes of the ATM network. The objective of this study is to understand the effect of different levels of clock noise on the synchronization performance of the signal exiting the ATM network when SRTS method is used to reconstruct the signal frequency. See [1] for details of the SRTS method.

THE SIMULATION MODEL

We consider two architectures for synchronizing the clocks at the entrance and exit of the ATM network. These synchronization architectures will induce different levels of noise on the clocks used in the SRTS method. The two synchronization architectures are the following:

1. Each node is synchronized by a stratum 2 or stratum 3 Building Integrated Timing Supply (BITS) clock, which is directly synchronized by a collocated Primary Reference Source (PRS)
2. Each node is synchronized by a reference signal from a remote PRS.

The BITS clock is the most accurate and stable clock at a given location. It is used as the reference to which all other collocated clocks are synchronized. A PRS is a clock which has a long-term accuracy of one part in 1011 with verification to UTC ([2]). The two synchronization architectures are shown in Figure 2.

We use TDEV masks to specify different levels of clock noise. TDEV is the square root of TVAR. (See [7] for details of TVAR and its relation to other variances). The ANSI T1.101 TDEV mask for wander generation of a stratum 2 or 3 clock (see [2]) is used as the maximum level of noise in clocks at the entrance and exit nodes of the network when a collocated PRS is used to synchronize the BITS clocks at these nodes (case 1). When the nodes are synchronized by a remote PRS (case 2), we use two TDEV masks to simulate two levels of maximum noise in the node clocks. The higher level of noise is taken from the TDEV interface mask of T1.101 [2] and the lower level of noise is from the TDEV mask of T1.105.09 [3]. These three TDEV masks are shown in Figure 3.

We used two methods of generating clock noise from the TDEV masks: The fractional Brownian motion method in [4] and the successive random additions method in [5]. The method in [4] is memory-intensive and is better suited for simulations of short time periods. The method in [5] was used for longer simulation periods (integration times of thousands of seconds).

We used the DS1 (Digital Signal level 1 in the North American Digital Hierarchy) with an associated nominal bit rate of 1.544 Mbps as the CBR signal entering the ATM network.

SIMULATION RESULTS

The SRTS method itself induces noise on the signal exiting the ATM network even when there is no noise present in the clocks of the entrance and exit nodes. The attributes of this induced noise depend on the frequency of the signal entering the ATM network, as well as the frequency of the network clock used to construct the time stamps. However, most of the power of this SRTS "signature" noise is in the high frequency region and most of it will be attenuated by a low-pass filter in actual SRTS implementations. The TDEV signatures are shown in Figure 4 for two cases: (a) The DS1 entering the ATM network has a nominal frequency (1.544 MHz) (b) the DS1 entering the ATM network has a +30Hz offset from the nominal frequency. A network clock frequency of 2.43MHz was used in all simulations.

To see how clock noise affects the DS1 phase in the SRTS method, we used the TDEV curves given in Figure 5 to simulate clocks with high, intermediate, and low levels of noise relative to the SRTS signature noise.

The TDEV of the DS1 exiting the ATM network follows the SRTS signature TDEV up to some integration time (in the higher frequency region) and then follows the clock noise TDEV for larger values of integration time (in the lower frequency region). The higher the noise level, the sooner the DS1 phase TDEV begins to follow the noise TDEV. Figure 6(a) (for a DS1 with the nominal frequency) and Figure 6(b) (for a DS1 with a +30 Hz offset) show these trends.

Next, we simulated the synchronization performance of the DS1 exiting the ATM network when the clock noise is generated according to various ANSI T1 TDEV masks ([2], [3]). Figure 7 shows the TDEV of a simulated clock and the TDEV mask used to generate the clock noise. The high degree of coincidence of the two TDEV curves show that the generated clock noise is consistent with the corresponding TDEV mask. Simulated noise from the other two TDEV masks showed a similar consistency.

Figure 8(a) and Figure 8(b) show the TDEV of the simulated DS1 phase resulting from clock noise generated from different TDEV masks. The TDEV of the DS1 phase approximately follows the TDEV of the clocks.

Finally, we also investigated the effect of noise in the source input signal on the performance of the timing of the signal recreated at the exit node. The TDEVs of the source signals having low, intermediate, and high levels of noise for this part of the study are shown in Figure 9. Figure 10 shows the TDEVs of the simulated phase of the DS1 at the exit node, subject to the various levels of source noise. Figure 10 also includes the intrinsic SRTS noise signature.

The behavior of the TDEV curves for the phase of the DS1 is very similar to the behavior of the curves for the DS1 produced when there is noise on the network clocks (Figure 6). At small integration times (high frequencies), the curves more or less follow the characteristic curve of the SRTS method. As the integration time of the TDEV is increased further, signals with more noise depart from the characteristic SRTS curve sooner than signals with less noise. In all cases, once the TDEV curve of a DS1's phase departs from the SRTS curve, it remains at noise levels characteristic of the noise generated on the source.

At small integration times, there appears to be some filtering of the source noise on the DS1 at the exit node. This effect is explained by the operation of the SRTS method, in which a single time stamp represents the time at which 3,008 bits have been received at the entrance node. Low-to-moderate levels of noise at time scales less than that of the 3,008-bit frame are eclipsed by the signature of the SRTS method itself. High levels of noise at these time scales will be attenuated by this effect, but will produce more noise than the signature of the SRTS method. A low-pass filter in a realistic implementation of the SRTS method would reduce the high-frequency peak of the method, and would presumably attenuate this short-time-scale noise further.

CONCLUSIONS

The SRTS method introduces noise on to the DS1 phase leaving the ATM network even when there is no noise in the entrance and exit node clocks. The attributes of this noise depend on the frequency of the signal entering the ATM network and the frequency of the network clock used to construct the time stamps. Most of this SRTS "signature" noise power is in the high frequency and will be attenuated by a low-pass filter used in SRTS implementations.

When there is noise in the entrance and exit node clocks, the TDEV of the DS1 phase follows the SRTS TDEV "signature" only in the high frequency region and begins following the noise TDEV in the lower frequency region. The higher the level of clock noise, the higher the threshold frequency at which the TDEV of DS1 phase begins to follow the clock noise TDEV. This behavior is also evident when there is noise on the source signal itself.

ACKNOWLEDGMENTS

REFERENCES

1. R.C. Lau and P.E. Fleischer, "Synchronous Techniques for Timing Recovery in BISDN," 1992 IEEE Globecom Conference Proceedings, Vol. 2, pp.814-820, 1992.
2. Synchronization Interface Standard, ANSI T1.101, (Draft, 1998).
3. Synchronous Optical Network (SONE) – Network Element Timing and Synchronization, ANSI T1.105.09, 1996.
4. N. Jeremy Kasdin, Todd Walter, "Discrete Simulation of Power Law Noise," IEEE Frequency Control Symposium, 1992, pp. 274-283.
5. Richard F. Voss "Random Fractal Forgeries," Fundamental Algorithms for Computer Graphics, Ed. R.A. Earnshaw, 1985, Springer-Verlag, pp.805-835.

6. Jacques Rutman, "Characterization of Frequency Stability in Precision Frequency Sources," Proceedings of the IEEE, Vol. 79, No. 6, June 1991, pp.952-960.

7. David W. Allan, Marc A. Weiss, and James L. Jespersen, "A Frequency-Domain View of Time-Domain Characterization of Clocks and Time and Frequency Distribution Systems," 45th Annual Symposium on Frequency Control - 1991, pp.667-678.
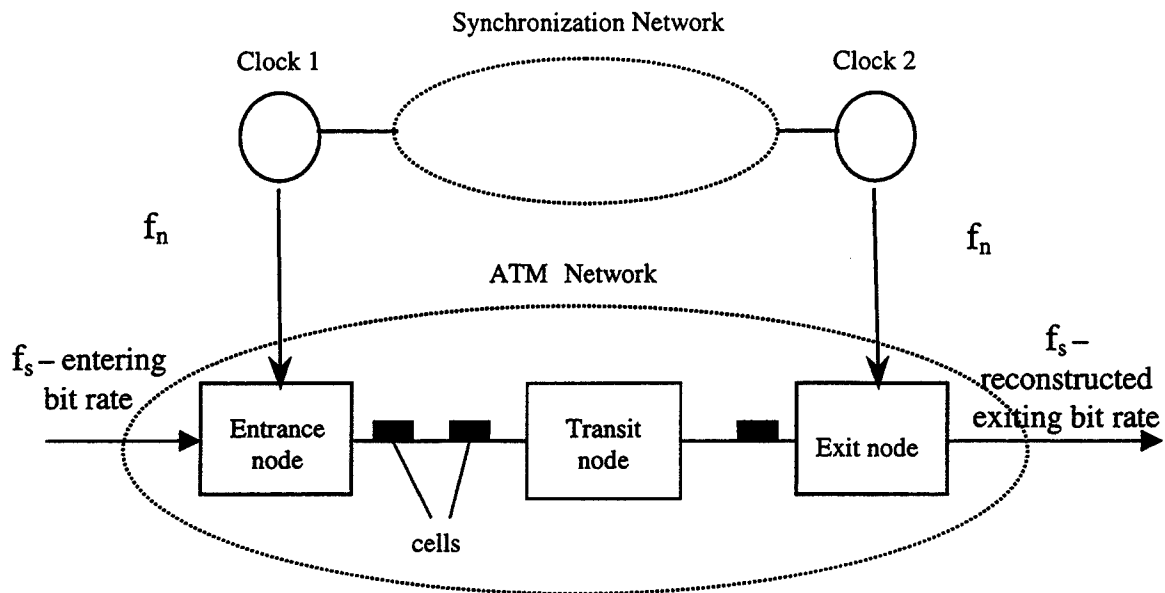
Figure 1. SRTS method for transporting CBR traffic over an ATM network.

(1)   (2)
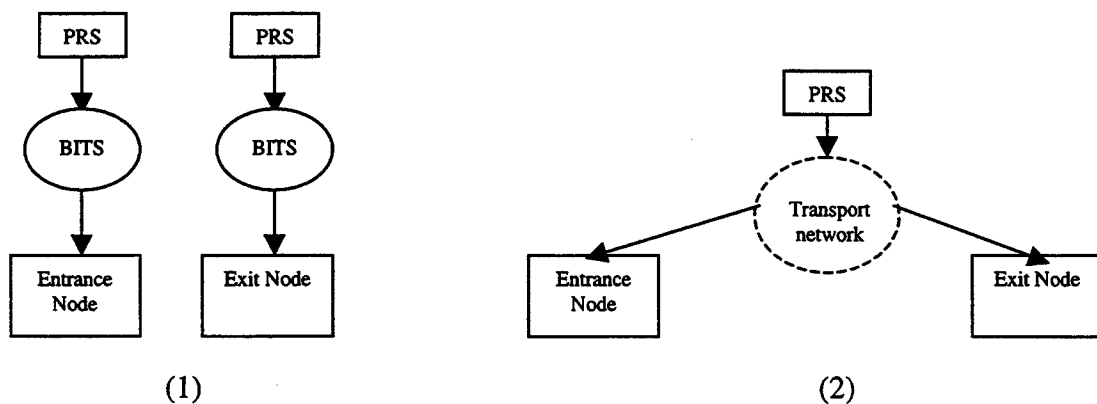
Figure 2. Two architectures for synchronizing the entrance and exit node clocks.

417
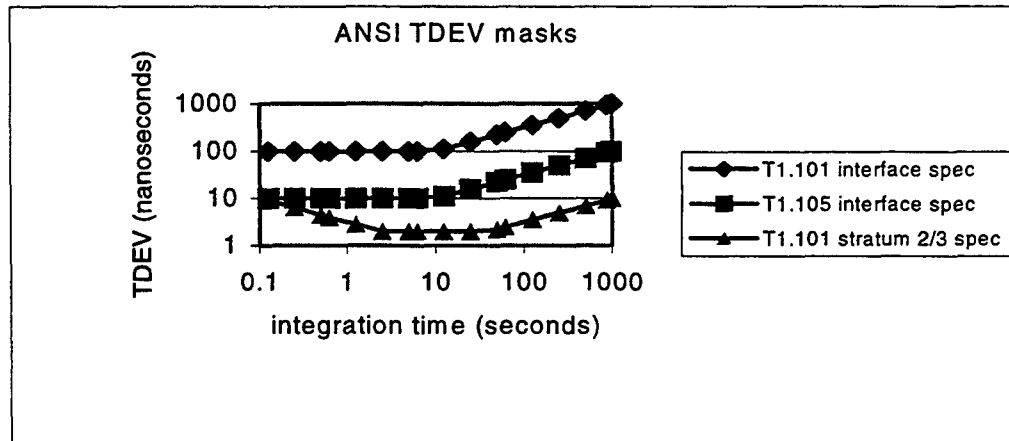
Figure 3. ANSI TDEV masks used to simulate clock noise.
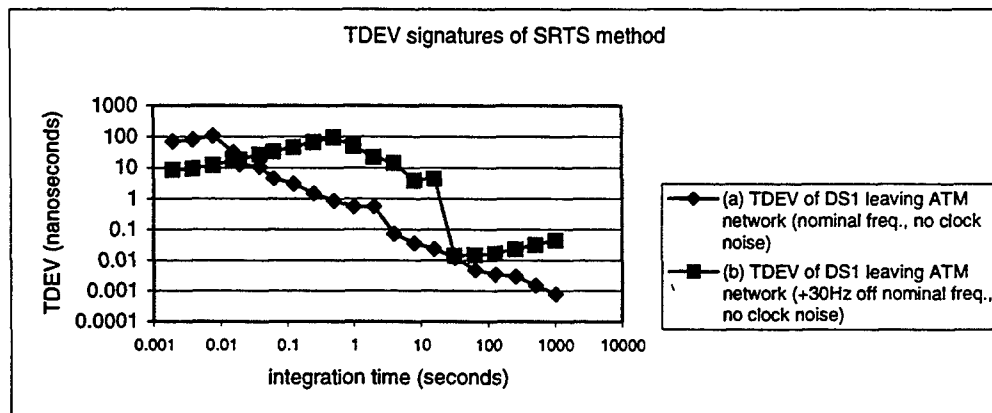
Figure 4. TDEV of DS1 leaving ATM network when there is no noise in any clock:
      (a) entering DS1 has nominal frequency
      (b) entering DS1 has +30Hz frequency offset from nominal.
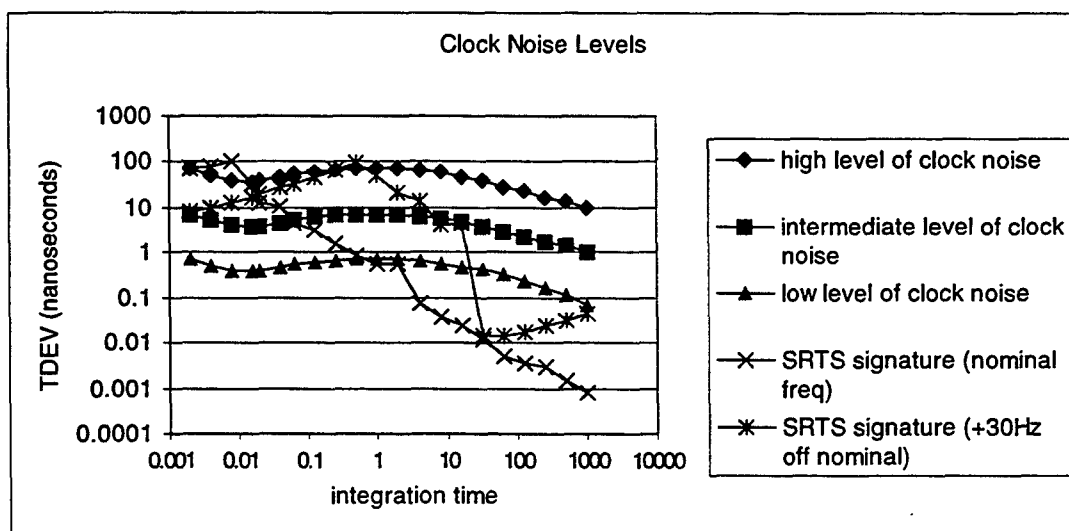
Figure 5. TDEV of different levels of clock noise and TDEV of the SRTS signatures.

418
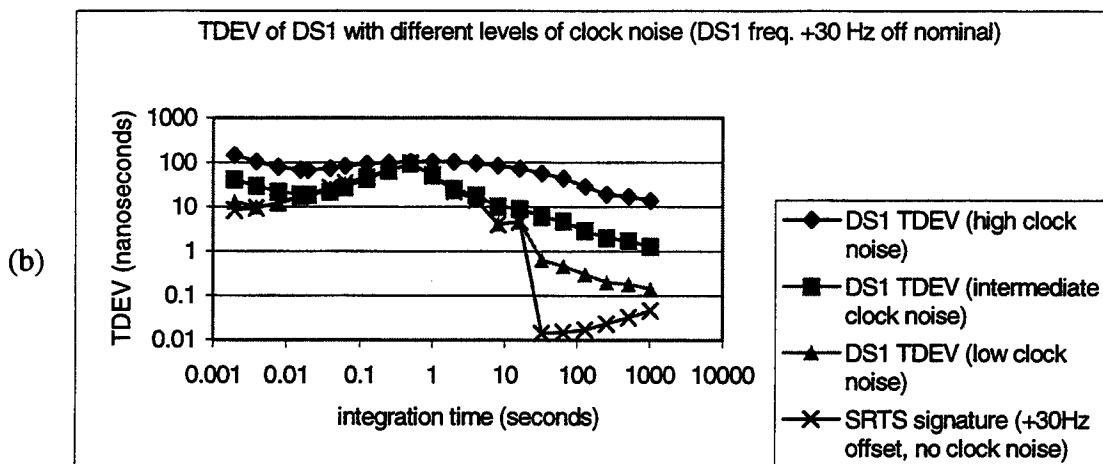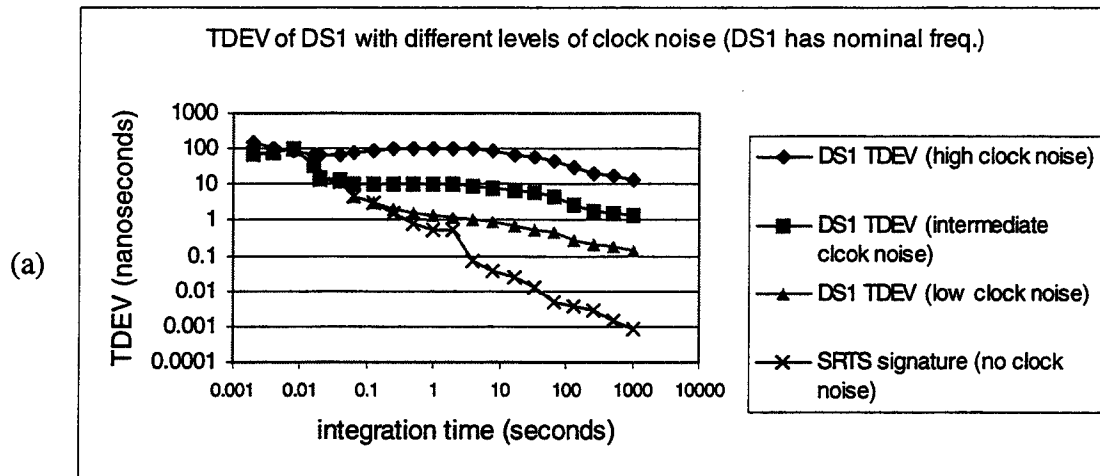
Figure 6. TDEV of DS1 phase resulting from different levels of clock noise
   (a) Entering DS1 has nominal frequency
   (b) Entering DS1 has +30 Hz offset from nominal frequency.
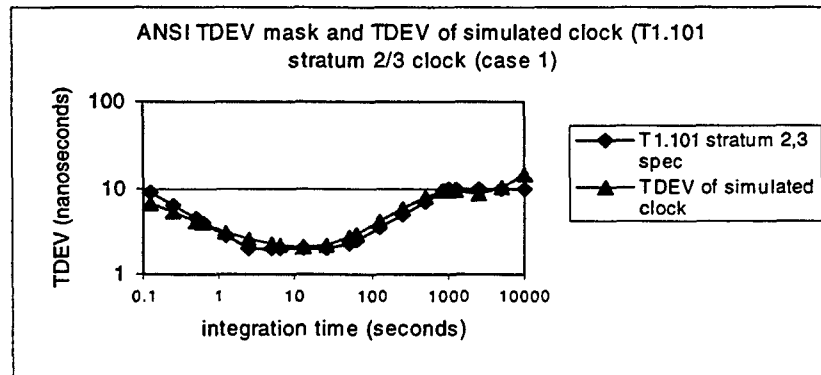
Figure 7. TDEV mask used to simulate the clock noise and TDEV of simulated clock (T1.101 stratum 2 or stratum 3 clock).
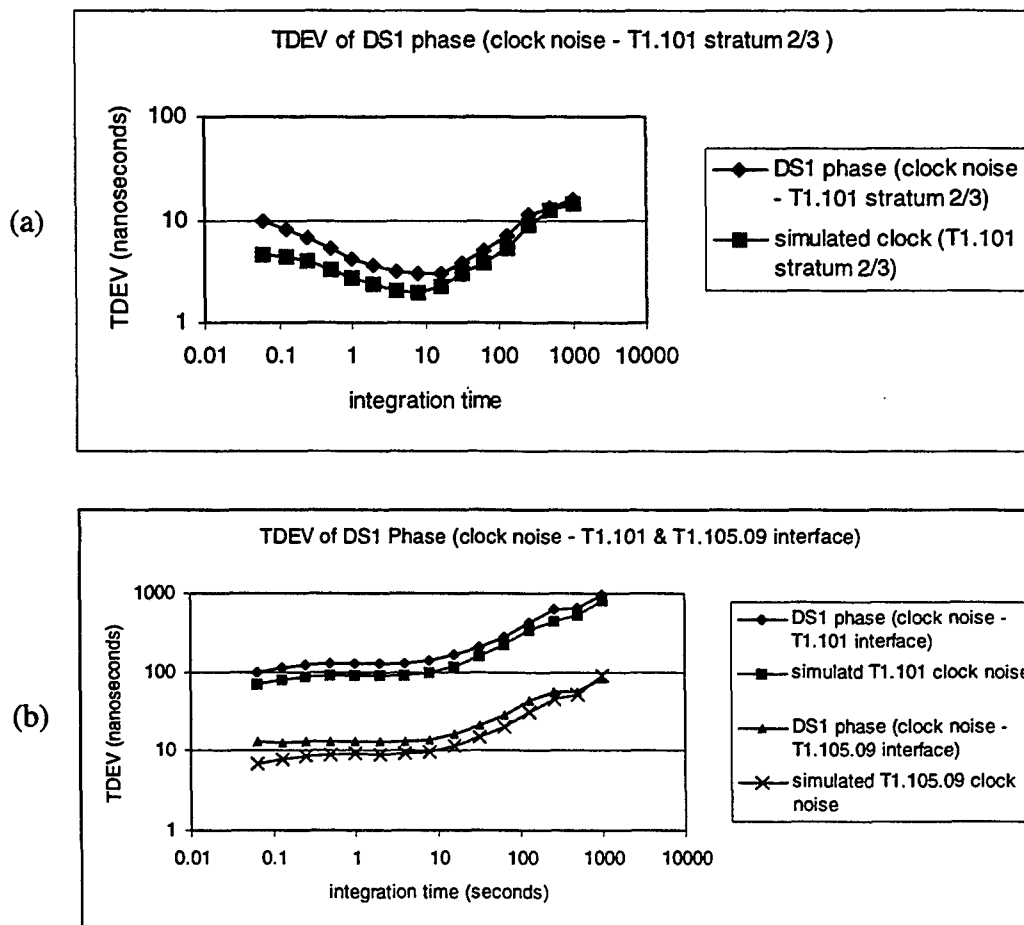
Figure 8. TDEV of simulated DS1 resulting from clock noise
(a) Generated from T1.101 stratum 2/3 TDEV mask
(b) Generaged from T1.101 and T1.105.09 interface TDEV masks.
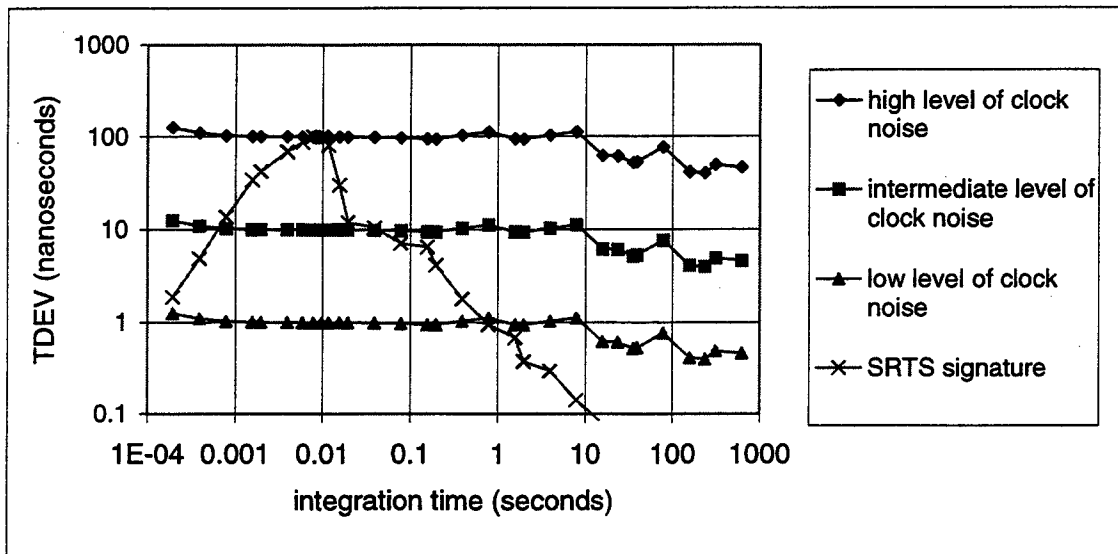
Figure 9. TDEV of various levels of source noise.
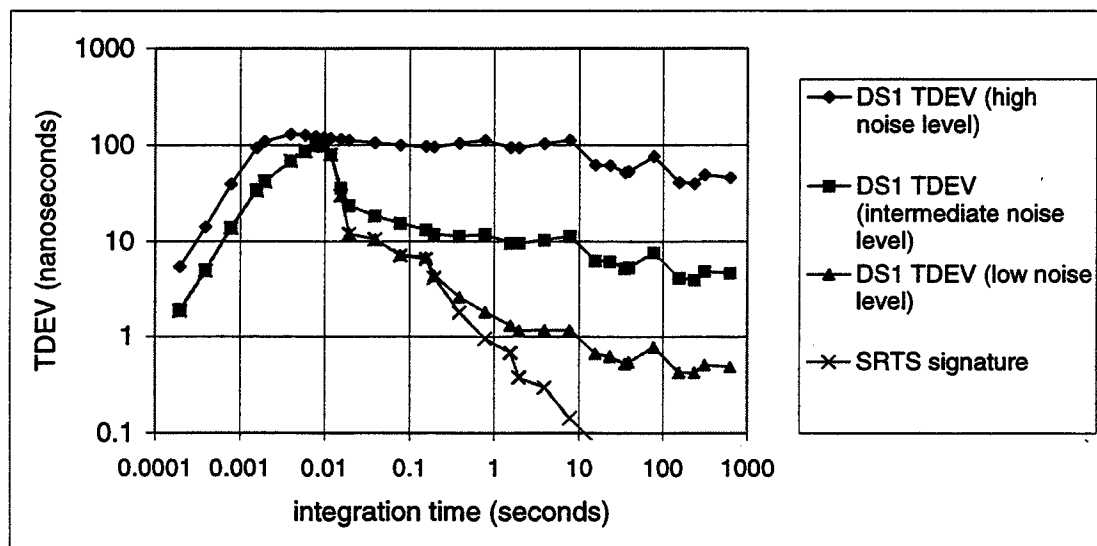
Figure 10. TDEV of DS1 phase resulting from various levels of noise on source.

THE SYNCHRONIZATION OF THE SPANISH R&D NETWORK*

J.Palacio, F. Javier Galindo, T. López, L. Batanero
Real Instituto y Observatorio de la Armada
Cecilio Pujazón s/n, 11.110 San Fernando, Spain
tel +34-956-599-286 fax +34-956-599-366
e-mail: jpalacio@roa.es

C. Tomás
RedIRIS, Centro Comunicaciones CSIC RedIRIS
Serrano 142, 28006 Madrid, Spain
tel + 34-91-585-5150 fax +34-91-564-7421
e-mail: celestino.tomas@rediris.es

Abstract

RedIRIS is the Spanish academic network for research and development funded by the National Plan for R&D (Plan Nacional de I&D) and managed by the Centro de Comunicaciones CSIC RedIRIS, which depends on the Scientific Research Council (Consejo Superior de Investigaciones Científicas). Since September 1996 Real Instituto y Observatorio de la Armada (ROA) has been in charge of the synchronization of the RedIRIS network, using the NTP protocol. We have also been responsible of the installation of two Stratum 1 time servers, one at the network operational center in Madrid and the second at ROA in San Fernando. Some modifications on the software and the kernel have been made. In this paper we present an overview of the results of these modifications on the performance of the service and studies on its accuracy and accessibility.

INTRODUCTION

The Network Time Protocol is fully described and explained in [1] [2] [3] [4]. This protocol is used to synchronize the local area network of Real Instituto y Observatorio de la Armada (ROA). ROA is connected to the Spanish R&D network (RedIRIS) through the Red Informatica de Andalucia (RICA) using a point-to-point connection of 64 Kbs. ResIRIS provides the users of the network the necessary support for infrastructure and services.

RedIRIS

On 1988, the National Plan for R&D started a horizontal special program IRIS for the Interconnection of Computer Resources (Interconexión de los Recursos Informáticos) of universities and research centers, and until the end of 1993 this program was managed by Fundesco. From 1991, when the first promotion stage was finished, IRIS became what RedIRIS actually is: the national academic and research network, still funded by National Plan for R&D and nowadays managed by the Scientific Research Council (Consejo Superior de Investigaciones Científicas). RedIRIS is the main tool of the National Program of Applications and Telematic Services and will assume the responsibility of providing the required network services and actual and future support to the infrastructure, according to the main objectives of the program. About 300 institutions are nowadays connected to RedIRIS, mainly universities and R&D Centers. The services offered by RedIRIS to the Spanish academic and research community require the support of a basic infrastructure of transport technologically adapted to the requirements of the connected centers. These services are provided in collaboration with other academic networks and other international forums.

The operational Center of RedIRIS is located in Madrid, the capital of Spain. Its backbone gives connectivity to each of the 17 main Regions Spain is administratively divided in. The regional administrations are in charge of the deployment of the network inside their respective territory. In order to harmonize the configuration and to get the better results from the Network, RedIRIS organized working groups whose tasks are to study some of the services of the net. One of these WGs is IRIS-NTP, whose responsibility is to study the performances of the implementation of the protocol in the network.

ROA

ROA is the responsible to maintain and distribute the Official Time Scale, UTC(ROA). This Time Scale is produced by an ensemble of commercial cesium clocks and disseminated by the HF Time Signal Broadcast Service, the Telephone Distribution System (using the European standard code), GPS Time Scale comparisons, and NTP. Inside Spain, ROA is the pioneer center in having a Stratum 1 synchronizing its LAN.

ROA has three Stratum 1 NTP servers operating inside its LAN. All of them are PCs using Linux as the operating system and running NTP protocol.

RedIRIS' NTP SERVICE

The synchronization NTP service of RedIRIS is supported by three Stratum 1: hora.rediris.es, titac.fi.upm.es and hora.roa.es. All of them are PCs that receive precise time from a GPS receiver. The first one is located at the RedIRIS operational center, but is managed by ROA. The second one is placed at Universidad Politécnica de Madrid and managed by its Computational Center. The later is placed at ROA. RedIRIS network topology is like a star whose center is Madrid and whose 17 sides correspond to each of the Spanish Regions (see Figure 1). ROA is placed in one end of the Andalusian arm, so the shorter synchronization distance of a computer of the network connected on the other arms of the star is the one that

connects it with hora.rediris.es.

ROA SERVER

As mentioned above, ROA has three Stratum-1 servers constituted by PCs running Linux and NTP protocol. Hora.roa.es was the first computer to be adapted to be an NTP server. A GN-72 FURUNO GPS was used as time tag and precise time supplier. The original NTP distribution was modified as a result of a study to accommodate the synchronization needs with the signals we have at hand.

SOFTWARE

To use the 1 Pulse Per Second (1PPS) coming from GPS, a PPS_ROA device driver was written. In this, one serial port was used to get the NMEA code from GPS, and the functions of the UART of the second serial port were modified to eliminate any other duties than those relating to the DCD status line. One can select the edge of the 1PPS incoming signal to originate the interruption that transfers the variables to the 'hardpps' subroutine which calculates the time and frequency offset of the clock. An IOCTL was included to adapt the information coming from the PPS_ROA driver, at daemon level, because the original 'ciogetev' subroutine was written for SunOS, and there was a need to translate it for Linux.

As the driver needs to be continuously debugged while in the development state, it was rewritten to be included as a module. This allowed us to make changes without modifying and compiling the kernel and it gave us more flexibility in programming. As a predominant result, the frequency correction has been divided into two tasks:

- a coarse frequency correction that is made by the kernel, and

- a fine correction that is made by the Time daemon.

The time that the clock spends in synchronizing, when the daemon is started, is reduced following this procedure:

a) when PPS_ROA module is installed, it gives the kernel the frequency offset of the clock derived from continuous measurements of phase offsets; and

b) when the daemon is started, the coarse frequency correction is already made and all that it must do is make a fine correction of few parts per million.

Following this procedure, the offset of the computer scale is within few microseconds two hours after the daemon's start. Figure 2 shows the offsets of a computer started with an initial offset of 20 milliseconds, following the explained procedure and the original NTP procedure.

HARDWARE

The explained setup uses one of the external serial ports to get the time code and the other serial port for the time synchronization signal. When we need to use these external ports for controlling other laboratory devices, a PC card was designed to use a Motorola ONCORE VP

GPS receiver. The NMEA output from the GPS is sent to the PC bus using a UART. Its 1PPS signal is split to get an external monitoring output of the injected signal in the proper ISA BUS IRQ line. See Figure 3 for more details. An external 1PPS, coming from other precise time source can be applied to the card, being then the IRQ line controller.

RESULTS

We have made some measurements using the PC card described above. Installed in a PC with Pentium, a 1PPS from a cesium clock was supplied as an external reference. A subroutine allows us to record the cycle count of the PCC immediately after a 1PPS arrives the computer and the corresponding IRQ is attended. Figure 4 plots the differences of the readings with the mean, multiplied by the period of the frequency of the crystal. This demonstrates that, using the reading of PCC as the internal time reference, an uncertainty of 1.3 microseconds is obtained with a single measurement and a time stability of 47.6 ns is expected for 64 s intervals (see Figure 5).

Another experiment was carried out measuring the time differences between the time provided to the computer, and a signal produced by changing the status of the DTR line of the UART when the IRQ is attended. Figure 6 plots these differences. When the activity of the computer is low, a usual mean offset of 9 microseconds is obtained, that is mainly due to latency of the call to get the time of the system [5] and other contributions related to hardware delays. This offset increases when the activity is higher, as shown in Figure 6, where the computer has a higher network information transference. Figures 7 and 8 show Allan time deviations of these measurements.

Having access to two Primary NTP servers with precise time from GPS, assuming that the time offset between the GPS is less than one microsecond, we can measure the asymmetry of the link. Using the rawstats files one can determine the delay of the outgoing and returning path. Figure 9 shows the asymmetry of the round trip and the filtered offsets measured in one of the NTP servers. These asymmetries are assumed as increments of the offset to the server and consequently as phase jumps of the internal clock by a client computer. This figure also shows that the daemon filter removes short-term variations of the round trip.

Information about the daily performance of the service can be found at: http:/hora.rediris.es/ntp/stats. From this page the offsets of the Stratum 1 and 2 servers and some of 3's can be obtained, giving clear information as to its performance.

An NTP service has also been established, with the collaboration of the Instituto de Ciencias de Mar de Barcelona, aboard the Spanish Navy's Oceanographic Ship *Hesperides*. This service is been evaluated while serving in the Antarctica Continent.

ACKNOWLEDGMENT

[1] D. L. Mills, *Internet time synchronization: the Network Time Protocol*, IEEE Trans. Communications COM-39, 10 (October 1991), 1482-1493.

[2] D. L. Mills, *Network Time Protocol (Version 3) specification, implementation and analysis.* Network Working Group Report RFC-1305, University of Delaware, March 1992, 113 pp.

[3] D. L. Mills, *Unix kernel modifications for precision time synchronization*, Electrical Engineering Department Report 94-10-1, University of Delaware, October 1994, 24 pp.

[4] D. L. Mills, *Improved algorithms for synchronizing computer network clocks*, IEEE/ACM Trans. Networks (June 1995), 245-254.

[5] D. L. Mills, *Precision synchronization of computer network clocks*, ACM Computer Communication Review 24, 2 (April 1994), 28-43.
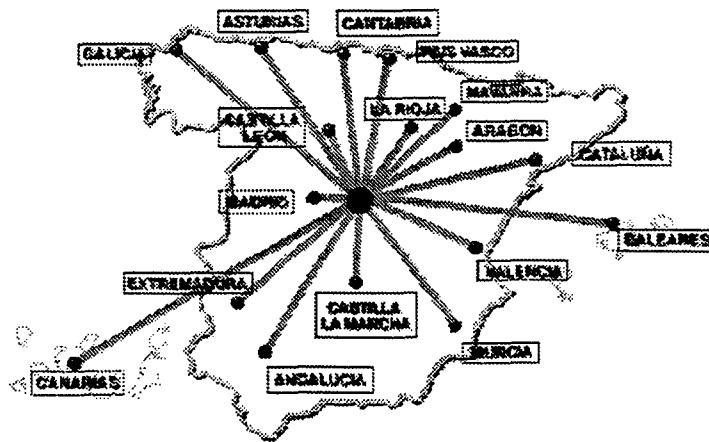
Figure 1: RedIRIS Network topology
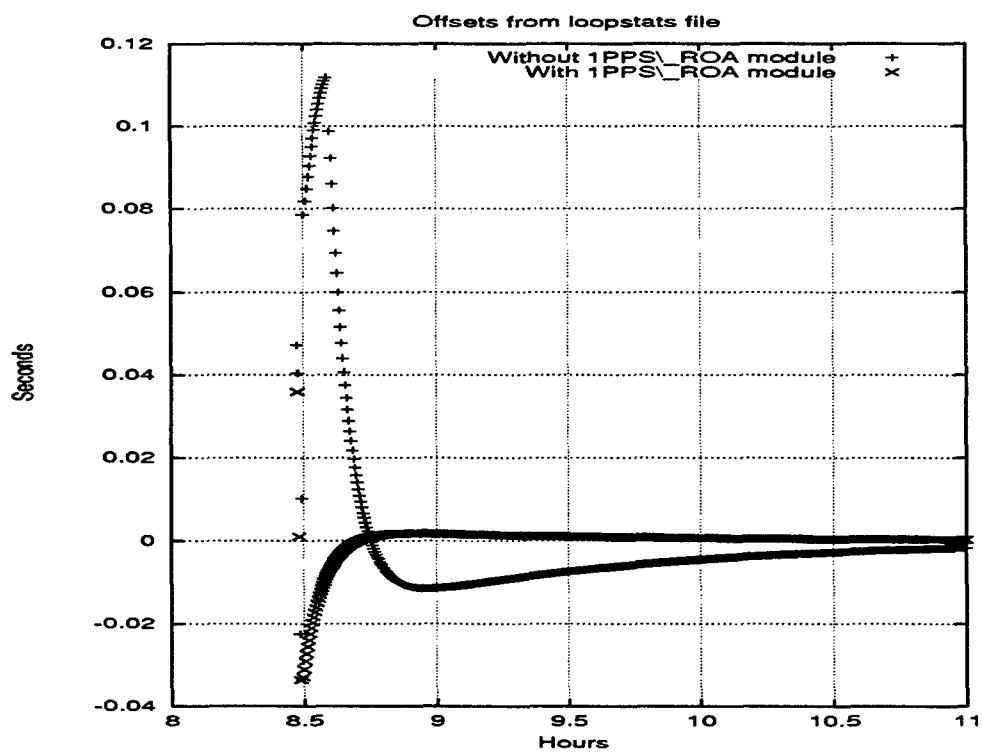
Figure 2: Initial transient response

428
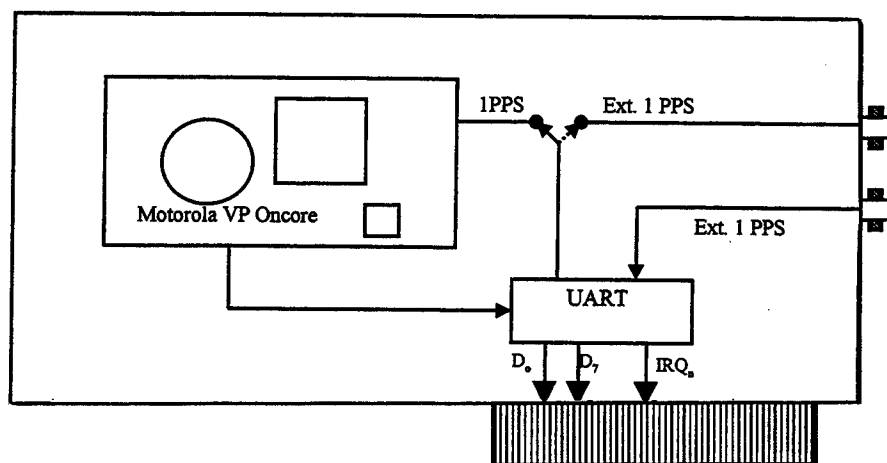
Figure 3: Diagram of the PC card prototype
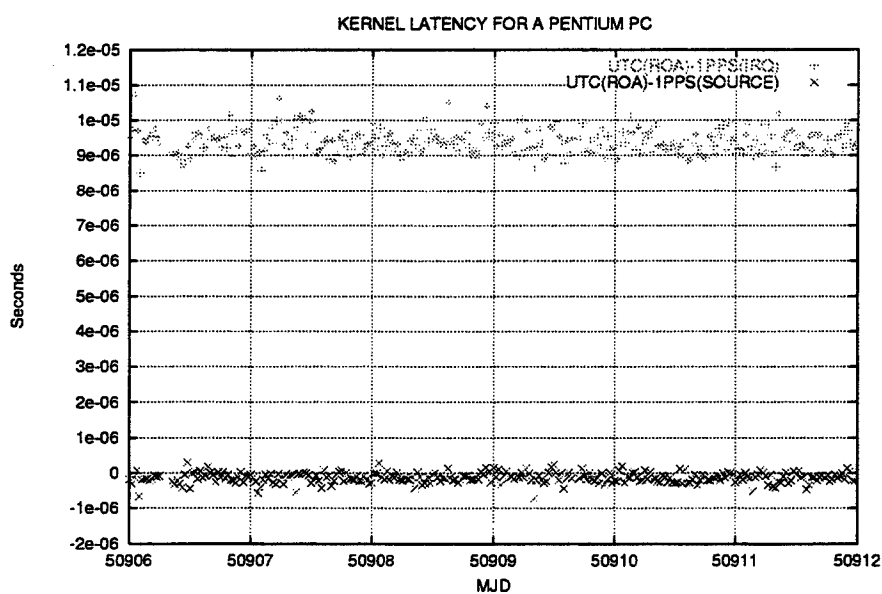
Figure 4: Time offset between 1PPS(input) and 1PPS(IRQ)
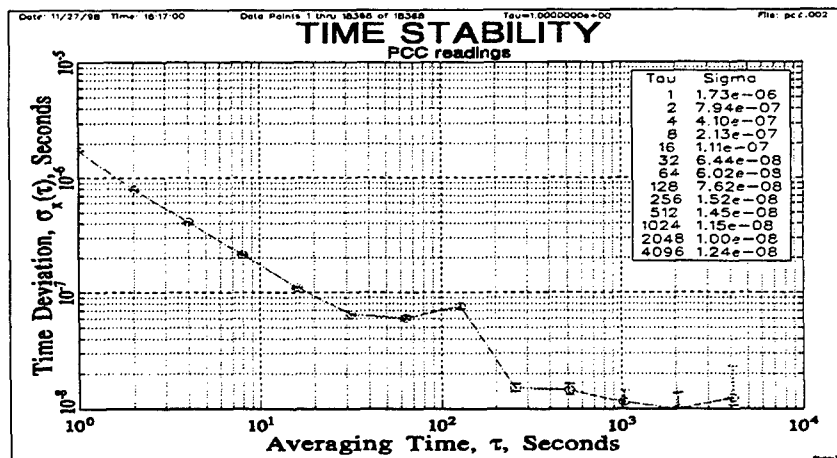
Figure 5: TDEV of PCC time stamps
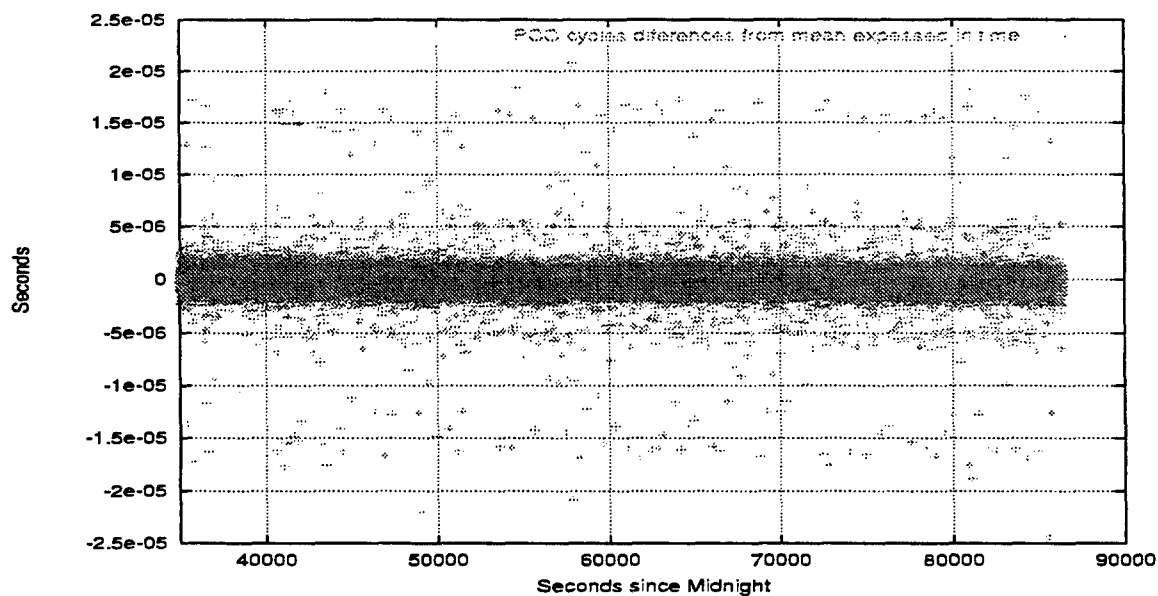
Figure 6: PCC stamps readings changed to time

430
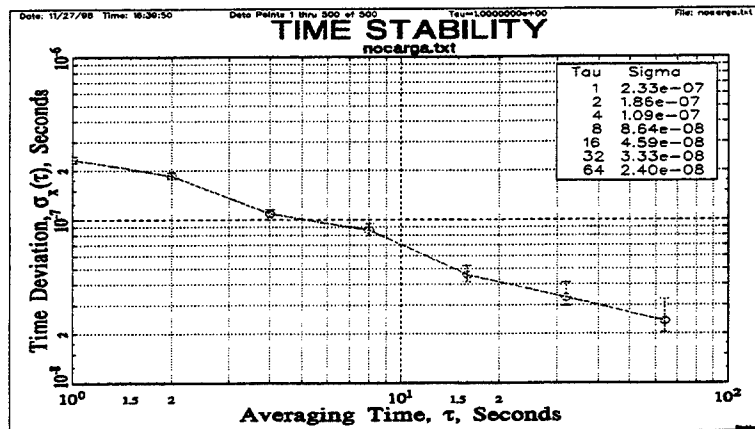
Figure 7: TDEV of time offsets with low activity
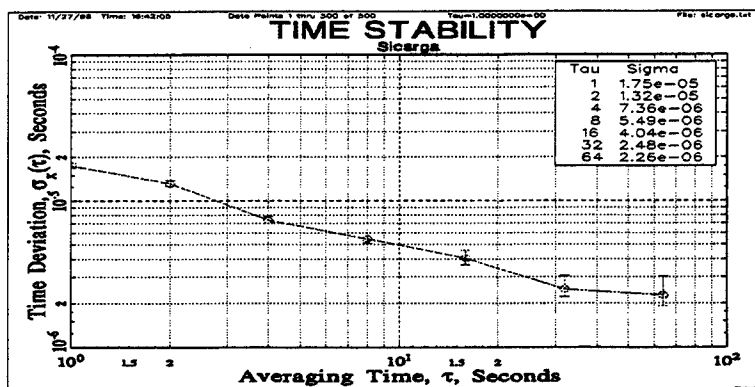
Figure 8: TDEV of time offsets with high activity
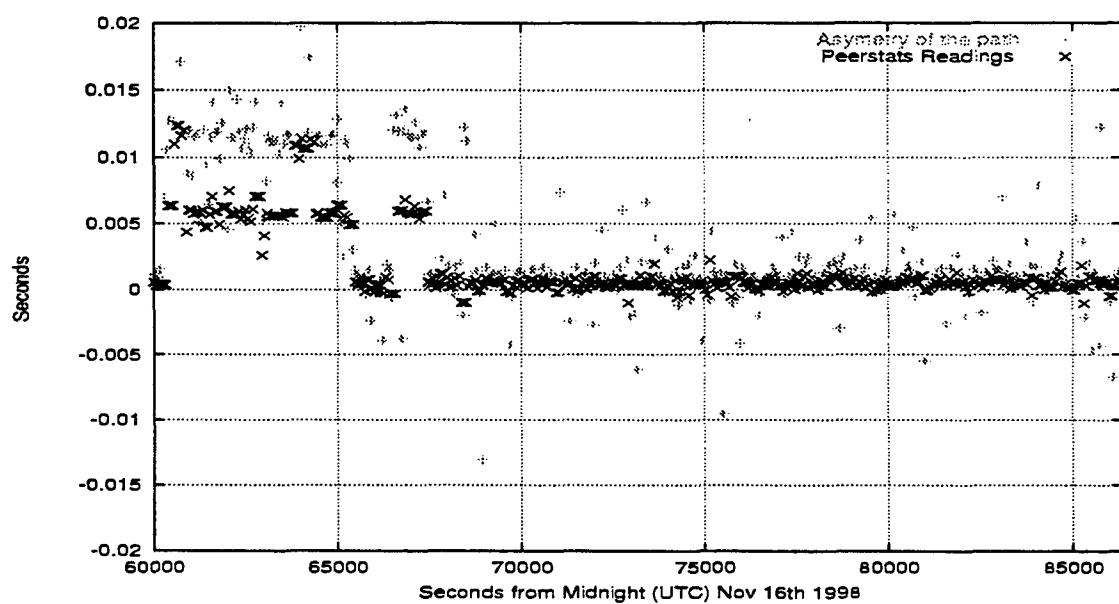
Figure 9: Asymmetry on the link and measured offset of the peer

PSEUDO-RANDOM CODE CORRELATOR TIMING ERRORS DUE TO MULTIPLE REFLECTIONS IN TRANSMISSION LINES

F. G. Ascarrunz*, T. E. Parker†, and S. R. Jefferts†
*University of Colorado, Boulder, CO, USA
†National Institute of Standards and Technology
Boulder, CO 80803, USA

Abstract

Multiple reflections in transmission lines can cause an amplification of timing errors associated with the delay sensitivity to environmental effects of the transmission lines. This multiplicative effect arises because the timing error in an early/late code correlator is a function of the relative RF carrier phase, the relative power levels, and the relative time delay between the direct and relected signal.

INTRODUCTION

The theoretical analysis of the timing errors introduced by the correlator sensitivity to multipath signals is well known [1,2]; however, the correlator timing errors due to multiple signal propagation in transmission lines has not been fully appreciated by the timing community. Multiple reflections of a spread-spectrum-modulated signal in a cable can cause large biases in the correlation function. These biases are tracked by the delay-locked loop (DLL), resulting in timing errors. Multiple reflections of a sinusoidal signal can be characterized by the voltage standing wave ratio (VSWR). Destructive or constructive interference may occur depending on the length of the transmission line, the source and load terminations, and the frequency of the signal. In a similar manner a spread spectrum signal will be influenced by the presence of a reflected signal that has an arbitrary delay, phase, and amplitude with respect to the direct signal.

MULTIPLE REFLECTIONS IN TRANSMISSION LINES

Multiple reflections in transmission lines can occur when there is a mismatch in impedance and a signal reflects off the load back toward the source. If the backward propagating signal is reflected forward again, it will become an interfering reflected signal that is smaller in amplitude, delayed in time, and arbitrary in phase as compared to the direct signal. If the reflections occur at the ends of the transmission line, the multipath signal is delayed from the direct signal by twice the propagation delay of the transmission line. For simplicity we will assume that the reflections occur at the ends of the transmission line and only one interfering signal is dominant. This is not necessarily
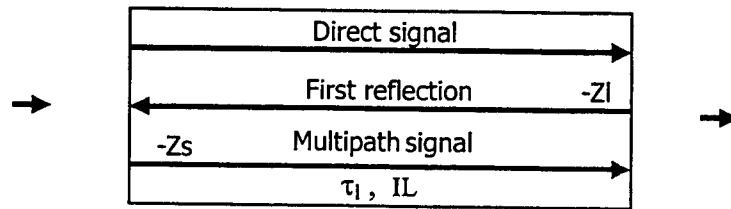
Figure 1. Graphical representation of a cable.

true because damage or dielectric imperfections along the length of the transmission line may cause an impedance change that results in multiple reflections. Figure 1 is a graphical representation of a cable, with a direct signal and an interfering signal that results from reflections due to an impedance mismatch at the ends of the cable. Z_s is the return loss of the source and Z_l is the return loss of the load. The power of the direct signal is P and the power of the reflected interfering signal is P_m. The cable has an electrical length τ_l and the insertion loss is IL. The relation between the power level of the direct signal and the level of the reflected signal is given by

$$P_m = P - 2 \cdot IL - Z_s - Z_l. \tag{1}$$

EARLY/LATE CODE CORRELATOR

A simplified model of a noncoherent early/late (E/L) correlator is described below. The complete derivations of these equations are presented in references [1,2]. In Figure 2, the E/L code loop detector is displayed in its simplest form. The input signal Y(t) is split and is the input to the early and the late correlator channels. The reference pseudo-random code sequence (PN) to the early and late correlators is spaced by a chip. The time variable is t, the reference sequence time estimate is T, and T_c is the chipping period. In both the early and late correlation channels, the output of the correlator is band–pass filtered and squared. The code detector error signal $S(\varepsilon)$ is the difference of the early and late correlation channel outputs. The error signal $S(\varepsilon)$ is driven to zero by the DLL in normal tracking operation. The tracking loop error is (t-T) and is given by ε.
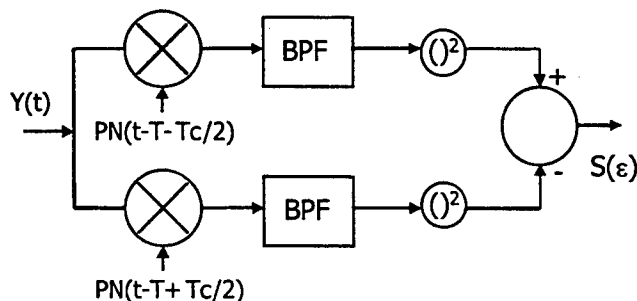
Figure 2. Code loop detector model.

The input signal Y(t) is the sum of the direct signal and one interfering signal resulting from a reflection off the ends of a cable as described in the preceding section. Y(t) is given by

$$Y(t) = \sqrt{2P} \cdot PN(t - T) \cdot \cos(2\pi f \cdot t + \phi)$$
$$+ \sqrt{2P_m} \cdot PN(t - T - \tau_m) \cdot \cos(2\pi f \cdot t + \phi + \phi_m) \qquad (2)$$

where f is the direct signal carrier frequency, ϕ is the carrier phase of the direct signal, τm is the time delay of the reflected interfering signal with respect to the direct signal, and ϕm is the relative carrier phase between the direct and the interfering signal.

The error signal from the code loop detector S(ε) is given by

$$S(\varepsilon) = P \cdot R_{PN}^2 (\varepsilon - \tfrac{T_c}{2}) + P_m \cdot R_{PN}^2 (\varepsilon + \tau_m - \tfrac{T_c}{2})$$
$$+ 2P \cdot R_{PN}(\varepsilon - \tfrac{T_c}{2}) \cdot P_m R_{PN}(\varepsilon + \tau_m - \tfrac{T_c}{2}) \cdot \cos(\phi_m)$$
$$- P \cdot R_{PN}^2 (\varepsilon + \tfrac{T_c}{2}) - P_m \cdot R_{PN}^2 (\varepsilon + \tau_m + \tfrac{T_c}{2})$$
$$- 2P \cdot R_{PN}(\varepsilon + \tfrac{T_c}{2}) \cdot P_m R_{PN}(\varepsilon + \tau_m + \tfrac{T_c}{2}) \cdot \cos(\phi_m) \qquad (3)$$

when the input to the system is Y(t) as described in equation 2. The function $R_{PN}(\varepsilon)$ is the auto-correlation function of PN(t-T). The magnitude of the timing error is a function of ϕ_m, RF carrier phase between direct and reflected signals, τ_m the time delay between the direct and reflected signal, and P_m/P the ratio of reflected signal power level to direct signal power level.

During tracking mode the delay lock loop adjusts the time estimate of the reference, T, such that S(ε) is zero. A plot of the correlator loop detector error is shown in Figure 3 for the case where there is no interfering signal present. A plot of the correlator loop detector error is shown in Figure 4 for the case where a reflected interfering signal is present. Note that the S(ε) function is distorted and that there is a timing error bias. The timing error during tracking is given by solving for ε for the condition S(ε)=0.

Since the magnitude of the timing error is a function of ϕ_m, τ_m, and P_m/P, the
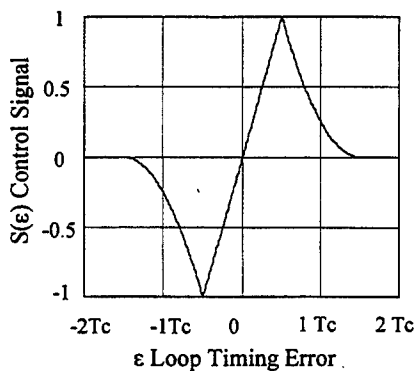
Figure 3. S(ε) without multipath.

Figure 4. S(ε) with multipath.

435
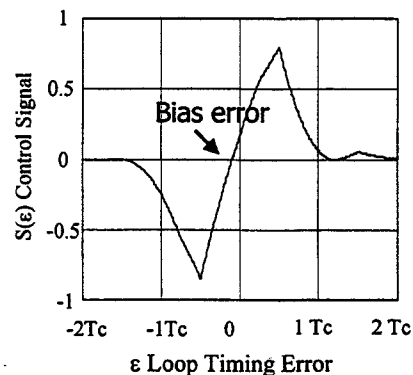
timing error will be a function of the propagation path through the circuit elements as well as a function of the various termination impedances when multiple reflections are present. If the timing error did not change, a simple calibration procedure could be established to eliminate the bias; however, small changes in propagation path or termination impedance may occur due to environmental effects and the calibration procedure would be ineffective. A plot of the timing error as a function of τ_m is shown in Figure 5, for the case of an interfering signal that is 30 dB lower in power than the direct signal. The carrier frequency is 70 MHz and the chip rate is 2.5 MHz. Note that a 7 ns propagation delay can cause a 13 ns delay change as measured by the correlator.
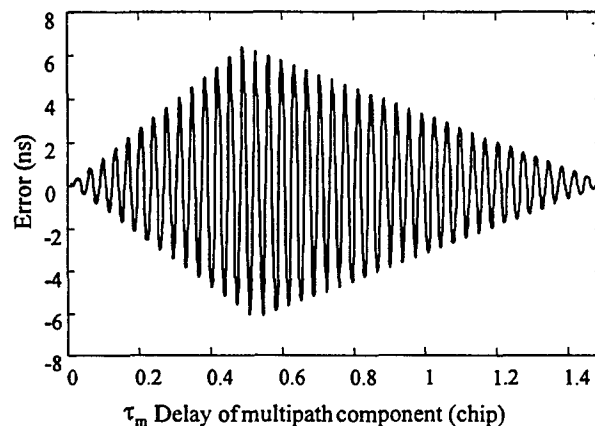
Figure 5. Timing error due to multipath, as a function of the electrical length of a cable.

In addition, you can increase the length of the propagation path, and the correlator, depending on the RF carrier phase, may measure a shorter delay. In the next section a more dramatic numerical example will be presented to illustrate how small physical delay changes due to environmental effects such as the temperature coefficient of a cable can be amplified by the correlator into unexpectedly large timing errors in a GPS receiver.

A GPS EXAMPLE

The relative RF carrier phase between the direct and reflected signals is a function of the propagation path and the source and load terminations. Aging, temperature, and other environmental effects affect the propagation delay through the cable and give rise to larger than expected timing errors. For example, consider a typical GPS timing receiver system that is composed of an antenna and low noise amplifier, a 30 m low loss cable, and a receiver located indoors. The carrier frequency is 1575 MHz and the C/A code has a chip rate of 1.023 MHz that corresponds to chip period of 978 ns. A good cable may have a delay temperature coefficient of 7 ppm/°C. The propagation delay through the 30m cable is 110 ns and will have variations on the order of 0.8 ps/°C. Assuming that the multi-path signal in the cable is caused by impedance mismatch at the antenna and receiver and that it is 30 dB attenuated with respect to the direct signal, we

436

can calculate the timing error for a 10 °C temperature rise of the cable. The propagation of the direct signal will change by 8 ps and the propagation of the multi-path signal will change by 16 ps. The correlator, however, will indicate a change of −800 ps. This example does not illustrate a minimum or maximum error. The magnitude of the error for the same cable and temperature excursion will be different for a small increase or decrease in overall length.

CONCLUSION

Propagation of multiple reflections in transmission lines can cause larger than expected timing errors. These timing errors are a function of the propagation path and are sensitive to environmental effects such as aging, temperature, and humidity. Good matching and care in component selection are essential in trying to minimize multiple reflection signal propagation. Temperature compensation of these timing errors may not be effective, because the temperature coefficient of delay is also a function of the propagation path. In fact, the temperature coefficient of the phase delay through a system is not the same as the temperature coefficient of delay as measured by a PN code correlator.

In some systems, sweeping the carrier frequency can be used to evaluate the magnitude of the multipath environment. In other systems, a careful selection of high phase stability cable and a judicious choice of cable length may minimize the multipath problems.

REFERENCES

1. Holmes, J. K., *Coherent Spread Spectrum Systems*, John Wiley and Sons, Inc., New York, 1982.
2. Van Dierendonck, A. J., "GPS Receivers," *Global Positioning Systems: Theory and Applications*, Vol. 1, American Institute of Aeronautics and Astronautics, Inc., Washington, 1996.

THE TIME DISTRIBUTION SYSTEM FOR THE WIDE AREA AUGMENTATION SYSTEM (WAAS)

William J. Klepczynski
Innovative Solutions International, Inc.
1608 Spring Hill Road, Suite 200, Vienna, VA 22181, USA
(202) 651-6970, *Bill.Klepczynski@faa.gov*

Abstract

This paper describes the functions, requirements, and objectives of the Time Distibution System (TDS). It should be pointed out that the WAAS TDS has not yet been developed because it is a componentof the final phase of WAAS development. However, WAAS Phase 1 allows for the inclusion of the TDS into the WAAS if it is developed before the final phase of WAAS.

The TDS will be located at the U.S. Naval Observatory (USNO). It will be used to provide the offset data between WAAS Network Time (WNT) and Coordinated Universal Time (UTC). The offset data will then be passed on to the WAAS Master Station (WMS) for transfer to the Geostationary Uplink Station (GUS) and broadcast to users of precise time through the WAAS Signal-in-Space (SIS).

INTRODUCTION

The WAAS has a secondary mission of time distribution [1]. UTC(USNO), Coordinated Universal Time as determined by the Master Clock at the USNO, represents the approved time standard source for the WAAS. Time distribution will be accomplished by providing users with a time offset between WNT and UTC. This time offset will be determined at the United States Naval Observatory (USNO) by a Time Distribution System (TDS). The TDS receives WAAS messages from the geostationary satellites within its view and computes the time difference between the epoch time of the start of a WAAS message and the 1 Pulse Per Second (PPS) of the USNO Master Clock which is the physical realization of

UTC(USNO), the time reference for GPS Time. The data collected from each observed satellite by the TDS receiver are passed on to a USNO data acquisition system. The data are then transferred to the WAAS Master Stations (WMS) through an interface between the WAAS and the USNO. The WMS collects the WNT/UTC offset and creates a Type 12 Message that is then sent to the Geostationary Uplink Station (GUS) which transmits it to the geostationary satellite (GEO). The purpose of the Type 12 Message is to provide time users with an accurate source of time referenced to UTC.

TDS DESCRIPTION

The TDS receiver is a specially modified WAAS receiver that functions in a fashion similar to a GPS Time Transfer Unit. It receives the message from a satellite and reconstructs the WNT time that corresponds to that message and then compares that time to the time being input to the TDS from the USNO Master Clock.

The TDS contains an antenna, receiver, and modem. The TDS Antenna receives the WAAS SIS from the GEO satellites. The TDS Receiver collects the WAAS SIS observable and forwards WAAS GEO navigation message and WNT/UTC offset data to a processor. The receiver will output a data string that contains WNT offset data. As shown in Figure 1, an interface between the USNO Processor and the WAAS Message Center Processor (MCP) will communicate the WNT/UTC offset back to the WAAS system.

The data, produced by measuring each GEO satellite 1 PPS epoch with respect to UTC(USNO), are collected and recorded for computation of correction parameters to WNT. The satellite epoch beginning time will be converted to WNT by utilizing the time offset and drift numbers from the WAAS SIS. The TDS then passes the values of all satellites being tracked to the USNO data acquisition system in a format compatible with USNO reduction programs. The collection of WNT-UTC(USNO) time differences is performed by the WAAS Operations and Maintenance (O&M) function for inclusion by the WMS in WAAS Message 12. Message 12 is not intended for navigation.

Users within the WAAS Service Volume can acquire the WAAS GEO SIS and utilize the correction parameters contained in Message 12 to determine their local receiver time with respect to UTC to within an accuracy of 20 nanoseconds. Since the GEO moves very little in the sky with respect to the user, the use of a high gain antenna will be very effective in mitigating the effects of interference.

TDS REQUIREMENTS

Origin of the Requirements

TDS requirements are originally defined in FAA-E-2892B (Specification for the WAAS), paragraph 3.2.8.2. This was originally a Phase 1 requirement; however, due to funding constraints it was deferred and is now contained in SOW Option 3, paragraph 3.2.3.

- FAA-E-2892B, paragraph 3.2.8.2: "*WNT/UTC Time Maintenance*. The WNT offset error from UTC (after correction as defined in paragraph 3.1.3.9.2.2.12.2) shall be less than 20 nanoseconds."

- SOW Option 3, paragraph 3.2.3: "*Option 3 Time Distribution System (TDS) Implementation*. This option shall remain valid for the duration of the WAAS contract. Under the requirements of the Phase 1 WAAS the contractor shall include the TDS in: System Level Documentation - CDRL A121, Configuration Item Level Documentation - CDRLs A042, A043, Interface Control Documentation - CDRL A052, Interface Requirements Specification - CDRL A019, System Orientation Manual - CDRL A123 and the System/Segment Design Document - CDRL A018. Upon exercise of Option 3 the TDS shall be implemented. The contractor is not required to resubmit the Configuration Item Development Specification (A042) and the Interface Control Document (A052) until Option 3 is exercised. The generation of the WAAS Signal in Space Message Type 12, shall be implemented in Phase 1 if WNT/UTC offset information in accordance with the above documentation is provided as GFI."

Description of the Requirement

The requirement states: The WAAS Network Time (WNT) offset from UTC shall be less than 20 nanoseconds. The TDS will include a standard WAAS receiver/antenna. It will be located at the USNO which will determine WNT and compare it with UTC(USNO). The offset will be requested by the WMS for inclusion in the Type 12 message. A TDS Interface Control Document will be required to describe the relation of the TDS with other external systems and equipment.

Justification of the Requirement

The TDS is needed in order for the WAAS to fulfill its secondary mission of time distribution, accomplished by providing users with a time offset between WNT and UTC. The TDS will be valuable to the non-navigation community for synchronizing power grids and telecommunications networks on which the WAAS is dependent. Additionally, it will be of value to other systems within the FAA, such as Automatic Dependent Surveillance (ADS) and ADS-B (Broadcast). Furthermore, the TDS will provide a link with other international Satellite-Based Augmentation Systems (SBAS) through a knowledge of their time offsets with UTC and, therefore, WNT.

TDS OBJECTIVES

WNT, as measured from the GEO SIS epoch timing, is controlled to very close tolerances to the GPS time epoch and will be maintained to a highly accurate time offset with respect to UTC(USNO). The TDS performs a time difference between the GEO beginning of message epoch times and an accurate 1 pulse per second (1 PPS) strobe from the USNO time reference system (Master Clock), which denotes the beginning of a UTC second mark.

Users within the WAAS Service Volume which also have a TDS can acquire the WAAS GEO SIS and utilize the correction parameters contained in Message 12 to determine the offset of their local reference time from UTC to within an accuracy of 20 nanoseconds. WNT provides for the user a continuous, accurate, and redundant timing signal which is not affected by Selective Availability. In addition, if a high gain antenna is used, a TDS receiver should be able to mitigate the effects of interference on the received signal.

DISCUSSION

GPS has become one of the primary means for distribution of time throughout the world. Several manufacturers have developed special timing systems to be used in conjunction with GPS signals. These systems are often called GPS Time Transfer Units (TTUs). Unfortunately, there are no WAAS timing systems in existence. However, the WAAS receivers used at the WAAS Reference Stations (WRS) provide the necessary hardware to allow the development of a WAAS TDS based on the knowledge which has been gained in the development of GPS TTUs.

By placing a scaled-down version of the WAAS Reference Station receiver at the USNO and using the USNO Master Clock as the local reference for the receiver, it is possible to determine the offset between the timed messages coming from the GEO based on WNT and UTC(USNO). The TDS Receiver provides sufficient output data through an RS232 port to allow the calculation of this difference. The

calculations can be done on site at the USNO using a PC system and a time interval counter which is compatible with other USNO timing systems. The results of these calculations will then be passed on to the USNO Data Acquisition System for storage and computation of average values. The WAAS WMS will then retrieve the necessary data for inclusion in the WAAS Message 12 by an Internet connection to the MCP or in a manner to be mutually agreed to by Raytheon and USNO such that the operational concept for the WAAS is satisfied.

Prior to start of operations with the TDS, it will be placed at the USNO for a trial period of data acquisition. During this period, a thorough analysis of the data will be performed in order to verify and validate that all calibration constants have been correctly evaluated through independent checks.

ACKNOWLEDGMENTS

REFERENCES

[1] W. J. Klepczynski, *"The role of time and frequency in the Wide Area Augmentation System (WAAS),"* Proceedings of the 12th European Frequency and Time Forum, 10-12 March 1998, Warsaw, Poland.

BIBLIOGRAPHY

The following WAAS documents provided input for this article.

Specification for the Wide Area Augmentation System (WAAS), FAA-E-2892C.

System Specification for the Wide Area Augmentation System (WAAS), CDRL Sequence No. A121-001B.

System/Segment Design Document for the Wide Area Augmentation System, CDRL Sequence No. A018-001B.

Prime Item Development Specification, Time Distribution Subsystem for the Wide Area Augmentation System (WAAS), CDRL Sequence No. A052-003, 14 March 1997.

Interface Control Document, Time Distribution Subsystem for the Wide Area Augmentation System (WAAS), CDRL Sequence No. A052-004, 16 March 1997.

Antenna
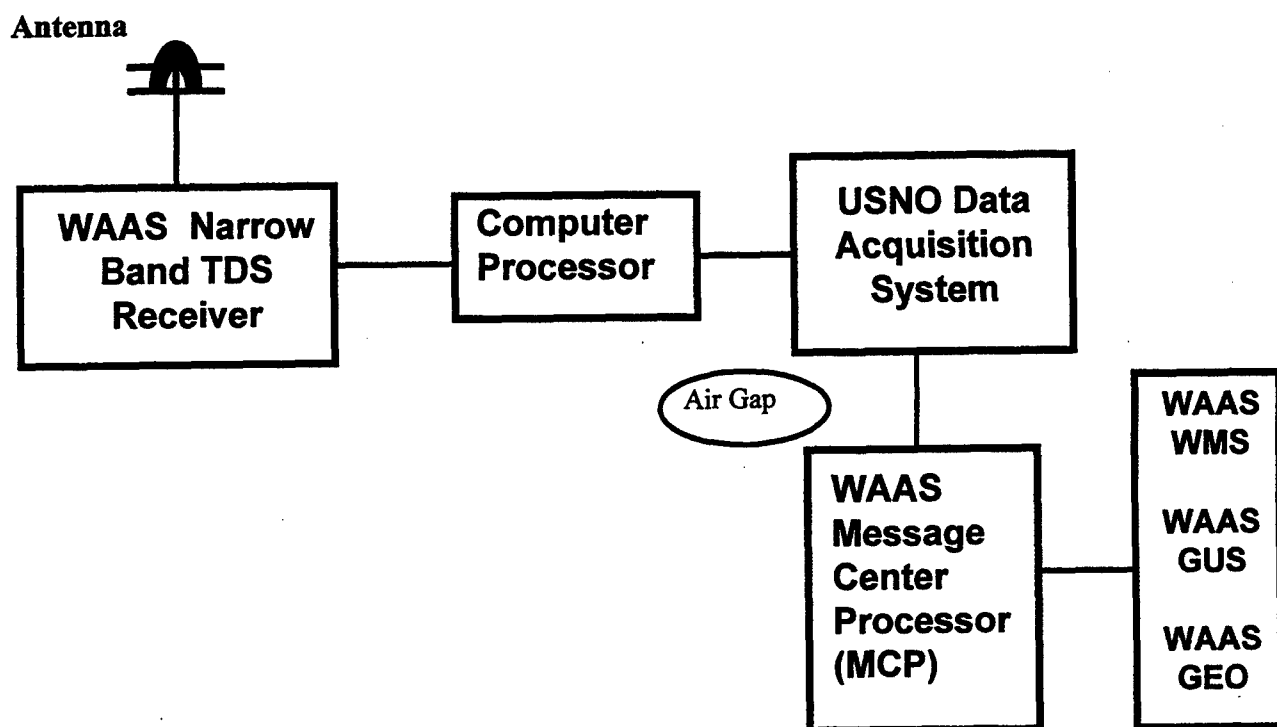
Figure 1 – Architecture of the Time Distribution System (TDS)

Questions and Answers

DENNIS McCARTHY (USNO): My question is regarding the specifications for the WAAS net time. You said it would have worldwide availability. So do you have any numbers on what you expect the specifications will be with respect to GPS time?

WILLIAM KLEPCZYNSKI (ISI): The specification for WAAS net time with regard to GPS time calls for 50 nanoseconds, because that allows the seven meters or so that will allow for a safe navigation in certain conditions.

DENNIS McCARTHY: Is that the only specification on the net time?

WILLIAM KLEPCZYNSKI: No, the second specification on WAAS net time is that it be within 20 nanoseconds of UTC USNO.

DENNIS McCARTHY: Okay, 20 nanoseconds of UTC USNO.

WILLIAM KLEPCZYNSKI: And 50 nanoseconds of GPS time.

JOERG HAHN (DLR): I was listening to some of the problems with the funding of the WAAS system. Can you tell me something about this?

WILLIAM KLEPCZYNSKI: I can not tell you that; I have no idea. Actually, I am a technical type, and I was away on travel and had just come back. All I can say is that unofficially I know that Congress has not been very happy the way the FAA officials have been documenting their budget and things like that. So they have been slapped on the hand a little bit here and there. What the net fallout is, I honestly do not know, at this point in time, just because I have not been at the office for at least a week now. I know that there were some major meetings taking place this week to describe the budget, but I do not know what the result is.

ON THE PROBLEMS OF SYSTEM TIME GENERATION FOR A FUTURE GNSS2

J.H. Hahn

DLR, Institut für Hochfrequenztechnik
Postfach 1116, D-82230 Oberpfaffenhofen, Germany
joerg.hahn@dlr.de

P. Tavella

Istituto Elettrotecnico Nazionale G. Ferraris
Strada delle Cacce 91 I-10135 Torino, Italy
tavella@tf.ien.it

Abstract

For any satellite navigation system clock synchronization to a system common time is a requirement of utmost importance. There are some features, being of particular interest, which are studied here. For clock comparisons one- and two-way methods can be applied. In the present conventional systems GPS & GLONASS systems, only the first method is actively in use. Improvements in several areas are expected in scenarios applying two-way and inter-satellite-links (ISL).

For generation of the system time scale (STS) with one or some chosen types of clocks the ensemble solution is the most stable and reliable. There are several and sometimes different constraints for the realization of a STS for navigation or timing users.

In this paper we discuss the impact of clock comparison measures and of STS generation peculiarities on the development of a 2nd generation Global Navigation Satellite System (GNSS2). We give simulation results of a STS and induced navigation/timing user clock error in a possible GNSS2 scenario, defined by (Case 1) 15 Inclined Geosynchronous Satellites (IGSO) equipped with a RAFS (space Rb) each + 3 Geostationary Satellites (GEO) equipped with an H-Maser, and 4 ground stations operating with a Cs-frequency standard, where both inter-satellite and two-way links are adopted. It will be shown that for the navigation user the error contribution due to the clocks can reach a value of about 0.7 ns (1σ), with an update interval of 30 min in this particular scenario. Satellite constellations equipped with H-Maser give better results. For time dissemination purposes, the UTC steering policy will be addressed and an error

reaching 27 ns (1σ) is expected in the above scenario. Finally we also investigated a constellation using Ultra Stable Quartz Oscillators on-board the satellites (Case 2). We show that such a configuration could also satisfy the needs of navigation/timing users.

INTRODUCTION

For the designer of a new civil navigation system, i.e. GNSS2 the time keeping in such a complex system plays a major role. Much experience in this field was gained by the GPS developers over the past years. Only if the mutual clock synchronization between the satellite clocks is realized within a high level of precision can the navigation user solve for its own antenna position. This would enable also time dissemination to the scientific timing community or other commercial services. But to use such a feature to a high extent, some efforts have to be made to ensure the accuracy of the STS.
For navigation purposes only, a system as realized with the current GPS and GLONASS could almost live with its own free system time scale. But as written in the GPS-Interface Control Document, the timing user is a specified customer, and GPS-time & UTC dissemination is one of the system goals. This concerns GLONASS too, and a link to UTC had to be established in both systems.

For civil navigation purposes more or less relaxed requirements on the long-term stability of the STS could be specified if we consider the opportunity to have regularly and safe contacts to the satellites. This is also a cost factor. Now, for a future GNSS2 some decisions have to be made:

1. Do we need / wish to distribute a high accurate and stable time scale ?
2. In which terms this time scale has to be optimized, and what is the impact on the system design ?
3. How to find the most cost-effective solution ?

In order to answer such questions we identified some tasks which have to be studied very carefully:

- selection of the satellite clock type: Cs, Rubidium Atomic Freq. Standard (RAFS), H-Maser, Ultra Stable Oscillator (USO, quartz)
- clock synchronization method (one- & two-way)
- STS generation, ensemble technique preferred
- measurement rate & clock parameter update rate

For a GNSS2 in the present development phase also inter-satellite-ranging (ISR) is studied. Combined with a dedicated satellite constellation such a scenario can benefit from the opportunity to increase the measurement and update rate sufficiently. This could also help to decrease the requirements on the clock stability: much cheaper and more reliable clocks, i.e. USOs could be considered.

In a first step we investigated a clock scenario (Case 1) with 15 RAFS and 3 H-Maser clocks in orbit (European space-qualified versions each), and 4 Cs-clocks on ground. Both ISL and two-way links had been adopted. The User Equivalent Range Error (UERE, see below) clock requirement was 0.7 ns (1σ). We will show the results of this simulation and discuss possible system design constraints and simplifications. At the end we give another simulation result where USOs have been considered on-board the satellites (Case 2).

SYNCHRONIZATION METHOD AND SCENARIO

There are two different synchronization methods available which can be used for clock synchronization, namely one- and two-way methods. The advantage of the first is its simplicity in operation, but it is strongly correlated to the position error of the two participating stations. This can be avoided with two-way methods requiring active stations at both sites. A more detailed description can be found elsewhere. To meet a compromise between both methods the so–called two-way pseudo cross-link had been proposed. This mode works like a two-way cross-link: both stations send a signal wrt. the other station, but the transmission from one station is delayed by a certain interval τ_{wait}. Such an operation can be of highest interest in an ISL-scenario, where only one satellite transmits, others are listening. After a certain interval the transmit/receive configuration is changed and so on. The clock comparison between two satellites is depicted in **Fig. 1**.

Applying a pseudo cross-link the clock offset $T_{n,m}$ in [s] between two stations (satellites) can be determined in the same manner as with a cross-link by just subtracting the offset due to the clock rate during the interval τ_{wait} :

$$T_{n,m} = \frac{PR_m - PR_n}{2} - \frac{\Delta\tau_{n,m}}{2} - y \cdot \tau_{wait} - \tau_{rel\,n.m}$$

Eq. 1

PR_m & PR_n being the time intervals between the transmitted and received signal (recorded as one-way pseudoranges in [s]) as measured at both m & n sites, $\Delta\tau_{n,m}$ is the asymmetric delay in [s], y is the rate between both clocks in [s/s], $\tau_{rel,n.m}$ relativistic delay in [s]. The waiting interval depends on the number of satellites involved in such a system. The accuracy will mainly depend on a decrease of the asymmetry term, which itself consists of the

- geometric
- atmospheric (iono- + troposphere).
- Sagnac effect
- instrumental (transmitter + receiver, receiver noise)

differential delays. Clearly it can be seen that there is a requirement for stable clocks at both stations at least over the whole waiting period (i.e. some seconds till 2 min.)

Using such measured clock offsets the STS is generated. This scenario applies essentially highly accurate two-way data. Additionally, clock offset solutions from the Kalman filter for ephemeris determination (pure one-way solution) can be used in a weighted combination to the more accurate two-way measured clock offsets. Getting such data the STS can be computed as an appendix to the orbital Kalman filter.

STS AND ITS GENERATION

For navigation, dating, and maybe time dissemination purposes, the existence of a system reference time scale is compulsory in a GNSS2. The clocks of each satellite shall then be synchronized to the common reference time scale. This is necessary in particular for:
- providing correct information on the clock status in the navigation message,
- having a common reference time for scheduled system operation activities,
- evaluating satellite ephemeris,
- disseminating a reference time scale to different users.

The system time reference can be an independent time scale with the unique request of being the common reference for all the GNSS2 (space, ground, and users segments). In the civil as well as military standards, the use of the UTC is recommended and, actually, UTC has a wide diffusion.

The solutions adopted to define a STS are usually twofold:

- The first is the *master clock* solution, where one of the system clocks is chosen to be the *master* and it defines the time scale for all the system. Such a solution seems to be preferred in GLONASS.
- On the other hand, the STS can be defined as an ensemble time scale obtained from a suitable average of *all the system clocks* either on ground or on-board. This second solution is adopted in GPS-time and it has evident advantages in reliability and stability.

As far as stability is concerned, it can be demonstrated that an ensemble time has better stability than any single clock participating to the ensemble, at least for some particular values of integration time τ.

STABILITY ?

The STS constitutes the reference time scale versus which the errors of all the single clocks are estimated. The better the reference time, the better are the estimations of the clock errors. Moreover, all the system clocks are synchronized to the STS and they have to locally reproduce, in real-time, the STS. The STS will in fact be available only in deferred time because a certain delay is introduced due to the need of gathering clock data and of computing the ensemble time. To this aim, a prediction of STS and of each single clock behavior is necessary. The more stable the STS, the more it is predictable and thus better reproduced, in real-time, by each single clock. In addition, if the system time is more stable than any single clock, it would be almost sure that any observed anomaly in the time offset between a satellite clock and STS can be ascribed to the satellite clock, and thus corrective actions can be taken.

ACCURACY ?

As far as the navigation is concerned, the STS accuracy defined as the degree of agreement versus UTC is not a compulsory demand. System clocks could be all very fast and delivering a time unit far from the SI-definition, but, if all the system clocks were coherent in such a system, navigation accuracy would not be damaged. Thus, the agreement with UTC seems not necessary in principle, but it results in some related benefits:

- The first is the **very long-term stability**. It was stated that the STS has to be stable, but clock stability depends on the integration time τ, so the integration time τ over which optimize stability has to be chosen. A different choice of the clock weights results in a different stability of the ensemble time. Due to the aim of the STS of being a measurement reference and also for practical reasons due to measurement availability, with the Case 1 a study was performed by choosing to optimize the stability of the STS in the range of medium-/long-term integration times, i.e. $10 \leq \tau \leq 30$ days, not longer. It is also very difficult to optimize to stability over months or years with the clocks commercially available currently, due to the difficulties in estimating their very long-term behavior. Conversely, UTC, which is the ultimate reference time, has the best stability in the very long-term by definition and by its fundamental aims. Therefore, ensuring the agreement of the STS versus UTC means also ensuring the very long-term stability. In this case the accuracy can be seen as a long-term warranty that the system time is not degrading. Moreover, for practical reasons, it seems surely easier to maintain the agreement with an existing and well disseminated time scale, rather than creating a completely independent one. In addition, there are recommendations of standardization organizations as the CIPM, ITU, and military, as NATO, explicitly asking to use UTC as reference [1] - [3].
- The strongest remark anyway comes from the fact that a GNSS2 could be also a mean for **disseminating UTC** in almost real-time around the world. This clearly asks for a close agreement versus UTC. The current request in Europe for a system disseminating UTC is very strong and not only restricted to metrological institutions. The existence of a reference time scale with easy access, cheap, and accurate is requested by telecommunication companies, scientific laboratories and astronomical observatories, industries that synchronize their computers, banks, watch sellers, transportation systems, and so on. As a matter of fact, the market of Rb-standards disciplined to a GPS receiver that locks the frequency of the Rb-standard to the GPS time scale is still growing and new users are still arising. In such a case, since UTC exists only *"after the fact,"* and results are available with a delay of one month, the STS must ensure the best metrological qualities in the meantime, when UTC is still not known. This is another reason suggesting that the STS should be optimized over an integration time τ of about 10-20 days, i.e. the mean time before the publication of UTC results.

A possible easy and cheap solution to maintain agreement versus UTC, and also for sake of reliability and of safety, could be the frequent comparison of the STS versus a local intermediate time scale chosen among the *real-time* approximations of UTC versus which the STS could be more frequently compared (the same role of UTC(USNO) in GPS). This will be considered in Case 2.

EXPECTED FEATURES

The use of a STS not only based on the signal of a single clock, but obtained from an "ensemble" of oscillators ensures a better performance in terms of stability, accuracy, and reliability. This is true for any ensemble time. The case of an ensemble including also satellite clocks by means of ISL offers some peculiarities and advantages:

- Clocks are kept in more stable conditions. In fact, once they are appropriately insulated from temperature gradients, the environment is less noisy for vibration and e.m. disturbances. The clock behavior should then be more stable than on Earth and the same for the resulting ensemble time.
- Minor correlation among clocks is expected being spread on different satellites. Thus, the independence of clocks should be ensured and this avoids the appearance of correlated noises that degrade the quality of the ensemble time and whose detection is difficult.
- In case of optical links, the clock comparison schedule is guaranteed, since there will be no obstacles causes by bad weather. Therefore, the clock comparison series doesn't contain unexpected *missing data* with all the subsequent statistical problems of data reconstruction.
- On the other hand, the series of data may be not evenly spaced and measurement data can be not directly on the standard date requested for the computation of the ensemble time. Therefore, an appropriate smoothing and optimal estimation technique is necessary.
- The measurement uncertainty can be dependent on the geometry of ISL and, thus, not be constant. Moreover, multiple contemporary ISLs are possible, providing a redundant set of clock comparisons that should be processed by an appropriate least-squares estimator.

From the uncertainty of the clock inter-comparisons performed by ISL, from the intrinsic metrological qualities of the used clocks, and from the statistical capabilities of the ensemble algorithm, the qualities of the ensemble time can be estimated and validated by simulations. It is expected that

- ISL can guarantee clock comparisons with a subnanosecond uncertainty,
- Clocks on-board and on Earth could be atomic commercial standards with a medium-long-term stability up to the level of 10^{-14},
- The average algorithm could lead to an improvement of a factor $\sqrt{N}$ on the metrological qualities (N - number of clocks, $N = 22$ in Case 1, $N = 83$ in Case 2 as given below).
- It can be shown that the uncertainty on individual clock offsets from STS at the update epoch is negligible due to the low measurement uncertainty and large number of data which can be handled by means of appropriate smoothing and optimal estimation techniques, etc.

The resulting ensemble time scale could thus reasonably reproduce the UTC, in real-time, with a time error comprised in some tenths of nanoseconds .

GENERAL DEFINITION

Several ingredients are necessary. Apart from the smoothing on measurements data, the STS has to be defined as a weighted average of clock readings, where clock weights are to be appropriately fixed. Moreover, since time or frequency steps are to be avoided to ensure stability, each time that a clock enters or leaves the ensemble, a correction is necessary. Such a correction needs the prediction of the clock frequency, and thus mathematical tools typical of the signal processing analysis have to be introduced. Moreover, to ensure reliability, often an upper limit of weight is introduced. In addition, to avoid any degradation of the stability and reliability of the ensemble time, any check on possible anomalies in the clock behavior is necessary. Lastly, the offsets between each clock and STS are obtained and can be used to update the satellite clocks.

The basics of the average algorithm will not be given here, seeming to be commonly known to this community. The here-applied definition of an ensemble time is at the basis of most algorithms for ensemble time scales currently used and that have differently added some other stability improvements [4] - [6].

RESULTS

Simulation results will be given in the following for both assumed GNSS2-scenarios (Case 1, Case 2) as given in the introduction.

STS STABILITY – CASE 1

The stability of the 22 simulated clocks and of the STS is reported in **Fig 2**. The integration intervals from 10^4 s (~2.5 hours) up to 10^7 s (~100 days) are chosen, which constitute the range of interest either for the ISL periodicity or for the update interval of STS and on-board clocks. It can be easily extended down to 10^2 s, if necessary, because the noise affecting clocks from 10^2 s to 10^4 s is a white frequency (WFM) or random walk phase noise (RWPM) for all the clocks considered. It can be seen that the instabilities of the different RAFS follow more or less the same pattern, so is for H-Maser and Cs clocks.

It was decided to optimize the STS stability over the medium-long-term to provide a time reference useful for the estimation of single clock behavior and for maintaining an agreement versus UTC. To this aim, the instability over $\tau = 30$ days is of particular interest because it determines the weight of the clock in the computation of the ensemble STS. As expected, since long-term stability has to be optimized, the weights attributed to Cs clocks will be larger than the others. In particular it appears that due to the presence of linear frequency drift, the weights attributed to RAFS are almost negligible, compared to the Cs-weights. This stresses the fact that if long-term stability is to be obtained, then clocks with good long-term stability have to be used and the best solution is using Cs-standards.

It means that in reality the weighted average is mostly driven by Cs clocks, while the other clocks add a small gain. Nevertheless, the STS inherits a small frequency drift that generates a low instability. Such residual drift is very low and should not cause a problem from the stability point of view. From such considerations, it appears that the STS has more or less the same behavior of Cs clocks (WFM plus random walk frequency noise - RWFM), but at a lower level. From such simulation tests, it can be assumed that the instability of the STS would be mostly due to WFM for 10^4 s $\leq \tau \leq 20$ days and RWFM for $\tau \geq 20$ days.

STS ERROR & UTE – CASE 1

With the STS stability as estimated before, the uncertainty on the STS prediction can be evaluated by using the theory of random walk and the associated uncertainty. Let's suppose that the STS computation has an updating period equal to T_{STS}. The error gained by STS was evaluated, see **Tab. 1**. This means that, if STS is updated at least once a day, the uncertainty in the STS prediction remains below the level

of 5 ns. This error is below the level of the corresponding errors in predicting RAFS and Cs-clock offsets, but it is worse than the error gained by an H-Maser. On the other hand, the stability of STS continues to increase for observation times up to 20 days, while the stability of an H-Maser can be deteriorated by the frequency drift. Such STS could then be a good long-term reference for estimating frequency offsets and drift of RAFS and H-Maser, but it can hardly be a good reference for estimating the long-term behavior of Cs clocks. Such results strongly depend on the fact that the long-term stability of STS can only be ensured by the 4 Cs standards, and an ensemble STS obtained with only four clocks cannot exhibit better accuracy.

In case the time dissemination purpose was to be fulfilled, the STS should provide an accurate information of time, and the error versus the UTC has to be estimated. In fact UTC is known only a posteriori and if STS runs freely between one UTC update and the other, it can accumulate a large time error only due to its random noise, which is mostly due to the WFM. Therefore, in case the UTC steering was possible only any 30 days, the gained error after 30 days could amount to about 27 ns. It could be worthwhile, for sake of accuracy and also for safety, considering the possibility of using another real-time UTC approximation as a second reference useful for a more frequent and accurate steering of STS, as done in GPS with UTC(USNO).

T_{STS}	$u_{STS, max}$
5 min	0.3 ns
15 min	0.5 ns
30 min	0.7 ns
1 hour	1.0 ns
...	...
24 hours	5.0 ns

Tab. 1: STS uncertainty for different update intervals in Case 1

The uncertainty on the clock offset wrt. STS of a single satellite clock is equal to the User Time Error (UTE). The knowledge of the offset of any single clock versus STS in real-time is limited by at least two sources of uncertainty: the uncertainty due to the limited knowledge and predictability of the behavior

- of the single clock
- of the STS.

By assuming that STS and clocks on-board are updated with the same periodicity denoted by T_{STS}, it appears that $t - t_0$, i.e. the time since the last update, can vary in the region $0 < t - t_0 < T_{STS}$. The behavior of the total uncertainty for the three different types of clocks is reported in **Fig. 3**. In case of H-Maser, the uncertainty is dominated by the uncertainty due to STS noise, in case of RAFS and of Cs clocks, the larger contribution is due to the RAFS or Cs clocks themselves. The result of the overall (UTE) clock error evaluation for the different

T_{STS}	$u_{UTE,maser, max}$ [ns]	$u_{UTE,RAFS, max}$ [ns]
5 min	0.3	0.7
15 min	0.5	1.2
30 min	0.7	1.7
1 hour	1.0	2.4
...	...	...
24 hours	5.0	12.4

Tab. 2: Maximum values of the overall clock error (UTE) for different satellite clocks wrt. STS(1σ) – Case1

satellite clocks of the selected scenario is given in **Tab. 2** for $t - t_0 = T_{STS}$.

CLOCK ERRORS ON NAVIGATION SOLUTION, UERE CLOCK COMPONENT – CASE 1

The UERE combines the individual satellite errors to an overall error, and is defined following [7] as that component of system accuracy being independent of location and time that represents the receiver ranging error among the four satellites in view that provide the lowest Geometric Dilution of Precision (GDOP)-value. The uncertainty in evolution of the STS between two updates is not of importance for the UERE clock component. This can be explained with the fact that the STS error evolves in the same manner for all system clocks, thus, producing only a common bias. This bias, because it is common to all satellite pseudo-ranges, plays no role for the navigation user's position solution. Thus, the corresponding STS clock error can be excluded. The UERE clock uncertainty $u_{UERE(M),clock}$ by tracking $M \geq 4$-satellites ($M = 4$ for the classical definition, $M > 4$ for today's state-of-the art receivers) with individual satellite clock uncertainties $u_{x_i(t)}$, can be estimated with

$$u_{UERE(M),clock} = \frac{\sqrt{\sum_{i=1}^{M} u_{x_i(t)}^2}}{M} \quad ; M \geq 4$$

Eq. 2

The result for $M = 4$ is given in **Tab. 3**. In the last column the case of 4 H-Maser clocks has been shown for comparison. The good impact of such a constellation is quite visible.

STABILITY AND UERE IN A USO SCENARIO WITH CASE 2

In this case we considered a scenario with 83 clocks, namely 64 USOs (on-board Low Earth Orbiting (LEO)-satellites), 9 RAFS in orbit and 1 H-Maser, 9 Cs on ground

# H-maser	0	1	2	3	4
# RAFS	4	3	2	1	0
T_{STS}	U_{UERE} [ns]	U_{UERE} [ns]	U_{UERE} [ns]	U_{UERE} [ns]	U_{UERE} [ps]
5 min	0.30	0.26	0.21	0.15	3
15 min	**0.55**	0.48	0.39	0.28	6
30 min	0.80	**0.69**	**0.56**	0.40	8
1 hour	1.10	0.95	0.78	**0.55**	11
2 hours	1.60	1.38	1.13	0.80	16
...	...	...	...	...	...
24 hours	5.70	4.94	4.03	2.85	93

Tab. 3: UERE(4) cock error (1σ) for different clock combinations vs. update interval – Case 1

with the typical stability pattern as given in **Fig. 4**.

We concentrated on the short-term here, because the considered USOs have their best stability even in this observation range, a low measurement and update interval (up to 5 min) can be expected from the ISL-scenario, and steering to UTC can be maintained by frequent comparison of the STS versus a local real-time approximation of UTC versus which the STS could be very frequently compared. The application of USOs would make a system less expensive and increases reliability. Different STSs were examined:

- STS with all the 83 clocks;
- STS with all the clocks except USO;
- STS with USO only,

all optimized for τ = 1000 s. The instabilities obtained are illustrated in **Fig. 5** adding also the typical ADEV pattern of USO and H-Maser. It can be seen that an optimization on τ = 1000 s, gives the larger weight to the H-Maser (99%), and at τ = 1000 s the stability of STS is very similar to that of the H-Maser. Nevertheless, the presence of the USOs gives a large impact on the long-term behavior of the STS which inherits a frequency drift.

If the USOs are excluded the short-term is not worse, but the long-term is much better. It must also be stressed that in case the H-Maser is only one, so the STS largely relies on such a unique clock giving a very high weight and such a situation could raise some reliability problems.

The last STS is obtained with the USOs only. It can be seen that the stability of such STS is very similar to the USO instability, but at a lower level due to the high number of USOs at one's disposal. The solution of not using USOs in the STS could result in better stability. By plotting the instability of the clocks together with that of STS obtained without USOs in **Fig. 6**, it can be seen that the instability of the STS is much lower than those of the single clocks over the optimized interval of τ = 1000 s, apart from the H-Maser case, whose instability is more or less the same of the STS. For the observation intervals 100 s < τ < 10000 s, the dominating noise of the STS is a WFM corresponding

# USO	0	1	2	3	4
# RAFS	4	3	2	1	0
T_{STS}	U_{UERE} [ns]	U_{UERE} [ns]	U_{UERE} [ns]	U_{UERE} [ns]	U_{UERE} [ns]
5 min	0.30	0.26	0.21	0.15	0.03
15 min	**0.55**	**0.48**	0.41	0.31	0.17
30 min	0.80	0.73	**0.66**	**0.57**	**0.47**
1 hour	1.10	1.17	1.23	1.29	1.35
...	...	...	...	...	...
24 hours	5.70	87.64	123.81	151.58	175

Tab. 4: UERE(4) cock error (1σ) for different clock combinations vs. update interval – Case 2

454

to RWPM, so the uncertainty analysis of the STS follows the same approach as described above. Finally the UERE clock component for the different satellite clock combinations have been calculated as given in **Tab. 4.**

CONCLUSION

In both study cases ISL and two-way clock comparisonhavebeen considered. The proposed pseudo cross-link should be further investigated, being of interest for future ISL-scenarios in general. The low measurement uncertainty (of course also depending on the frequencies and signal structure, transmitting power etc. used) and the large number of redundant data handled by means of appropriate smoothing and optimal estimation techniques led to the assumption that the uncertainty on each clock offset wrt. STS is negligible at the update epoch. This approach has to be examined in more detail through numerical simulations.

We have shown that an ensemble time scale should be preferred for a GNSS2's STS. This ensemble can be generated as a weighted average of the mutual clock difference readings. In Case 1 the long-term optimization of STS has been stressed to enable UTC-reproduction by the STS itself. The simulated STS uncertainty can reach a value of up to 5 ns, the UTE is 5 ns for an H-Maser and about 12 ns for a RAFS, all values after one day. The UERE clock requirement can be met with an update interval not larger than 30 min in all combinations. More H-Masers would relax the update constraints. In case 2 the STS's short-term has been optimized. It has been shown that while generating the STS the USOs should better be excluded. But these clocks show a good (and cost-effective, reliable) influence on the UERE clock uncertainty in such a considered ISL-scenario within shorter integration times. With an update interval not larger than 15 min the requirement can still be satisfied in any combination.

It has been discussed why the steering of STS to UTC is so important. The UTC-dissemination with a future GNSS2 must be addressed in the development phase, because there are requests from many users world-wide. The ISL-scenario in general has a good impact and offers some more possibilities on the time-keeping system of the considered GNSS2.

ACKNOWLEDGMENT

REFERENCES

[1] Comptes rendus des séances de la quinziieme Conférence Générale des Poids et Mesures, Paris, 1975
[2] ITU-T Telecommunication standardisation sector of ITU, International Telecommunication Union, Definition and terminology for synchronisation networks, 1996.
[3] Recommendation CIPM 1996, Comite International des Poids et Mesures, Comptes rendus 85th meeting, Paris, 1996.
[4] L. A. Breakiron: Timescale algorithms combining cesium clocks and hydrogen masers, in Proc. 23th Precise Time and Time Interval Meeting, Los Angeles, CA, 1991, pp. 297-305.
[5] S. R. Stein: Advances in time scale algorithms, in Proc. 24th Precise Time and Time Interval Meeting, Washington, DC, 1992, pp. 289-298.
[6] C. Thomas, P. Wolf, P. Tavella: Time scales, Monographie BIPM 94/1, Bureau International des Poids et Mesures, Sèvres, France, 1994.
[7] TECHNICAL CHARACTERISTICS OF THE NAVSTAR GPS, developed by the NATO Navstar GPS Technical Support Group, Sept. 1989.
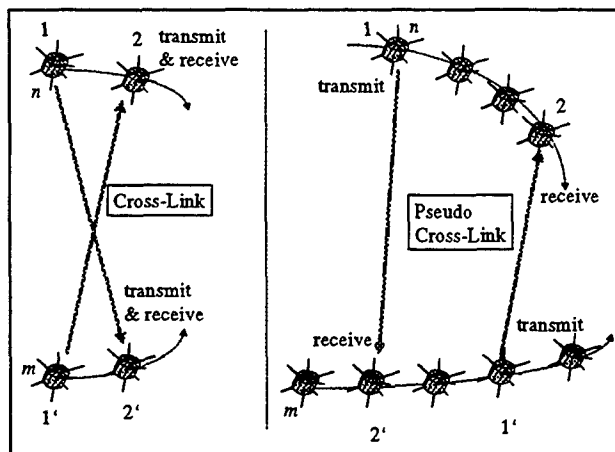
Fig. 1: Two-way cross-link and pseudo cross-link between two satellites
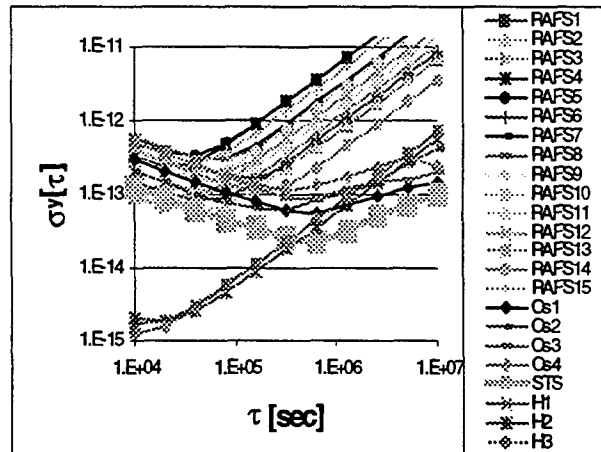
Fig. 2: Allan Deviation (ADEV) of the STS together with that of the 22 simulated clocks in Case 1
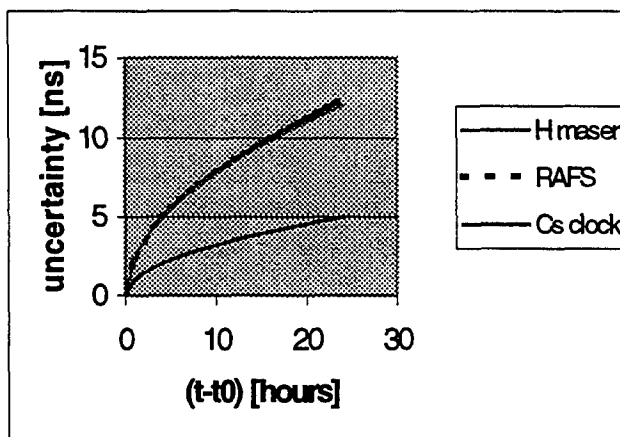
Fig. 3: Total uncertainty on the clock offset wrt. STS (UTE clock component) vs. time since the last update
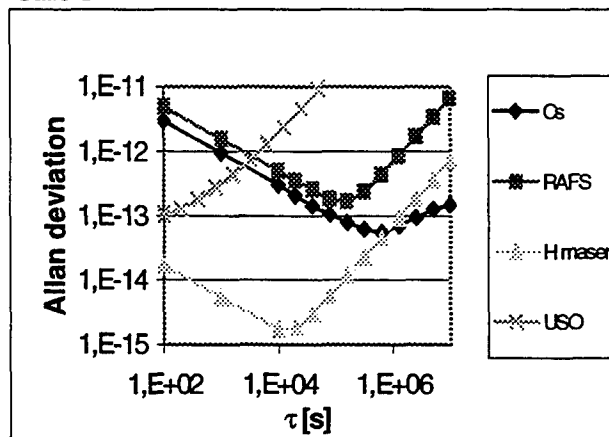
Fig. 4: Typical instabilities of the clocks considered in Case 2
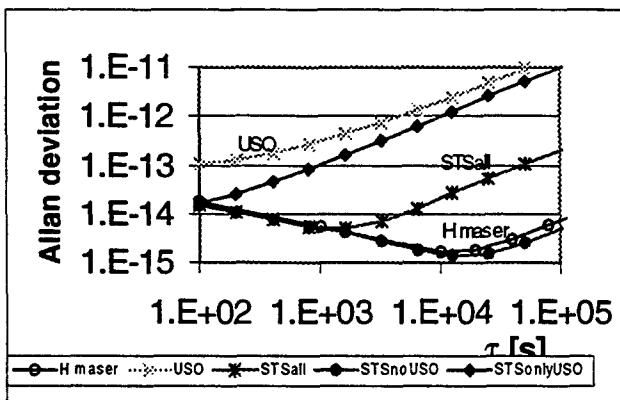
Fig. 5: Instability of the STS in Case 2 obtained with different ensembles of clocks & typical ADEV pattern of USO and H-maser
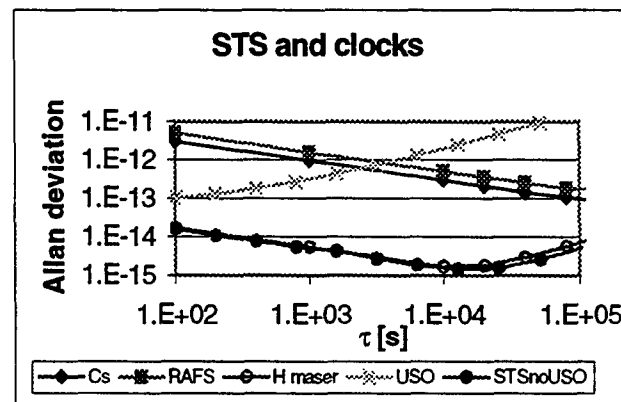
Fig. 6 Plot of the instability of the clocks used together with that of STS in Case 2 obtained without USO

456

Questions and Answers

DENNIS McCARTHY (USNO): Could you comment on how this would work with existing systems, or if you have considered that?

JOERG HAHN (DLR): We have not considered that. We only know that within GPS we have the two satellites where inter-satellite links are considered. We only have seen one simulation study – I think from The Aerospace Corporation. I do not remember all the numbers now, but it is the only thing I have seen on this, no other studies.

Of course, if the people here would listen to us, we would be quite thankful for any help in such investigations.

THE ROLE OF TIME AND FREQUENCY IN THE MTSAT SATELLITE-BASED AUGMENTATION SYSTEM (MSAS)

Toru Ishita, NEC Corporation, Tokyo, Japan

Aileen S. Nii, ISI Satellite Navigation Division, Inc., Vienna VA

Abstract

The MTSAT Satellite-based Augmentation System (MSAS) is a satellite-based augmentation system (SBAS) for navigation. The MSAS is one of several applications that shares the use of the Multifunctional Transport Satellite (MTSAT), a geostationary earth orbiting (GEO) satellite, which will be launched by the Japanese Ministry of Transport in August 1999. The MSAS design is based on the development of the US Wide Area Augmentation System (WAAS) and therefore may be familiar to those who are acquainted with the WAAS. Time and frequency play a critical role in four areas within MSAS, and these areas are the focus of this paper.

Firstly, MSAS performs several functions. One – it collects data from the NAVSTAR Global Positioning System (GPS); two – it provides an independent ranging signal from MTSAT to supplement the navigation signals from the GPS constellation; three - it provides differential corrections to improve the navigation capability of the GPS; four – it provides the offset of MSAS Network Time (MNT) from Coordinated Universal Time (UTC); and five – it provides system integrity information to the user. With these functions, the MSAS can become the primary means of time distribution and synchronization within Japan and other areas under the footprint of the MTSAT. The accuracy and precision attainable by MSAS is critically dependent on the performance of the time and frequency subsystems in the four areas of discussion.

The first area of discussion is the manner in which the data recording system tags its observations. Accurate recording of the time of observations is essential in order to measure the timeliness (latency) of all transmitted information. This information is based on algorithms that derive their input from data collected from a network of eight data collection sites, including four Ground Monitoring Stations (GMS) and four Monitor and Ranging Stations (MRS). Each GMS/MRS has three independent, free-running cesium-beam frequency standards.

The second is the discussion of the method of deriving the MNT and keeping it close to GPS Time. The MSAS, through the Master Control Stations (MCS), maintains MNT, its own local time scale, and is steered to a real-time estimate of GPS Time. Only an estimate of GPS Time can be made because GPS Time is affected by Selective Availability (SA). It is essential to have a uniform time scale as a reference in order to derive differential corrections that improve the

accuracy that can be obtained from the GPS Standard Positioning Service (SPS).

The third topic of discussion is the manner in which the MSAS navigation message from the MTSAT is controlled and transmitted. The signals transmitted from the MTSAT, which can be used as a supplemental ranging source to GPS, must be emitted in synchronization with GPS signals in order to make them compatible within a common navigation solution.

The last area of discussion is the secondary mission of the MSAS. Like the WAAS [1], it is to provide UTC. It does this by comparing MNT, which is synchronized to GPS Time, with UTC, as maintained by a UTC provider. For the WAAS, it is the US Naval Observatory (USNO). Although the Japanese Civil Aviation Bureau (JCAB) has yet to make a decision to provide the time distribution service, the procedures for obtaining, calculating, and transmitting the offsets of MNT from UTC, as part of the MSAS navigation message, is described.

INTRODUCTION

In the past, history tells us that navigation systems have depended on time, and therefore timekeepers have looked to navigation systems for the distribution of time, accurately and timely. Today, the crux of the GPS relies upon a highly evolved clock technology. However, unlike navigators, who need four GPS satellites by which to navigate, timekeepers only need one GPS satellite to determine time if they know their position. The observations of only one satellite will also allow timekeepers to remotely synchronize clocks around the world.

The MSAS is one of the most recent developments in the evolution of navigation systems. While it is somewhat similar to other differential GPS systems in concept, the MSAS provides the JCAB and the air navigation community a significantly higher level of performance than the GPS SPS and other differential systems dependent upon GPS. Based on the augmentation methods utilized by the MSAS, it provides not only improved accuracy, but also increased availability, integrity, and continuity of service. It accomplishes this by continually monitoring GPS transmissions from the GMSs/MRSs and by transmitting an augmented message from the MTSAT 1 presently, and MTSAT 2 and other GEO satellites in the future. The signal from the MTSAT, while sharing the same frequency as the GPS L1 frequency, is different in format and bit rate.

THE MSAS PROCESS

The MSAS process is illustrated in the diagram of Figure 1. There are four GMSs distributed throughout Japan at the JCAB's Area Control Centers (ACC) in Sapporo, Tokyo, Fukuoka,and Naha (in Okinawa). Two MRSs are collocated at the MCSs at Kobe and Hitachi-Ohta, and two MRSs, in Australia and Hawaii, respectively. Each GMS and MRS consists of three independent subsystems or sets of ground monitoring equipment (GME). Each GME consists of a cesium-beam frequency standard, a 12-channel, dual frequency MSAS-GPS receiver and a wide and a narrow band GPS receiver that continually track all GPS satellites and GEO satellites available to them. The data obtained at these ground-monitoring stations (GMS/MRS) are transmitted to two MSAS master control stations (MCS) where the MSAS navigation messages and MSAS Network Time are formed. Each MCS consists of three major subsystems – the Central Processing Facility (CPF), the Navigation Earth Station (NES), and the Monitor

and Control (M&C). The navigation messages contain information on satellite orbits, the current state of the ionosphere, system health, and timing information. Each MCS passes the navigation message to two Ground Earth Stations (GES), where it is uplinked by one GES to the MTSAT 1, the Phase 1 GEO satellite, which then transmits it to the user. The MTSAT Tracking and Telemetry Control (TTC) facility is also collocated with the GES and MCS at the Aeronautical Satellite Control Center (ASC) sites in Kobe and Hitachi-Ohta. The ASC provides shelter, power, and operations and maintenance services for all systems located at the site.

Each GMS/MRS performs the functions of data collection, reasonability check, data processing, and data transfer. Each GMS/MRS consists of triple redundant GMEs that collect three, independent sets of data, including GPS satellite observables and GEO satellite observables, and transmits the data to the CPFs at both MCSs in the system. Independence of the data sets is ensured by gathering the observable parameters through independent sets of equipment that are necessary to support the verification function performed by the CPF at the MCS. Prior to transmitting data to the MCSs, each GME verifies the reasonability of its collected data. Failed data are marked as having failed the reasonability test and are then forwarded to the MCSs. To ensure the availability of the data at each MCS, each GMS/MRS transmits data to each MCS through two independent communications networks, known as the Network Communications System (NCS) in the MSAS.

At each MCS, the CPF performs the functions of corrections processing, satellite orbit determination, integrity determination, and the verification, validation, and the MSAS message generation. Once per second, the CPF collects the data received from all GMSs/MRSs and processes them to support the functions described above. This processing is performed on all available GME data and results in the transmission of a formatted, 250-bit, MSAS message once per second. These MSAS messages are sent to both NESs. The timing of MSAS processing is scheduled to allow broadcast of the resulting MSAS message from the MTSAT coincident with the following GPS 1-second Coarse/Acquisition (C/A) code epoch. The MSAS validates the Signal-in-Space (SIS) by checking the downlinked messages to ensure that they are identical to those transmitted to the MTSAT and by comparing navigation position solutions from MSAS and GPS with the surveyed GMS/MRS locations. From each M&C console, control over the MSAS can be exercised via a computer-human interface. To avoid conflicts, only one MCS and, therefore, only one M&C subsystem console attended by the Controlling Operator, can be designated as the controlling MCS at any one time within the MSAS.

The initial MSAS design for Phase 1 implementation has two MCS/GES/TTC combinations that perform the functions of broadcast and ranging. Each MCS has one CPF that formats the 250-bit MSAS message. In MSAS, there is the advantage of the MCS facility collocated with the GES/TTC facilities, and it is that that improves the availability of MSAS messages. Each NES, which includes the MSAS Signal Generator (MSG), selects one CPF as its message source and encodes the received message using a half rate forward error correcting (FEC) convolution code. The resulting 500-bit message is modulated on a GPS-type signal and uplinked to the MTSAT. Both GESs serve the MTSAT; one operates as the primary uplink, and the other operates as a hot standby. The two GESs serving the MTSAT are operationally independent and located at geographically diverse ASCs separated by a minimum of 300

miles. Each ASC facility currently services only one GES. When there are at least two GEO satellites, each GEO satellite will be served by two GESs, one from each ASC site. The MTSAT "bent pipe" transponder shifts the frequency of the signal and broadcasts it to the MSAS users. The transition between primary and backup GES is initiated, when necessary, to maintain the availability of the MSAS SIS.

The NES ranging function is accomplished by transmitting a signal to the users on the GPS L1 frequency with the following information: (1) a precisely timed Pseudo-Random Noise (PRN) code that is assigned to each GEO satellite and (2) a precise ephemeris that is contained in the GEO satellite navigation message, which is sent periodically in the broadcast function. This signal structure is achieved in a similar manner to that of GPS, except that the precise timing of the PRN code is carried out on the ground rather than on the GEO satellite or the MTSAT, in this instance. This function will allow the users to apply the MTSAT as another GPS satellite, thereby increasing overall system availability.

TIME AND THE GMS/MRS

The recording of the time of observations is an area of concern for the MSAS. All observations are made at the independent GMSs/MRSs. In order to ensure a uniform time basis at each GMS/MRS, a clock based on GPS Time is used as the reference.

Each GMS/MRS contains three GMEs that identify three identical threads. These threads are required for sufficient redundancy to provide data to the MCS in the event a single failure in the GMS/MRS occurs. In addition to other commercial-off-the-shelf (COTS) components contained in the GME, there is a cesium-beam frequency standard (Atomic Clock).

The frequency standard needs to meet certain specifications to be useful in the MSAS architecture. The functional requirements include:
- Accuracy
- Settability
- Stability
- Single Side Band Phase Noise
- Warm-up Time.

Accuracy shall be at least 2×10^{-12} with no aging for the life of the cesium tube, so that it can be tuned to a specified frequency. The frequency standard provides each MSAS receiver a 10 MHz sinusoidal wave reference signal with a stability of at least 2×10^{-13} over 24 hours in order to accurately compare the MTSAT signals with GPS Time. The GME frequency standards require communication via RS-232 interface to the data collection processor (DCP) for interrogation and parameter adjustments.

The 10 MHz output from the cesium-beam frequency standard is input to a GPS receiver that provides a 1 PPS output used as the epoch of observations. Figure 2 is a diagram of the role of the cesium-beam frequency standard in the GME at a GMS/MRS. **The receiver clock is set to GPS Time at start-up.** Thus, GME receivers are approximately synchronized to the level of several microseconds. **The output data stream of each MSAS monitor receiver contains a parameter that has the offset of the receiver 1 PPS from GPS Time.** After that the output 1 PPS is governed by the rate of the input cesium clock. In

essence, **the output from the GPS receiver is a free-running clock**. This is necessary for the formation of an independent time scale.

TIME AND THE CPF IN THE MCS

The CPF and M&C in the MCS embodies processing equipment necessary to perform the Corrections and Verification (C&V) and Monitor and Control (M&C) functions, respectively. There is also a GPS clock for synchronization with GPS and equipment to interface the MCS with the NCS communication circuits. There are two MCSs in the Phase 1 MSAS. The quantities are planned for increase in subsequent phase(s). The end-phase MSAS is projected to have up to at least four MCSs.

The CPF performs several functions. Those involving time, directly or indirectly, include:
- Determine GPS/GEO satellite orbits
- Monitor SIS performance
- Generate MNT
- Generate MNT/UTC offset message
- Generate MSAS messages.

The data from all three GMEs for each GMS/MRS are sent to each of two (for redundancy) corrections processors (CP) in the CPF subsystem and the data from each GME at a single GMS/MRS are compared. The clocks are monitored relative to each other to determine if one clock is "bad"; that is, it checks to see if it has a significant change in offset. The current Phase 1 design does not estimate the frequency offset between GME clocks. This is the start of the formation of the MNT, which is described in the next section.

MSAS NETWORK TIME

In order for the MSAS signal to supplement the GPS navigation signals, the MSAS transmissions must be synchronized to them, i.e., GPS Time. This is accomplished by establishing MSAS Network Time as the reference time for the MSAS. The MNT is steered to GPS Time. Measurements from all GMEs at all GMSs/MRSs are sent to each CPF at the MCSs, of which there are two in Phase 1. Each CP at each CPF has an MNT algorithm, and computes a potentially independent MNT time scale from the data received from the GMSs/MRSs. All "good primary clocks" involved in the GME measurements that a CPF CP receives are used to form the MNT time scale. This time scale is then steered to the GPS with the same algorithm.

At the CPF CP, the GPS satellite and GEO satellite orbits and clocks are calculated along with the input GME ground clocks relative to the MNT_i time scale (the localized MNT time scale of CP_i) [2]. The raw MNT_i time scale is an average of all the "good" input GME ground clocks. The output of the orbit determination program and clock filters is used to estimate the localized MNT_i-to-GPS offset. The difference between each GPS Space Vehicle (SV) clock solution and the broadcast ephemeris clock solution is an estimate of the MNT_i-to-GPS offset. Once per day, a linear fit to these offsets is calculated to determine MNT_i bias and frequency offset with respect to the GPS time scale. The MNT_i frequency is

steered once per day based on this estimate. The steering command is designed to drive the offset to zero. The steering filter (MSAS Phase 1 version) daily computes a linear-fit estimate between MNT and GPS. Step one compares the GPS clock solutions (given in MNT) with the broadcast ephemeris clocks that give estimates of the GPS clocks in the GPS time scale with SA corruption added. This difference is used as the input to the MNT to GPS estimation filter every 30 seconds.

Each CPF synchronizes its MNT_i of its master CP via a communications link to all other CPFs. At every pre-established time interval (Phase 1 interval is 5 minutes), the CPF exchange MNT_i via their estimate of all SV clocks. For each common SV clock estimate, the difference is a measurement of the bias offset between each MNT_i. Let MNT be the average of all MNT_i Thus, at any time interval, MNT_i can be measured as the average of these SV clock differences. The MNT algorithm described above is implemented in each CP at the CPFs.

The MSAS messages include fast and slow corrections that are transmitted by the MTSAT. Fast corrections shall be determined for each GPS SV. This is accomplished by using the long-term correction message, which is broadcast from the MTSAT to remove the long-term clock offset in frequency from the extrapolated fast correction. Note that the total of the long-term and fast corrections must be added together before comparisons between the two CP outputs can be made.

It is estimated that the once-per-day steering may not be sufficient to keep MNT close to GPS Time. Therefore, the hardware steering will be supplemented by correction messages within the MSAS navigation messages. There will be slow correction messages and fast correction messages that are transmitted by the MTSAT. The slow correction will be updated once every five minutes and will take care of the major part of the correction. The fast correction will be issued every second and will compensate for the effects of SA. This steering filter described above has to be able to follow the GPS time scale because the GPS time scale is steered to UTC in a "bang-bang" method [3].

TIME AND THE MTSAT

The cesium clock at the NES will be slaved to the MNT. Once per day, the CPF will issue commands to steer the NES clock in order to reduce any offset from GPS Time. The NES clock controls the synchronization of the MSAS navigation message from the MTSAT.

The schematic relationship and the flow of data and time from the CPF through the NES (an MSAS subsystem), the GES, and the MTSAT at the ASC are illustrated in Figure 3. The MSG in the NES provides a C/A PRN code plus an MSAS message signal as a 70 MHz Intermediate Frequency (IF) to the upconverter. The IF is converted to the RF uplink frequency; then the GES amplifies it and transmits the signal to the MTSAT. The K-band uplink is received by the MTSAT and translated to the L1 and K-band downlinks, which are broadcast in right-hand circular polarization (RHCP) earth coverage beams to users and the GES. The GES receives the downlink L1 and K-band signals from the MTSAT. The signals are amplified and the K-band is converted to L2, and the L1 and L2 signals are provided to the NES.

The NES receiver accepts C/A PRN code signals at the L1 and L2 frequencies from the GES. The NES receiver measures code and carrier phase pseudorange data for both input signals. This information is sent to the NES processors and MSG, which have algorithms and hardware that develop time, frequency,

and phase feedback correction signals. The processor also FEC encodes the MSAS message. These correction signals adjust the time, frequency, and phase of the C/A PRN code signal to take out the uplink range, range rate, and ionospheric effects. The MSG also combines the FEC-encoded MSAS message data with this uplink-corrected C/A PRN code, which is provided as an IF signal to the upconverter in the NES. The frequency standard provides precise and stable frequency references for all the converters, signal generators, and receivers in the GES and NES. The frequency offset of the 5 and 10 MHz output shall be settable over a range of +/- 1 x 10^{-9} . The Settability requirement is only applicable for the frequency standard at the NES, because this must be able to compensate for any drift in the MTSAT's local translation oscillator.

The GES transmits signals from the NES containing integrity and correction data along with a GPS-like ranging signal to the MTSAT. The NES receives signals from the MTSAT at both K-band, which is translated to L2 frequency, and L1 frequencies. The NES controls the uplink power levels to protect against uplink interference and variations in transmission losses. The NES provides frequency translation of the uplinked signal to K-band and translation of K-band downlink signal to L2 frequency.

The MTSAT subsystem is a satellite in geostationary orbit in space, at a longitude of 140 degrees East.

THE MSAS TIME DISTRIBUTION SYSTEM (M-TDS)

Like the WAAS, the MSAS has the capability to provide a time distribution service. Time distribution is accomplished by providing users with a time offset between MNT and UTC. This time offset is determined by the UTC provider and passed to the MSAS MCS through an interface between the MSAS and the UTC provider. Although the JCAB has yet to select the UTC provider, the description below provides the general approach and implementation of an M-TDS. The MCS collects the MNT/UTC offset and creates a Type 12 message, which is then sent to the GES, which transmits it to the MTSAT. The purpose of the Type 12 message is to provide time users with a more accurate source of time referenced to UTC. The UTC provider does this by determining the time offset between the MTSAT SIS epoch, which is MNT, and UTC. The UTC, as determined by the Master Clock at the UTC provider, represents the approved time standard source for MSAS.

The M-TDS is an independent system located at the UTC provider facility. The M-TDS acquires the MSAS messages from the MTSAT within view of the UTC provider facility and performs a time difference between the MTSAT beginning-of-message epoch times and an accurate 1 PPS from the UTC provider time reference (the Master Clock at the UTC provider facility). The Master Clock also provides a stable 10 MHz frequency source to the M-TDS receiver.

The M-TDS contains an antenna, MSAS receiver, and modem. The M-TDS antenna receives the MSAS SIS from the MTSAT. The M-TDS receiver collects the MSAS SIS observables and forwards the MSAS navigation message and MNT/UTC offset data to the UTC provider processor. The output data string from the receiver contains the MNT offset data. The M-TDS modem provides the interface between the UTC provider processor and the MCS to communicate the MNT/UTC offset data back to the MSAS.

The data, produced by measuring each GEO satellite 1 PPS epoch with UTC (from the UTC provider), are collected and recorded for computation of correction parameters to MNT. The satellite epoch beginning time will be converted to MNT by utilizing the time offset and drift numbers from the MSAS SIS. The M-TDS then passes the values of all satellites being tracked to the UTC provider data acquisition system. The collection of MNT/UTC offset is performed by the M&C function for inclusion by the CPF in MSAS Message 12.

The M-TDS relates MNT to UTC (from the UTC provider). The primary purpose of the M-TDS is to provide the MNT/UTC offset data to the MCSs for the subsequent MSAS SIS broadcast to time users who require precise reference to UTC. Users at remote locations within the MSAS Service Volume can acquire the MTSAT SIS and utilize the correction parameters contained in Message 12 and their local receiver time to determine UTC to within an accuracy of 20 nanoseconds. Message 12 is not intended for navigation. Until the M-TDS is implemented, Message 12 will not contain any data.

MSAS AND THE TIMEKEEPING COMMUNITY

The MSAS will provide time within the Japanese Flight Information Region for the recording of all events. It will also provide a very stable timing signal for the timekeeping community. The MSAS timing signal will not be affected by SA. Since time is broadcast from the MTSAT, a GEO satellite, it will be relatively stationary to a user on the ground. Thus, a high-gain antenna can be used to provide a very good signal to the stationary user. The offset of MNT from UTC is transmitted within the MSAS navigation message. The signal will be available continuously.

Such a signal provides some unusual capabilities for the timekeeping community. **It should allow the development of more economical timing systems utilizing its signals.** Cheaper crystals can now be used in systems that rely on atomic standards as their flywheel while they integrate GPS time to remove the effects of Selective Availability. Because of the absence of SA, **it will be possible to almost instantaneously detect any pathological behavior in a system providing time.** With GPS, one has to wait to see if the transients are due to SA or anomalous clock behavior. If one is within the footprint of two GEOs within the same SBAS transmitting Message 12, one can have **an immediate redundancy check.** This can be used as an extremely robust check for many timed systems.

ACKNOWLEDGEMENTS

REFERENCES

1. W. J. Klepczynski, "The Role of Time and Frequency in the Wide Area Augmentation System (WAAS)," Proceedings of the 12th European Forum of Time and Frequency, March 1998.
2. S. Peck, C. Griffith, V. Reinhardt, J. Tekawy, W. Bertiger, B. Haines, G. M. R. Winkler, "WAAS Network Time Performance and Validation Results," Proceedings of ION GPS-97, September 1997.

3. C. H. McKenzie, W. A. Feess, R. H. Lucas, H. Holtz and A. L. Satin, "GPS-UTC Time Synchronization," Proceedings of the 21st Annual Precise Time and Time Interval (PTTI) Applications and Planning Meeting, November 29, 1989.

BIBLIOGRAPHY

The following MSAS and WAAS documents provided input for this article.

MTSAT Satellite-Based Augmentation System (MSAS) Specifications, dated December 20, 1996

System/Segment Specification for the MTSAT Satellite-based Augmentation System, SDRL Sequence No. MS104-01-002, dated 8 May 1998

System/Segment Design Document for MTSAT Satellite-based Augmentation System, SDRL Sequence No. MS202-01-002, dated 15 July 1998
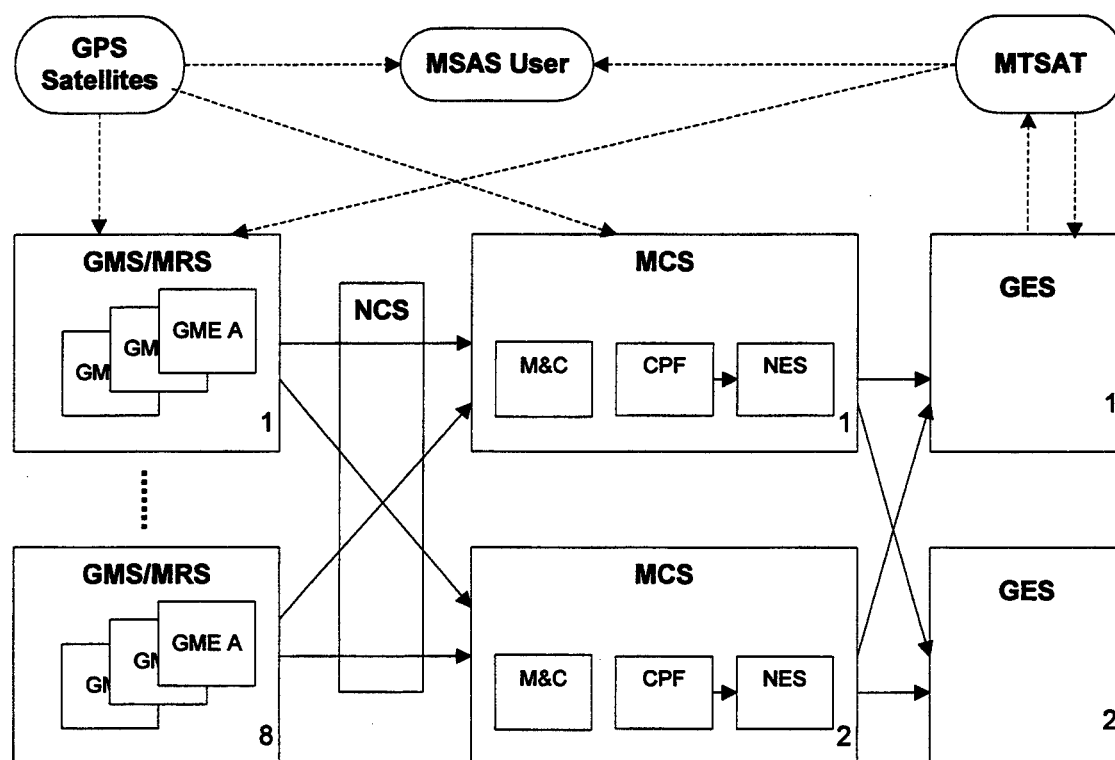
Figure 1. The MSAS Process
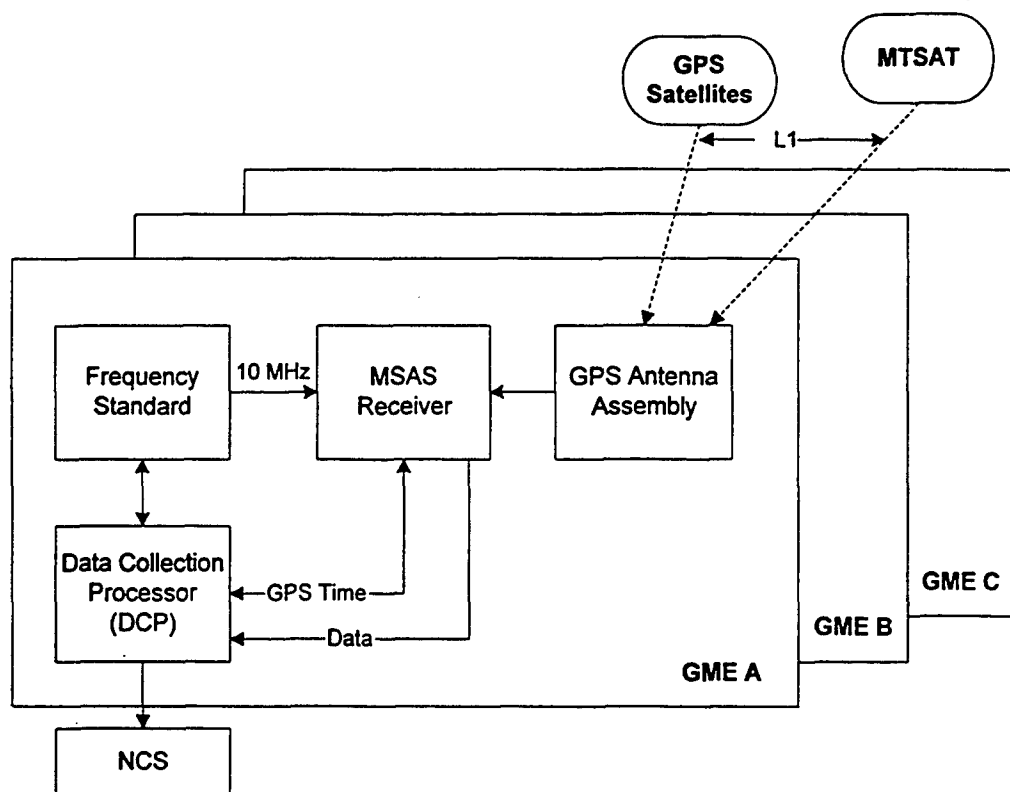
Figure 2. Role of the Frequency Standard in the GME Configuration
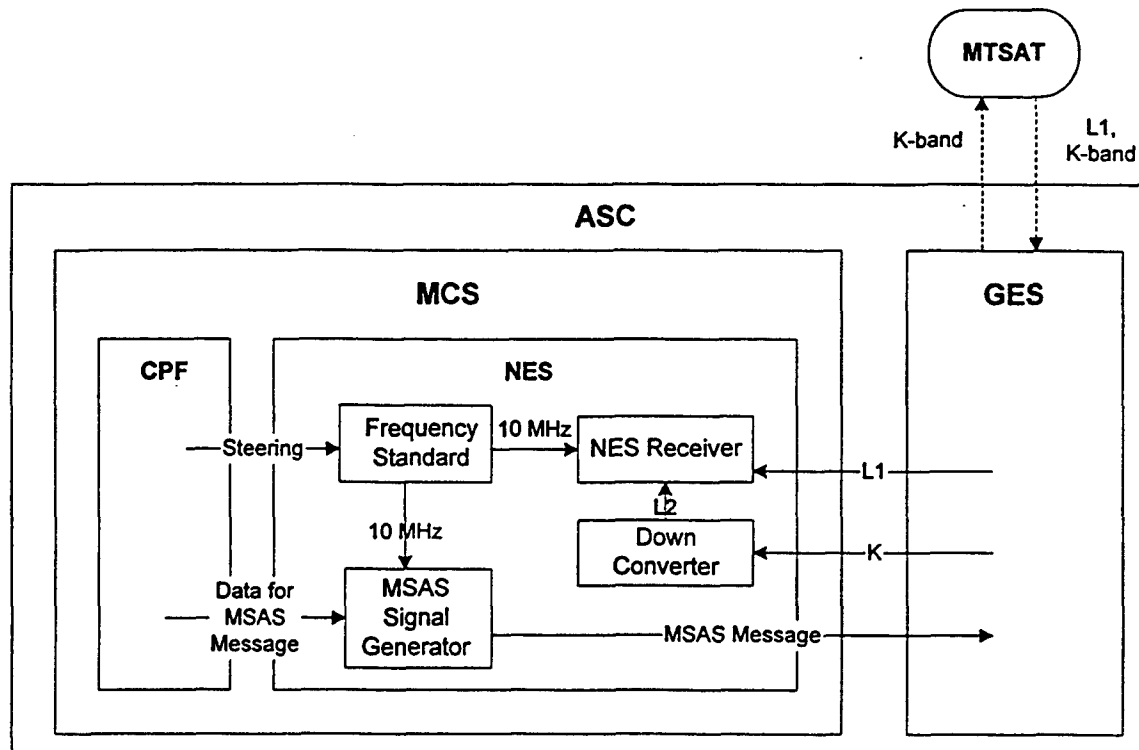
Figure 3. Role of Data and Time at the ACS

THE ROLE OF TIME AND FREQUENCY IN EGNOS (EUROPEAN GEOSTATIONARY NAVIGATION OVERLAY SYSTEM)

A. Job*, J. Legenne*, M. Brunet**, J-M. Pieplu***, A. Batchelor****

* European Space Agency (ESA): 18, avenue E. Belin, 31401 Toulouse, France

** Centre National d'Études Spatiales (CNES): 18, avenue E.Belin, 31401 Toulouse, France

*** Alcatel: 105 avenue du général Eisenhower, 31037 Toulouse, France

**** Racal Research Limited, Reading, Berkshire RG2 0SB, England

Abstract

The European Geostationary Navigation Overlay System (EGNOS) is being developed in Europe to provide GPS and GLONASS regional augmentation services to aviation, maritime, and land users. EGNOS will provide the following services: i) GEO-based GPS-like Ranging signals to improve the availablity and continuity of GPS and GLONASS navigation services. ii) Ground Integrity Channel (GIC) to improve the integrity of GPS- and GLONASS-based navigation and position determination for safety-critical applications. And iii) Wide-Area Differential corrections (WAD) to improve the accuracy of GPS-SPS and GLONASS. Additionally, EGNOS will disseminate accurate time to users, synchronized to GPS, GLONASS, and UTC time scales. The paper provides an overview of EGNOS ground-segment architecture, gives requirements related to time aspects, and describes preliminary analysis and performances through test trials. It also covers initial results achieved in the frame of the EURIDIS program, conducted by CNES, after several months of measurements.

INTRODUCTION

The commission of the European Union (CEU), Eurocontrol, and the European Space Agency (ESA), which together form the European Tripartite Group (ETG), jointly defined the European Navigation per Satellite Program, whose first step is GNSS-1.

GNSS-1 is based on the enhancement of the existing GPS and GLONASS navigation per satellite systems, respectively operated by the US and Russian Departments of Defense. The basic principle of GNSS-1 relies on the addition of a ground-segment, which will process and deliver GPS and GLONASS differential corrections and integrity data to users, and on new geostationary satellites. The EGNOS program was defined by the ETG in 1994-1995. Its initial phase has just ended with the system Preliminary Design Review (PDR), while the implementation phase is about to start. EGNOS service is expected to be delivered in the year 2002 to Civil Aviation, Land Mobile, and Maritime users.

The role of time and frequency in EGNOS is of paramount importance, since any synchronization error would be derived into navigation error. This paper gives a brief overview of EGNOS architecture, including its main functions. It also provides time requirements as specified at system level, and describes the design and expected performances of time functions.

DESCRIPTION OF THE MAIN EGNOS FUNCTIONS AND ARCHITECTURE

The EGNOS system will provide the following functions:

- GEO Ranging: Transmission of GPS-like signals from GEO satellites (INMARSAT-III AOR-E and IOR, and the ESA ARTEMIS satellites). This will augment the number of navigation satellites available to the users and, in turn, the availability of satellite navigation.

- GNSS Integrity Channel (GIC): Broadcasting of integrity information. This will increase the availability of GPS / GLONASS / EGNOS safe navigation service up to the level required for civil aviation non-precision approaches.

- Wide Area Differential (WAD): Broadcasting of differential corrections. This will increase the GPS / GLONASS / EGNOS navigation service performance, mainly its accuracy, up to the level required for precision approaches down to CAT-I landing.

EGNOS Architecture

To ease the understanding of the role of time functions, this section provides a summary description of the EGNOS architecture. The EGNOS is composed of four segments: ground segment, space segment, user segment, and support facilities.

- The EGNOS Space Segment is composed of transponders embarked on board GEO satellites.

- The EGNOS User Segment consists of GNSS Standard receivers developed according to RTCA MOPS DO-229.

- The EGNOS Support Segment includes some facilities needed to support System Development, Operations, and Qualification.

- Finally, the EGNOS Ground Segment as described below.

EGNOS Ground Segment Overview

The EGNOS Ground Segment consists of *Ranging and Integrity monitoring Stations* (RIMS), which are connected to a set of redundant control and processing facilities called *Mission Control Center* (MCC). The MCC determines the integrity, ephemeris and clock differential corrections for each monitored satellite and ionospheric delays, and generates GEO satellite ephemeris. This information is sent in a message to the *Navigation Land Earth Station* (NLES), to be up-linked along with the GEO Ranging Signal to GEO satellites. These GEO satellites downlink these data on the GPS Link 1 (L1) frequency with a modulation and coding scheme similar to the GPS one. All ground Segment components are interconnected by the *EGNOS Wide Area Communications Network* (EWAN).

Please refer to [3], [4] and [5] for more detailed information concerning EGNOS overall architecture.

SYSTEM REQUIREMENTS ON TIME ASPECTS

The Navigation mission of EGNOS would basically not have required for the system any explicit reference to an external time scale. EGNOS being based on differential principles, all measurements and data are referred to an internal EGNOS Network Time (ENT) whose performance requirements shall be derived exclusively from navigation accuracy performance requirements. Therefore, system requirements do not address for instance any ENT stability performance.

System Specification requires EGNOS ENT to be steered within 50ns of GPS system time; this is a requirement derived from Signal In Space (SIS) specification of RTCA MOPS and ICAO SARPS. Even if the GPS reference is not well known because not directly accessible (with SA on SPS signals), this steering requirement is not very stringent and mostly specified to be compatible with the maximum capacity of the message (256m) used to correct the GPS satellite clock.

The above requirement will also allow the use of one particular mode of navigation, called Ranging, where differential corrections are not used and the user can mix in its navigation solution GPS and EGNOS GEO signals whose time references are closely related enough if maintained within the specified range. For this mode EGNOS has specified an UERE (User Equivalent Range Error) of 25m (95%) for the GEO Ranging signal; this error encompasses:
- ENT-GPS time offset error
- ENT-GEO time transfer error
- GEO-User range error.

The ENT-GEO time transfer error is specified to be less than 10ns (maximum), after offset and drift correction provided in EGNOS GEO message #9. This particular requirement is of special interest for a precise time broadcast function in real time.

Effectively, beside its principal navigation mission, EGNOS signals may be used as a means to broadcast ENT, which is a PTTI source closely related to GPS time and to UTC.

For the UTC connection, EGNOS will provide in message # 12, as required in SIS specification, the time difference and the drift between ENT and UTC. But, in discrepancy with the SIS requirement, the real-time offset will not be provided in relation with UTC, which is a "paper" time, but with a physical primary clock of a European laboratory participating in UTC.

EGNOS system presently requires that ENT shall be within 20ns of UTC; this shall be understood as the uncertainty on the time difference with UTC(k), because the UTC-UTC(k) time difference is not under EGNOS control and not available in real time. When this latest information is made available to EGNOS (real time or with prediction) EGNOS will revisit the performance requirement.

The following sections will provide in response to the requirements, a description of each time functions, and the expected performances, based on analysis and experiment.

EGNOS SYSTEM OVERVIEW RELATED TO TIME

Both GPS and GLONASS use Time Difference of Arrival (TDOA) as the basis for the formation of receiver-to-satellite range measurements. Therefore, accuracies of the receiver and satellite clocks involved have a direct impact on the range measurement accuracy achieved. Both GPS and GLONASS satellites provide information in their broadcast navigation messages that enable system users to correct for satellite clock errors; i.e. the offset of individual satellite clocks from the nominal satellite system time-scale. These corrections are accurate to within a few nanoseconds. However, in the case of GPS, they do not account for Selective Availability (SA) dither, and unless they are estimated and removed, they will degrade user-positioning performance. Furthermore, for high integrity applications it is desirable to produce independent estimates of the satellite clock errors, in order to monitor the broadcast corrections.

In order to determine highly accurate estimates of satellite clock errors and disseminate them to system users, the EGNOS system performs three basic clock functions located in the Central Processing Facility:

- RIMS clock synchronization and generation of the EGNOS Network Time (ENT);
- Steering of ENT to GPS time;
- Determination of the satellite clock offsets from ENT;
- Estimation of the difference between ENT and UTC.

Figure 1 below describes the links between EGNOS sub-systems related to time functions.
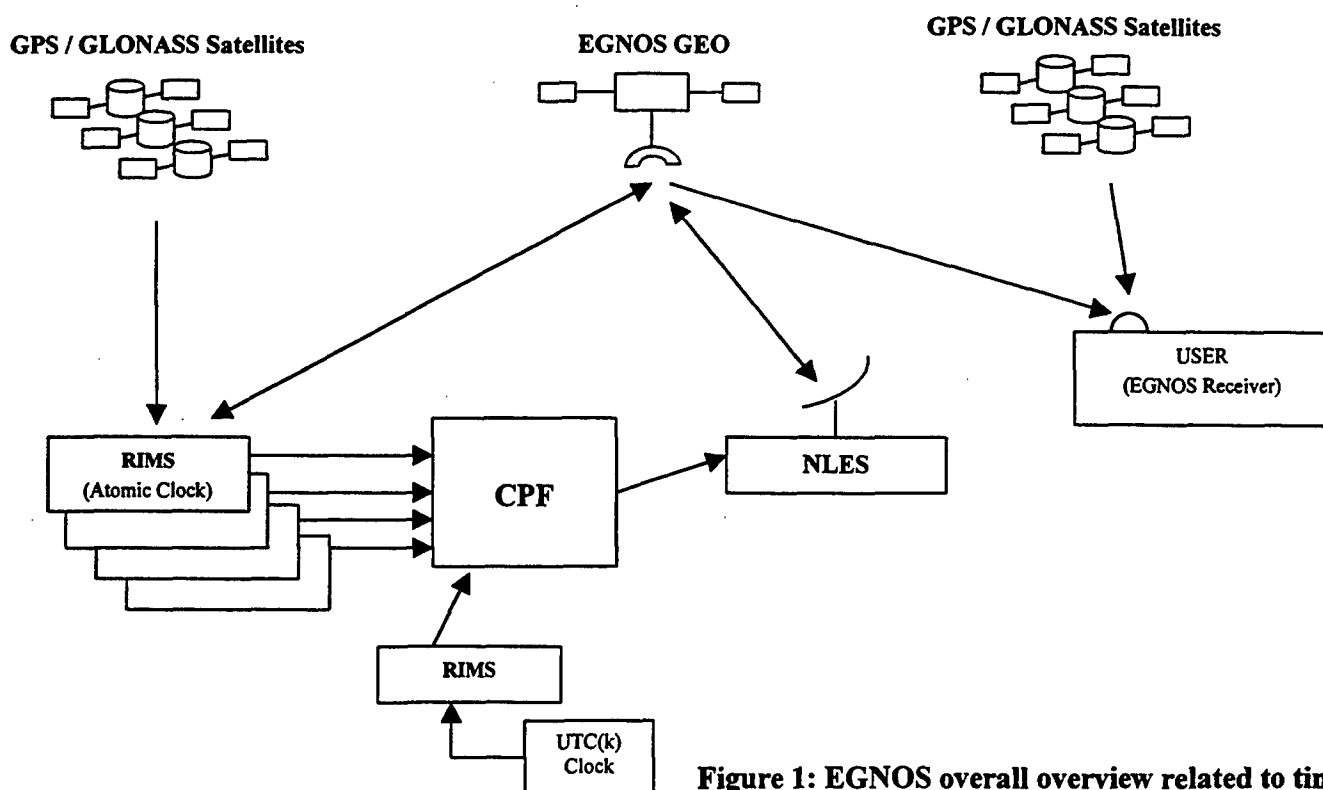

Figure 1: EGNOS overall overview related to time

RIMS Clock Synchronization and Generation of ENT

RIMS clock synchronization is performed using the *composite-clock* technique. In the composite-clock technique, ENT is defined as the implicit ensemble mean of all RIMS clocks and the synchronization process generates estimates of the offset and drift of each RIMS clock relative to it. These estimates can then be used to reference all RIMSs' pseudo-range measurements to ENT. This synchronization process is necessary in order to allow simultaneously observed pseudo-range measurements from multiple RIMS to be combined in the function that estimates satellite clock errors (see below).

A simpler, alternative synchronization technique is the *master-clock* technique, whereby one RIMS clock is nominated to provide the network time and all other RIMS clocks are synchronized to that clock. The composite-clock method has two significant advantages over this approach. Firstly, the master clock approach has a single point of failure; if the master clock is lost, ENT is lost. In contrast, the composite-clock ENT is maintained as long as there are two clocks in the ensemble. Secondly, the stability of ENT provided by the master-clock method is of course limited to the stability of the master clock itself. With the composite clock technique, the stability of ENT becomes the stability of the implicit ensemble mean of all of the RIMS clocks. Assuming an ensemble of n identical, independent, clocks, this gives a $\sqrt{n}$ improvement in stability. This last feature of the composite clock has the important side effect of increasing the ability of the system to detect and isolate clock failures.

The composite clock algorithm is executed by means of a Kalman filter. The filter measurement data comprises a linearly independent set of *common-view* observations with minimum a priori variance. A common-view observation for a pair of RIMS is formed by subtracting simultaneously observed pseudo-range measurements to a common satellite. Before subtraction, the pseudo-ranges are *pre-processed* to remove RIMS antenna-to-satellite antenna geometric ranges and reduce unwanted errors, such as multipath delays and thermal noise. The resulting common-view observations represent direct measurements of the RIMSs' clock offsets plus residual errors.

The filter states comprise the offsets and drifts of each RIMSs' clock relative to a hypothetical *ideal* time-scale. The consequence of this formulation is that the filter provides estimates the offsets and drifts relative to the *implicit*, weighted average of all of the RIMS clocks. This implicit ensemble mean essentially defines the EGNOS time-scale, ENT. The relative weighing of clocks used within the filter is dependent upon several factors, but is largely determined by the process noise models associated with each of the clocks. These models characterize RIMS clock stability.

Since only clock difference measurements are available to the filter, the filter model has unobservable components that cause secular growth trends in the state error covariance matrices. Special measures must be employed to remove these trends, otherwise they will eventually lead to numerical instability within the filter. It can be shown that, once the secular growth trends due to the unobservable components of the system model have been removed from the covariance matrix, the resulting covariance describes the errors in the filter state estimates relative to the implicit ensemble mean, *not* the ideal time-scale. Full details of the composite clock algorithm can be found in [1].

Steering of ENT to GPS Time

In order to limit the dynamic range of the satellite clock corrections, thereby reducing the size of the WAD clock messages and improving the efficiency of the message dissemination process, it is necessary to steer ENT to the GPS time-scale. Steering of ENT to the GPS time-scale is performed using a second-order, low-pass digital filter. The steering input signal is an instantaneous estimate of the ENT–GPS time-scale offset. This is computed from the estimated satellite clock offsets from ENT and the GPS broadcast satellite clock corrections, which are estimates of the satellite clock offsets from the GPS time-scale. The cut-off frequency of the filter is chosen to provide the best reduction of Selective Availability (SA), whilst avoiding significant lags due to the relative drift of ENT with respect to the GPS time-scale. The more stable ENT is, the lower the cut-off frequency can be set and the greater the reduction of SA.

The EGNOS system baseline will easily meet the ENT-GPS time-scale steering requirement of <50 nsec. The *all cesium* scenarios examined demonstrate that a steering accuracy of < 3 nsec can be achieved. These results must be treated with caution, since they are based upon synthetic data sets with idealized models of SA and RIMS clocks. However, the results are consistent with other findings, such as those quoted in [2].

Steering accuracy of < 3 nsec will allow ENT realizations from different CPFs to be synchronized autonomously, without need for a dedicated ENT-A to ENT-B synchronization function. However, if such a function is required, experimentation with real and synthetic data has shown that synchronization of different ENTs can easily be achieved with an accuracy of better than 3nsec (2σ). This is the system requirement imposed to make CPF switchovers transparent to EGNOS users.

Satellite Clock Corrections

Satellite clock corrections and correction rates are computed using all available pseudo-range and Doppler measurements from the pre-processing function. The measurements are referenced to ENT using the RIMS synchronization parameters and then collected into groups by satellite. For each satellite, weighted least-squares estimates of its clock's offset and rate-of-change with respect to ENT are computed. The offsets are later separated by low-pass filtering, similar to that used for the ENT steering function (described below), into the slow and fast components which comprise the satellite clock correction messages. The rate-of-change estimates are used to project the corrections forward in time by the expected system latency.

Broadcast ENT through Geostationary Earth Orbit (GEO) Satellites

The satellite fast and slow clock corrections are disseminated to EGNOS users in via the GEO satellite in separate messages. The EGNOS user receiver decodes these messages and reconstitutes the combined satellite clock offsets from ENT for each of satellite it tracks and applies them to its pseudo-ranges, together other WAD corrections provided by EGNOS. In this way, the ENT time-scale replaces the GPS-, or GLONASS-, time-scale in the receiver's navigation solution. Hence, not only does the receiver compute an improved estimate of position, because of the WAD corrections, it also computes an estimate of its internal receiver clock offset from ENT.

Once available on the ground, ENT has to be accurately transferred on board GEO satellites. Indeed, the GEO time is defined at the output of the GEO payload, precisely at the L1 antenna center of phase. This function is ensured by the so-called Long-Loop, a servo-control mechanism, based on the near symmetry between the up and down links from the NLES to the GEO satellite.

UERE on ENT

A fixed user equipped with an EGNOS receiver could obtain ENT in real time through one or several GPS-corrected signals or GEO channel. The accuracy of this information is directly the User Range accuracy as indicated in the table below:

Range accuracy in m (1σ)	GPS	GEO
UDRE (orbit + clock)	0.65	1.0
Ionospheric error	0.50	0.50
Tropospheric error	0.20	0.20
Receiver noise	0.50	1.0

Multipath (45° elev.)	0.25	0.25
GPS latency	0.42	-
UERE (5° elev.)	4.1	4.1
UERE (20° elev.)	1.8	2.1
UERE (90° elev.)	1.0	1.3

Table 1: EGNOS User Equivalent Range Error (UERE)

A user able to control properly its multipath environment (or mitigate the multipath through several channels) will obtain a total time transfer accuracy in the range of 4 to 6 ns (1σ).

Estimation of the Difference between ENT and UTC Time Scales

UTC means Coordinated Universal Time. It is a coordinated time scale, obtained from a combination of data from about 230 clocks kept by 65 laboratories spread worldwide. UTC is made available in the form of time differences with respect to local time UTC(k) of laboratory k. The computation is carried out in deferred-time for the standard dates, currently every five days, and the results are published monthly by the BIPM in *Circular T* in the form of time differences [UTC − UTC(k)]. UTC is therefore available in deferred time on a monthly basis. Only UTC(k) are maintained permanently in about 48 time centers.

UTC being a theoretical average of many clocks around the world, it is not possible to establish a direct link between ENT and UTC. Instead, it is necessary to use a physical clock participating to the elaboration of UTC.
Therefore, the time difference between ENT and UTC can be broken down into 2 terms:

ENT − UTC = [ENT − UTC(k)] + [UTC(k) − UTC]
(k standing for any European laboratory participating to the elaboration of UTC)

475

UTC (k) – UTC

The time differences [UTC – UTC(k)] are made available on a monthly basis by the BIPM through the Circular T, and are out of the scope of EGNOS.

Performances of the time difference [UTC – UTC(k)] is as follows:

- IUT and CCDS Recommendation is to keep [UTC – UTC(k)] within 100 ns (1σ),
- The estimated uncertainty for the time differences [UTC – UTC(k)] is currently at the level of 10ns (1σ), provided in deferred time by *Circular T.*
- The estimated uncertainty of a prediction of the time difference [UTC – UTC(k)] depends on the period of prediction, and could be in the range of 20 ns (1σ).

ENT – UTC (k)

To synchronize ENT and UTC(k), an EGNOS RIMS will be co-located with lab k to be physically connected to its atomic clock (with interfaces at 10 MHz and 1pps levels). EGNOS RIMS synchronization module will estimate directly the time difference between ENT and RIMS(k) with an uncertainty of less than 3ns (2 σ). The time difference will be broadcast with message type 12 with the above uncertainty.

PRELIMINARY PERFORMANCE OVERVIEW THROUGH TEST TRIALS

Early Test System

In order to investigate the performance of the CPF clock functions, a wide range of experiments were conducted. These experiments utilized both recorded GPS data sets, collected simultaneously from a network of receivers distributed throughout Europe, and synthetic data sets produced using Racal Research's in-house GPS data generator. The synthetic data sets were required in order to provide truth data for clock errors and SA. The synthetic data generator provides a comprehensive model of GPS pseudo-range error sources. Furthermore, to ensure realism, its error models were calibrated against recorded data sets.

RIMS Synchronization Experiments

The EGNOS system requirement for RIMS clock synchronization accuracy is 3nsec 2σ. Experiments using both real and synthetic GPS data sets have shown that the EGNOS system baseline will meet this requirement, provided that RIMS multipath is not excessive.

The above conclusion was drawn after evaluation of the clock synchronization filter with multiple test scenarios. These scenarios were designed to investigate the following factors:

- (i)   size and density of RIMS network;
- (ii)   use of both precise and GPS broadcast ephemerides for computation of the geometric ranges to satellites;
- (iii)   use of single- and dual-frequency data ionospheric delay error modelling;
- (iv)   variation in filter update rates; and
- (v)   variation in the satellite elevation cut-off angle below which pseudo-range measurements are ignored.

Figure 2 shows a typical example of synchronization errors for a synthetic, fifteen RIMS, scenario, with each RIMS equipped with a high-quality cesium clock. The synthetic data used were calibrated against data recorded with high-quality, dual-frequency, geodetic receivers and antennas. The figure shows the errors in the realizations of ENT computed from each RIMS clock using the filter synchronization parameters.
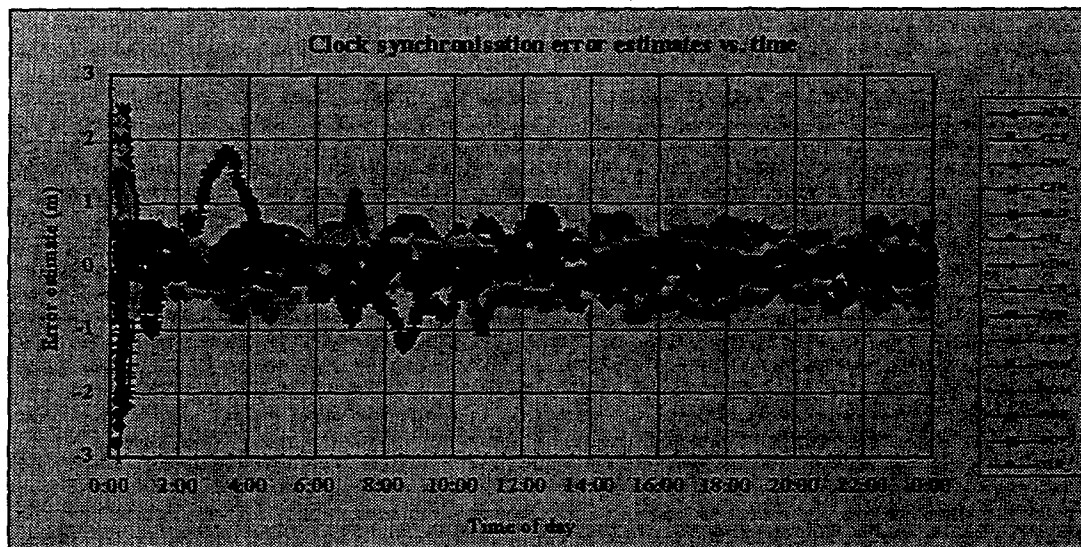
Figure 2: Typical RIMS synchronization performance

Satellite Clock Error Estimation

Independent experiments have been carried out in order to determine the accuracy of the satellite clock corrections. The experiments have demonstrated that RMS errors of about 0.5m are to be expected with the EGNOS system baseline design. As with the other results quoted, high-quality, dual-frequency, geodetic receivers and antennas are assumed. Similar test scenarios were used to those described for the RIMS clock synchronization function.

ENT to GPS Time Scale Steering

An example of the steering filter's performance is shown in below in Figure 3. Three, seven RIMS scenarios are shown: SYN-4(7), all high quality cesium; SYN-5(7), all high-quality rubidium; and SYN-6(7), a mixed scenario with one cesium and six rubidium clocks.

Figure 3 illustrates the high steering accuracy that can be achieved when high quality cesium clocks are used. The EGNOS system baseline, containing fifteen such clocks, will easily meet the ENT-GPS time-scale steering requirement of <50 nsec. Indeed, the *all Cesium* scenarios examined demonstrated that a steering accuracy of <3 nsec can be achieved, provided at least five high-quality Cesium clocks are present in the ensemble. These results must be treated with some caution, since they are based upon synthetic data sets with idealized models of SA and RIMS clocks. However, the results are consistent with other findings, such as those quoted in [2].

Another interesting feature of Figure 3 is that it illustrates the relationship between the stability of ENT and the choice of steering filter cut-off frequency. To reduce SA significantly, a very long time constant is required in the steering filter. This in turn requires that the relative drift between the ENT and GPS time-scales over periods commensurate with this time constant is very small. For the mixed and all-rubidium ensembles, SYN-5(7) and SYN-6(7) respectively, this is not the case, and leads to the biases seen in the steering errors for these ensembles. Reducing the time constant removes these biases, but at the expense of allowing SA to *leak* through.

Steering accuracy of <3 nsec will allow ENT realizations from different CPFs to be synchronized autonomously, without need for a dedicated ENT-A to ENT-B synchronization function. However, if such a function is required, experimentation with real and synthetic data has shown that synchronization of different ENTs can easily be achieved with an accuracy of better than 3nsec 2σ.
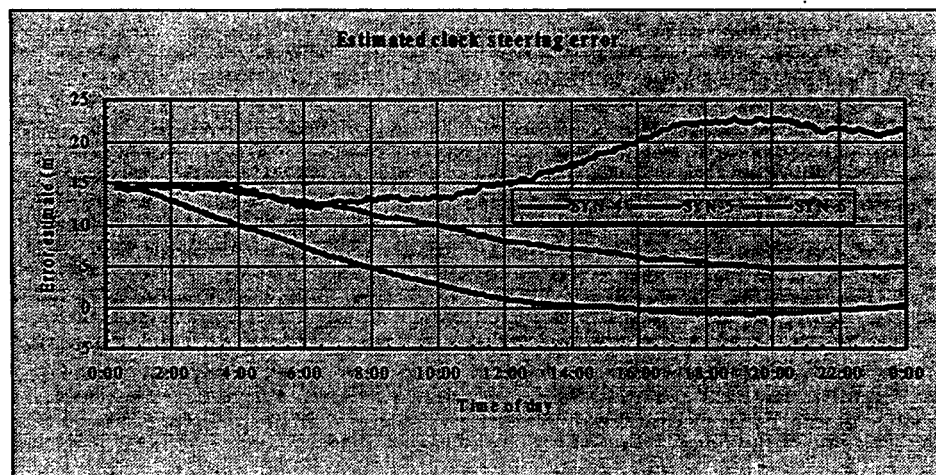
Figure 3: typical ENT steering results (cut-off frequency 2×10⁻⁵Hz)

EURIDIS RANGING

Since July 1995, CNES has conducted the development of EURIDIS, a test-bed representative of the EGNOS Ranging using INMARSAT 3 AOR-E navigation payload.

EURIDIS Ground Segment

EURIDIS Ground Segment is based on the following Figure 4:

- Three Geostationary Ranging Stations (RIMS) forming a large-based triangle: Aussaguel near Toulouse, Kourou in French Guyana and Hartebeeshoek in South Africa.

- a Mission Control and processing Center (MCC) located at the CNES site in Toulouse (France) for processing and ground segment monitoring,

- a Navigation Land Earth Station (NLES) in charge of generating the GEO ranging signal,

- a communication network dedicated to EURIDIS.
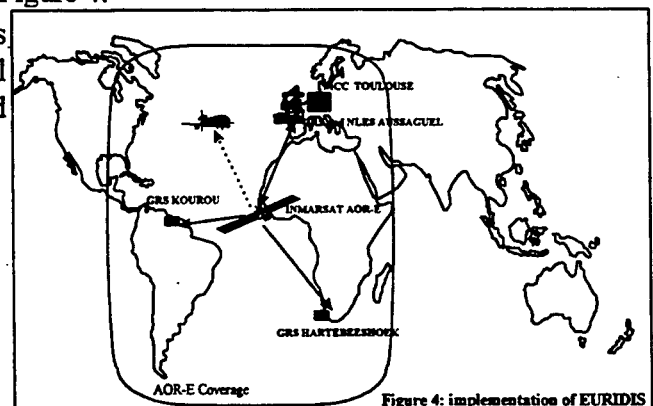
Figure 4: implementation of EURIDIS

478

EURIDIS Performance (Ref. [8])

Even with the limited infrastructure, the objective has been given to EURIDIS to demonstrate the Ranging performance of EGNOS: 25m (95%). To meet this required accuracy on the GEO UERE, the following requirements have been derived:

- the GPS time must be known within 20 ns (1σ)
- the time transfer to the GEO must be achieved with an error less than 20 ns (1σ)

EURIDIS and CNES(NRT2) GPS time estimates

Figure 5: EURIDIS GPS Time restitution

- in order to determine the GEO satellite position with an accuracy less than 7.5 m(1σ), each RIMS must be synchronized within 10 ns (1σ).

GPS Time Restitution

With many limitations with regards of EGNOS (use of only one reference station, without correction of GPS broadcast orbits, etc.), the

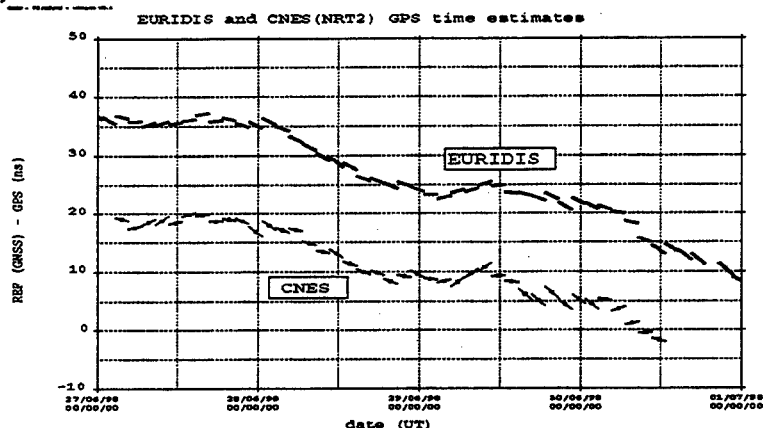| Error source	Euridis (1 σ)	NRT 2 (1 σ)
SA dither	1 ns	1 ns
GPS position	9 ns	9 ns
Troposphere	1 ns	1 ns
Ionosphere	3 ns	3 ns
Antenna position	1 ns	1 ns
Receiver noise	< 1 ns	< 1 ns
Filtered GPS multipath	1 ns	1 ns
Antenna, cables	2 ns	1 ns
Total	9,9 ns	9,7 ns

Table 2: expected uncertainty budgets of GPS Time restitution for EURIDIS and CNES (NRT2)

uncertainties are expected to be less than 10ns (1s) (cf. Table 2). These results were compared with a CNES independent chain using a GPS time-oriented receiver (NRT2, four channels). Figure 5 plots EURIDIS and CNES results from June 27 to July 1 1998. We can observe a systematic difference of 16 ns with a standard deviation of 1ns. The bias is not consistent with Table 2 error budget, and further experiments are planned to determine the origin of this bias. The variation of GPS time is also under study and could be correlated with the ionospheric corrections.

GPS Time Transfer to the GEO

The GEO time is defined at the output of the GEO payload, precisely at the L1 antenna center of phase. This precise time must be synchronized to the GPS time with an accuracy of 10ns(1σ). That function is ensured by a servo-control technique, based on the near symmetry between the up and down links NLES-GEO. One original feature of EURIDIS Long Loop was rather to apply a time bias corresponding to the drift between GEO time and GPS time as observed from Aussaguel RIMS. In order to ensure the independence between GEO time and the orbit restitution process, the Long Loop reference time, fully mastered by the MCC, is used as GEO transmission time estimate in the orbit

restitution filter. A navigation payload simulator was specifically developed by SEXTANT in order to test the behavior of the EURIDIS Long Loop on the ground test bench. It simulates the RF interfaces with the Long Loop equipment including satellite movement, ionospheric delays on C1, C2 and L1 links, and satellite clock drift. Excellent results were obtained, showing performances of ± 5 ns peak to peak over 24 hours of simulation.

With real INMARSAT 3 AOR-E satellite, it is not possible to measure directly the quality of the GEO time transfer and to verify the error budget, which was evaluated to be 10.8 ns (1σ) in a previous paper [7]. A global performance is available with UERE evaluation.

GEO UERE Performance

From a user point of view, UERE is the only parameter that matters, as it translates into a positioning error, when the geometry of the satellites is known. UERE usually include all the terms having an impact on the user positioning error. In EURIDIS, down link propagation and user receiver errors are not considered. UERE thus only characterizes time synchronization and orbit errors coming from EURIDIS ground segment. It represents errors coming either from the GEO orbit or from the time synchronization onboard the GEO satellite.

UERE is computed every second in the ground segment in Aussaguel as part of the integrity checks. Long– term UERE in Aussaguel (over approximately one day) was found to be 4m RMS (13.3 ns). Another estimation of UERE, has been done using Kourou measurements. UERE was found to be 6 m RMS (see Figure 6). Discontinuities that can be observed don't come

UERE for the GEO in KOUROU (6 m RMS)

Figure 6

from the signal itself, but are due either to orbit updates (every 12 hours) or to time correction models sent to the user (also every 2 hours).
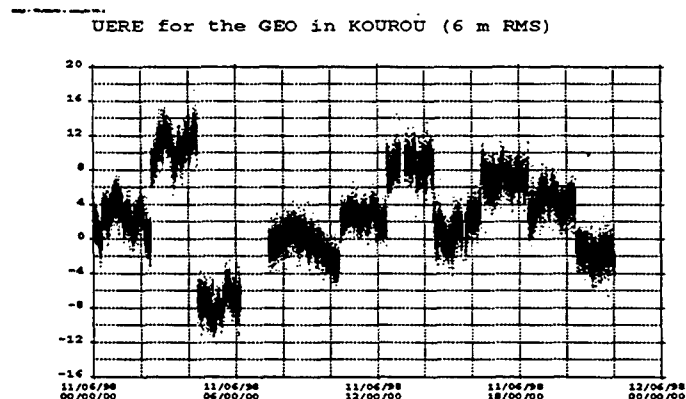
The EURIDIS UERE signals is under evaluation at Sèvres near Paris with BIPM time as reference, and then will be performed at Washington with USNO-MC clock reference.

CONCLUSION

As described in this paper, the role of time and frequency is of paramount importance in EGNOS. Any synchronization error would be derived into navigation error. To answer to these stringent constraints:

- A very stable ENT will be generated and steered to GPS Time with an accuracy estimated to better than 3 ns.
- EGNOS RIMS clocks will be synchronized to ENT with an accuracy of 3ns (2σ).
- ENT will be transferred very accurately to GEO satellites with the long-loop process.

Additionally, EGNOS will provide in real time the difference between ENT and UTC(k). Based on EGNOS GEO signals, users with GNSS multi-channel receivers will have the capability to synchronize very accurately their clocks.

REFERENCES

[1]   Brown, K.R., *The theory of the GPS composite clock*, Proc. ION GPS-91, pp. 223-241.

[2]   Peck, S. et al, *WAAS network time performance and validation*, Proc. ION GPS97, pp 1123-1131.

[3]   J. Benedicto et al, *EGNOS: the European Satellite Based Augmentation to GPS and GLONASS*, Proc. GNSS98.

[4]   D. Flament et al, *EGNOS, The European Based Augmentation to GPS and GLONASS-mission and system architecture*, Proc. GNSS98.

[5]   J-M. Pieplu et al, *EGNOS algorithms performances status and experiment activities*, Proc. GNSS98.

[6]   P. Gouni et al, *Time and frequency aspects in EURIDIS*, Proc. EFTF-96.

[7]   H. Secretan et al, *EURIDIS performances assessment*, Proc. GNSS98.

VALIDATION OF A TIME OF TRANSMISSION MONITOR SUITE FOR MEASUREMENT OF THE OFFSET BETWEEN LORAN-C TRANSMISSIONS AND UTC

Lt. Lee S. Putnam
United States Coast Guard Navigation Center
7323 Telegraph Rd., Alexandria, VA 22315
lputnam@navecen.uscg.mil

Abstract

The U.S. Loran-C system is an integral part of the national infrastructure for the dessimination of precise time and ime interval. In 1997 the U.S. Coast Guard Loran Support Unit located in Wildwood, New Jersey, developed a Time of Transmission Monitor (TOTM) suite. The TOTM suite will be used to measure the average daily offset between UTC and the time of transmission of a Loran-C station. Direct measurement of the time of transmission of the Loran-C signal with respect to UTC will allow the Coast Guard to more tightly couple the Loran-C system to UTC. This paper will discuss the effort, jointly undertaken by the U.S. Coast Guard and the U.S.Naval Observatory, to implement and validate the TOTM equipment suite.

INTRODUCTION

Loran-C is a long-range radionavigation system, which is operated in the United States by the U.S. Coast Guard. The U.S. Loran-C system is operated in concert with Loran-C stations in Canada and with a Russian CHAYKA station to provide radionavigation coverage for the entire continental United States and most of the sub-arctic areas of Alaska and Canada.

The primary requirement for operation of the Loran-C system is to provide the maritime and general aviation community with a long-range radionavigation service. However, the Loran-C system is also recognized as a component of the national Precise Time and Time Interval (PTTI) infrastructure. Synchronization of Loran-C transmissions with Coordinated Universal Time (UTC) allows the Loran-C system to be used for the dissemination of UTC. Cesium-based oscillators provide each Loran-C station with a highly stable source for derivation of the 100 kHz carrier frequency. This allows the Loran-C system to be used as a precise time interval source.

Public Law 100-223, enacted by Congress in 1987, requires timing of Loran-C master transmissions to be held to within 100 nanoseconds of UTC. Control of the offset between Loran-C master transmissions and UTC has traditionally been accomplished using far-field Time Of Arrival (TOA) information measured by the U.S. Naval Observatory (USNO) using Loran-C timing receivers at various locations throughout the country. The TOA of the Loran-C master

signals observed by the receiver at a given location is compared to the UTC standard maintained by USNO at that location. The offsets for each Loran-C master transmission are analyzed over a period of time to determine the relationship between the Time Of Emission (TOE) of the master signal and UTC. Once sufficient analysis has been accomplished to establish the Loran-C TOE/UTC relationship, adjustments can be made in the form of either master oscillator frequency changes or TOE changes.

Holding the offset between UTC and each Loran-C master TOT to within 100 nanoseconds has been a difficult task. Data gathered using far-field receivers are prone to systematic noise resulting primarily from changes in the propagation path delay. Short-term as well as long-term changes in the propagation path affect the time required for the Loran-C signal to travel from the transmitting site to the far-field receiver. Short-term effects, noticeable over several days, are predominately the result of weather fronts moving through the propagation path. Long-term effects are seasonal in nature and are noticeable over several months. Diurnal changes can also be recognized, however, averaging a set of samples taken over a twenty-four hour period can mitigate these.

As a means of improving the quality of the data available for control of the offset between UTC and the Loran-C master TOE, the U.S. Coast Guard Loran Support Unit located in Wildwood, New Jersey, has developed a Time Of Transmission Monitor (TOTM) suite. Two prototype installations of the TOTM equipment have been under evaluation over the past year at Loran Station Williams Lake, Canada, and at Loran Station Seneca, New York.

TIME OF TRANSMISSION MONITOR

The prototype TOTM suite consists of a GPS timing receiver, a time interval counter, a reference time generator (RTG), and a clamp-on current transformer. With the exception of the RTG, the components are all commercially available. The U.S. Coast Guard Loran Support Unit developed the RTG.

484
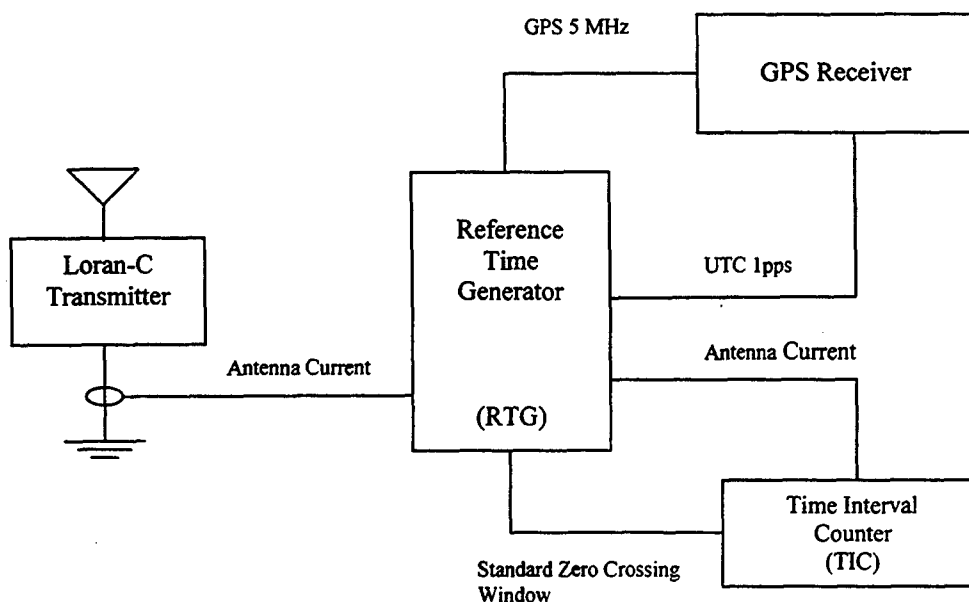
GPS Timing Receiver

The GPS timing receiver provides 1PPS and 5 MHz waveforms that are stabilized to UTC (GPS) with an accuracy of 40 nanoseconds RMS.

Time-Interval Counter

The time-interval counter has time base stability on the order of 2.5×10^{-9} and measurement resolution of 750 picoseconds. It can also perform limited statistical computations on up to 1 million measurement samples.

Reference Time Generator

The RTG provides a means of generating a Standard Zero Crossing (SZC) window at the Loran-C rate being measured. The SZC window is calibrated to a UTC reference provided by a 1PPS reference.

Clamp-on Current Transformer

The clamp-on current transformer provides a means of obtaining a sample from the transmitting antenna current. The antenna current sample is provided to the TIC for use in the offset measurement.

TOTM Functional Description

The Time Of Transmission Monitor suite is designed to measure the offset between UTC and the start of the first of sixteen pulses in a Loran-C Group Repetition Interval (GRI). To accomplish this, the 5 MHz output of the GPS timing receiver is used by the Reference Time Generator to develop a Standard Zero Crossing (SZC) window that is calibrated to UTC and which occurs at the same rate as the Loran-C transmission that is being measured. The SZC window can be used for direct measurement of the Standard Zero Crossing of the transmitted Loran-C pulse. The SZC window is provided to the start input of the Time Interval Counter (TIC), while the Antenna Current waveform from the clamp-on current transformer is provided to the stop input.

The TIC samples a time difference between the SZC window and the Standard Zero Crossing of the antenna current waveform once every GRI. For the Loran-C rate 59900 microseconds, this results in approximately 721,000 measurement samples in a twenty-four hour period. The TIC uses simple statistically analysis to determine the mean and standard deviation of the each twenty-four hour sample set.

TOTM VALIDATION

Loran Support Unit completed installation of two prototype TOTM suites at Loran Stations Williams Lake, British Columbia, and Seneca, New York, in the fall of 1997. The installation at Loran Station Williams Lake was accomplished to fill a need for UTC offset data for that station that was not otherwise available. The prototype installation at Loran Station Seneca was accomplished to provide us with the ability to compare the data set gathered from the TOTM

suite against the data set obtained from the tradition far-field measurement method. Evaluation of the data obtained from these two installations began shortly thereafter.

Early comparison of the data sets gathered from the two sites led to the following observation: the data set from the Williams Lake installation had much less noise than did the data set from Seneca. We hypothesized that the increase in noise in the Seneca data was the result of a more aggressive oscillator management protocol being used for that station. Early in 1998 we set out to prove this. For a period of two months we discontinued adjustments to the 9960-Master oscillator. We found that the apparent noise in the measurement diminished significantly, confirming our hypothesis. This information was used to modify our control protocol for the 9960-Master oscillator. Data obtained for the period following these changes show a reduction in noise in both the USNO data set and the TOTM data set.

## Comparison of the Seneca TOTM and USNO Data Sets

Acceptance of the TOTM measurement method required validation ot the method beyond a theoretical analysis. Historically, the U.S. Naval Observatory has provided the Coast Guard with daily measurement of the offsets between UTC and the Loran-C master station transmissions. In February of 1998, the Coast Guard and USNO agreed to conduct a joint validation of the TOTM measurement method.

Early comparison of the TOTM and USNO far-field data revealed a difference in the offsets being reported by the two measurement systems. There was also a significant difference in the degree of noise seen in the two measurement sets, the USNO far-field data showed a much higher degree of noise. This led us to believe that the most likely source of error in the two measurement systems was the propagation model being used in the far-field measurement method.

In an attempt to eliminate or significantly reduce this potential source of error, a joint USNO and Coast Guard experiment was conducted during March 1998. Three sets of near far-field measurements were taken within a 17-mile radius of Seneca, New York. The measurements compared the Time Of Arrival (TOA) of the Loran-C transmission from Seneca against a Hewlett Packard 5071 Cesium Frequency Standard that had been calibrated to UTC at USNO. An Austron 2100 Loran-C receiver was used to receive the Seneca transmission. This experiment proved to be inconclusive. The inherent cumulative errors of the suite used for the near far-field measurement proved to be greater than the precision needed to validate the TOTM suite.

To resolve the differences seen in the data from the TOTM and USNO measurements, we returned to analysis of the data itself. For a period of time from June through September 1998 it appeared as if there was a fairly constant offset between the two measurement sets. This led us to speculate on the presence of a systematic error that had not yet been accounted for. As time passed, it became apparent that the differences that we were seeing were not constant. In October of 1998, the data began to converge.

9960-Master Seneca New York
UTC Offset Measurements
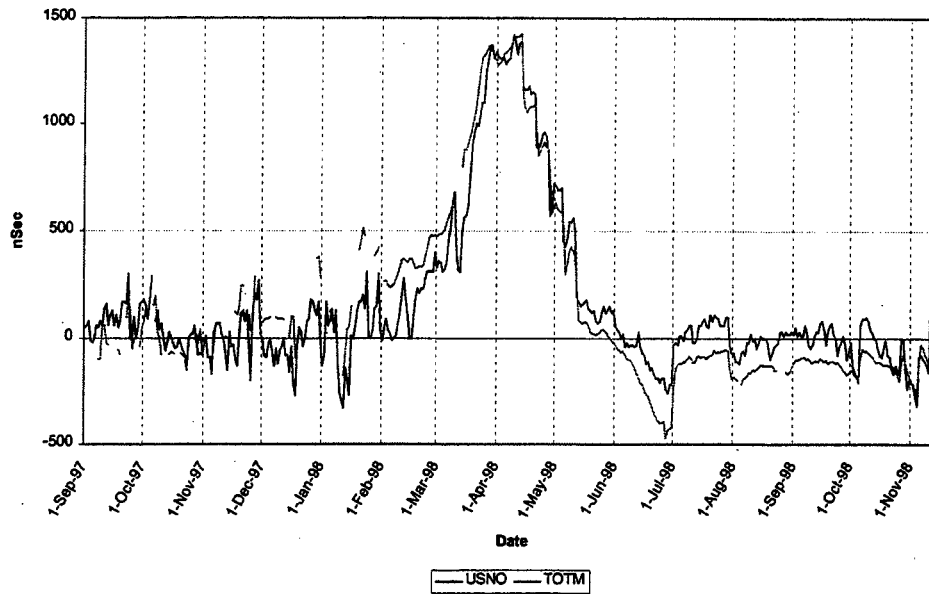
A long-term analysis of the two data sets over the entire fourteen-month sample period reveals a clear trend. The two data sets converge and diverge over the course of the year and cross twice a year.

USNO - PTOTM @ Seneca
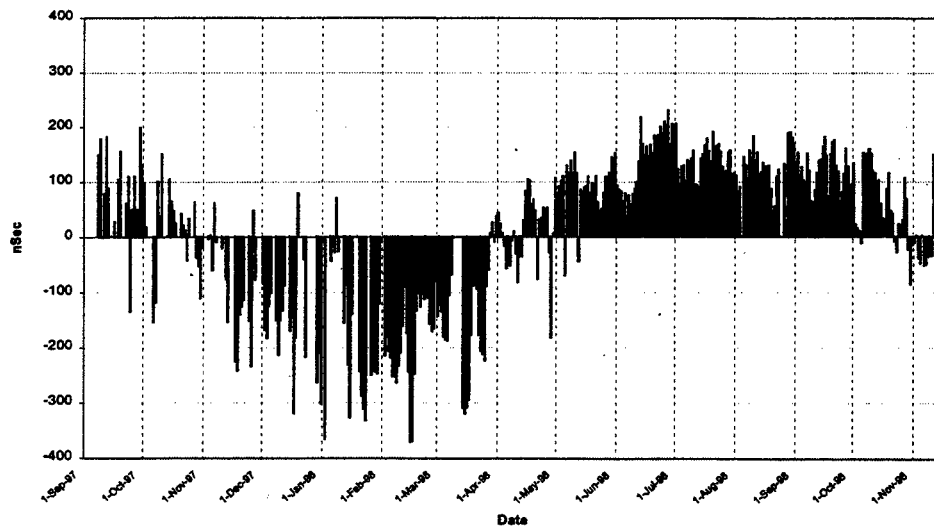
A plot of the daily differences between the two data sets over the fourteen-month period makes the annual trend very apparent.

487

Once the annual trend in the daily differences between the two measurement systems was identified, analysis of the overall effect of the phenomenon was conducted. We found that the mean of the daily differences taken over a twelve-month period (approximately one cycle) is on the order of 12 –15 nanoseconds. However, the standard deviation of the mean is rather high at 140 nanoseconds. Upon further analysis of the data, we noticed that the two measurement systems react differently to a time step. When a two-day period following each Loran-C time step is removed from the data sets, the mean remained nearly the same, while the standard deviation improved significantly. This indicated that there is good long-term correlation between the two measurement systems.

The next step was to identify the source of the annual trend. Our initial hypothesis was that, because of the seasonal nature of the trend, it must be related to changes in the propagation path delay. This led ⋮ us to analyze the method used to resolve the far-field Time Of Arrival (TOA) measurements into Time Of Emission (TOE) UTC offsets. We found that the TOA offset data are converted to TOE offset data by applying a constant value, which represents the predicted propagation path delay and the near-far field transition. Application of a constant does not permit the propagation path model to adapt to seasonal changes in the propagation path delay. This was clearly a source of significant error in the far-field measurement method that would not be present in the time of transmission measurement method.

CONCLUSIONS

From analysis of the data obtained over the past fourteen months from the two measurement systems, the following conclusions can be made:

(1) there is a difference in the measurement system that is cyclical in nature with a period of approximately one year,

(2) the most probable source of the difference seen in the two measurement systems is the lack of compensation for seasonal changes in the propagation model applied to the far-field measurements,

(3) the mean of the daily differences seen in the two measurement systems is small, indicating that there is good long-term correlation between the two systems,

(4) the TOTM measurement system provides data that contain far less noise than the data obtained from far-field measurements,

(5) implementation of the TOTM measurement data as the primary means of control for Loran-C Master station timing would be advantageous in termsof our ability to improve the synchronization of the Loran-C system with UTC

(6) continuation of far-field measurement capability is desirable to ensure long-term stability of the system and to provide data for long-term analysis of the effect of changes in the propagation path.

ACKNOWLEDGMENTS

REFERENCES

1. M.J. Campbell and E.A. Paulus, *U.S. Coast Guard Prototype Time Of Transmission Monitor (PTOTM)*, Proceedings Of The Twenty-Sixth Annual Technical Symposium, International Loran Association (1997).

2. L.W. Campbell, R.H. Doherty,andJ.R. Johler, *Loran-C System Dynamic Model Temporal Propagation Variation Study*, U.S. Department of Transportation, 1979.

3. S.N. Samaddar, *The Theory Of Loran-C Ground Wave Propagation – A Review*, U.S. Coast Guard.

-Note-
The views expressed herein are those of the author and are not to be construed as official or reflecting the views of the Commandant, U.S. Coast Guard, of U.S. Department of Transportation.

Questions and Answers

ED BUTTERLINE (Symmetricom): I have a question related to the future of LORAN. I hear a rumor that the Coast Guard has requested $100 million from Congress to perform deferred maintenance and extend the life of the system up to 2006 or 2008. But the last official words I have seen or heard is that the system is going to die in the year 2000. What is the future of the system as you now know it as we are sitting here right now?

LT. LEE PUTNAM (USCG): Unfortunately, I am the Public Relations Officer at NAVSAT. No, I have the answer to this question, and every time I give a talk, for some reason; I do not know why; 1996 Federal Radionavigation Plan stated that the Coast Guard will discontinue operation December 31st of the year 2000. That same year, Congress mandated that a study be conducted by the Department of Transportation on the cost and benefits of continuing LORAN beyond that time. That study was completed this spring by Booz-Allen and Hamilton, Incorporated, and was forwarded by the Secretary of Transportation to Congress.

The study recommended continuation of LORAN beyond 2015. The Commandant of the Coast Guard, the head of the FAA and some upper level management people in the department made a recommendation to the Secretary that LORAN be continued to 2008. The Coast Guard has gone forward with a budget request this year for recapitalization money for the year 2000.

One of the things the Coast Guard said was we have a system that is 25 years old and has not had significant recapitalization since it was established, and it is not going to make it past 2000.
We still operate HP 5061s that you can not get tubes for anymore unless you get remanufactured ones, so there are obviously some things that have to be replaced. So because of that, we said we need $107 million over a five-year period to recapitalize the system if we are going to continue to operate beyond 2000. So there is a budget line item request of approximately 34 million for the year 2000.
That is basically where we are at this point. That line item is under review and there has been no formal decision from the Secretary as to where we are going to go forward.

ED BUTTERLINE: My concern is that there was a flaw in the Booz-Allen and Hamilton study, that it did not consider a major piece of the national infrastructure as a user of LORAN. That oversight, I think, should be corrected and should have some effect, and what I am talking about is the use of LORAN as a timing source by the national telecommunications infrastructure. That is certainly a significant piece of the national infrastructure, and while it does not depend a hundred percent on LORAN, it does use it as a backup system. It was not reflected in the Booz-Allen and Hamilton study.

LT. LEE PUTNAM: I would agree with you that it is not adequately reflected in the study. I do not want to argue on behalf of Booz-Allen and Hamilton, but I do know that they did make an attempt to get input from that community. The attempt was met with one reply from a major telecommunications concern – let me retract that, it was met with two. One of the replies was withdrawn. I do not know the reason and I do not know how to answer your concern. But I do agree with you. The Coast Guard feels the same way, that we are part of the national infrastructure for dissemination of UTC and also for frequency. That was not reflected in the study very well.

DEMETRIOS MATSAKIS (USNO): For the honor of the USNO, I think I should correct something that you said. I do not think there was any trouble with our measurements taken on our LORAN calibration

trip; I think the problem, the reason it was inconclusive, was due to unmeasurable propagation delays which could have been modeled with considerable theoretical effort that we had not gone through yet. Although it is certainly the case that if we ever do another calibration trip, we will go with even more equipment and do an even better job for you – which we are happy to provide.

PTTI '98 ATTENDEES LIST

Brent K. Andberg
Headquarters Marine Corps, PP&O
Space Plans and Policy
HQMC/PP&O/PLI, 2 Navy Annex
Washington, DC 20380-1775
Tel: 703.614.3706
Fax: 703.614.1420
bandberg@notes.hqi.usmc.mil

Douglas Arnold
TrueTime, Inc.
2835 Duke Ct.
Santa Rosa, CA 95407
Tel: 707.528.1230
Fax: 707.527.6640

Franklin Ascarrunz
Spectra Dynamics Inc.
1212 Main St.
Lewisville, CO 80027
Tel: 303.665.1852
Fax: 303.604.6088
Franklin@spectradynamics.com

Glenn J. Atkinson
AlliedSignal
4060 E. Bijou St.
Colorado Springs, CO 80909
Tel: 719.597.8326
Fax: 719.380.7144
glenn.atkinson@alliedsignal.com

Jacques Azoubib
BIPM
Pavillon de Breteuil
92312 Sevres
France
Tel: 33 1 45 077 062
Fax: 33 1 45 077 059
jazoubib@bipm.fr

Thomas B. Bahder
ARL
2800 Powder Mill Road
Adelphi, MD 20783
Tel: 301.394.2044
Fax: 301.394.2103
bahder@arl.mil

Richard G. Bailey
Datum Bancomm Timing
6781 Via del Oro
San Jose, CA
Tel: 408.547.4161
rbailey@bt.datum.com

Thomas Bartholomew
TASC
131 National Bus. Pkwy
Annapolis Junction, MD
Tel: 301.483.6000
Fax: 301.604.0500
trbartholomew@tasc.com

Francoise S. Baumont
Observatoire De La Cote D'Azur
CERGA REO
Avenue Nicolas Copernic
Grasse 06130
France
Tel: 33 49 340 5338
Fax: 33 49 340 5333
baumont@obs-azur.fr

Ronald L. Beard
Naval Research Laboratory
4555 Overlook Ave., SW
Code 8150
Washington, DC 20375
Tel: 202.461.7054
Fax: 202.767.2845
beard@juno.nrl.navy.mil

Patrick D. L. Beasley
DERA Malvern
St. Andrew's Road
Great Malvern, WORC5,
England
Tel: 44 168 489 6692
Fax: 44 168 489 5057
prcork@dera.gov.uk

Jacques Beser
3S Navigation
4 Executive Circle, Ste 200
Irvine, CA 92614
Tel: 949.862.5900
Fax: 949.862.5908
jbeser@aol.com or nav3s@aol.com

Jimmie Brad
Naval Research Laboratory
4555 Overlook Ave., SW
Washington, DC 20375-5320
Tel: 202.404.4023
Fax: 202.767.4050
brad@juno.nrl.navy.mil

Lee A. Breakiron
U.S. Naval Observatory
Time Service Department
3450 Mass Ave. NW
Washington, DC 20392
Tel: 202.762.1092
Fax: 202.762.1511
lab@tycho.usno.navy.mil

Darrin L. Brendel
DCS Corporation
2221 Camino del Rio S.
San Diego, CA 92108
Tel: 619.681.1890, ext. 227
Fax: 619.681.1899
dbrendel@dcscorp.com

David Briggs
Datum-FTS
34 Tozer Rd.
Beverly, MA 01915
Tel: 978.927.8220
Fax: 978.927.4099
dbriggs@ftsdatum.com

Michel M. Brunet
European Space Agency
18 Avenue Edward Belin
31401 Toulose Cedex 4
France
Tel: 33 561 273 345
Fax: 33 561 282 613
michel.brunet@cnes.fr

Carine Bruyninx
Royal Observatory of Belgium
Avenue Circulaire #3
Brussels B-1180
Belgium
Tel: 32 2 373 0292
Fax: 32 2 374 9822
cbruyninx@oma.be

Carolyn Bryant
NRL
4555 Overlook Ave, SW
Washington, DC 20375
Tel: 202.767.2595
Fax: 202.767.2845
bryant@juno.nrl.navy.mil

James A. Buisson
Antoine Enterprises Inc.
6220 Julian Lane
Mineral, VA 23117
Tel: 202.404.7062
Fax: 202.767.2845
buisson@juno.nrl.navy.mil

Eric A. Burt
U.S. Naval Observatory
Time Service Department
3450 Mass Ave. NW
Washington, DC 20392
Tel: 202.762.0308
Fax: 202.762.1511
burt@atom.usno.navy.mil

Ed Butterline
Symmetricom
1461 Carlisle Road
North Brunswick, NJ 08902
Tel: 732.246.7891
Fax: 732.246.7277
ebutterline@symmetricom.com

Malcolm D. Calhoun
Jet Propulsion Laboratory
M/S 298
4800 Oak Grove Drive
Pasadena, CA 91109
Tel: 818.354.9763
Fax: 818.393.6773
malcolm.d.calhoun@jpl.nasa.gov

James Camparo
The Aerospace Corp
M2-253
PO Box 92957
Los Angeles, CA 90009
Tel: 310.336.6944
Fax: 310.336.7055
james.c.camparo@aero.org

James A. Carlson
Institute for Defense Analysis
1801 N. Beauregard St.
Alexandria, VA 22311
Tel: 703.845.2389
Fax: 703.845.6722

Peter E. Cash
Datum/FTS
58 Cogswell Ave
Beverly, MA
Tel: 978.927.8220
Fax: 978.927.4099
pcash@ftsdatum.com

Tom Celano
Timing Solutions Corp
5335 Sterling Dr., #B
Boulder, CO 80301
Tel: 303.939.8481
Fax: 303.443.5152
tpcelano@timing.com

Harold Chadsey
U.S. Naval Observatory
Time Service Department
3450 Mass Ave. NW
Washington, DC 20392
Tel: 202.762.1450
Fax: 202.762.1511
hc@planck.usno.navy.mil

Ching-Haur Chang
Telecommunication Labs of
Chunghwa Telecom
Natl Std Time & Freq Lab.
12, Lane 551, Min-Tsu Road Sec. 5
Yang-Mei, Taoyuan Taiwan 326
ROC
Tel: 886 3 424 4246
Fax: 886 3 424 5474
changc@ms.chttl.com.tw

Randolph T. Clarke
U.S. Naval Observatory
Time Service Department
3450 Mass Ave. NW
Washington, DC 20392
Tel: 202.762.1500
Fax: 202.762.1511
rtc@smart.usno.navy.mil

494

Pierre J. Claudon
Observatoire De La Cote D'Azur
CERGA Service Temps Frequence
2130 Route De L'observatoire -
Caussols
06460 St Vallier De Thiey
France
Tel: 33 493 405 424
Fax: 33 493 405 433
claudon@obs-azur.fr

John Conkle
Absolute Time Corporation
800 Charcot Ave #110
San Jose, CA 95131
Tel: 408.383.1515
Fax: 408.383.0706
john@absolutetime.com

Franco Cordara
Istituto Elettrotecnico Nazionale
Strada Delle Cacce 91
Turin
Italy
Tel: 39 011 39191
Fax: 39 011 3919259
cordara@tf.ien.it

David T. Crater
U.S. Air Force/2SOPS
Navigation Analysis (DOAN)
300 O'Malley Ave, Suite 41
Schriever AFB, CO 80912
Tel: 719.567.2541
Fax: 719.567.2671
craterdt@schriever.af.mil

Leonard S. Cutler
Hewlett-Packard
3500 Deer Creek Road
MS 26M-9
Palo Alto, CA 94304
Tel: 650.857.5259
Fax: 650.813.3384
Len_Cutler@hpl.hp.com

Theodore C. Dass
ITT
6974 Los Reyes Circle
Colorado Springs, CO 80918-6009
Tel: 719.567.3928
Fax: 719.567.3927
dasstc@afmc.fafb.af.mil

John A. Davis
NPL CTM
Queens Road, Teddington,
Middlesex, TW11 0IW London
United Kingdom
Tel: 44 181 943 7137
Fax: 44 181 943 7138
John.Davis@npl.co.uk

Gerrit de Jong
NMi Van Swinden Laboratorium
Section Time and Frequency
654 P.O. Box
Delft 2600 AR
Netherlands
Tel: 31 15 269 1623
Fax: 31 15 261 2971
GdeJong@NMi.nl

Edoardo Detoma
AlliedSignal Technical Services
Corso Montecucco 95
Torino 10141
Italy
Tel: 39 11 385 4579
Fax: 39 11 242 0372
detomae@tin.it

James A. DeYoung
U.S. Naval Observatory
Time Service Department
3450 Mass Ave. NW
Washington, DC 20392
Tel: 202.762.0290
Fax: 202.762.1511
dey@herschel.usno.navy.mil

William A. Diener
Jet Propulsion Laboratory
Frequency and Time
4800 Oak Grove Dr.
Pasadena, CA 91109
Tel: 818.354.6670
Fax: 818.393.6773
bdiener@jpl.nasa.gov

Gary L. Dieter
Boeing
440 Discoverer Ave.
Ste 38
Schriever AFB, CO 80912-4438
Tel: 719.567.3176
Fax: 719.567.2664
dietergl@afmc.fafb.af.mil

Robert Douglas
National Research Council
M36
Ottawa Ontario
Canada
Tel: 613.993.5186
Fax: 613.952.1394
rob.douglas@nrc.ca

Gregor Dudle
Swiss Federal Office of Metrology
Electricity, Acoustic and Time Section
Lindenweg 50
CH-3003 Bern-Wabern
Switzerland
Tel: 41 31 323 3298
Fax: 41 31 323 3210
gregor.dudle@eam.admin.ch

James Early
Trimble
610 Herndon Pkwy
Herdon, VA
Tel: 703.904.1030
Fax: 703.904.1040
jim-early@trimble.com

495

Christopher R. Ekstrom
U.S. Naval Observatory
Time Service Department
3450 Mass Ave. NW
Washington, DC 20392
Tel: 202.762.0066
Fax: 202.762.1511
ekstrom@atom.usno.navy.mil

Henry F. Fliegel
The Aerospace Corp
2350 E. El Segundo
El Segundo, CA
Tel: 310.336.1710
Fax: 310.336.5036
fliegel@courier1.aero.org

Hugo Fruehauf
Odetics Telecom
1585 S. Manchester Ave.
Anaheim, CA 92802
Tel: 714.780.7960
Fax: 714.780.7696

Michael Garvey
Datum/FTS
34 Tozer Rd.
Beverly, MA
Tel: 978.927.8220
rmgarvey@fts.datum.com

Robert M. Graham
Sandia National Laboratories
PO Box 5800
MS 0665
Albuquerque, NM 87185-0665
Tel: 505.845.0434
Fax: 505.844.6096
rmgraha@sandia.gov

Christopher J. T. Gregerson
U.S. Naval Observatory
Requirements
515 N. Columbus St. #2
Alexandria, VA 22314-2215
Tel: 202.762.1506
Fax: 202.762.1461
ctjg@spica.usno.navy.mil

Jeffrey C. Elmer
Larus Corporation
306 Barnhill Road
West Chester, PA 19382
Tel: 610.692.5693
Fax: 610.701.0775
clmerj@erols.com

Efrain Flores-Colon
SPAWAR Systems Center
53560 Hull St.
San Diego, CA 92152
Tel: 619.524.3152
Fax: 619.524.2074
efrain@spawar.navy.mil

Michael J. Full
NIMA
USAF SMC/CZD
2435 Vela Way #1613
El Segundo, CA 90245
Tel: 310.383.0289
michael.full@losangeles.af.mil

Dick Gast
TRAK Microwave
4726 Eisenhower Blvd.
Tampa, FL 33634
Tel: 813.884.1411
rgast@trak.com

Clive Green
Quartzlock
Gothic, Plymouth Rd., Totnes
Devon TQ9 SLH
United Kingdom
Tel: 44 1 803 862062
Fax: 44 1 803 867962
clivegreen@quartzlock.com

Peter Grognard
IMEC
VKDM
Kapeldreef 75
Leuven B-3001
Belgium
Tel: 32 16 281 791
Fax: 32 16 281 515
grognard@imec.be

Sheila Faulkner
SFA Inc.
3159 Patrick Henry Drive
Falls Church, VA 22044
Tel: 703.532.6411
Fax: 703.532.6338
bopenyan@aol.com

Gerald L. Freed
ITT Industries
Aerospace/Communications Div
100 Kingsland Rd
Clifton, NJ 07014-1993
Tel: 973.284.2104
Fax: 973.284.3394
gfreed@acdnj.itt.com

Ivan J. Galysh
Naval Research Laboratory
4555 Overlook Ave., SW
Washington, DC 20375
Tel: 202.404.7060
Fax: 202.767.2845
galysh@juno.nrl.navy.mil

Glen Gibbons
GPS World
859 Willamette St.
Eugene, OR 97401
Tel: 541.984.5286
Fax: 541.344.3514
ggibbons@advanstar.com

Charles A. Greenhall
Jet Propulsion Laboratory
4800 Oak Grove Dr.
MS 298-100
Pasadena, CA 91109
Tel: 818.393.6944
Fax: 818.393.6773
charles.greenhall@jpl.nasa.gov

Mark J. Gunzelman
U.S. Naval Observatory
3450 Massachusetts Avenue, NW
Washington, DC 20392-5420
Tel: 202.762.1479
Fax: 202.762.1461
mjg@spica.usno.navy.mil

Joerg H. Hahn
DLR Oberpfaffenhofen
Institute of Radio Frequency
Technology
Postbox 1116
Wessling Bavaria D-82230
Germany
Tel: 49 815 328 2335
Fax: 49 815 328 1135
joerg.hahn@dlr.de

Yuko Hanado
Communications Research
Laboratory
4-2-1 Nukui-kita-machi Koganei
Tokyo
Japan
Tel: 81 42 327 7568
Fax: 81 42 327 6689
yuko@crl.go.jp

Gildas H. Herman
Temex Telecom
29 Avenue de la Baltique
Les Ulis 91953
France
Tel: 33 1 69 822 007
Fax: 33 1 64 464 550
gildas_herman@compuserve.com

Douglas W. Hogarth
20241 194th Pl., NE
Woodinville, WA 98072-8889
Tel: 425.788.1507
doug@niceties.com

Robert Horton
WR Inc.
710A W. 4th St.
Pueblo, CO 81003
Tel: 719.595.9880
Fax: 719.595.9890
robert@fleetpc.com

Stacy J. Huser
USAF/2SOPS
Navigation and Timing Analysis
5770 Innsbrook Place, #1303
Colorado Springs, CO 80918
Tel: 719.264.1409
husersj@schriver.af.mil

Steven T. Hutsell
U.S. Naval Observatory
USNO AMC
400 O'Malley Avenue, Ste 44
Schriever AFB, CO 80912-4044
Tel: 719.567.6740
Fax: 719.567.6763
steven.hutsell@schriever.af.mil

Michito Imae
Communications Research
Laboratory
Standards and Measurements
Division
4-2-1, Nukuikita Koganei
Tokyo 184-8795
Japan
Tel: 81 42 327 7566
Fax: 81 42 327 6689
imae@crl.go.jp

Jeffrey S. Ingold
AlliedSignal Technical Services
VLBI
1 Bendix Road
Columbia, MD 21045
Tel: 410.964.7188
Fax: 410.964.7187
jsingold@atscv1.atsc.allied.com

T. Jay Jayawardena
AT&T
101 Crawfords Corner Road
Rm 2C-424
Holmdel, NJ 07733
Tel: 732.949.9584
Fax: 732.949.0830
tj@att.com

Kenneth J. Johnston
U.S. Naval Observatory
3450 Massachusetts Avenue, NW
Washington, DC 20392-5420
Tel: 202.762.1513
Fax: 202.762.1461
kjj@astro.usno.navy.mil

David M. Judge
U.S. Naval Observatory
Time Service Department
3450 Mass Ave. NW
Washington, DC 20392
Tel: 202.762.1427
Fax: 202.762.1511
dmj@laplace.usno.navy.mil

Sarunas K. Karuza
The Aerospace Corp
PO Box 92957
MS M1 111
Los Angeles, CA 90009
Tel: 310.336.6837
Fax: 310.336.6225
sarunas.k.karuza@aero.org

Sonia U. Kim
3S Navigation
4 Executive Circle, Ste. 200
Irvine, CA 92614
Tel: 949.862.5900
Fax: 949.862.5908
nav3s@aol.com

Wendy L. King
U.S. Naval Observatory
Time Service Department
3450 Massachusetts Avenue, NW
Washington, DC 20392-5420
Tel: 202.762.1577
Fax: 202.762.1511
wendy@newton.usno.navy.mil

Dieter Kirchner
Technical University Graz
Inffeldgasse 12
A-8010 Graz
Austria
Tel: 43 316 873 7441
Fax: 43 316 46 3697
kirchner@inw.tu-graz.ac.at

William J. Klepczynski
ISI
1608 Spring Hill Rd.
Vienna, VA 22182
Tel: 202.651.7670
Fax: 202.651.7699
wklepczy@aol.com

Douglas E. Koch
Naval Research Laboratory
4555 Overlook Ave., SW
Washington, DC 20375
Tel: 202.404.7067
Fax: 202.767.2845
koch@juno.nrl.navy.mil

497

Paul Koppang
Datum
1711 Holt Rd.
Tuscaloosa, AL
Tel: 205.553.0038
pak@wwisp.com

Paul F. Kuhnle
Jet Propulsion Laboratory
4800 Oak Grove Drive
MS 298-100
Pasadena, CA 91109
Tel: 818.354.2715
Fax: 818.393.6773
Paul.F.Kuhnle@jpl.nasa.gov

Francois Lahaye
Natural Resources - Canada
615 Booth
Ottawa Ontario
Canada
Tel: 613.995.4488
Fax: 613:995.3215
Francois.Lahaye@geod.emr.ca

G. Paul Landis
SFA
4555 Overlook Ave., SW
Washington, DC 20375
Tel: 202.404.7061
Fax: 202.767.2845
landis@juno.nrl.navy.mil

Marie M. Largay
Naval Research Laboratory
4555 Overlook Ave., SW
Code 8153
Washington, DC 20375
Tel: 202.767.9133
Fax: 202.767.2845
largay@juno.nrl.navy.mil

Dennis G. Larsen
U.S. Naval Observatory
3450 Massachusetts Avenue, NW
Washington, DC 20392-5420
Tel: 202.762.1538
Fax: 202.762.1461
dgl@spica.usno.navy.mil

Albert Leong
The Aerospace Corp
2350 E. El Segundo Blvd.
El Segundo, CA 90245
Tel: 310.336.2328
Fax: 310.336.2385
albert.leong@aero.org

Sigfrido M. Leschiutta
I.E.N.
Strada delle Cacce 91
10135 Torino
Italy
Tel: 39 011 3919543
Fax: 39 011 346384

Judah Levine
NIST
Dept of Commerce MS 847
325 Broadway
Boulder, CO 80303
Tel: 303.497.3903
Fax: 303.497.6461
jlevine@boulder.nist.gov

Wlodzimierz Lewandowski
BIPM
Pavillon de Breteuil
92312 Sevres
France
Tel: 33 1 45 077 063
Fax: 33 1 45 077 059
wlewandowski@bipm.fr

David R. Lewis
DoD
2003 Compton Ct.
Annapolis, MD 21401
Tel: 301.668.6701

Gene E. Long
Brandywine Communications
PO Box 260
Ridge, MD 20680
Tel: 301.872.4490
gel@mail.ameriec.net

Douglas R. Lowrie
EG&G
35 Congress St.
Salem, MA 01970
Tel: 978.745.3200
Fax: 978.741.4923
dlowrie@egginc.com

Leo A. Mallette
Hughes
2309 S. Santa Anita Ave.
Arcadia, CO 91006
Tel: 310.364.9243
Fax: 310.364.9048
lmallette@mail.hac.com

Willard A. Marquis
Lockheed Martin Missiles and Space
GPS IIR Operations
2825 Bethune Ct.
Colorado Springs, CO 80920-5123
Tel: 719.567.3936
Fax: 719.567.3927
Willard.Marquis@lmco.com

David A. Masiero
Coast Guard NAVCEN
7323 Telegraph
Alexandria, VA 22315
Tel: 703.313.5872
Fax: 703.313.5805
dmasiero@navcen.uscg.mil

Demetrios N. Matsakis
U.S. Naval Observatory
Time Service Department
3450 Mass Ave. NW
Washington, DC 20392
Tel: 202.762.1587
Fax: 202.762.1511
dnm@orion.usno.navy.mil

Dennis D. McCarthy
U.S. Naval Observatory
3450 Mass Ave. NW
Washington, DC 20392
Tel: 202.762.1837
Fax: 202.762.1563
dmc@maia.usno.navy.mil

Thomas McCaskill
Naval Research Laboratory
4555 Overlook Ave., SW
Washington, DC 20375
Tel: 202.404.7068
Fax: 202.767.2845
mccaskill@juno.nrl.navy.mil

Angela D. McKinley
U.S. Naval Observatory
Time Service Department
3450 Mass Ave. NW
Washington, DC 20392
Tel: 202.762.1457
Fax: 202.762.1511
amd@simon.usno.navy.mil

Marvin Meirs
FEI
55 Charles Lindbergh Blvd.
Mitchell Field, NY 11553
Tel: 516.794.4500
Fax: 516.794.4340

Martin W. Mellor
Charles Stark Draper Laboratory
Systems Engineering
555 Technology Square
Cambridge, MA 02139-3563
Tel: 617.258.2184
Fax: 617.258.3737
mmellor@draper.com

Debbie Melnick
Meetings Verbatim
PO Box 941221
Atlanta, GA 31141
Tel: 707.925.0204

Filippo Messina
Observatorio Astronomico di Cagliari
(CAO)
Str. 54 Loc. Poggio dei Pini
Capoterra 09012
Italy
Tel: 39 70 7118 0212
Fax: 39 70 725 425
messina@ca.astro.it

Brent E. Miller
Litton TASC
131 National Business Pkway
Annapolis Junction, MD
Tel: 301.483.6000, ext.2088
bemiller@jswg.org

Mihran Miranian
U.S. Naval Observatory
Time Service Department
3450 Mass Ave. NW
Washington, DC 20392
Tel: 202.762.1452
Fax: 202.762.1511
mm@aitken.usno.navy.mil

George M. Misko
GPS World
101 Fieldcrest Ave
Edison, NJ 08837
Tel: 732.225.9500
Fax: 732.225.0211
gmisko@advanstar.com

Don Mitchell
TrueTime, Inc.
2835 Duke Ct.
Santa Rosa, CA 95407
Tel: 707.528.1230
Fax: 707.527.6640

David C. Monton
Applied Research Laboratory
University of Texas
10000 Burnet Rd.
Austin, TX
Tel: 512.835.3831
dmonton@arlot.utexas.edu

Angelyn Moore
Jet Propulsion Laboratory
MS 238-540
4800 Oak Grove Dr.
Pasadena, CA 91109
Tel: 818.354.5434
Fax: 818.393.6686
Angelyn.W.Moore@jpl.nasa.gov

Raymond Moskaluk
Hewlett-Packard Co.
Santa Clara Division (TMO)
5301 Stevens Creek Blvd
M/S 52U/26
Santa Clara, CA 95052
Tel: 408.553.3319
Fax: 408.553.6891
ray_moskaluk@hp.com

Leonardo Mureddu
Cagliari Astronomical Observatory
(CAO)
Str. 54 Loc. Poggio dei Pini
Capoterra (CA)09012
Italy
Tel: 39 70 711 80214
Fax: 39 70 725 425
mureddu@ca.astro.it

Tamara A. Myers
Naval Research Laboratory
4555 Overlook Ave., SW
Washington, DC 20375
Tel: 202.404.7069
Fax: 202.767.2845
myers@juno.nrl.navy.mil

Lisa M. Nelson
NIST
Time and Frequency Div.
325 S. Broadway
Boulder, CO 80303-3328
Tel: 303.497.3446
Fax: 303.497.6461
lnelson@boulder.nist.gov

Robert A. Nelson
Satellite Engineering
Research Corporation
7701 Woodmont Ave., Ste 208
Bethesda, MD 20814
Tel: 301.657.9641
Fax: 301.657.9642
robtnelson@aol.com

Jerry R. Norton
Johns Hopkins University
APL
Johns Hopkins Road
Laurel, MD 21104
Jerry_Norton@jhuapl.edu

499

Karen F. O'Donoghue
NSWCDD
Code B35
17320 Dahlgren Rd.
Dahlgren, VA
Tel: 540.653.1567
Fax: 540.653.8673
kodonog@nswc.navy.mil

Jay Oaks
Naval Research Laboratory
4555 Overlook Ave., SW
Washington, DC 20375
Tel: 202.767.1434
oaks@juno.nrl.navy.mil

Christopher J. Olszewski
AT&T
101 Crawfords Corner Road
Rm 2C-424
Holmdel, NJ 07733
Tel: 732.949.2149
Fax: 732.949.0830
colszewski@att.com

Allen (Skip) W. Osborne
Allen Osborne Associates
756 Lakefield Rd., Bldg. J.
Westlake Village, CA 91361
Tel: 805.495.8420
Fax: 805.373.6067

Terry N. Osterdock
Absolute Time Corporation
800 Charcot Ave #110
San Jose, CA 95131
Tel: 408.383.1520
Fax: 408.383.0706
terry@absolutetime.com

Joseph W. Ouellette
Litton/PRC
222 N. Sepulveda Blvd.
Ste 1310
El Segundo, CA 90245
Tel: 310.363.2023
Fax: 310.363.2023
joe.ouellette@losangeles.af.mil

Juan Palacio
Real Observatorio de la Armada
Seccion de Hora
Cecilio Pujazon s/n
San Fernando Cadiz E-11.100
Spain
Tel: 34 956 599 286
Fax: 34 956 599 366
jpalacio@roa.es

Paul Paquet
Royal Observatory of Belgium
Avenue Circulaire #3
Brussels B-1180
Belgium
Tel: 32 2 373 0249
Fax: 32 2 374 9822
paquet@oma.be

Thomas E. Parker
NIST
Time and Frequency Division
325 Broadway
Boulder, CO 80803
Tel: 303.497.7881
Fax: 303.497.6461
tparker@bldrdoc.gov

Ralph Partridge
Los Alamos Nat'l Laboratory
141 San Ildefonso Road
Los Alamos, NM 87544
Tel: 505-662-6585
72311.440@compuserve.com

William H. Paul
U.S. Army TECOM NRO-DT-T
White Sands Missile Range, NM
Tel: 505.679.9220

Peter Z. Paulovich
SPAWARSYSCEN Charleston
PO Box 1376
Norfolk, VA 23501-1376
Tel: 757.396.0287
Fax: 757.396.0518
paulovip@spawar.navy.mil

Alexander H. N. Pawlitzki
TimeTech
Nobelstrasse 15
D-70569 Stuttgart
Germany
Tel: 49 711 678080
Fax: 49 711 6780899

George R. Peters
Lockheed Martin Mission Systems
GPS
700 N. Frederick Road
Gaithersburg, MD 20879
Tel: 301.240.5489
Fax: 301.240.6073
george.peters@lmco.com

Gerard Petit
BIPM
Pavillon de Breteuil
92312 Sevres
France
Tel: 33 1 45 07 70 67
Fax: 33 1 45 07 70 59
gpetit@bipm.fr

Vince Pham
SPAWAR San Diego
53560 Hull St.
San Diego, CA 92152
Tel: 619.553.3010
Fax: 619.553.3460
vpham@spawar.navy.mil

Ed Powers
U.S. Naval Observatory
Time Service Department
3450 Mass Ave. NW
Washington, DC 20392
Tel: 202.762.1451
Fax: 202.762.1511
powers@drake.usno.navy.mil

Lt. Lee Putnam
U.S. Coast Guard Navigation Center
7323 Telegraph Road
Alexandria, VA 22315
Tel: 703.313.5861
Fax: 703.313.5805
lputnam@navcen.uscg.mil

Jim Ray
U.S. Naval Observatory
3450 Massachusetts Ave, NW
Washington, DC 20392-5420
Tel: 202-762-1444

William J. Riley
EG&G
35 Congress St.
Salem, MA 01970
Tel: 978.745.3200
Fax: 978.741.4923
wriley@egginc.com

Pascal Rochat
Temex
Vauseyou 29
Neuchatel
Switzerland
Tel: 41 1 32 7321660
Fax: 41 1 32 7321667
temex@vtx.ch

Edward Rodemsky
Trimble
610 Herndon Pkwy
Herndon, VA
Tel: 703.904.1030
Fax: 703.904.1040
ed-rodemsky@trimble.com

Ronald C. Roloff
Advanced Technical Resources
8005 McKenstry Dr.
Laurel, MD 20723
Tel: 301.225.3636
Fax: 301.853.0246
rroloff@clark.net

Jessica L. Roma
Infinity Systems Engineering
6440 Gemstone Way
Colorado Springs, CO
Tel: 719.567.6362
Fax: 719.567.6660
jroma@infinity.whit.org

Lisa Rumphrey
TrueTime, Inc.
2835 Duke Ct.
Santa Rosa, CA 95407
Tel: 707.528.1230
Fax: 707.527.6640

Bill Ryan
DISA
10701 Parkridge Blvd.
Reston, VA 20191
Tel: 703.438.3177
ryanw@ncr.disa.mil

Jim Saret
Saret Associates
9 Delphi Circle
Andover, MA 01810
Tel: 978.475.9332
Fax: 978.475.9332
jimsaret.sa@worldnet.att.net

Wolfgang Schaefer
TimeTech
Nobelstrasse 15
D-70569 Stuttgart
Germany
Tel: 49 711 678080
Fax: 49 711 6780899

Thomas Schildknecht
University of Bern
Astronomical Institute (AIUB)
Sidlerstrasse 5
Bern CH-3012
Switzerland
Tel: 41 31 631 85 91
Fax: 41 31 631 38 69
Thomas.Schildknecht@aiub.unibe.ch

Lara Schmidt
U.S. Naval Observatory
Time Service Department
3450 Mass Ave. NW
Washington, DC 20392
Tel: 202.762.0289
Fax: 202.762.1511
lss@ramsey.usno.navy.mil

Richard E. Schmidt
U.S. Naval Observatory
Time Service Department
3450 Mass Ave. NW
Washington, DC 20392
Tel: 202.762.1578
Fax: 202.762.1511
res@tuttle.usno.navy.mil

William H. Schuh
ITT/FSC
PO Box 5228
VAFB, CA 93437
Tel: 805.734.8232, ext. 63166
Fax: 805.734.8232, ext. 66997

George A. Shaton
DoD
CANX, QS11 Ste 6690
Ft. Meade, MD 20755-6690
Tel: 301.688.7322

Paul Skoog
TrueTime, Inc.
2835 Duke Ct.
Santa Rosa, CA 95407
Tel: 707.528.1230
Fax: 707.527.6640
PSkoog@truetime.com

William E. Smith
Datum Corp
Efratom Time & Frequency Division
3 Parker
Irvine, CA 92618
Tel: 949.598.7615
Fax: 949.598.7650
besmith@efratom.com

Armin Soering
Deutsche Telekom AG
Zentrale, TN236-5
Am Kavalleriesand 3
Darmstadt 64295
Germany
Tel: 49 6151 834549
Fax: 49 6151 833834
soering@topmail.de

Samuel R. Stein
Timing Solutions Corp
5335 Sterling Dr., #B
Boulder, CO 80301
Tel: 303.939.8481
Fax: 303.443.5152
srstein@timing.com

Mark A. Strain
TRAK Microwave
4726 Eisenhower Blvd.
Tampa, FL 33634
Tel: 813.884.1411
Fax: 813.884.0981
mstrain@trak.com

Donald Stribling
AlliedSignal
4060 E. Bijou St.
Colorado Springs, CO 80909
Tel: 719.637.6780
Fax: 719.380.7144
don.stribling@alliedsignal.com

Miranda Swan
Quartzlock
Gothic, Plymouth Rd., Totnes
Devon TQ9 SLH
United Kingdom
Tel: 44 1 803 862062
Fax: 44 1 803 867962
quartzlock@quartzlock.com

Thomas B. Swanson
U.S. Naval Observatory
Time Service Department
3450 Massachusetts Avenue, NW
Washington, DC 20392-5420
Tel: 202.762.1458
Fax: 202.762.1511
swanson@atom.usno.navy.mil

Richard L. Sydnor
Jet Propulsion Laboratory
2983 Zane Grey Terrace
Altadena, CA 91001
Tel: 626.794.6848
sydnor@pacbell.net

Philip E. Talley, Jr.
Sax Freeman Associates
Naval Research Laboratory
Naval Space Technology
1022 Eagle Crest
Macon, Georgia 31211
Tel: 912.745.3415
petalley@mylink.net

Patrizia Tavella
Istituto Elettrotecnico Nazionale
Strada delle Cacce 91
10135 Torino
Italy
Tel: 39 011 391 9235
Fax: 39 011 391 9259
tavella@tf.ien.it

Eddie Thompson
746TG Holloman AFB
1466 Vander Griff Rd.
Holloman AFB, NM 88330
Tel: 505.679.1714
ethompson@mailgate .46tg.af.mil

Massimo Tinto
Jet Propulsion Laboratory
4800 Oak Grove Dr.
Pasadena, CA 91109
Tel: 818.254.0798
Fax: 818.393.4643
Massimo.Tinto@jpl.nasa.gov

Robert L. Tjoelker
Jet Propulsion Laboratory
MS 298-100
4800 Oak Grove Drive
Pasadena, CA 91109
Tel: 818.354.1873
Fax: 818.393.6773
tjoelker@fridge.jpl.nasa.gov

Fred Torcaso
U.S. Naval Observatory
Time Service Department
3450 Mass Ave. NW
Washington, DC 20392
Tel: 202.762.1456
Fax: 202.762.1511
torcaso@random.usno.navy.mil

Minh Q. Tran
U.S. Naval Observatory
Time Service Department
3450 Mass Ave. NW
Washington, DC 20392
Tel: 202.762.0913
Fax: 202.762.1511
mtran@tsee11.usno.navy.mil

Peter A. Tyler
Geco-Prakla
Solbraveien 23
1370 Asker
Norway
Tel: 47 66 788000
Fax: 47 66 788500
tyler@oslo.geco-prakla.slb.com

Jacques Vanier
University of Montreal
Montreal
Canada
Tel: 514.425.5055
Fax: 514.425.5055
jacques.vanier@sympatico.ca

Francine M. Vannicola
U.S. Naval Observatory
Time Service Department
3450 Mass Ave. NW
Washington, DC 20392
Tel: 202.762.1455
Fax: 202.762.1511
fmv@cassini.usno.navy.mil

Francois Vernotte
Observatoire de Besancon
Laboratoire Temps-Frequence
41 bis avenue de l'Observatoire - B.P.
1615
Besancon Cedex 25010
France
Tel: 33 381 666 922
Fax: 33 381 666 944
francois@obs-besancon.fr

James D. Voss
Spectracom Corporation
101 Despatch Drive
East Rochester, NY 14445
Tel: 716.381.4827
Fax: 716.318.4998
JamesDVoss@aol.com

Steven Waite
WR Inc.
710A W. 4th St.
Pueblo, CO 81003
Tel: 719.595.9880
Fax: 719.595.9890
gpsman@fleetpc.com

June E. Watanabe
Litton/PRC
222 N. Sepulveda Blvd.
El Segundo, CA 90245
Tel: 310.252.8024
Fax: 310.252.4345

Joe White
Naval Research Laboratory
Code 8151
4555 Overlook Ave., SW
Washington, DC 20375
Tel: 202.767.5111
Fax: 202.767.4050
white@juno.nrl.navy.mil

Victor S. Zhang
NIST
Time and Frequency Div.
325 Broadway
Boulder, CO 80303
Tel: 303.497.3977
Fax: 303.497.6461
vzhang@boulder.nist.gov

Warren F. Walls
Femtosecond Systems, Inc.
690 Arbutus Street
Golden, CO 80401
Tel: 303.462.0799
Fax: 303.462.0766
femtosecond@uswest.net

Kevin A. Waters
DoD
Washington, DC
Tel: 202.688.7526

Ray Williamson
Femtosecond Systems, Inc.
690 Arbutus Street
Golden, CO 80401
Tel: 303.462.0799
Fax: 303.462.0766
femtosecond@uswest.net

Dai Zhongning
Singapore Productivity and
Standards Board
National Measurement Center
2 Bukit Merah Central
PSB Building 159835
Singapore
Tel: 65 278 6666
Fax: 65 274 5413
lsy@psb.gov.sg

S. Clark Wardrip
SFA, Inc.
726 Foxenwood Dr.
Santa Maria, CA 93455
Tel: 805.937.6448
Fax: 805.937.9601
skyclark@aol.com

Marc A. Weiss
NIST
325 Broadway
Boulder, CO 80303
Tel: 303.497.3261
Fax: 303.497.6461
MWeiss@boulder.nist.gov

Andy Wu
The Aerospace Corporation
El Segundo, CA 91364
Tel: 310.336.0437
Fax: 310.336.5076
andy.wu@aero.org

James F. Zumberge
Jet Propulsion Laboratory
4800 Oak Grove Dr.
Pasadena, CA 91109
Tel: 818.354.6734
Fax: 818.393.4963
James.F.Zumberge@jpl.nasa.gov